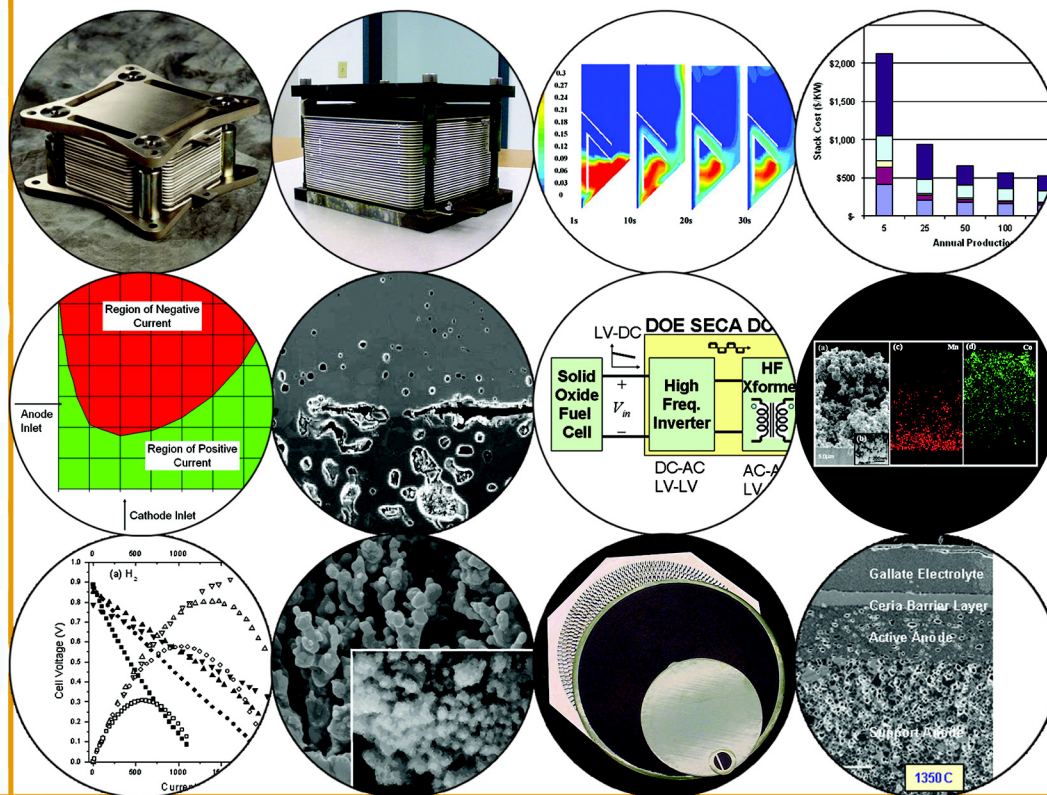


2004 Office of Fossil Energy Fuel Cell Program Annual Report

FUEL CELL



ANNUAL REPORT





National Energy Technology Laboratory

626 Cochrans Mill Road
P.O. Box 10940
Pittsburgh, PA 15236-0940

3610 Collins Ferry Road
P.O. Box 880
Morgantown, WV 26507-0880

One West Third Street, Suite 1400
Tulsa, OK 74103-3519

P.O. Box 750172
539 Duckering Bldg./UAF Campus
Fairbanks, AK 99775-0172

Mark C. Williams
Fuel Cell Technology Manager
304-285-4747
mark.williams@netl.doe.gov


*Visit the SECA website at:
www.seca.doe.gov*

*Visit the NETL website at:
www.netl.doe.gov*

Customer Service **1-800-553-7681**



**U.S. Department of Energy
Office of Fossil Energy**

Printed in the United States on recycled paper 

September 2004

2004 Office of Fossil Energy Fuel Cell Program Annual Report

September 2004

CONTENTS

I	Introduction.....	1
II	SECA Industry Teams	9
1	Acumentrics Corporation: Development of a Low-Cost 10-kW Tubular SOFC Power System	11
2	Cummins Power Generation: 10-kW Solid Oxide Fuel Cell Power System Commercialization	15
3	Delphi Automotive Systems LLC: Solid State Energy Conversion Alliance Delphi SOFC	19
4	FuelCell Energy, Inc.: Thermally Integrated High Power Density SOFC Generator	23
5	GE Hybrid Power Generation Systems: Solid State Energy Conversion Alliance (SECA) Solid Oxide Fuel Cell Program	27
6	Siemens Westinghouse Power Corporation: Small-Scale Low-Cost Solid Oxide Fuel Cell Power Systems	33
III	SECA Core Technology Program	37
A	Materials	39
1	Argonne National Laboratory: SOFC Research and Development	39
2	Ceramatec, Inc.: Metal Interconnect for SOFC Power Systems	44
3	Functional Coating Technology, LLC: Composite Cathode for High Power Density Solid Oxide Fuel Cells	47
4	GE Hybrid Power Generation Systems: Materials and Process Development Leading to Economical High-Performance Thin-Film Solid Oxide Fuel Cells	51
5	Georgia Tech Research Corporation: Functionally Graded Cathodes for Solid Oxide Fuel Cells	55
6	Lawrence Berkeley National Laboratory: Development of Metal-Supported SOFC	61
7	National Energy Technology Laboratory: Advanced Fuel Cell Development	66
8	NexTech Materials, Ltd.: Continuous Process for Producing Low-Cost, High-Quality YSZ Powder	71
9	Oak Ridge National Laboratory: Reliability and Durability of Materials and Components for Solid Oxide Fuel Cells	75
10	Pacific Northwest National Laboratory: SOFC Compressive Seal Development at PNNL	81
11	Pacific Northwest National Laboratory: Reduction of Carbon Formation from Nickel Catalysts Using Nickel-Gold Surface Alloys	85
12	Pacific Northwest National Laboratory: SOFC Anode Materials Development at PNNL	90
13	Pacific Northwest National Laboratory: SOFC Cathode Materials Development at PNNL	93
14	Pacific Northwest National Laboratory: SOFC Interconnect Materials Development at PNNL	97
15	Sandia National Laboratories: Reliable Seals for Solid Oxide Fuel Cells	101
16	Southwest Research Institute: Surface-Modified Ferritic Interconnect Materials for Solid Oxide Fuel Cells	105
17	University of Pittsburgh: Fundamental Studies of the Durability of Materials for Interconnects in Solid Oxide Fuel Cells (SOFCs)	109
18	University of Utah: Cathodes for Low-Temperature SOFC: Issues Concerning Interference from Inert Gas Adsorption and Charge Transfer	115
19	University of Washington: Advanced Measurement and Modeling Techniques for Improved SOFC Cathodes	119

III SECA Core Technology Program (Continued)

B Fuel Processing	125
1 Argonne National Laboratory: Technology Development in Support of the Solid State Energy Conversion Alliance	125
2 Los Alamos National Laboratory: Diesel Reforming for Solid Oxide Fuel Cell Auxiliary Power Units	128
3 National Energy Technology Laboratory: Fundamental Reforming Studies - Role of Catalytic O ₂ Supports on Fuel Reforming	135
4 National Energy Technology Laboratory: Hexaaluminate Reforming Catalysts	138
5 National Energy Technology Laboratory: Diesel Fuel Reforming Kinetics	141
6 Northwestern University: Operation of Solid Oxide Fuel Cell Anodes with Practical Hydrocarbon Fuels	147
C Power Electronics	153
1 Oak Ridge National Laboratory: Trade Study for Integrating Numerous SECA SOFC Modules	153
2 Texas A&M University: Development of a New Class of Low-Cost, High-Frequency Link Direct DC-to-AC Converters for SOFCs	157
3 Virginia Polytechnic Institute and State University: Low-Cost Soft-Switched DC/DC Converter for Solid Oxide Fuel Cells	161
D Modeling & Simulation	167
1 Georgia Institute of Technology: An Integrated Approach to Modeling and Mitigating SOFC Failure	167
2 Pacific Northwest National Laboratory: SOFC Model Development at PNNL	173
3 TIAX LLC: Solid Oxide Fuel Cell Manufacturing Cost Model: Simulating Relationships between Performance, Manufacturing, and Cost of Production	178
4 University of Florida: Determination of Electrochemical Performance and Thermo-Mechanical-Chemical Stability of SOFCs from Defect Modeling	183
E Controls & Diagnostics	191
1 University of Illinois: An Investigation to Resolve the Interaction between Fuel Cell, Power Conditioning System and Application Load	191
F Manufacturing	199
1 GE Hybrid Power Generation Systems: Tape-Calendering Manufacturing Processes for Multi-Layer Thin-Film Solid Oxide Fuel Cells	199
2 University of Utah: A Low-Cost Process for the Synthesis of Nanosize Ytria-Stabilized Zirconia (YSZ) by Molecular Decomposition	203
IV Fuel Cell Systems	207
1 FuelCell Energy, Inc.: Molten Carbonate Fuel Cell Product Design Improvement	209
2 Siemens Westinghouse Power Corporation: High-Temperature Solid Oxide Fuel Cell Development	213

V Hybrids	217
1 FuelCell Energy, Inc.: Direct Fuel Cell/Turbine Power Plant	219
2 GE Hybrid Power Generation Systems: Solid Oxide Fuel Cell Hybrid System for Distributed Power Generation	223
VI Advanced Research	229
1 California Institute of Technology: Enhanced Power Stability for Proton-Conducting Solid Oxide Fuel Cells	231
2 Ion America Corporation: Optimization and Demonstration of Solid Oxide Regenerative Fuel Cell (SORFC)	236
3 Lawrence Livermore National Laboratory: Direct Carbon Conversion Fuel Cell	240
4 Pacific Northwest National Laboratory: High Temperature Electrochemistry Center	245
5 University of Utah: Active Cathodes for Super-High Power Density Solid Oxide Fuel Cells through Space Charge Effects	251
VII SBIR, HBCU, & UCR Projects	255
1 Boston University: Bi-Layer p-n Junction Devices for Coal-Based SOFC Interconnections	257
2 Boston University: Materials System for Intermediate-Temperature SOFC	262
3 Brown University: Spouted Bed Electrodes for Direct Utilization of Carbon in Fuel Cells	267
4 Ceramatec, Inc.: Lanthanum Gallate Electrolyte Based Intermediate-Temperature Solid Oxide Fuel Cell Development	271
5 Ceramatec, Inc.: Advanced Net-Shape Insulation for Solid Oxide Fuel Cells	274
6 Duke University: Carbon Ionic Conductors for Use in Novel Carbon-Ion Fuel Cells	278
7 Georgia Institute of Technology: Novel Electrode Materials for Low-Temperature Solid Oxide Fuel Cells	281
8 Materials and Systems Research, Inc.: LSGM-Based Composite Cathodes for Anode-Supported, Intermediate-Temperature (600-800°C) Solid Oxide Fuel Cells	285
9 Materials and Systems Research, Inc.: A Metallic Interconnect for Intermediate-Temperature Planar Solid Oxide Fuel Cells (SOFCs)	289
10 MesoScribe Technologies, Inc.: Advanced Thermal Spray Fabrication of Solid Oxide Fuel Cells	294
11 NexTech Materials, Ltd.: Novel Ceria-Based Materials for Low-Temperature SOFCs	299
12 NexTech Materials, Ltd.: Low-Cost Spray Deposition for SOFC Manufacturing	302
13 NexTech Materials, Ltd.: Highly Textured Composite Seals for SOFC Applications	305
14 Northwestern University: A Novel Integrated Stack Approach for Realizing Mechanically Robust SOFCs	309
15 Southern University and A&M College: Dense Membranes for Anode-Supported All-Perovskite IT-SOFC	314
16 TDA Research: Sorbents for the Removal of Odorants from Natural Gas	318
17 University of Akron: Carbon-based Fuel Cell	321
18 Virginia Tech: Modeling and Design for a Direct Carbon Fuel Cell with Entrained Fuel and Oxidizer	323

VIII Novel Generation327

 1 Ramgen Power Systems, Inc.: Development and Testing of a Rotating Supersonic Shock
 Compressor329

Acronyms & Abbreviations333

Primary Contact Index339

I Introduction

I Introduction

Fossil fuels have been instrumental in establishing the modern power generation and transportation components of the United States economy, and the extensive infrastructure in place for these fuels ensures that they will continue to be an important energy resources for a long time to come. However, in light of environmental and energy security concerns, advanced technologies for electric power generation and transportation are being developed to reduce or eliminate emissions and improve efficiency, thereby reducing our nation's growing need to import fossil fuels. One technology with high potential to satisfy these goals is the fuel cell.

Fuel cells have the potential to fundamentally change the nature of electric power generation. They use electrochemistry rather than combustion to produce high-quality power with greatly reduced emissions. Fuel cells designed to operate on pure hydrogen emit only electricity, water, and heat. However, in the absence of an extensive hydrogen production and delivery infrastructure, fuel cells that can operate on available fossil fuels such as natural gas, gasoline, and diesel are needed to accelerate the commercialization of this clean and efficient technology.

Under the leadership of the National Energy Technology Laboratory (NETL), government, industry and academia partners are developing solid oxide fuel cells and advanced system concepts for generating stationary power from fossil fuels. Targeted applications for introduction of these technologies include utility, industrial, commercial, and residential markets. The current focus of the Fuel Cell Program is on developing solid oxide fuel cells through the Solid State Energy Conversion Alliance (SECA).

The Fuel Cell Program efforts support several Administration initiatives: the Hydrogen Fuel initiative, the Energy Security initiative, the Clear Skies initiative, and the Global Climate Change initiative. Because they are able to operate on conventional fuels such as natural gas, solid oxide fuel cells are an important bridging technology, proving the benefits of fuel cell technology while the hydrogen economy is in its early stages of development. Through significantly higher efficiencies than those of currently dominant technologies such as internal combustion engines, gas turbines, and steam turbines, solid oxide fuel cells represent an opportunity to reduce fossil fuel consumption and dependence on foreign energy sources. Finally, solid oxide fuel cells greatly reduce emissions of both criteria pollutants and greenhouse gases, contributing to environmental sustainability.

NETL is pleased to present this FY 2004 Fuel Cell Program Annual Report. Projects sponsored by the Office of Fossil Energy are advancing the frontiers of solid oxide fuel cell research. The objectives and accomplishments of each project funded under the Fuel Cell Program are described in abstract format.



*Rita Bajura, Director,
NETL*



*Ralph Carabetta, Director,
Strategic Center for Coal*

The Fossil Energy Fuel Cell Program is managed at the National Energy Technology Laboratory, under the Strategic Center for Coal.

Fuel Cell Research and Development at NETL

In partnership with the private sector, NETL is developing fuel cells for stationary applications in the utility, industrial, commercial, and residential markets. The program elements discussed below are the focus of current work.

Solid State Energy Conversion Alliance. SECA was initiated in 1999 as a unique alliance between government, industry, and the scientific community. SECA promotes the development of environmentally friendly solid oxide fuel cells using widely available fossil fuels, thereby facilitating an affordable, clean and reliable source of electric power for virtually all markets. The alliance includes government agencies, commercial developers, universities, and others committed to the development of low-cost, high power-density, solid-state fuel cells for a broad range of applications. SECA's approach is mass customization of a common 3- to 10-kilowatt module. Fuel cells built from core modules will meet the needs of diverse markets—from stationary power generation, to the military, to the transportation sector. Two DOE national laboratories, NETL and the Pacific Northwest National Laboratory, are the driving forces behind SECA.



From L to R: Wayne Surdoval (SECA Coordinator), Joseph Strakey (Director, Office of Coal and Power Research and Development), and Mark Williams (Technology Manager, Fuel Cells)



Fuel Cell Turbine Hybrids. The Hybrids Program provides research advances in fuel cell turbine hybrid systems by linking technologies to generate electricity from natural gas at high efficiencies. Power-producing systems that contain a combination of high-temperature fuel cells and gas turbines have the potential for ultra-high efficiency in converting fossil fuels to electricity. The combined efficiency of a hybrid system can be raised to greater than 70 percent, and NO_x emissions are essentially eliminated.

Fuel Cell Systems. This program targets near-term distributed generation—the modular design of fuel cells for convenient placement of the power source near the customer. The goal of this program is to develop low-cost, simple and modular fuel cell power generation systems for the distributed generation, repowering, industrial, and commercial markets.

Electrochemical Engineering. The High Temperature Electrochemistry Center (HiTEC) was formed in 2002 to provide crosscutting, multidisciplinary research that leads to advanced electrochemical technologies to minimize the environmental consequences of using fossil fuels in energy generation. This program supports all areas of the fuel cell program by developing electrochemical energy-conversion technologies, such as energy storage using electrochemical concepts, reversible fuel cells, and membranes. The program objectives are to reduce fuel cell stack costs, shorten development time, and increase fuel flexibility of fuel cell turbine hybrids.

Meeting Our Nation's Energy Initiatives

Our fuel cell R&D program is poised to support the goals and integration of the Administration's key energy initiatives: Hydrogen Fuel, Energy Security, Clear Skies, and Global Climate Change.

Hydrogen Fuel Initiative. This initiative will reduce the growing dependence on foreign oil by developing the technology for commercially viable hydrogen-powered fuel cells to power cars, trucks, homes and businesses with no pollution or greenhouse gases.

Different types of fuel cells are optimized for different fuels, but all fuel cells need hydrogen for the electrochemical reaction that produces electric power. Since SECA fuel cells are able to easily reform hydrogen carrier fuels such as natural gas, the SECA fuel cell can also operate on conventional fuels. In this sense, they are a bridge to the hydrogen economy, and lessons learned in the development and application of SECA fuel cells will help to accelerate the transition to hydrogen fuel cells.

Energy Security. America's energy security is threatened by our dependence on foreign oil. Two-thirds of the 20 million barrels of oil Americans use each day is used for transportation. Fuel cell vehicles offer the best hope of dramatically reducing our dependence on foreign oil. Early market penetration of SECA auxiliary power units will enhance the applicability and usefulness of fuel cells in cars, trucks, and recreational vehicles, as well as stimulate consumer acceptance. Successes by SECA will synergistically impact the integration and progression of hydrogen production, distribution infrastructure, and fuel cell vehicles. Fuel cells will also alleviate compelling electrical system security aspects by reducing vulnerability and increasing reliability.



Clear Skies Initiative. This initiative cuts power plant emissions of the three worst air pollutants (nitrogen oxides, sulfur dioxide, and mercury) by 70 percent. This initiative uses a "cap and trade" program which models the most successful clean air law – the 1990 Clean Air Act's acid rain program.

Power production from fossil fuels using fuel cells is an attractive option because it results in fewer and lower emissions than are generated by the combustion process used by conventional technologies. The absence of combustion greatly reduces the formation of pollutants, including nitrogen oxides, sulfur oxides, hydrocarbons, and particulate matter.

Global Climate Change. Through this initiative, the U.S. will develop a new tool to measure and credit emissions reductions while at the same time recommend reforms that protect and provide transferable credit for emission reductions. This initiative cuts greenhouse gas intensity by 18 percent over the next 10 years.

Fuel cells also release less carbon dioxide than traditional power plants and could focus the development of carbon capture and storage technologies to stabilize long-term greenhouse gas levels in the atmosphere. Widespread use of fuel cell technology could make a significant improvement in air quality and reduced greenhouse gas emissions in the U.S.

Key Program Accomplishments

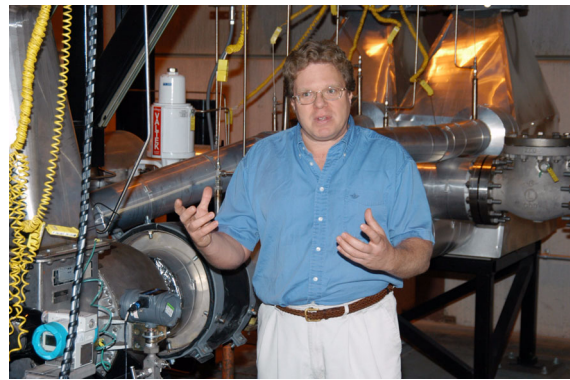
NETL Opens Fuel Cell/Turbine Hybrid Research Facility

The Hybrid Performance Facility — called the Hyper facility — is now fully operational at the NETL. This one-of-a-kind facility, developed by NETL's Office of Science and Technology, will be used to develop control strategies for the reliable operation of fuel cell/turbine hybrids.

Combined systems of turbines and fuel cells are expected to meet power efficiency targets that will help eliminate, at competitive costs, environmental concerns associated with the use of fossil fuels for producing electricity and transportation fuels.

A fuel cell is an electrochemical device that produces electricity from hydrocarbon fuels without combustion, while a turbine produces electricity when steam or hot gases expand, spinning the turbine blades. When the two energy conversion devices are combined into an integrated power-producing system, the combined system achieves fuel efficiency and emissions performance that are beyond the reach of any single standalone system.

In addition to planned NETL studies, the Hyper facility and modeling results are available for public research collaboration. Collaboration with academic, non-profit, or commercial research groups can be arranged under a variety of cooperative programs, such as a Cooperative Research and Development Agreement (CRADA), and student or visiting scholar programs. Several industry and academic partnerships are now in place, including support from Woodward Governor Company, West Virginia University, Georgia Tech, and others.



Dave Tucker, a scientist and researcher at NETL, stands in front of the Hyper research facility.

World's First Coal Mine Methane Fuel Cell Powers Up in Ohio

In a novel pairing of old and new, FuelCell Energy of Danbury, Connecticut, has begun operating the world's first fuel cell powered by coal mine methane. The demonstration harnesses the power of a pollutant - methane emissions from coal mines - to produce electricity in a fuel cell.

"We believe this technology can reduce coal mine methane emissions significantly while producing clean, efficient, and reliable high-quality power," Secretary of Energy Spencer Abraham said. "This has the dual benefit of reducing greenhouse gases while supporting our energy security by generating power from readily available domestic fuels."

The technology supports the Administration's initiative to reduce America's dependence on foreign oil by developing commercially viable fuel cells to power cars, trucks, homes and businesses. Because it's fueled by coal mine methane - a greenhouse gas that could otherwise be released to the atmosphere - the demonstration project also supports the Global Climate Change initiative.

The demonstration at the Rose Valley coal mine methane test site in Hopedale, Ohio, features FuelCell Energy's innovative Direct FuelCell[®] technology. The 200-kW power plant generates enough electricity to supply an average of 40 homes. A successful demonstration could pave the way to the use of fuel cells to mitigate coal mine methane emissions while producing power at high efficiency and very low emissions.

SECA Industry Team Approaches Phase I Performance Targets

General Electric (GE) Hybrid Power Generation Systems of Torrance, CA, is nearing their SECA Phase I cell module performance target for solid oxide fuel cell development. With a modified electrode composition and microstructure, the GE fuel cell module achieved 276 mW/cm^2 at the design current of 428 mA/cm^2 and 88% fuel utilization using simulated autothermal reformat, nearly meeting the SECA Phase I target power density of 300 mW/cm^2 at the same conditions. A fuel utilization of 95% was achieved with 64% hydrogen and balance nitrogen at 800°C . A more detailed report of progress made in this area is discussed in "II.5: Solid State Energy Conversion Alliance Solid Oxide Fuel Cell Program."



Some of the NETL Fuel Cell Project Managers are shown here. From L to R: Magda Rivera; Travis Shultz; Shawna Toth; Don Collins; and Bruce Utz, Director of the Power Systems Projects Division

Acumentrics Begins Alaska Fuel Cell Field Test

In a field test co-funded by the U.S. Departments of Energy and Defense, Acumentrics of Westwood, Mass., initiated start-up of a microtubular solid oxide fuel cell at the Exit Visitor's Center of Glacier Park, AK. The test validates the feasibility of using SOFCs in remote areas to produce both heat and electricity from propane. The Acumentrics design combines ceramic mini-cylinders, each roughly the diameter of a magic marker, into a 10-kilowatt module that could offer exceptional ruggedness and quicker start-ups than other systems, making the fuel cell especially applicable for residential markets, military applications, broadband communication networks, and auxiliary power units for heavy-duty trucks.



Randy Gemmen, a scientist and researcher at NETL, oversees tests at the NETL Fuel Cell Test Bed.

SECA Industry Team Improves Power Density

Siemens Westinghouse Power Corporation (SWPC) fabricated a planar solid oxide fuel cell that demonstrated 30% higher power density than their previous seal-less tubular design. Recognizing that the seal-less tubular cell design would not meet the SECA cost and performance targets, SWPC combined the seal-less feature and a flattened cathode with integral ribs to increase the power density and to reduce the size of the cell. The ribs reduce the current path length by acting as bridges for current flow, and they form air channels that eliminate the need for air feed tubes. Due to the shorter current path, the cell design has lower cell resistance and higher power output than tubular cells. A five-channel cell with the new design achieved voltage stability over more than 1000 hours of operation at 1000°C and 85% fuel utilization. This project is discussed in detail in "II.6: Small-Scale Low-Cost Solid Oxide Fuel Cell Power Systems."

New Computer Modeling Center for Solid State Energy Conversion Alliance

SECA Industry Teams now have a powerful computational platform on which to design and optimize solid oxide fuel cell systems. The modeling center is located at the Pacific Northwest National Laboratory, where some

of the most advanced SOFC software packages are developed under the SECA Core Technology Program. SOFC software packages enable the modeling and analysis of cell electrochemistry, temperature profiles, fuel and air stream flow characteristics and stress distributions. The SECA Modeling Center will facilitate the efficient analysis and modification of existing SOFC cell and stack designs to enhance both performance and reliability. In addition, these tools may be used to define precisely the safe-operation envelope needed in planning an effective system controls strategy.

Delphi Tests Generation 3 Solid Oxide Fuel Cell

Delphi Automotive Systems, LLC, of Troy, MI, in partnership with Pacific Northwest National Laboratory, successfully tested its 30-cell Generation 3 SOFC stack with a fuel that simulated hydrogen-rich gas derived from coal. The stack, which has half the thickness and weight of its predecessor, achieved a power density of 500 mW/cm^2 at 0.7 volts/cell and 750°C . The test demonstrated the feasibility of building a well-sealed fuel cell module from thin metallic cassettes fabricated by high-volume manufacturing processes such as stamping, brazing, and laser welding used in the automotive industry. With further development and optimization of stack performance to reach SECA targets, several Generation 3 modules will be assembled into a 3-5 kW SOFC prototype for use with a range of fuels in applications such as heating and air conditioning for homes, offices, and vehicles. More about this project can be found in "II.3: Solid State Energy Conversion Alliance Delphi SOFC."



Dave Berry, a scientist and researcher at NETL, discusses the fuel processing work being performed under the SECA program at NETL.

II SECA Industry Teams

II SECA Industry Teams

II.1 Development of a Low-Cost 10-kW Tubular SOFC Power System

Norman Bessette

Acumentrics Corporation

20 Southwest Park

Westwood, MA 02090

Phone: (781) 461-8251; Fax: (781) 461-8033; E-mail: nbessette@acumentrics.com

DOE Project Manager: Don Collins

Phone: (304) 285-4156; E-mail: Donald.Collins@netl.doe.gov

Objectives

- Design a common low-cost generator to meet all chosen markets.
- Develop an anode-supported micro-tubular cell capable of twice the power density presently achieved.
- Design, build, and test an inverter with 94% efficiency for conversion from direct current (DC) to alternating current (AC).
- Test prototype of a natural gas fueled unit meeting and exceeding Solid State Energy Conversion Alliance (SECA) goals.

Approach

- Remove precious metals from anode connection brazes which are stable and conductive in the necessary operating environment.
- Improve anode conductivity and stability to allow a greater power per unit length of cell tube.
- Decrease solid oxide fuel cell (SOFC) generator component costs through advanced manufacturing techniques.
- Develop a control topology utilizing Controller Area Network bus (CANBUS) architecture to decrease overall instrumentation and control cost.
- Develop the AC/DC high-efficiency conversion end building off our existing 98%-efficient DC/DC regulator.

Accomplishments

- **Fuel Cell Power Increased by 33%:** Through the development of an advanced power take-off concept, the Acumentrics Tubular SOFC has resulted in a power increase of 33% over the existing cell design. This has been achieved by a proprietary contact technique allowing power take-off from both ends of the cell tube. This breakthrough results in a reduction in overall cost/kW of the system of approximately 25%.
- **Brazed Electrical Connection Meets SECA Cost Target:** The electrical take-off from the anode of Acumentrics' tubular SOFC had been accomplished prior to this SECA project utilizing a braze material adding over \$1,300/kW to the product cost. Under a SECA task, a number of braze materials and mixtures have been tested, with one achieving the necessary performance requirements while only adding \$1/kW to the overall system cost, thereby reducing the system cost by over \$1,300/kW.
- **Prototype DC/AC Inverter Achieves Over 96% Efficiency:** Acumentrics has developed a DC/DC regulator capable of achieving over 98% efficiency and also prototyped a DC/AC inverter stage that is over

98% efficient. The full system has been verified to achieve over 96% efficiency (excluding transformer), which is above the DOE-sponsored energy challenge requirements.

- **Stable Cell Performance Exceeds 6000-hr Operation:** Demonstrated over 6000 hours stable cell performance with average degradation rate below 0.25%/500 hours, nearly achieving the 2010 Phase III SECA goal of 0.1%/500 hours.
- **Improved Anode Conductivity Increasing Power by 10%:** Cells which had an additional high nickel contact layer added to the inner diameter of the fuel cell tube have shown an improvement of 10% in power over standard cells with current collected at one end of the tube.

Future Directions

- **Evaluate a DC/AC Inverter with Greater Than 95% Efficiency:** By demonstrating the integration of an inverter capable of over 95% efficiency versus the market standard of 82-90%, overall system efficiencies can rise by nearly 5 percentage points. This improvement in overall efficiency can be taken as fuel savings to reduce the overall cost of electricity (COE). Another option is to operate the fuel cell stack at a lower cell voltage point, thereby increasing the individual cell power and decreasing the number of fuel cells required and the overall capital cost.
- **Complete the System Design Capable of Achieving SECA Cost Targets:** The overall system design for a generator capable of achieving SECA cost goals is nearing completion. Upon completion of this design, the detail cost requirements of each subsystem will be validated and a work breakdown structure for each major subsystem will be developed. Trade-offs for performance and cost in each major area will be made to allow for a machine capable of penetration into the largest number of markets.
- **Reduce the Operating Temperature to 650-700°C:** By demonstrating an SOFC equal in performance at 650-700°C to one at 800°C, all materials of construction will reduce in cost dramatically, as will overall size due to reduced amounts of insulation. By reducing the operating temperature to or below 700°C, stainless steel materials can be substituted where only high-temperature alloys were suitable previously, which could result in greater than a six-fold reduction in cost.

Introduction

The Acumentrics SECA project has focused on the design and manufacture of micro-tubular SOFC power systems approaching twice the power density now achieved by state-of-the-art anode-supported tubular designs. These units will be capable of entry into the telecommunication, remote residential, and military markets. Operation on fuels including natural gas and propane will be developed for the telecommunication and remote residential markets. Operation on liquid fuels, including diesel and JP-8, will be developed for the military markets.

Working with Acumentrics to define market segments and market requirements are a number of key investors that are strategic players in their respective markets. They include:

- Chevron Texaco for remote markets and liquid fuels.

- Northeast Utilities and NiSource for integration in the natural gas and electricity infrastructure.
- Sumitomo Corporation of Japan for introduction and product definition into the Japanese market.

Approach

To achieve the final SECA goal of a manufactured unit cost of less than \$400/kW, work can focus on increasing cell power, thereby decreasing the number of cells per kilowatt, or it can focus on decreasing the cost of each component. With such an aggressive goal, work must focus on both paths. To increase cell power, work is centered on improved materials as well as enhancements in geometry. Cells with increased anode conductivities to decrease electrical bus losses are being investigated. Improved conductivity of cathodes is also being investigated to decrease the potential loss associated with the electrochemical reaction on the air side. Increases in cell tube diameter as well as

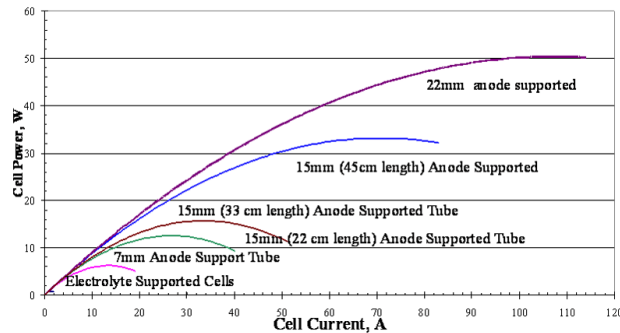


Figure 1. Cell Power Trend

multiple contact points along the length are also being studied.

For subsystem cost reductions, the machine is divided into four major sub-systems: the SOFC generator, the control system, the power conditioning system, and the fuel and airflow system. In the SOFC generator, advanced materials and manufacturing techniques are being investigated, including metal injection molding as well as metal stampings. Vacuum cast insulation to near net shape is also being considered. For the control system, a CANBUS architecture is being developed as well as integration of control of all valves and power electronics. For the power electronics sub-system, the focus is on improving the overall DC/AC conversion efficiency to avoid excessive losses which compromise overall system efficiency and require more cells and therefore more cost. In the air and fuel sub-system, removal of redundant components as well as qualification of equivalent components at lower cost are the paths chosen.

Results

To improve cell power, advancements have been made in the tube anode conductivity as well as connection points. Figure 1 shows the cell power trend with time of the Acumentrics anode-supported design. The first curve represents older designs built on electrolyte-supported tubes producing only 1 W/tube. The technology was then developed to build anode-supported cells, which enabled an immediate increase to 7 W/tube. This 700% jump is a result of two major factors. The first is a decrease in electrolyte thickness from 300 microns to less than 30 microns, which causes a significant reduction in

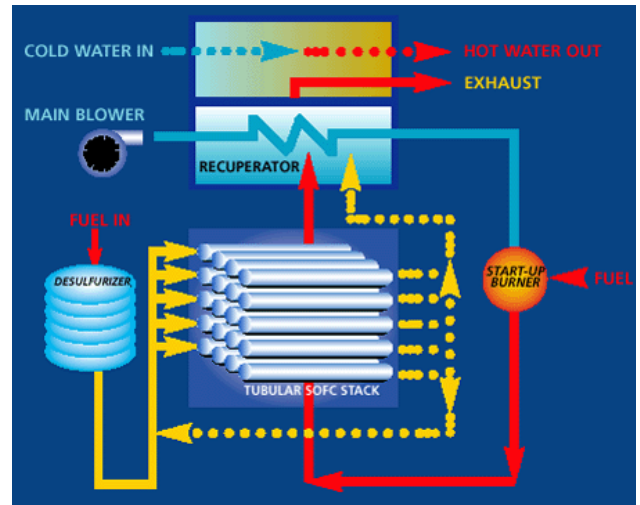


Figure 2. Acumentrics Tubular SOFC Steam Reformed System Overview

cell resistance. The second is an increased anode support thickness, allowing for a lower voltage drop cell bus. The next power increases were geometry-related, allowing 12 W/tube by increasing to 15 mm diameter and then 16 W/tube, which has now increased to 20 W/tube by increasing length. Further work will move to increase the diameter to 20-25 mm with some length increase with an ultimate goal of 50 W/tube.

To improve overall system efficiency, a steam-reformed natural gas fuel system was developed to replace the existing partial oxidation system. This was made feasible by the development of a dual-chamber manifold system that allowed for capture of not only the inlet fuel but also the effluent fuel. This effluent stream provides the necessary water for steam reformation, thereby increasing the overall fuel concentration and system performance. Figure 2 shows the overall system diagram, which shows a percentage of the cell effluent reintroduced with the new fuel while the remaining percentage is combusted to provide preheating for the air stream as well as additional combined heat and power capabilities.

To decrease generator cost, major reductions have been made in braze connection part and material costs as well as recuperator costs. The original Acumentrics design had a brazed connection to the anode for current collection which was made



Figure 3. Cell Braze Cap Development

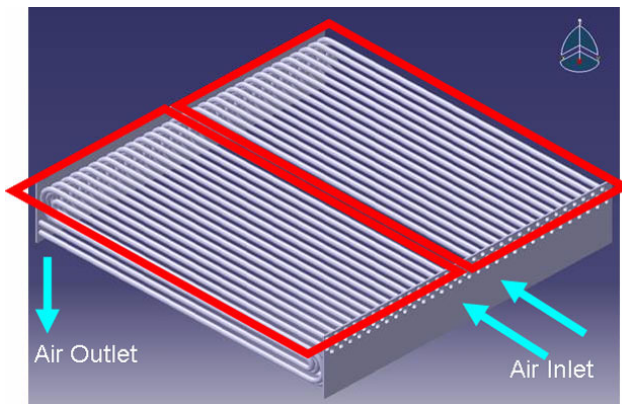


Figure 4. Bent Tube Recuperator Design

with a precious metal braze material. This resulted in a cost of over \$1300/kW. Under the first phase of this project, two braze materials have been developed and validated for performance and longevity which are each under \$1/kW. The cell itself was brazed to a nickel connection cap machined from solid stock nickel, resulting in a cost of over \$6/cell. During the initial phase of this project, a new stamped design was developed which is under \$0.65/cell, with further reductions expected. Figure 3 shows the existing and newly developed designs. For recovering the heat from the fuel cell stack, the recuperator design prior to the SECA project was a welded three-pass design of high-temperature super alloys which required welding of over 900 tube ends. A new design has been developed with a lower-cost material consisting of a bent tube geometry, reducing the welding requirements by over 67%. A schematic is seen in Figure 4.

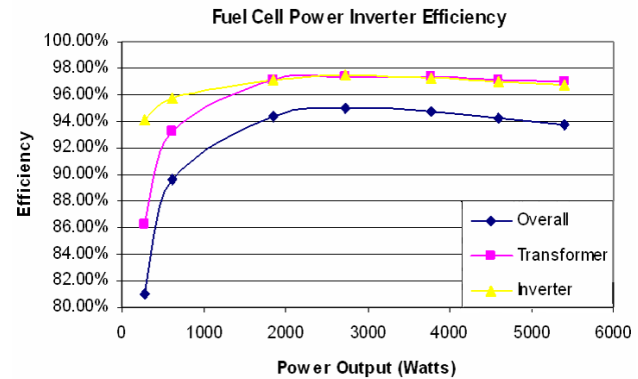


Figure 5. Fuel Cell Power Inverter Efficiency

To boost the overall system efficiency, a DC/AC inverter was developed which has an overall conversion efficiency of over 94%. Figure 5 shows the efficiency and its trend over the 0 to 5 kW level. This unit, when fully developed, has the ability to replace an existing inverter package that is 86-87% efficient. This would then result in a boost in overall generator system efficiency of over 3 points. Another advantage of this design is the usage of many components being developed for the 48 V automotive conversion which is occurring at this time. This will allow for leveraging of the volume cost reductions seen in the automotive industry into the fuel cell industry.

Conclusions

Considerable advancements have been made in the first year of the Acumentrics' SECA project. Cell power advancements have been made exceeding 300%. Cost reductions in certain key fuel cell stack components have resulted in decreases of over \$1000/kW. Advances in system efficiency and DC/AC efficiency have also been realized to allow achievement of the SECA performance goals. Further work on all of these tasks will be performed to achieve the ultimate goal of \$400/kW.

FY 2004 Publications/Presentations

1. "Status of the Acumentrics SOFC Program", N.F. Bessette, Presented at the Annual SECA conference, Boston, MA., May 11, 2004.

II.2 10-kW Solid Oxide Fuel Cell Power System Commercialization

Daniel Norrick (Primary Contact), Eric Barringer

Cummins Power Generation

1400 73rd Avenue NE

Minneapolis, MN 55432

Phone: (763) 574-5301; Fax: (763) 528-7253; E-mail: Daniel.a.norrick@cummins.com

DOE Project Manager: Don Collins

Phone: (304) 285-4156; E-mail: Donald.Collins@netl.doe.gov

Subcontractors: SOFCo, Alliance, Ohio

Objectives

- The objective of this Cummins Power Generation (CPG) and SOFCo-EFS Holdings LLC (SOFCo) project is to demonstrate the Solid State Energy Conversion Alliance (SECA) Phase 1 solid oxide fuel cell (SOFC) objectives through technical progress in the following areas:
- SOFC stacks that achieve target performance and stability and that can be manufactured in volume at the target cost.
- A waterless catalytic partial oxidation (CPOX) reforming process that can efficiently and cost effectively convert natural gas or propane into a hydrogen-rich synthesis gas.
- SOFC hot box subsystem design (insulated enclosure containing SOFC stacks, manifolds, heat exchangers, start-up burner, and reformer) that is compact and can be mass-produced at a cost meeting the Phase 1 cost target.
- SOFC system balance of plant, including air and fuel supply systems, that meets the cost and reliability targets.
- A control system for the SOFC power system, including regulation of fuel and air flows and management of electrical power generation and load sharing. Control system must function in conjunction with an energy storage system through start-up, steady-state and transient loads, and shut-down, including emergency shut-down without damage to the SOFC stack.
- An efficient electrical power conditioning system to convert DC voltages and invert them to produce useable AC output.

Approach

The CPG-SOFCo approach coordinates development in the following major areas:

- Planar SOFC cell, interconnect, and stacks
- Planar SOFC manufacturing and scale-up
- Dry CPOX fuel reforming
- Fuel cell balance-of-plant (BOP)
- Fuel cell and power electronics system controls
- Power conditioning

Specifically, the CPG-SOFCo team is conducting the following work:

- Develop and evaluate advanced solid oxide fuel cells that provide the required performance and are compatible with the SOFCo ceramic interconnect.
- Use a progression of stack tests to validate the development of materials and assembly methods for useable stacks that can achieve high fuel utilization (good sealing) and low degradation rates.
- Develop a CPOX reforming process and scale-up to system-sized units.
- Design and develop a hot box subsystem which can be delivered to CPG for integration into complete SOFC power systems.
- Develop control hardware and software required to regulate system operation.
- Integrate the BOP components, hot box subsystem, and controls into a working development prototype. Operate the prototype with stack simulators to shake down the system, followed by installation of SOFC stacks and operation of the full prototype.
- Evaluate and refine the lessons learned from the prototype system to design, construct, and test the deliverable SECA Phase 1 system.

Accomplishments

- Advanced electrolyte-supported cells demonstrated improved cell performance. These cells meet the interim performance targets defined for Phase 1 of the SECA project.
- Degradation of short stacks was reduced to <4% per 500 hours. Fuel utilization in excess of 80% with natural gas reformat was demonstrated. These results confirmed the viability of SOFCo's stack assembly method, the materials used for seals, and electrical contacts between the cells and interconnects.
- Dry (waterless) CPOX reforming for natural gas and propane were successfully demonstrated. The bench-scale CPOX reactor was scaled up for use in a kilowatt-scale prototype system. Long-term testing with natural gas showed stable operation for more than 2500 hours, and stacks operated on the reformat demonstrated no problems through 2000 hours of testing.
- A kilowatt-scale prototype hot box was constructed incorporating two stack simulators. The hot box subsystem was successfully integrated with the BOP components in the test facility at CPG.
- The kilowatt-scale C1 prototype has been operated successfully on reformed pipeline natural gas. Testing on the C1 prototype validated system models and control algorithms and provided valuable information on system transient response.

Future Directions

- Refine the composition and microstructure of the electrodes for the advanced electrolyte-supported cell as required to achieve the Phase 1 target performance.
- Use instrumented short stacks and continued optimization of materials to assemble stacks that further reduce the non-cell contributions to resistance and power degradation rates.
- Complete the design and development of a robust tall stack assembly for the system prototype to be delivered to DOE at the end of Phase 1.
- Scale the CPOX reformer to 6 kWe and complete testing using natural gas. Testing will be used to establish operating parameters and control requirements.
- Complete the design and construction of the deliverable hot box subsystem. Assemble the hot box and deliver to CPG.
- Complete the specification and procurement of the balance of plant for the deliverable system.
- Complete the final tailoring and development of the DC converters for the fuel cell and battery system.
- Complete the development and integration of the control system with the fuel cell, balance of plant, and power electronics.

Introduction

Solid oxide fuel cell power systems offer the potential to generate electrical power from hydrogen or hydrocarbon fuels cleanly and efficiently. The objective of the CPG-SOFCo project is to design and develop a 3-10 kW SOFC-based power system that can be competitive with existing small diesel generating systems in terms of cost and package size, but offer significant benefits in efficiency, emissions, lower noise and vibration. Achieving these objectives requires advancement in five major areas:

- Cell, interconnect, and SOFC stack performance and robustness
- Optimizing manufacturing processes for production of cells, interconnects, and stack assemblies
- System design, thermal integration, and packaging of the hot components and sub-systems including stacks, fuel reformer, heat exchangers, and insulation system
- Control system for regulating air and fuel flows to the stacks in proportion to electrical load and operating temperatures, and for managing electrical load distribution between the fuel cell and batteries during steady-state and transient loading
- Electrical power conditioning, including DC voltage boosts (converters) and DC to AC power (inverter)

The team has made significant progress in all five areas during 2004 and is on plan to meet the objectives of Phase 1 of the SECA project.



Figure 1. Improved Performance of SOFC Stacks

Results

Development work during 2004 has substantially improved cell performance, primarily through the introduction of scandia-stabilized zirconia electrolytes to improve ionic conductivity and reduce cell area specific resistance (ASR). Through this work, ASRs have been reduced by a factor of three and are approaching the Phase 1 target value. [Figure 1.]

Typical stack power degradation at constant voltage has been improved to 3% per 500 hours, nearing the Phase 1 target of 2% per 500 hours. [Figure 2.]

Dry (waterless) CPOX reforming for natural gas and propane (LP gas) were successfully demonstrated. The bench-scale CPOX reactor was scaled up for use in a kilowatt-scale prototype system. Long-term testing with natural gas showed stable operation for more than 2500 hours, and stacks operated on the reformate demonstrated no problems through 2000 hours of testing. [Figure 3.]

A progression of stack tests at 5 cells, 20 cells, and 47 cells, respectively, has validated the stack assembly process and the integrity of the stack sealing system. Target fuel utilization of 80% has been demonstrated on stacks of all sizes.

Design and manufacturing work to scale up the ceramic interconnect from approximately 10 by 10 cm to 15 by 15 cm is on track to produce high-quality parts meeting design requirements.

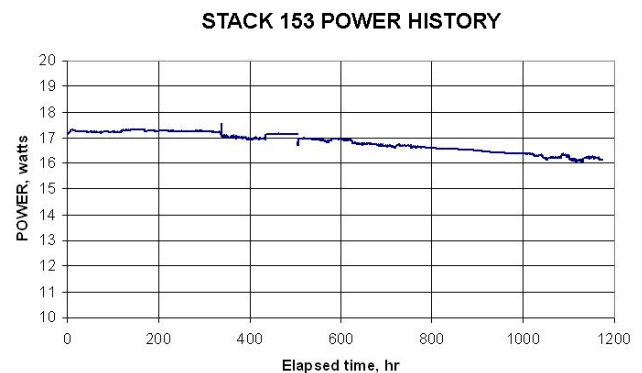


Figure 2. Improved Degradation Performance of SOFC Stacks; Calculated Average Degradation 2.9% per 500 Hours

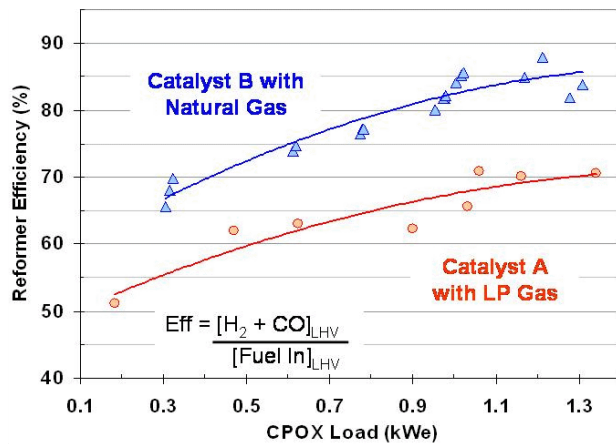


Figure 3. High-Efficiency CPOX Operation on Natural Gas and Liquefied Petroleum (LP) Gas

Testing of a kW-scale demonstrator unit at CPG in Minneapolis has provided valuable information validating system modeling and control strategy. During testing, CPG-developed controls exhibited excellent steady-state and transient stability and response.

CPG demonstrated a high-efficiency DC-DC boost system which will be used to control current flow and voltage supply to the inverter section from the fuel cell stacks and from the batteries. [Figure 4.]

Conclusions

- Electrolyte-supported cells with ScSz electrolytes provide improved SOFC performance.
- Planar SOFC stacks in the range of 50 repeat units can be constructed and successfully operated at high fuel utilizations.
- A dry (waterless) catalytic partial oxidation reformer system can provide a suitable fuel stream from commercial natural gas without sulfur removal and without forming carbon.

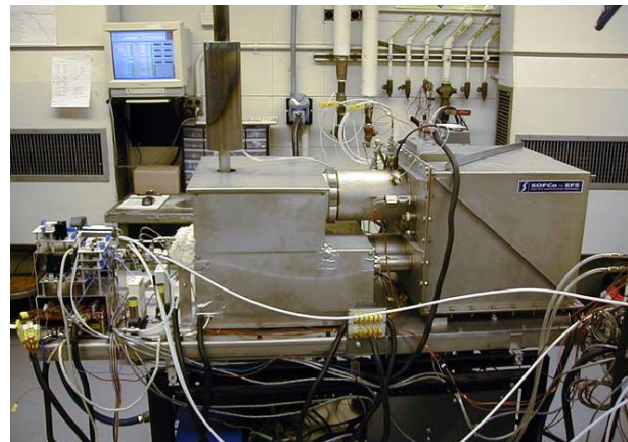


Figure 4. kW-Scale SOFC Development Prototype System

- A compact kilowatt-scale SOFC power system can be started and operated within design parameters in both steady-state and transient operating modes.
- DC-DC voltage conversion can be accomplished at high (98%) efficiency with simple, producible, and cost effective inductor-based DC-DC boost.

FY 2004 Publications/Presentations

1. R. Goettler, T. Cable, K. Kneidel, T. Morris and E. Barringer, "SOFCo Planar Solid Oxide Fuel Cell Development Status," 2003 Fuel Cell Seminar Abstracts, pp. 902-905, November 2003.
2. L. Xue, E. Barringer, T. Cable, R. Goettler and K. Kneidel, "SOFCo Planar Solid Oxide Fuel Cell," International Journal of Applied Ceramic Technology, Volume 1, Number 1, pp. 16-23, February 2004.
3. D. Norrick, "10kWe SOFC Power System Commercialization Program Progress," SECA Annual Workshop, May 11, 2004, Boston, MA.

II.3 Solid State Energy Conversion Alliance Delphi SOFC

Steven Shaffer (Primary Contact), Mike Faville, Sean Kelly, Karl Haltiner, Subhasish Mukerjee, David Schumann, Gail Geiger, Kevin Keegan, Larry Chick, John Absmeier

Delphi Automotive Systems LLC

5725 Delphi Drive

Troy, Michigan 48098

Phone: (585) 359-6615; Fax: (585) 359-6061; E-mail: steven.shaffer@delphi.com

DOE Project Manager: Magda Rivera

Phone: (304) 285-1359; E-mail: Magda.Rivera@netl.doe.gov

Subcontractors: Battelle/Pacific Northwest National Laboratory, Richland, WA; Electricore, Inc., Indianapolis, IN

Objectives

- Develop a 5-kW solid oxide fuel cell (SOFC) power system for a range of fuels and applications.
- Develop and demonstrate technology transfer efforts on a 3-10 kW stationary distributed power generation system that incorporates endothermic reforming of methane and natural gas.
- Initiate development of a 5-kW system for later mass-market automotive auxiliary power unit application which will incorporate endothermic reforming of gasoline.

Approach

- Develop and test major subsystems and individual components as building blocks for applications in targeted markets.
- Integrate major subsystems and individual components into a “close-coupled” architecture for integrated bench testing.
- Integrate major subsystems and individual components into a stationary power unit (SPU) for the stationary market.
- Integrate major subsystems and individual components into an auxiliary power unit (APU) for the transportation market.

Accomplishments

- Gen 3 cassettes (repeating units for stack) were successfully fabricated and tested. The Gen 3 cassettes have a 50% reduction in thickness and weight compared to Gen 2 cassettes. The cassettes are fabricated using high-volume manufacturing processes like stamping, brazing and laser welding.
- Over twenty Gen 2 stack subsystems were built and tested. Power densities of 420 mW/cm² at 0.7 V/cell at 750°C were achieved in the stack laboratory with simulated recycle reformat. Thermal cycling tests in a furnace with 60 minutes heat-up from room temperature to 750°C demonstrated five thermal cycles with minimal degradation.
- Demonstrated 1617 W gross power in a Gen 2 APU. Solid model design geometry, computational fluid dynamics (CFD), finite element analysis (FEA), and thermal analysis were completed for the Gen 3 APU. Particular attention was placed on system pressure drop and thermal management concerns.
- Thirty-cell Gen 3 stacks were fabricated and tested. Power densities of greater than 500 mW/cm² at 0.7 Volts/cell at 750°C were achieved with simulated reformat.

- Extensive CFD analysis was completed on the integrated component manifold (ICM), process air module (PAM), and cathode air heat exchanger (CHEX) to reduce pressure drops within specified allocations and improve the temperature gradients in the SOFC plant.
- A new commercial combustible gas sensor has been sourced, and prototype samples have been ordered for possible implementation as part of the safety and diagnostics system.
- The catalytic partial oxidation (CPOx) reformer (see Figure 1) has been further developed. Both gasoline and methane CPOx reformers are under test. We are currently developing the endothermic methane/natural gas and gasoline reformer technology. This technology will be utilized in the SPU demonstration system.

Future Directions

- Test a cart-based endothermic reformer/stack system in Q3, 2004.
- Design a full-scale development system (6000 watts gross desired) during Q3-Q4, 2004.
- Design, build and test a full-scale SPU demonstration system during Q1-Q3, 2005.
- Prepare/finalize the detailed system cost estimate during Q1-Q2, 2005.
- Test the Delphi Demonstration System A SPU and operation of the system at the DOE National Energy Technology Laboratory (NETL) site in Q4 2005.

Introduction

The objective of this project is to develop a 5-kW solid oxide fuel cell power system for a range of fuels and applications. Delphi is developing a 3-10 kW system for stationary distributed power generation applications that incorporates endothermic reforming of natural gas. Delphi is also initiating development of a 5-kW system for later use in a mass-market automotive auxiliary power unit. The automotive unit will incorporate endothermic reforming of gasoline.

These two complementary systems will introduce fuel cell systems to the market for both distributed power generation of AC systems for electric power, and transportation systems for advanced automotive power trains. Developing both industrial and transportation applications based on similar components increases the potential production volumes of the components and therefore reduces the potential cost.

Approach

Delphi's approach is to evaluate components and subsystems at increasingly integrated levels. The system integration levels are Level 0, Level I, and Level II, as shown in Figure 2. Level 0 integration represents the individual testing and development of the major subsystems and components. Level I integration represents the close coupling of the major system modules such that all major system functions are represented and functional during the test. Level II integration represents the final product package, integration, and function for the SOFC power plant or APU (shown in Figure 3). In the laboratory, a stand is employed to hold the product and facilitate fuel, air, electrical, and exhaust connections, but the intended construction and function of the system should be representative of product intent at this integration level.

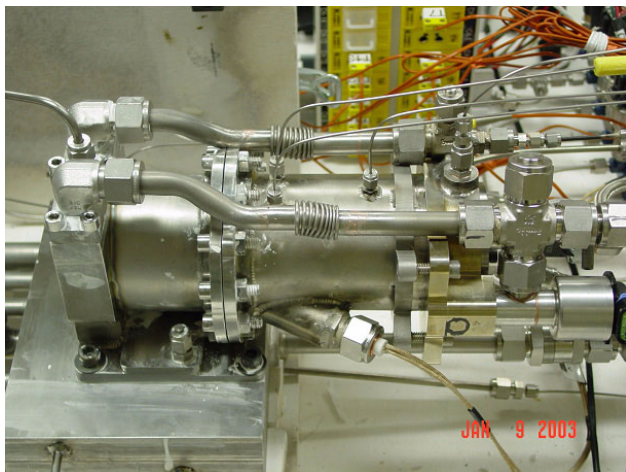


Figure 1. Tubular CPOx Reformer Assembly

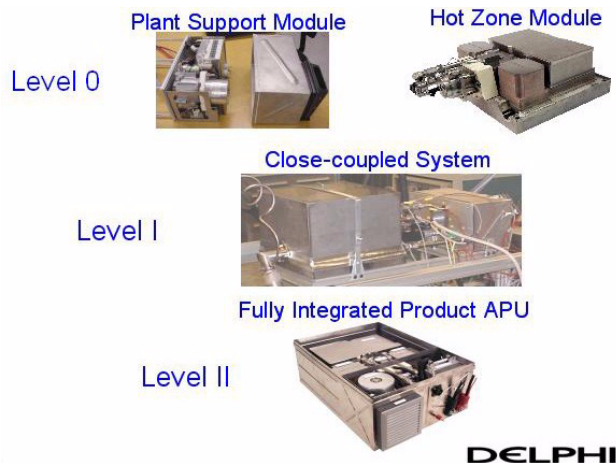


Figure 2. SOFC System Development Levels

Results

At the system level, several changes have been made to the Gen 3 physical plant mechanization. They include addition of anode tail gas recycle function, addition of fixed burner air bypass, and separate process air and system cooling air (purge air) streams. These changes are important in improving the efficiency of both the stack and the balance-of-plant.

Key achievements in stack development included the fabrication of over twenty Gen 2 stack subsystems. Gen 3 cassettes were successfully fabricated that have much lower mass when compared to the Gen 2 stack design. Major progress in process development of stamping, brazing and laser welding led to the fabrication of hundreds of cassettes for stack build and test.

Gen 3 short stacks were fabricated and tested successfully. A 3-cell stack was thermally cycled 30 times in a furnace. Thirty-cell stacks were built and tested successfully. Power density of greater than 500 mW/cm^2 was achieved with simulated reformat at 750°C . A Gen 3, 15-cell stack was successfully thermally cycled 10 times in a furnace with minimal degradation in power. Figure 4 shows a Gen 3 30-cell stack. The stack is 3.5 liters and 13 kg.

Fundamental cell development focused on improving cathode performance. Lanthanum strontium ferrite and lanthanum strontium cobalt ferrite cathodes have demonstrated good power

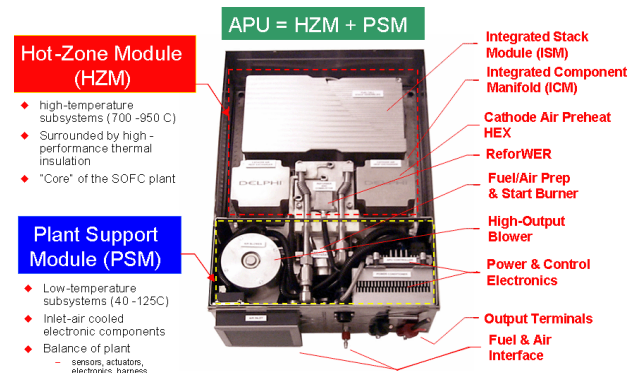


Figure 3. SOFC APU System Modules

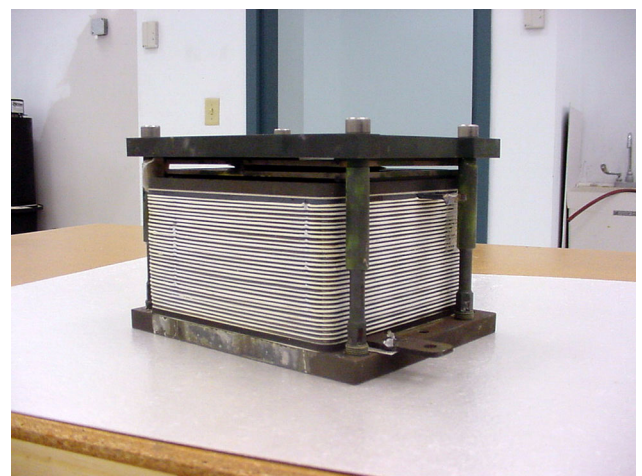


Figure 4. Gen 3 Solid Oxide Fuel Cell 30-cell Stack

densities in fundamental testing as well as in stacks. Key issues related to cathode degradation were studied in the presence of chromia- and alumina-forming alloys. Durability tests on intermediate and full-sized stacks were carried out successfully for over 1000 hours. The tests underscored the degradation in power due to the interaction of chromia with the cathode in interconnect designs containing chromia-forming alloys. Controlled experiments on intermediate-sized, 1-cell stacks with non-chromia-containing interconnects showed minimal degradation in the same time periods.

Fundamental interconnect development focused on understanding and studying the viability of concepts that would provide an alternative to using chromia-containing alloys in the stack. Fundamental development of seals demonstrated improved performance from reinforced glass seals.

Conclusions

- Improved thermal management, reduced package size, and improved gaskets at high-temperature interfaces are key to dramatically improved output power and system efficiency.
- The addition of anode tail gas recycle, addition of fixed burner air bypass, and separate process air and system cooling air (purge air) streams are designed to address capability gaps in current system hardware.
- Fundamental stack development was targeted towards improving sealing, interconnects and overall stack durability (continuous and thermal cycling) while increasing power density.

FY 2004 Publications/Presentations

1. November 2003: Fuel Cell 2003, Miami Beach: Extended Abstract and Presentation, SOLID OXIDE FUEL CELL STACK FOR AN AUXILIARY POWER UNIT: A DEVELOPMENT UPDATE, Subhasish Mukerjee, Steven Shaffer, James Zizelman, Delphi Corporation; L. Chick, V. Sprenkle, K.S.Weil, K. D. Meinhardt, D.M.Paxton, J.E.Deibler, Pacific Northwest National Laboratory Operated by Battelle

2. November 2003: Fuel Cell 2003, Miami Beach: Extended Abstract only, DELPHI'S GENERATION 2 SOFC APU SYSTEM: FROM GASOLINE TO ELECTRIC POWER, Subhasish Mukerjee, Steven Shaffer, James Zizelman, Delphi Corporation
3. May 2004: SECA Annual Workshop, Boston: Presentation only, DEVELOPMENT UPDATE ON DELPHI'S SOLID OXIDE FUEL CELL SYSTEM, Steven Shaffer, Delphi Corporation
4. June 2004: 2nd International Fuel Cell Science, Engineering & Technology Conference, RIT, Rochester, NY: Presentation only, DEVELOPMENT UPDATE ON DELPHI'S SOLID OXIDE FUEL CELL SYSTEM, Steven Shaffer, Delphi Corporation

Patents

Patent applications submitted: The US Patent Office serial numbers:

- 10/769164
- 10/793302
- 10/797301
- 10/801740

Patent issued:

- The US Patent Office Grant Number 6744235

II.4 Thermally Integrated High Power Density SOFC Generator

Pinakin Patel (Primary Contact), Brian Borglum, Peng Huang

FuelCell Energy, Inc. (FCE)

3 Great Pasture Road

Danbury, CT 06813

Phone: (203) 825-6072; Fax: (203) 825-6273; E-mail: ppatel@fce.com

DOE Project Manager: Magda Rivera

Phone: (304) 285-1359; E-mail: Magda.Rivera@netl.doe.gov

Subcontractors: Versa Power Systems, Des Plaines, Illinois (GTI, MSRI, UU)

Objectives

Research and development in Phase I shall focus on the research, design and manufacture of a planar solid oxide fuel cell (SOFC) power generator for stationary applications (3-10 kW) using natural gas as the standard fuel. Goals of the Phase I project include:

- Design of a thermally integrated, internal reforming fuel cell stack and compact balance-of-plant (BOP) package and system.
- Development of optimal cell structure having the target power density (300 mW/cm^2) and durability at lower operating temperatures ($\leq 800^\circ\text{C}$).
- Development of fuel processing system for operation on U.S. natural gas as the baseline fuel and initiation of development of fuel processing systems for broadly available fuels such as diesel.
- Prototype testing of natural gas (baseline fuel) fueled unit meeting the minimum Solid State Energy Conversion Alliance (SECA) technical requirements.

Approach

The research and development to achieve the above goals is organized in the following tasks:

- **System Design & Analysis** – In this task, work shall focus on prototype design, system-level modeling and analysis. Work will also concentrate on fuel processor subsystem development and thermally integrated power system development.
- **Cell Design, Development and Optimization** – In this task, work shall focus on improvements in cell performance through material changes and refinements. Composition and morphology of the anode, electrolyte, and cathode will be addressed to increase cell performance. Thermo-mechanical modeling of cells will be performed.
- **Stack Design and Development** – In this task, work shall focus on the development of 3-10 kW stack design to resolve manifold design and stack thermal issues and improve stack performance. Focus of work will be on the internal reforming stack design.
- **Product Development and Packaging** – Work shall concentrate on the integration of SOFC subsystems (electrical BOP and mechanical BOP) with SOFC stacks to maximize electrical efficiency and to reduce heat losses, overall system weight, and cost.
- **Process Development for Cost Reduction** – Work shall focus on SOFC cost reduction by manufacturing process improvements and adaptation of mass production techniques.
- **Prototype Test and Evaluation** – Work shall focus on the test and evaluation of the prototype system against the minimum SECA technical requirements.

Accomplishments

- In an endurance cell test using FCE's direct fuel cell (DFC) hardware, the internal reforming efficiency of methane fuel was over 95% with excellent stability (7000 hours of operation).
- The highest power density of 1.9 W/cm² at 800°C on button cell and 1.4 W/cm² at 750°C on 10 x 10 cm cell on hydrogen fuel (ideal conditions) has been achieved.
- An 80-cell tower, assembled using 4 stacks, produced 3.5 kW DC power.
- A kW-class SOFC system was designed, built and operated on natural gas fuel with a net system efficiency of up to 35%.

Future Directions

- Complete 3-kW baseline system design for natural gas fueled SOFC and initiate 10-kW advanced system design.
- Optimize electrode functional layers.
- Reduce cell operating temperature to 700°C.
- Validate alternate fabrication processes to improve cell performance and reduce cost.
- Develop high power density stack design incorporating modeling results, and advance gaskets and internal reforming cell design.

Introduction

The FCE team has initiated its technology development efforts. The efforts in this period focused on the critical technology development areas to meet the SECA program goals for the 3-10 kW SOFC generator. The FCE team has made significant progress in cell, stack and system technology areas and has met all planned milestones. In addition, the Team, FuelCell Energy and subcontractors, Versa Power Systems, including Gas Technology Institute (GTI), Materials and Systems Research, Inc. (MSRI) and University of Utah (UU), has developed and integrated a strategic R&D plan, milestones and efforts to ensure the achievement of SECA goals.

Approach

The FCE team is focusing on developing a 3-10 kW planar, thin-film, anode-supported SOFC system operating at 700°C, with a power density of >0.5 W/cm² at 0.7 V/cell by Phase III. The Phase I effort will focus on development of cell and stack designs, leading to a prototype 3-10 kW system operating on natural gas fuel, with lower heating value efficiency target of up to 40% and a degradation rate of <2%/1000 hours.

The cell technology approach is based on the record-setting performance achieved by MSRI and FCE. The baseline cell materials will be Ni/YSZ cermet for anode, yttria-stabilized zirconia (YSZ) as electrolyte and lanthanum strontium manganite (LSM) or other ceramic for cathode. In the stack design, internal and external manifold designs will be evaluated, innovative seal designs will be adopted, and internal reforming combined with radiative and convection cooling will be developed. A 3-kW baseline system and an advanced 10-kW system will be developed using the kW-class system under development within the FCE team.

Results

Cell Development: Cell development was focused on intermediate-temperature (700-750°C), planar, anode-supported SOFC technology. Significant progress in cell materials, design, scale-up, and fabrication has been made. Performance of SOFC trilayer (positive electrolyte negative) was improved significantly by improving the functional layer design. The highest power density of 1.9 W/cm² at 800°C on button cell and 1.4 W/cm² at 750°C on 10 x 10 cm cell on hydrogen fuel was achieved. Internal reforming of methane to hydrogen is a key to high power density cell operation. An internal reforming cell (100 cm² area) was assembled using

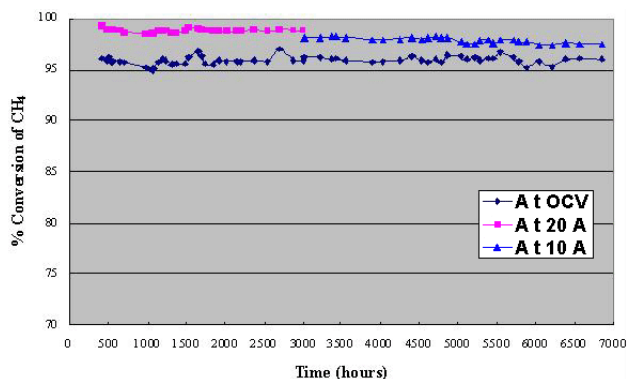


Figure 1. Stability of Internal Reforming of Methane - Excellent Stability of Internal Reforming

FCE's DFC hardware. The cell exhibited good reforming efficiency (>95% at 700°C) and excellent stability during 7000 hours of operation (Figure 1). As expected, the internal reforming efficiency increased as the operating current increased.

Conventional SOFC cell (trilayers) manufacturing requires multiple firing steps. These steps are complex, requiring elaborate process control and expensive equipment. FCE's single-fire process offers a significant cost savings. The single-fire trilayer processing technology was improved with greater reproducibility in performance. Cell sizes fabricated ranged from button size up to 20 x 20 cm. The cell and stack test results successfully validated the viability of the process.

Stack Development: The SOFC stack design was scaled up from 5 to 20 cells per stack, incorporating larger area (120 cm²) cells. Figure 2 shows a 20-cell stack, which is comprised of commercially available materials with matched thermal expansion coefficients. The individual cells of a 20-cell stack at 750°C and 0.5 A/cm² exhibited excellent performance. The average cell voltage was 0.85 V with a voltage spread of less than 20 mV. An 80-cell tower consisting of 4 stacks of 20 cells each was built and tested. This 4-stack tower produced 3.5 kW DC power after conditioning. Thermal cycling capability of two 20-cell stacks was validated through five thermal cycles each.

Seal technology is the key area for stack development to meet the SECA goals. Several gasket materials and designs, such as mica, glass and



Figure 2. 20-cell SOFC Stack - This Stack Is a Building Block for an 80-cell Tower

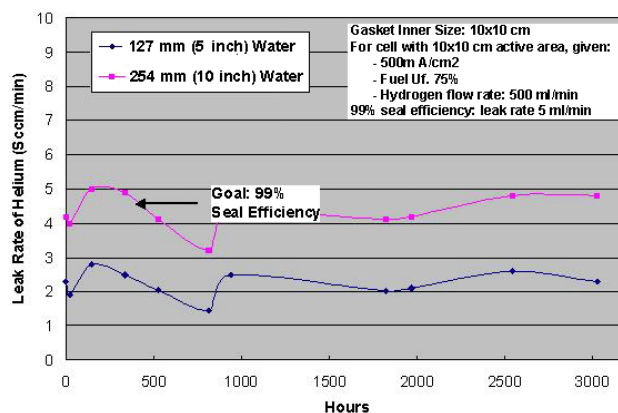


Figure 3. Gasket Development Test Results - The 3000-hour Test Showed Acceptable Seal Performance

other composite materials, were identified, and their evaluation was initiated. A new composite gasket, PH-1 gasket, was developed using FCE's DFC technology as a foundation and showed very promising results. For gaskets with inner perimeter 10 cm x 4 cm, the leak rates were 2-3 ml/min for air and 6-7 ml/min for simulated helium at backpressure of 15 inches water, only about a sixth that of a mica gasket with the same size. Over 3000 hours endurance testing of PH-1 on simulated fuel side, operation indicated excellent seal performance, as shown in Figure 3.



Figure 4. 2-kW Aurora System

System Development: Preliminary design of baseline 3-kW system was initiated. The design is based on FCE's 2-kW Aurora system with technical input from the parallel California Energy Commission project. The system will be natural gas fueled and operate in a grid parallel mode. It will incorporate a room temperature desulfurizer for natural gas. The advanced system (10 kW) will incorporate features to further reduce system cost. Such features may include anode recycle (hot, cold or selective), dual voltage output (DC and AC) for telecom applications, low-cost cell and stack designs, etc.

Figure 4 shows the prototype Aurora system. It incorporates significant design advances in thermal integration and management and power conditioning. Segregation of the heat sources (stacks and afterburner) has been accomplished through the

creation of two physically separate zones. The stack zone has a single 80-cell stack tower at its center with other components located in close proximity to the vertical faces of the stack. The integrated module zone exchanges heat from the afterburner to the prereformer and other regenerative exchangers. With this design, heat flows in the system can be varied and directed to specific components, allowing for maximum operational control and thermal management of the system. The result is a system with the capability to operate with higher fuel utilization, as well as a significantly higher level of electrical and cogeneration efficiency. In addition to the advances in performance, the system has also been designed to facilitate maintenance with quickly replaceable modules. The test results on natural gas fuel showed that a peak electrical efficiency of up to 35% is feasible with this system.

Conclusions

- The technology development of the planar SOFC cell, stack and system indicate that the higher power density (300-500 mW/cm²) operation is facilitated by internal reforming. FCE's internal reforming technology was validated through a 7000-hour cell test.
- The 80-cell tower concept using 4 stacks of 20 cells each offers a low-cost, near-term option to build 3-10 kW size SOFC systems.

Publications

1. P. Patel, Thermally Integrated High Power Density SOFC Generator, SECA Annual Conference, Boston, MA, May 11-13, 2004.
2. B. Borglum, Planar SOFC Development Status at FuelCell Energy, Solid Oxide Fuel Cell Forum, Lucerne, Switzerland, June 28 - July 2, 2004.

II.5 Solid State Energy Conversion Alliance (SECA) Solid Oxide Fuel Cell Program

Nguyen Minh (Primary Contact), Ray Andrews, Tony Campbell
GE Hybrid Power Generation Systems
19310 Pacific Gateway Drive
Torrance, CA 90502-1031
Phone: (310) 538-7250; Fax: (310) 538-7250; E-mail: nguyen.minh@ps.ge.com

DOE Project Manager: Travis Shultz
Phone: (304) 285-1370; E-mail: Travis.Shultz@netl.doe.gov

Objectives

- Develop a fuel-flexible and modular system (3 to 10 kW) that can serve as the basis for configuring and creating low-cost, highly efficient, and environmentally benign power plants tailored to specific markets.
- Demonstrate a prototype system of the baseline design with desired cost projections and required operating characteristics (Phase I); assemble and test a packaged system for a selected specified application (Phase II); field test a packaged system for extended periods (Phase III).

Approach

Phase I

- Establish a baseline system concept and analyze its performance characteristics.
- Perform a cost study to estimate system costs.
- Develop a robust, reliable, high-performance solid oxide fuel cell (SOFC) stack technology amenable to low-cost manufacturing.
- Develop a fuel processor as a pre-reformer for processing a variety of fuels.
- Evaluate system thermal management to establish a suitable recuperation scheme for the system.
- Develop and implement a flexible control structure incorporating required sensors.
- Identify a flexible low-cost power management subsystem.
- Evaluate component integration.
- Assemble and test a prototype system to demonstrate performance meeting the program requirements.

Accomplishments

System Design and Analysis

- A conceptual 5-kW system has been designed, and its performance and operating characteristics have been analyzed. When fully developed, the estimated system efficiency on natural gas is about 40%. A failure modes and effects criticality analysis for the system has been completed.
- Preliminary prototype system design, including analysis of initial baseline design, was completed.

Cost Estimate

- Projected cost estimates were updated and cost report submitted.

Stack Technology Development

- Several module and stack tests of the SECA stack design were conducted. A single-cell module, running at 88% fuel utilization in simulated autothermal reforming (ATR) reformat containing 7% methane, achieved a power density of 0.276 W/cm² at the SECA design current of 0.428 A/cm². This compares favorably with the target of 0.300 W/cm² under the same operating conditions.
- Extraordinarily high fuel utilization (95%) has been demonstrated with the half sealed stack design.
- A 10-cell stack of the SECA stack design was tested and achieved a peak power of 503 W.
- A design iteration on the stack was performed. The new design retains the positive features of the previous design and incorporates new features to improve thermal cycling and sealing.
- The fuel cell cathode was improved. Initial performance improvements of 20% were observed, and the new cathode retains its performance at approximately 1/3 the thickness of the standard cathode.

Fuel Processing

- The ATR pre-reformer has been designed. The pre-reformer was built and tested, and operation was demonstrated with natural gas and propane. The pre-reformer meets all the requirements of the SECA system.

Control and Sensor Development

- A strategy for the control subsystem has been selected and tailored to meet the required system performance and operation characteristics. A multi-level design, including top-level supervisory algorithms and active controls, was developed and implemented in software to manage the various control system tasks.

Thermal Management

- Detailed design of the system heat exchangers was initiated.
- Two concepts for the system tail-gas burner were evaluated. Both were found to be viable solutions and the prototype solution was downselected.

Power Electronics

- System power electronics were fabricated and tested. The power electronics achieved efficiency >94% over a wide range of power (3-6 kW).

Prototype Assembly

- A preliminary prototype system design has been completed, including flow sheet, heat and material balance, package drawing, and bill of materials.
- System schematic was developed and configuration management controlled.
- Bill of materials was also developed and controlled in parallel to the system schematic.

Future Directions

- Kilowatt-class stacks will be built and operated to demonstrate required performance.
- Evaluation and development of all system components will be completed.
- The test plan for the prototype system will be finalized.
- Integrated operation of stack with fuel reformer will be demonstrated.
- Prototype component and subsystem testing will be completed.

- Prototype system will be assembled.
- Final audited cost estimate will be completed and submitted.
- Prototype testing will be conducted at GE according to the test plan.

Introduction

This project focuses on developing a low-cost, high-performance solid oxide fuel cell (SOFC) system suitable for a broad spectrum of power generation applications. The overall objective of the project is to demonstrate a fuel-flexible, modular 3-to-10-kW system that can be configured to create highly efficient, cost-competitive, and reliable power plants tailored to specific markets. The key features of the SOFC system include a fuel-flexible pre-reformer; a low-cost, high-power-density SOFC stack; integrated thermal management; and suitable control and power management subsystems. When fully developed, the system is expected to meet the projected cost of \$400/kW.

Approach

The SOFC system is a stationary power module (3 to 10 kW) capable of operating on different fuels. The system consists of all the required components for a self-contained unit, including fuel cell stack, fuel processing subsystem, fuel and oxidant delivery subsystem, thermal management subsystem, and various control and regulating devices.

- The SOFC is a compact arrangement of anode-supported cells (fabricated by the GE tape-calendering process) and metallic interconnects. The stack design is based on an advanced concept that maximizes cell active area and minimizes sealing. The fuel cell can operate directly on light hydrocarbon fuels and incorporates materials for high performance at reduced temperatures (<800°C). These characteristics provide a low-cost, fuel-flexible fuel cell suitable for operating under various conditions. The tape calendering process for manufacturing thin-electrolyte, anode-supported cells is a potentially low-cost, mass-customization technique suitable for high-volume production and automation using available commercial equipment.

- The fuel processor is a catalytic reactor that pre-reforms the hydrocarbon fuel before the gas is fed to the SOFC stack.
- The main thermal management components provide means to utilize the excess heat of the exhaust gases of the SOFC to supply heating to the incoming air and fuel as well as generating steam.
- The control system has a flexible structure that can be modified or optimized for different applications.

The project consists of three phases. Phase I of the project focuses on developing system components having the required operating characteristics, resolving critical technological issues, and demonstrating a prototype system. The Phase I work concentrates on system design and analysis, cost study, stack technology development, fuel processing development, controls and sensors, power electronics, and system prototype assembly and testing. Phase II will demonstrate a packaged system selected for a specified application and further improve technology and assess system cost. Phase III will extend the Phase II effort to field test a packaged system for extended periods to verify the required performance, cost, reliability, and lifetime for commercial uses.

Results

System Design and Analysis: A six-sigma performance analysis for a Phase III target of 40% was performed, including required variabilities from 13 major subsystem parameters. A performance variability analysis of the Phase I conceptual system was performed, including estimated variabilities from 11 major subsystem parameters. Four concepts were compared to the baseline system. The baseline system concept was selected for the conceptual system design. A failure modes and criticality effects analysis for most of the system has been performed. Part-load models for all system

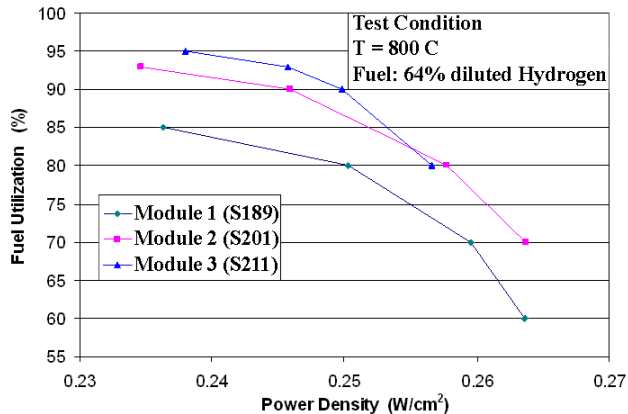


Figure 1. SOFC Module Fuel Utilization

components have been developed and incorporated into a system part-load performance model; this will be used to predict the most efficient operational point and the maximum power rated operational point.

Stack Technology Development: A stable fuel utilization of 95% was achieved with 64% hydrogen and balance N₂ at 800°C (Figure 1). At this utilization, a reasonable performance was also achieved: 0.67 V at 0.356 A/cm², for a power density of 0.238 W/cm². Several single-cell modules and multi-cell stacks of the baseline design were tested. Significant performance improvements have been observed in these tests. For example, under dilute hydrogen at 88% fuel utilization, a power density of 0.193 W/cm² was demonstrated at a cell voltage of 0.722 V. While under ATR fuel and the same fuel utilization, the power density was 0.230 W/cm² at 0.722 V. At the design current in ATR fuel, the module achieved a power density of 0.276 W/cm² at 88% fuel utilization, which approaches the target of 0.300 W/cm². Testing of several stacks of the baseline design was performed. One 5-cell, one 6-cell, and two 10-cell stacks were tested with a peak of 75% fuel utilization and maximum power of 0.5 kW. Following the completion of the testing, a risk review was conducted on the stack design. The review identified several major risks, and an improved stack design was then developed. Performance of cathodes has been improved, reducing cathode polarization to ~200 milliohm-cm². The cathode polarization area specific resistance (ASR) is plotted in Figure 2 as a function of cathode thickness for both baseline cathode and modified

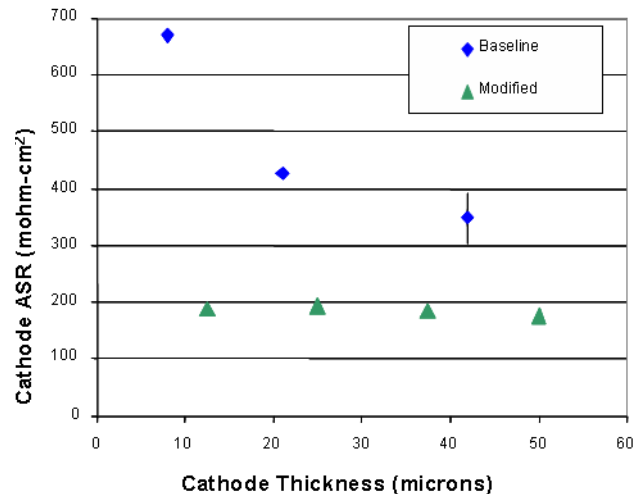


Figure 2. Polarization ASR Measured at Different Thickness for Baseline and Modified Cathodes

cathode. The modifications produced two benefits: 1) the ASR was reduced by over 50%, and 2) low ASR was maintained at lower cathode thicknesses, which reduces materials and processing cost.

Fuel Processing: Two generations of the ATR external fuel processor design were completed, built, and tested. A photograph of the final ATR processor is shown in Figure 3. The ATR prototype was operated for 42 hours with 9 start/stop cycles. Eight tests were performed using pipeline natural gas, and one was performed using commercial-grade propane. The major operational parameters varied during testing were oxygen-to-carbon ratio, steam-to-carbon ratio, process gas inlet temperature, and reformate mass flow rate. The fuel processor met or exceeded most of the performance targets at the inlet specifications. The reactor demonstrated its ability to reform an alternative fuel (propane) for six continuous hours with no apparent loss of conversion efficiency.

Control and Sensor Development: A multi-level design was developed to manage the various control system tasks. The general control system architecture for this design consists of top-level supervisory algorithms that determine setpoints based on user settings and system conditions. These setpoints are provided to a set of active controls that handle setpoint tracking and disturbance rejection. The baseline control strategy developed in simulation



Figure 3. ATR Fuel Processor

has been updated to facilitate software development and testing. The requirements for the control software are that it execute in real-time and is robust. The target update rate for the control software is currently 0.01 seconds. Preliminary testing with all of the input A/D data, BIT check, supervisory controls, active controls, and output D/A shows that the software can execute in the range of 0.0002 to 0.0003 seconds. Therefore, significant margin exists for execution of the software in the real-time environment. The robustness of the real-time control software was verified by extended continuous operation (>40 hours), and several failure mode investigations were performed such as loss of controller or host PC power.

Thermal Management: The primary components of the thermal management subsystem include a combustor, cathode air preheater, steam generator, and fuel processor reactant preheaters. Combustor development activities have focused on determining system design considerations necessary to operate either a catalytic-type burner or a more conventional, diffusion-type burner. The analysis completed to date shows that both combustor options represent viable approaches to tail-gas combustion. A catalytic approach was chosen for the prototype system to

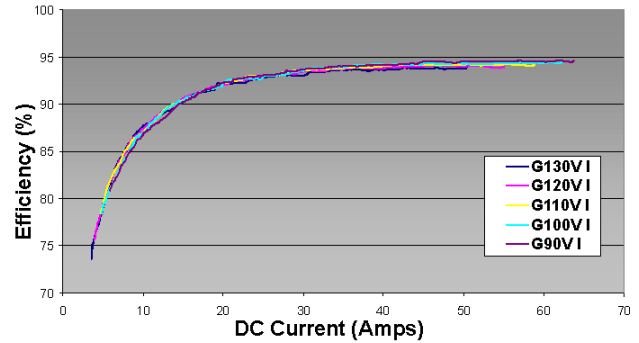


Figure 4. Inverter Efficiency Curve

allow increased design flexibility. Activities related to the cathode air preheater were focused on two areas: 1) the procurement of a heat exchanger and 2) determination of heat exchanger sizing methodology to accommodate off-design operation.

Power Electronics: Efficiency testing was conducted on two prototype inverters at GE. This data was necessary for down-selecting an inverter that will be used in the prototype system. Overall inverter efficiency is calculated as the total AC power output of the unit divided by the total DC power input. Efficiency curves were generated for multiple DC input voltages. The efficiency for the selected inverter is generally above 94% for DC power greater than 3 kW (Figure 4). The measurement uncertainty for the efficiency is calculated to be approximately $\pm 0.25\%$, but the results have been consistent throughout the testing of the inverter.

Prototype System Assembly: The prototype system will be assembled based on the concept design developed in this project. The prototype system design will at conclusion include process and instrumentation diagrams; system heat and material balances at rated conditions and off-design points; defined startup and shutdown procedures; failure mode and effects analysis; specified, designed, and identified components; designed control system; and designed thermal management system. The initial prototype system schematic was devised. The schematic created a baseline for prototype system analysis activity and the bill of materials (BOM). The BOM lists each component shown on the schematic, quantities, technical parameters to be used

for hardware identification, and the owner responsible for that component. Layout concepts for the prototype system have been developed utilizing actual component design drawings for those items that have been identified to date and derived conceptual design models for unidentified components.

Conclusions

- A conceptual design of the SECA system for stationary (residential) applications has been developed.
 - SOFC modules and stacks of the baseline design have been built and operated and show significant performance improvements. Extraordinarily high fuel utilizations up to 95% in 64% H₂-36% N₂ at 800°C have been demonstrated.
 - An ATR pre-reformer for the SECA system has been designed, built and tested on two types of fuels and meets the system requirements.
 - A multi-level design for the control subsystem, including top-level supervisory algorithms and active controls, has been developed and implemented in software for the SECA system.
- Efficiencies of >94% for inverters have been demonstrated to meet the SECA system requirement.
 - A preliminary design for the prototype system has been developed. Schematic and BOM for the system have been established.

FY 2004 Publications/Presentations

1. N. Q. Minh, "Development of Solid Oxide Fuel Cell Systems for Power Generation Applications", 2003 Fuel Cell Seminar Abstracts, Courtesy Associates, Washington, DC, 2003, p. 892.
2. A. B. Campbell, J. F. Ferrall, N. Q. Minh, "Solid Oxide Fuel Cell Power System", VF-007232, 29th Annual Conference of the IEEE Industrial Electronics Society, Roanoke, VA, November 2-6, 2003.
3. N. Q. Minh, "SECA Solid Oxide Fuel Cell Program", presented at the SECA Annual Workshop and Core Technology Program Peer Review in Boston, MA, May 11-13, 2004.

II.6 Small-Scale Low-Cost Solid Oxide Fuel Cell Power Systems

Shailesh D. Vora

Siemens Westinghouse Power Corporation

1310 Beulah Road

Pittsburgh, PA 15235

Phone: (412) 256-1682; Fax: (412) 256-1233; E-mail: Shailesh.Vora@siemens.com

DOE Project Manager: Don Collins

Phone: (304) 285-4156; E-mail: Donald.Collins@netl.doe.gov

Subcontractors: Fuel Cell Technologies, Ltd., Kingston, Ontario, Canada; Blasch Precision Ceramics, Albany, NY

Objective

- To develop a commercially viable 5-10 kWe solid oxide fuel cell power generation system that achieves a factory cost goal of \$400 per kWe.

Approach

- Improve cell performance through new cell design and new materials.
- Lower operating temperature from 1000°C to 800°C.
- Eliminate internal fuel reformers through on-cell reformation.
- Develop low-cost high-volume manufacturing processes.
- Use low-cost module materials due to lower operating temperature.
- Simplify balance-of-plant (BOP) design by elimination of parts.

Accomplishments

- Fabricated high power density (HPD) seal-less planar cells. A new design that combines the seal-less feature and a flattened cathode with integral ribs was chosen. The ribs reduce the current path length by acting as bridges for current flow. This cell design, due to shorter current path, has lower cell resistance and hence higher power output than tubular cells.
- Demonstrated 30% higher power density for HPD cells compared to tubular cells.
- Demonstrated over 1000 hours voltage stability for HPD cells at 1000°C and 85% fuel utilization.
- Developed bundling technique for HPD cells. Bundles with up to 11 HPD cells were fabricated.
- Completed module design for a 5-kWe proof-of-concept system with HPD cells. Module design for the proof-of-concept unit was completed with identification and layout of components. Number and type of cells required to obtain the required power output were finalized.

Future Directions

- Optimize HPD cell design in terms of number of channels and dimensions.
- Develop cell materials for operation at 800°C.
- Improve cell performance through optimized cell design and new materials.
- Assemble and test proof-of-concept system.

Introduction

The objective of this project is to develop a standard high-performance, low-cost solid oxide fuel cell (SOFC) system that can be manufactured in high volume for application in a number of different end uses, including residential power generation and auxiliary power units (APUs) in commercial and military transportation applications. This project is a ten-year, three-phase project with prototype SOFC systems being tested at the end of every phase. Performance and cost improvements made during each phase will be incorporated in each prototype, and products based on each prototype will be made ready for market entry as they become available.

Approach

We have identified key technical issues that must be resolved to achieve low-cost commercial SOFC systems. We will focus on cost reductions and performance improvements to transform today's SOFC technology into one suitable for low-cost mass production of small systems for multi-market applications. The key advances identified are:

- Improved cell performance through design and materials innovations to double the power and thus reduced cost per kW
- On-cell reformation of natural gas fuel to eliminate high-cost internal reformer components
- Sulfur-tolerant anodes to eliminate the fuel desulfurization system
- Use of low-cost insulation and containment vessels by lowering the system operating temperature
- High-efficiency (95%) power conditioning systems to improve overall system electrical efficiency
- Cost-effective fuel processing systems for operation of the standard SOFC module on alternate fuels

In addition to the key advances noted above, adoption of more automated mass production techniques for cell, module and BOP manufacturing will ensure overall SOFC system cost effectiveness.



Figure 1. Cylindrical and HPD Cells

Results

Prior to the start of the project, it was recognized that Siemens Westinghouse's seal-less tubular cell design would not be able to meet the cost and performance targets of the program. A need to develop a cell with higher power density and compact design was identified. A new design that combined the seal-less feature and a flattened cathode with integral ribs was chosen. This new design, referred to as high power density (HPD) SOFC, has a closed end similar to the tubular design. The ribs reduce the current path length by acting as bridges for current flow. The ribs also form air channels that eliminate the need for air feed tubes. This cell design, due to shorter current path, has lower cell resistance and hence higher power output than tubular cells.

Analytical modeling was initiated to optimize the number of ribs (channels) for maximum power and mechanical stability despite thermal stresses during operation. Based on initial results, HPD cell designs with five channels (HPD5) and 10 channels (HPD10) were selected for cell preparation to develop manufacturing processes and test electrical performance.

Several HPD5 and HPD10 cells were fabricated and tested for electrical performance. Figure 1 shows cylindrical and HPD cells. HPD5 cells showed over 30% higher power density compared to cylindrical cells, with the target being 100% more power density for the 10-year program. Figure 2 shows voltage versus current density comparison for cylindrical and HPD5 cells. Figure 3 shows voltage

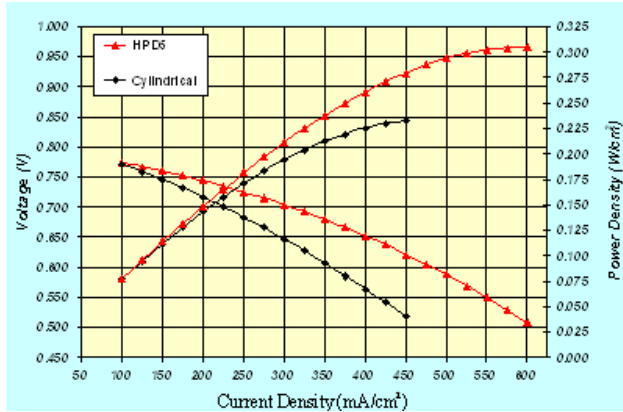


Figure 2. Voltage versus Current Density Comparison for Cylindrical and HPD Cells

stability of HPD5 cell over more than 1000 hours of operation.

Efforts were also directed towards the development of cell-to-cell connections to bundle cells. A bundle with 11 HPD5 cells was fabricated for demonstration purposes. Tensile tests to measure the mechanical viability and integrity of connections were conducted with acceptable results.

Conceptual design of a 5-kWe proof-of-concept system for residential applications was completed. Siemens Westinghouse worked closely with Fuel Cell Technologies (FCT), a partner in module and BOP development, on this task. The overall thrust of the task was to start from the existing residential

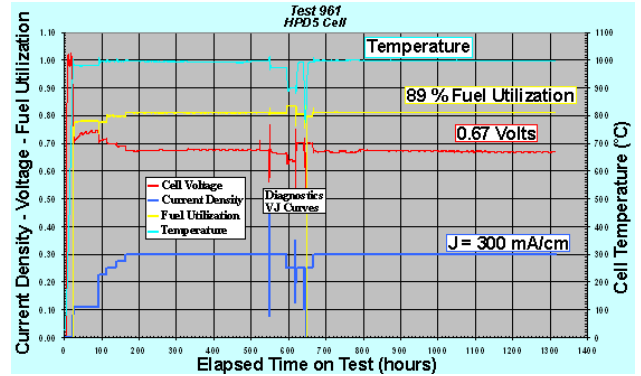


Figure 3. Voltage versus Time Plot for HPD5 Cell

prototype system design and develop concepts to simplify the system.

Conclusions

Fabrication processes for HPD cells were established, and electrical testing showed significant improvement in power density over cylindrical cells.

FY 2004 Publications/Presentations

1. S. D. Vora, SECA Program at Siemens Westinghouse, Presented at SECA Annual Workshop and Peer Review Meeting, May 11-13, 2004, Boston, MA

III SECA Core Technology Program

III.A Materials

III.A.1 SOFC Research and Development

Michael Krumpelt (Primary Contact), Thomas Kaun, Terry A. Cruse, Mark C. Hash
Argonne National Laboratory
9700 S. Cass Avenue
Argonne, Illinois 60439
Phone: (630) 252-8520; Fax: (630) 252-4176; E-mail: krumpelt@cmt.anl.gov

DOE Project Manager: Lane Wilson
Phone: (304) 285-1336; E-mail: Lane.Wilson@netl.doe.gov

Objectives

- Explore the mechanisms of chromium-related solid oxide fuel cell (SOFC) performance degradation.
- Explain why chromium poisoning appears to be more severe at 700°C than at 800°C.

Approach

- Determine and compare cell performance degradations with different interconnect materials and temperatures.
- Measure chrome contents in cathodes from cell tests and in cathodes that were equilibrated in contact with bipolar plate materials.
- Determine weight loss of chrome oxide at different water concentrations in the gas phase.

Accomplishments

- SOFC performance degradation due to chromium poisoning of the cathodes was shown to indeed be faster at 700°C than at 800°C.
- Three different mechanisms were identified that can cause chromium poisoning, with oxyhydroxide evolution from the bare metal being responsible for the accelerated effect at 700°C.
- Thermogravimetric analyses have unequivocally shown that weight loss attributed to oxyhydroxide volatility is proportional to the water content in the gas phase.
- Chromium volatility is lower from compounds like MnCr_2O_4 or LaCrO_3 .
- Lanthanum ferrite cathodes were shown to be more severely affected by chromium poisoning than lanthanum manganite.

Future Directions

- The reason for the diminished cathode performance will be investigated.
- Methods for diminishing the chromium migration will be explored.
- The nature of the chrome species in the cathode and whether solid-state diffusion is related to the oxide conductivity of the cathode will be explored.

Introduction

Chromium contamination of SOFC cathodes has been observed by several groups of researchers developing stacks with metallic bipolar plates. When a chromium source is present, the cells exhibited significant performance declines, leading to speculation that chromium contamination may “poison” the cathode performance. Hilpert et al. have attributed the chromium transport to the formation of volatile oxyhydroxide species that form when chromium-containing steels are exposed to oxygen and water at elevated temperatures (1, 2). The oxyhydroxide (primarily $\text{CrO}_2(\text{OH})_2$ (3)) can form either by reaction of the surface oxide with oxygen and water, or by direct reaction of metallic chromium (4), which then deposits at the active cathode sites (5). A good overview of many issues associated with metallic-based interconnects is provided by Quadackers (6). Other issues being considered are cathode/electrolyte interactions and compositions (7). In addition to vapor-phase transport, because the interconnect is in direct contact with the cathode, chromium may also diffuse into the cathode by a solid-state mechanism. In this report we present the results of work addressing the degradation of cell performance in the presence of different steels, the chemical reactivity of steels with cathode materials and volatilization from various chromium sources.

Approach

The primary approach used to investigate chromium poisoning of the SOFC cathode was to operate SOFC cells at a constant potential of 0.7 volts and observe performance degradation. SOFCs of 2.5 cm X 2.5 cm and similar-sized samples of either 430 SS, EBrite, or Crofer 22 APU were used. Additionally, metal particles of the same alloy were placed on top of the cathode. Next, a Pt mesh current collector was placed on top of the cathode and particles, followed by the metallic plate with slits cut in it. Cells with lanthanum strontium iron oxide (LSF), lanthanum strontium manganese oxide (LSM), or an A-site-deficient LSF were operated at 700°C and 800°C. Air at 2% humidity was used as the cathode gas and hydrogen, with 3% humidity, as the anode gas. The cells were operated until 50% of the initial current was supported at 0.7 volts.

Postoperation analysis was done by scanning electron microscopy (SEM), and Cr distribution was determined by energy dispersive x-ray spectroscopy (EDS).

A second set of experiments examined the weight loss of Cr_2O_3 , MnCr_2O_4 and LaCrO_3 by thermogravimetric analysis. Alumina was used as a standard to correct for any buoyancy effects. Runs were carried out at 700°C and 800°C using 3 mol% or 25 mol% H_2O in a carrier gas of 20% O_2 in Ar, with a flow rate of 50 sccm. The materials were allowed one hour to equilibrate with respect to environment prior to data collection.

Results

Results of the cell tests are shown in Figures 1a and 1b. Figure 1a shows polarization curves of a cell with an LSM cathode and a 430 SS interconnect at 700°C after 2, 48, 144, 168, and 216 hours of operation. The polarization curve declines quite rapidly, and after 200 hours only half the initial current was sustained. Figure 1b shows the cell current at 0.7 V versus the operation time at 800°C and at 700°C. While the cell current at 700°C was significantly smaller than at 800°C, consistent with a higher resistance at lower temperatures, both cells show a significant decrease in current. However, the decline at 700°C appears more rapid than at 800°C, implying increased poisoning at lower temperature.

Similar results were observed with both E-Brite and Crofer 22 APU materials. SEM was used to examine the degraded cells, with EDS used to determine the chromium content through the cathode. Figure 2 provides SEM images, Figure 3 the corresponding chromium profiles, of the cross section of three cells with different cathodes, all tested with Crofer 22 APU. An LSM cathode, Figure 2a, had very little chromium after 200 hours, while the different LSF cathodes, Figures 2b and 2c, had much higher chromium after 50 hours, with the heavily A-site-deficient LSF having the highest chromium content.

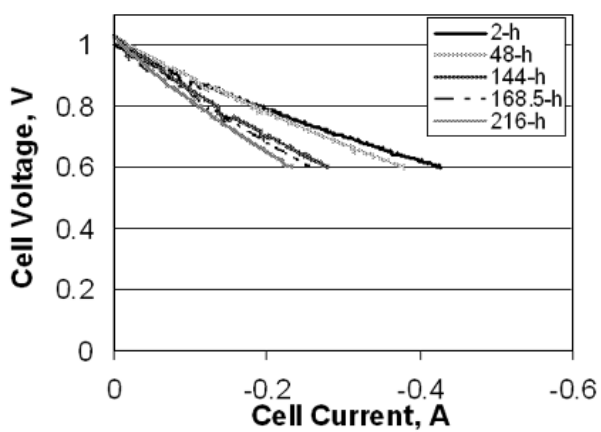
Thermogravimetric Analysis

Shown in Figure 4 are the mass losses from chromia powder measured by thermogravimetric analysis in flowing air at 700°C and 800°C with either

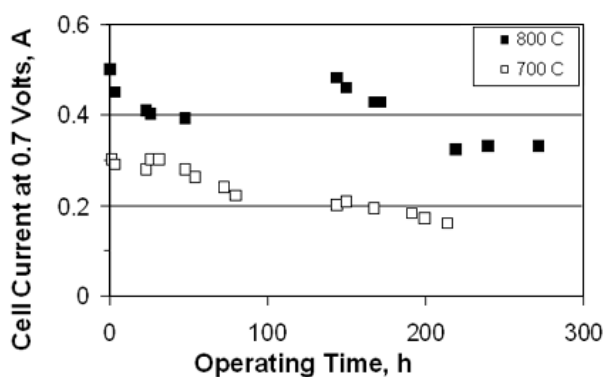
3 or 25% water in the air. Chromia clearly reacts with oxygen and water to form a volatile species, and based on thermodynamic analysis this should be primarily $\text{CrO}_2(\text{OH})_2$. The material loss is on the order of micrograms per hour and shows dependence on both temperature and water content of air.

Discussion

Having examined the issue of chromium poisoning from several different perspectives, it appears that no single mechanism may be completely responsible for the interactions between stainless steel and SOFC cathodes. The volatile oxyhydroxide species can form by a reaction of air and steam with



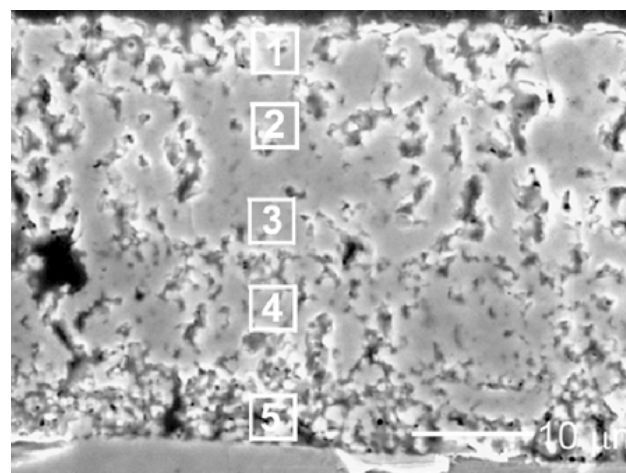
(a)



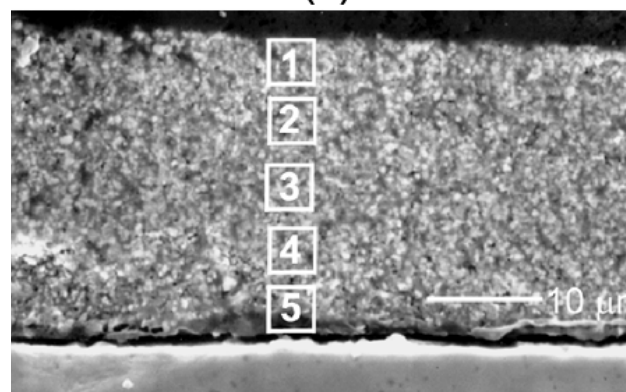
(b)

Figure 1. (a) Polarization Curves of InDec Cell #17 with LSM and 430 SS at 700°C and 2% Humid Air, Showing Ongoing Performance Cecline, and (b) Cell Current at 0.7 V for Two SOFCs with LSM Cathode, 430 SS and Humid 2% Air, One at 700°C and the Other at 800°C

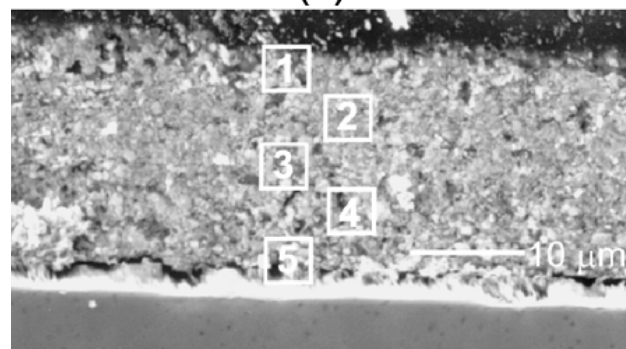
the bare metal or with the protective chromium oxide layer. The reaction with the metal is thermodynamically favored and appears to be faster. Poisoning of cathodes is more rapid at 700°C because the interconnect surface is essentially bare. At



(a)



(b)



(c)

Figure 2. SEM of (a) LSM Cathode, (b) LSF Cathode, and (c) A-site-deficient LSF Operated at 800°C with a Crofer 22 APU Interconnect

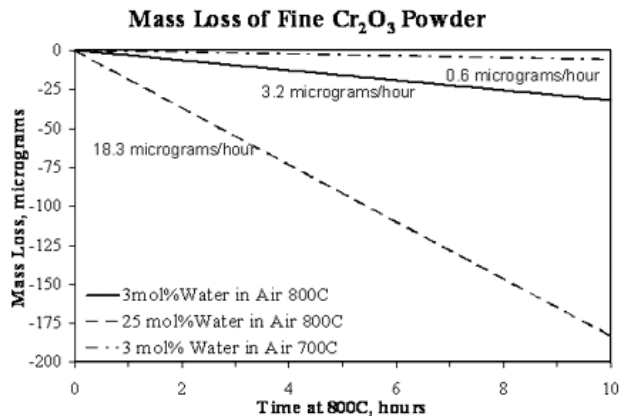


Figure 4. Comparison of the Mass Loss from Chromia under Various Conditions; the Species of Mass Loss is Expected to be CrO₂(OH)₂

800°C, the metal surface oxidizes to form a protective oxide scale, which is less reactive with oxygen and steam.

However, solid-state diffusion also seems to play a role in the migration of chromium. In both the cell tests and the solid-state equilibrations, the chromium levels were highest in the sub-stoichiometric LSF, followed by stoichiometric LSF and LSM. It is well known that the oxide ion conductivity decreases in that order. Since oxide ion conductivity will not affect the gas-phase diffusion, migration must be by a surface mechanism.

Conclusions

While ferritic stainless-steel-based interconnects are potentially attractive for planar SOFCs, it appears that interactions/reactions involving chromium in either the alloy or the protective scale can interact with the cathode materials. Therefore, the surface of any metallic interconnects will need to either be chromium-free or have chromium in a more stable form, such as a spinel or perovskite phase. However, the long-term relative stability of such materials has not yet been sufficiently examined.

References

- Hilpert, K., D. Das, M. Miller, D. H. Peck and R. Wei, J. Electrochem. Soc., Vol. 143, No. 11, pp. 3642-3647 (1996).

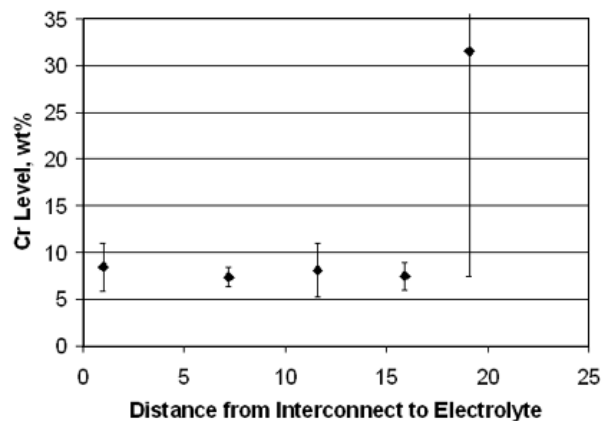
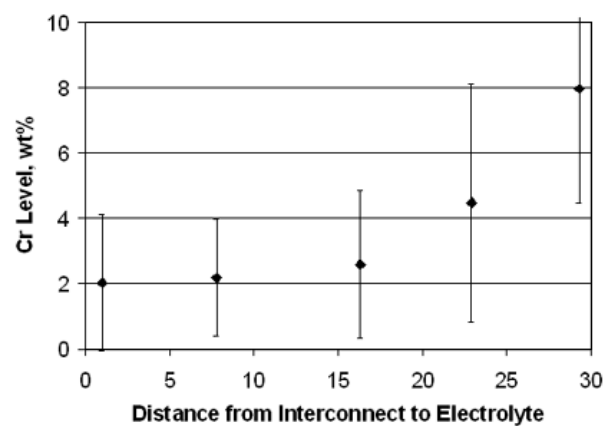
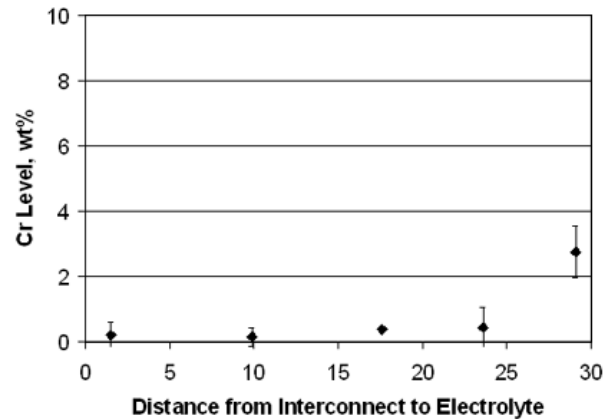


Figure 3. Charts Corresponding to the Chromium Content Determined by EDS for Points 1 through 5 for Each Cathode

2. Gindorf, C., L. Singheiser, and K. Hilpert, *Steel Research*, Vol. 72, pp. 528-533, (2001).
3. Ebbinghaus, B. B., *Combustion and Flame*, Vol. 93, pp. 119-137 (1993).
4. Fryburg, G., F. Kohl, and C. Stearns, *J. Electrochemical Soc.*, Vol. 121, pp. 952958 (1974).
5. S. P. Jiang et al., *J. European Ceramic Society*, Vol. 22, pp. 361-373 (2002).
6. Quadackers, W. J., J. Piron-Abellan, V. Shemet, and L Singheiser, *Materials at High Temperatures*, Vol. 20, No. 2, pp. 115-127 (2003).
7. Matsuzaki, Y. and I. Yasuda, *J. Electrochem. Soc.*, Vol 148, No. 2, pp. A126A131 (2001).

III.A.2 Metal Interconnect for SOFC Power Systems

S. (Elango) Elangovan (Primary Contact), Shekar Balagopal, and Insoo Bay

Ceramatec, Inc.

2425 South 900 West

Salt Lake City, UT 84119-1517

Phone: (801) 978-2162; Fax: (801) 972-1925; E-mail: Elango@ceramatec.com

DOE Project Manager: Lane Wilson

Phone: (304) 285-1336; E-mail: Lane.Wilson@netl.doe.gov

Objectives

- Select a surface treatment process for commercial ferritic stainless steel to reduce oxide scale growth rate.
- Optimize treatment process conditions to provide a conductive, stable scale.
- Measure the scale properties in solid oxide fuel cell (SOFC) relevant conditions.

Approach

- Select a heat treatment process to achieve a thin, dense scale of a conductive oxide composition.
- Measure scale conductivity in air at target operating temperature.
- Evaluate scale morphology under fuel cell operating conditions.

Accomplishments

- The surface treatment was found to reduce the scale growth rate as determined by thermogravimetry at 750°C. The treated metal coupons showed a parabolic rate constant of $5 \times 10^{-9} \text{ gm}^2/\text{cm}^4/\text{hr}$, compared to $7 \times 10^{-8} \text{ gm}^2/\text{cm}^4/\text{hr}$ for uncoated coupons. The low oxidation rate of treated interconnects will enable achieving the target fuel cell operating life of 40,000 hours.
- Scale resistance was 10 milliohm-cm² in air at 750°C and less than one milliohm-cm² in humidified hydrogen.
- Scale morphology was characterized as a function of treatment process and test conditions relevant to fuel cell operation.

Future Directions

- Optimize the surface treatment to mitigate the effect of simultaneous exposure to hydrogen and air on opposite sides of the metal interconnect.
- Evaluate chromium evaporation characteristics of the stainless steel as a function of surface treatment.

Introduction

Interconnects perform essential functions in a fuel cell stack: namely, electrical connection between adjacent cells and separation of air and fuel. In many cases, they also provide structural support for the stack. The use of commercial alloy offers the potential for low-cost interconnect components. This allows achieving the DOE target of low-cost, modular fuel cell stacks.

The SOFC interconnect must simultaneously satisfy several functional requirements. These functions require materials with high electronic conductivity for the series connection of individual single cells, gas impermeability to separate fuel and oxidant gases, chemical stability and conductivity over a large oxygen concentration range in order to maintain integrity in both the fuel and air atmospheres. Thermal expansion match with the rest

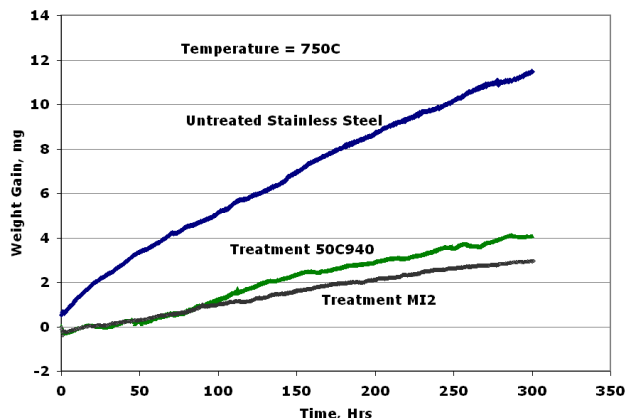


Figure 1. Thermogravimetry of Ferritic Stainless Steel Coupons

of the cell elements is desired. Metal interconnects are very desirable from the viewpoints of manufacturing cost in addition to other functional requirements, provided that the high conductivity can be maintained at the operating conditions. Metal interconnects also lend themselves to ease of fabrication of gas channels and greater control over dimensions to help improve the conformity as well as uniform reactant distribution to ensure uniform current density, high fuel utilization and high fuel efficiency. The use of thin metallic sheets will also reduce overall weight in the fuel cell system. High thermal conductivity of metal interconnects will help distribute the heat generated during the operation of the cell, thereby reducing the cooling air requirement as well as eliminating thermal stress failure of ceramic components caused by sharp thermal gradients.

The principal requirements of metal interconnects can be summarized as follows:

- 1) thermal expansion match with other cell components,
- 2) oxidation resistance in air and fuel at the operating temperature,
- 3) conductive interface (scale) in air and fuel atmospheres,
- 4) prevention of reactivity with electrode materials to form insulating compounds,
- 5) low volatility of major or minor constituents that poison electrode activity,
- 6) compatibility with anode and cathode environments,
- 7) uniformity in contact with the cells,
- 8) thermal cycle capability, and
- 9) low cost.

The present work focuses on the development and

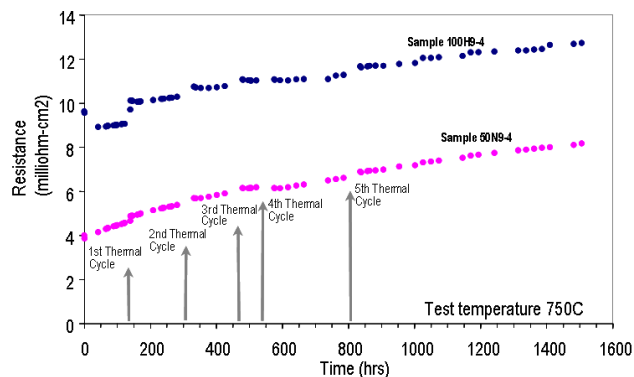


Figure 2. Resistance of Coupon Couples in Air at 750C

evaluation of conductive oxide scale on commercial ferritic stainless alloys.

Approach

A commercial stainless steel alloy was selected. The surface oxide scale was modified using an appropriate coating and heat treatment process to provide a dense conductive oxide scale. The growth rate, resistivity, and morphology of the scale were determined as a function of time for the various surface treatment conditions. The evaluations were made both in single-atmosphere (air or fuel) or dual-atmosphere (air and fuel on the opposite sides) conditions.

Results

Thermogravimetry of a 400-series commercial stainless steel was performed. Both untreated and treated coupons were evaluated. Two types of treatments were done. The first one was to heat treat the coupon to grow a controlled, dense oxide scale layer (treatment 50C940). In a second variation, an additional treatment was done to provide a stable chromium oxide composition as the outer layer (treatment MI2). The comparison of the oxide scale growth, via weight gain, is shown in Figure 1. The pre-grown oxide layer was found to reduce the scale growth significantly, while the second treatment provided an additional reduction in scale growth rate.

The resistances of the coupons were measured after they were surface treated. Two coupons were sandwiched using a conductive perovskite (e.g., cobaltite) as the contact paste. The change in

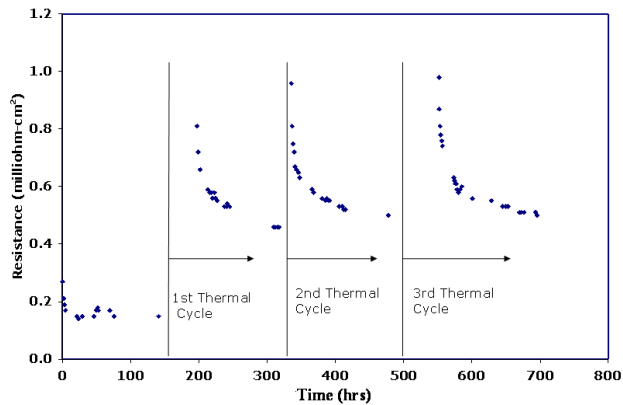


Figure 3. Resistance of Coupon Couples in Humidified Hydrogen at 750°C

measured resistance values of the coupon couples at 750°C in air is shown in Figure 2. The coupons were subjected to several thermal cycles. Similar measurements were also made in humidified hydrogen using nickel paste as the contact layer, shown in Figure 3. In both atmospheres, the resistance values were below 10 milliohm-cm², meeting the interconnect resistance target.

Earlier work showed that the oxide scale on the air side is disrupted when the opposite side is exposed to hydrogen at the target cell operating temperature. In order to evaluate the effect of dual-atmosphere exposure, resistance of a coupon couple was measured as one coupon was exposed to dual atmosphere. The test arrangement and the results of a test using the graded scale composition are shown in Figure 4. The low resistance measured under realistic exposure condition is encouraging although additional work is needed in characterizing possible change in scale morphology under such conditions.

Conclusions

- Surface treatment to commercial ferritic stainless steel is shown to reduce the oxidation rate in air at SOFC operating temperature.
- The resistance values of the stainless interconnect meet the target.
- Exposure to dual atmospheres disrupts the oxide scale on the air side, and the graded scale layer provides a promising approach. Further work is

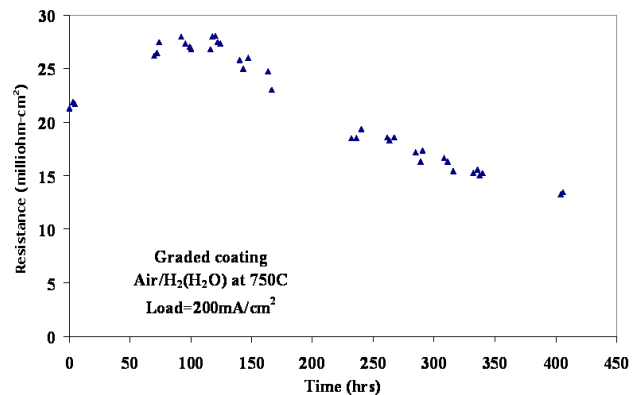
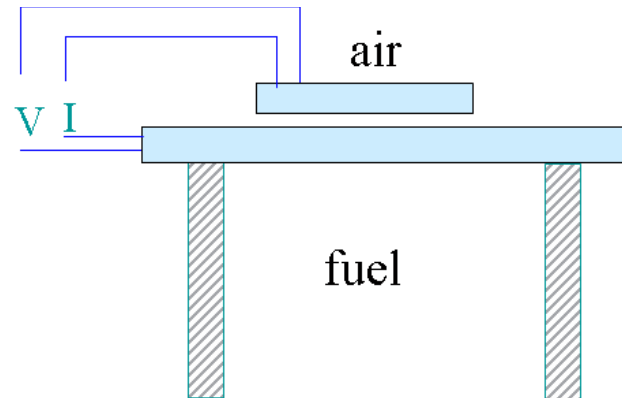


Figure 4. Test Configuration and Resistance of Coupon Couples in Dual Atmosphere

planned to evaluate the scale morphology. The work will also be extended to study the chrome evaporation from the interconnect that could poison the cathode during stack operation.

FY 2004 Publications/Presentations

1. "Evaluation of ferritic stainless steel interconnects for use as metal interconnects for solid oxide fuel cells," S. Elangovan et al., Journal of Materials Engineering and Performance, Vol. 13, No. 3, June 2004.
2. SECA Annual Workshop and Core Technology Program Peer Review Workshop, Boston, MA, May 2004.
3. SECA Core Technology Program Review Meeting, Albany, NY, September 2003.

III.A.3 Composite Cathode for High Power Density Solid Oxide Fuel Cells

Ilwon Kim (Primary Contact), Scott Barnett, Yi Jiang, Zhongliang Zahn, Dan Gostavic

Functional Coating Technology, LLC.

1801 Maple Ave. Suite 5320

Evanston, IL 60201

Phone: (847) 467-5376; Fax: (847) 467-5378; E-mail: ikim@fctnet.com

DOE Project Manager: Lane Wilson

Phone: (304) 285-1336; E-mail: Lane.Wilson@netl.doe.gov

Objectives

- Determine the electrochemical reaction kinetics of (La,Sr)(Co,Fe)O₃ (LSCF)-based cathode.
- Develop novel cathode structures.
- Determine the reactions between LSCF and zirconia. Develop a strategy to avoid reactions between LSCF and zirconia and promote electrochemical reactions.
- Determine the sensitivity of performance to sintering conditions.
- Demonstrate the feasibility of the LSCF composite cathode for use in high-performance solid oxide fuel cells (SOFCs) operating at low temperature.
- Determine the structural stability at operating temperature.

Approach

- Utilize idealized cathode structure to study the reaction pathway and rate-limiting steps for LSCF.
- Investigate LSCF-GDC (gadolinia-doped ceria) composite cathode structure that can help take advantage of the best properties of each material.
- Study the reaction of LSCF and zirconia and its effect on reaction kinetics.
- Determine the sensitivity of LSCF performance with respect to sintering conditions.
- Use GDC interfacial layer to prevent reaction, and study reaction kinetics at both idealized and practical interfaces.

Accomplishments

- Feasibility of LSCF-GDC cathode for high-performance SOFC has been well demonstrated. For low-temperature SOFC, a Ni-SDC (samarium-doped ceria) anode-supported cell with ceria electrolyte showed power density over 1 W/cm² at 623°C. Ni-YSZ anode-supported cell with yttria-doped zirconia (YSZ) electrolyte and a GDC interlayer showed 0.85 W/cm² and 1.6 W/cm² at 700°C and 800°C, respectively.
- For symmetric composite cathode samples, the LSCF-GDC cathode sample with GDC interlayer exhibited 0.3 Ω/cm² at 650°C, more than 50% lower resistance than a similarly fabricated LSCF-GDC sample without GDC interlayer.
- Basic kinetic data was obtained for LSCF using porous symmetric samples and the Adler-Lane-Steel (ALS) model.
- Screen printing processes have been developed for the interlayer and composite cathode for scale-up in the future.
- Initial attempts at accelerated testing have been made for symmetric cells as well as a Ni-YSZ anode-supported cell operating under elevated temperature.

Future Directions

- In order to determine long-term (40,000 hours) stability and compatibility with other SOFC components in a cost-effective way, a protocol for accelerated testing needs to be developed.
- Process scale-up for the anode-supported cell is needed.

Introduction

Reduction of SOFC operating temperature plays a key role in reducing stack cost by allowing the use of low-cost metallic interconnects and new approaches to sealing. Reported results for anode-supported SOFCs show that cathode polarization resistance is one of the primary barriers to achieving high power densities at operating temperatures $\leq 700^\circ\text{C}$. For example, one prior study of thin-electrolyte SOFCs showed that the low-current cathode interfacial resistance, R_I , was 70-85% of the total cell resistance from $550\text{-}800^\circ\text{C}$ [1]. Thus, there is considerable current interest in new cathodes, other than the standard $(\text{La,Sr})\text{MnO}_3$ (LSM)-YSZ compositions, for solid oxide fuel cells (SOFCs) that can operate at temperatures $\leq 700^\circ\text{C}$.

While the search for new cathode materials is valuable, there are known materials that show considerable promise for low-temperature applications. In particular, compositions containing $(\text{La,Sr})(\text{Co,Fe})\text{O}_3$ (LSCF) have been shown via impedance spectroscopy [2, 3, 4] to provide far superior performance compared to $(\text{La,Sr})\text{MnO}_3$ (LSM) cathodes. For example, low-current polarization resistances measured for LSCF-GDC cathodes on YSZ electrolytes are $\approx 0.3 \Omega\text{cm}^2$ at 600°C and $\approx 0.03 \Omega\text{cm}^2$ at 700°C [3]. Despite these fundamental advantages, there has been little attempt to incorporate these cathodes into anode-supported SOFCs. This is due in part to the potential difficulties with this material. First, LSCF reacts readily with zirconia (at least for Co-containing compositions) to form resistive interfacial zirconate phases, severely limiting cathode performance [5]. Second, processing temperatures are low enough that progressive sintering during longer-term cell operation may compromise long-term stability.

Approach

This work includes a fundamental study of electrochemical reactions at controlled LSCF-YSZ

interfaces. Chemical reaction between LSCF and zirconia has been studied, and methods for mitigating the reactions, such as the inclusion of an interfacial ceria layer, have been investigated. A novel cathode composite structure has been developed, and demonstrations of their high performance under low temperature were done using Ni-based anode-supported cells. As a means to test the long-term stability of porous LSCF-based structures under SOFC operating conditions, initial attempts have been made at accelerated testing of symmetric cells as well as anode-supported cells under elevated temperature.

Results

The LSCF reaction kinetics has been studied using impedance arc from electrochemical impedance spectroscopy (EIS) characterization of symmetric half-cells. The half-cells of LSCF with thickness in the range of $30 \mu\text{m}$ were screen printed on both sides of bulk single-crystal YSZ electrolyte. The ALS model was used to fit the data, taking into account that for a mixed ionic conductor such as LSCF, the reaction zone is extended beyond three-phase boundaries. In this case, with an infinitely thick layer boundary condition, chemical resistance is expressed as follows:

$$R_{\text{chem}} = (RT/2F^2)[\tau/(1-\varepsilon)aC_o^2D^*k]^{1/2} \quad [6]$$

Thick LSCF films should be appropriate for this model. Figure 1 shows a typical experimental impedance arc from LSCF/YSZ samples with fittings based on the ALS model. The fitting indicated a relatively good agreement with the ALS model, with estimated bulk diffusion coefficient and surface reactivity on the order of $D^* \sim 1 \times 10^{-8}$ and $k \sim 1 \times 10^{-5}$, respectively, which are on the same order of magnitude as those of similar materials such as LSC. However, the accuracy of the fitting was limited by high-frequency arc interfering on the left hand side of the arc. The source of high-frequency arc is unclear.

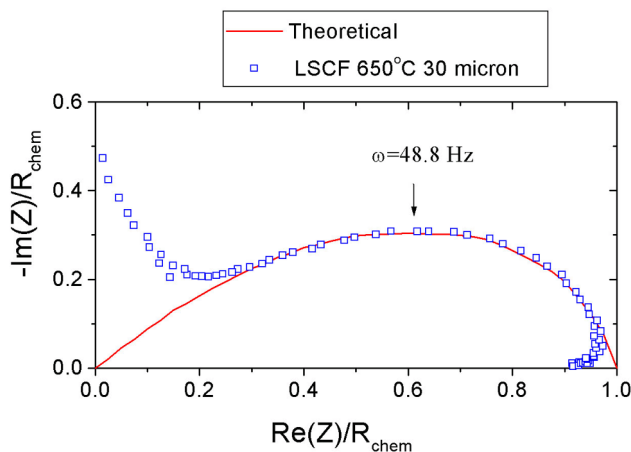


Figure 1. A Typical Experimental Arc from LSCF/YSZ Samples with Fittings Based on ALS Model

The dependence of the interfacial impedance of LSCF-GDC symmetric cathodes on sintering temperature was studied, with sintering temperatures varying from 900°C to 1100°C. The effect of sintering temperature is clear, with impedance decreasing as the sintering temperature increases, reaching minimum impedance of 0.6 Ω at 700°C and 0.17 Ω at 800°C for sintering temperature of 1025-1050°C. While this value is an order of magnitude higher than that achieved in previous work [3], it is likely that the value is limited by LSCF-YSZ reaction as well as the microstructure not being optimized for active reaction surface area. Further increases in sintering temperature increased the impedance, reaching $\sim 3.5 \Omega\text{cm}^2$ at 1100°C. This is likely due to sintering of pore structure as well as further reaction between LSCF-YSZ.

Figure 2 compares the polarization resistance of LSCF-GDC cathode with and without GDC interlayer vs. inverse temperature from the symmetric half-cell samples. The resistances correspond to 0.3 Ωcm^2 and 0.7 Ωcm^2 at 650°C with and without GDC, respectively, for the single interface case of typical cells. The slope of the graph with inverse T for both of the samples are almost identical, indicating that the GDC interlayer does not have significant effect on the rate-limiting step.

Figure 3 shows the button cell performance at various temperatures for the Ni-YSZ anode-supported cell with YSZ electrolyte / GDC interlayer

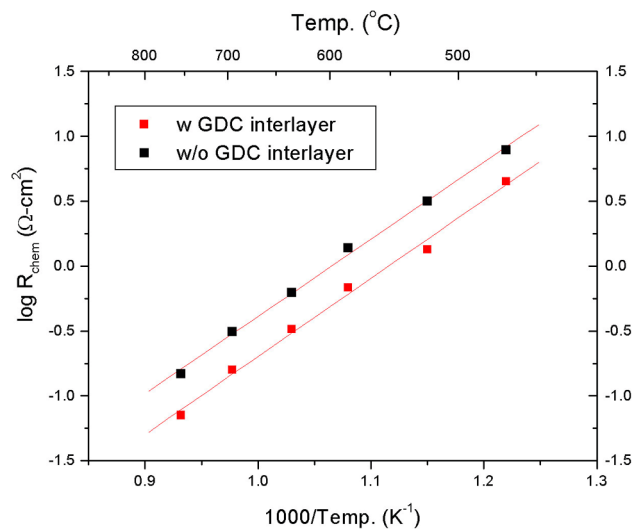


Figure 2. Polarization Resistances of LSCF-GDC Cathode with and without GDC Interlayer vs. Inverse Temperature

/ LSCF-GDC cathode. The thicknesses of YSZ electrolyte and GDC interlayers are 8 μm and 3 μm , respectively. Both the GDC layer and LSCF-GDC cathode were screen printed. As shown in Figure 3 (top), open circuit potentials (OCPs) are close to theoretical values corresponding to air on the cathode side and 3% $\text{H}_2\text{O}-\text{H}_2$ fuel on the anode side. The maximum power densities at 800°C and 700°C are about 1.6 W/cm^2 and 0.8 W/cm^2 , respectively (Figure 3, bottom). AC impedance analysis results showed that at 800°C, the ohmic resistance is about 0.13 Ωcm^2 , while the total electrode resistance including the anode and cathode is about 0.17 Ωcm^2 . At 700°C, they are 0.215 Ωcm^2 and 0.26 Ωcm^2 , respectively. In order to evaluate the performance of the cathode under lower temperature, Ni-SDC anode-supported cells were used with SDC electrolyte and LSCF-GDC cathode. An excellent power density of $\sim 1 \text{ W}/\text{cm}^2$ was obtained at 623°C, indicating substantially better performance compared to the Ni-YSZ supported cell with YSZ electrolyte shown above. This and subsequent EIS tests on the Ni-SDC cells indicated that the cathode performance is not a limiting factor on the performance of the cells under operation temperature as low as 600°C. In fact, the open circuit voltage at 623°C was only $\sim 0.9 \text{ V}$, suggesting that even better performance is probable with LSCF-GDC cathode, if it were not due to the electronic conductivity of SDC.

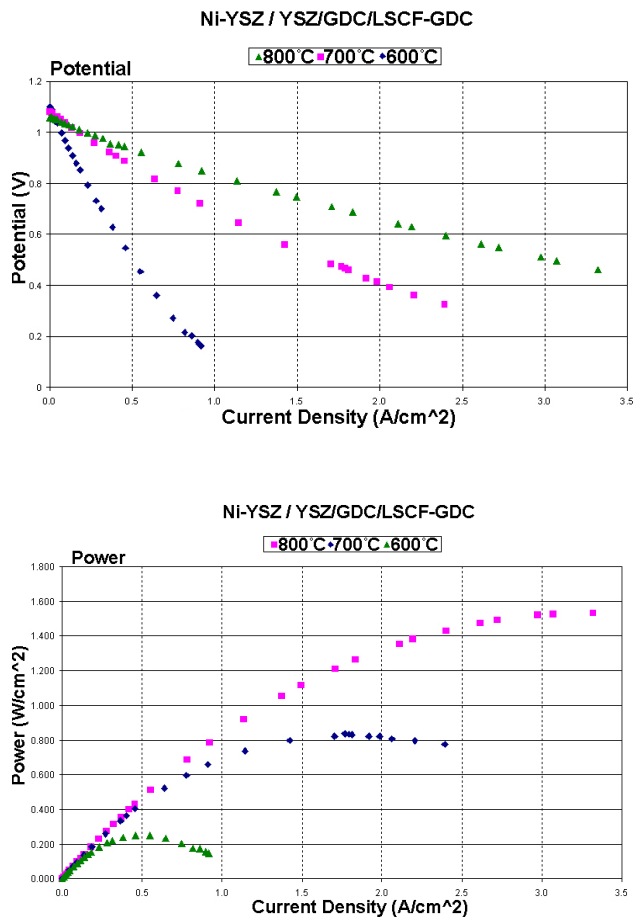


Figure 3. (top) Performance of Ni-YSZ Anode-Supported Cell with YSZ Electrolyte / GDC Interlayer / LSCF-GDC - Potential
(bottom) Power Density Plot of the Same Cell

Conclusions

The feasibility of LSCF-GDC composite cathode for low-temperature, high-performance SOFCs has been amply demonstrated. For further development, long-term stability and compatibility of the LSCF need to be verified, preferably via appropriate accelerated testing.

References

1. T. Tsai and S.A. Barnett, *Solid State Ionics* 98, 191 (1997).
2. V. Dusastre and J.A. Kilner, *Solid State Ionics*, 126 (1999) 163.
3. E.P. Murray and S.A. Barnett, *Solid State Ionics*, 148, (2002) 27.
4. E. Perry Murray, and S.A. Barnett, in: S.C. Singhal, and M. Dokiya (Eds.), *Solid Oxide Fuel Cells VI*, The Electrochemical Society Proceedings Series, Pennington, NJ, 1999, p. 369.
5. Steele, et al. *Solid St. Ionics* 135 (2000) 445.
6. SA. Adler, J.A. Lane, and B.C.H. Steel, *J. Electrochem. Soc.*, 143, 3554 (1996)

III.A.4 Materials and Process Development Leading to Economical High-Performance Thin-Film Solid Oxide Fuel Cells

Nguyen Minh (Primary Contact), Jie Guan

GE Hybrid Power Generation Systems

19310 Pacific Gateway Drive

Torrance, CA 90502-1031

Phone: (310) 538-7250; Fax: (310) 538-7250; E-mail: nguyen.minh@ps.ge.com

DOE Project Manager: Lane Wilson

Phone: (304) 285-1336; E-mail: Lane.Wilson@netl.doe.gov

Objectives

- Develop a fabrication process for anode-supported solid oxide fuel cells (SOFCs) based on lanthanum gallate electrolytes.
- Identify and evaluate high-performance cathodes for gallate-based SOFCs.
- Demonstrate a gallate-based SOFC that is capable of achieving high performance at reduced temperatures (550 to 800°C).

Approach

- Develop the tape-calendering process to fabricate lanthanum gallate electrolytes.
- Screen cathode materials using cells with self-supported lanthanum gallate electrolytes.
- Modify electrode microstructures and processing parameters to improve electrochemical performance of selected cathode materials.
- Fabricate and characterize thin gallate electrolyte/nickel anode bilayers (also referred to as anode-supported thin gallate electrolyte structures).
- Optimize fabrication process parameters to improve bilayer quality, especially density of the gallate electrolyte.
- Integrate cathodes with thin gallate electrolyte/anode bilayers into single cells and evaluate cell performance at reduced temperatures.
- Analyze cell performance losses and project performance capability.

Accomplishments

- Thin gallate electrolyte structures were fabricated using a tape-calendering process. Fabrication parameters such as raw materials characteristics, tape formulations, and sintering conditions were evaluated. Dense gallate electrolytes with thickness in the range of 10-50 microns were obtained. Use of ceria interlayers with thickness of 3~10 microns between gallate electrolytes and Ni-containing anodes was implemented in the fabrication process.
- Raw material characteristics were found to be critical in the fabrication of thin gallate layers. With high-surface-area lanthanum gallate materials, densification of the thin electrolyte was achieved at sintering temperature of 1350°C.
- Interaction between Ni in anode and lanthanum gallate electrolyte was observed during bilayer fabrication. Decreasing the sintering temperature and increasing the thickness of the ceria barrier layer reduced the migration of Ni from the anode to the gallate electrolyte.

- A high-performance cathode based on $\text{Sr}_{0.5}\text{Sm}_{0.5}\text{CoO}_3$ (SSC) was developed. Performance in the temperature range of 600~800°C was characterized. Low electrode polarization of ~0.23 ohm-cm² was achieved at 600°C.
- Performance of thin gallate electrolyte/anode bilayers integrated with high-performance cathodes was characterized. Tested cells generally showed poor performance because of low cell open circuit voltages (OCVs) and interactions between NiO of the anode and the thin gallate electrolyte during fabrication.
- Analysis of performance losses in tested single cells indicated the potential of high cell power densities (up to 1 W/cm²) at 600°C.

Future Directions

- This project was completed in December 2003. No additional work is planned.

Introduction

The program goal is to advance materials and processes that can be used to produce economical, high-performance solid oxide fuel cells (SOFCs). The overall objective is to demonstrate an SOFC that is capable of achieving extraordinarily high power densities at reduced temperatures. An integrated approach to develop a high-performance, reduced-temperature SOFC is based on the development of materials and structures that result in superior electrolyte and electrode properties. These properties, when combined, are capable of increased performance in the 550 to 800°C temperature range while maintaining function integrity up to 1000°C for short periods.

Approach

The approach is to focus on developing high-performance electrolyte and cathode structures and integrating these structures as thin layers in an anode-supported cell for reduced-temperature (550 to 800°C) operation. The high-performance electrolyte in this project is based on high-conductivity lanthanum gallate [1]. The fabrication of anode-supported thin gallate electrolyte cells is based on the tape-calendering process.

The anode-supported thin electrolyte structure consists of a thin electrolyte (10-50 micron) made of $\text{La}_{0.8}\text{Sr}_{0.2}\text{Ga}_{0.8}\text{Mg}_{0.15}\text{Fe}_{0.05}\text{O}_3$ (LSGMF) or $\text{La}_{0.8}\text{Sr}_{0.2}\text{Ga}_{0.8}\text{Mg}_{0.2}\text{O}_3$ (LSGM). Under the gallate electrolyte is a thin interlayer of ceria that is incorporated to prevent the possible reaction between electrolyte and NiO in the anode. The electrolyte and interlayer are supported by an anode structure

consisting of a thin active anode and a thick support anode, both made of Ni-ceria cermet. To improve the quality of the bilayer, efforts are focused on starting material modification and layer structure engineering as well as sintering temperature optimization. Approaches for developing high-performance cathodes include assessing new electrode materials, engineering microstructures, and modifying processing parameters.

Results

Project results are summarized in this section. During the initial development work, fabrication feasibility was explored with available lanthanum gallate powders. It was found that the anode-supported thin gallate electrolyte structure could be fabricated using the tape-calendering process by modifying tape formulations. However, electrolyte densification could only be achieved at higher temperatures (>1450°C). Analysis of the cell microstructure revealed that the electrolyte layer made of coarse gallate materials (surface area ~0.6 m²/g) contained large grain size and undesired porosity. A considerable amount of Ni was also found in the electrolyte even though a ceria interlayer was used between the electrolyte and the Ni-ceria anode. Similar results on Ni migration were also reported in the literature [2].

To address these issues, several variables such as raw material characteristics, thickness of gallate electrolyte and ceria interlayer, and sintering temperatures were investigated to improve electrolyte densification and reduce Ni migration. For instance, to reduce Ni migration during the fabrication process, ceria barrier thickness was

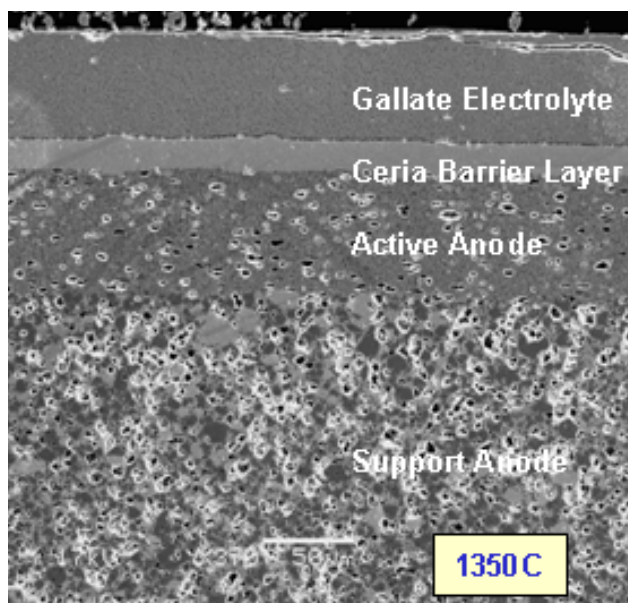


Figure 1. Anode-Supported Thin Gallate Electrolyte Structure Fabricated with Tape-Calendering Process

increased to about 8~10 microns and sintering temperature was reduced to 1350°C. The LSGMF electrolyte thickness was also increased to about 50 microns to minimize the possible defects such as pinholes and micro-cracks. As shown in Figure 1, the fabricated bilayer shows dense and continuous structure of ceria barrier layers and gallate electrolytes. Examination of the electrolyte surface and cross-section did not detect significant defects such as pinholes and micro-cracks.

However, in a close examination of polished cross-sections of the fabricated bilayer, Ni-containing phase was reduced but still noticeable (Figure 2), especially at the gallate/ceria interface, even though the ceria interlayer (~10 micron) appeared to be dense and continuous. It is interesting to note that Ni-containing phase was not observed inside the ceria layer except at the interface between gallate electrolyte and the ceria interlayer.

The cathode compositions were selected based on catalytic activity, conductivity, stability, and compatibility with electrolyte at both processing and operating temperatures. Based on the performance screening tests with samarium strontium cobaltite ($\text{Sm}_x\text{Sr}_{1-x}\text{CoO}_3$) and lanthanum strontium ferrite

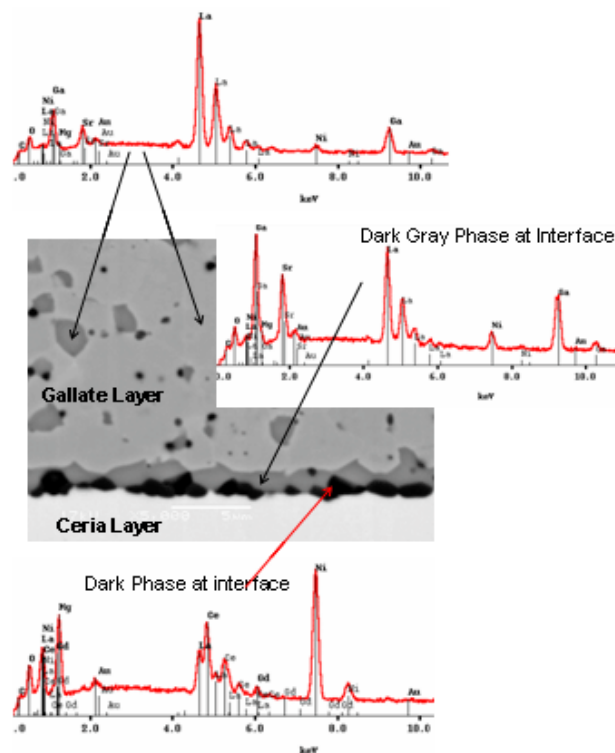


Figure 2. Composition Analysis Showing Ni Migration and Interaction with Gallate Electrolyte

(La-Sr-Co/Fe- O_3) materials, the cathode development and evaluation efforts were focused on $\text{Sr}_{0.5}\text{Sm}_{0.5}\text{CoO}_3$ (SSC).

To improve the SSC cathode performance, SSC powder characteristics and processing parameters such as temperature, thickness, and ink solid loading (for screen printing of cathodes on bilayers) were optimized. Cathodic polarizations were reduced to $\sim 0.23 \text{ ohm}\cdot\text{cm}^2$ at 600°C with a processing temperature of 1000°C.

In most of the tested cells, the OCVs under N_2/air were about 80-120 mV, indicating good gas tightness of the electrolyte. However, under H_2/air , the OCVs were less than 850 mV compared to the theoretical value of $\sim 1100 \text{ mV}$. The exact causes of the low cell OCVs remain unclear. One hypothesis is that the electrolyte (due to interaction among ceria, NiO and LSGMF) might become mixed conductive under reducing atmospheres. Another hypothesis is that the test cell might crack upon reduction due to its low mechanical strength.

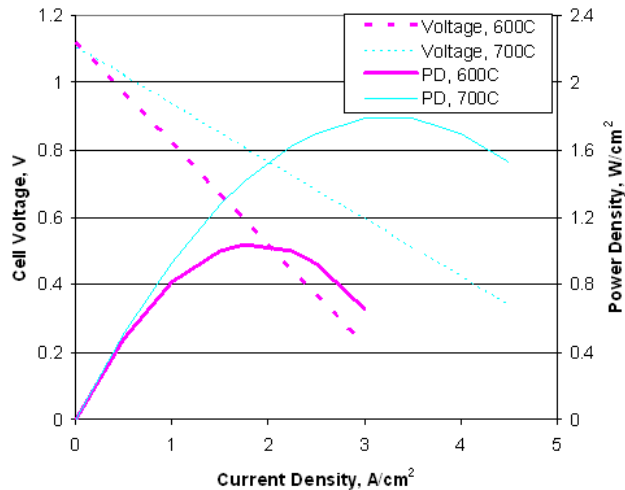


Figure 3. Projected Performance of Anode-Supported 10-micron LSGMF Cells with the Following Conditions: SSC cathode ASR: 0.23 ohm-cm² at 600°C, 0.1 ohm-cm² at 700°C; Conductivity of LSGMF Electrolyte: 0.024 S/cm at 600°C, 0.072 S/cm at 700°C; Anode ASR: 0.07 ohm-cm² at 600°C and 700°C; Air as Oxidant, Hydrogen (2% Humidification) as Fuel

Given the high performance of the SSC cathode and low resistance of highly conductive thin-LSGMF electrolytes, integration of the cathode and the anode-supported thin-LSGMF electrolyte structure is expected to give high cell performance at reduced temperatures if the issues of materials interaction and low mechanical strength can be resolved. Shown in Figure 3 is the projected performance at 600°C and 700°C of a cell with the SSC cathode, 10-micron LSGMF electrolyte, and an anode with polarization equivalent to that of YSZ/Ni anodes for yttria-stabilized zirconia (YSZ) electrolytes. As can be seen, a power density of 1 W/cm² should be feasible if the issues relating to thin gallate structure fabrication can be resolved.

Conclusions

Characteristics of lanthanum gallate materials suitable for thin electrolyte structure fabrication were defined in this project. Bilayers with thin and dense lanthanum gallate electrolyte supported on a nickel/ceria anode were successfully fabricated by tape calendaring. In the fabrication process, interaction between NiO and lanthanum gallate electrolyte was observed. The interaction was reduced with a ceria interlayer between the electrolyte and the anode. Performance of cathodes based on Sr_{0.5}Sm_{0.5}CoO₃ (SSC) was evaluated and improved with material characteristics modification and processing parameters engineering. The improved cathode exhibited excellent performance with cathode polarization of ~0.23 ohm-cm² at 600°C. The high-performance SSC cathode and thin gallate electrolyte structures were integrated into single cells, and cell performance was characterized. Tested cells generally showed poor performance because of low cell OCVs. Analysis of cell performance indicated the possibility of achieving high power densities (e.g., 1 W/cm² at 600°C) if the issues relating to thin gallate electrolyte fabrication can be resolved.

References

1. T. Ishihara et al., "Nickel-Gd-Doped CeO₂ Cermet Anode for Intermediate Temperature Operating Solid Oxide Fuel Cells Using LaGaO₃-Based Perovskite Electrolyte", *Solid State Ionics*, Vol. 132, p. 209, 2000.
2. S. Elangovan et al, "Lanthanum Gallate Electrolyte for Intermediate Temperature Operation", *Electrochemical Society Proceeding*, Vol. 2003-07, p. 299, 2003.

III.A.5 Functionally Graded Cathodes for Solid Oxide Fuel Cells

Meilin Liu (Primary Contact), Harry Abernathy, Erik Koep, Yin Liu, and Jian Dong

Georgia Tech Research Corporation

Atlanta, GA 30332-0245

Phone: (404) 894-6114; Fax: (404) 894-9140; E-mail: meilin.liu@mse.gatech.edu

DOE Project Manager: Lane Wilson

Phone: (304) 285-1336; Fax: (304) 285-4403; E-mail: Lane.Wilson@netl.doe.gov

Objectives

- Elucidate the oxygen reduction mechanism that occurs at the cathode of a solid oxide fuel cell (SOFC) using electrochemical performance measurements and *in-situ* spectroscopic techniques.
- Identify the rate-limiting step of the oxygen reduction mechanism under desired operating conditions.
- Develop a model to predict cathode performance considering cathode material, microstructure, and operating conditions.
- Use results from experiments and model calculations for more rational design of cathode microstructure and material.
- Optimize the performance of a mixed ionic/electronic conductor (MIEC) cathode.

Approach

- Prepare fuel cell samples with well-defined cathode surfaces using standard micro-fabrication techniques to quantify and vary the relative amounts of different reaction areas.
- Examine, *in-situ*, the presence of adsorbed oxygen species and the change in the surface structure of candidate fuel cell cathode materials under various operating conditions using Fourier transform infrared emission spectroscopy (FTIRES) and Raman microspectroscopy.
- Fabricate cathodes graded in both composition and microstructure using a combustion chemical vapor deposition (CCVD) process.
- Test the performance of all generated samples using electrochemical impedance spectroscopy (EIS).
- Develop mathematical models to simulate various possible oxygen reduction reaction schemes.
- Use computer modeling to calculate the potential and current distributions throughout the SOFC electrolyte and cathode under different operating conditions and geometrical configurations.

Accomplishments

- Patterned platinum electrodes were fabricated with feature sizes varying from 2-100 μm on yttria-stabilized zirconia (YSZ) substrates. The patterned electrodes were tested using EIS.
- Patterned lanthanum strontium manganese oxide (LSM) electrodes were fabricated with a 2 μm feature size on YSZ substrates. The patterned electrodes were tested using EIS.
- Infrared emission spectra were recorded using FTIRES for $\text{Sm}_{0.5}\text{Sr}_{0.5}\text{CoO}_3$ (SSC), $\text{La}_{1-x}\text{Sr}_x\text{FeO}_3$ (LSF), $\text{La}_{1-x}\text{Sr}_x\text{CoO}_3$ (LSC), and $\text{La}_{1-x}\text{Sr}_x\text{MnO}_3$ (LSM) cathode materials as a function of temperature, oxygen partial pressure, and applied potential. Peaks attributed to adsorbed superoxide (O_2^-) and peroxide (O_2^{2-}) ions were observed in the spectra, indicating that during oxygen reduction on these cathodes, the oxygen molecule reduces before dissociating into oxygen atoms.

- An atomic force microscope (AFM) tip was used to enhance the Raman scattering signal of our Raman micro-spectrometer. This tip-enhanced Raman scattering (TERS) effect has increased the sensitivity of the Raman system to analyze the surface of our candidate cathode materials.
- Successfully created electrodes with compositional and structural gradients by changing precursor composition and needle size in our CCVD system. The cathode consisted of three porous layer structures, with about 5 μm thick 60 wt.% LSM–40 wt.% gadolinia-doped ceria (GDC) fine agglomerates (0.5 μm diameter) at the bottom (close to YSZ electrolyte), followed by 5 μm thick 30 wt.% LSM–30 wt.% LSC–40 wt.% GDC fine agglomerates (0.5 μm diameter), and topped with 15 μm thick 60 wt.% LSC–40 wt.% GDC coarse agglomerates (2–3 μm diameter) on the air side.
- The current and potential distributions through the SOFC electrolyte have been analyzed under different geometrical configurations.
- Several oxygen reduction reaction mechanisms have been proposed and are currently in the evaluation phase.

Future Directions

- Generate and test different micro-patterned electrode configurations to quantify the relative reactivity of different possible reaction sites.
- Further analyze the FTIRES spectra to obtain reaction kinetics parameters to be used in our mathematical models.
- Use Raman and infrared spectroscopy to identify the specific catalytic site where the oxygen molecule is reduced and dissociates.
- Introduce microstructural and compositional variations into the computer modeling.
- Quantitatively analyze porosity of each layer of the functionally graded cathodes produced by CCVD and correlate microstructure with processing conditions.

Introduction

As the operating temperature of a solid oxide fuel cell (SOFC) is lowered to reduce the system costs, the cathode/electrolyte interface begins to limit the cell performance. Various processes are associated with this interface: the transport of oxygen gas through the porous cathode, the adsorption of oxygen onto the cathode surface, the reduction and dissociation of the oxygen molecule (O_2) into the oxygen ion (O^{2-}), and the incorporation of the oxygen ion into the electrolyte for it to be transported across to the anode. A strictly electronic conductor cathode permits the reduction of oxygen to occur only at the triple phase boundary (TPB) between the oxygen gas, the cathode, and the electrolyte. By using a mixed ionic/electronic conductor (MIEC) as a cathode material, the electrochemically active area extends from just the TPB to the entire cathode surface.

This project comprises four research areas:
(1) the fabrication and testing of micro-patterned

cathodes to compare the relative activity of the TPB to the rest of the cathode surface, (2) the use of Fourier transform infrared emission spectroscopy (FTIRES) and Raman spectroscopy to analyze the oxygen reduction mechanism on the cathode surface, (3) the use of mathematical modeling to predict cathode performance based on different geometries and microstructures, and (4) the fabrication of cathodes that are graded in composition and microstructure to generate large amounts of active surface area near the cathode/electrolyte interface while creating a network of larger pores further from the interface to accommodate gas flow.

Approach

Micro-patterned electrodes were fabricated on YSZ substrates using standard photolithographic processes. Each test sample features an array of identical electrodes covering a surface area of 36 mm^2 . The procedure was first demonstrated using platinum electrodes, after which LSM electrodes were fabricated. The LSM patterned electrodes were

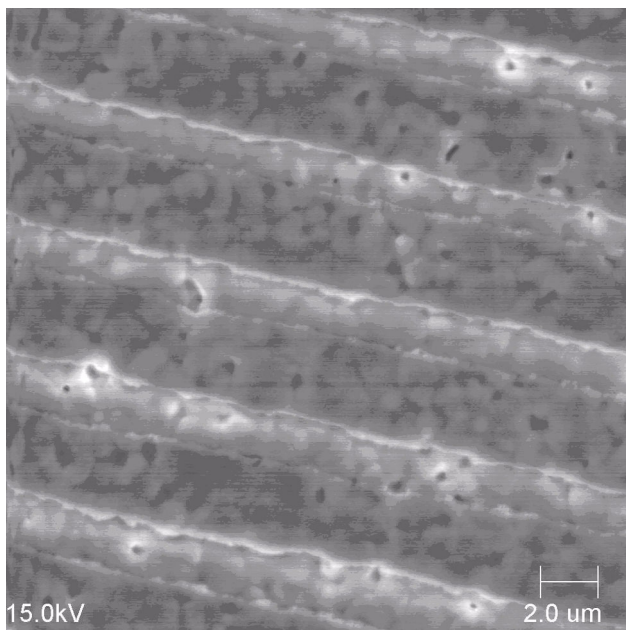


Figure 1. LSM lines on the YSZ electrolyte showing good TPB resolution. LSM electrode width is 2 μm with an electrode thickness of 0.25 μm .

characterized using electrochemical impedance spectroscopy (EIS). Characteristic impedance loops were generated from which the cathode/electrolyte interfacial resistance was calculated as a function of temperature and TPB length.

For the spectroscopic studies, porous films of candidate cathode materials (LSM, LSF, LSC, SSC) were painted on YSZ substrates and placed in a chamber designed for *in-situ* FTIRES experiments. Emission spectra from the cathode surface were recorded as a function of applied potential, partial pressure, and temperature. For kinetics information, emission spectra were taken continuously as the atmosphere inside the chamber was switched from argon to a desired oxygen partial pressure and then back again to argon. Further, Raman microspectroscopy was used to confirm the peak assignments made from the FTIR emission spectra and to analyze the surface structure of the cathode.

The current and potential distributions through the cathode and electrolyte were calculated using finite element analysis in Femlab software. The initial model was composed of a dense electrolyte covered by an air channel and dense electrode, a representative model for cells with patterned

electrodes. The steady-state distributions were calculated initially with the TPB being the only active region for electrochemical reactions (the case when a pure electronic conductor such as Pt is used as the electrode). The activity of regions other than the TPB (e.g., when a mixed conductor is used as an electrode) and porosity in the cathode will be added after optimization of the present geometry.

Combustion chemical vapor deposition (CCVD) was used to fabricate SOFC cathode films of variable composition and microstructure. In this process, a fuel containing a precursor to the desired oxide composition is sprayed through a flame at the end of a needle and deposited onto a substrate. Two approaches were attempted to control the composition and porosity of the deposited layer: (1) varying the needle-tubing size and the concentration of a precursor/fuel solution, and (2) using a solid oxide powder/fuel suspension rather than a solution. The deposited oxide films were mixtures of LSM (an electronic conductor), GDC (an ionic conductor), and LSC (a mixed ionic/electronic conductor). Three layers of varying composition and porosity were deposited on each YSZ substrate. The performance of each functionally graded cathode was characterized using EIS.

Results

We have succeeded in depositing both platinum and LSM patterned electrodes on YSZ substrates of varying feature size. By reducing the feature size, the amount of TPB can be increased rapidly while maintaining the same amount of surface area. Figure 1 shows a scanning electron micrograph of patterned electrode lines 2 μm in width. This resolution is critical to accurately quantify the dependence of cathode performance on TPB length. The cathode/electrolyte interfacial resistance was calculated from the characteristic impedance loops shown in Figure 2(a). Figure 2(b) shows the interfacial conductance (the inverse of the resistance) plotted as a function of the TPB length. This figure demonstrates the expected trend that as the relative amount of electrochemically active area (the TPB) increases with respect to total surface area, the conductivity of the electrode also increases. An expected plateau of LSM impedance at large TPB lengths was not accurately resolved, indicating that for a

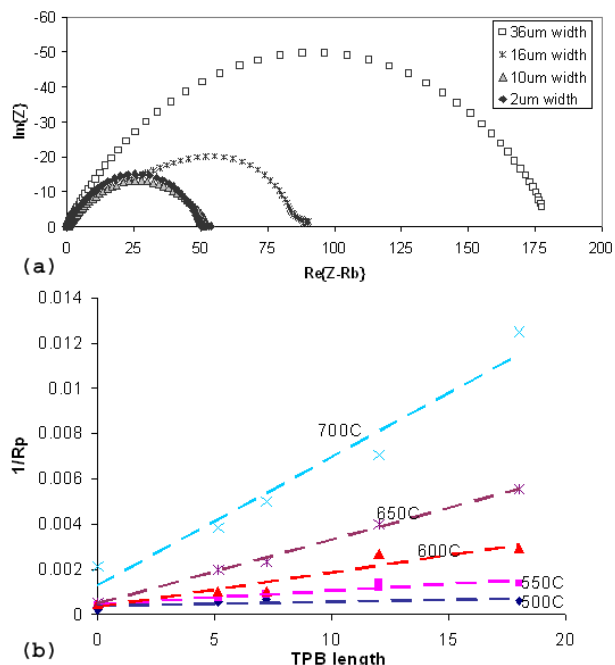


Figure 2. (a) Typical impedance loops of patterned LSM electrodes at 700°C. (b) Plot of interfacial conductance versus TPB length.

predominately electronic conductor such as LSM, the active region of the TPB extends less than 1 μm from the TPB itself. One micron is half of the current minimum possible feature size. Process parameters are being developed to fabricate LSM electrodes with sharply reduced feature sizes through the use of electron-beam lithography.

Figure 3 shows a typical series of emission spectra of an SSC cathode as the atmosphere switches from argon to 1% oxygen. As the sample is exposed to an oxygen-containing environment, the baseline shifts from horizontal to curved, and a series of peaks emerge from the baseline. For purposes of clarity, the spectra obtained as the atmosphere was switched from 1% oxygen back to argon have been omitted; however, the baseline does indeed reverse from curved back to horizontal, and the peaks in the 800 to 1250 cm^{-1} region slowly disappear. The baseline shift has been attributed to changes in the properties of the bulk electrode material and will be analyzed at a later time. The spectral features from 1400 to 1800 cm^{-1} and from 2300 to 2500 cm^{-1} are common to water vapor and carbon dioxide and thus result from random fluctuations in the carbon dioxide

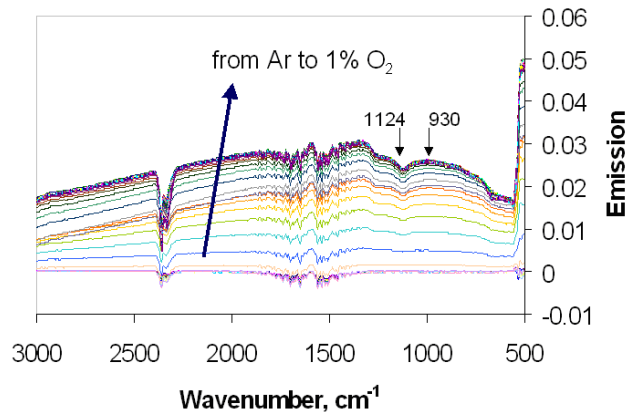


Figure 3. FTIR emission spectra for SSC pellet at 700°C as sample atmosphere changes from argon to 1% oxygen. All spectra are compared to a background spectrum measured in argon.

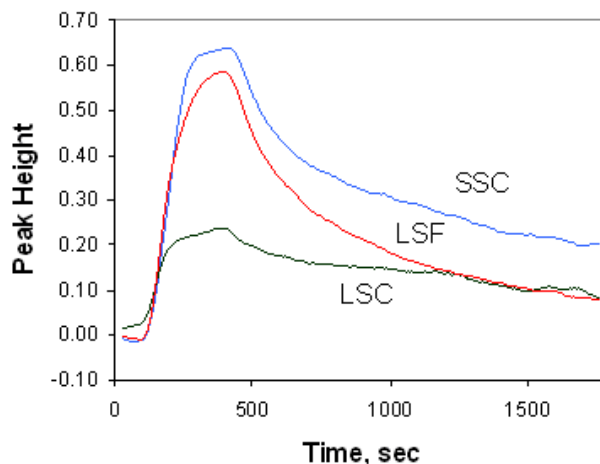


Figure 4. Plot of the height of 1124 cm^{-1} peak during gas switching experiment from argon to 1% O_2 and back to argon for different cathode materials at 600°C.

and water vapor concentrations between the emission sample chamber and the FTIR detector. The only peaks that related directly to the change in atmosphere were those located between 800 and 1250 cm^{-1} . The peaks at approximately 1236 and 1124 cm^{-1} were assigned to adsorbed superoxide (O_2^{1-}) species, while the features around 930 cm^{-1} were attributed to adsorbed peroxide (O_2^{2-}) species. The presence of the reduced oxygen molecular species on the surface demonstrates that for oxygen reduction on this cathode material, the adsorbed O_2 molecule is reduced before it dissociates. Further,

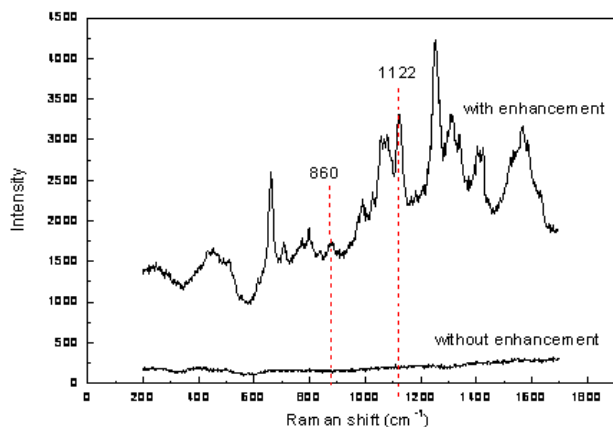


Figure 5. Raman spectra of thin film LSM with and without the tip enhancement.

since the reduced oxygen species are observable on the surface, the rate-limiting step for this mechanism is not the initial reduction of O_2 . Further studies are necessary to discern which step after the initial reduction is the exact rate-limiting step.

To quantify the concentration of adsorbed oxygen species on the surface, the height of the 1124 cm^{-1} superoxide peak was calculated by subtracting away the curved baseline. Figure 4 shows the change in the 1124 cm^{-1} peak intensity as the atmosphere was switched from pure argon to 1% O_2 for five minutes and then back to argon for SSC, LSF, and LSC at 600°C . SSC had the greatest intensity, indicating the largest concentration of surface species and thus the greatest amount of oxygen reduction activity of the three materials. This result is consistent with electrochemical performance data of the three materials under similar operating conditions. This time-dependent data is being further analyzed to obtain kinetic parameters of the oxygen reduction mechanism, which can be used for our mathematical modeling of the system.

Shown in Figure 5 are the Raman spectra of a thin LSM film with and without the presence of an atomic force microscope (AFM) tip near the film surface. It can be seen that the presence of the AFM tip dramatically enhanced the intensity of the Raman scattering signal; many new peaks appeared in the spectrum. The two peaks at 860 and 1122 cm^{-1} are considered to be surface-adsorbed peroxide and superoxide species. Further investigations into these

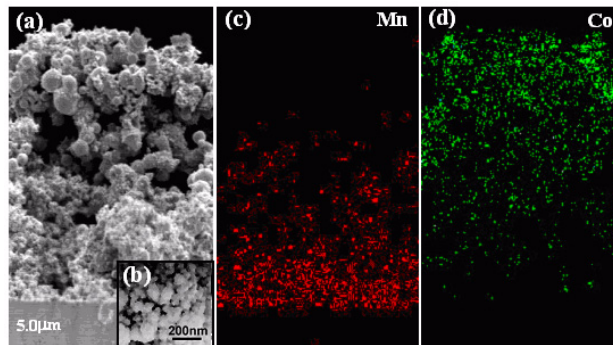


Figure 6. (a) Cross-sectional fracture surface of the functionally graded cathode fabricated on an YSZ pellet using a combustion CVD process, (b) Higher magnification image of the cathode showing the nanostructure, (c) EDS dot mapping showing manganese distribution on the cross-section surface, and (d) EDS dot mapping of cobalt distribution.

tip-enhanced Raman scattering (TERS) spectra should yield valuable information about the exact structure of the cathode surface.

Shown in Figure 6(a) is a cross-sectional view (as fractured) of a half-cell with composite cathode supported by a $240\text{ }\mu\text{m}$ thick dense YSZ electrolyte. The cathode, fabricated by CCVD, consists of three porous layer structures and is graded in both microstructure and composition, with about $5\text{ }\mu\text{m}$ thick 60 wt.% LSM–40 wt.% GDC fine agglomerates ($0.5\text{ }\mu\text{m}$ diameter) at the bottom (close to YSZ electrolyte), followed by $5\text{ }\mu\text{m}$ thick 30 wt.% LSM–30 wt.% LSC–40 wt.% GDC fine agglomerates ($0.5\text{ }\mu\text{m}$ diameter), and $15\text{ }\mu\text{m}$ thick 60 wt.% LSC–40 wt.% GDC coarse agglomerates ($2\text{--}3\text{ }\mu\text{m}$ diameter) on the top (air side). The two bottom layers are actually nanostructured, as shown in the inset Figure 6(b), offering extremely high surface area for oxygen reduction. Energy dispersive spectroscopy (EDS) dot mapping revealed the compositional changes on the cross-sectional micrograph. As shown in Figure 6(c), manganese content gradually declined from YSZ/LSM–GDC interface to LSC–GDC airside, while the cobalt signal exhibited the opposite trend as shown in Figure 6(d). The manganese-rich layers provide fast electrochemical reaction rates, high chemical stability, and a satisfying match in thermal expansion coefficient with YSZ electrolyte. Meanwhile, the

large interconnected pore channels within the coarse top layer facilitate oxygen gas mass transport through the cathode. The cobalt-rich top layer has high conductivity for efficient current collection.

Conclusions

Standard electrochemical testing of normal SOFC samples compares the overall performance of candidate cathode materials without directly revealing the reasons for the differences in performance between materials. By incorporating micro-patterned electrodes into our standard SOFC electrochemical testing and supplementing this testing with *in-situ* spectroscopic techniques, we have created a system to identify where, how, and to what extent the cathode reactions occur for different materials under different operating conditions. By deducing the rate-limiting step of the oxygen reduction mechanism, we can more specifically design more catalytically active cathode materials. Then, by quantifying the relative electrochemical reactivity of the different active regions of the cathode, we can use mathematical modeling to optimize the microstructure of the cathode. Finally, further refinement of the CCVD process will also allow us to create these optimized microstructures from the desired materials.

Publications

1. Y. Liu, S. Zha, and M. Liu, "Novel Nanostructured Electrodes Fabricated by Combustion CVD", *Advanced Materials* 16 (2004) pp.256-260.
2. Y. Liu, W. Rauch, S. Zha, and M. Liu, "Fabrication of Nanostructured Electrodes for Solid Oxide Fuel Cells Using Combustion CVD", *Solid State Ionics* 166 (2004) pp.261-268.
3. Y. Liu, C. Compson, and M. Liu, "Nanostructured and Functionally Graded Cathodes for Intermediate Temperature Solid Oxide Fuel Cells", *Journal of Power Sources*, in press.
4. Y. Liu, M. Liu, "Porous Electrodes for Low-temperature Solid Oxide Fuel Cells Fabricated by a Combustion Spray Process", *Journal of the American Ceramic Society*, in press.
5. Y. Liu, S. Zha, and M. Liu, "Fabrication of Nanostructured Electrodes for SOFCs Using a Combustion CVD Process", presented in *204th Meeting of The Electrochemical Society*, Orlando, FL, U.S.A., October 12-16, 2003.
6. Q. Wu, H. Abernathy, and M. Liu, "FTIR Studies of Oxygen Reduction Reaction on SOFC Cathode Materials", presented in *204th Meeting of The Electrochemical Society*, Orlando, FL, U.S.A., October 12-16, 2003.
7. Y. Liu, C. Compson, M. Liu, "Functionally Graded Cathodes for Intermediate Temperature Solid Oxide Fuel Cells", presented in *205th Meeting of The Electrochemical Society*, San Antonio, TX, U.S.A., May 9-14, 2004.
8. E. Koep, C. Compson, Z. Zhou and M. Liu, "A Photolithographic Process for Investigation of Electrode Reaction Sites in Solid Oxide Fuel Cells", *Solid State Ionics*, Under review May, 2004.
9. Y. Liu, S. Zha, and M. Liu, "Nano-composite Electrodes Fabricated by a Particle-Solution Spraying Process for Low-Temperature SOFCs", *Chem. Mater.*, accepted.

Patents

1. Y. Liu and M. Liu, "A Combustion Spray Process for Fabrication of Films and Coatings", US Provisional Patent Application, filed.

III.A.6 Development of Metal-Supported SOFC

Steven J. Visco (Primary Contact), Lutgard C. De Jonghe

Lawrence Berkeley National Laboratory

Materials Sciences Division B62R203

Berkeley, CA 94720

Phone: (510) 486-5821; Fax: (510) 486-4881; E-mail: sjvisco@lbl.gov

DOE Project Manager: Lane Wilson

Phone: (304) 285-1336; E-mail: Lane.Wilson@netl.doe.gov

Objectives

- Reduce the cost and increase the reliability of solid oxide fuel cell (SOFC) components through the introduction of inexpensive metal supports.
- Improve SOFC electrode performance through metal salt infiltration.
- Develop anti-corrosion coatings for stainless steel components to inhibit scale growth and Cr volatilization and to maintain high electronic conductivity.

Approach

- Develop low-cost coating technology for stainless steel components.
- Infiltrate cobalt nitrate into reproducible lanthanum strontium manganite (LSM) and LSM/YSZ air electrode structures.
- Conduct long-term testing of metal-infiltrated cells to determine aging effects.
- Determine and optimize sintering profiles for LSM-YSZ cathodes to match with sintering of yttria-stabilized zirconia (YSZ) thin-film electrolyte.
- Determine baseline power curves for alternative anodes on cathode-supported cells.

Accomplishments

- Doubled the performance of anode- and cathode-supported SOFCs at reduced operating temperature (650°C).
- Developed anti-corrosion coating based on reaction of Mn-Co spinel with stainless steel; this coating reduced corrosion rate by a factor of 10 and survived 120 rapid thermal cycles with no evidence of spallation.
- Developed a unique method to infiltrate anode and cathode catalysts into porous structures in a **single processing step**, producing sufficient catalyst loading for high-performance electrodes. A wide range of perovskite compositions can be produced from this proprietary technology. A fine-grained structure that is highly catalytic is produced, leading to excellent performance.
- Long-term testing (100 hours) of metal-nitrate-infiltrated cells has indicated stable performance for this period of time. Longer-term (1000 hours) tests will be performed in the next quarter.
- Successfully determined and modified sintering profiles for LSM-YSZ substrates to match YSZ thin-film electrolyte, and consequently produced high-quality cathode-supported cells.
- Used cathode-supported cells to evaluate alternative anodes (sulfur tolerant). Initial testing at Lawrence Berkeley National Laboratory (LBNL) indicates that further development of alternative anodes is needed.

Future Directions

- Determine the window of stability for electrode enhancement by nano-infiltration: examine the effects of temperature, degree of infiltration, and chemical composition on long-term stability of performance boost, and recommend an operational range for the improved electrodes.
- Set up equipment for the accurate determination of volatile Cr species produced when moist air reacts with stainless steel. This is a critical parameter for the commercialization of low-cost fuel cell stacks having stainless steel components.
- Determine the effect of anti-corrosion coatings on Cr volatilization from stainless steel.
- Determine the window of stability for the use of steel components in high-temperature solid oxide fuel cells from 600 to 900°C for both stationary power applications (50,000 - 100,000 hours) and transportation applications (5,000 - 10,000 hours).

Introduction

The main goal of the LBNL project is to support industrial Solid State Energy Conversion Alliance (SECA) teams in their effort to commercialize solid oxide fuel cell technology that meets the SECA performance and cost targets. In order to achieve the aggressive SECA goals, it is necessary to reduce the cost of solid oxide fuel cell components through the introduction of inexpensive materials while maintaining the high levels of performance possible with thin-film electrolytes. Developers are also compelled to lower the operating temperature of SOFC systems while maintaining high system efficiency. Accordingly, in FY 2004 the LBNL core effort is focused on the use of catalyst infiltration to improve electrode performance at low temperature, the development of cathode-supported architectures for sulfur-tolerant anodes, and electrochemical characterization of the improved electrodes during transient and extended operation

Approach

Among the complexities of SOFC development is the high degree of interactivity between SOFC materials at the processing temperature and/or during cell operation. This interaction can negate improvements made to isolated components and lead to fuel cell or stack failure. Accordingly, the LBNL team uses a highly integrated approach for the development of low-cost SOFC components, testing improvements on realistic cell structures with close attention to the manufacturability of technical innovations. The LBNL team also talks routinely with component manufacturers to assess

the commercial viability of its SOFC improvements. The LBNL group uses standard electro-analytical techniques for the characterization of fuel cell components such as AC impedance spectroscopy, potentiostatic and galvanostatic evaluation, as well as current-interrupt and related electrochemical techniques. Our group has also fabricated a sensitive transpiration apparatus to determine the Cr volatilization rates for coated and uncoated stainless steel samples. In this way, we can determine the effectiveness of coatings developed at LBNL in terms of the electronic conductivity of the coating, compatibility with anode and cathode composition, oxidation resistance, and minimization of Cr evaporation in the fuel cell environment. It is anticipated that technical innovations developed at LBNL and careful characterization of structures fabricated with such improvements will lead to successful technology transfer to the industrial teams.

Results

In order to ensure long life for SOFC stacks, a number of developers are considering reducing the fuel cell operating temperature from 800-900°C to 600-800°C. Since ionic transport and electrode kinetics are thermally activated, the power density of fuel cell stacks decreases with temperature. Accordingly, the LBNL team has been developing nano-catalysts that can be infiltrated into the fuel cell electrodes to boost the low-temperature performance and thereby offset the negative effect of lower operating temperature on power density. As can be seen in Figure 1, the peak power density of an anode-supported thin-film SOFC cell was *increased by a*

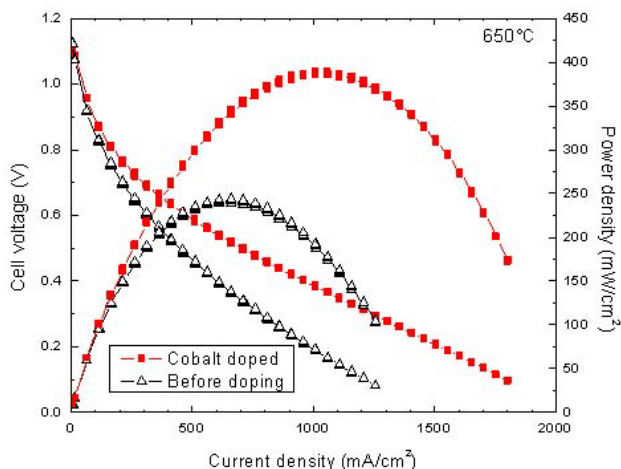


Figure 1. 650°C Performance of Anode-Supported Thin-Film Cell with LSM-YSZ Cathodes

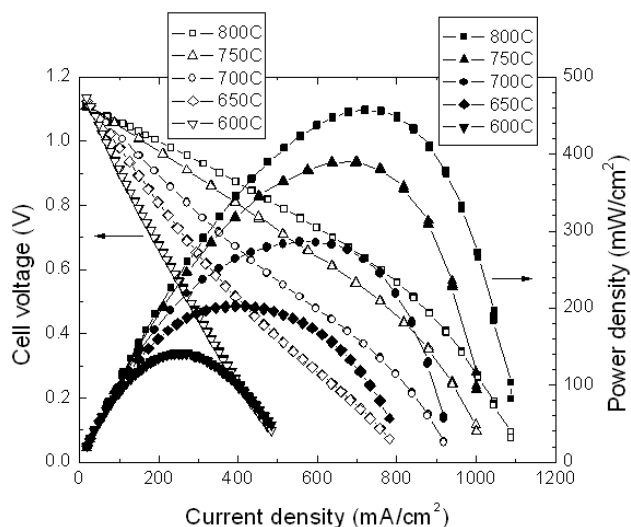
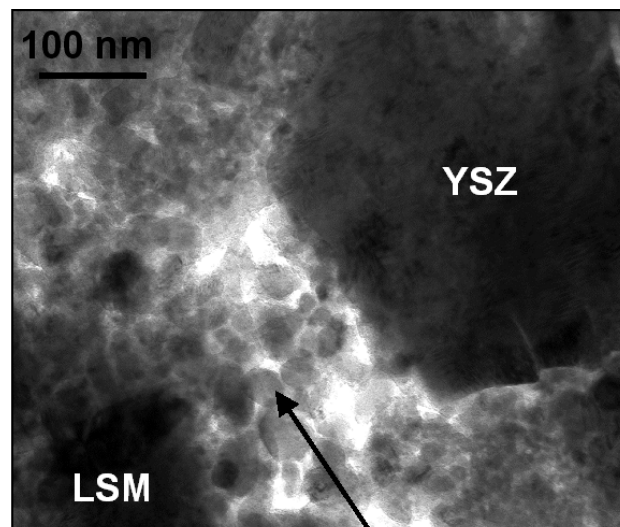


Figure 2. 600-800°C Performance of Cathode-Supported SOFC with Catalyst Infiltration

factor of 2 at 650°C. We have seen similar performance improvements for both anode- and cathode-supported thin-film SOFCs (Figures 1 & 2). A key issue for this approach is that the improvement in power density at reduced temperatures is stable over the operating lifetime of the SOFC stack. The LBNL group is currently investigating the time-dependence of the performance of electrodes having nano-catalyst infiltration. LBNL has also done transmission electron microscope (TEM) investigations of electrode structure as a function of catalyst infiltration; as can be seen from Figure 3, the



Co-(La,Mn,O) Particles, 10-60 nm

Figure 3. TEM Image of Infiltrated Nano-Catalysts after 100 Hours at 800°C

presence of 10-60 nm catalyst centers is observed in the modified structure. Such modified electrodes have been tested for periods of 100 hours continuous operation with no indication of performance deterioration. However, longer tests of 1000 hours or more are needed to project the long-term stability of the modified low-temperature electrodes.

The LBNL team has also developed process technology for the fabrication of cathode-supported SOFCs. This work was initiated to support the development of alternative anodes for sulfur-tolerant SOFCs. To date, the majority of work in sulfur-tolerant anodes has been focused on SrTiO₃-based electrodes. However, the titanate electrodes tend to react with the YSZ electrolyte when co-fired in an anode-supported geometry. Consequently, the LBNL group launched the development of cathode-supported cells so that alternative anodes can be bonded to the cathode-supported structure at reduced temperatures. As can be seen from Figure 2, the performance of the cathode-supported SOFC is quite reasonable at temperatures as low as 650°C. Initial testing of alternative anodes on the cathode-supported cells indicates that further improvements are needed.

Another critical issue for the development of SOFC stacks utilizing metal components is the

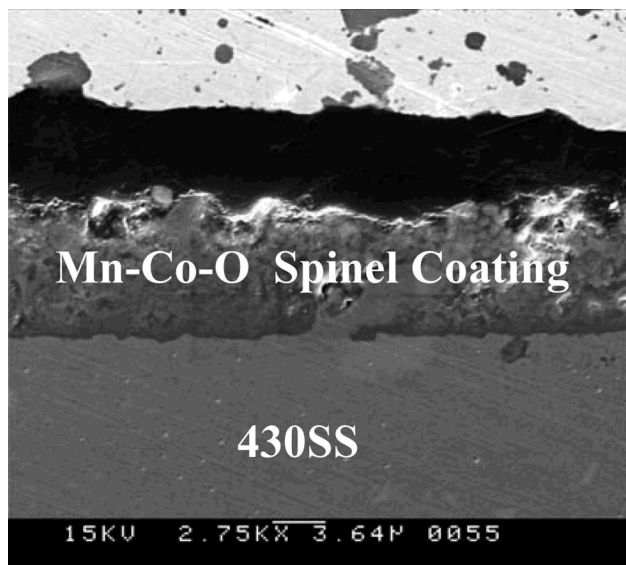


Figure 4. Protective Coating on Stainless Steel after 120 Rapid Thermal Cycles between Room Temperature and 800°C

development of low-cost coatings to reduce the oxidation of the metal as well as block the vaporization of volatile $\text{Cr}(\text{OH})_2\text{O}_2$ produced from the reaction of moist air with the Cr_2O_3 scale. The LBNL group developed a technique whereby a colloidal MnCo_2O_4 powder is spray-coated onto 430 stainless steel and bonded at 850°C. At 850°C, this coating exhibits a **factor of 10 improvement in oxidation rate and resistivity** compared with the uncoated 430 stainless steel. Another critical aspect of any coating is its ability to withstand thermal cycling. Coated and un-coated 430 stainless steel samples were subjected to 120 rapid thermal cycles; the uncoated samples showed significant spallation of the chromia scale, while the coated samples showed no evidence of thermal cycling damage (see Figure 4).

Future work will include refinement of the metal infiltration process and long-term testing of the stability of the performance improvement. We have completed the assembly of the transpiration measurement apparatus and will initiate studies on the volatilization of Cr from coated and un-coated stainless steel samples. As we continue to improve electrode performance at reduced temperatures and the behavior of steel components in aggressive environments, we will then initiate testing of small

SOFC stacks incorporating such improvements to assess the viability of the technology for transfer to the industrial teams.

Conclusions

- Infiltration of catalytic metal nitrates into porous fuel cell electrodes improves the peak power performance by as much as a factor of 2 at reduced temperatures.
- Anti-corrosion coating based on reaction of Mn-Co spinel with stainless steel reduces the corrosion rate by a factor of 10, exhibits much higher electronic conductivity than the native scale, and survives hundreds of rapid thermal cycles with no evidence of spallation.
- Long-term testing (100 hours) of metal nitrate-infiltrated cells indicates stable performance. Longer-term (1000 hours) tests will be performed in the next quarter.
- The performance of cathode-supported thin-film cells is quite reasonable, but somewhat lower than anode-supported structures
- Initial testing at LBNL indicates that further development of alternative anodes is needed.

FY 2004 Publications/Presentations

1. *Protective Coating on Stainless Steel Interconnect for SOFCs: Oxidation Kinetics and Electrical Properties*, Xuan Chen, Peggy Y. Hou, Craig P. Jacobson, Steven J. Visco, and Lutgard C. De Jonghe, submitted to Solid State Ionics.
2. *Catalyst-Infiltrated Supporting Cathode for Thin-film SOFCs*, Keiji Yamahara, Craig P. Jacobson, Steven J. Visco, and Lutgard C. De Jonghe, submitted to Solid State Ionics.
3. *Ionic Conductivity of Stabilized Zirconia Networks in Composite SOFC Electrodes*, Keiji Yamahara, Tal Z. Sholklapper, Craig P. Jacobson, Steven J. Visco, and Lutgard C. De Jonghe, submitted to Solid State Ionics.
4. *Development of Low-Cost Metal Supported SOFCs*, Steven J. Visco, Craig P. Jacobson, Lutgard C. De Jonghe, 2003 Fuel Cell Seminar, November 3-7, 2003, Miami Beach, Florida.

5. *Co-Fired Cathode Supported Thin Film IT-SOFC*, Ionel C. Stefan, Keiji Yamahara, Mariza Marrero-Cruz, Craig P. Jacobson, Steven J. Visco, and Lutgard C. De Jonghe, Electrochemical Society 2003 Meeting, Orlando, Florida.
6. *The Effect of Lithium Doping on Ceria-Based Electrolyte Materials*, Craig P. Jacobson, Mariza Marrero-Cruz, Eric P. Hong, Steven J. Visco, and Lutgard C. De Jonghe, 8th International Symposium on Ceramics in Energy Storage and Power Conversion Systems, January 28, 2004.
7. *Modification of Electrode Architectures for Reduced Temperature SOFCs*, Craig P. Jacobson, Keiji Yamahara, Liming Yang, Steven J. Visco, and Lutgard C. De Jonghe, 8th International Symposium on Ceramics in Energy Storage and Power Conversion Systems, January 28, 2004.
8. *Improving the Electrochemical Performance of Metal Supported SOFCs*, Craig P. Jacobson, Steven J. Visco, and Lutgard C. De Jonghe, 8th International Symposium on Ceramics in Energy Storage and Power Conversion Systems, January 28, 2004.
9. *Co-Fired LSM Supported Thin-Film SOFCs with Infiltrated Catalysts*, Lutgard C. De Jonghe, Keiji Yamahara, Craig P. Jacobson, and Steven J. Visco, 6th European Solid Oxide Fuel Cell Forum.
10. *Alloy Supported Thin-Film SOFCs*, Lutgard C. De Jonghe, Craig P. Jacobson, Steven J. Visco, 6th European Solid Oxide Fuel Cell Forum.
11. *Interfaces in Solid Oxide Fuel Cells*, Lutgard C. De Jonghe, Keiji Yamahara, Craig P. Jacobson, and Steven J. Visco, Lake Louise 2003.

Special Recognitions & Awards/Patents Issued

1. United States Patent 6,682,842, January 27, 2004, Composite electrode/electrolyte structure, Steven J. Visco, Craig P. Jacobson and Lutgard C. De Jonghe.
2. United States Patent 6,740,441, May 25, 2004, Metal current collect protected by oxide film, Craig P. Jacobson, Steven J. Visco, and Lutgard C. De Jonghe.
3. United States Patent Application, Planar electrochemical device assembly, June 17, 2004, Craig P. Jacobson, Steven J. Visco, and Lutgard C. De Jonghe.
4. United States Patent Application, Electrochemical cell stack assembly, February 5, 2004, Craig P. Jacobson, Steven J. Visco, and Lutgard C. De Jonghe.

III.A.7 Advanced Fuel Cell Development

Randall Gemmen (Primary Contact), Chris Johnson, Steven Zitney

National Energy Technology Laboratory (NETL)

3610 Collins Ferry Rd.

Morgantown, WV 26507

Phone: (304) 285-4536; E-mail: Randall.Gemmen@netl.doe.gov

Subcontractors: Fluent, Inc., Morgantown, WV; Drexel University, Philadelphia, PA; University of Utah, Salt Lake City, UT

Objectives

- Develop and validate advanced models for fuel cell analysis and design.
- Apply models for advanced fuel cell development.
- Transfer modeling capability to Solid State Energy Conversion Alliance (SECA) development teams and Core Technology Program participants.
- Analyze performance of solid oxide fuel cells (SOFCs) under dynamic loading.
- Develop capability to integrate computational fluid dynamics (CFD)-based fuel cell models with process models.
- Test perovskite coatings for fuel cell interconnects.

Approach

- Advance commercial CFD codes (FLUENT) to include fuel cell electrochemistry.
- Obtain model validation data using button cells representative of SECA technology.
- Apply new codes to investigate dynamics of SOFC operation.
- Integrate 3-D SOFC CFD model into process model of auxiliary power unit (APU).
- Apply doped LaCrO₃ coatings to standard interconnect material substrates and investigate coating properties and usefulness for SECA technologies.

Accomplishments

- First-generation fuel cell code has been released to SECA members (core and vertical teams).
- Model comparisons to button cell validation data have shown good agreement and have shown that specimen parameter changes (e.g., electrolyte thickness) can cause significant changes to model parameter values.
- Application of dynamic models has shown that circulating current conditions can exist within a cell/stack following certain common types of load changes.
- Developed capability to integrate FLUENT CFD models with Aspen Plus (Aspen Technology, Inc., Cambridge, MA) process simulation models.
- LaCrO₃ coatings were achieved having acceptable levels of area specific resistance (less than 0.1 ohm/cm²) during short-term tests.

Future Directions

- Develop reforming capability within these advanced fuel cell models.
- Apply codes to investigate fuel cell design parameter sensitivity.

- Expand testing to include larger cells (e.g., 10 cm x 10 cm).
- Begin study of mechanical failure limitations of SOFC by developing high-temperature strain gage technology.
- Investigate mechanisms for silicon build-up under LaCrO_3 -coated interconnects and determine if its oxide layer can be avoided or minimized through dopants.

Introduction

Because a fully functional hydrogen economy will take many years to create, the U.S. DOE is supporting the development of solid oxide fuel cells through the Solid State Energy Conversion Alliance (SECA) program as a way to efficiently use existing fossil fuel resources. The goal of this program is to provide low-cost fuel cell systems for mass markets. To achieve this goal will require new and innovative SOFC designs and materials. To assure success will require improved design tools and material data. The work performed here will address both needs by providing improved detailed modeling tools and new interconnect material options for SOFC design engineers.

Approach

Modeling

NETL has been developing fuel cell models using the FLUENT (Fluent Inc., Lebanon, NH) commercial software code. In this third phase (FY 2004) of development, further enhancements to the code allow for improved speed and accuracy in the analysis of cells and stacks by enabling the code to run in parallel mode on clusters of computers. In addition, internal reforming modeling capability will be added. This tool has been made available to SECA developers and to participants in the SECA Core Technology Program (Prinkey, 2004). To further improve the analysis of SECA and other fuel cell systems, NETL computational scientists, building on collaborations with NETL contracted activities, have developed the capability to integrate detailed FLUENT CFD models with Aspen Plus (Aspen Technology, Inc., Cambridge, MA) process simulation models (Zitney et al., 2004). Coupled CFD and process simulations provide a better understanding of the fluid mechanics that drive overall performance and efficiency of fuel cell systems. In addition, the analysis of the fuel cell

using CFD is not done in isolation but within the context of the whole fuel cell process.

Dynamic Load Studies

Both model and experimental studies are used to investigate the performance of fuel cells under dynamic loads. It has already been made clear that the chemical kinetics at the cathode can degrade fuel cell performance (Jorgensen et al., 2000). While much about basic kinetics at the electrode/electrolyte interface is unknown, it can be expected that this is non-linear, thereby making the steady-state results from Jorgensen et al. incomplete. This project will examine these effects and compare to steady-state results to quantify any variances and to investigate cell properties that may change specifically resulting from dynamic loads.

Perovskite Interconnect Coatings

Use of lanthanum chromite coatings on metallic interconnect alloys may reduce the material costs for SOFC stacks considerably. This work will experimentally evaluate LaCrO_3 -based coatings for application to SOFC systems. In FY 2004, we continued to study the film properties of LaCrO_3 films deposited by RF magnetron sputtering. We have also obtained Ca-doped LaCrO_3 thin films deposited by DC-magnetron sputtering on the Cr-containing stainless steel and nickel-based high-temperature alloy substrates (SS 446, Inconel 600). After sputtering, the alloy samples with deposited film were annealed at 800°C for 2 hours. A number of analytical techniques (x-ray diffraction, scanning electron microscope, atomic force microscope, nanoindentation, Raman, and area specific resistance measurements) were used to characterize film properties such as phase formation, film morphology, mechanical properties and film resistance. We are also pursuing alternative low-cost methods of depositing chromite-based films, focusing at this point on dip-coating using “Pechini” solutions.

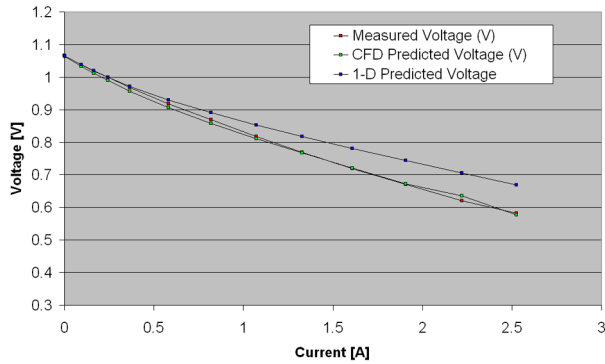


Figure 1. FLUENT Model Validation with Button Cell Data

Results

Modeling

Results from one of the validation studies of the new FLUENT SOFC model are shown in Figure 1. The results show very good agreement. To perform the validation effort, NETL has derived a consistent method for assessing the model parameters whereby the resistance of the electrolyte layer is first assessed based on measured cell data and resistivity data from the literature, followed by a calculated assessment of the exchange current from the data at low current density given an assumption of the contact resistance. Three loss mechanisms—electrolyte, cathode exchange current, and contact resistance—dominate the cell behavior.

Results from a detailed modeling study of a prototype short stack of SOFC cells operating in a crossflow configuration are shown in Figures 2-3. The study was used to demonstrate the present capability of the new model prior to release of the model to SECA partners in June of 2004. At this time, many SECA members (vertical and core) have downloaded the model, and NETL will continue to support their use of the model through updates and enhancements.

The Aspen Plus-FLUENT Integration Toolkit was applied to a SECA APU process simulation coupled with a 3-D planar SOFC CFD model. Detailed discussion of capability and results can be found in Zitney et al., 2004. This new capability is

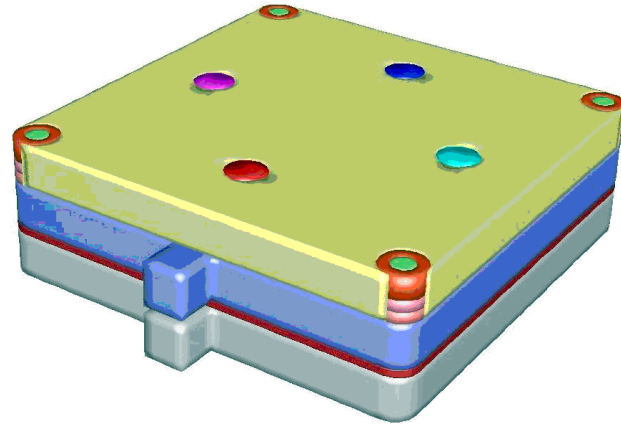


Figure 2. Test Case Geometry for FLUENT Model of an SOFC Cell

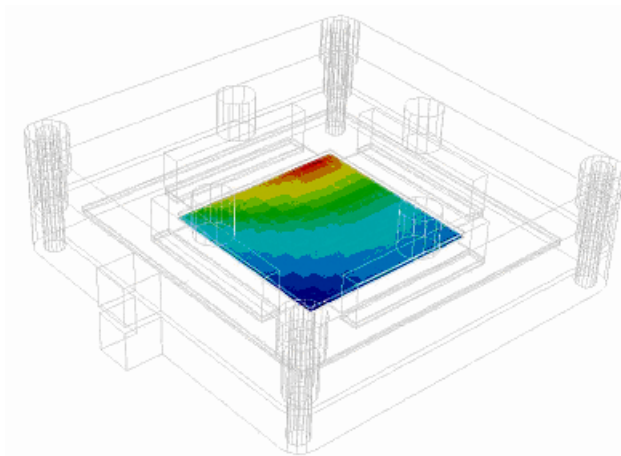


Figure 3. Sample FLUENT Model Results—Current Density Contour Plot

now available to help design and evaluate concepts for DOE's FutureGen program.

Dynamic Load Studies

The effect of applying transient loads on an SOFC cell was studied (Gemmen and Johnson, 2004). Some novel results are shown in Figure 4 for a representative "SECA technology" cell, showing the current density over the cell at the moment following load decrease. As can be seen, an internal current circulation condition can exist within the cell in spite of having lost external load. Such conditions are found to be due to temperature variations within the cell that control local Nernst voltages within the cell. With such variables driving potential conditions

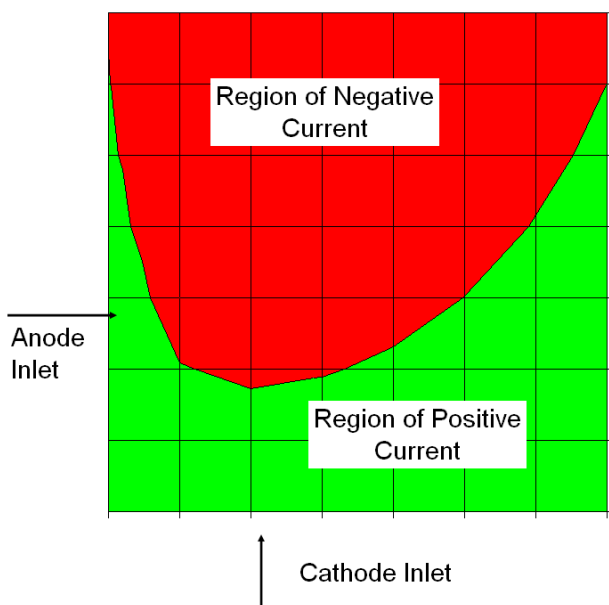


Figure 4. Cell Current Density Following Unload Event Showing Current Reversal

existing within the cell, an internal current circulation is produced. Such conditions have not been reported in prior work and may very well be of interest to SOFC designers who need to ensure that proper reducing and oxidizing conditions remain on the anode and cathode, respectively, at all times.

Perovskite Interconnect Coatings

We reported last year that the “as deposited” chromite films were amorphous as confirmed by x-ray diffraction (XRD). After annealing at 700°C for 1 hour, the amorphous film transformed to LaCrO₃ perovskite structure. Two transformations occurred during the amorphous-to-perovskite structure transition: the first is the amorphous-to-LaCrO₄ monoclinic structure transformation at 495°C, and the second is a LaCrO₄-to-LaCrO₃ orthorhombic structure transformation at 780°C (note that there is loss of oxygen in this transition). The second phase transition is accompanied by a fairly large volume decrease, which unfortunately results in the formation of porous structure for the LaCrO₃ perovskite thin film. Energy dispersive x-ray (EDS) analysis of the films prior to annealing showed that the “as deposited” film was oxygen-deficient relative to the chromite stoichiometry. This led us to anneal

the films in a low partial pressure of oxygen, with the idea being that if we were far enough away from the composition of LaCrO₄, we could avoid the intermediate phase formation and thus obtain a denser film. XRD and AFM data indeed show that we have changed the reaction pathway and have obtained a smaller-grain, denser film. Further work is necessary to determine if we do in fact obtain a film that is dense enough to act as an adequate protective layer.

Resistivity measurements were carried out on a number of samples annealed both in air and in low oxygen partial pressure atmospheres. The results show initially that all samples have area specific resistances (ASR) at acceptable levels (less than 0.1 ohm/cm²), with the low oxygen annealed sample initially performing the best. However, when the samples are exposed to air annealing for 100 hours, the ASR values increase, and the samples that were initially annealed in air become the best performers. We believe the reason for this is that the denser films change the kinetics of oxide growth under the perovskite layer to favor the formation of continuous silica layers (silica being present in most alloys as a trace element). Work is now being done to try and confirm this hypothesis.

Conclusions

Great progress is being made to provide new, advanced tools for fuel cell design. Basic model development is complete, with enhancements underway to add additional capabilities and enable integration with process models. These tools are now being validated using data from SOFC developers and from NETL test facilities. Collaboration with SECA developers and Core Technology participants is underway to validate the model and to provide the tools for their use. Validation of the model for single cells and cell stacks will be continued.

Insight to the dynamic behavior of SOFC systems is also being advanced. New fuel cell models that include the capability to calculate current reversal show that certain load transients can induce current circulation within the cell. Such conditions should be considered by fuel cell engineers during the design of these systems.

Finally, previous work on the perovskite films has shown the basic transformation behavior of LaCrO_3 perovskite coatings under conditions typical of SOFC operation. The understanding of these transformations has led us to change the annealing atmosphere to avoid detrimental intermediate phases. It was found that changing these processing conditions does improve film quality. ASR measurements, however, suggest that Si in the substrate alloys may be detrimental to conductivity of the film/substrate combination. Understanding of this problem is one aspect of future work. Work has also progressed to Ca-doped chromite films. Doping of the perovskite films is known to increase conductivity.

References

1. Prinkey, M.T. (2004), "FLUENT Model for SOFC Analysis", presented at the 2004 SECA Program Workshop, Boston, MA.
2. Gemmen, R.S. and C. Johnson (2004), "Dynamics of Solid Oxide Fuel Cell Operation," Paper No. FUELCELL2004-2475, ASME Second International Conference on Fuel Cell Science, Engineering, and Technology, Eds. R. Shah and S.G. Kandlikar, Rochester NY, June 13-16, 2004, pp. 229-235.
3. Jorgensen, M.J., P. Holtappels, and C.C. Appel (2000), "Durability Test of SOFC Cathodes," J. Appl. Electrochemistry, V. 30, 4.
4. Zitney, S.E., M.T. Prinkey, M. Shahnam, and W.A. Rogers (2004), "Coupled CFD and Process Simulation of a Fuel Cell Auxiliary Power Unit," Paper No. FUELCELL2004-2490, ASME Second International Conference on Fuel Cell Science, Engineering, and Technology, Eds. R. Shah and S.G. Kandlikar, Rochester NY, June 13-16, 2004, pp. 339-345.

FY 2004 Publications/Presentations

1. Prinkey, M.T. (2004), "FLUENT Model for SOFC Analysis," presented at the 2004 SECA Program Workshop, Boston, MA.
2. Gemmen, R.S. and C. Johnson (2004), "Dynamics of Solid Oxide Fuel Cell Operation," Paper No. FUELCELL2004-2475, ASME Second International Conference on Fuel Cell Science, Engineering, and Technology, Eds. R. Shah and S.G. Kandlikar, Rochester NY, June 13-16, 2004, pp. 229-235.
3. Zitney, S.E., M.T. Prinkey, M. Shahnam, and W.A. Rogers (2004), "Coupled CFD and Process Simulation of a Fuel Cell Auxiliary Power Unit," Paper No. FUELCELL2004-2490, ASME Second International Conference on Fuel Cell Science, Engineering, and Technology, Eds. R. Shah and S.G. Kandlikar, Rochester NY, June 13-16, 2004, pp. 339-345.
4. Orlovskaya, N., A. Coratolo, C. Johnson, and R.S. Gemmen (2004), "Structural Characterization of LaCrO_3 Perovskite Coating Deposited by Magnetron Sputtering on an Iron Based Chromium Containing Alloy as a Promising Interconnect Material for SOFCs," Journal of the American Ceramic Society, Accepted for publication.
5. Johnson, C., R.S. Gemmen, N. Orlovskaya (2004), " LaCrO_3 Thin Films Deposited by Rf Magnetron Sputtering on Stainless Steel Materials," presented at The 28th International Conference and Exposition on Advanced Ceramics and Composites, January 2004.

III.A.8 Continuous Process for Producing Low-Cost, High-Quality YSZ Powder

Scott L. Swartz, Ph.D. (Primary Contact), Michael Beachy, and Matthew Seabaugh

NexTech Materials, Ltd.

404 Enterprise Drive

Lewis Center, OH 43035

Phone: (614) 842-6606; Fax: (614) 842-6607; E-mail: swartz@nextechmaterials.com

DOE Project Manager: Shawna Toth

Phone: (304) 285-1316; E-mail: Shawna.Toth@netl.doe.gov

Objectives

- Develop a robust process for producing yttrium-stabilized zirconia (YSZ) powder that can be tailored to meet the Solid State Energy Conversion Alliance (SECA) Industry Team needs.
- Produce YSZ powder in 5-10 kg batches, and demonstrate reproducibility of the process.
- Demonstrate the advantages of tailoring YSZ powder characteristics to specific requirements of fabrication processes used in solid oxide fuel cell (SOFC) manufacture.
- Demonstrate that the process provides YSZ powder at low manufacturing cost.

Approach

- Use chemical precipitation methods to produce hydroxide precursors that can be converted into crystalline YSZ via thermal treatments.
- Use ball milling and attrition milling methods to reduce particle size of YSZ powders to below one micron.
- Use uniaxial and isostatic pressing methods followed by sintering to produce ceramic samples for density and ionic conductivity measurements.

Accomplishments

- Established a homogeneous precipitation process for preparing an yttrium-zirconium hydrous oxide precursor, which can be converted to crystalline YSZ via calcination.
- Established calcination and milling methods to prepare YSZ powders with controlled surface area and particle size distribution.
- Demonstrated that YSZ powder produced by the process can be sintered to densities greater than 98 percent theoretical at temperatures less than 1400°C.
- Demonstrated sintered YSZ ceramics with high ionic conductivity (>0.08 S/cm at 800°C), equivalent to the best values reported in the literature.
- Demonstrated that the manufactured cost of YSZ powder produced using the process will be less than \$25 per kilogram at large production volumes.

Future Directions

- Continued process refinements aimed at increasing performance and reducing manufacturing cost. The emphasis of these studies will be on higher-cost unit operations, improving low-temperature sintering capability, and demonstrating process reproducibility.
- Demonstration of advantages of using tailored YSZ powders in fabrication processes used for the manufacture of SOFCs. This will involve fabrication of planar SOFC components using tailored YSZ powder and testing of the performance of these components.

- Production of evaluation samples of YSZ electrolyte powder, NiO/YSZ anode powder, and/or SOFC components produced from these powders for evaluation by SECA Industry Teams and Core Technology Program participants.
- Continual updates to the manufacturing cost analyses, incorporating process refinements that are implemented.

Introduction

One of the current barriers to reducing the manufacturing cost of SOFCs is the high cost of some of the critical raw materials. The availability of a low-cost, highly reliable and reproducible supply of engineered raw materials is needed to assure successful commercialization of SOFC technology. The yttrium-stabilized zirconia (YSZ) electrolyte material is a primary ingredient for two of the three layers comprising an SOFC element: the dense electrolyte layer and the porous nickel-based cermet (Ni/YSZ) anode layer. In addition, YSZ often is used as a performance-enhancing additive to lanthanum strontium manganite (LSM)-based cathode layers. In practice, the same YSZ raw material is used for each of the component layers, even though different fabrication processes are used for each layer. Significant opportunities for performance optimization and cost reduction would be possible if the YSZ raw material were tailored for each component layer. The project focuses on the development of YSZ powder synthesis technology that is “tailored” to the process-specific needs of different SOFC designs being developed under DOE’s Solid State Energy Conversion Alliance (SECA) program.

Approach

NexTech’s approach to developing a low-cost YSZ electrolyte powder production process is based on the following principles: (1) the process must be scalable to high volume (500 tons per year) production at a cost of less than \$25/kilogram; (2) the process must be sufficiently versatile so that powder characteristics can be tailored to a specific customer’s requirements; (3) the process must be reliable, providing consistent batch-to-batch quality; and (4) the process must provide a relatively pure YSZ powder that meets performance criteria relative to particle size, surface area, sintering activity, and ionic conductivity. The process being developed in

this project is based on homogeneous precipitation (see Figure 1). With homogeneous precipitation, the pH and solids content remain constant throughout the process, which is the key to achieving uniformity and reproducibility of the finished product. Another attribute of the homogeneous precipitation process is that it can be made continuous with constant replenishment of the feed solutions. This provides considerable cost and reliability advantages relative to current chemical synthesis processes.

In the project, synthesis studies are being conducted to identify optimum precipitation conditions for producing hydrous oxide precursors. These precursors then are processed into YSZ powders by washing and drying of the precipitates, calcination of the dried precursor to form a crystalline YSZ powder with targeted surface area ($\sim 10 \text{ m}^2/\text{gram}$), and milling of the calcined YSZ powder to sub-micron particle size. The YSZ powders are subjected to a comprehensive characterization protocol involving x-ray diffraction, chemical analyses, particle size distribution, surface area measurements, and sintering studies. Performance of sintered YSZ ceramics is being assessed by density measurements, ionic conductivity measurements, mechanical property measurements, and scanning electron microscopy.

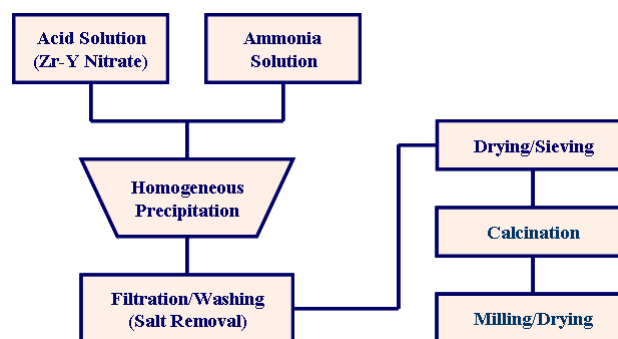


Figure 1. Homogenous Precipitation Process for YSZ Powder

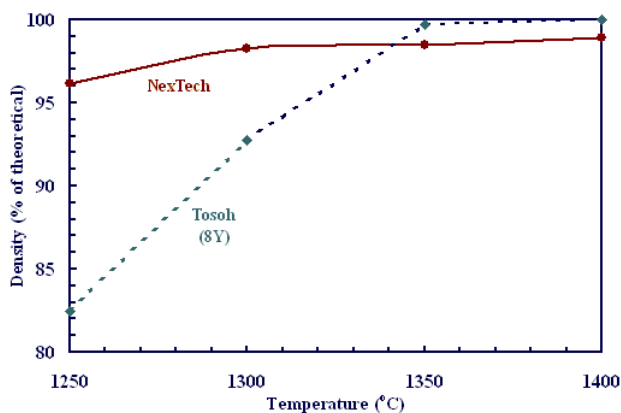


Figure 2. Sintering Performance of Experimental YSZ Powder, Compared to Commercially Available YSZ Powder

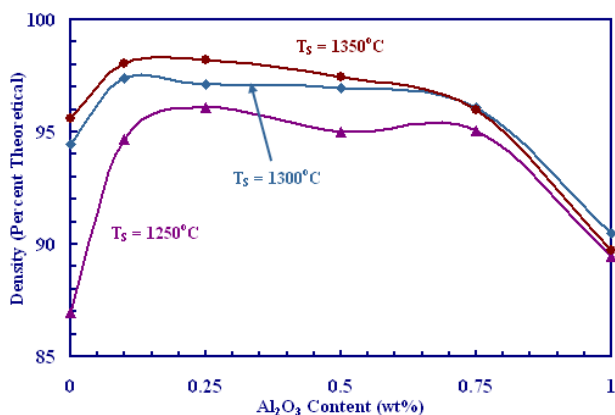


Figure 3. Effect of Al_2O_3 Content on Sintering Performance of Experimental YSZ Powder

Results to Date

In this project, NexTech has demonstrated a laboratory-scale continuous (homogeneous) precipitation process for YSZ electrolyte powder with equivalent, and in some ways superior, performance to YSZ powder that is commercially available from non-domestic suppliers. Key results to date are discussed below:

- The initial precipitation conditions were shown to have a profound effect on the performance of fully processed (calcined and milled) YSZ powders. After optimization of precipitation conditions, YSZ powders were produced that exhibited excellent low-temperature sintering performance compared to the current industry-

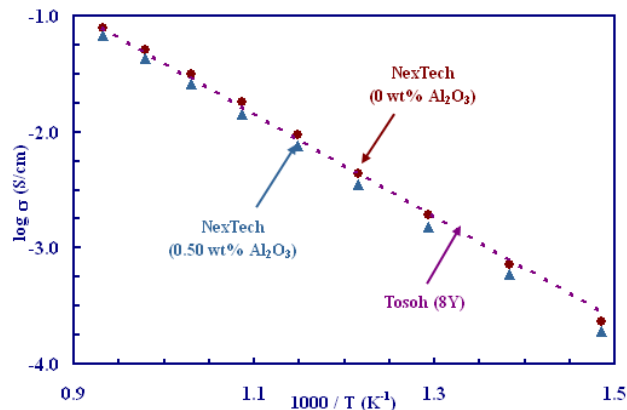


Figure 4. Ionic Conductivity Data for YSZ Ceramics

standard YSZ powder (Tosoh 8Y). This is shown in Figure 2. Densities of >96 percent theoretical were achieved with a sintering temperature of 1250°C, compared to a density of <82 percent theoretical for the commercial YSZ powder.

- NexTech also demonstrated improved densification through doping with alumina (Al_2O_3), nickel oxide (NiO) and manganese oxide (Mn_2O_3) dopants, especially at low sintering temperatures (less than 1300°C). The optimum Al_2O_3 dopant concentration appears to be in the range of 0.25 to 0.50 weight percent, as shown in Figure 3.
- Ionic conductivities of sintered YSZ ceramics are essentially the same for ceramics derived from experimental and commercial YSZ powders (see Figure 4). Alumina dopants resulted in a slight reduction of conductivity, whereas NiO and Mn_2O_3 dopants resulted in more significant reductions of ionic conductivity.
- A manufacturing cost analysis confirmed that YSZ powder prepared by NexTech's homogeneous precipitation process could be manufactured at a cost of less than \$25 per kilogram (see Figure 5). This analysis was based on a production volume of 500 metric tons per year, which is a fraction of the volume necessary when SOFCs are in full-scale production.

Conclusions

- Homogeneous precipitation is a promising route for the continuous synthesis of hydrous oxide

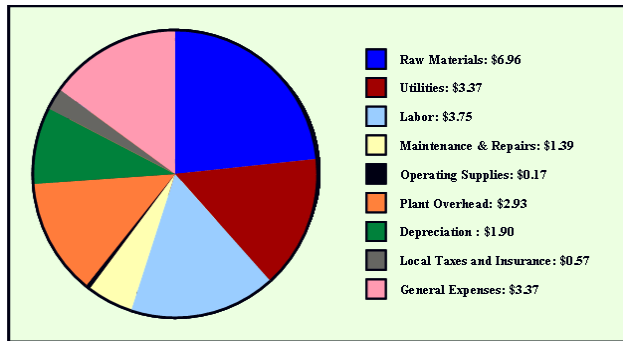


Figure 5. Results of Manufacturing Cost Analysis

precursors to high-quality YSZ powders. The initial precipitation conditions had a profound effect on downstream milling performance (after calcination) and on subsequent sintering and electrical performance. Important synthesis variables include concentrations of the precipitant solutions, feed rates during precipitation, and the pH during precipitation.

- The processing of the precipitated hydroxide slurries prior to drying was critically important to achieving high-performance YSZ powders. For aqueous processing, surfactants were required to allow hydroxide precipitates to be dried directly from aqueous suspensions. An alternative approach, based on solvent exchange of the precipitated hydroxides into isopropyl alcohol prior to drying, also was demonstrated.

- Several oxide dopant strategies were identified that led to significant improvements in sintering performance of YSZ ceramics. Dopants such as aluminum oxide, nickel oxide, and manganese oxide all were found to increase ceramic densities, especially with low sintering temperatures (~1200 to 1300°C). These dopants also led to a reduction of ionic conductivity, which suggests a trade-off between dopant concentration, low-temperature sinterability, and ionic conductivity.
- Based on a manufacturing cost analysis, YSZ powders prepared by the homogeneous precipitation process can be manufactured at a cost of less than \$25 per kilogram at high production volumes. This analysis identified specific unit operations where cost can be reduced upon further optimization.

FY 2004 Publications/Presentations

1. S.L. Swartz, et al., *Continuous Process for Low-Cost, High-Quality YSZ Powder*, SECA Annual Workshop and Core Technology Program Peer Review Workshop (May 12, 2004).
2. S.L. Swartz, et al., *Continuous Process for Low-Cost, High-Quality YSZ Powder*, SECA Core Technology Program Review Meeting (October 1, 2003).

III.A.9 Reliability and Durability of Materials and Components for Solid Oxide Fuel Cells

Edgar Lara-Curzio (Primary Contact), Miladin Radovic and Rosa Trejo

Oak Ridge National Laboratory

1 Bethel Valley Rd.

Oak Ridge, TN 37831-6969

Phone: (865) 574-1749; Fax: (865) 574-6098; E-mail: laracurzioe@ornl.gov

DOE Project Manager: Travis Shultz

Phone: (304) 285-1370; E-mail: Travis.Shultz@netl.doe.gov

Objectives

- Characterize mechanical properties-namely elastic moduli, biaxial strength and fracture toughness-of typical anode and electrolyte materials as a function of temperature, level of porosity and environment (reducing or oxidizing).
- Evaluate the magnitude of the residual stress in solid oxide fuel cell (SOFC) anode-electrolyte bilayers.
- Study the effect of thermal cycling on mechanical properties of materials and components for SOFCs.

Approach

- The elastic properties of electrolyte materials (yttria-stabilized zirconia [YSZ] and gadolinium-doped ceria [GDC]) and anode materials (NiO-YSZ and Ni-YSZ) were determined as a function of temperature in different environments using a resonant ultrasound spectrometer (RUS).
- The stochastic distribution of biaxial strengths and fracture toughness of Ni-based anode materials and YSZ electrolytes were determined up to 800°C in H₂ and air. Biaxial strength was determined using the ring-on-ring test method, while fracture toughness was determined according to the double-torsion test method. Experimental fixtures to carry out these tests at elevated temperatures and controlled environments were designed and fabricated at Oak Ridge National Laboratory (ORNL).
- The magnitude of residual stresses in YSZ/NiO-YSZ and YSZ/Ni-YSZ bilayers was determined as a function of temperature by X-ray diffraction (XRD).
- The effect of thermal cycling on the mechanical properties of Ni-based anode materials was investigated by subjecting test specimens to thermal cycling followed by determination of biaxial strength and elastic properties at ambient conditions. Thermal cycling tests were carried out in controlled environments using equipment developed at ORNL.

Accomplishments

- Developed methodologies and experimental facilities for determination of elastic properties, fracture toughness and biaxial strength of SOFC materials in controlled environments as a function of temperature. The methodologies developed are based on the use of RUS, ring-on-ring testing to determine equibiaxial strength and double-torsion to determine fracture toughness.
- Determined the elastic properties, biaxial strength and fracture toughness of tape cast YSZ electrolyte materials, as well as Ni-based anode materials, before and after hydrogen reduction as a function of porosity and temperature, in reducing and oxidizing environments. Strength results were analyzed using Weibull statistics and correlated to microstructural features that act as strength-limiting flaws. Results have been compiled in a user-friendly database.

- Determined changes in the magnitude of the elastic properties of GDC, which are induced by the creation of oxygen vacancies, as a function of exposure time in a reducing environment using RUS.
- Found that microcracking induced by thermal cycling results in a decrease in the elastic properties and strength of Ni-based anode materials.
- Determined the magnitude of residual stresses in YSZ/NiO-YSZ and YSZ/Ni-YSZ bilayers as a function of time in air and in H₂.

Future Directions

- Evaluate the effect of thermal cycling on microstructure, residual stresses and mechanical properties of materials and components for SOFCs.
- Evaluate crack growth rates in YSZ, NiO-YSZ and Ni-YSZ cermets as a function of temperature, porosity and specimen thickness.
- Characterize mechanical properties of cathode material (lanthanum strontium manganite [LSM]) as a function of porosity and temperature.
- Determine the thermal shock resistance of YSZ, Ni-YSZ cermets and YSZ/Ni-YSZ bilayers as a function of temperature, porosity and specimen thickness.
- Evaluate the thermal and creep properties of Ni-YSZ cermets.

Introduction

The durability and reliability of SOFCs depend not only on their electrochemical performance, but also on the ability of their components to withstand mechanical stresses that arise during processing and service. Specifically, the mechanical reliability and durability of SOFCs are determined by the stress distribution in, and the stochastic distribution of strengths of, their components. The stress distribution is a complex function of several parameters, including geometry of the SOFC, temperature distribution and external mechanical loads. Furthermore, residual stresses induced during processing as a result of mismatch in the thermoelastic properties of SOFC components, and evolution of stresses during service, will also affect durability and reliability. The determination of the stress distribution in SOFC materials and components typically requires the use of computational tools (e.g., computational fluid dynamics and finite-element stress analyses), which in turn requires knowing the physical and mechanical properties of the materials and components. The stochastic distribution of strengths of SOFC materials is primarily determined by the type and distribution of strength-limiting flaws, which are either intrinsic to the material or introduced during processing and/or manufacturing. Because flaws can

grow with time, it is expected that the distribution of strengths will also evolve with time. Knowledge of the distribution of stresses in, and strengths of, SOFC materials and components is essential to predict their durability and reliability.

Approach

Because most SOFC components consist of thin membranes, the determination of their physical and mechanical properties poses experimental challenges. As part of this project, a resonant ultrasound spectrometer (RUS) was adapted to determine the elastic moduli of SOFC materials at elevated temperatures and in different environments. For example, the elastic moduli of YSZ, GDC, NiO-YSZ and Ni-YSZ were determined in air and in a reducing environment (a gas mixture of 4% H₂ + 96% Ar) at temperatures up to 800°C.

Components of planar SOFCs are mainly subjected to biaxial states of stress that result from the thermal expansion mismatch among the SOFC constituents and from temperature gradients induced during operation. Thus, it has been customary to determine the biaxial strength of SOFC materials using the concentric ring-on-ring flexural-loading configuration. The results of the biaxial test are analyzed using Weibull statistics to determine the

parameters of the distribution of strengths, namely Weibull modulus and characteristic strength. In order to evaluate the mechanical properties of Ni-based anode materials in controlled environments (e.g., reducing environment), a unique experimental system was designed and built. The same experimental system is used to determine fracture toughness by the double-torsion test method.

XRD is used to determine the magnitude of residual stresses in bilayers of NiO-YSZ/YSZ as a function of temperature, before and after hydrogen reduction.

Both in stationary and transportation applications, SOFCs will be subjected to thermal cycling associated with start-up and shut-down cycles. The evolution of stresses that will develop in SOFCs as a result of thermal cycling is expected to impact the service life of SOFCs. Thus, experimental equipment for subjecting SOFC components to thermal cycling was developed at ORNL and used to investigate the effect of thermal cycling on the properties of YSZ and NiO-YSZ materials.

Results

The elastic moduli (Young's and shear) of 8 mol% YSZ were found to decrease with temperature between 25 and 600°C. Above 600°C, they were found to increase slightly with temperature up to 1000°C. The peaks associated with resonant frequencies, obtained by RUS, were found to be very broad at temperatures between 200°C and 600°C, suggesting high damping (internal friction) in YSZ at these temperatures. Results of characterization studies using Raman spectroscopy and XRD did not reveal any phase transformation at these temperatures. Thus, the atypical trend of the elastic moduli and the increase in mechanical damping with temperature could be related to mechanically induced mobility of vacancies due to reorientation of elastic dipoles formed between oxygen vacancies and Y (dopant) ions. However, additional work is needed to ascertain the source of this behavior. Similar property-temperature trends were observed for fracture toughness and biaxial strength. The elastic moduli of NiO-YSZ were determined in air as a function of temperature, while the elastic moduli

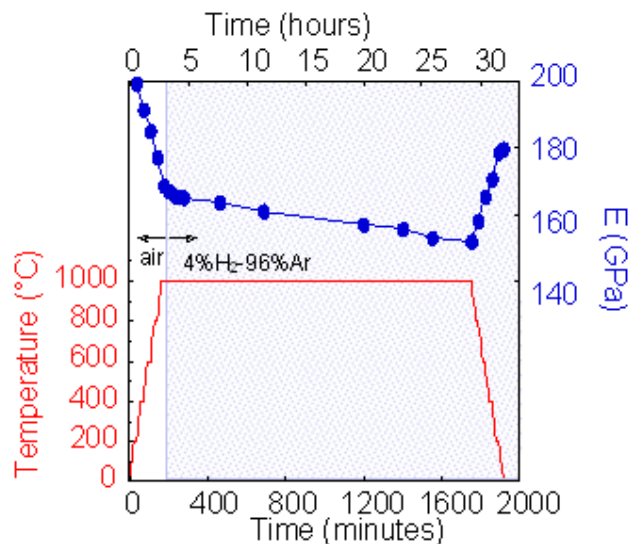


Figure 1. Young's Modulus of GDC as a Function of Temperature and Reduction Time at 1000°C in 4% H₂-96% Ar Gas Mixture

of Ni-YSZ anodes were determined in a gas mixture of 4% H₂ + 96% Ar as a function of temperature. Similar moduli-temperature trends were found for both NiO-YSZ and Ni-YSZ, although the initial decrease in elastic moduli in the temperature interval between 25°C and 600°C is less pronounced than for the case of YSZ.

GDC is considered to be a good electrolyte candidate material because of its high ionic conductivity at elevated temperatures. However, when GDC is exposed to low partial pressures of oxygen or reducing environments, the oxygen vacancy concentration in GDC increases with time. For example, it was found (Figure 1) that at a constant temperature of 1000°C in a gas mixture of 4% H₂ + 96% Ar, the Young's modulus of GDC decreases with time as a result of the increase in oxygen vacancy concentration.

The characteristic biaxial strength and Weibull moduli for NiO-YSZ precursor for SOFC anode were determined from the results of ring-on-ring tests in air as a function of porosity for different temperatures. Also, the characteristic biaxial strength and Weibull moduli for Ni-YSZ (Figure 2) were determined in a gas mixture of 4% H₂ + 96% Ar as a function of porosity and temperature. These results show that the characteristic biaxial strength of

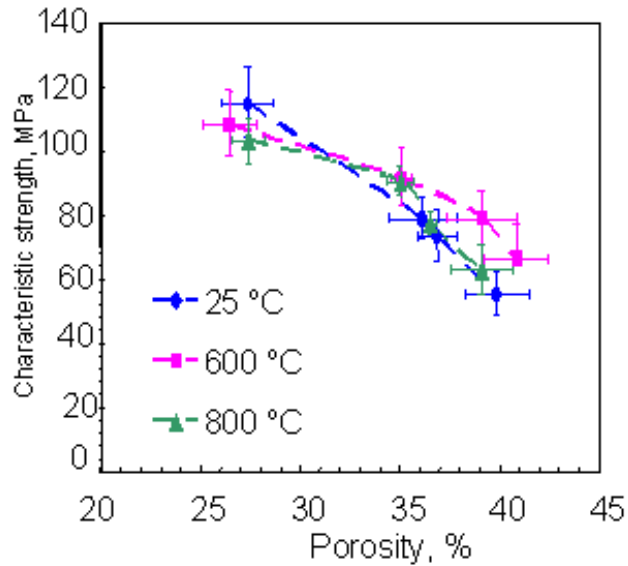


Figure 2. Characteristic Biaxial Strength of Ni-YSZ as a Function of Porosity at 25°C, 600°C and 800°C. Error bars for characteristic strength represent upper and lower 95% confidence bounds. Error bars for porosity represent one standard deviation.

these materials decreases with porosity at all temperatures. On the other hand, the characteristic biaxial strength is slightly higher at elevated temperatures than at room temperature.

Ni-based anode materials were subjected to thermal cycling between 20°C and 800°C in a gas mixture of 4% H₂-96% Ar. Each thermal cycle consisted of heating up to 800°C at a constant rate of 30°C/min, soaking at 800°C for 2 hours and cooling in 90 minutes to ambient temperature at the natural cooling rate of the furnace. The changes induced by thermal cycling on Young's and shear moduli were determined at room temperature by impulse excitation, while biaxial strength was determined by ring-on-ring testing, and the results were analyzed using Weibull statistics. It was found that both the elastic moduli and biaxial strength decrease with the number of thermal cycles, as shown in Figure 3. For example, the characteristic strength of these materials decreased by as much as 25% after 81 cycles. Scanning electron microscopy of the thermally cycled samples revealed the formation of small microcracks, predominantly between YSZ and Ni grains. Thus, the observed changes in mechanical

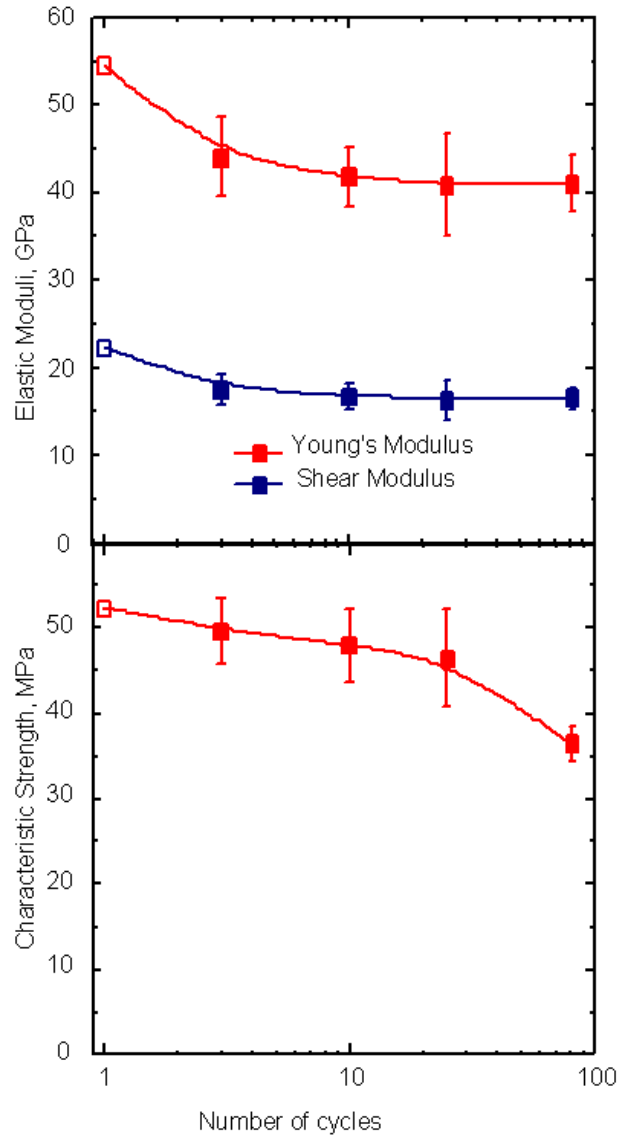


Figure 3. Elastic Properties (top) and Characteristic Biaxial Strength (bottom) of the Ni-YSZ Anode as a Function of Number of Thermal Cycles in Hydrogen

properties can be attributed to the initiation and propagation of microcracks resulting from the difference in thermal expansion behavior of Ni and YSZ grains.

The residual stresses in bilayers of YSZ and NiO-YSZ were determined as a function of temperature from XRD spectra in air and in a gas mixture of 4% H₂ and 96% Ar. The residual stresses in the 10- μ m thick layer of YSZ before and after reduction of the NiO-YSZ layer are plotted in

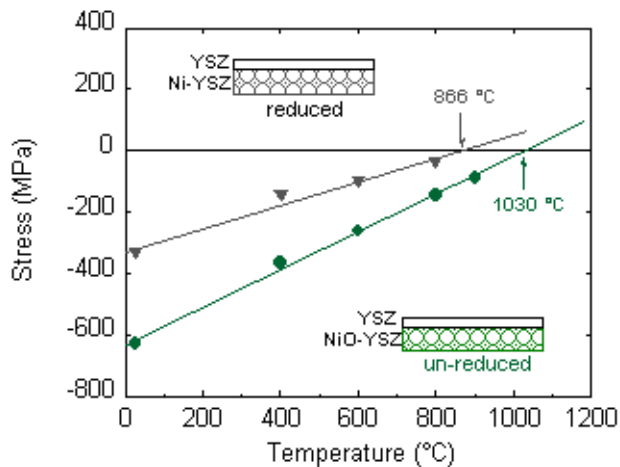


Figure 4. Residual Stresses in Bilayers of YSZ/NiO-YSZ before and after Reduction in Hydrogen

Figure 4. These results show that residual stresses in YSZ are compressive and that in both cases their magnitude decreases with temperature. The compressive residual stresses at room temperature are large, i.e. ≈ 600 and ≈ 400 MPa before and after hydrogen reduction, respectively. It was also found that the zero-stress temperature was lower than the co-sintering temperature, most likely due to creep-induced stress relaxation at elevated temperatures.

Conclusions

- It was found that the biaxial strength of both NiO-YSZ and Ni-YSZ decreases with porosity, but does not depend significantly on temperature, at least up to 800°C . The magnitude of the elastic constants and fracture toughness of these materials decreases significantly with temperature in the 25°C - 600°C range.
- The elastic properties of YSZ and GDC were characterized as a function of temperature by RUS in air. It was found that Young's and shear moduli of YSZ decrease with temperature between 25°C and 600°C and that they increase slightly with higher temperature up to 1000°C . The Young's modulus of GDC was determined by RUS in air and was found to decrease almost linearly with temperature. When exposed to a gas mixture of 4% H_2 -96% Ar at 1000°C , the Young's modulus of GDC was found to decrease

continuously with time due to an increase in the concentration of oxygen vacancies.

- The elastic moduli and biaxial strength of Ni-based anode materials were found to decrease with the number of thermal cycles due to formation of small microcracks predominantly between Ni and YSZ grains.
- It was demonstrated that XRD is a powerful technique to determine the magnitude of residual stresses in multilayers of SOFC materials. The residual stresses in NiO-YSZ/YSZ bilayers were determined as a function of temperature before and after hydrogen reduction. It was found that residual stresses in YSZ layer are compressive and relatively large and that their magnitude decreases with temperature. It was also found that magnitude of compressive residual stresses in the YSZ layer decreases after hydrogen reduction.

References

1. ASTM 1499
2. A. Migliori and J. L. Sarrao, Resonant Ultrasound Spectroscopy: Applications to Physics, Materials Measurements and Nondestructive Evaluation, John Wiley and Sons, New York, (1997)
3. E. R. Jr. Fuller, "An Evaluation of Double-Torsion Testing – Analysis" in Fracture Mechanics Applied to Brittle Materials, ASTM Special Technical Publication No 678 Edited by Freiman S. W., ASTM, Philadelphia (1997)
4. A. Atkinson and A. Selcuk, "Strength and Toughness of Tape-Cast Yttria-Stabilized Zirconia", J. Am. Ceram. Soc., 83, 2029 (2000)

FY 2004 Publications/Presentations

1. M. Radovic, E. Lara-Curzio, L. Riester, "Comparison of Different Experimental Techniques for Determination of Elastic Properties of Solids", *Mater. Sci. Eng. A368* (2004) 56-70.

2. M. Radovic and E. Lara-Curzio “Changes in Elastic Properties of SOFC Anode Materials during the Reduction of NiO to Ni in Hydrogen”, *J. Amer. Ceram. Soc.* (2004) in press.
3. M. Radovic and E. Lara-Curzio, “Mechanical Properties of Tape-Cast Nickel-Based Anode Materials for Solid Oxide Fuel Cells Before and After Reduction in Hydrogen”, submitted for publication.
4. M. Radovic, E. Lara-Curzio, B. Armstrong, L. Walker, P. Tortorelli and C. Walls, “Kinetics of the Hydrogen Reduction of NiO/YSZ and Associated Microstructural Changes” in “28th Cocoa Beach Conference on Advanced Ceramics and Composites Ceramics”, Eds. M. Readey and E. Lara-Curzio., Engineering and Science Proceedings, Vol. 25, The American Ceramic Society (2004) in press.
5. M. Radovic, E. Lara-Curzio, R. Trejo, B. Armstrong and C. Walls, “Elastic Properties, Equibiaxial Strength and Fracture Toughness of 8mol%YSZ Electrolyte for SOFC”, *ibid* 4.
6. E. Lara-Curzio, M. Radovic and B. Armstrong, “Effect of Hydrogen Reduction on the Thermomechanical Properties of Ni-Based Anodes for Solid Oxide Fuel Cells”, Invited Lecture at 28th Cocoa Beach Conference on Advanced Ceramics and Composites Ceramics, Cocoa Beach, FL (2004).
7. M. Radovic, E. Lara-Curzio, T. Zhen and B. Armstrong, “Effect of Thermal Cycling on the Mechanical Properties of the Ni-Based Materials for SOFCs”, presented at 106th Annual Meeting and Exposition of American Ceramic Society, Indianapolis, IN (2004).
8. E. Lara-Curzio, T. Watkins, R. Trejo, C. Luttrell, M. Radovic, J. Lannutti and D. England, “Effect of Temperature and H₂-Induced Reduction on the Magnitude of Residual Stresses in YSZ-NiO/YSZ Bi-Layers”, *ibid* 8.
9. M. Radovic, E. Lara-Curzio, B. Armstrong, P. Tortorelli and L. Walker, “Effect of Hydrogen Reduction on the Microstructure and Elastic Properties of Ni-Based Anodes for SOFCs”, Proceedings of the 106th Annual Meeting and Exhibition of the American Ceramic Society, Indianapolis, The American Ceramic Society (2004) in press.
10. M. Radovic, E. Lara-Curzio, B. Armstrong and C. Walls, “Elastic Properties, Biaxial Strength and Fracture Toughness of Nickel-Based Anode Materials for Solid Oxide Fuel Cells”, *ibid* 9.

III.A.10 SOFC Compressive Seal Development at PNNL

Yeong-Shyung “Matt” Chou (Primary Contact), Jeff Stevenson

Pacific Northwest National Laboratory

P.O. Box 999, MS K2-44

Richland, WA 99352

Phone: (509) 375-2527; Fax: (509) 375-2186; E-mail: Yeong-Shyung.Chou@pnl.gov

DOE Project Manager: Lane Wilson

Phone: (304) 285-1336; E-mail: Lane.Wilson@netl.doe.gov

Objectives

- Develop inexpensive seals for solid oxide fuel cell (SOFC) stacks that offer low leak rates and excellent reliability during long-term operation and thermal cycling.
- Improve understanding of degradation mechanisms affecting seal performance, including intrinsic materials degradation in the SOFC environment and interactions with other SOFC components.

Approach

- Perform preliminary evaluation of seal concepts.
- Prepare and test seal materials and designs under SOFC-relevant conditions (atmosphere and temperature).
- Evaluate tested seal components to improve understanding of degradation processes during seal operation.

Accomplishments

- Developed inexpensive “hybrid” compressive seal based on mica paper with glass-ceramic interlayers.
- Demonstrated low leak rate and stability of hybrid seals during long-term testing with extensive thermal cycling.

Future Directions

- Complete investigation of long-term seal performance/reliability.
- Evaluate and optimize mica/glass “composite” version of hybrid seal.
- Study degradation and reactions at mica/interconnect interfaces during aging in SOFC environments.

Introduction

Planar SOFC stacks require adequate seals between the interconnect and cells in order to prevent mixing of the oxidant and fuel gases and to prevent leaking of gases from the stack. In addition, these seals must also allow the stack to be thermally cycled repeatedly (between ambient conditions and the operating temperature). Several different approaches to sealing SOFC stacks are available, including rigid, bonded seals (e.g., glass-ceramics); compliant seals (e.g., viscous glass); and compressive seals (e.g., mica-based composites). Rigid seals typically soften and flow slightly during stack fabrication (at a

temperature above the operating temperature) but then become rigid (to avoid excessive flow or creep) when cooled to the operating temperature. The thermal expansion of rigid seals must be closely matched to the other stack components in order to avoid damaging the stack during thermal cycling. Compliant seals attempt to simultaneously perform the sealing function and prevent thermal stress generation between adjacent components. Compressive seals typically utilize materials such as sheet-structure silicates that do not bond adjacent SOFC components; instead, the sealing material acts as a gasket, and gas-tightness is achieved by applying a compressive force to the stack. Both compliant and

compressive seals potentially improve the ability of the stack to tolerate thermal expansion mismatch between the various stack components.

Previous Core Technology Program seal development work at Pacific Northwest National Laboratory (PNNL) has focused on a novel “hybrid” mica-based compressive seal concept. Initial development efforts focused on hybrid seals based on naturally cleaved Muscovite mica sheets, which offered leak rates several orders of magnitude lower than those measured with “plain” mica compressive seals. The seals, however, did not exhibit the desired thermal cycle stability as the leak rates tended to increase with increasing thermal cycles. Microstructural characterization of cycled seals revealed undesirable degradation of the Muscovite mica due to coefficient of thermal expansion (CTE) mismatch with the mating materials. Improvements in thermal cycle stability have been obtained with seals based on Phlogopite mica paper, which has a higher “x-y” CTE (~11 ppm/°C) than Muscovite mica (~7 ppm/°C). Recent seal work has focused on optimizing Phlogopite paper-based hybrid seals to maintain low leak rates during thermal cycling under reduced applied compressive loads (6 to 100 psi).

Approach

Candidate seals were evaluated by studying seal quality (i.e., leak rate or open circuit voltage) as a function of temperature, gas pressure and composition, and applied compressive load. For leak rate measurements, the seal assemblies were placed between an Inconel600 pipe and an alumina substrate. A compressive load was applied throughout the tests, including the heating and cooling cycles. The leak rates were determined with high-purity helium, maintaining a 2 psi differential. Thermal cycling was conducted between 100°C and 800°C, with 2-hour dwells at 800°C. Open circuit voltage (OCV) tests were also conducted using electroded dense 8YSZ electrolyte pressed between an Inconel cap and an alumina base support; in these tests, the mica seals were located between the 8YSZ and the Inconel fixture. Stability and resistance to chemical interaction with other SOFC components were evaluated through thermogravimetric analysis, x-ray diffraction, electron microscopy, and optical microscopy.

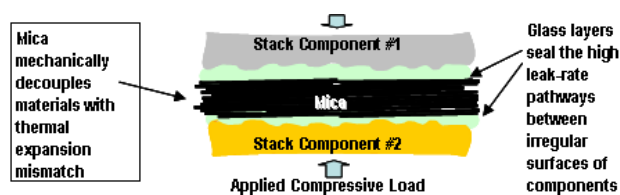


Figure 1. Schematic Illustration of Hybrid Mica Seal; Mica paper is in center of seal with glass layers on each side to fill mica/stack component interfaces

Results

The glass-mica paper hybrid seals consist of commercially available Phlogopite mica paper sandwiched between thin layers of a proprietary SOFC glass-ceramic seal material covered under United States Patents 6,430,966 and 6,532,769. The seals were fabricated by inserting the mica paper between polymer tapes (prepared by conventional tape casting techniques) which contained the glass-ceramic powder. Sealing was accomplished by placing the tri-layer tape/mica/tape structure between the stack components to be sealed. The configuration was subsequently heat-treated (typically to 830°C) to soften the glass sufficiently to cause bonding to the component surfaces. Final seal thickness was typically ~100-200 μm (Figure 1).

Performance

Results for thermal cyclic leak rate tests on a 2”x 2” hybrid seal (1 layer of mica paper sandwiched between glass-ceramic surface layers) are shown in Figure 2. When compressed at ~25 psi or more, the seals exhibited extremely low leak rates and excellent stability during repeated thermal cycling. It is important to emphasize that, in these tests, the materials adjacent to the seal had a significant CTE mismatch (Inconel600, with a CTE of ~16-17 ppm/K, vs. alumina, with a CTE of ~8-9 ppm/K). As a point of comparison, similar tests using a glass-ceramic seal alone between these materials resulted in seal failure after a single thermal cycle.

Results for OCV testing of a 2”x 2” seal compressed at 100 psi are shown in Figure 3. The OCV measurements were conducted using dilute moist hydrogen “fuel” vs. air, for which the

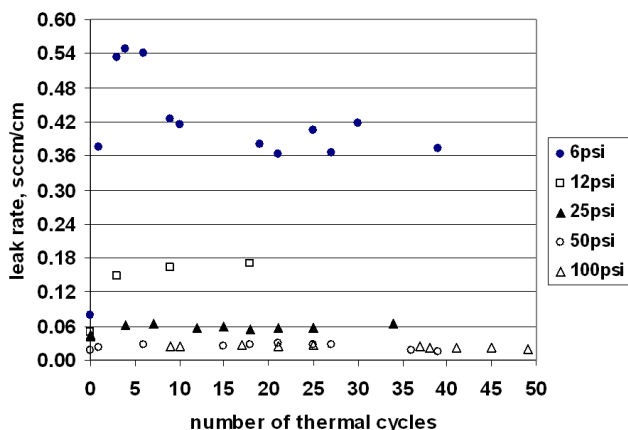


Figure 2. Leak Rates at 800°C of a 2'' x 2'' Hybrid Phlogopite Mica Seal Pressed under Various Compressive Loads

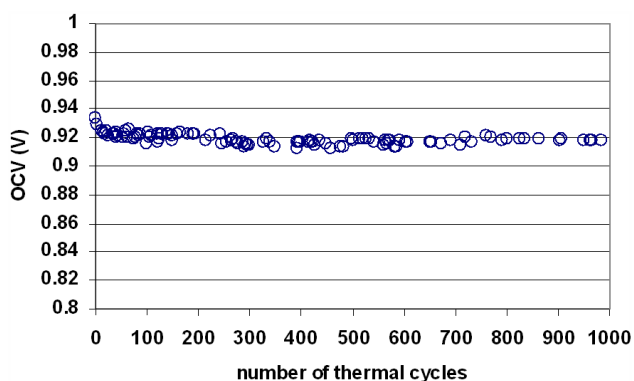


Figure 3. OCV Results for Thermal Cycle Tests on 2'' x 2'' 8YSZ Plate with Hybrid Phlogopite Mica Seal Compressed at 100 psi

calculated Nernst voltage at 800°C is 0.932-0.934 V. Over 1000 thermal cycles (heated from 100°C to 800°C in 30 minutes), the OCV decreased by less than 2%.

It should be noted that the leak rates shown in Figure 2 were measured at 2 psid; reduction of the pressure drop across the seal results in a linear decrease in leak rate. A typical example is shown in Figure 4 for a 2'' x 2'' hybrid Phlogopite mica pressed at 12.5 psi; the data in Figure 4 were taken after 19 thermal cycles. For pressure drops of 0.1-0.2 psid, the seal leak rate was ~0.02 sccm/cm.

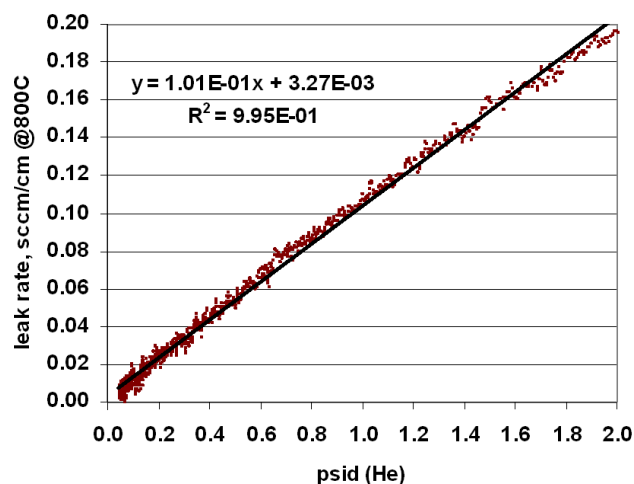


Figure 4. Effect of Differential Pressure on the Leak Rate of a 2'' x 2'' Hybrid Phlogopite Mica Seal Pressed at 12.5 psi; Measurement was taken after 19 thermal cycles

Conclusions

Inexpensive, easy-to-fabricate “hybrid” mica paper/glass compressive seals were found to offer stable, low leak rates under relatively low applied compressive stress during isothermal and thermal cyclic exposure conditions.

FY 2004 Publications

1. Y-S Chou, J. W. Stevenson, “Novel infiltrated Phlogopite mica compressive seals for solid oxide fuel cells,” *Journal of Power Sources* (in press) (2004).
2. Y-S Chou, J. W. Stevenson, “Long-term thermal cycling of Phlogopite mica based compressive seal for solid oxide fuel cells,” in *Developments in Fuel Cells and Lithium Ion Batteries, Ceramic Transactions* vol. 161 (2004), edited by Arumugan and Manthiram (in press).
3. Y-S Chou, J. W. Stevenson, “Infiltrated Phlogopite micas with superior thermal cycle stability as compressive seals for solid oxide fuel cells,” in *Developments in Fuel Cells and Lithium Ion Batteries, Ceramic Transactions* vol. 161 (2004), edited by Arumugan and Manthiram (in press).

FY 2004 Presentations

1. J. W. Stevenson, P. Singh, K. Meinhardt, L. Chick, C. Coyle, Y-S Chou, S. Weil, and G. Yang, "SOFC seals: technology challenges and status," 28th International Cocoa Beach Conference, Symposium II: International Symposium on Solid Oxide Fuel Cell Materials and Technology, Cocoa Beach, Florida, 2004.
2. Y-S Chou and J. W. Stevenson, "Long-term thermal cycling and open circuit voltage testing of Phlogopite mica-based compressive seals for solid oxide fuel cells," 106th Annual Meeting of the American Ceramic Society, Indianapolis, Indiana, April 18-22, 2004.
3. Y-S Chou and J. W. Stevenson, "Infiltrated Phlogopite micas with superior thermal cycle stability as the compressive seal for solid oxide fuel cells," 106th Annual Meeting of the American Ceramic Society, Indianapolis, Indiana, April 18-22, 2004.
4. Y-S Chou, J. W. Stevenson, and P. Singh, "Development of compressive seals for solid oxide fuel cells," SECA CTP Program Review, Boston, Massachusetts, May 11-13, 2004.

III.A.11 Reduction of Carbon Formation from Nickel Catalysts Using Nickel-Gold Surface Alloys

David L. King (Primary Contact), Yong Wang, Ya-Huei (Cathy) Chin, Robert Rozmiarek, Jianli (John) Hu

Pacific Northwest National Laboratory

P.O. Box 999

Richland, WA 99352

Phone: (509) 375-3908; Fax: (509) 375-2186; E-mail: david.king@pnl.gov

DOE Project Manager: Don Collins

Phone: (304) 285-4156; E-mail: Donald.Collins@netl.doe.gov

Objectives

- Develop methods to minimize carbon formation from nickel catalysts during hydrocarbon reformation
- Quantify effect of gold addition to nickel catalyst surface on catalyst activity and activity maintenance
- Identify role of gold in controlling nickel surface properties through surface characterization techniques
- Extend catalyst modification concepts to Ni anodes, enabling partial on-anode reforming of natural gas

Approach

- Baseline supported nickel catalyst (Ni/MgAl₂O₄) performance in reforming methane and butane
- Quantify effect of gold addition on carbon formation and reforming activity
- Develop analytical methodology to characterize nickel surface
- Verify methane reforming kinetics with Ni/YSZ (nickel/yttria-stabilized zirconia) anode
- Quantify effect of gold addition on carbon formation and reforming activity with nickel anode catalyst

Accomplishments

- Demonstrated that addition of gold to supported nickel catalyst at sub-monolayer coverage significantly retards carbon formation
- Showed that sufficient gold to retard carbon formation from nickel results in a decrease in catalyst activity of ~65-85%, and methane conversion is more affected by Au addition than butane conversion
- Determined that H₂ chemisorption provides the best method to correlate Ni availability with catalyst activity
- Identified a method based on N₂O chemisorption that may provide means to quantify step sites
- Determined that step site poisoning model does not fully explain results

Future Directions

- Obtain kinetic data for on-anode reforming to support model development
- Evaluate effect of gold addition to Ni/YSZ for methane reforming on activity and carbon formation
- Identify best methods for adding gold onto Ni/YSZ
- Evaluate effect of other additives to improve nickel anode performance (alkaline earth, Sn, Ce) as well as alloys such as Ni-Cu
- Evaluate efficacy of natural gas pre-reforming with modified Ni catalysts
- Measure activity of doped strontium titanate as sulfur-tolerant steam reforming catalyst

Introduction

The objective of this project is to determine whether alloying the surface of nickel catalysts with low concentrations of gold is an effective strategy to retard carbon formation under realistic conditions of catalyst operation for fuel reforming. The nickel-gold catalyst can be seen as a prototypical system which, when understood, could lead to alternate metal modifications of the nickel catalyst. Understanding the surface properties of the modified nickel catalyst is key to understanding and quantifying the activity and carbon resistance.

Of particular interest is the addition of gold to the nickel anode of the solid oxide fuel cell (SOFC). There is a desire to carry out on-anode reforming of natural gas directly on the anode, reducing or eliminating a pre-reformer, but carbon formation is a concern. Moreover, steam reforming on the anode is an endothermic process, and a highly active anode may develop severe temperature gradients. Therefore, reducing the activity of the anode toward steam reforming is desirable. Addition of gold to the nickel anode is attractive due to its ability to reduce carbon formation and catalyst activity.

Approach

A test reactor system was developed for steam reforming of supported nickel catalysts. The activity and activity maintenance of the catalysts in reforming both butane and methane were quantified and correlated with available nickel surface sites. The effect of addition of gold at various concentrations was also quantified in terms of activity and activity maintenance. Other tools were used to quantify the amount of carbon produced on these catalysts. Various surface analysis methods were evaluated to identify means to characterize the nickel surface, in order to both determine total available sites as well as distinguish unique sites such as step sites.

Recent research by the team has focused on quantifying the activity of the nickel SOFC anode toward methane steam reforming. This work was carried out in collaboration with core technology personnel with expertise in modeling. Our catalyst testing results will provide kinetic data for a model

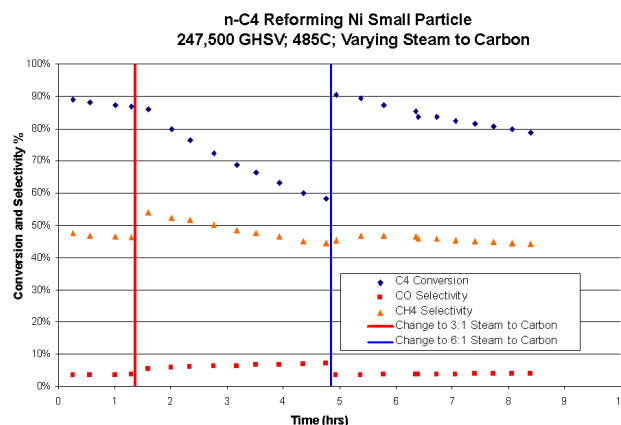


Figure 1. Supported Nickel Catalyst Shows Rapid Deactivation in Butane Reforming

that will be used to predict thermal gradients on the catalyst as a result of methane on-anode reforming using a conventional nickel anode. Significant effort was expended to make sure that the kinetic data were free of heat and mass transport limitations. This model will provide guidance regarding necessary nickel anode activity reduction in order to reduce thermal gradients across the anode surface. Research on the effect of addition of gold to the nickel anode on reduction in steam methane reforming was begun, and preliminary activity data obtained.

Results

Initial studies quantified the activity and deactivation of a supported nickel catalyst of defined crystallite size toward butane reforming at high flow rate (space velocity) and relatively low temperature. This work was done to corroborate previously published studies^{1,2} and to quantify the effect of gold addition on activity. Initial performance is shown in Figure 1, which shows activity decline at 485°C with both 6:1 and 3:1 steam:carbon (S/C) ratios. The activity could be recovered by a one-hour steam/hydrogen treatment. Figure 2 shows the effect of addition of 0.4 wt.% gold to the nickel catalyst on activity and activity maintenance. This shows clearly that the conversion was essentially stable over several hours for both 6:1 and 3:1 S/C ratios, although at lower steam content (S/C = 1.5), some decline in activity was observed. A decrease in activity by at least a factor of 3 was observed following gold addition. Figure 3 shows the effect of gold addition on steam reforming of methane over

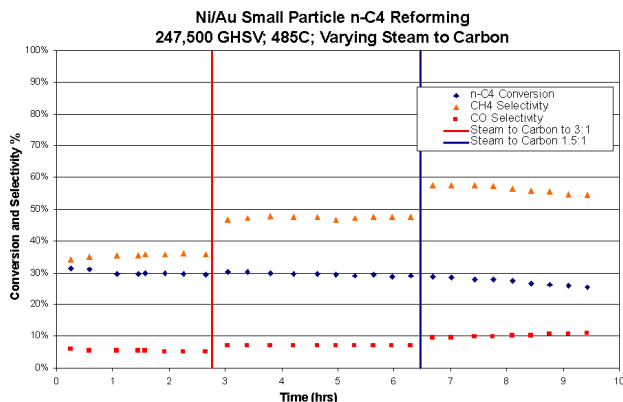


Figure 2. Addition of 0.4% Gold to Nickel Catalyst Eliminates Deactivation by Carbon Formation

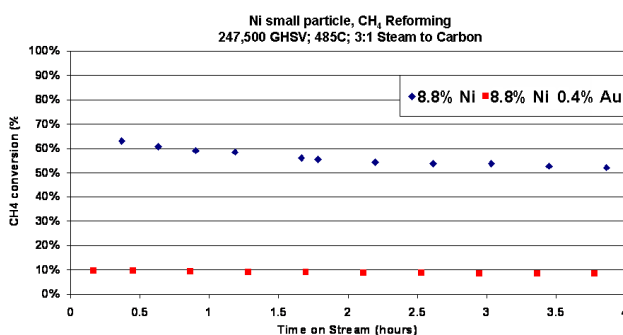
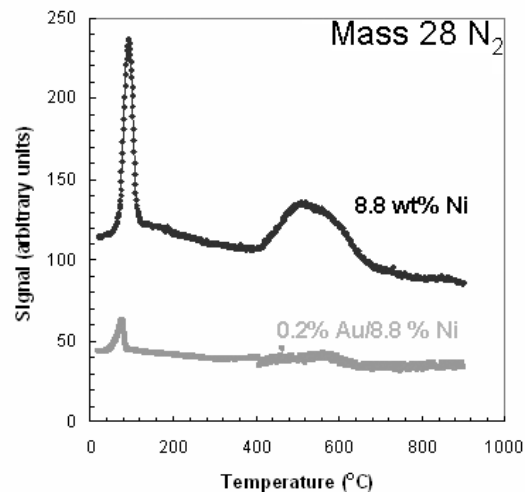


Figure 3. Effect of Gold Addition to Nickel Catalyst on Steam Reforming of Methane

this same catalyst (8.8% Ni/MgAl₂O₄). Again, addition of gold at 0.4 wt.% substantially retards deactivation on the nickel catalyst. In this case, the reduction in activity is at least a factor of 6, a greater reduction than in the case of butane.

One of the challenges in adding gold (Au) to nickel is to determine the location of gold and its form, i.e. is it on the nickel or is it simply on the support, and if on the nickel is it present as single atoms or aggregates. We used x-ray photoelectron spectroscopy (XPS) to establish the presence of Au on the surface of a 15.8 wt.% Ni/MgAl₂O₄ catalyst by showing a decrease in the nickel signal that is greater than would be expected if a bulk alloy formed or if gold were not associated with nickel. Hydrogen chemisorption measures the available surface nickel. Addition of gold drastically reduces the apparent nickel surface area, probably by altering the adsorption properties of the adjacent nickel sites by electronic effects. The decrease in activity for both



	N ₂ O	N ₂
Ni	9583	3500
Ni-Au	3430	366

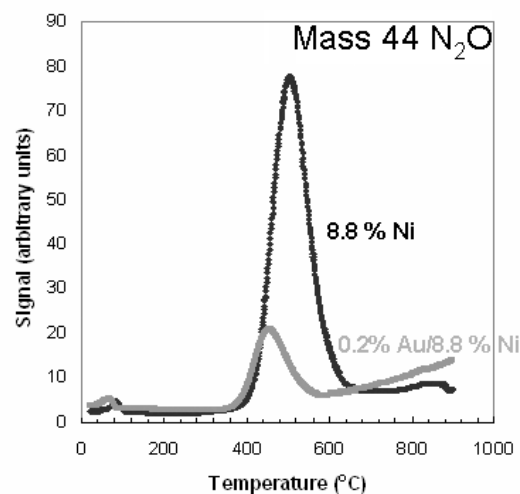


Figure 4. N₂O TPD over 8.8% Ni-0.2% Au/MgO-Al₂O₃ Catalyst

butane and methane reforming on addition of gold correlates with the decrease in hydrogen chemisorption property.

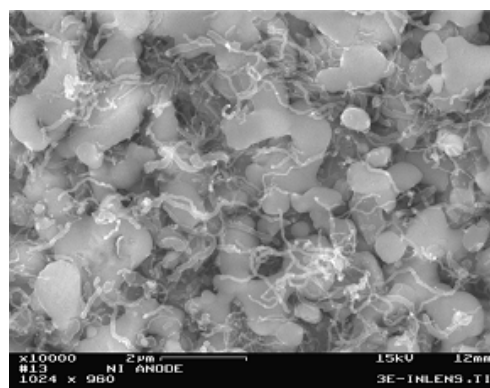
Attempts to characterize specific Ni surface sites have focused on the adsorption of nitrous oxide (N₂O) on both nickel and nickel-gold catalysts. N₂O may physically adsorb on nickel sites, or it may dissociate, with the oxygen forming a surface metal oxide site, and release nitrogen gas (N₂, mass 28). Highly active sites are expected to dissociate N₂O, whereas less active sites on nickel may simply chemisorb the N₂O molecule intact. Figure 4

compares the N_2 and N_2O signals following interaction and temperature-programmed desorption (TPD) from the surface of a 8.8 wt.% Ni/MgAl₂O₄ catalyst with and without 0.2 wt.% Au. The 8.8% Ni sample shows significant peak intensity for both N_2O and N_2 . Addition of 0.2 wt.% Au decreases both peaks, but the N_2 peak is more severely reduced, which is consistent with gold preferentially depositing on the most active nickel sites. We continue to investigate N_2O TPD as a method to characterize the nickel surface.

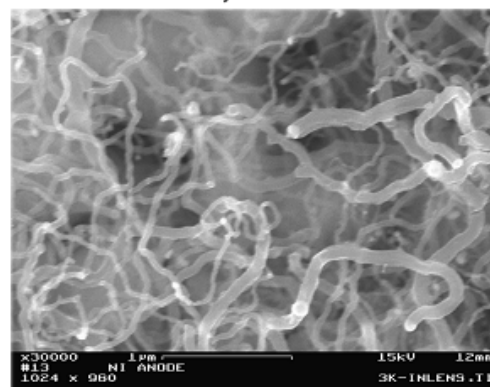
On-anode reforming of natural gas is a challenge, especially due to the presence of higher hydrocarbons in addition to the methane. Preliminary studies of butane reforming verified this challenge. We have observed deactivation through carbon formation even at S/C ratios as high as 6/1. The deposition of carbon on the anode is easily observed visually. Figure 5 shows that the carbon formed from reforming of butane on the Ni/YSZ anode is primarily filamentary carbon (carbon nanotubes). The bright spot in the lowermost picture, taken at 50,000 magnification with backscattering, indicated that a small particle of nickel is located at the tip of the filament. This is consistent with carbon growth proceeding from the base of the nickel particle and displacement of the particle from the surface of the anode.

Conclusions

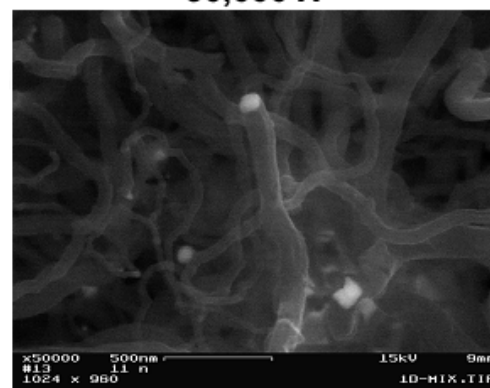
- Carbon formation can occur with nickel-based catalysts, even when thermodynamics predict that carbon should not be formed. This is a result of competing kinetics between carbon deposition and removal.
- Addition of gold to the surface of a nickel catalyst results in significantly retarding deactivation through carbon formation, simultaneously decreasing reforming activity. The effect of gold addition on the decrease in methane steam reforming appears to be greater than the effect on higher hydrocarbon (butane) reforming.
- Hydrogen chemisorption appears to be the best method to characterize the available surface of nickel catalyst, in order to correlate surface sites with catalytic activity. This is true of both Ni and Ni/Au catalysts. Addition of gold to the nickel



10,000 X



30,000 X



Back Scattered Image + SE
Image 50,000 X

Figure 5. Scanning Electron Micrograph of Spent Ni-YSZ Anode Shows Presence of Filamentary Carbon and Evidence for Nickel at Tip of Carbon Filament

surface significantly retards chemisorption of gases such as H_2 and N_2O .

- N_2O adsorption followed by temperature-programmed desorption appears to be a promising

method to distinguish between and quantify highly active and less active Ni surface sites.

References

1. H.S. Bengaard, J.K. Norskov, J. Sehested, B.S. Clausen, L.P. Nielsen, A.M. Molenbroek, J.R. Rostrup-Nielsen; "Steam Reforming and Graphite Formation on Ni Catalysts". *J. Catalysis* 209 (2002) 365-384.
2. F. Besenbacher, I. Chorkendorff, B.S. Clausen, B. Hammer, A.M. Molenbroek, J.K. Norskov, I. Stensgaard; "Design of a Surface Alloy Catalyst for Steam Reforming". *Science* 279 (1998) 1913.

FY 2004 Publications/Presentations

1. David L. King, Yong Wang, Ya-Huei (Cathy) Chin, Robert Rozmiarek, John Hu; Reduction of Carbon Formation From Nickel Catalysts Using Nickel-Gold Surface Alloys. Presented at SECA Core Technology Program Review Meeting, Albany NY, October 1, 2003.
2. David L. King, Yong Wang, Ya-Huei (Cathy) Chin, Robert Rozmiarek, John Hu; Reduction of Carbon Formation From Nickel Catalysts Using Nickel-Gold Surface Alloys. Presented at SECA Core Technology Program Review Meeting, Boston MA, May 12, 2004.
3. Ya-Huei (Cathy) Chin, David L. King, Yong Wang, Robert Rozmiarek, John Hu; Surface Modification Of Supported Nickel Catalysts For Steam Reforming Of Hydrocarbons. Presented at the 26th Annual Symposium on Applied Surface Analysis, Pacific Northwest National Laboratory, Richland WA, June 17, 2004.

III.A.12 SOFC Anode Materials Development at PNNL

Olga Marina (Primary Contact), Jeff Stevenson

Pacific Northwest National Laboratory

P.O. Box 999, MS K2-44

Richland, WA 99352

Phone: (509) 375-2337; Fax: (509) 375-2186; E-mail: Olga.Marina@pnl.gov

DOE Project Manager: Lane Wilson

Phone: (304) 285-1336; E-mail: Lane.Wilson@netl.doe.gov

Objectives

- Develop solid oxide fuel cell (SOFC) anode compositions which will satisfy advanced anode requirements including redox tolerance, sulfur tolerance, and carbon tolerance while offering low polarization losses and long-term stability.
- Improve understanding of mechanisms affecting anode performance, including both intrinsic factors (e.g., composition, microstructure) and extrinsic factors (e.g., S poisoning).

Approach

- Synthesize, process, and characterize candidate SOFC anode compositions.
- Utilize carefully controlled SOFC testing (half-cell and full-cell) to quantify performance of anode compositions under SOFC exposure conditions.
- Evaluate effects of redox cycling and exposure to sulfur compounds and hydrocarbon fuels on anode performance.

Accomplishments

- Demonstrated improved sulfur tolerance for Pacific Northwest National Laboratory's (PNNL's) ceramic composite anode relative to traditional nickel/yttria-stabilized zirconia (Ni/YSZ) SOFC anodes.
- Improved understanding of roles played by ceria and titanate phases in composite anode.

Future Directions

- Evaluate performance and stability of ceramic anode in various hydrocarbon fuels.
- Improve mechanistic understanding of effects of sulfur and carbon on anode performance.

Introduction

The current state-of-the-art anode material is a Ni/YSZ cermet (a composite of Ni metal and YSZ ceramic). Overall, this material offers many good properties, including high electrical and thermal conductivity, reasonable thermal expansion, and chemical and dimensional stability in the fuel gas environment. While Ni/YSZ is satisfactory for cells operating on clean, reformed fuel, advanced SOFC designs are likely to place additional constraints on the anode, such as tolerance of highly oxidizing

environments and/or the capability of tolerating significant quantities of sulfur and/or hydrocarbon species in the fuel stream. Ni/YSZ anodes are not stable in oxidizing environments at high temperature. To simplify SOFC system requirements, it is desirable that the anode material be stable not only while exposed to the fuel environment during operation, but also when exposed to more oxidizing conditions (i.e., air) during system startup and shutdown.

Previous work at PNNL has resulted in the development of a promising 2-phase ceramic anode based on a mixture of doped strontium titanate and doped ceria. Optimized compositions in this system offer excellent dimensional and chemical stability during redox cycling, appropriate coefficient of thermal expansion (CTE), and good electrocatalytic activity towards hydrogen reduction. Stable performance with 25 ppm H₂S present in a hydrogen fuel stream was also demonstrated.

Approach

Composite ceramic anode powders in the Sr-La-Ti-Ce-O system were prepared (both by single-step co-synthesis and by mixing separately prepared powders) by glycine/nitrate combustion synthesis. The powders were calcined and then attrition milled to reduce the average particle size to less than 0.5 μm . The resulting powders were characterized by dilatometry, x-ray diffraction (XRD), energy dispersive spectroscopy (EDS), scanning electron microscopy (SEM), and transmission electron microscopy (TEM). Electrode inks were prepared by mixing the powder with a commercial binder in a 3-roll mill, and then screen-printed in a circular pattern onto YSZ pellets or membranes. The screen-printed electrodes were sintered in air at 900-1000°C. A platinum paste current collector grid was screen-printed on the top of the electrode.

The cells were mounted between two vertical alumina tubes and isolated from the environment by sealing with gold rings when heated to 900°C in air. After that, fuel was introduced into the anode compartment to reduce the anode. The opposite side of the cell was supplied with air. Experiments were performed at atmospheric pressure in the temperature range 550-900°C. Electrochemical measurements were carried out using a Solartron 1280 frequency response analyzer in combination with a Solartron 1286 potentiostat or an Arbin BT4 potentiostat.

Results

Electrolyte-supported single cells (160 μm 8YSZ electrolyte) with ceramic anodes were tested in fuel gas containing 290-1000 ppm H₂S over 500 hours; results are shown in Figures 1-3. It was found that

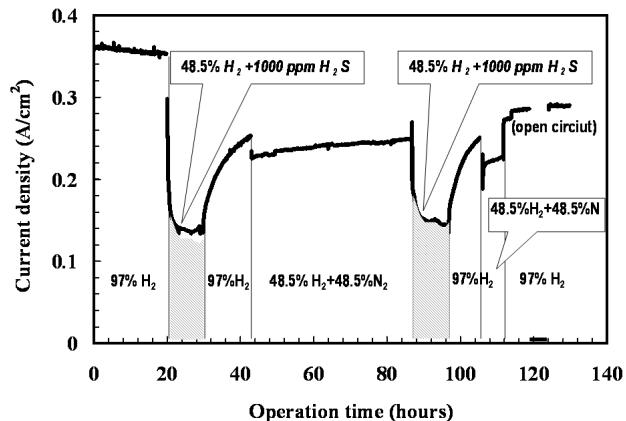


Figure 1. Effect of H₂S additives on performance of the 160- μm YSZ electrolyte-supported cell with La-doped SrTiO₃/La-doped ceria composite anode (prepared in one synthesis step) and lanthanum strontium ferrite (LSF20) cathode with a samarium-doped ceria (SDC) interlayer. T=850°C. Cell voltage = 0.7 V.

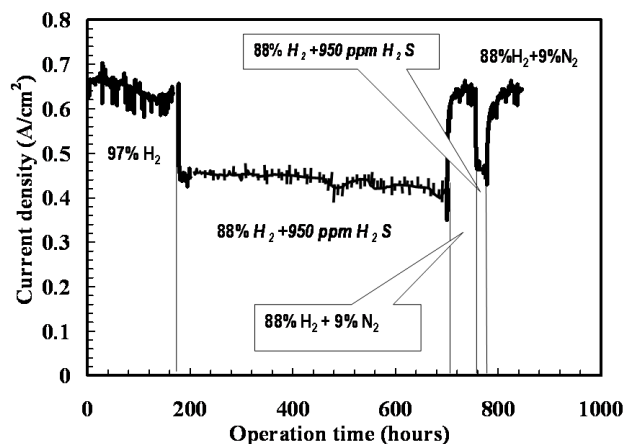


Figure 2. Effect of H₂S additives on performance of the 160- μm YSZ electrolyte-supported cell with a La_{0.35}Sr_{0.65}TiO₃/Ce_{0.7}La_{0.3}O_{1.85} composite anode (prepared by mixing of the oxides in a 7:3 mole ratio) and LSF20 cathode with a SDC interlayer. T=850°C. Cell voltage = 0.3 V.

the cell performance decreased by 40% in the presence of 1000 ppm H₂S (Figure 1) at a cell voltage of 0.7 V, by 30% in the presence of 950 ppm of H₂S at a cell voltage of 0.3 V (Figure 2), and by only 9% in the presence of 280 ppm of H₂S at a cell voltage of 0.3 V (Figure 3). When H₂S was removed from the fuel stream, the composite anodes self-recovered without requiring cleaning with either hot

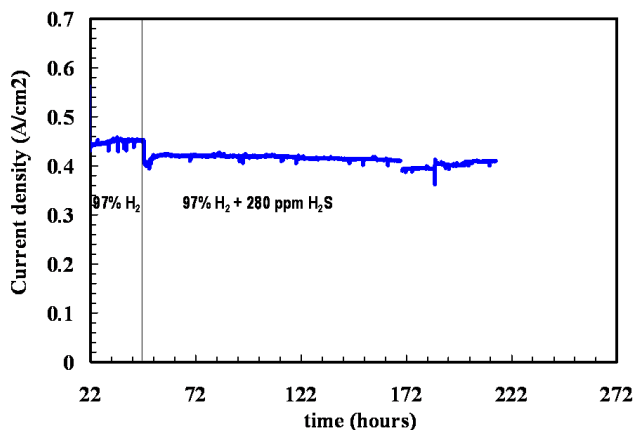


Figure 3. Effect of H₂S additives on performance of the 160- μ m YSZ electrolyte-supported cell with a La_{0.35}Sr_{0.65}TiO₃/Ce_{0.5}La_{0.5}O_{1.75} composite anode (prepared by mixing of the oxides in a 5:5 mole ratio) and LSF20 cathode with a SDC interlayer. T=850°C. Cell voltage = 0.3 V.

air or hot steam. Visually, no sulfur deposits were found on the anodes after cooling in H₂. Some yellowish deposits were found on the alumina test fixture. After returning to clean moist hydrogen, some performance decrease (up to 18%) was noticed. This degradation may be related to: i) Pt current collector poisoning due to Pt_xS formation (visual color change was observed), ii) partial Pt current collector delamination from the anode, iii) ceramic anode degradation in the presence of H₂S, and/or iv) cathode degradation with time. It should be noted that no degradation in the anode performance with time in wet hydrogen was observed in half-cell measurements.

Conclusions

Composite ceramic anodes show better stability of performance than Ni/YSZ anodes when H₂S is present in the fuel stream. Studies are in progress to more fully ascertain the conditions under which performance degradation occurs, and the specific mechanisms which lead to degradation.

FY 2004 Publications/Presentations

1. OA Marina, MS Walker, JW Stevenson, "Development of Ceramic Composites as SOFC Anodes," in 2003 Fuel Cell Seminar: Fuel Cells - Reliable, Clean Energy, November 3-7, 2003, Miami Beach, Florida. pp. 340-343. Fuel Cell Seminar, Washington, DC.
2. OA Marina, JW Stevenson, LR Pederson, "Development of Ceramic Composites as SOFC Anodes," Invited speaker at 55th Pacific Coast Regional & Basic Science Division Meeting of the American Ceramic Society, October 20, 2003, Oakland, CA.
3. OA Marina, "Development of Advanced SOFC Anodes," presented at the SECA Core Technology Program Review Meeting, May 11-13, 2004, Boston, MA.

III.A.13 SOFC Cathode Materials Development at PNNL

Steve Simner (Primary Contact), Mike Anderson, Jeff Stevenson

Pacific Northwest National Laboratory

P.O. Box 999, MS K2-44

Richland, WA 99352

Phone: (509) 375-4577; Fax: (509) 375-2186; E-mail: steven.simner@pnl.gov

DOE Project Manager: Lane Wilson

Phone: (304) 285-1336; E-mail: Lane.Wilson@netl.doe.gov

Objectives

- Develop solid oxide fuel cell (SOFC) cathode materials and microstructures offering low polarization losses and long-term stability at intermediate SOFC operating temperatures (650-800°C).
- Improve understanding of mechanisms affecting cathode performance, including both intrinsic factors (e.g., composition, microstructure) and extrinsic factors (e.g., Cr poisoning).

Approach

- Synthesize, process, and characterize candidate SOFC cathode compositions.
- Utilize carefully controlled SOFC testing to quantify performance of SOFC cathode materials on anode-supported cells.
- Evaluate effects of various interconnect alloys and Cr sources on cathode performance.

Accomplishments

- Developed an improved button cell test fixture design. Evaluated effects of alloy interconnect materials on cathode performance.
- Evaluated effects of Cr vapor species on cathode performance.

Future Directions

- Complete investigation into effects of alloy oxide scale composition on cathode performance.
- Investigate effects of cathode/contact layer chemistry and microstructure on Cr poisoning.
- Improve understanding of cathode “burn-in” phenomenon during initial cell operation.

Introduction

Minimization of electrode polarization processes (especially cathodic polarization) represents one of the greatest challenges to be overcome in obtaining high, stable power densities from SOFCs. Cathodic polarization exhibits a high activation energy relative to the other internal power losses (e.g., electrolyte ohmic losses), so the need to improve cathode performance becomes increasingly important as the targeted SOFC operating temperature is reduced. The severe environmental conditions experienced by the cathode during operation greatly reduce the

number of likely candidate materials. In particular, the cathode material must be stable at the SOFC operating temperature in air, and it must have high electronic conductivity, high catalytic activity for oxygen molecule dissociation and oxygen reduction, and a thermal expansion compatible with the SOFC electrolyte (usually yttria-stabilized zirconia, YSZ). Chemical interactions with the electrolyte and interconnect materials must be minimal. In addition, the cathode material must have a porous microstructure so that gaseous oxygen can readily diffuse through the cathode to the cathode/electrolyte interface. This porous morphology must remain

unchanged during SOFC operation over the lifetime of the cell.

For high-temperature SOFCs operating at around 1000°C, the preferred cathode material is Sr-doped lanthanum manganite, LSM, which offers adequate electrical conductivity and electrocatalytic activity, reasonable thermal expansion, and stability in the SOFC cathode operating environment. For SOFCs operating at substantially lower temperatures, such as 650-800°C, alternative cathode materials may be required, since lanthanum manganite does not appear to be a satisfactory choice due (at least in part) to its low ionic conductivity and slow surface oxygen exchange kinetics. Alternative perovskite compositions—typically containing La on the A site and transition metals such as Co, Fe, and/or Ni on the B site—have received attention. In general, they offer higher oxygen ion diffusion rates and exhibit faster oxygen reduction kinetics at the electrode/electrolyte interface than lanthanum manganite. In recent years, Pacific Northwest National Laboratory (PNNL) has developed an optimized Sr-doped lanthanum ferrite (LSF) cathode which delivers high power density in anode-supported cells (~1.2 W/cm² at 800°C and ~0.8 W/cm² on button cells at 750°C; measured at 0.7 V; fuel is 97% H₂/3% H₂O; oxidant is air; low fuel and air utilization). In recent work at PNNL, interactions between candidate SOFC cathode materials (LSM and LSF) and a state-of-the-art interconnect alloy (Crofer22APU) were evaluated using single-cell electrochemical testing, x-ray diffraction (XRD), and scanning electron microscopy/energy dispersive x-ray (SEM/EDS). The effects of Cr vapor species on these cathode materials were also investigated.

Approach

Cathode powders were synthesized using the glycine-nitrate combustion technique. The powders were processed to obtain the desired particle size distribution, and then applied to anode-supported YSZ membranes with a samarium-doped ceria (SDC) interlayer. The resulting cells were placed into test fixtures, and current-voltage data were recorded from 700-850°C. For long-term tests, the cells were held at 0.7 V and periodically subjected to current sweeps from 0-7 A. A mixture of 97% H₂-3% H₂O was flowed to the anode at 200 sccm, and

air to the cathode at 300 sccm. For alloy interaction tests, alloy current collectors were used on the cathode side (tests were also performed with Pt current collectors to provide an idealized performance baseline). After cell tests were completed, the cells were analyzed by SEM/EDS. Cathode material/alloy interactions were also studied using high-temperature XRD (HTXRD).

Results

Significant degradation of performance was observed when a commercial SOFC interconnect alloy (Crofer22APU) was used as the cathode current collector in a newly designed button cell fixture. (The primary advantage of this new test fixture over conventional button cell fixtures lies in the fact that it does not depend on expensive (and unrealistic) sintered platinum cathode current collectors. Instead, it utilizes actual candidate current collector materials for SOFC stacks, thereby providing a means of assessing interactions between interconnect, contact, and cathode materials). Degradation was not observed when Pt was used as the current collector. Potential sources of degradation include solid-state reaction of the alloy oxide scale (Cr₂O₃ and (Mn,Cr)₃O₄ spinel) with the cathode material, and reaction of volatile Cr species with the cathode material. While both cathode materials showed a significant decrease in performance over a relatively limited period of operation, the mechanisms of the degradation appear to vary from one cathode material to another.

LSF Cathode. Figure 1 indicates cell performance data utilizing an LSF-20 cathode with a Crofer cathode current collector at 750°C and 0.7 V. The data is compared to a similar cell with a Pt current collector. The Crofer-containing cell indicated rapid degradation in performance, whereas the sample utilizing the Pt current collector showed typical performance characteristics for LSF-based cells (cell conditioning over 100-200 hours followed by stable performance). SEM/EDS analysis of the tested cathode revealed Cr distributed throughout the LSF cathode and also in the SDC interlayer. HTXRD of an LSF-20 film on Crofer foil during heating in air at 800°C for 72 hours indicated the formation of a high Fe-containing oxide (SrFe₁₂O₁₉). These results suggest that the Cr diffuses into the

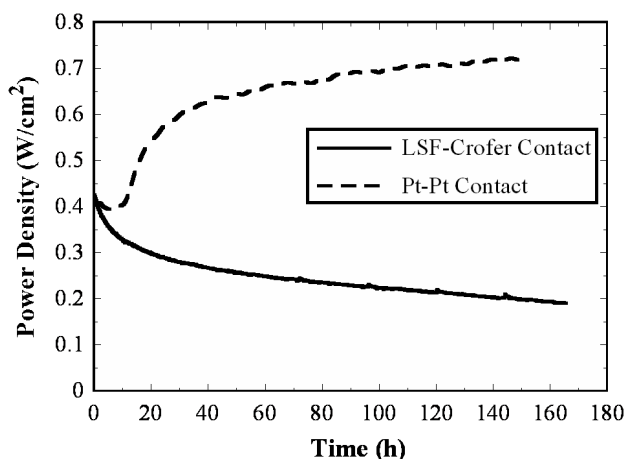


Figure 1. Test Results for Cells with LSF Cathode

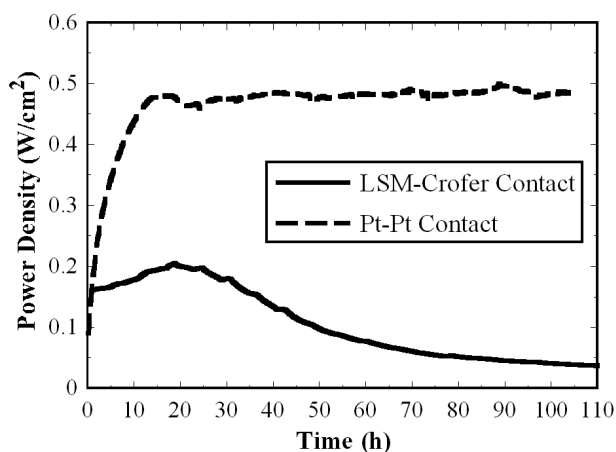


Figure 2. Test Results for Cells with LSM Cathode

LSF perovskite, where it presumably displaces Fe cations on B sites in the ABO_3 lattice structure.

LSM Cathode. Figure 2 indicates cell performance data for LSM/Crofer and LSM/Pt cells; again, there was significant disparity between the two samples. Without the Crofer alloy, LSM indicated a typical conditioning effect followed by stable performance of ~ 500 mW/cm². When Crofer was utilized as the cathode current collector, an initial “burn-in” was also observed, but within 20 hours of testing the cell began to severely degrade. SEM/EDS analysis of the tested cathode revealed no discernible Cr within the LSM cathode, but within the SDC-20 interlayer, as much as 5 atomic % Cr was detected. HTXRD indicated no discernible reaction products between the Crofer foil and LSM cathode

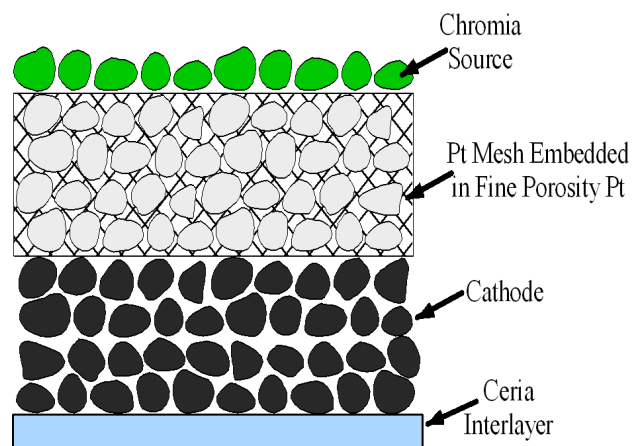


Figure 3. Schematic Illustration of Test Configuration for Cr Vapor Tests

even after 120 hours at 800°C. Adjacent to the Crofer wire, approximately 1-2 atomic % Cr was apparent, and SEM did indicate a segregated high Cr phase (possibly $SrCrO_4$).

Cr Vapor Tests. Tests evaluating the effect of Cr vapor species on cathode performance were performed by physically separating the Cr vapor source (Cr_2O_3 , $MnCr_2O_4$, or Sr-doped lanthanum chromite) from the cathode (test configuration shown schematically in Figure 3). Preliminary results found that degradation rates were dependent on the Cr source ($Cr_2O_3 > MnCr_2O_4 > Sr$ -doped lanthanum chromite). It is believed that this trend in degradation rate correlates with the Cr volatilization rate for each source. Cr_2O_3 is known to exhibit higher Cr volatilization rates than lanthanum chromite, and tentative calculations indicate that $MnCr_2O_4$ has a volatilization rate intermediate between the other oxides.

Conclusions

The performance of LSM and LSF cathodes at intermediate temperatures can be affected by the presence of Cr-containing materials (alloys and oxides). Both solid-state and vapor-phase interactions have been observed for cells tested with a commercial Cr-containing interconnect alloy. Studies are in progress to more fully ascertain the conditions under which performance degradation occurs and the specific mechanisms which lead to degradation.

FY 2004 Publications/Presentations

1. M.D. Anderson, J.W. Stevenson and S.P. Simner, "Reactivity of Lanthanide Ferrite SOFC Cathodes with YSZ Electrolyte," *Journal of Power Sources*, **129** [2] (2004) 188.
2. S.P. Simner, M.D. Anderson and J.W. Stevenson, "La(Sr)FeO₃ Cathodes with Marginal Cu Doping," *J. Am. Ceram. Soc.*, in press (2004).
3. S.P. Simner, J.F. Bonnett, M.D. Anderson and J.W. Stevenson, "Low Temperature Sinterability of La(Sr)FeO₃ Cathodes on YSZ," *Solid State Ionics*, in press (2004).
4. S.P. Simner, J.F. Bonnett, M.D. Anderson and J.W. Stevenson, "Enhanced Low Temperature Sintering of (Sr, Cu) Doped Lanthanum Ferrite Cathodes," *Solid State Ionics*, in press (2004).
5. S.P. Simner, M.D. Anderson and J.W. Stevenson, "Development of Anode-Supported SOFCs and Low Temperature Cathodes," 2003 Fuel Cell Seminar, Miami Beach, Florida, November 3-7, 2003.
6. S.P. Simner, J.F. Bonnett, M.D. Anderson and J.W. Stevenson, "Lanthanum Ferrite Cathode Development at PNNL," 2003 ASM Materials Solutions Conference and Exposition, Pittsburgh, Pennsylvania, October 13-15, 2003.

III.A.14 SOFC Interconnect Materials Development at PNNL

Zhenguo "Gary" Yang (Primary Contact), Guanguang Xia, Prabhakar Singh, and Jeff Stevenson

Pacific Northwest National Laboratory

P.O. Box 999, MS K2-44

Richland, WA 99352

Phone: (509) 375-3756; Fax: (509) 375-2186; E-mail: zgary.yang@pnl.gov

DOE Project Manager: Lane Wilson

Phone: (304) 285-1336; E-mail: Lane.Wilson@netl.doe.gov

Objectives

- Develop cost-effective, optimized materials for intermediate-temperature solid oxide fuel cell (SOFC) interconnect and interconnect/electrode interface applications.
- Identify and understand degradation processes in interconnects and interconnect/electrode interfaces.

Approach

- Screening study of conventional and newly developed alloys (chemical properties, electrical properties, mechanical properties, cost).
- Investigation of degradation of alloy interconnect materials and their interfaces under SOFC operating conditions.
- Development of improved interconnect materials (surface modification, bulk modification, cathode/interconnect contact materials).

Accomplishments

- Completed dual atmosphere oxidation study on selected Ni-based alloys.
- Evaluated effects of moisture on oxidation of Crofer22APU ferritic stainless steel.
- Evaluated compatibility and electrical resistance of cathode/contact paste/interconnect components.

Future Directions

- Evaluate dual atmosphere oxidation of alloys using simulated reformat on fuel side.
- Complete study evaluating electrical properties and chemical stability of cathode/contact paste/interconnect structures.
- Develop optimized protective oxide layers to minimize electrical resistance and Cr volatility at surfaces of alloy-based interconnects.

Introduction

With the reduction in SOFC operating temperatures, low-cost, high-temperature oxidation alloys have become promising candidates to replace lanthanum chromite, a ceramic that can withstand operating temperatures in the 1000°C range. To improve the understanding of the advantages and limitations of alloy interconnects, Pacific Northwest National Laboratory (PNNL) has been engaged in

systematic screening studies to identify and evaluate potential candidate materials and to examine in detail the materials issues that must be resolved. These issues include chromia scale evaporation; scale electrical resistivity in the long term; corrosion under interconnect dual exposure conditions; and scale adherence and compatibility with the adjacent components, such as seals, electrodes and/or electrical contact layers.

Approach

Following earlier work on ferritic stainless steels, the oxidation behavior of nickel-based alloys was investigated under SOFC interconnect dual exposures. Specifically, the alloy samples were exposed to flowing moist air (~3% water) and moist hydrogen (also ~3% water) at 800°C in a specially designed dual atmosphere test apparatus for 300 hours. After testing, the scale morphology, chemistry, and elemental distributions were studied via x-ray diffraction (XRD), scanning electron microscopy (SEM), and energy dispersive spectroscopy (EDS), and compared with standard test samples exposed to air only at 800°C. To study the effects of water vapor in air on the oxidation behavior of Crofer22APU under single and dual exposures, a coupon was oxidized under moist hydrogen vs. moist air exposure. For alloy/cathode compatibility studies, reaction couples and electrical resistance couples were prepared and tested in air at elevated temperatures.

Results

The work on oxidation behavior of selected nickel-based chromia-forming alloys (Haynes230, Hastelloy S, and Haynes242) under the hydrogen/air dual environment indicated that the dual exposure led to an oxidation behavior on the air side that differed from that observed in air only, while the oxidation behavior on the fuel side was similar to that found in fuel only. However, unlike ferritic stainless steels that often suffer localized attack at the air side via accelerated growth of iron oxide nodules, a uniform scale was observed on Hastelloy S after a duration of 300 hours at 800°C under dual exposure conditions (Figures 1 - 3). The dual atmosphere exposure produced a uniform, fine chromia-dominated scale at the air side that also contained a small amount of spinel. In comparison, the scale grown on the sample that was exposed to moist air at both sides appeared less uniform, and NiO was also observed in the scale.

Similar behavior was also observed for Haynes230 under the hydrogen/air dual environment. A uniform chromia-dominated scale grew on the air side and contained a small amount of spinel. In comparison, the scale grown on a sample

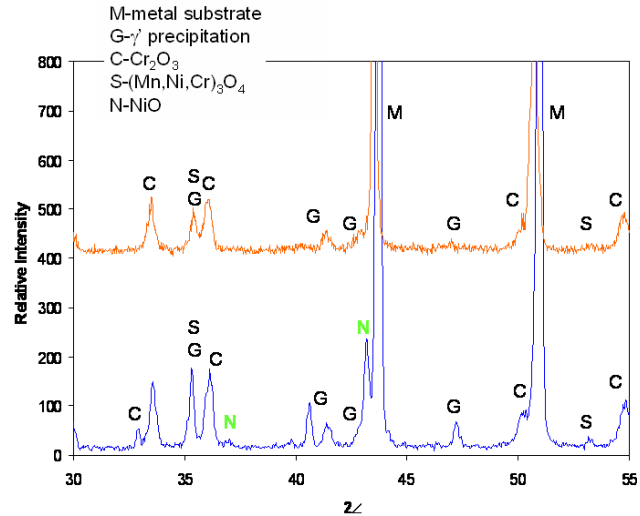


Figure 1. XRD Pattern of the Airside Scale Grown on Hastelloy S after Oxidization at 800°C for 300 Hours under a Moist Hydrogen/Moist Air Dual Exposure, Compared with Scale Grown in Air Only

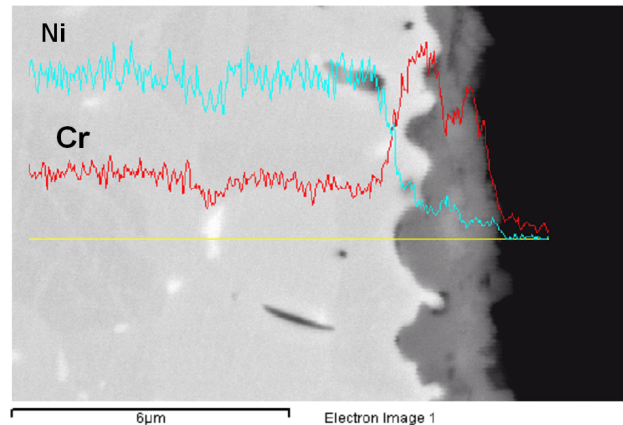


Figure 2. SEM Micrograph of the Airside Scale Grown on Hastelloy S after Oxidization at 800°C for 300 Hours under a Moist Hydrogen/Moist Air Dual Exposure

that was exposed to air on both sides appeared less uniform, with occasional regions of NiO as a top layer of the scale.

For Haynes242, XRD indicated that the scale grown on the sample that was exposed to moist air at both sides was less uniform and contained more NiO than the scale grown on the air side under dual atmosphere exposure. Overall, it appears that, for

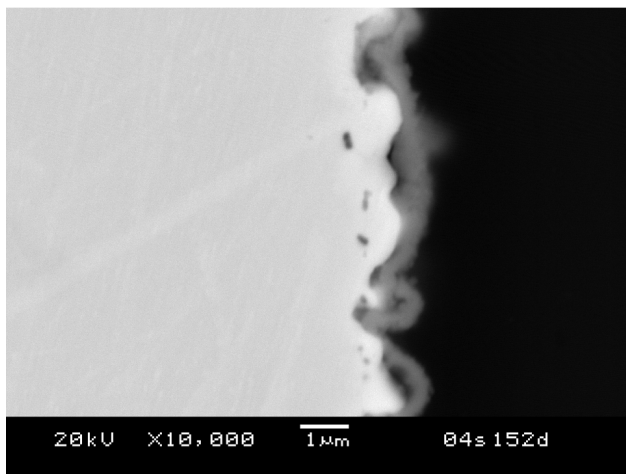


Figure 3. SEM Micrograph of the Airside Scale Grown on Hastelloy S after Oxidization at 800°C for 300 Hours in Moist Air Only

Ni-based superalloys with sufficient chromium, e.g. Haynes230 and Hastelloy S, dual exposure tends to facilitate the formation of a uniform chromia-dominated scale.

For Crofer22APU, a ferritic stainless steel, it was found that the scale grew homogeneously on the air side of Crofer22APU during the isothermal oxidation under moist hydrogen/air dual environment at 800°C, but contained a significant amount of iron in the top spinel layer, i.e. $(\text{Mn,Cr,Fe})_3\text{O}_4$. When the air (ambient, containing 1% H_2O) was replaced by moist air (3% H_2O) on the air side (i.e. moist hydrogen/air dual environment), the increased water partial pressure on the air side further accelerated the anomalous oxidation, resulting in nucleation and growth of hematite in the scale that led to a localized attack. In contrast, a uniform scale comprised of chromia-rich sublayer and $(\text{Mn,Cr})_3\text{O}_4$ spinel top layer was observed on the Crofer22APU sample that was exposed to moist air at both sides.

Studies on the chemical compatibility between cathode/contact paste/interconnect components indicated that, among different perovskites, lanthanum manganite facilitates formation of a spinel layer at the contact interface which acts as a barrier to mitigate Cr migration into the perovskite. For example, after 300 hours exposure to air at 800°C, a dense, uniform $(\text{Cr,Mn})_3\text{O}_4$ layer formed at the contact interface between a coupon of Crofer22APU

and $\text{La}_{0.8}\text{Sr}_{0.2}\text{MnO}_3$ paste. EDS analysis indicated ~0.5% Cr in the manganite, which was much lower than the percentage (8-10% Cr) found in lanthanum ferrite contact pastes. The migration of Cr into the perovskite likely resulted in formation of SrCrO_4 . The formation of strontium chromate was confirmed by XRD on powder mixtures of Cr_2O_3 and perovskites that were heat-treated at 800°C in moist air for 300 hours.

Conclusions

Under the SOFC interconnect dual exposures, the oxidation behavior of high-temperature oxidation-resistant alloys on the air side can be quite different from that observed in single atmosphere exposure. For ferritic stainless steels with a relatively low Cr percent (<23%), dual exposure enhances iron transport and in some cases leads to the formation of Fe_2O_3 hematite-rich nodules in the scale. Increased water vapor in air further accelerates the anomalous oxidation behavior of ferritic stainless steel on the air side. For Ni-based alloys, the dual exposure inhibits the growth of NiO in the scale on the air side and thus facilitates the formation of uniform, protective scale. When in contact with chromia-forming alloy interconnects, manganite perovskites facilitate the formation of a $(\text{Cr,Mn})_3\text{O}_4$ layer, which mitigates Cr migration and decreases contact resistance.

FY 2004 Publications

1. Yang Z, Xia G, Singh P, Stevenson JW. "Effects of Water Vapor on the Anomalous Oxidation Behavior of Ferritic Stainless Steels under Solid Oxide Fuel Cell Operating Conditions," submitted to Acta Mater.
2. Yang Z, Xia G, Singh P, Stevenson JW. "Anomalous Oxidation Behavior of Ni Based Alloys under Solid Oxide Fuel Cell Interconnect Exposure Conditions," submitted to Script Mater.
3. Yang Z, Walker MS, Singh P, Stevenson JW, Norby T. "Oxidation Behavior of Ferritic Stainless Steels under Solid Oxide Fuel Cell Interconnect Exposure Conditions," *J. Electrochem Soc*, in print.

4. Yang Z, Hardy JS, Walker MS, Stevenson JW. "Structure and Electrical Conductivity of Thermally Grown Scales on Ferritic Fe-Cr-Mn Steel for SOFC Interconnect Applications," *J. Electrochem Soc*, in print.
5. Yang Z, Singh P, Stevenson JW. "Anomalous Corrosion Behavior of Stainless Steels under Solid Oxide Fuel Cell Interconnect Exposure Conditions," *Electrochem & Solid State Lett* 2003; 6:B35.
6. Yang Z, Walker MS, Singh P, Stevenson JW. "Investigation of Oxidation-Resistant Alloy Interconnects for Use in Planar SOFC," 2003 *Fuel Cell Seminar Abstracts*, Courtesy Associates, Washington, D.C. (2003).
2. Yang Z, Xia G, Singh P, Stevenson JW, "Interconnect Development," 2004 SECA Workshop, Boston, May 11-14, 2004.
3. Yang Z, Xia G, Walker MS, Singh P, Stevenson JW, "Anomalous Oxidation Behavior of Oxidation Resistant Alloys under SOFC Interconnect Dual Exposure Conditions," 133rd Annual Meeting of TMS, Charlotte, NC, March 15-17, 2004.
4. Yang Z, Xia G, Meinhardt KD, Weil KS, Singh P, Stevenson JW, "Evaluation of Crofer22 APU for SOFC Interconnect Applications," 2003 ASM Mater. Sol. Conf. & Exp., Pittsburgh, October 15-17, 2003.
5. Yang Z, Singh P, Stevenson JW, Walker MS, Xia G, "Corrosion of Ferritic Stainless Steel Interconnect under Dual Atmospheres," 2003 ASM Mater. Sol. Conf. & Exp., Pittsburgh, PA, October 15-17, 2003.

FY 2004 Presentations

1. Yang Z, Hardy JS, Paxton DM, Singh P, Stevenson JW, Walker MS, Weil KS, Xia G, "Application of High Temperature Oxidation Resistant Alloys for SOFC Interconnect Applications: Status and Challenges," 133rd Annual Meeting of TMS, Charlotte, NC, March 15-17, 2004. (Invited)

III.A.15 Reliable Seals for Solid Oxide Fuel Cells

Ronald E. Loehman (Primary Contact), Mathieu Brochu, Raj Tandon, Terry Garino, Bryan Gauntt
Sandia National Laboratories, MS 1349
Albuquerque, NM 87185-1349
Phone: (505) 272-7601; Fax: (505) 272-7304; E-mail: loehman@sandia.gov

DOE Project Manager: Don Collins
Phone: (304) 285-4156; E-mail: Donald.Collins@netl.doe.gov

Objectives

- Develop sealing techniques for solid oxide fuel cells (SOFCs) that are reliable and cost-effective.
- Determine performance-limiting features of different sealing approaches.
- Determine seal degradation mechanisms.
- Optimize seal properties.

Approach

- Glass matrix composite seals can be engineered to provide a wide range of chemical and mechanical properties.
- Composite approach allows glass and filler to be optimized independently.
- Glass phase is above its glass transition temperature (T_g) at SOFC operating temperature to reduce thermal and mechanical strains.
- Viscosity, coefficient of thermal expansion (CTE), etc. can be controlled by adding unreactive powder.
- Volume fraction of glass phase can be reduced to minimum for seal, which reduces reactivity with fuel cell materials.

Accomplishments

- Developed and tested over 30 glass compositions with different glass transition temperatures and expansion coefficients.
- Made glass-ceramic powder composites by varying glass and additive compositions and volume fraction of powder additive; demonstrated that we can vary CTE in controlled manner.
- Sealed different composites to yttria-stabilized zirconia (YSZ) electrolytes; demonstrated good adhesion and mechanical strength.
- Showed composite seals are resistant to damage from thermal cycling.
- Made similar glass matrix composites, but with metal powder additives; sealed them to SOFC parts and showed that we can vary the seal properties in a systematic manner.
- Tested seals at 800-850°C for up to 200 hours; showed adhesion is maintained.

Future Directions

- Conduct more thermal cycling and long-time exposure tests at service temperature.
- Determine effects of environmental exposure; e.g., reducing and oxidizing atmospheres.
- Test new seal compositions and joining parameters.
- Develop pressure rupture test as a quick screen for seal compositions and processes.

- Perform more fundamental mechanical tests on composite seal materials at operating temperatures; e.g., flexural strength and fracture toughness.
- Determine seal adhesion to SOFC parts such as YSZ substrates.
- Investigate shaping and forming methods for composite seals such as tape casting and screen printing.

Introduction

Development of reliable methods for sealing solid oxide fuel cell stacks presents the most challenging set of performance criteria in the entire field of ceramic joining. For SOFC applications, the requirements on the sealing method include:

1. Adhesion of the sealing material to fuel cell components from room temperature to as high as 1000°C
2. Provide a leak-tight seal at the SOFC operating temperature
3. Ability to maintain a seal while accommodating strains from SOFC components with different CTEs
4. Lack of adverse reaction between the sealing material(s) and the fuel cell components
5. Chemical and physical stability of the sealant at temperatures up to 1000°C in oxidizing and reducing atmospheres
6. Thermal shock tolerance
7. Electrically insulating for some SOFC designs

All of the above properties must be maintained for SOFC operating lifetimes of up to 40,000 hours. The list is written in approximate order of decreasing stringency. That is, no matter what the SOFC design, the seal must be adherent and leak tight. On the other hand, some stack designs may require joining only similar materials and, thus, a matched CTE seal may be sufficient. Note also that the requirements may be contradictory. For example, being leak tight and adherent at high temperatures suggests a refractory, stiff sealant, which may work against the requirement for thermal strain accommodation. Such situations are common, and seal developers know that seal design is specific to a particular component geometry and usually requires compromises among competing requirements.

Approach

Under DOE sponsorship, this project is developing an approach to sealing SOFCs that can be tailored to the specific requirements of the vertical teams in the DOE / Solid State Energy Conversion Alliance (SECA) program. The technique combines extensive capabilities in composites and ceramic joining that have been developed at Sandia over the past 15-20 years. In our judgment, relief of thermal expansion mismatch stresses will require SOFC seals to incorporate either a ductile metal or a high-viscosity glass that can relieve stresses through viscous creep. Other design and operational constraints on SOFCs, which as discussed above frequently are in opposition, severely restrict the options for seal materials. Based on our prior experience in ceramic joining and on results obtained so far on this project, we believe we have greatest design flexibility using ceramic-filled glasses and metal-filled glass composites. We have demonstrated that we can control properties such as glass transition temperature and thermal expansion coefficient by varying the compositions, amounts, and microstructures of the different phases. Design choices are guided by thermochemical and composite microstructural models that allow us to target specific seal properties for a given design. Several seal systems are showing promise in functional tests. In future work we will use our extensive background in modeling composite properties to optimize the compositions and structures for specific combinations of seal properties for best performance.

The specific tasks for this project include the following:

1. Consult with vertical teams to learn their specific requirements.
2. Synthesize candidate glasses.
3. Measure glass properties such as T_g, CTE, and possibly viscosity as a function of temperature.
4. Choose ceramic powder filler, particle size, and particle morphology.

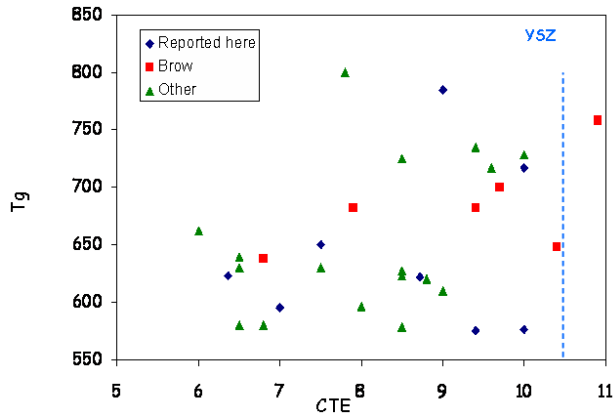


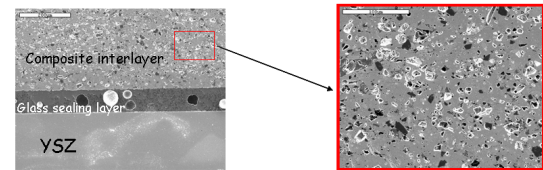
Figure 1. Glass Compositions Plotted as a Function of Glass Transition Temperature (T_g) and Coefficient of Thermal Expansion (CTE)

5. Design and make ceramic-filled glass composite sealants in a range of compositions and microstructures.
6. Make test seals with specified SOFC materials and measure strengths of bonded test specimens as a function of temperature.
7. Determine stability of seal over time at temperature by analyzing interfaces of specimens after long-term heating.
8. Measure deformation of candidate sealant-SOFC bilayers in situ as a function of temperature using an apparatus that is unique to Sandia.
9. Use measured properties (e.g., strains) as inputs to 3D finite element modeling computations to calculate stresses for different SOFC stack designs. Alternatively, we can provide the property data (e.g. strain vs. temperature data) to the vertical teams and they can do the computations themselves.
10. Apply property data, engineering data, and finite element simulations to design seals that minimize stresses (and to define practical limits for the stresses in SOFCs); transfer results to vertical teams as they are obtained.

Results

We have made over 30 different glass compositions with potential for the composite seal approach and measured their physical properties. Figure 1 shows the compositions on a plot of glass transition temperature (T_g) as a function of

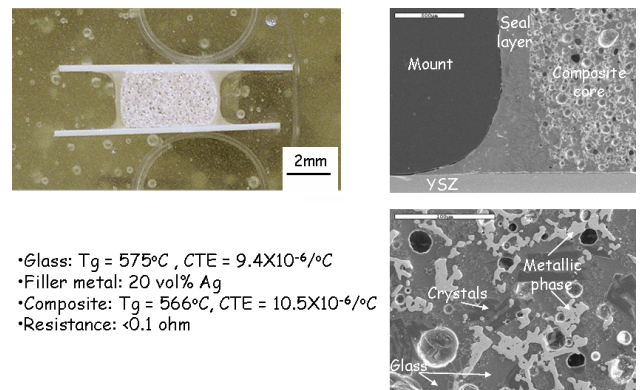
Liquid phase sintered composite layer sealed by two thin glass layers



- Ceramic: 70 vol% YSZ
- Glass: $T_g=703^\circ\text{C}$, $\text{CTE}=9.7 \times 10^{-6}/^\circ\text{C}$
- Composite CTE: $10.2 \times 10^{-6}/^\circ\text{C}$ (200-700°C)

Composite interlayer:
70vol% YSZ - 30vol% Glass
Note: no pressure applied

Figure 2. Glass-Ceramic Seal Bonded to YSZ Substrate with Thin Layer of the Same Glass as in the Composite



- Glass: $T_g = 575^\circ\text{C}$, $\text{CTE} = 9.4 \times 10^{-6}/^\circ\text{C}$
- Filler metal: 20 vol% Ag
- Composite: $T_g = 566^\circ\text{C}$, $\text{CTE} = 10.5 \times 10^{-6}/^\circ\text{C}$
- Resistance: $<0.1 \text{ ohm}$

Figure 3. Micrographs of glass-Ag composite showing that an electrically conductive seal can be obtained by adjusting the amount of the Ag. If the volume fraction of Ag is reduced, an insulating seal results.

coefficient of thermal expansion (CTE). The plot shows that we have glasses with a wide range of properties available.

Figure 2 shows several micrographs of a seal to YSZ that comprises a composite layer with 70 vol% YSZ powder and 30 vol% of one of our sealing glasses bonded with a thin layer of the same glass. The composite CTE has been adjusted to $10.2 \times 10^{-6}/^\circ\text{C}$. The seal adheres tightly to the YSZ and survived multiple thermal cycles up to 850°C .

Glass composite seals incorporating a ductile metal are particularly able to accommodate CTE mismatch stresses through deformation. Figure 3 is an example with 20 vol% Ag and the remainder one of our glasses. This composition is electrically

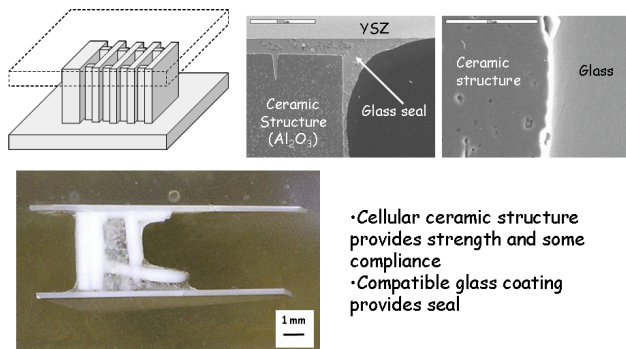


Figure 4. The Sandia-developed Robocasting technique, a type of freeform deposition, can make seals that combine ceramic and glass structures to optimize mechanical properties. In this example, a somewhat compliant cellular alumina structure provides mechanical support and the glass layer provides the seal.

conductive because the Ag is just above the percolation limit. We can obtain an insulating seal with almost the same mechanical properties by reducing slightly the amount of Ag.

We have used the Sandia-developed freeform fabrication technique known as Robocasting to make some demonstration seals. The idea is to show the range of ceramic-glass structures that are possible and that may be designed to optimize specific mechanical properties. In Figure 4, a cellular alumina structure provides mechanical support for the seal while the glass provides the hermetic seal to the YSZ. This seal proved particularly robust in thermal cycling tests.

Type of cast	Additive / vol%	Vol% Solid
Pure glass	N/A	65%
Glass-ceramic composite	14a / 30vol%	65%
Glass-metal composite	Ni / 30vol%	65%

Typical volume% solid of common tape cast is around 55-65%



Tape cast thicknesses 0.56 to 0.85mm (green)

Typically 0.5 to 1.5mm

Figure 5. Glass-powder composites can be prepared as green tapes similar to those used in microelectronic packaging. This approach allows more processing options.

Availability of manufacturing processes is always an issue in materials joining. Figure 5 illustrates some experiments that show that glass-ceramic composite seals can be formed using preforms that are tapecast using techniques common to microelectronic packaging. The green (unfired) tape can be cut to the shape required for the bond area and stacked so that the whole assembly is sealed and otherwise processed in a co-fire operation.

Conclusions

We have demonstrated the potential of the glass-powder composite approach for sealing SOFCs. We have shown that we can independently vary compositions and microstructures to achieve desired seal properties and that those properties can be targeted to seal different SOFC materials. We have demonstrated a number of techniques for applying the seals that would be practical in a manufacturing setting.

III.A.16 Surface-Modified Ferritic Interconnect Materials for Solid Oxide Fuel Cells

Bruce Lanning (Primary Contact), James Arps

Southwest Research Institute

6220 Culebra Road

San Antonio, TX 78238-5166

Phone: (210) 522-2934; Fax: (210) 522-6220; E-mail: blanning@swri.org

DOE Project Manager: Lane Wilson

Phone: (304) 285-1336; E-mail: Lane.Wilson@netl.doe.gov

Objectives

- Engineer a surface oxide scale on a ferritic stainless steel that is
 - Mechanically and chemically stable at 800°C in oxidizing and reducing environments, and
 - Electrically conductive to minimize stack internal resistance losses.
- Develop process for rendering the alumina scale electrically conductive (such as metal ion implantation) that is inherently scaleable for manufacturing.
- Demonstrate stable electrical conductivity of interconnects for an extended time (>1000 hours) at 800°C in contact with cathode materials ((La_{0.8}Sr_{0.2})FeO₃ [LSF] and (La_{0.6}Sr_{0.4})(Fe_{0.8}Co_{0.2})O₃).

Approach

- Formation and characterization of stable alumina/chromia scales on ferritic stainless steels, such as FeCrAlY and 430.
- Doping of near-surface layer with elements such as niobium, titanium, and yttrium to render the insulating alumina scale conductive.
- Exposure testing, via DC area specific resistance (ASR) and AC impedance measurements, of treated ferritic stainless steel samples at elevated temperatures (800°C) in air for up to 1000 hours, including elevated temperature testing/characterization of interconnect/LSF cathode diffusion.

Accomplishments

- Formed and demonstrated stable (up to 900°C), self-limiting scale on FeCrAlY in oxidizing environments and in contact with LSF cathode materials.
- Observed an order-of-magnitude decrease in ASR with the implantation of niobium or titanium at a dose of 1×10^{16} atoms/cm², as compared to un-doped FeCrAlY (resistance comparable to chromia-forming 430 SS).
- Established conduction mechanism of doped and un-doped FeCrAlY scales using AC impedance techniques and confirmed that results agreed with ASR measurements.
- Demonstrated stability of doped and un-doped FeCrAlY scales in contact with LSF cathode material at elevated temperatures (800°C) in exposure tests for 1000 hours.

Future Directions

- Conduct additional tests to establish optimum dopant concentrations (and type) in order to ensure low ASR and minimum effect due to bulk diffusion.
- Having established proof-of-concept of the proposed ion implantation methodology, the next step will be to develop more scaleable manufacturing processes that achieve the same oxide composition, e.g. magnetron sputtering, sol-gel or other similar processes.

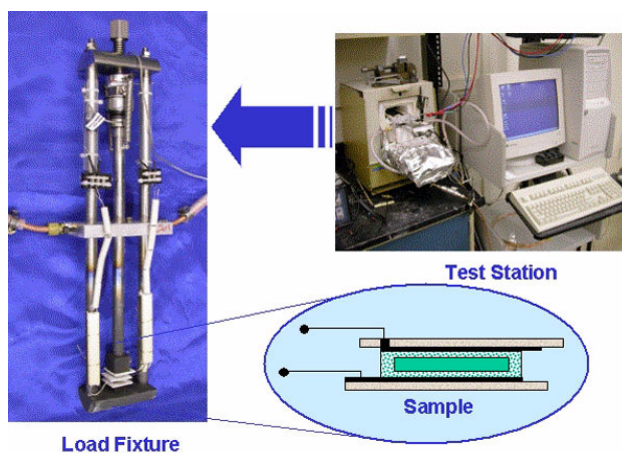


Figure 1. Load Fixture and Corresponding Test Station for High-Temperature DC ASR and AC Impedance Measurements

Introduction

Interconnects are a critical element of a solid oxide fuel cell (SOFC) assembly in that they must: 1) be easily formable and machinable; 2) be thermally matched to adjoining ceramic cell components; 3) have mechanical integrity and fracture toughness over prolonged periods of exposure to high temperature, reducing/oxidizing environments; and 4) develop surface scales that are not only stable and electrically conductive over a large O_2 concentration range, but prevent ion migration or gas permeation across the interconnect-electrode boundary. Although much work has focused on metal alloys for interconnect materials, particularly chromium alloys containing an oxide that is both oxidation resistant and electrically conductive, the thermal instability of typical native metal oxides allows interdiffusion of cations across the interconnect-electrode boundary that ultimately leads to degradation of SOFC performance. In particular, the volatility and corresponding outward diffusion tendencies of chromium cations in chromia scale-forming alloys lead to spallation and instability at the interconnect/electrode boundary.

Approach

A novel approach, based on ion implantation, was investigated to render the stable alumina scale on aluminum-containing ferritic alloys, such as

FeCrAlY, conductive. As part of the one-year effort, we implanted a series of pre-treated FeCrAlY stainless steel samples with niobium and titanium ions and, alongside sibling 430 stainless steel samples (as control), conducted both DC ASR and AC impedance measurements to evaluate ASR and conduction mechanisms. In addition to evaluating FeCrAlY and 430 scale formation and properties up to 900°C in air for 1,000 hours, the stability of the scales were evaluated in contact with LSF cathode materials. A specially designed load frame (fixture), shown in Figure 1, was designed and fabricated in order to accurately control the applied load at the contacting interfaces at the elevated temperatures for this investigation. Scale structure and composition were evaluated with x-ray diffraction (XRD) and energy dispersive x-ray (EDX)/Auger electron spectroscopy (AES), respectively.

Results

Oxidation kinetics for both FeCrAlY and a typical chromia-forming ferritic steel (430) were investigated. We confirmed, as part of our oxidation kinetics evaluation of FeCrAlY and 430 ferritic steel, the parabolic growth of a mixed chromia/alumina scale on FeCrAlY and a single chromia layer in the case of the 430 stainless steel; the outer contiguous layer of Al_2O_3 , in the case of FeCrAlY, formed a stable, self-limiting, protective scale. To render the alumina scale conductive, we then implanted either titanium or niobium ions into FeCrAlY scales to a fixed depth, varying only the thickness of the oxide. Area specific resistance (ASR) was measured as a function of temperature and time at temperature using both modified 4-point DC and AC impedance techniques. As a result of the relatively high lead/system resistance component of the overall ASR measurement, a consequence of the test configuration, a qualitative measurement of the DC resistance was obtained using an oxidized 430 SS specimen as a means for comparison. ASR for an un-doped FeCrAlY oxide scale (i.e., alumina) was more than an order of magnitude greater than the 430 control sample, whereas the ASR for the doped FeCrAlY oxide scale sample was comparable to the 430 control sample; hence, the resistance of a doped alumina scale on FeCrAlY was equal to the resistance of a chromia-scale forming alloy, such as 430 (typically $<0.1 \Omega\text{-cm}$).

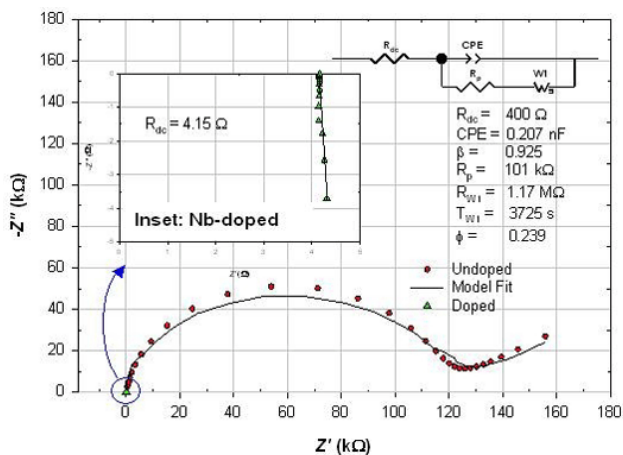


Figure 2. AC Impedance Plot for Un-doped and Nb-doped FeCrAlY Alumina Scales after 1000 Hours at 800°C in Air; Enlarged View around Origin Shown by Inset

Along with the DC ASR measurements, AC impedance measurements were used to assess basic conduction mechanisms across the various interfaces of the contact up to 800°C, providing confirmation of the effect of the dopant. Based on the AC impedance results, un-doped alumina scales exhibited mixed conduction and the transport-limited mechanisms of a high-impedance, solid-state electrolyte. Addition of niobium resulted in at least a two-order-of-magnitude reduction in resistance over the un-doped specimen. Niobium-doped alumina scales exhibited pure electronic conduction, as opposed to mixed ionic-electronic conduction, even after 1000 hours at 800°C. As shown in Figure 2, the DC resistance component was less than the system resistance (i.e., leads, junctions, etc.).

A diffusion couple experiment, placing a doped FeCrAlY alumina scale in contact with an LSF cathode material for 1000 hours at 800°C, confirmed the stability of the interface region. The entire diffusion couple specimen, along with fixture, was cross-sectioned and then polished prior to an EDX analysis to produce the elemental “dot” maps shown in Figure 3. No detectable cation interdiffusion took place across the contiguous alumina layer, and thickness of the scale layer remained essentially unchanged after 500 hours at temperature. This stability of the alumina scale on FeCrAlY is consistent with its reported long-term stability

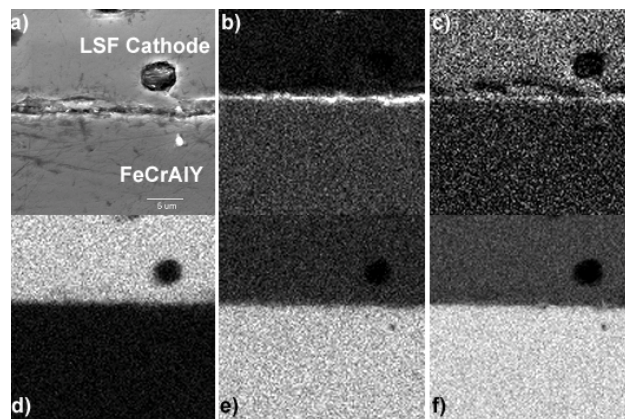


Figure 3. LSF/FeCrAlY Contact @ 800°C for 1000 Hours (intimate contact); SEM and X-ray Dot Maps for: a) SEM, b) Aluminum, c) Oxygen, d) Lanthanum, e) Chromium, and f) Iron

(~40,000 hours at 950°C) in advanced gas-cooled reactors for the nuclear industry.

Conclusions

Our results have clearly shown that dopant additions increase the electronic conductivity of alumina-forming scale alloys, such as FeCrAlY, transforming from a mixed ionic/electronic conduction mechanism. Just as importantly, the demonstrated stable formation of an alumina scale is a clear advantage over conventional pure chromia forming alloys for interconnect materials. Future work in this area would be to optimize the dopant addition/concentration and any possible effects of bulk dilution (although none were observed in the limited 1000 hour tests of this study), as well as the type of dopant addition; i.e., strontium and TiO₂ as opposed to pure titanium. Since we have proved the concept of this procedure (patent application submitted) the next step would be to develop more scaleable manufacturing processes that achieve the same oxide composition, e.g. by magnetron sputtering, sol-gel, or other similar processes.

References

1. Y. Larring et al., J. Electrochem. Soc. (2000) 147, 3251-3256.
2. W. J. Quadackers et al., Solid State Ionics (1996), 91, 55-67.

3. K. Hwang, P. Y. Hou and J. B. Gooderough, Solid State Ionics (2000), 129, 237.
4. M. J. Bennett, M. R. Houlton and G. Dearnaley, Corros. Sci. (1980) 20, 69-72.
2. 13th International Conference on Surface Modification of Materials by Ion Beams, September, 2003, San Antonio, TX.

FY 2004 Publications/Presentations

1. 2003 Fuel Cell Seminar, Miami, FL.

Special Recognitions & Awards/Patents Issued

1. One patent pending

III.A.17 Fundamental Studies of the Durability of Materials for Interconnects in Solid Oxide Fuel Cells (SOFCs)

Gerald H. Meier (Primary Contact), Frederick S. Pettit

Department of Materials Science and Engineering

848 Benedum Hall

University of Pittsburgh

Pittsburgh, PA 15261

Phone: (412) 624-9720; Fax: (412) 624-8069; E-mail: ghmeier@engr.pitt.edu, pettit@engr.pitt.edu

DOE Project Manager: Lane Wilson

Phone: (304) 285-1336; E-mail: Lane.Wilson@netl.doe.gov

Subcontractor: Jack L. Beuth

Department of Mechanical Engineering

Carnegie Mellon University

5000 Forbes Avenue

Pittsburgh, PA 15213-3890

Phone: (412) 268-3873; Fax: (412) 268-3348; E-mail: beuth@andrew.cmu.edu

Objectives

- To develop mechanism-based evaluation procedures for the stability of SOFC interconnect materials and to use these procedures to study and modify a group of alloys which have already been identified as candidate interconnect materials, i.e. ferritic stainless steels.
- To study fundamental aspects underlying the thermomechanical behavior of interconnect materials and develop accelerated testing protocols.
- To investigate the potential for the use of “new” metals as interconnect materials.

Approach

- Characterize exposed fuel cell interfaces.
- Study and attempt to control growth rates of chromia scales on Cr and ferritic alloys.
- Study the adhesion of chromia scales subjected to cyclic oxidation conditions in simulated fuel cell atmospheres.
- Investigate evaporation of Cr-oxide species both theoretically and experimentally.
- Measure stresses in oxide scales on ferritic alloys using x-ray diffraction (XRD).
- Perform indentation testing to evaluate interface adhesion of thermally grown oxide scales and deposited coatings.
- Develop a mechanism-based, accelerated testing protocol for evaluating the thermomechanical stability of oxides and coatings on metallic interconnects.
- Evaluate the possibility of reducing the oxidation rate of pure Ni.
- Evaluate the use of Fe-Ni alloys with low coefficient of thermal expansion (CTE) (Invar) as interconnects.
- Evaluate the use of coatings to limit oxide evaporation from chromia-forming interconnect alloys.

Accomplishments

- Characterized the oxidation behavior of a variety of ferritic stainless steels in simulated fuel cell atmospheres over the temperature range 700°-900°C.

- Discovered that exposure under some fuel cell operating conditions can promote sigma phase formation in some ferritic stainless steels.
- Adapted an indentation technique for measuring interfacial fracture toughnesses for oxides formed on interconnects and for coatings applied to interconnects.
- Used interfacial toughnesses measured in specimens subjected to short exposure times to estimate times for spontaneous spallation (failure) of chromia scales.
- Ascertained that it may be possible to modify the surface of pure nickel or to alloy Ni to allow its use as an intermediate-temperature interconnect material.

Future Directions

- Evaluate the oxidation behavior of ferritic stainless steels under dual atmosphere conditions, with one side of the specimen exposed to a simulated fuel cell cathode gas and the other side exposed to a simulated anode gas.
- Continue the development of indentation as an accelerated testing technique for chromia scales and deposited coatings.
- Continue the study of coatings to reduce oxide evaporation from chromia-forming alloys.
- Investigate Cr-free alloys as possible interconnect materials.

Introduction

Solid oxide fuel cells provide a potential way to generate electricity with high efficiency and low pollution. The operating principles of fuel cells have been known for over 100 years, and low-temperature fuel cells provided the electric power on all the Gemini and Apollo spacecraft. However, fuel cells have not achieved widespread commercial use for a number of economic and technical reasons.

One of the most important technical challenges for solid oxide fuel cells, which operate in the temperature range 700°-900°C, is the design of interconnects (current collectors). These components, in addition to electrically connecting individual cells in a stack, must separate the anode compartment of one cell from the cathode compartment of the adjacent cell. This means that one side of an interconnect is exposed to the fuel, typically hydrogen or hydrocarbons in which the oxygen partial pressure is low, and the other side is exposed to the oxidant, which is typically air

Interconnect material requirements include a variety of physical, chemical, and electrical properties. The optimal interconnect material would have the following properties:

1. Low electrical resistivity.

2. Impermeability to anode and cathode gases.
3. Stability in both anode and cathode gases under thermal cycling conditions.
4. Chemical compatibility with other cell components.
5. Close match in coefficient of thermal expansion with other components.
6. Good mechanical properties.
7. High thermal conductivity.
8. Ease of fabrication.
9. Low cost.

Ceramic interconnects usually have favorable values of properties 2, 3, 4, and 5. However, they are usually deficient in the other desired properties.

Metallic interconnects are attractive in that they have favorable values of properties 2, 6, 7, 8, and 9. With respect to property 7, although metallic materials have low electrical resistivity, they react with SOFC gases to form oxide layers, which generally have high electrical resistivity. Interconnect system resistance can be greatly increased by oxide layer thickening and spallation. Oxidation-resistant alloys are designed to form one of three protective oxides: alumina, silica, or chromia. Of these, the electrical resistivities of alumina and silica are much too high for interconnect applications.

Approach

The project consists of three major tasks aligned with its three objectives.

Task 1: Mechanism-based Evaluation Procedures

A variety of chromia-forming interconnect alloys are being subjected to thermal cycling in air, in simulated anode gas (Ar-H₂-H₂O) and with simultaneous exposure to air on one side and simulated anode gas on the other. Combined exposures have been shown at Pacific Northwest National Laboratory (PNNL) to often yield different behavior than exposures with the same gas on both sides of the specimen. Exposure temperatures range from 700°C to 900°C. Oxidation kinetics are being tracked by mass change measurements, and corresponding changes in oxide scale resistances are being measured. Exposed specimens are being examined in cross-section by scanning electron microscopy (SEM) to document changes in structure with exposure.

Methods are being studied to slow the growth of chromia scales on Cr and ferritic alloys with exposure in order to decrease the contribution of the scale to interconnect resistance. The ability of chromite coatings to reduce harmful CrO₃ evaporation from chromia-forming interconnect alloys is also being investigated. Specimens for this task and tasks 2 and 3 are being provided by PNNL, the National Energy Technology Laboratory (NETL) and Solid State Energy Conversion Alliance (SECA) Industrial Team members.

Task 2: Fundamental Aspects of Thermomechanical Behavior

Understanding the resistance of growing chromia scales to spallation requires a fundamental understanding of the mechanics of chromia adhesion. From a fracture mechanics standpoint, the adherence of protective oxide scales to alloy substrates is governed by 1) the stored elastic energy in the scale, which drives delamination, and 2) the fracture toughness of the alloy/oxide interface, which quantifies the resistance to fracture.

The stored elastic energy in the scale is increased by increases in the scale thickness (which can be

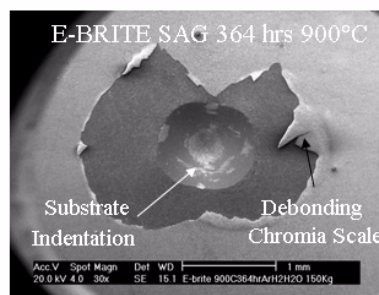
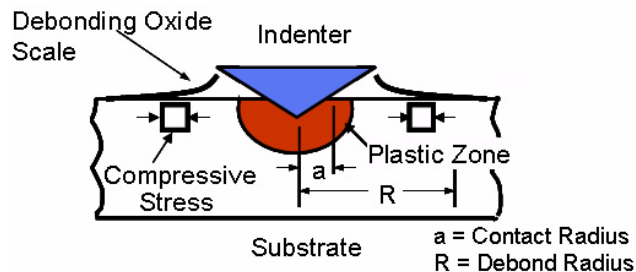


Figure 1. Indentation Fracture Testing Techniques Used to Study the Thermomechanical Behavior of SOFC Interconnects

measured by cross-section SEM) and increases in the residual stress in the scale. In this task, x-ray diffraction (XRD) is being used to measure stresses in chromia films formed on pure chromium and chromia-forming alloys after the exposures described for Task 1.

An indentation test (see Figure 1) is also being used to measure the fracture toughness of chromia/alloy interfaces for the same exposures. In the test, the chromia scale is penetrated by the indenter, and the plastic deformation of the underlying substrate induces compressive radial strains in the substrate. These strains are transferred to the coating, and the associated coating stress drives the extension of a roughly axisymmetric interface crack. The interfacial toughness can be determined from the results of a mechanics analysis of the indentation problem and a measurement of the delamination radius.

SOFCs must be able to operate for very long periods of time (e.g. 40,000 h with hundreds of thermal cycles). Clearly, testing interconnect alloy modifications over this time period is not feasible, and accelerated testing protocols are needed. In addition to subjecting specimens to exposures at higher temperatures and increasing thermal cycle frequency, XRD and indentation are being used as

accelerated testing techniques, yielding insight into scale durability after short exposure times.

Task 3: Alternative Material Choices

Metallic materials other than chromia-formers are being considered for use as low-temperature SOFC interconnects. Experiments similar to those described for Task 1 are being performed on pure Ni. Its only oxide, NiO, has no vapor species with high partial pressures, and it has a higher electrical conductivity than chromia. NiO should not even form in the anode gas. In addition, low-CTE, dispersion-strengthened Ni is being considered. The alternatives being considered are dispersing Y_2O_3 or Li_2O in Ni. The latter would also provide a potential source of Li^{+1} cations to dope the NiO scale.

Low-CTE Fe-Ni alloys (Invar) are also being considered. Because the CTE of Invar is substantially lower than that of typical ceramic SOFC components, increasing Ni content may be needed allow the interconnect CTE to be matched to that of SOFC ceramic components. Neither component of these alloys will form oxide in the anode gas. Evaporation of CrO_3 can be reduced by the use of coatings, as described above. This concept is also being pursued.

Results

Task 1: Mechanism-based Evaluation Procedures

The cyclic oxidation of three ferritic stainless steels has been evaluated under conditions pertinent to fuel cell operation. The alloys are (compositions in wt%):

- E-BRITE (Fe-26 Cr-1 Mo-0.2 Si)
- AL 453 (Fe-22 Cr-0.6 Al-0.3 Mn + 0.1Ce/La)
- Crofer (Fe-22Cr-0.5Mn-0.08 Ti-0.016P-0.06 La)

Cycle times of 1 hour were used, with exposure temperatures of 700°C and 900°C. The exposure environments included

- Dry Air (Simulated Cathode Gas)
- Air + 0.1 atm H_2O
- Ar/ H_2 / H_2O (Simulated Anode Gas) ($P_{O_2} = 10^{-17}$ atm at 900°C and 10^{-20} atm at 700°C)

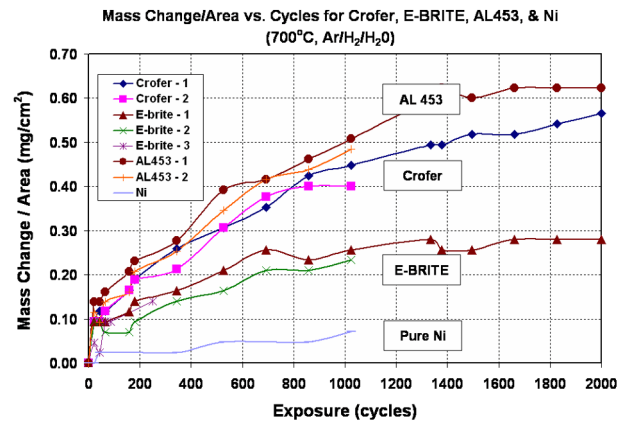


Figure 2. Cyclic Oxidation Data for Ferritic Alloys and Pure Ni Exposed in Simulated Anode Gas (Ar-4%, H_2 , H_2O) at 700°C

Figure 2 is a typical plot of mass change versus time for exposure in simulated anode gas at 700°C.

Exposure in air plus water vapor at 700°C and 900°C resulted in accelerated growth of chromia scales and accelerated oxide spallation from alloys that did not contain a reactive element (e.g. E-BRITE). External layers of $MnCr_2O_4$ were observed to form on Crofer at 900°C. These may result in reduced oxide evaporation. Oxide growth rates were substantially lower at 700°C than at 900°C. Sigma phase was observed to form at 700°C in the alloys with higher chromium concentration, e.g. E-BRITE. Typical microstructures of this alloy after exposure are presented in Figure 3. The sigma phase formation was more extensive in atmospheres containing water vapor. This phase must be avoided since it is very brittle and tends to crack, as indicated in Figure 3.

Task 2: Fundamental Aspects of Thermomechanical Behavior

Indentation testing to determine the fracture toughness of chromia scale/alloy interfaces has been performed on E-BRITE specimens exposed in wet air and simulated anode gas environments at 900°C. Specimens exposed in wet air for 100 hours and longer showed indentation-induced flaking of the chromia scale, indicative of a thin chromia scale and a non-uniform interfacial toughness. The size of the

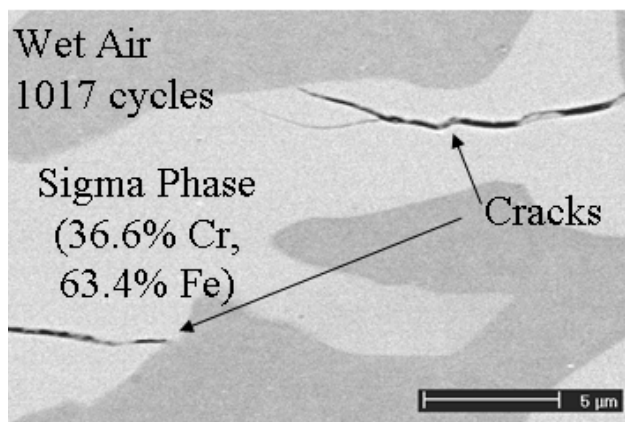
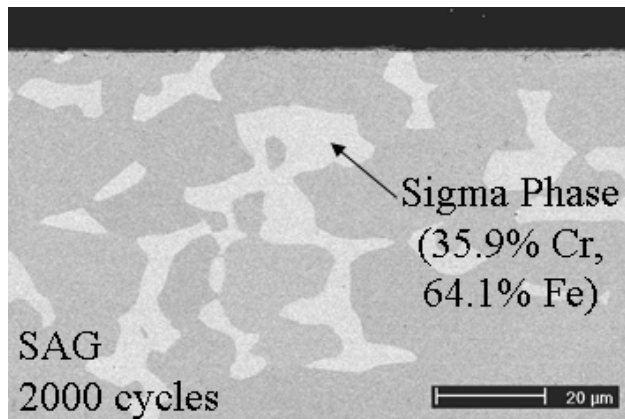


Figure 3. Micrographs Showing Sigma Phase Formation in E-BRITE at 700°C

region experiencing debonding did not change with exposure. This behavior is consistent with weight gain measurements and observations via optical microscopy of spontaneous flaking of chromia scales in these specimens.

Specimens exposed in simulated anode gas showed peeling of a comparatively thick, intact chromia scale (see Figure 1), with an increase in debond size with exposure. This behavior is also consistent with weight gain measurements and observations of a thickening chromia scale remaining attached to the alloy. Fracture mechanics analysis of the indent problem, coupled with residual stresses measured by XRD and oxide thicknesses measured by cross-section SEM, yielded interfacial fracture toughness values for these specimens. Toughness values for a specimen exposed for 364 hours in simulated anode gas and oxide growth data have

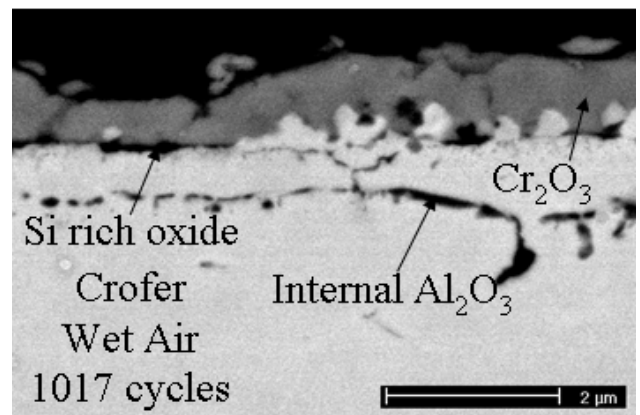
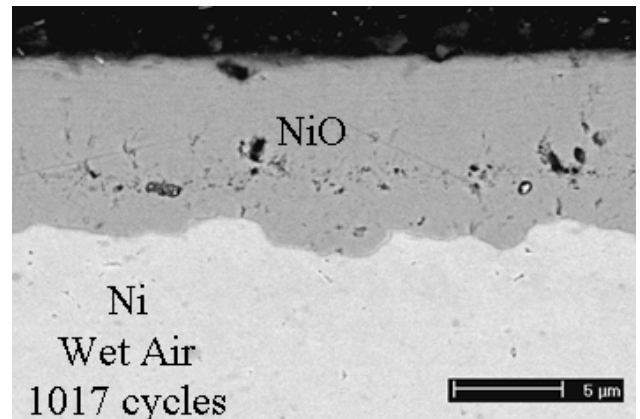


Figure 4. Comparison of Oxide Thickness for NiO and Cr₂O₃ formed at 700°C

been used to predict that spontaneous spallation will occur at approximately 800 hours. This prediction is consistent with observations of specimens exposed for 800 hours and more.

Task 3: Alternative Material Choices

Experiments are being carried out on pure Ni as a possible alternative interconnect material. Figure 2 includes the oxidation data for Ni in the simulated anode gas at 700°C. The Ni did not form an oxide layer in this gas. The small mass gain is believed to result from the dissolution of hydrogen and/or oxygen into the Ni. Figure 4 shows cross-sections of Ni and the ferritic alloys after exposure in moist air at 700°C. The NiO layer is approximately ten times thicker than the layers of Cr₂O₃. However, the NiO has a much higher electrical conductivity, so the actual contribution to the resistance of the system may actually be less for a Ni interconnect.

Conclusions

The aim of this project is to evaluate the chemical and thermomechanical stability of interconnect alloys in simulated fuel cell environments. The oxidation of three ferritic stainless steels has been characterized at both a typical operating temperature (700°C) and, to obtain more rapid results, at an elevated temperature (900°C). X-ray diffraction and indentation fracture testing have been used to characterize the mechanical durability of chromia scales grown on interconnect alloys. In addition to providing insights into mechanisms causing chromia spallation, these test techniques offer an alternative means of accelerating oxidation testing. The understanding gained from these tests will be used to suggest ways to optimize the properties of ferritic alloys. A parallel study is being carried out to evaluate the potential use of alternate interconnect alloys.

FY 2004 Publications/Presentations

1. G. H. Meier, F. S. Pettit, and J. L. Beuth, "Fundamental Studies of the Durability of Materials for Interconnects in Solid Oxide Fuel Cells," Phase I Topical Report on DOE Award: DE FC26 02NT41578, June 2003.
2. G. H. Meier, "Fundamental Studies of the Durability of Materials for Interconnects in Solid Oxide Fuel Cells," NETL Workshop on Solid Oxide Fuel Cells, Albany, NY, September 2003.
3. G. H. Meier, "Degradation of Materials in Solid Oxide Fuel Cells," ASM International, Materials Solutions, Pittsburgh, PA, October 2003.
4. J. L. Beuth, "Thermo-Mechanical Testing of SOFC Interconnect Alloy Durability," Materials Solutions, Pittsburgh, PA, October 2003.
5. G. H. Meier, "Fundamental Studies of the Durability of Materials for Interconnects in Solid Oxide Fuel Cells," NETL Workshop on Solid Oxide Fuel Cells, Boston, MA, May 2004.

III.A.18 Cathodes for Low-Temperature SOFC: Issues Concerning Interference from Inert Gas Adsorption and Charge Transfer

Anil V. Virkar

University of Utah

Department of Materials Science & Engineering

122 S. Central Campus Drive

Salt Lake City, UT 84112

Phone: (801) 581-5396; Fax: (801) 581-4816; E-mail: anil.virkar@m.cc.utah.edu

DOE Project Manager: Lane Wilson

Phone: (304) 285-1336; E-mail: Lane.Wilson@netl.doe.gov

Objectives

- To synthesize dense samples of perovskite mixed ionic electronic conductors (MIECs), including Sr-doped LaMnO₃ (LSM) (which is predominantly an electronic conductor with negligible ionic conductivity), Sr-doped LaCoO₃ (LSC) and Sr-doped LaFeO₃ (LSF).
- To investigate oxygen incorporation reaction by the proposed electrochemical method using mixtures of O₂ and N₂, as well as of O₂ and Ar.
- To fabricate anode-supported cells with MIEC + yttria-stabilized zirconia (YSZ) or MIEC + Sm-doped ceria (SDC) composite cathodes.
- To investigate cell performance and cathodic polarization as a function of temperature and composition of the oxidant.

Approach

- Synthesize LSM, LSC, and LSF powders by conventional methods as well as by combustion synthesis.
- Fabricate dense and porous samples of LSM, LSC, and LSF by pressing and sintering.
- Investigate oxygen exchange kinetics using the conductivity relaxation method.
- Fabricate patterned electrodes and measure charge transfer resistance as a function of three-phase boundary (TPB) length.
- Investigate the dependence of cell performance on oxygen partial pressure by using oxidants containing various mixtures of O₂ and an inert gas.

Accomplishments

- A new method of analysis was developed for the conductivity relaxation technique which facilitates the determination of the surface exchange coefficient and chemical diffusion coefficient.
- Using patterned electrodes of LSM on YSZ, it was demonstrated that the oxygen reduction reaction predominantly occurs at the TPB. Using this technique, charge transfer resistivity was measured as a function of temperature and oxygen partial pressure.
- Single cells were tested in various O₂ + N₂, O₂ + Ar, and O₂ + CO₂ gas mixtures.
- In 100% O₂ as oxidant and at 800°C, maximum power density as high as ~2.9 W/cm² was demonstrated.

Future Directions

The funded project has been completed, and no more work is planned. However, the following work is necessary for full evaluation of the proposed concept.

- Conduct experiments on the measurements of oxygen exchange coefficients and chemical diffusion coefficients on LSM, LSF, and LSC.
- Investigate the role of adsorption using patterned electrodes of LSF and LSC on YSZ and on other electrolytes such as ceria and Sr- and Mg-doped LaGaO₃ (LSGM).
- Investigate the role of chromium on the cathodic reaction using patterned electrodes.

Introduction

Typical oxidant in the operation of a solid oxide fuel cell (SOFC) is air, which contains 21% oxygen. When an SOFC is operating at a finite, nonzero current density, the oxygen content (partial pressure) close to the cathode/electrolyte interface is lower than that in pristine air. Also, when a stack is operated, the oxidant becomes depleted in oxygen, thus further lowering the oxygen content. In such cases, the oxygen content close to the cathode/electrolyte interface can be very low – perhaps approaching 2 to 4%, which means nitrogen is the predominant species at the cathode/electrolyte interface, where the cathodic reaction occurs. Low concentration of oxygen is expected to lead to low electrochemical reaction rate and lower performance. Under such conditions, the possible relative adsorption of nitrogen needs to be considered. Alternatively, regardless of the possible adsorption of nitrogen, relative decreased adsorption of oxygen needs to be taken into consideration. What is desired is a cathode material which preferentially adsorbs oxygen, thereby increasing the exchange current density.

The objective of this work was to investigate fundamental parameters that dictate cathodic charge transfer reaction rates of MIEC cathodes. This entailed investigation of the surface exchange coefficient and chemical diffusion coefficient of oxygen. In cathodes, which are predominantly electronic conductors such as LSM, the electrochemical reaction is expected to occur at the TPB. Investigation of the electrochemical reaction rate with such cathodes was conducted using patterned electrodes made by photo micro lithography. Finally, anode-supported button cells were made and tested in oxidants containing various oxygen concentrations.

Approach

Samples of MIEC materials such as LSC and LSF were fabricated as bars, both in a fully dense as

well as a porous form. The surface exchange coefficient was measured by the conductivity relaxation technique as a function of temperature and partial pressure of oxygen. Discs of yttria-stabilized zirconia were formed. Patterned LSM electrodes were deposited using photo micro lithography. The TPB was varied over a wide range, between 50 and 1200 cm⁻¹. Impedance spectra were obtained over a range of temperatures and oxygen partial pressures. Anode-supported button cells with Ni + YSZ anode, YSZ electrolyte and LSM + YSZ or LSC + SDC cathode were made. The cells were tested at 800°C with hydrogen as fuel and an oxidant containing various concentrations of oxygen.

Results

Figure 1 shows experimentally measured surface exchange coefficient as a function of oxygen partial pressure between ~0.02 and ~0.21 atm at 800°C on LSC using a porous sample. Note that the surface exchange coefficient increases with increasing oxygen partial pressure and then levels off, consistent with adsorption as a dominant step. Figure 2 is a scanning electron micrograph (SEM) of a patterned LSM electrode on a YSZ disc. The TPB was varied over a wide range by using different masks. On each disc, a counter electrode was deposited on the opposite face, and a reference electrode was wound along the cylindrical surface. Impedance spectra were measured over a range of temperatures and oxygen partial pressures. Figure 3 is an example of impedance spectra obtained. In this case, the impedance spectra were obtained on a sample of TPB length corresponding to 1200 cm⁻¹ as a function of oxygen partial pressure at 800°C. The intercept of the semi-circular arc on the x-axis gives the net charge transfer resistance. Note that as the oxygen partial pressure is increased, the charge transfer resistance decreases. Figure 4 shows the results of cell performance tests at 800°C using an anode-supported cell with LSC + SDC cathode. Note that power density as high as ~2.9 W/cm² could

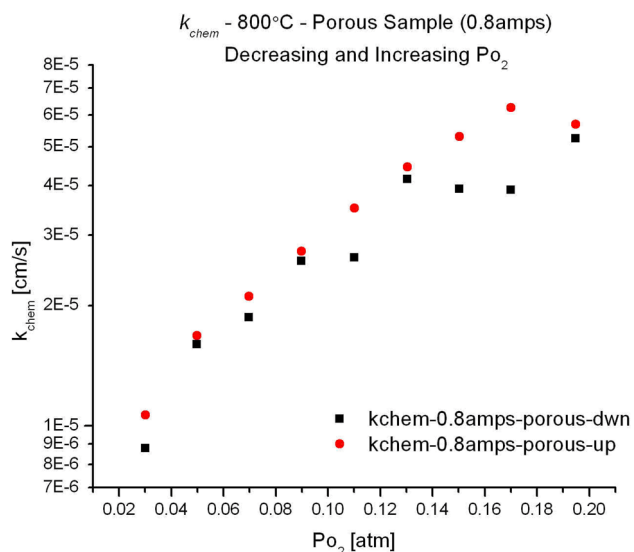


Figure 1. Plots of k_{chem} vs. PO_2 at 800°C, during both increasing and decreasing PO_2 , measured using porous sample. Note that at low values of PO_2 , the k_{chem} is virtually the same either during increasing PO_2 or decreasing PO_2 . The variance at high PO_2 may be experimental scatter. Note that k_{chem} increases with increasing PO_2 . It is anticipated that at high PO_2 , it will plateau out, consistent with Langmuir type adsorption.

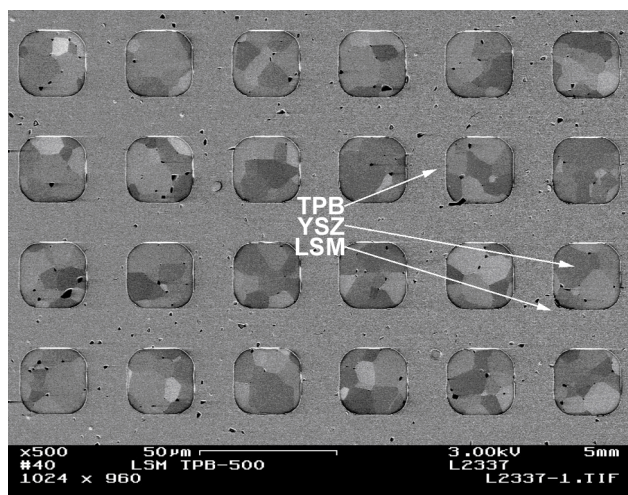


Figure 2. An SEM image of LSM patterned electrode deposited on a YSZ disc (deposited using the facilities at Pacific Northwest National Laboratories). The square regions are of YSZ, in which the grains can be seen. The rest of the region is the LSM coating. The l_{TPB} of this sample is 500 cm^{-1} .

**Impedance Spectrum of 1200 ITPB LSM Electrode
at 800 C for various partial pressure of Oxygen**

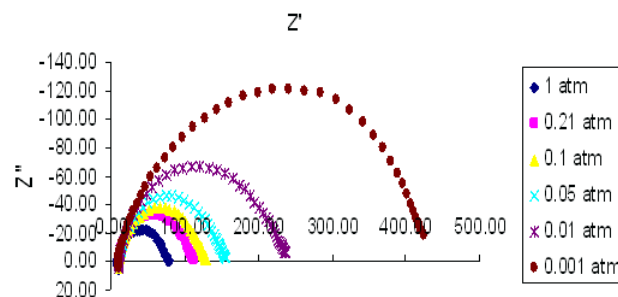


Figure 3. Impedance spectra on LSM patterned electrodes as a function of partial pressure of oxygen, PO_2 , in O_2 - N_2 gas mixtures as oxidant.

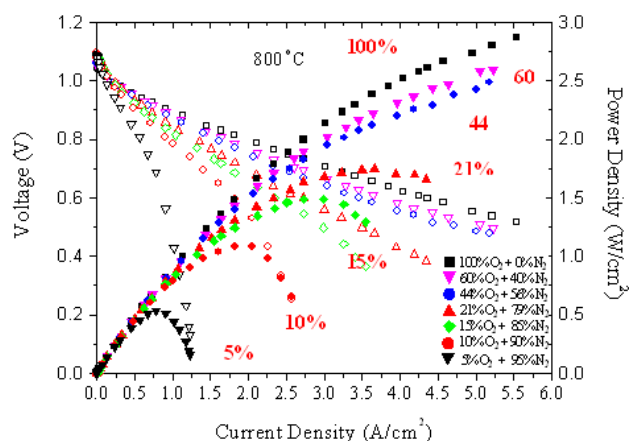


Figure 4. Voltage and power density vs. current density plots for a cell in oxidants of various compositions, ranging between ~5% O_2 + 95% N_2 to ~100% O_2 . Fuel: Hydrogen. Temperature: 800°C.

be achieved in pure oxygen. However, in an oxidant containing ~5% O_2 + ~95% N_2 , the power density is about 0.5 W/cm^2 . A large part of the decrease at high nitrogen concentration is related to the high charge transfer resistance at low oxygen concentrations. This result underscores the importance of investigating adsorption effects.

Conclusions

The principal objective of the work was to demonstrate the effects of oxygen content in the oxidant on parameters which determine cathodic

activity, namely surface exchange coefficient of MIEC materials and charge transfer resistance with predominantly electronic conductors as cathodes. These properties were investigated on LSC and LSM electrodes, respectively. The studies showed that both the surface exchange coefficient and charge transfer resistance are dependent on oxygen partial pressure. Single cells made and tested also showed that the performance increases with increasing oxygen partial pressure. The present work demonstrates a direct relationship between oxygen content and cathodic activation polarization and

explores its implications in governing cell performance. Power density as high as $\sim 2.9 \text{ W/cm}^2$ at 800°C was demonstrated.

FY 2004 Publications/Presentations

1. "Estimation of Charge Transfer Resistivity of $\text{La}_{0.8}\text{Sr}_{0.2}\text{MnO}_{3-\delta}$ (LSM) Cathode on $\text{Y}_{0.16}\text{Zr}_{0.84}\text{O}_{2-\lambda}$ (YSZ) Using Patterned Electrodes", R. Radhakrishnan, A. V. Virkar, and S. C. Singhal; accepted for publication in the Journal of the Electrochemical Society (2004).

III.A.19 Advanced Measurement and Modeling Techniques for Improved SOFC Cathodes

Stuart B. Adler (Primary Contact), Lilya Dunyushkina, Yunxiang Lu, and Jamie Wilson

Department of Chemical Engineering

University of Washington Box 351750

Seattle, WA 98115-1750

Phone: (206) 543-2131; Fax: (206) 685-3451; E-mail: stuardler@u.washington.edu

DOE Project Manager: Lane Wilson

Phone: (304) 285-1336; E-mail: Lane.Wilson@netl.doe.gov

Objectives

- Develop microelectrodes for improved isolation and measurement of the solid oxide fuel cell (SOFC) cathode overpotential (resistance) on cells having a thin electrolyte membrane.
- Develop nonlinear electrochemical impedance spectroscopy (NLEIS) for use in identifying what steps limit SOFC cathode performance.
- Generate a more detailed understanding of the electrochemistry governing SOFC cathodes, facilitating discovery and design of improved cathode materials and microstructures.

Approach

- Develop a MgO or MgO/spinel insulating mask layer which can regulate electrode/electrolyte contact with a spatial resolution of ± 50 microns.
- Develop a powder-based synthetic route for porous single-phase perovskite electrodes of the lanthanum strontium cobalt ferrite (LSCF) family, such that for a given bonding temperature one can vary surface area, porosity, and electrode morphology.
- Fabricate thin-film LSCF electrodes on ceria electrolytes, varying A/B ratio, electrolyte dopant type and concentration, and La/Sr ratio.
- Measure current-voltage (i - V) characteristics, impedance, and NLEIS response for both thin-film and porous perovskite electrodes.
- Model cathode performance and NLEIS characteristics using finite element analysis (FEA) methods, applied to thin-film and porous microstructures.

Accomplishments

- Demonstrated the insulation properties of screen-printed MgO/spinel as an insulating, thermal-expansion-matched mask layer.
- Conducted microelectrode half-cell measurements on both Pt/ceria and lanthanum strontium cobaltite (LSC)/ceria, and showed that the half-cell i - V characteristics and impedance add correctly to predict the response of a symmetric cell made from the same materials.
- Demonstrated frequency isolation of microelectrode half-cells.
- Completed i - V characteristics, impedance, and NLEIS measurements of porous $\text{La}_{0.8}\text{Sr}_{0.2}\text{CoO}_{3-\delta}$ (LSC-82) electrodes (symmetric cells on Sm-doped ceria) in air, including 1st and 3rd harmonic data.
- Developed a I - D FEA model for the harmonic response of LSC-82 to third harmonic, as required to analyze the measured harmonics above.

- Discovered an anomalous negative 3rd harmonic response for LSC-82, which is inconsistent with existing models for oxygen reduction and bulk transport.

Future Directions

- Measure and model NLEIS response of symmetric cells of laser-deposited LSC electrodes.
- Measure and model NLEIS response of *half-cells* (1st, 2nd, 3rd harmonic) of porous LSC, and interpret using 1-D model which incorporates surface diffusion.
- Develop thinner, more spatially resolved mask for use on thinner electrolytes.
- Examine role of processing on LSC/ceria interfacial bonding and resistance, as distinct from catalytic properties and transport to the interface.

Introduction

Many promising new cathode materials for solid oxide fuel cells incorporate *mixed conducting ceramics* (materials which carry both oxygen ions and electrons) in order to substantially enhance oxygen reduction at reduced temperature¹. For example, $\text{La}_{1-x}\text{Sr}_x\text{Co}_{1-y}\text{Fe}_y\text{O}_{3-\delta}$ (LSCF) cathodes utilize a significant portion of the electrode material surface, extending the reaction up to 10 microns from the electrode/electrolyte interface². While these electrodes have proven promising in early exploratory research, they are only empirically understood³, far from optimized^{4,5}, and can react unfavorably with the electrolyte^{6,7}. Significant materials development is required to bring these electrodes to commercial fruition.

In order to address these issues, we believe a new generation of diagnostic tools are required that can accelerate the screening, fabrication, optimization, and long-term performance evaluation of cathode materials. One issue we are currently addressing is improved isolation and measurement of the cathode resistance as distinct from the rest of the cell. Commercially viable SOFCs require thin electrolytes (10-150 μm), making it difficult to separate anode and cathode resistances using standard cell tests. We are developing microelectrodes that potentially offer improved accuracy, faster throughput, and broader screening capabilities, while maintaining the ability to test cells made by commercially relevant fabrication methods. The second issue we are working on is new experimental methods for distinguishing what factors limit cathode performance. Although electrochemical impedance spectroscopy (EIS) is widely used for cathode

development, results can be difficult to interpret in terms of mechanism and difficult to extrapolate to stack performance. We are currently developing extensions of EIS (NLEIS and electrochemical frequency modulation) that characterize the *nonlinear* cell response, potentially offering much higher resolution in terms of identifying rate-determining steps, separation of anode and cathode, and ability to predict cell performance based on half-cell measurements.

Approach

Figure 1 shows a schematic of the microelectrode cell design we are currently pursuing. The light area on the electrolyte surface is a mask

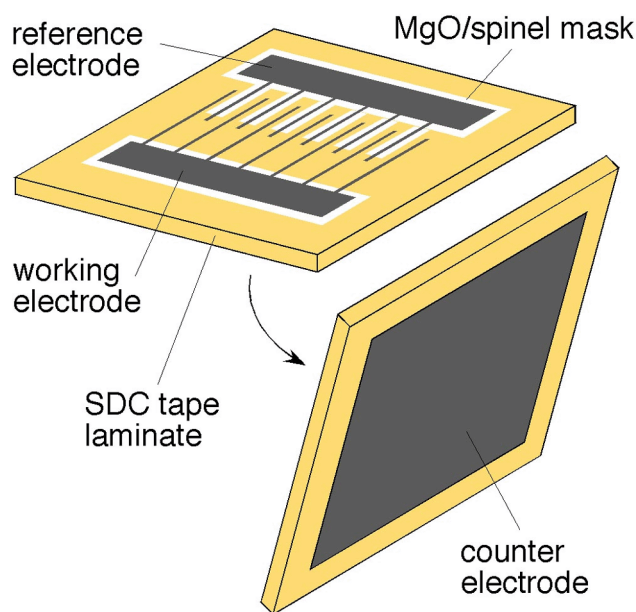


Figure 1. Cell Configuration of a Microelectrode Half-Cell

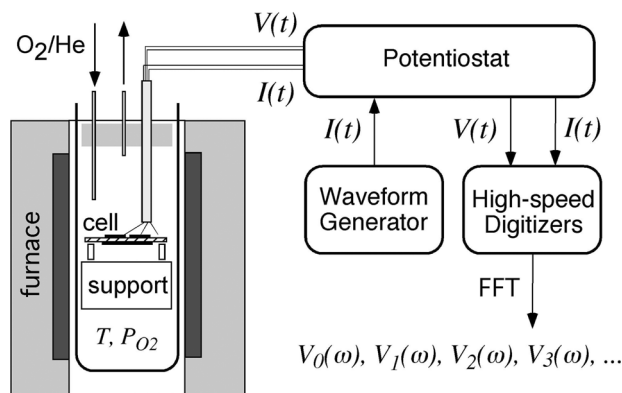


Figure 2. Schematic of NLEIS Experimental Apparatus

layer that regulates where the working and reference electrodes make contact to the electrolyte. In this way, the ohmic losses are well defined and confined to a region close to the working electrode (cathode) of experimental interest. Numerical simulations of this arrangement suggest that it provides a high degree of accuracy and frequency isolation. The mask layer is currently fabricated by screen printing and firing a MgO/spinel mixed powder ink onto a dense (fired) tape of Sm-doped ceria (SDC) electrolyte. The electrodes are subsequently processed onto the cell under the same conditions as any ordinary cell. Electrochemical measurements are then made, and performance is normalized to the actual area of the working electrode.

Figure 2 shows a schematic of our system for making NLEIS measurements. The frequency response analyzer normally used for impedance is replaced with a computer containing a sinusoidal signal generator and two synchronized high-speed analog-to-digital converters. The signal is used as the current set-point for a galvanostat, which measures and returns the current and voltage vs. time. These signals are then Fourier-transformed and analyzed to determine the magnitude and phase of any harmonics generated by the cell. These harmonics are analogous to those generated by a musical instrument around a base tone. One can tell which instrument is playing the same note (piano, oboe, violin) by the harmonics it generates. In our case, by constructing and solving physical models for the electrode's harmonic response, we can (in principle) tell which mechanism is correct by comparison of calculated and measured harmonics.

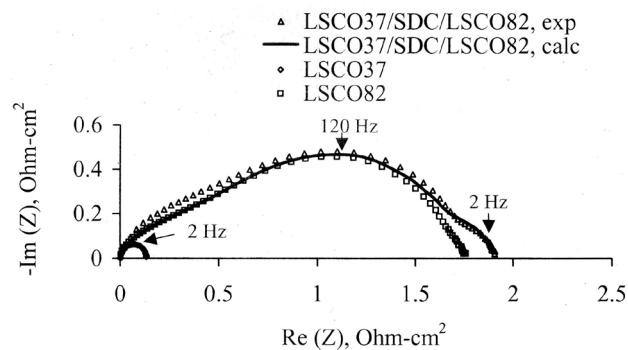


Figure 3. Impedance of LSC/SDC Cells in Air at 750°C

Results

Figure 3 shows the measured impedance of three cells. The first cell consists of a Sm-doped ceria (SDC) electrolyte, coated on one side with a full-sized (1 cm²) porous La_{0.3}Sr_{0.7}CoO_{3-δ} (LSC-37) electrode, and on the other with a full-sized porous La_{0.8}Sr_{0.2}CoO_{3-δ} (LSC-82) electrode. The other two cells are microelectrode half-cells consisting of LSC-37 and LSC-82 working electrodes, respectively, on SDC. Both half-cells have a 1-cm² LSC-82 counterelectrode. With the exception of the mask layer, the microelectrode half-cells were processed identically to the cell with full-sized electrodes. Due to differences in composition and processing temperature, the LSC-37 and LSC-82 electrodes have very different characteristics; the impedance magnitude of the LSC-82 electrode is about 10 times larger than that of the LSC-37 electrode, and it has a characteristic frequency approximately 100 times higher.

As shown in Figure 3, the impedance of the LSC-37/SDC/LSC-82 cell consists of two arcs, which presumably represent contributions of the two electrodes, respectively. In contrast, the microelectrode half-cells show only one arc, which differ from each other in resistance and frequency response. After area normalization, the impedance of the two half-cells were added, yielding a “calculated” impedance spectrum for a LSC-37/SDC/LSC-82 cell, assuming the same ohmic membrane resistance as the actual cell. The data lie nearly on top of each other, which is a testament to both the accuracy and frequency isolation of the microelectrodes, as well as the reproducibility of fabrication in this case.

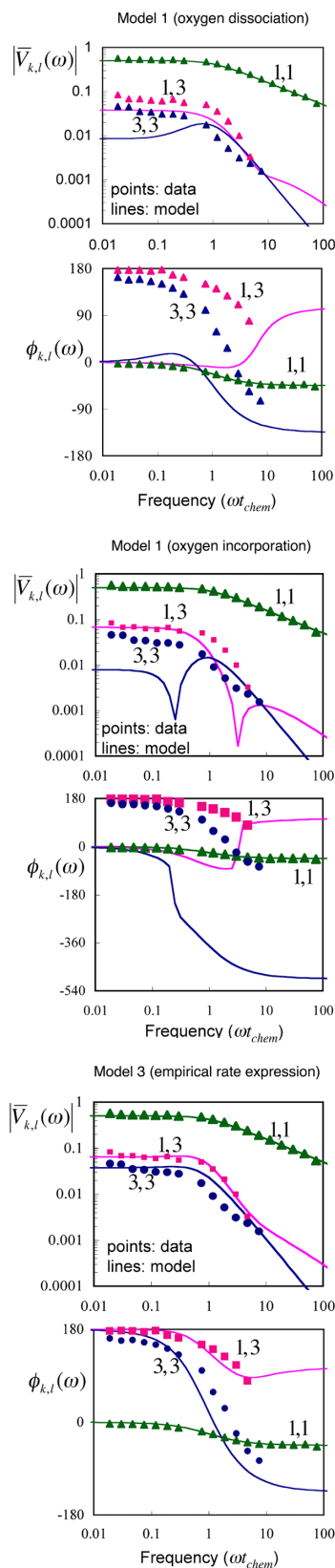


Figure 4. NLEIS Measurements of LSC-82/SDC at 750°C in Air

Moving on to NLEIS, Figure 4 shows Bode plots of the 1st (1,1) and 3rd (3,3) harmonic response of a symmetric LSC-82/SDC/LSC-82 cell in air at 750°C. Only the first and third harmonic signals are shown since the 2nd harmonic signal in this case was small due to the physical symmetry of the cell. Also shown is the 3rd-order contribution to the first harmonic (1,3), which can be thought of as a consistency check on the third harmonic. The data in the three columns are the same; the differences shown are various models for the response, which are explained below.

Figure 4 also shows calculated harmonics for the experimental results. All three models assume a bulk transport path for oxygen ions from the surface of the mixed conductor to the electrode/electrolyte interface, but make different assumptions about the mechanism of oxygen reduction. In the first model, oxygen reduction is assumed to be limited by oxygen dissociation. The second model assumes oxygen incorporation at the surface is limiting. Finally, the third column shows the predicted response assuming an empirical rate expression for oxygen reduction, which has never before been proposed.

The first thing to note is that all three of these models predict the same 1st harmonic (impedance). In other words, ordinary impedance (as a technique) does not provide any information that helps distinguish these various cases from each other. In contrast, the higher harmonics depend very strongly on the model assumptions. Clearly, model 1 (which is often assumed by workers) fails to predict many features of the data, even resulting in the wrong sign (180° phase difference) at low frequency. The second model is also wrong, predicting several nullifications (sign singularities) in the harmonic response, which are not observed. The best fit to the data appears to be model 3, but it is not yet clear if the improved fit is because the rate expression is correct, or merely because it is compensating for other false assumptions in the model (for example the neglecting of surface diffusion). We are currently investigating these issues.

Conclusions

Microelectrodes potentially offer an easy, low-cost way to isolate the performance of a particular electrode while maintaining the composition,

microstructure, and processing of that electrode as closely as possible to the electrode of interest.

NLEIS is a potentially useful and powerful new technique which provides higher resolution than traditional linear impedance for distinguishing specific mechanisms governing electrode response.

FY 2004 Publications/Presentations

1. J.R. Wilson, D.T. Schwartz, and S.B. Adler, "Nonlinear Electrochemical Impedance Spectroscopy for Solid Oxide Fuel Cell Cathode Materials," *submitted to Electrochimica Acta*.
2. L.A. Donyushkina, Y. Lu, and S.B. Adler, "Microelectrode Array for Isolating Electrode Polarization in Planar SOFC's," *in Preparation*.

Special Recognitions & Awards/Patents Issued

1. Charles W. Tobias Young Investigator Award of the Electrochemical Society (2004).

References

1. Lane, J. A.; Adler, S.; Middleton, P. H.; Steele, B. C. H. *Solid Oxide Fuel Cells (SOFC-IV)*, 1995; p 584-96.
2. Adler, S. B. *Solid State Ionics* **1998**, *111*, 125-134.
3. Steele, B. C. H.; Hori, K. M.; Uchino, S. *Solid State Ionics* **2000**, *135*, 445-450.
4. Steele, B. *Comptes Rendus De L Academie Des Sciences Serie Ii Fascicule C- Chimie* **1998**, *1*, 533-543.
5. Kleitz, M.; Petitbon, F. *Solid State Ionics* **1996**, *92*, 65-74.
6. Lau, S. K.; Singhal, S. C. *Proc. Corrosion* **1985**, *85*, 79.
7. Chen, C. C.; Nasrallah, M. M.; Anderson, H. U. *Proc. - Electrochem. Soc.* **1993**, *93-4*, 598-612.

III.B Fuel Processing

III.B.1 Technology Development in Support of the Solid State Energy Conversion Alliance

Michael Krumpelt (Primary Contact), Di-Jia Liu

Argonne National Laboratory

9700 S. Cass Avenue

Argonne, Illinois 60439

Phone: (630) 252-8520; Fax: (630) 252-4176; E-mail: krumpelt@cmt.anl.gov

DOE Project Manager: Norm Holcombe

Phone: (412) 386-4557; E-mail: Norman.Holcombe@netl.doe.gov

Objectives

- Improve the thermal stability of reforming catalyst for diesel fuel.
- Improve the sulfur tolerance of the catalysts.
- Characterize the catalytic activity.
- Determine long-term stability.

Approach

- Synthesize and characterize perovskites that are stable in hydrogen and oxygen and have redox chemistry on the "B" site.
- Explore the effects of different dopants on the A and B sites.
- Verify that the doped catalysts are chemically and thermally stable and relatively unaffected by sulfur-containing fuel.

Accomplishments

- A class of perovskites based on LaCrO_3 and LaAlO_3 and doped with 5% of a transition metal on the B site was found to have excellent activity for catalyzing the autothermal reforming of dodecane into a hydrogen-rich gas.
- The perovskites were shown to remain single phase in both reducing and oxidizing conditions, proving that the catalysis is occurring by redox chemistry on the B site and not on small metallic particles supported on an oxide matrix.
- The effect of 50 ppm of dibenzothiophene in dodecane was shown to be minimal.

Future Directions

- Optimize the composition of the catalysts in terms of activity for aromatics, aliphatics and other diesel components; cost; and sulfur tolerance.
- Determine the long-term stability.
- Work with a private sector organization on scaling up the process.

Introduction

Auxiliary power units (APUs) for heavy-duty vehicles could reduce emissions and conserve fuel where engines are kept running while drivers rest. An APU must have enough power to keep the cabin air-conditioned or heated in hot or cold climatic conditions, respectively, and may have to also supply electricity for refrigeration of loads. The amount of fuel needed will be significant, and drivers may resist having to refuel the APU with anything other than the diesel fuel used for the engine.

Converting diesel fuel into a hydrogen-rich gas that is suitable for solid oxide fuel cells is more challenging than converting gasoline because of the multi-cyclic aromatics and the aromatic sulfur compounds in diesel fuel. To break down these compounds, the operating temperature of the reformer needs to be raised, and the reforming catalyst needs to have a significant tolerance for sulfur. In making these statements, it is assumed that an autothermal reactor (ATR) [1] is used and that the diesel fuel is not desulfurized at the refinery.

When the operating temperature of the ATR exceeds about 800°C, catalyst stability becomes an issue. Noble metal catalysts such as rhodium, palladium or platinum on alumina or ceria not only lose some activity due to adsorption of hydrogen sulfide on the metal surface, but are further affected by evaporation and consolidation of the metal.

Approach

In earlier work at ANL to form noble metal ions, it was noticed that noble metals interact with supports containing oxide ion vacancies. It stands to reason, then, that the partial oxidation of hydrocarbon molecules might also be occurring on perovskite surfaces with B-site elements that can undergo redox reactions. Such catalysts would be expected to be more thermally stable than finely dispersed noble metals on alumina.

To be useful as an ATR catalyst, the perovskite must of course be chemically stable in oxidizing and reducing conditions. Lanthanum chromite and lanthanum aluminite meet that requirement. The first has some redox properties on the B site while the aluminite does not. However, doping with other

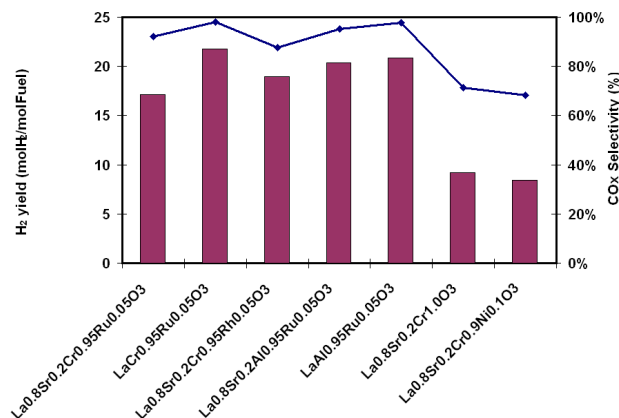


Figure 1. Hydrogen Yield (bar) and CO_x Selectivity (line) Obtained for Several Perovskite Catalysts during ATR Reforming

transition metal elements on the B site can make the surface more active. In this paper, we report results of doping chromite and aluminite with ruthenium.

Results

Shown in Figure 1 are the hydrogen yields and CO_x selectivities obtained under the ATR reforming condition of O₂/C = 0.5 and H₂O/C = 2. The ruthenium-doped lanthanum chromite is clearly much more active than the undoped chromite or the nickel-doped chromite. To our surprise, strontium substitution on the A- site seems to diminish the activity somewhat. Similarly, the aluminite-based perovskites with ruthenium doping on the B site performed very well, proving that the activity is associated with the B site doping and not the B site host. We also found that ruthenium-doped chromite has similar catalytic activity, as measured by the hydrogen yield and CO_x selectivity, to that of rhodium-doped perovskite during the reforming of dodecane. This is rather enlightening considering the significant difference in raw material cost. Further study, of course, is necessary to verify whether comparable performance can be achieved under a wider range of catalytic conditions or types of fuels.

One may ask whether the ruthenium or the rhodium is in fact substituted for chromium or aluminum in the perovskite lattice or present as metals or oxides on the surface. Efforts are underway to answer this question using extended x-ray absorption fine structure (EXAFS).

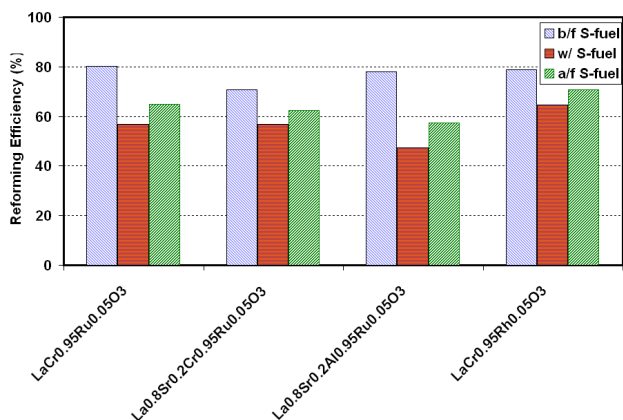


Figure 2. Total Reforming Efficiencies before, during, and after Exposure to DBT

Preliminary results indicate that the majority of the ruthenium and rhodium are anchored in the lattice.

One of the key challenges in diesel reforming is deactivation from sulfur poisoning. The current low-S diesel standard has sulfur content of 500 ppm with 350 ppm being typical. (In 2006, the sulfur limit drops to 15 ppm.) Unlike the case of gasoline, the organic sulfur compounds in diesel are from mainly polyaromatic molecules such as dibenzothiophene (DBT), methyl-dibenzothiophene, etc. These compounds are even harder to desulfurize and are expected to cause deactivation of reforming catalysts. Shown in Figure 2 are the total reforming

efficiencies of the ATR reaction over four perovskite catalysts before, during, and after exposure to the fuel containing the organic sulfur for 150 minutes. (The maximum reforming efficiency ranges from 81% to 87% depending on the product distribution between H₂ and CO.) The deactivation occurs over all the catalyst samples tested, albeit at different degrees. However, a significant recovery was also observed after the sulfur-contaminated fuel was replaced by S-free fuel.

Conclusions

Ruthenium-doped perovskites have been shown to be effective catalysts for the autothermal reforming of dodecane, and to retain a significant level of activity in the presence of sulfur. Whether multicyclic aromatics that constitute a few percent of diesel fuel can be reformed as well remains to be investigated.

References

1. M. Krumpelt, T. R. Krause, J. D. Carter, S. Ahmed, *Catalysis Today*, 77 (2002), 3-16.

III.B.2 Diesel Reforming for Solid Oxide Fuel Cell Auxiliary Power Units

Rodney L. Borup (Primary Contact), W. Jerry Parkinson, Michael A. Inbody, José I. Tafoya, and Dennis Guidry

Los Alamos National Laboratory

P.O. Box 1663

Los Alamos, NM 87545

Phone: (505) 667-2823; Fax: (505) 665-9507; E-mail: borup@lanl.gov

DOE Project Manager: Norm Holcombe

Phone: (412) 386-4557; E-mail: Norman.Holcombe@netl.doe.gov

Objectives

- Research and develop technologies for cost-effective and durable onboard diesel reformers for solid oxide fuel cell (SOFC) auxiliary power unit (APU) applications
- Examine experimentally the fundamentals of the diesel reforming process
 - Characterize the key parameters of the diesel reforming process
 - Fuel vaporization and mixing
 - SOFC anode exhaust recycle for water availability
 - Determine the factors that limit durability
 - Catalyst sintering and deactivation
 - Carbon formation during operation and startup
 - Develop and test processes to extend durability
 - Catalyst regeneration
- Develop models to provide a design and operation basis for a durable diesel reformer
 - Carbon formation models
 - System models to evaluate SOFC anode exhaust recycle

Approach

- Experimental measurements of diesel reforming in an adiabatic reactor
 - Simulate real-world diesel reformer operation and identify commercial design issues
 - Investigate and develop direct fuel injection and gas mixing
 - Evaluate the use of SOFC anode exhaust recycle on reactor operation, temperature profiles, carbon formation, and catalyst durability
 - Examine effects of fuel composition on operating parameters, outlet composition, and carbon formation
- Experimental measurements in an isothermal microscale reactor
 - Develop kinetic rate expression for carbon formation
 - Evaluate catalyst activity and develop rate expressions for diesel reforming
- Chemical models to interpret and codify experimental results
 - Develop chemical equilibrium model of carbon formation
 - Model reformer operation with SOFC anode exhaust recycle
 - Develop and apply kinetic models to describe details of diesel reforming process

Accomplishments

- Measured carbon formation
 - During isothermal diesel reforming simulating SOFC anode exhaust recycle
 - During adiabatic diesel reforming with anode exhaust recycle
 - Post-characterization of carbonaceous materials
- Measured catalyst surface area reduction during reforming of diesel fuel(s)
 - Measured radial and axial profiles of catalyst surface area after operation
- Measured axial temperature profiles for various operating conditions during adiabatic reforming of diesel fuel
- Measured diesel reforming characteristics simulating SOFC anode exhaust recycle
 - High adiabatic temperatures (>800°C) at low recycle rates (20%)
 - Increasing recycle rates moves oxidation downstream in reformer
- Refined carbon formation model to solve issues with convergence and user interface

Future Directions

- Experimental Measurements and Process Developments
 - Carbon formation
 - Quantify as a function of catalyst and recycle ratio
 - Define diesel components that contribute to high carbon formation rates
 - Examine additive effects (e.g., ethanol) on carbon formation
 - Investigate stand-alone startup and processes to avoid carbon formation
 - Develop carbon removal/catalyst regeneration processes
 - Catalyst sintering and deactivation
 - Develop reformer operational profiles that reduce catalyst sintering
 - Stabilize active catalyst particles
 - Reformer durability and hydrocarbon breakthrough effect on SOFC
 - Incorporate SOFC ‘button’ cell operating on reformat
 - Examine sulfur effect on reforming kinetics and carbon formation
- Modeling
 - Refine carbon formation models
 - Improve model by incorporating user carbon enthalpies
 - Develop ‘user-friendly’ interface
 - Examine system effects of anode recycle such as efficiency and parasitic losses
- Technology Transfer
 - Disseminate results via publications and presentations
 - Make carbon formation model available for Solid State Energy Conversion Alliance (SECA) teams

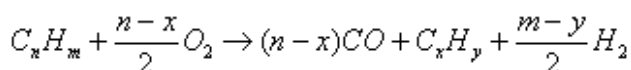
Introduction

The use of a solid oxide fuel cell (SOFC) to provide auxiliary power for diesel trucks can increase fuel efficiency and reduce emissions by reducing

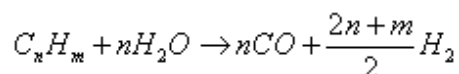
diesel engine idling time. The potential high-volume market for a SOFC auxiliary power unit (APU) could provide the driver for high-volume manufacturing to reduce the cost of a SOFC module, a key goal of the SECA Program. The logical fuel of choice for a

diesel truck SOFC APU is diesel fuel. SOFCs are being researched that directly oxidize hydrocarbon fuels, but the power densities are lower than SOFCs that use the products of reforming diesel fuel: H₂, CO, CO₂, H₂O, N₂, and hydrocarbons such as methane. Since the SOFC is the costly component of the system, increasing the power density provides benefits in reducing volume, mass, and cost that can offset the cost and complexity of adding a diesel reformer to the system. The objective of this project is to research and develop the technology to enable that diesel reformer to be cost-effective and durable.

Diesel fuel can be reformed into a H₂/CO-rich fuel feed stream for a SOFC by autothermal reforming (ATR), a combination of partial oxidation (POx),



and steam reforming (SR),



The typical autothermal reformer is an adiabatic, heterogeneous catalytic reactor, and the challenges in its design and operation, particularly durable operation, on diesel fuel are manifold. These challenges begin with the vaporization and mixing of diesel fuel with air and steam where pyrolysis can occur and improper mixing leads to hot spots and incomplete conversion. Changes in diesel fuel composition such as seasonal changes affect the reactor residence time for complete conversion and the optimal operating conditions. Carbon formation during operation and startup can lead to catalyst deactivation and fouling of downstream components, reducing durability. The exotherm of the POx reaction can generate temperatures in excess of 800°C [1], where catalysts rapidly sinter, reducing their lifetime. This exothermic temperature rise can be reduced by the endotherm of steam reforming, but this requires the addition of water along with design to balance the kinetic rates. Water addition also helps to reduce carbon formation, so a key issue becomes the source of the water onboard the vehicle. Our research begins to address these issues through an experimental and modeling examination of the fundamentals of these processes. The intent is to

provide a design and operation basis for a durable diesel reformer for a SOFC APU.

Approach

Our approach is to develop a fundamental understanding of the parameters that affect the design, operation, and durability of an onboard diesel fuel reformer for a SOFC APU. We employ experimental measurements in diesel reformer reactors and microscale reactors along with development and application of chemical models to interpret and codify experimental results. Experimental measurements of diesel reforming are made in an adiabatic heterogeneous catalytic reactor to simulate real-world diesel reformer operation and to identify commercial design issues. The reactor was used to investigate and develop direct diesel fuel injection for effective fuel vaporization and mixing with air and steam. The reactor was instrumented to measure axial profiles through the catalyst volume for examination of the effects of fuel constituents on reactor performance, catalyst surface area as a function of time and temperature, and the effects of SOFC anode recycle. Carbon formation was mapped as a function of operating conditions (S/C, O/C) and quantity of SOFC anode recycle. Following the experiments, the catalyst surface area was measured using Branauer-Emmett-Teller (BET) surface area measurement and carbonaceous deposits were characterized with thermogravimetric analysis.

Experiments conducted in the adiabatic reactor were complemented by experiments conducted in a well-controlled and well-defined isothermal microscale reactor, which can be used for measurements of kinetics of diesel reforming. The isothermal experiments were used to measure carbon formation rates for both partial oxidation and steam reforming conditions over a range of temperatures.

We are developing models of the diesel reforming process and system. An equilibrium chemical code has been developed and is being further refined to model the equilibrium conditions for carbon formation as a function of operating conditions, fuel composition, and thermodynamics of deposited carbon species. The equilibrium model was expanded to model the effect of SOFC anode recycle on the diesel reformer outlet composition and

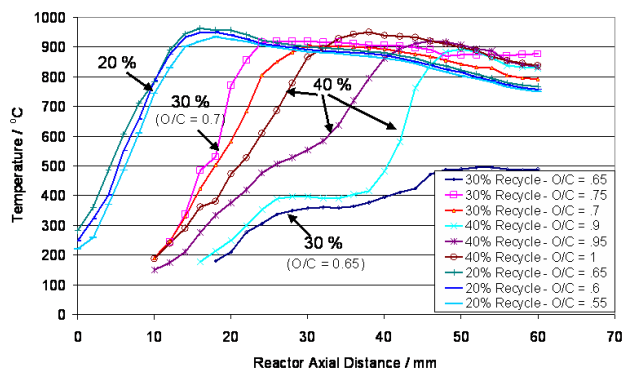


Figure 1. Axial temperature profiles measured during diesel reforming for simulated anode exhaust recycle ratios of 20% (O/C = 0.55, 0.60, 0.65), 30% (O/C = 0.65, 0.70, 0.75) and 40% (O/C = 0.90, 0.95, 1.00). Adjusted O/C with recycle ratio to obtain similar operating temperatures. Fuel was low-S Swedish diesel fuel. Pt/Rh supported catalyst, 1.5" diameter. Residence time ~ 50 msec.

temperatures. These models serve as a beginning for development of kinetic models to more accurately describe the measured temperature profiles and the diesel reforming process and to serve as a basis for optimal design of diesel reformers.

Results

A key factor in the successful operation of a commercial or experimental diesel reformer is effective vaporization of the diesel fuel and its mixing with air and steam. The challenge arises because of the propensity of diesel fuel to pyrolyze upon vaporization. This problem was solved in the experimental adiabatic reactor by using direct fuel injection through a commercial (BETE PJ8) nozzle. The air, steam, and SOFC anode recycle components were injected through an annulus around the fuel nozzle. Good mixing of the fuel and air streams was verified by thermal imaging of the outlet catalyst face. Good fuel distribution was observed at flow rates greater than 24 g/min fuel flow. Thus, the fuel turndown is limited by the flow distribution from the nozzle. Fuel/steam/air preheat was limited to below 180°C to prevent either clogging of the fuel nozzle by pyrolysis or unsteady fuel flow caused by vapor lock. The adiabatic reactor was modified further to measure axial temperature profiles through the catalyst volume

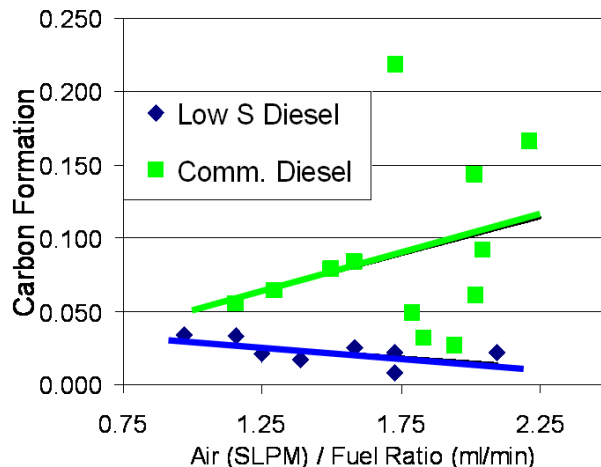


Figure 2. Carbon formation as a function of air/fuel ratio measured during adiabatic diesel reforming at 35% SOFC anode exhaust recycle ratio.

during operation. The catalysts used were Pt/Rh supported on an yttria-stabilized zirconia (YSZ) reticulated foam. This configuration of the adiabatic reactor was used in the following experiments.

Recycle of the SOFC anode exhaust into the diesel reformer is a simple method to supply water for steam reforming without an external water supply. The effect of SOFC anode exhaust recycle on diesel reforming was investigated by injecting a H₂/N₂/H₂O mixture into the operating adiabatic reactor. This mixture simulates SOFC anode exhaust by substituting H₂ for the H₂ and CO content of a real exhaust and N₂ for the N₂ and CO₂ content. Figure 1 shows axial temperature profiles measured through a Pt/Rh-supported catalyst in diesel reforming of low-sulfur Swedish diesel fuel for simulated SOFC anode exhaust recycle rates of 20%, 30%, and 40%. The oxygen to carbon ratio (O/C) was increased as the recycle flow was increased in order to maintain the reformer outlet temperatures between 750 and 850°C. The temperature profiles for 20% recycle show the temperature rise from the oxidation reactions starting at the catalyst inlet and peaking about 10 mm downstream. The temperature profiles for 30% and 40% recycle rates show the temperature rise from oxidation moves downstream to about 10-20 mm from the catalyst inlet. Higher recycle ratios require an increase in the O/C to achieve a similar adiabatic temperature because of the increased flow of inert species.

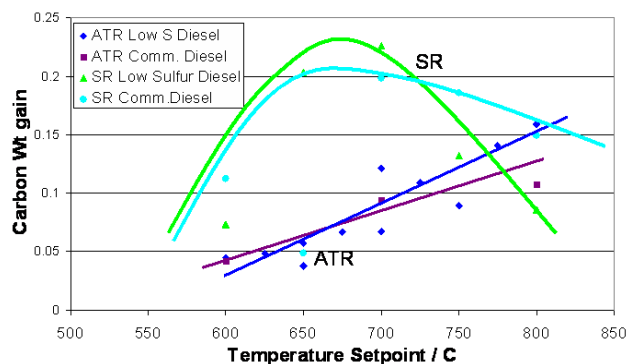


Figure 3. Carbon formation measured as a function of temperature in the isothermal microcatalyst reactor for ATR conditions ($O/C = 1.0$, $S/C = 0.34$) simulating 35% SOFC anode exhaust recycle ratio and for steam reforming conditions ($O/C = 0.0$, $S/C = 1.0$).

Experiments were conducted using the adiabatic reactor to investigate the effect of fuels and, for each fuel, to map the outlet gas composition and carbon formation as a function of operating condition. Figure 2 shows measured carbon formation in adiabatic diesel reforming of low-S Swedish diesel fuel and commercial diesel fuel as a function of air-fuel ratio. Carbon formation with the commercial diesel fuel was on average three times higher than that for the low-S Swedish diesel fuel. Carbon formation increased with increasing air flow and temperature for commercial diesel fuel, while carbon formation decreased with increasing air flow and temperature for low-S Swedish diesel fuel.

Experiments were conducted using an isothermal microscale reactor to clarify the effects of temperature and specific operating conditions on carbon formation rates. Figure 3 shows carbon formation as a function of temperature for autothermal reforming (ATR) ($O/C = 1.0$, $S/C = 0.34$) and for pure steam reforming ($O/C = 0.0$, $S/C = 1.0$) of low-S Swedish diesel fuel and commercial diesel fuel. These measurements were taken over a period of 5 hours in the microscale reactor held at a constant temperature in a tube furnace. The ATR conditions simulate similar adiabatic measurements for a SOFC anode recycle of 35%. Under these ATR conditions, carbon formation increases linearly with temperature, contrary to equilibrium predictions.

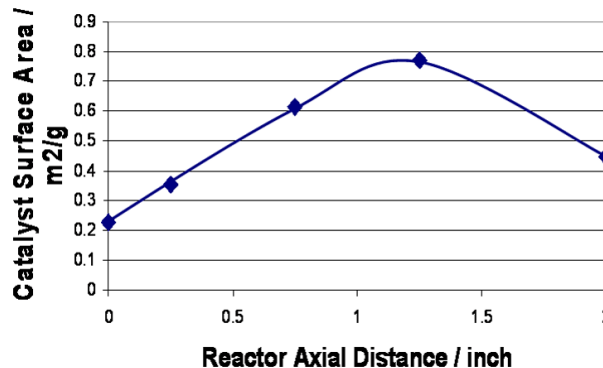


Figure 4. Axial profile of catalyst surface area (radially averaged) after adiabatic diesel reforming at 35% anode recycle by BET.

Carbon formation in steam reforming conditions appears to be limited by kinetic rates as the temperature increases to a carbon formation maximum at 700°C; then, at higher temperatures, carbon formation decreases with increasing temperature as predicted by equilibrium. In these experiments, the carbon formed during reforming was collected downstream of the catalyst and did not adhere to the Pt/Rh catalyst surface. However, carbon has been observed on the surface of Pt/Al₂O₃ catalysts in other diesel reforming measurements [10].

For a SOFC APU, a diesel reformer should convert all of the hydrocarbons in the fuel to CO, CO₂, and CH₄. In practice, hydrocarbon breakthrough is observed after 500 to 1000 hours of operation and is ascribed to loss of catalyst surface area [2,3]. A cylindrical catalyst used in the adiabatic reformer for diesel reforming measurements at a simulated anode recycle rate of 35% was sectioned axially and radially, and the catalyst surface area of each section was measured using BET. Table 1 lists the measured catalyst surface areas and the percentage remaining of the fresh surface area of ~ 4.3 m²/g. The axial profile (radially averaged) of the catalyst surface area after testing is shown in Figure 4. Catalyst surface areas are approximately constant across the catalyst but are smaller at the inlet than at longer axial distances. This is an indication that the high temperatures observed from the oxidation reaction could be sintering the catalyst at the reactor inlet.

Table 1. Catalyst surface areas measured at radial and axial locations of a Pt/Rh catalyst on a cylindrical YSZ foam support after adiabatic diesel reforming experiments with a simulated SOFC anode exhaust recycle rate of 35%. Surface areas were measured with BET. Table entries are formatted as surface area in m²/g (percent remaining of the average fresh catalyst surface area of 4.3 m²/g).

Depth (inch)	Radius (inch)				
	-0.56	-0.28	0.00	0.28	0.56
0.00	0.208 (4.8)	0.274 (6.4)	0.284 (6.6)	0.259 (6.0)	0.168 (3.9)
0.25	0.200 (4.6)	0.447 (10.4)	0.290 (6.7)	0.466 (10.8)	0.460 (10.7)
0.75	0.435 (10.1)	0.756 (17.6)	0.582 (13.5)	0.538 (12.5)	0.764 (17.8)
1.25	0.575 (13.4)	0.913 (21.2)	0.800 (18.6)	0.837 (19.5)	0.727 (16.9)
2.00	0.578 (13.4)	0.398 (9.3)	0.586 (13.6)	0.304 (7.1)	0.363 (8.4)

Conclusions

Diesel fuel reforming has been conducted under isothermal conditions and under adiabatic conditions to examine the oxidation and reforming reactions, operational conditions, catalyst activity and durability, and carbon formation. Carbon formation has been modeled for equilibrium conditions and has been measured during isothermal and adiabatic diesel reforming operation.

Diesel reforming with adiabatic operation has simulated SOFC anode recycle, without other additional water, with operation at about 30-40% recycle reasonably successful in terms of diesel conversion, carbon formation and catalyst temperature control. Temperature profiles inside the catalyst have been measured for a number of recycle rates and oxygen/carbon ratios and for various fuels, including commercial diesel and low-sulfur diesel. Increasing recycle rates moves oxidation downstream in the reformer, as does commercial diesel fuel compared with low-sulfur diesel fuel. High adiabatic temperatures (>800°C) are generally

observed at low recycle rates (20%). Operation with 30-40% recycle rate appears to be a good trade-off between high adiabatic temperatures and larger reactor volume.

Isothermal carbon formation measurements from steam reforming (O/C = 0.0, S/C = 1.0) appear to show both kinetic and equilibrium effects, with a maximum amount of carbon formation at about 700°C, for both commercial diesel fuel and low-sulfur diesel fuel. Autothermal reforming (O/C = 1.0, S/C = 0.36) measurements made isothermally show increasing carbon formation with increasing temperature, in contrast to equilibrium predictions. Adiabatic operation shows lower carbon formation for higher operating temperatures for low-sulfur diesel fuel, but higher carbon formation for higher operating temperatures for commercial diesel fuel.

References

1. Ahmed, S., Presentation to Department of Energy, Washington, DC, May 01, 2003
2. Borup, R.L., Inbody, M.A., Tafoya, J.I., Guidry, D.R., Vigil, W.J., Semelsberger, T.A., DOE Hydrogen, Fuel Cells & Infrastructure Technologies Program Review and Peer Evaluation Meeting, Berkeley, CA, May 21, 2003
3. Kopasz, J.P., Applegate, D., Miller, L., Rossignol, C., DOE Hydrogen, Fuel Cells & Infrastructure Technologies Program Review and Peer Evaluation Meeting, Berkeley, CA, May 21, 2003.
4. Berry, D.A., Shekhawat, D., Gardner, T.H., Shamsi, A., DOE SECA – Solid State Energy Conversion Alliance Core Technology Review Meeting, Albany, NY, October 1, 2003

FY 2004 Publications/Presentations

1. Diesel and Gasoline Reforming for Fuel Cell Systems, Rodney L. Borup, W. Jerry Parkinson, Michael A. Inbody, José I. Tafoya, Will J. Vigil, Troy A. Semelsberger, and Dennis R. Guidry, Fuel Cell Seminar, Miami, November 3-6, 2003

2. Fuel Composition Effect on Fuel Cell Reformer Performance and Light-off, Rodney L. Borup, Michael A. Inbody, José I. Tafoya, Troy A. Semelsberger, Will J. Vigil, and Dennis R. Guidry, 224th National Meeting of the American Chemical Society, August 20, 2003
3. Hydrocarbon Reforming for Fuel Cell Systems: Fuel Effects on Fuel Processor and Light-off, Rodney L. Borup, Michael A. Inbody, José I. Tafoya, Will J. Vigil and Dennis R. Guidry, National Meeting of the American Institute of Chemical Engineers, San Francisco, November 17-19, 2003
4. Fuels Testing in Fuel Reformers for Transportation Fuel Cells, Rodney L. Borup, Michael A. Inbody, José I. Tafoya, Troy A. Semelsberger, Will J. Vigil, and Dennis R. Guidry, 2003 SAE Powertrain & Fluid Systems Conference, Pittsburgh, October 27-30, 2003
5. Fuels Testing in Fuel Reformers for Transportation Fuel Cells, Rodney L. Borup, Michael A. Inbody, José I. Tafoya, William J. Vigil, and Troy A. Semelsberger, SAE International Paper #: 03FFL-253
6. Diesel Reforming with SOFC Anode Recycle, Rodney L. Borup, W. Jerry Parkinson, Michael A. Inbody, José I. Tafoya, and Dennis R. Guidry, Electrochemical Society, San Antonio, May 9-14, 2004
7. SOFC Anode Recycle Effect on Diesel Reforming, Rodney L. Borup, W. Jerry Parkinson, Michael A. Inbody, José I. Tafoya, and Dennis R. Guidry, American Institute of Chemical Engineers, New Orleans, April 26-29, 2004.

III.B.3 Fundamental Reforming Studies - Role of Catalytic O₂ Supports on Fuel Reforming

David A. Berry (Primary Contact) and Maria Salazar Villaphando (WVU)

U. S. Department of Energy

National Energy Technology Laboratory

P. O. Box 880

3610 Collins Ferry Road

Morgantown, WV 26507-0880

Phone: (304) 285-4430; Fax: (304) 285-4469; E-mail: David.Berry@netl.doe.gov

Subcontractor: West Virginia University (WVU), Morgantown, WV

Objectives

- Search for long-duration reforming catalysts in the development of auxiliary power units.
- Investigate the role of oxygen-conducting supports in reforming of diesel fuel compounds and their role in decreasing carbon formation and/or increasing sulfur tolerance.

Approach

- Several sample matrices of ceria-based catalysts will be studied to elucidate the effects of the following variables on the rate of carbon formation and conversion:
 - Support type (CeO₂ and Al₂O₃)
 - Catalyst type (Pt, Ni, Rh)
 - Dopant concentration in the oxygen ion conductor
 - Dopant type (La, Gd) in the oxygen ion conductor
 - Ionic conductivity
 - Oxygen storage capacity vs. ionic conductivity
- Catalyst characterization will include ionic conductivity, oxygen storage capacity, surface area, dispersion, crystal size, crystal phase and surface composition.
- Catalytic activity and selectivity will be determined for partial oxidation of hydrocarbons (POH) as a function of temperature, CH₄/O₂ and space velocity.
- Post reaction analysis of the catalysts will include transmission electron microscopy (TEM) and/or scanning electron microscopy (SEM), surface area, crystal size and crystal phase.
- Labeled reaction mixtures and labeled doped ceria catalysts will be tested during isotopic studies.
- Post reaction analysis by nuclear reaction analysis and secondary ion mass spectroscopy is planned to complement the isotopic studies.
- Studies related to sulfur tolerance are planned for the second stage of this project.

Accomplishments

- Experimental facilities were constructed, including two catalytic flow reactors conditioned to operate with liquid fuels and liquid products, mass spectrometer and Auto Chem 2910 analytical instruments.
- A comprehensive test matrix was developed to examine most relevant variables.
- Catalytic experimental tests and catalyst characterization have been initiated.
- Partial oxidation of methane was conducted on Rh/Al₂O₃ as a function of temperature.

- Catalytic activity of Pt/CeO₂ during partial oxidation of methane was examined.
- Surface area of catalysts was determined, and results showed values in the range of 30-60 m²/g.
- A review paper was presented at the Second International Conference on Fuel Cell Science, Engineering and Technology.
- Merit review was presented.

Future Directions

- Study the role of oxygen-conducting supports to increase sulfur tolerance.
- Investigate the effects of supported metal alloys and their role in decreasing carbon deposition and/or increasing sulfur tolerance.
- Further investigate catalysts that are able to mitigate carbon formation and or increase sulfur tolerance.

Introduction

Ceria-based catalysts are being investigated in order to fundamentally understand the role of oxygen-conducting supports in reforming of diesel fuel compounds and their role in decreasing carbon deposition. Ceria-based catalysts have shown ability to decrease carbon formation during partial oxidation of hydrocarbons (1,2). It has been speculated that this property is due to their high oxygen ion mobility. In this project, this assumption will be further investigated. This project is in an early stage, and most of the work conducted so far includes the set-up of experimental facilities and elaboration of experimental plan.

Approach

Ceria-based catalysts will be investigated, and the amount of deposited carbon will be determined as function of support type (CeO₂ and Al₂O₃), catalyst type (Pt, Ni, Rh), dopant type (La, Gd), dopant concentration, ionic conductivity and oxygen storage capacity. Catalytic activity and selectivity as a function of temperature, CH₄/O₂ and space velocity will be determined during the POH reactions.

Characterization of ceria-based catalysts will include ionic conductivity, oxygen storage capacity, surface area, dispersion, crystal size, crystal phase and surface composition. Post reaction analysis will include surface area and particle size, and selected samples will be analyzed by SEM to investigate types of carbon.

Isotopic exchange studies will be performed in order to obtain a mechanistic understanding of the influence of the oxygen ion mobility on the mitigation of carbon formation. Labeled reaction mixtures and doped ceria catalysts will be used in these experiments. Post reaction analysis of the catalysts by nuclear reaction analysis and secondary ion mass spectroscopy will allow quantifying the role of lattice oxygen in the formation of carbon.

Results

Table 1 shows product composition as a function of temperature for the partial oxidation of methane on Rh/Al₂O₃. The reaction was conducted at CH₄/O₂=2 and space velocity = 60,000 cm³h⁻¹g⁻¹. The catalytic activity tests were performed at different temperatures ranging from 450°C to 850°C, and catalysts were kept for 1 hour at each temperature. The conversion of methane and the production of CO and H₂ are increasing as a function of temperature. The concentration of CO₂ is higher at lower temperatures and lower at higher temperatures. This

Table 1. Partial Oxidation of Methane over Rh/Al₂O₃ (60,000 cm³h⁻¹g⁻¹)

Mol (%)	450°C	550°C	650°C	750°C	800°C	850°C
CH ₄	6.68	5.15	3.22	2.09	1.25	0.74
CO	0.51	3.00	5.44	6.90	7.95	8.67
CO ₂	3.25	2.34	1.25	0.68	0.33	0.07
H ₂	4.90	8.95	12.21	14.59	16.36	17.52

agrees with the reaction mechanism proposed for the partial oxidation of methane. It is suggested that it occurs in two steps: in the first step, combustion of methane takes place, producing CO₂ and H₂O; in the second step, synthesis gas is produced via CO₂ and steam reforming reactions of un-reacted methane. It is also suggested that the CO₂ reaction is slower than the steam reforming, which explains the higher concentrations of CO₂ at lower temperature (3).

Table 2 shows the product composition for the partial oxidation of methane, conducted on Rh/CeO₂ at 850°C for 5 hours, space velocity = 21,000 cm³h⁻¹g⁻¹ and CH₄/O₂=2.

Table 2. Partial Oxidation of Methane over Pt/CeO₂ at 850°C (21,000 cm³h⁻¹g⁻¹)

Compound	Mol (%)
CH ₄	1.92
CO	8.44
CO ₂	0.16
H ₂	17.21

Conclusions

This project has just recently started and it is in an early stage. Although it is too early to quantify, limited testing of ionically conductive supported catalysts shows a trend towards less carbon formation than is observed in non-conductive supported catalysts.

References

1. Applied Catalysis A: General 225(2002) 63-75.
2. Applied Catalysis B: Environmental 19 (1998) 267.
3. Catalysis Letters Vol. 91, Nos. 1 2 November 2003.

FY 2004 Publications

1. "Synthesis gas by partial oxidation and the role of oxygen-conducting supports: A review" was accepted for publication as proceedings from the Second International Conference on Fuel Cell Science, Engineering and Technology (2004).

FY 2004 Presentations

1. Presentation at the Second International Conference on Fuel Cell Science, Engineering and Technology. June 16, 2004. "Synthesis gas by partial oxidation and the role of oxygen-conducting supports: A review".

III.B.4 Hexaaluminate Reforming Catalysts

Todd H. Gardner (Primary Contact), Dushyant Shekhawat and David A. Berry

U. S. Department of Energy

National Energy Technology Laboratory

3610 Collins Ferry Road

P.O. Box 880

Morgantown, WV 26507-0880

Phone: (304) 285-4226; Fax: (304) 285-0943; E-mail: Todd.Gardner@netl.doe.gov

Objectives

- Develop a durable, low-cost middle distillate reforming catalyst with improved thermal stability and greater resistance toward carbon formation.
- Evaluate activity and selectivity of transition metal doped hexaaluminate catalysts.
 - Correlate activity and selectivity at various levels of transition metal doping.
 - Evaluate the thermal stability and reductive resistance of hexaaluminate catalyst systems.
 - Evaluate carbon formation characteristics.

Approach

- Synthesize and characterize transition metal doped hexaaluminate catalysts.
- Evaluate catalyst activity by turnover frequency (TOF) with model fuel compounds.
- Examine the effect of transition metal doping level on activity and selectivity.
- Examine carbon formation characteristics by post experiment analysis.
- Evaluate long-term stability.

Accomplishments

- Set up new test facilities for continuous unattended operation (operation up to 982°C and 80 psig).
- Synthesized $\text{LaCoAl}_{11}\text{O}_{19}$, $\text{LaFeAl}_{11}\text{O}_{19.5}$, $\text{LaNiAl}_{11}\text{O}_{19}$ catalyst samples.
- Identified optimal processing conditions for active phase formation and maximum surface area.
- Performed reductive stability experiments on $\text{LaCoAl}_{11}\text{O}_{19}$, $\text{LaFeAl}_{11}\text{O}_{19.5}$, and $\text{LaNiAl}_{11}\text{O}_{19}$ using temperature-programmed reduction (TPR) in 5 vol% H_2/Ar .
- Performed partial oxidation activity and selectivity screening experiments on the $\text{LaNiAl}_{11}\text{O}_{19}$ catalyst with CH_4 ; O/C = 1.0 at 850°C and 2 atm.
- Demonstrated 165 hours of operation on $\text{LaNiAl}_{11}\text{O}_{19}$ catalyst with CH_4 partial oxidation; O/C = 1.0 at 850°C and 2 atm.

Future Directions

- Improved catalyst durability:
 - Optimize active metal dopant level.
- Improved catalyst activity:
 - Evaluate activity and selectivity of platinum group metal doped hexaaluminate catalysts.
- Improved carbon formation resistance:
 - Evaluate the effect of alkaline earth doping on carbon formation.

- Improved sulfur resistance:
 - Evaluate the effects of high-temperature operation on sulfur resistance.
- Evaluate bi-metallic dopant combinations for sulfur resistance.

Introduction

The most promising route to hydrogen production from middle distillate fuels is catalytic reforming. For this application, the National Energy Technology Laboratory (NETL) is developing a new class of catalysts based on hexaalumina. Hexaalumina is of interest primarily due to its layered spinel structure that has been shown to be stable at high temperatures (1, 2). Catalytically active metals are doped directly into the structure, resulting in a highly dispersed catalyst system that has been shown to possess reductive stability (3, 4). This project is in its early stages with new test facilities having been constructed and initial catalyst synthesis and characterization having been undertaken.

Approach

A series of catalysts based on transition metal doped hexaalumina, with the general formula $AB_yAl_{12-y}O_{19-z}$, were prepared by co-precipitation from nitrate salt precursors. Catalyst activity, selectivity and reductive resistance will be investigated as a function of A-site (A = La, Ca, Sr and Ba) and B-site (B = Co, Fe, Ni, Rh, Pt, Pd) dopant type and concentration.

Methane partial oxidation will be used to initially screen catalysts for activity and selectivity. N-tetradecane and 1-methyl naphthalene will be utilized as model diesel fuel compounds. Catalyst activity will be measured fundamentally by TOF. Conversion activity, selectivity and carbon formation characteristics will be investigated at various temperatures, O/C ratios and space velocities. Catalyst reductive resistance will be assessed by TPR.

Characterization of hexaalumina catalysts will include active surface area determination, average crystallite size, active phase and surface composition. Post reaction analysis will consist of temperature-programmed oxidation (TPO) and scanning electron microscopy (SEM) for carbon forms and active surface area.



Figure 1. Catalyst Test Facility

Results

Figure 1 shows the new test facility that was constructed and instrumented for continuous and unattended operation. The facility consists of two isothermal fixed-bed reactors capable of operation at 982°C and 80 psig. Online gas phase analysis is determined by gas chromatograph-flame ionization detector (GC-FID) and mass spectrometer. The units are capable of simultaneous water and liquid hydrocarbon feeds. TPR and TPO of catalyst samples can be performed in-situ.

The reduction resistance of $LaCoAl_{11}O_{19}$, $LaFeAl_{11}O_{19.5}$, $LaNiAl_{11}O_{19}$ catalysts was determined by TPR in 5 vol% H_2/Ar . Figure 2 is a plot comparing the TPR spectra for these catalyst samples. $LaCoAl_{11}O_{19}$ showed a single reduction peak at 1093°C, indicating the reduction of Co^{+2} to Co^0 . $LaFeAl_{11}O_{19.5}$ showed two reduction peaks; the first, located at 407°C, is the reduction of Fe^{3+} to Fe^{2+} . The second peak, located at 1098°C, is the reduction of Fe^{2+} to Fe^0 . $LaNiAl_{11}O_{19}$ exhibited a single broad reduction peak at 1017°C, indicating the reduction of Ni^{2+} to Ni^0 . All samples exhibited a high degree of reduction stability.

Figure 3 shows the conversion activity and selectivity for CH_4 partial oxidation over

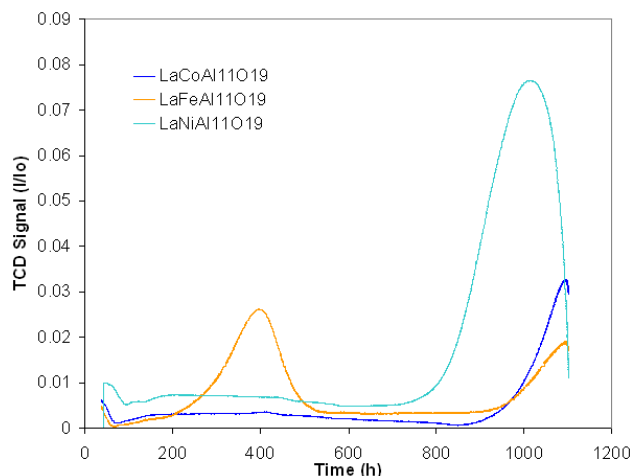


Figure 2. TPR of $\text{LaCoAl}_{11}\text{O}_{19}$, $\text{LaFeAl}_{11}\text{O}_{19.5}$, $\text{LaNiAl}_{11}\text{O}_{19}$ Catalysts in 5 vol% H_2/Ar

$\text{LaNiAl}_{11}\text{O}_{19}$, conducted at $\text{O/C} = 1.0$, $T = 850^\circ\text{C}$, $P = 2$ atm and gas hourly space velocity = $16,713 \text{ cm}^3\text{h}^{-1}\text{g}^{-1}$. The catalyst was first pre-reduced in 5 vol% H_2 at 900°C for 1 hour. The selectivity toward H_2 and CO ($\text{H}_2/\text{CO} = 2.0\text{-}2.1$) was stable over 165 hours of operation. An average CH_4 conversion of 87% was obtained..

Conclusions

Hexaaluminate catalysts exhibited a high degree of reductive stability as determined by TPR. CH_4 partial oxidation experiments on $\text{LaNiAl}_{11}\text{O}_{19}$ indicate that this catalyst is very active for partial oxidation and exhibits a high selectivity toward H_2 and CO .

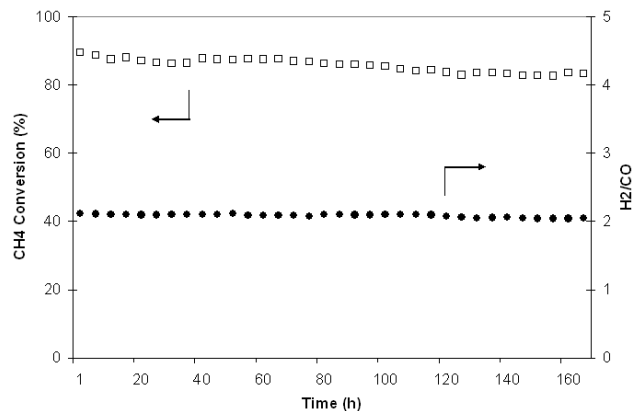


Figure 3. CH_4 Conversion and Selectivity of $\text{LaNiAl}_{11}\text{O}_{19}$

References

1. Machida, M., Shiomitsu, T. and Eguchi, K., *J. Solid State Chem.* 95 (1991) 220-223
2. Machida, M., Eguchi, K. and Arai, H., *J. Catal.* 103 (1987) 385-393
3. Xu, Z., Zhen, M., Bi, Y. and Zhen, K., *Catal. Lett.* 64 (2000) 157-161
4. Xu, Z., Zhen, M., Bi, Y. and Zhen, K., *Appl. Catal. A: Gen.* 198 (2000) 267-273

FY 2004 Publications/Presentations

1. Chemical Engineering Seminar, presentation to West Virginia University in April
2. SECA Core Conference Review
3. Partial Oxidation of n-Tetradecane over LaNi -Hexaaluminate, accepted to AIChE conference in November

III.B.5 Diesel Fuel Reforming Kinetics

Dushyant Shekhawat (Primary Contact), David A. Berry, and Todd H. Gardner

U. S. Department of Energy

National Energy Technology Laboratory

P. O. Box 880

3610 Collins Ferry Road

Morgantown, WV 26507-0880

Phone: (304) 285-4634; Fax: (304) 285-4469; E-mail: Dushyant.Shekhawat@netl.doe.gov

Objectives

- Provide kinetic reaction rate and process information of diesel fuel reforming to support the development of auxiliary power units (APUs) in commercial diesel truck transport and other related applications

Approach

- Propose initial kinetic network for individual model compounds
- Develop intuitive kinetic models for individual model compounds
- Conduct combinatorial fuel compound studies
- Develop surface response maps for binary fuel mixtures
- Correlate fuel reforming rates (versus process conditions) and catalyst type for individual and combined diesel constituents (surrogate diesel fuel)

Accomplishments

- Conducted combinatorial fuel compound studies
- Developed surface response maps for steam reforming (SR), partial oxidation (POX) and autothermal reforming (ATR) over Pt catalysts for single-component fuels
- Proposed probable kinetic schemes for different hydrocarbons

Future Directions

- Conduct ternary fuel compound studies
- Evaluate other fuel compounds within a classification to examine if similar reforming behavior exists
- Develop intuitive kinetic models for individual model compounds and benchmark fuel for particular catalyst types
- Continue evaluation of carbon formation
- Collaborate with Los Alamos National Laboratory to provide carbon deactivation kinetics
- Obtain experimental reactor performance data to validate reaction models and provide for fuel reactant mixing modeling capability suitable for CFD modeling codes
- Develop a detailed kinetic model that incorporates CFD

Introduction

The fuel processor is a critical component of fuel cell systems. The processor must be able to provide a clean, tailored synthesis gas to the fuel cell stack for long-term operation. Key characteristics desired

for the processor (and the system) include low cost, high efficiency, maximum thermal integration, low maintenance intervals, and acceptable startup and transient response. There are several barrier issues that must be overcome to achieve these characteristics. Carbon formation, particularly upon

startup, must be minimized to avoid coking of the catalysts in the reformer and downstream fuel cell. Fuels containing sulfur can poison both the reforming catalysts and the fuel cell anode. High thermal mass components (some of which may have heat-ramp restrictions) can limit startup times and transient response. And finally, cost targets must be achieved to ensure commercial success.

Fundamental understanding for design and operation of reformers is important for successful technology development. One of the most fundamental engineering design parameters that can be measured in the laboratory is the intrinsic kinetics of a catalyst system. Once established for a particular feedstock and catalyst system, kinetics can be coupled with computational fluid dynamics (CFD) code to effectively design, optimize, and minimize hydrocarbon slip in autothermal reformer systems. In principle, the kinetics of NO_x formation, sulfur poisoning, carbon formation and catalyst aging can be added to allow for a complete predictive model for reformer performance and operation.

However, modeling of reforming systems is extremely complicated. Diesel fuel consists of a complex, variable mixture of hundreds of hydrocarbon compounds, containing mainly olefins, saturates and aromatics. Empirical expressions for space velocity or simple power law-type models are typically used to design reformers. Unfortunately, these tend to be limited to a specific catalyst, fuel composition, and operating point. Therefore, the development of validated predictive models that can account for variations in these parameters is necessary.

For the autothermal reforming of diesel with steam and oxygen, a complex reaction network is expected. Elucidation of this network and the development of a generalized complex network model for platinum catalysts will be the initial focus of this body of work. The overall kinetic approach employed will balance the level of detail that can accurately be accommodated by CFD code with the ability to easily update kinetic parameters for a new catalyst system.

Approach

To select an appropriate model, it is necessary to understand the reaction mechanisms and pathways for the chemical system. One approach to gaining that understanding is surface response mapping. This is a statistical technique used to map characteristic responses (e.g. yield, conversion, carbon buildup, etc.) to input variables (O₂/C, H₂O/C, temperature, space velocity, etc.) over a defined region. It identifies the significance of parameters and their interactions. Also, it provides data that can lead to validation of kinetic models and can test the statistical significance of proposed reaction pathways. As the most important mechanisms and reaction pathways are defined, appropriate models will be selected. Kinetic measurements of binary components or individual reaction systems will be developed and used to validate the model. This will initially be done for a platinum catalyst and extended to other catalyst systems as needed to complete the model.

A fixed bed reactor system was used to conduct the experiments. The reactor was operated continuously at steady state. γ -Alumina-supported platinum (0.611 wt%) catalyst (surface area 103 m²/g) was used in this study as a base catalyst. A summary of reaction conditions is given in Table 1.

Table 1. Experimental Conditions

	ATR	SR	POX
O ₂ /C	0.3	0.0	0.5
H ₂ O/C	1.5	3.0	0.0
T (°C)	750 - 850	750 - 850	750 - 850
GHSV (h ⁻¹)	50,000 - 150,000 20,000 - 65,000*	50,000 - 150,000 20,000 - 65,000*	50,000 - 150,000 20,000 - 65,000*
*If 1-methylnaphthalene is in feed			

A mixture of two model compounds from different hydrocarbon classes, e.g. one from aromatics and one from paraffins, will be used to understand the combinatorial effects of feed components. Tetradecane, decalin, and 1-methyl-naphthalene are identified as model

compounds to represent paraffins, naphthenes, and aromatics, respectively, found in diesel. A rotatable-central-composite design will be used for process optimization. Each combination of model compounds representing two different organic classes in diesel will undergo autothermal, partial oxidation, and steam reforming at the temperature and space velocity range given in Table 1.

A gas chromatography technique was used to identify and separate the reaction products. The gases (N₂, O₂, CO, CO₂, and CH₄) were analyzed using a thermal conductivity detector (TCD), and the gaseous hydrocarbons were analyzed using a flame ionization detector (FID). Gas chromatography (Perkin Elmer's AutoSystem XL) coupled with mass spectrometry (Perkin Elmer's TurboMass Gold) was used to quantify and identify the complex liquid hydrocarbon product mixture that formed at various hydrocarbon conversions. Product yield is reported as a percentage of the theoretical yield based on moles of carbon in hydrocarbon fed to the reactor. For example, the yield of product A (H₂, CO, and CO₂) can be defined as

$$\text{Yield of A (\%)} = \frac{\text{Moles of A produced}}{N \times \text{moles of hydrocarbon fed to the reactor}} * 100$$

where N is the number of carbons in hydrocarbon fuel used in this study. In some cases, H₂ yields may be higher than 100% since steam reforming and water gas shift reaction also contribute in H₂ production apart from hydrocarbons.

Results

Statistical Analysis of Reforming Process

The yields of individual species from hydrocarbon reforming, which depend on the space velocity and reaction temperature, can be described by the equation

$$z = b_0 + b_1x + b_2y + b_{11}x^2 + b_{22}y^2 + b_{12}xy \quad (1)$$

where z is the yield of individual species after completion of the reaction, x is temperature (K), y is gas hourly space velocity (GHSV)(hr⁻¹), and b₀...b₂₂ are the coefficients of the model. The coefficients of Equation 1 were estimated by making use of the responses of experiments for the standardized values of x and y which varied in the range given in Table 1. Relationships between yield (z) and two quantitative variables x (space velocity) and y (reaction temperature) are represented by response surface curves as shown in Figures 1-5. Coefficients of quadratic Equation 1 are summarized in Table 2 for H₂ and CO yields from autothermal reforming of various types of raw materials used in this study. Quadratic fit of data from response surface mapping was excellent (>90%).

Different hypothetical reaction schemes of the process are established based on the response surface methodology studies. Each of the proposed kinetic schemes is being evaluated with respect to the experimental results using an iterative predictor-corrector method based on the Himmelblau-Jones-Bischoff technique [2, 3]. The following criteria are

Table 2. Coefficients of Quadratic Equations for Autothermal Reforming of Model Components

Fuel	X	Coefficients						R ²
		b ₀	b ₁	b ₂	b ₁₁	b ₂₂	b ₁₂	
Tetradecane + Decalin	H ₂	-2205.8	3.97	6.7e ⁻⁴	-1.8e ⁻³	-5.3e ⁻¹⁰	-6.8e ⁻⁷	92.2
	CO	-838.5	1.56	-9.5e ⁻⁴	-7.0e ⁻⁴	-2.2e ⁻⁹	1.1e ⁻⁶	95.6
1-Methylnaphthalene + Decalin	H ₂	-3237.1	5.62	3.1e ⁻³	-2.4e ⁻³	1.9e ⁻¹⁰	-3.3e ⁻⁶	98.0
	CO	-1953.6	3.44	1.1e ⁻³	-1.5e ⁻³	-1.2e ⁻⁹	-9.3e ⁻⁷	94.9
Tetradecane + 1-Methylnaphthalene	H ₂	-4678.5	9.12	-5.7e ⁻³	-4.4e ⁻³	8.3e ⁻⁹	4.4e ⁻⁶	95.0
	CO	17.95	-0.028	-2.3e ⁻³	3.7e ⁻⁵	6.9e ⁻¹⁰	2.0e ⁻⁶	93.0

being utilized to assess the validity of the model: calculated rate constants (positive values and follow Arrhenius Law), minimized value of objective function, and calculated profile of species concentration variations.

Earlier in this project, individual model compounds representing each homologous series present in diesel were evaluated to understand their reforming properties over Pt catalysts [1]. It was noted that each model compound behaved differently kinetically upon reforming under similar conditions. The hydrogen production rates at the same conditions were observed in this order: Aromatics \ll Naphthenes $<$ Paraffins. Hydrocarbon product distributions depended greatly on the model compound, type of reforming performed, and the process parameters (space velocity and reaction temperature).

This year, we conducted binary fuel compound studies to understand the combinatorial effects of feed components. Therefore, surface response maps were developed for steam reforming, partial oxidation and autothermal reforming over Pt catalysts for three binary fuel mixtures (n-tetradecane + 1-methylnaphthalene, decalin + 1-methylnaphthalene, and n-tetradecane + decalin).

Figures 1-3 show the effect of temperature and space velocity on the yields of H_2 , CO, and CO_2 from the autothermal reforming of 1-methylnaphthalene (aromatic) + n-tetradecane (paraffin). Figures 4-5 show the yields of H_2 from the autothermal reforming of 1-methylnaphthalene + decalin (naphthene) and n-tetradecane + decalin, respectively. Generally, the yields of H_2 and CO increase with increasing reaction temperature and decreasing space velocity. However, the yields of CO_2 from autothermal reforming decrease with increasing temperature because the lower temperatures favor the water-gas-shift reaction, while the reverse of the water-gas-shift reaction is facilitated at higher temperatures.

Difference in the relative reactivity of components in a binary mixture as well as the type of reforming performed play important roles in the reforming of a binary mixture representing a diesel fuel to produce syngas. Overall yields from a binary

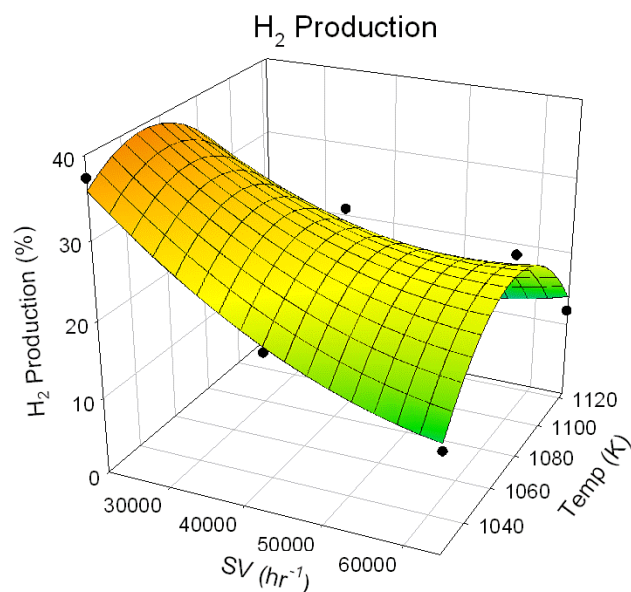


Figure 1. Yield of H_2 from ATR of n-tetradecane + 1-methylnaphthalene ($O_2/C = 0.3$ and $S/C = 1.5$)

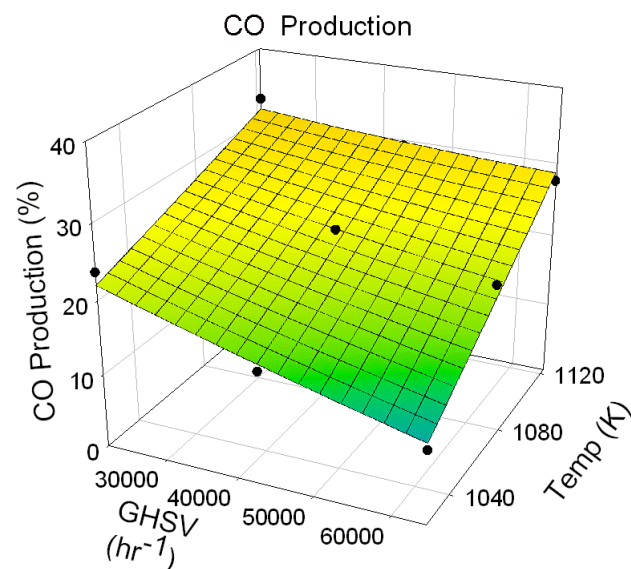


Figure 2. Yield of CO from ATR of n-tetradecane + 1-methylnaphthalene ($O_2/C = 0.3$ and $S/C = 1.5$)

diesel mixture are not simply the sum of yields from individual fuel components. Relative reactivity of one fuel component considerably affects the conversion pattern of others as well as the overall product distribution. Larger effects on reforming are noticed for greater differences in reactivity of binary components. For example, aromatics are relatively less reactive compared to paraffins; hence, the

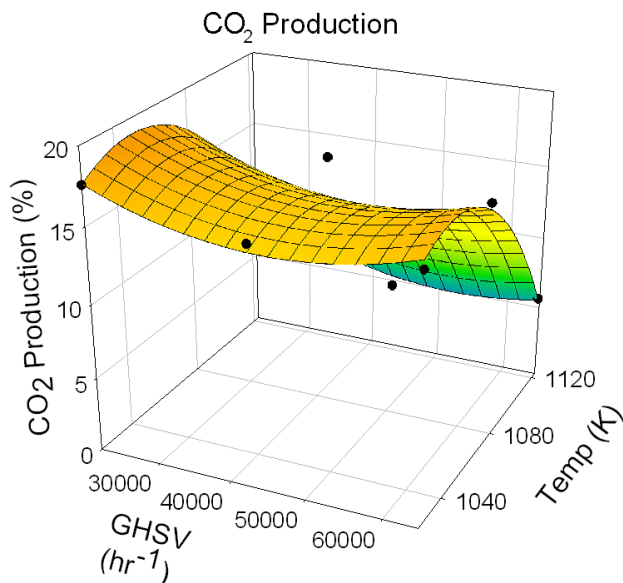


Figure 3. Yield of CO₂ from ATR of n-tetradecane + 1-methylnaphthalene ($O_2/C = 0.3$ and $S/C = 1.5$)

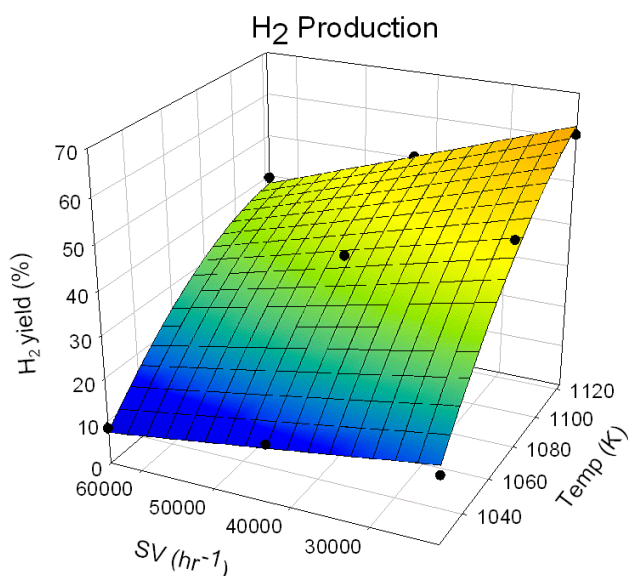


Figure 4. Yield of H₂ from ATR of 1-methylnaphthalene + decalin ($O_2/C = 0.3$ and $S/C = 1.5$)

highly reactive paraffins would consume available O₂ in POX and ATR reactions. Therefore, conversion of highly reactive fuel components proceeds towards completion and produces

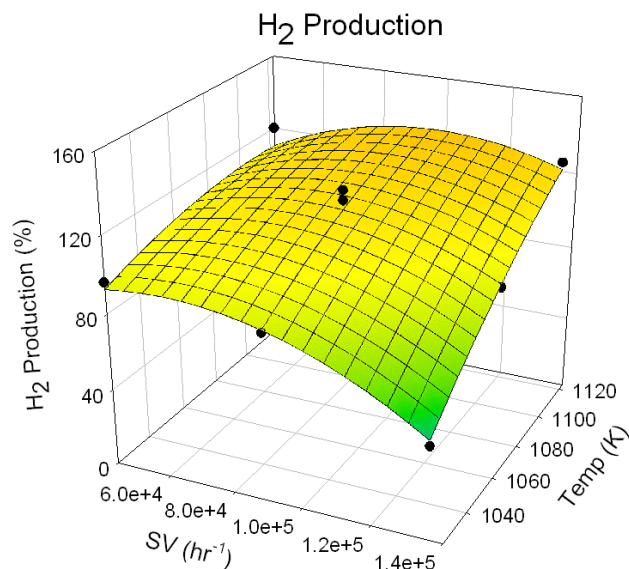


Figure 5. Yield of H₂ from ATR of n-tetradecane + decalin ($O_2/C = 0.3$ and $S/C = 1.5$)

combustion products, while not enough O₂ is spared for the less reactive component. Consequently, the less reactive component is predominantly subjected to pyrolysis reaction.

Partial oxidation reforming was affected significantly by the difference in the reactivity of fuel components, while steam reforming was not affected much from the difference in reactivity of fuel components since water was present in abundance in steam reforming. Autothermal reforming was somewhere in the middle.

Side reactions specific to one component play an important role in the reforming of a mixture. For example, aromatics are more prone to coking upon reforming; therefore, the presence of aromatics in the mixture can lower the yields of syngas over time due to catalyst deactivation. Also, the catalyst surface-component interaction may play an important role in the reforming of a mixture. For example, aromatics have an abundance of pi-electrons, so they may occupy catalyst active sites for longer time due to pi-complexation between d-orbitals in the metal and pi-electrons. Hence, there won't be enough reactive sites available for the desired reaction to occur.

Conclusions

- Overall yields are not the sum of yields from individual fuel components.
- Relative reactivity of one fuel component considerably affects the conversion pattern of others.
- The greater the difference in relative reactivity, the larger the effect.
- Conversion of highly reactive fuel components proceeds towards completion.
- Reverse of water gas shift reaction dominates at high temperatures.
- Partial oxidation reforming is affected significantly by the difference in reactivity of fuel components.
- Highly reactive components consume available O₂, produce combustion products.
- O₂ not spared for the less reactive component, pyrolysis reaction dominates.
- Steam reforming not affected much by the difference in reactivity of fuel components.

References

1. D.A. Berry, D. Shekhawat, T.H. Gardner, "Development of Predictive Models for Diesel-Based Fuel Processors", 2003 Annual Merit Review Meeting of Hydrogen, Fuel Cells & Infrastructure Technologies Program, Department of Energy Office of Energy Efficiency, Berkeley, CA, May 18-22, 2003.
2. J. Font, A. Fabregat, "Testing a Predictor-Corrector Integral Method for Estimating Parameters in Complex Kinetic Systems Described by Ordinary Differential Equations", *Computers Chem Engng*, 21(7) (1997) 719-731.
3. D.M. Himmelblau, C.R. Jones, K.B. Bischoff, "Determination of Rate Constants for Complex Kinetic Models", *Ind. & Eng. Chem. Fundamentals*, 6(4) (1967) 539-543.

III.B.6 Operation of Solid Oxide Fuel Cell Anodes with Practical Hydrocarbon Fuels

Scott A. Barnett (Primary Contact), Jiang Liu, Yuanbo Lin

Northwestern University

Dept. of Materials Science

2220 Campus Drive

Evanston, IL 60208

Phone: (847) 491-2447; Fax: (847) 491-7820; E-mail: s-barnett@northwestern.edu

DOE Project Manager: Daniel Driscoll

Phone: (304) 285-4717; E-mail: Ddrisc@netl.doe.gov

Objectives

- This work was carried out to achieve a better understanding of how solid oxide fuel cell (SOFC) anodes work directly with hydrocarbon fuels, examining both basic mechanisms and feasibility of this approach for SOFC stacks.
- Another objective was to use the basic information on hydrocarbon-anode reactions to better understand how SOFCs work with partially reformed fuel gas that contains residual hydrocarbons.
- Since real fuels contain sulfur, one goal was to examine the effects of sulfur on SOFC performance.
- The work also aimed to further develop not only Ni-YSZ (yttria-stabilized zirconia) anodes, but also ceramic-based anode compositions.

Approach

- SOFCs were fabricated using conventional ceramic processing methods, with both conventional Ni-YSZ anodes and novel ceramic anodes.
- Structural and chemical measurements of SOFC anodes were carried out in order to verify anode structure and composition and to detect coking.
- Differentially-pumped mass spectrometry was used for product-gas analysis, both with and without cell operation.
- Impedance spectroscopy was used in order to understand electrochemical rate-limiting steps.
- Life tests over a wide range of conditions were used to establish the conditions for stable operation or coking of anode-supported SOFC stacks directly on methane.
- Redox cycling was carried out on ceramic-based anodes.
- Tests on sulfur tolerance of Ni-YSZ anodes were carried out.
- The results from the various measurements above were analyzed together to obtain a more complete picture of fuel-anode interactions.

Accomplishments

- Direct methane power densities as high as 0.5 W/cm² at 700°C and 1.25 W/cm² at 800°C have been achieved. It is clear that further improvements are possible.
- Good fits to the open circuit voltage (OCV) data for various fuel compositions were obtained based on equilibrium calculations.

- Electrochemical impedance spectroscopy (EIS) measurements carried out during SOFC operation suggested that anode polarization was substantially larger for methane than for hydrogen. These results indicate that gas diffusion in the anode support played an important role in determining cell performance.
- Mass spectrometer measurements showed that the expected reaction products – H₂, H₂O, CO, and CO₂ – all increased with increasing cell current density. The dominant products at 800°C were H₂ and CO, in agreement with thermodynamic predictions. However, the thermodynamic predictions could not directly explain the lack of coking during direct methane operation.
- We have mapped out the stability region for direct methane operation. At lower temperatures, ≤700°C, stable operation without coking occurs over a wide range of current densities, whereas at higher temperatures, increasingly large currents are required to avoid coking and cell failure.
- A much wider stability range was achieved using fuel gases containing diluted methane such as would be present in partially reformed methane.
- Degradation of cell performance was observed for H₂S-contaminated H₂ fuel at 800°C, but surprisingly, the degradation was negligible at 700°C.
- Ceramic-based anodes showed good fuel flexibility with hydrogen, methane, ethane, propane, and butane, and excellent cell stability in redox cycling with hydrogen-air and propane-air.

Future Directions

No additional work is planned, but open issues include:

- Further work is needed to more fully characterize the S poisoning effects observed and to develop ways to minimize these effects.
- Further work is needed to develop detailed models of methane interactions, particularly diffusion and reaction processes within SOFC anodes.
- The present results have suggested new means for improving the stability of Ni-YSZ anodes in hydrocarbon fuels – these should be pursued.
- The direct methane SOFC should be studied as a means for low-cost, high-efficiency production of hydrogen by electrochemical partial oxidation.
- Ceramic anodes should be implemented in anode- or cathode-supported cells in order to verify that high power densities and stable operation can be achieved.

Introduction

Fuel cell power plants have been successfully demonstrated many times, but the high cost of these systems has prevented commercialization. One of the key factors that contribute to this high cost is a lack of fuel flexibility. Fuel cells generally operate only on hydrogen, which is neither readily available nor easily stored. Ideally, fuel cells should be able to utilize conventional hydrocarbon fuels ranging from natural gas to propane to gasoline. To utilize hydrocarbons, fuel cell power plants usually employ fuel reforming, which converts fuels into hydrogen that can be used directly. Reforming and exhaust-gas recirculation (which provides the steam for reforming) lead to additional plant complexity and

volume, increasing cost. Real fuels also contain sulfur contaminants that typically poison fuel cell anodes, decreasing performance. Thus, adsorbents must be used to remove the sulfur, and the adsorbent materials must be changed or regenerated after they become saturated. Based on the above arguments, fuel cell system cost could be substantially reduced if the fuel cells themselves could operate directly on real fuels.

Recent reports have described SOFC operation directly on methane and natural gas. These results have challenged traditional views that large amounts of steam are required to prevent carbon deposition on Ni-containing anodes. Heavier hydrocarbons such as propane, butane, and even gasoline have been used

directly in SOFCs^{1,2}, although it was necessary in this case to utilize alternate anode compositions, replacing the Ni with either Cu or a conducting ceramic. Prior to this study, there had been little attempt to understand the mechanisms whereby direct-hydrocarbon SOFCs operate.

Approach

In the Phase I project, we have studied the reaction mechanisms of hydrocarbons on two kinds of anodes: conventional Ni-based anodes and ceramic-based anodes. The effects of sulfur impurities and of redox cycling were also considered. The project was aimed both at achieving an understanding of the interactions between real fuels and SOFC anodes, and at providing information required to operate SOFCs directly on hydrocarbon fuels. In particular, we have carried out detailed studies of the operation of Ni-YSZ anodes in methane-containing fuels, including cell tests, impedance spectroscopy, mass spectrometric studies of anode exhaust gas, studies of open circuit voltages, studies of the addition of H₂S to the fuel, and lifetime studies designed to determine useful direct-methane operating conditions. In addition, new ceramic-based anodes have been developed that provide good performance without coking with a range of hydrocarbon fuels and are also extremely tolerant of redox cycling.

Results

Extremely good performance was achieved for direct-methane SOFCs. Figure 1 shows typical voltage and power density vs. current density of a SOFC operated on methane. The maximum power density was 1.25 W/cm² at 800°C. Note that operation in methane was not stable under some conditions, especially high *T* and low *J*; this is discussed further below. The open circuit voltage (OCV) in methane increased with increasing temperature, opposite of the usual trend shown for hydrogen. This trend agrees reasonably well with the OCV predicted based on the equilibrium anode gas composition.

Gd-doped ceria (GDC) electrolyte cells with (La,Sr)(Cr,V)O₃-GDC anodes were operated in various fuels. Power densities were lower than

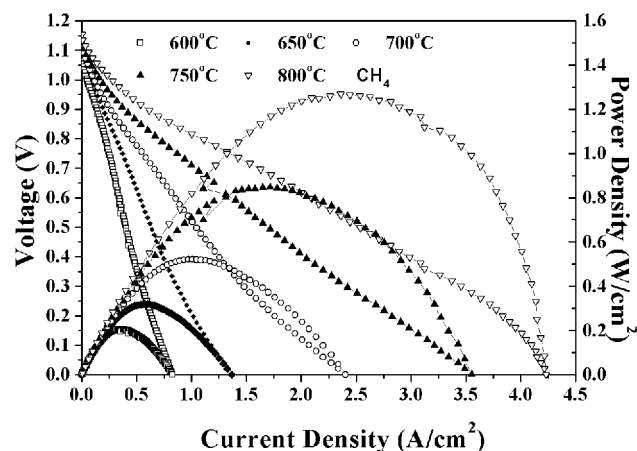


Figure 1. Voltage and Power Density vs. Current Density of a SOFC Operated on Humidified Methane

shown in Figure 1; e.g., with propane fuel the values were 120 mW/cm² at 650°C and 150 mW/cm² at 750°C. However, the low values were primarily due to the high resistance of the thick GDC electrolyte, and a more detailed analysis indicates that these electrodes have low enough resistances to allow much higher power densities. The cells were also successfully operated with hydrogen, methane, ethane, propane, and butane fuels at 700°C with similar power densities. Note that similar results have been obtained in cells with doped SrTiO₃-based anodes.

Electrochemical impedance spectroscopy (EIS) measurements were also done. The first real-axis intercepts, at 0.26 Ωcm² (600°C) and 0.10 Ωcm² (700°C), agreed well with the expected ohmic resistance of the 10-20 μm thick YSZ electrolyte. Each spectrum appeared to consist of a large higher-frequency depressed arc and a small lower-frequency arc, which both decreased in size with increasing temperature. The high-frequency arcs were larger for methane than for hydrogen, whereas the lower-frequency arcs appeared to change relatively little with fuel composition. The higher-frequency arc also changed with H₂ partial pressure (results not shown), suggesting that this arc was associated with the anode.

The following protocol was used to quantitatively determine the stability region. First, the cell was operated in hydrogen for more than 24 h to reduce the anode and fully stabilize the cell performance.

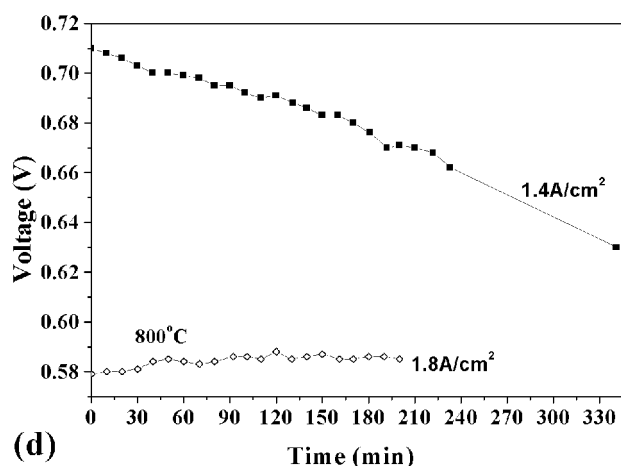
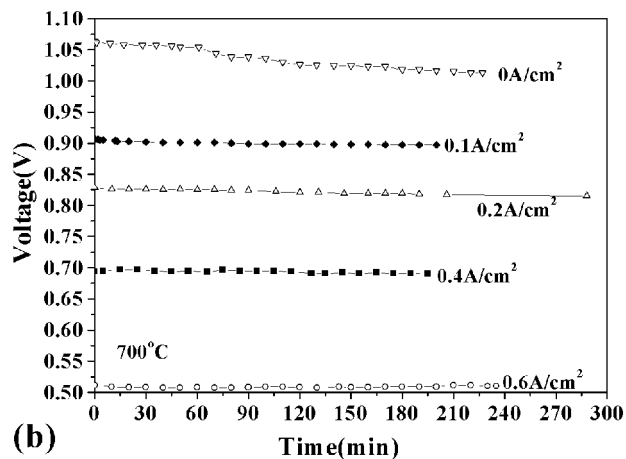


Figure 2. Cell Voltage versus Time at Constant Current J for SOFCs Operated in Humidified Methane at 700°C (a) and 800°C (b); the Cells Were Operated at Different J Values for 3-6 h in Each Step, Starting at High J and Reducing J in Steps

Second, the fuel was switched to methane with the cell maintained near the maximum power point. After the switch to methane, the V value at constant J dropped by $\approx 20\%$ to a new steady-state value. The drop was expected based on the I - V curves in Figure 1. Third, J was maintained constant near the maximum power point for >3 h, long enough to observe whether V was stable. Fourth, J was reduced and maintained constant for >3 h. This latter step was repeated until V became unstable.

Figure 2 shows results taken in this way at 700 and 800°C. As shown in Figure 2a (700°C), stability in methane was excellent as long as a minimum cell current density $J \sim 0.1$ A/cm² was maintained. It was

only at $J=0$ that V decreased gradually over several hours. Thus, the critical current density J_c was $0 < J_c < 0.1$ A/cm² at these temperatures. The results were similar at 750 and 800°C (Figure 2b), but much larger critical current values, i.e. 0.8 A/cm² $< J_c^{750} < 1.2$ A/cm² and 1.4 A/cm² $< J_c^{800} < 1.8$ A/cm², were needed to maintain stable operation. These results imply that the SOFC oxygen ion current was at least partially responsible for preventing coking and thereby maintaining stable operation. We believe that J_c increased with increasing T because of the increasing rate of methane cracking above $\approx 700^\circ\text{C}$.³

Initial attempts have been made to examine the effect of methane concentration on stability. This is relevant to understanding SOFC operation in partially-reformed hydrocarbon fuels, where there will be significant amounts of methane present. In these initial experiments, the effect of methane concentration alone was examined (i.e. without introducing any other reforming species) by using a 50% methane - 50% Ar mixture. The results at 800°C showed that the cell was fairly stable except for $J=0$, a remarkable improvement from the 800°C result in 100% methane (Figure 2b). This result indicates a surprisingly strong dependence on methane concentration. Further work is needed to fully characterize and understand this effect.

Mass spectrometer measurements of the anode exhaust gas were carried out to determine the nature of the anode reaction products. Figure 3 summarizes the product gas concentration results derived from the mass spectrometer data. Each of the species H₂, CO, CO₂, and H₂O increased with increasing J , but the increases in H₂ and CO were substantially larger. Note that an artifact in the mass spectrometer data, the so-called “zero blast” effect, caused the mass spectrometer to underestimate the size of low-mass peaks such as hydrogen. Thus, we believe that the hydrogen concentration should actually be larger than CO. Figure 3 is in reasonable agreement with thermodynamic calculations of the equilibrium anode exhaust gas composition.

Experiments were carried out testing the ability of ceramic anodes to withstand hydrogen-air and propane-air cycling. Figure 4 shows the result for propane-air cycling, with the cell maintained at a constant current of 200 mA/cm². The cell was

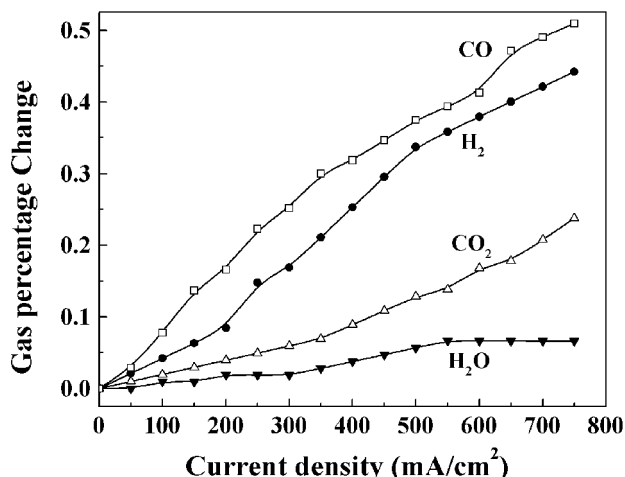


Figure 3. Changes in the Concentrations, in Percent, of Various Species versus SOFC Current Density during Operation in Humidified Methane at 800°C, Derived from Mass Spectrometer Data

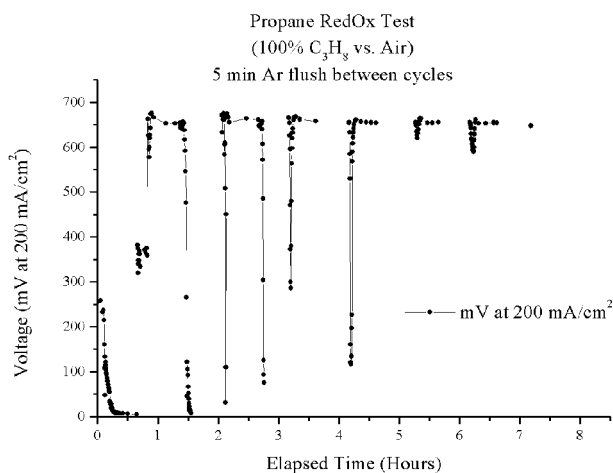


Figure 4. Propane-Air Redox Cycling Result for a Ceramic Anode SOFC

operated for ≈ 30 min in fuel, then the fuel flow was stopped and air allowed to enter the fuel compartment. The cell voltage and current rapidly dropped to zero. After ≈ 30 min, the fuel flow was re-started, whereupon the cell voltage and current rapidly returned to close to their original values. This cycle was repeated several times with similar results. Note that the transients at the beginning of fuel flow may be related to the time required to fully flush any air from the fuel lines. A total of 30 redox cycles were carried out during this cell test with no evidence of cell degradation. These results strongly

indicated that ceramic-based anodes avoid problems with redox cycling.

Ni-YSZ anode-supported cell tests were carried out using H₂ fuel with 10 ppm H₂S. The cell test protocol was as follows: the cell was first run in dry pure H₂, then exposed to 10 ppm H₂S in H₂ during stable operation, and finally allowed to reach steady-state performance after returning to pure H₂. The effect of H₂S was minor at 700°C, but there was a substantial degradation at 800°C. This result is rather surprising based on prior results for 750-1000°C, suggesting that sulfur poisoning is exacerbated as the temperature is reduced.⁴ More work is needed to understand this result.

Conclusions

Operation of Ni-YSZ anode-supported SOFCs directly on methane was studied, along with ceramic anode cells tested in a variety of hydrocarbon fuels. The results are beginning to provide a clearer picture of how these cells operate. The following are the main conclusions:

- Power densities as high as 0.5 W/cm² at 700°C and 1.2 W/cm² at 800°C have been achieved during direct methane operation. High open circuit voltages and large limiting currents are key reasons for the good performance in methane.
- The high-frequency impedance arc, probably associated with the anode, was substantially larger for methane than for hydrogen.
- The results suggest that SOFC performance is strongly dependent on gas diffusion and hence on anode parameters including thickness, porosity, and tortuosity.
- The SOFCs were stable without coking at $T \leq 700^\circ\text{C}$, except at very low current densities. At higher temperatures, increasingly large currents were required to avoid coking and cell failure.
- Mass spectrometer measurements showed that H₂ and CO were the main reaction products, with H₂O and CO₂ minor products – all the products increased with increasing cell current density. While these results were in general agreement with thermodynamic predictions, the lack of coking during direct methane operation was not.

- The results suggest that coke-free SOFC operation was achieved due to kinetic limitations on the methane cracking reaction, particularly at low temperature. It is suggested that oxidation of hydrogen, produced by methane reforming by reaction products within the anode, is an important electrochemical reaction; the resulting steam helps remove solid carbon, thereby suppressing coking at high current densities. Detailed modeling of diffusion and reaction processes within the anode is needed.
- The ability of these cells to produce syngas ($H_2 + CO$) with simultaneous electrical power generation makes them interesting for low-cost production of hydrogen.

References

1. J. Liu, B. Madsen, and S.A. Barnett, *Electrochem. Solid State Letters* 5, (2002) A122.
2. S. Park, R.J. Gorte, and J.M. Vohs, *Applied Catalysis A* 200, (2000) 55-61.
3. C.M. Finnerty, N.J. Coe, R.H. Cunningham, and R.M. Ormerod, *Catalysis Today* 46, (1998) 137.
4. Y. Matsuzaki and I. Yasuda, In *Proc. 7th Int. Symp. On Solid Oxide Fuel Cells* (Yokokawa, H. and Singhal, S.C., Editors), *Electrochem. Soc.*, p 769 (2001).

FY 2004 Publications/Presentations

1. A Atkinson, S Barnett, RJ Gorte, JTS Irvine, AJ McEvoy, MB Mogensen, S Singhal, J Vohs, "Advanced Anodes for High Temperature Fuel Cells," *Nature Materials* 3, 17-27 (2004).
2. Yuanbo Lin, Zhongliang Zhan, Jiang Liu, and Scott Barnett, "Direct Operation of Solid Oxide Fuel Cells with Methane Fuel," *Solid State Ionics*, submitted.
3. Presentation at the SECA program review, Sacramento, CA, February, 2004.

III.C Power Electronics

III.C.1 Trade Study for Integrating Numerous SECA SOFC Modules

*Burak Ozpineci (Primary Contact), Donald J Adams, Leon M. Tolbert
Oak Ridge National Laboratory, National Transportation Research Center
2360 Cherahala Blvd.
Knoxville, TN 37932
Phone: (865) 946-1329; Fax: (865) 946-1262; E-mail: ozpinecib@ornl.gov*

*DOE Project Manager: Don Collins
Phone: (304) 285-4156; E-mail: Donald.Collins@netl.doe.gov*

Subcontractors: MESTA Electronics, N. Huntingdon, PA

Objectives

- Identify power topologies that can be used to integrate numerous solid oxide fuel cell (SOFC) modules to supply much higher power than a single module can supply.
- Evaluate the pros and cons of each topology.
- Compare different topologies with respect to each other.

Approach

- Identify the requirements of a power converter for a fuel cell interface.
- Study the electrical supply characteristics of fuel cells.
- Identify power converter topologies with multiple inputs.
- Analyze the possible effects of using several fuel cell modules using multi-input power converters.
- Evaluate the possibility of modifying control to suit the load-varying voltage output of the fuel cells for better fuel cell utilization.

Accomplishments

- Identified five different families of power converter topologies that can be used to integrate numerous SOFC modules.
- Listed the pros and cons for each power converter topology.
- Developed a level reduction technique applied to multilevel converters integrating several fuel cell modules to increase the fuel cell utilization.
- Built a comparison matrix to compare all these power converter topologies with respect to cost, fault tolerance, reliability, etc.
- Completed a draft report.

Future Directions

- Complete the final report.
- Follow the literature for a possible addition to the five power topologies included in this project.

Introduction

The U.S. Department of Energy's Solid-State Energy Conversion Alliance (SECA) program is targeting solid oxide fuel cell (SOFC) modules in the 3-10 kW range to be made available for residential applications. In addition to residential use, these modules can also be used in apartment buildings, hospitals, etc., where a higher power rating would be required. For example, a hospital might require a 250-kW power supply. To provide this power using the SOFC modules, 25 of the 10-kW modules would be required. These modules can be integrated in different configurations to yield the necessary power. This report will show five different approaches for integrating numerous SOFC modules and will evaluate and compare each one with respect to cost, control complexity, ease of modularity, and fault tolerance.

Approach

The static and dynamic characteristics of SOFCs have been studied to identify the power converter requirements. With these in mind, several multi-input power converter systems have been studied to make sure they will be suitable for integration of numerous SOFCs. Using these converter topologies, the possible effects of integrating several fuel cell modules have been analyzed. Then, these topologies have been compared with respect to cost, control complexity, reliability, availability (at power system and device levels), fault tolerance, modularity (ability to isolate portions of the system for service or add power generation capacity while other portions of the complete system are still functioning), energy conversion efficiency, and ease of mass customization to enable mass production to drive down costs.

While studying the power converter topologies, it was found that there is a possibility of modifying controls to suit the load-varying voltage output of the fuel cells for better fuel cell utilization. To achieve this, a control technique was also developed and analyzed using simulation and some experimentation using batteries instead of fuel cells.

Results

The five power converter topologies selected for integrating numerous fuel cells are series configuration, dc-link configuration, high-frequency ac-link distribution, cascaded multilevel configuration, and multilevel configuration. A matrix given below compares these configurations with respect to each other.

	A	B	C	D	E
a	1	3	3	3	5
b	1	4	4	4	5
c	4	2	2	2	3
d	1	1	1	1	5
e	5	1	1	1	1
f	5	1	2	2	2
g	1	3	3	2	4
h	1	2	2	2	2

- A. Series configuration
 B. Cascaded multilevel configuration
 C. Multilevel configuration
 D. DC link configuration
 E. High-frequency ac (hfac) link configuration
- a. Cost (capital and operating): (1-Less expensive, 5-More expensive)
 b. Control complexity (1-Less complex, 5-More complex)
 c. Reliability (1-More reliable, 5-Less reliable)
 d. Availability (at power system and device levels) (1-Better availability, 5-Worse availability)
 e. Fault tolerance (1-More fault tolerant, 5-Less fault tolerant)
 f. Modularity (ability to isolate portions of system for service or add power generation capacity while other portions of the complete system are still functioning) (1-More modular, 5-Less modular)
 g. Energy conversion efficiency (1-More efficient, 5-Less efficient)
 h. Ease of mass customization to enable mass production to drive down costs (1-Easier, 5-More difficult)

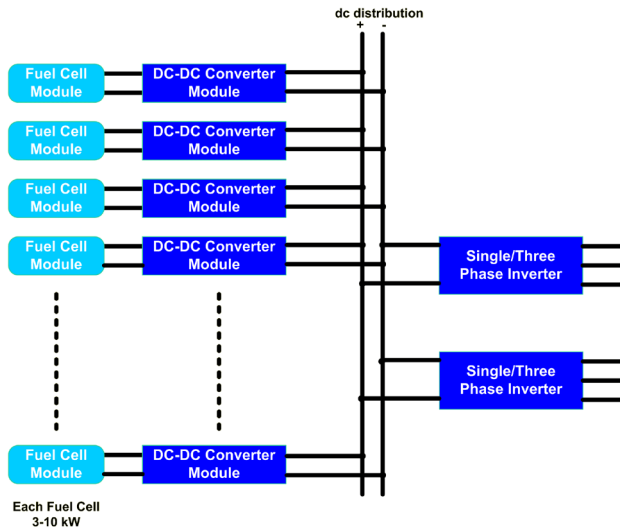


Figure 1. Block Diagram of the DC Distribution Configuration

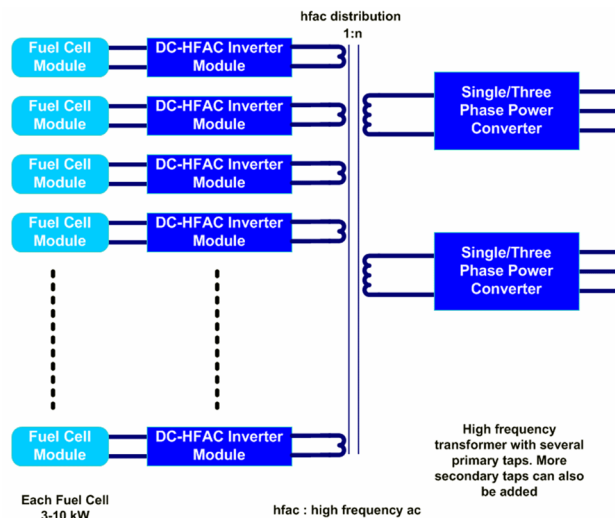


Figure 2. Block Diagram of the hfac Distribution Configuration

Figures 1 and 2 show the block diagrams of the DC link configuration and the hfac link distribution configuration, respectively.

The output voltages of fuel cells vary with load current. The power converter does not always operate at full-load at rated fuel cell voltage. As the load current decreases, the fuel cell output voltage increases. This causes challenges in the converter design since the converter switches have to be derated to accommodate the higher voltages. When numerous fuel cell modules are integrated, as the

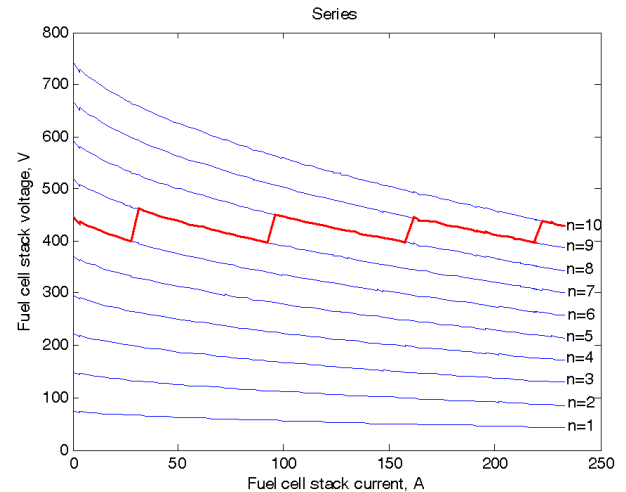


Figure 3. Static Characteristics for up to 10 Fuel Cells in Series and Level Reduction Technique Figure 4. One Phase of a Cascaded Three-Level Inverter

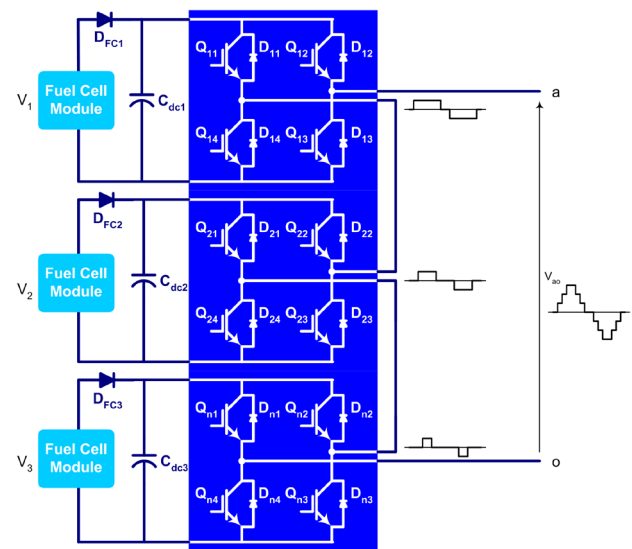


Figure 4. One Phase of a Cascaded Three-Level Inverter

load current decreases, some number of fuel cells can be taken off-line so that the remaining fuel cells can still provide the same power but at a voltage close to the rated value. This is called the level reduction control technique. A cascaded multilevel dc-dc converter is the best choice for this operation. Figure 3 shows the static characteristics of 1 to 10 fuel cells in series and how the level reduction works as the current decreases. As seen in this figure, even though fewer fuel cells are used, they can still supply the required power. Since level reduction technique

keeps the fuel cell output voltage lower, lower voltage rated devices can be used in the converters.

Figure 4 shows a cascaded multilevel inverter, which can also be controlled with the level reduction technique. In this case, the inverter switches are turned on and off by a fundamental frequency sine-triangle comparison technique developed for this converter which reduces the inverter levels (or takes fuel cells off-line) automatically, when needed.

Conclusions

Novel multiple-input converter topologies for fuel cells have been reviewed, and they have been compared with each other.

With level reduction control technique exploiting the V-I characteristics of fuel cells, the need for derating power semiconductors in fuel cell systems is eliminated. By inhibiting some of the fuel cells and using the inhibited fuel cells in other applications, like charging batteries, the system efficiency and the fuel cell utilization increase. If these fuel cells are left idling, then the life expectancy of the system increases. In addition to these benefits, using a multilevel converter also brings the advantages of modularity and increased reliability.

For the multilevel inverter, a fundamental switching sine-triangle comparison method is introduced. This method decreases the complexity of

the level reduction control for the multilevel inverters by eliminating the need for storing separate switching angle look-up tables for multilevel inverters for each number of dc sources.

The level reduction technique is also applicable to other fuel cell-fed multilevel inverters.

FY 2004 Publications/Presentations

1. B. Ozpineci, L. M. Tolbert, "Multiple input converters for fuel cells," Annual Meeting of IEEE Industry Applications Society, October 2004, Seattle, Washington.
2. B. Ozpineci, L. M. Tolbert, Z. Du, "Optimum fuel cell utilization with multilevel inverters," IEEE Power Electronics Specialists Conference, June 2002, Aachen, Germany.
3. B. Ozpineci, L. M. Tolbert, G. J. Su, Z. Du, "Optimum fuel cell utilization with multilevel converters," IEEE Annual Applied Power Electronics Conference and Exposition, February 22-26, 2004, Anaheim, California.
4. B. Ozpineci, Z. Du, L. M. Tolbert, D. J. Adams, D. Collins, "Integrating multiple solid oxide fuel cell modules," IEEE Industrial Electronics Conference, November 2-6, 2003, Roanoke Virginia.

III.C.2 Development of a New Class of Low-Cost, High-Frequency Link Direct DC-to-AC Converters for SOFCs

Dr. Prasad Enjeti

Texas A&M University

Department of Electrical Engineering

College Station, TX 77843-3128

Phone: (979) 845-7466; Fax: (979) 845-6259; E-mail: enjeti@ee.tamu.edu

DOE Project Manager: Don Collins

Phone: (304) 285-4156; E-mail: Donald.Collins@netl.doe.gov

Objectives

- To develop a new and innovative power converter technology suitable for solid oxide fuel cell (SOFC) power systems in accordance with the Solid State Energy Conversion Alliance (SECA) objectives.
- To realize a cost-effective fuel cell converter which operates under a wide input voltage range and output load swings with high efficiency and improved reliability.

Approach

- Employ state-of-the-art power electronic devices configured in two unique topologies to achieve direct conversion of DC power (24-48 V) available from a SOFC to AC power (120/240 V, 60 Hz) suitable for utility interface and powering stand-alone loads.
- Investigate the feasibility of two direct DC-to-AC converter topologies and their suitability to meet SECA objectives.

Accomplishments

- A 3-kW converter has been successfully constructed and tested. An overall efficiency (from fuel cell input DC to 120 V AC output) of 90% was measured. There is still room for improvement by reducing the transformer leakage and by improving the four-step switching strategy of the bidirectional switches.
- Due to absence of dc-link capacitors, a low-profile converter construction can be adopted, resulting in a higher-density package.
- An optimized 2nd order input filter at the input terminals guarantees the fuel cell input current is nearly devoid of current ripple.

Future Directions

- The converter construction and design will be further optimized for higher efficiency.
- The usage of silicon carbide (SiC) semiconductors will facilitate the converter operation at higher temperature. This needs to be explored further.

Introduction

This project proposes to design and develop a new class of power converters (direct DC to AC) to drastically improve performance and optimize the cost, size, weight and volume of the DC-to-AC converter in SOFC systems. The proposed topologies employ a high-frequency link, direct

DC-to-AC conversion approach. The direct DC-to-AC conversion approach is more efficient and operates without an intermediate dc-link stage. The absence of the dc-link results in the elimination of bulky, aluminum electrolytic capacitors, which in turn leads to a reduction in the cost, volume, size and weight of the power electronic converter.

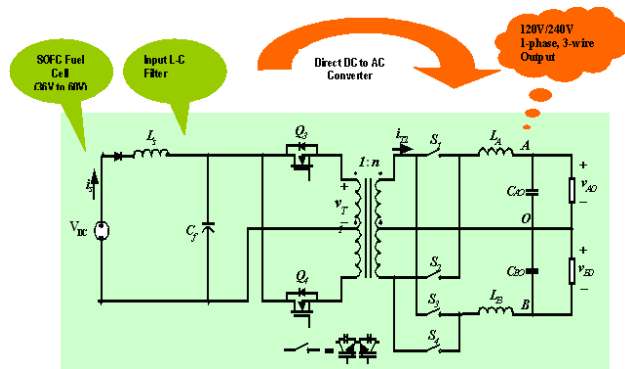


Figure 1. Proposed Voltage Source Type Direct DC-to-AC Converter for SOFC without a Battery

The feasibility of two direct DC-to-AC converter topologies and their suitability to meet SECA objectives have been investigated. Laboratory prototype converters (3-5 kW) have been designed and tested in Phase 1.

Approach

Figure 1 shows the complete topology of the first direct DC-to-AC converter. In this approach, the fuel cell DC input voltage is processed via a high-frequency link MOSFET (metal-oxide-semiconductor field-effect transistor) converter via transformer isolation.

The high-frequency transformer provides isolation as well as facilitates the step-up in voltage. The secondary side converter is composed of bi-directional switches, which directly convert to low-frequency AC output. Two MOSFET switches (Q3 and Q4) are connected in push-pull fashion for converting the SOFC voltage (36 V) to high frequency, and the secondary transformer is interfaced with switches S1 to S4 to transform direct DC to 1-phase 120-V/240-V, 60-Hz, 3-wire AC output.

From the technical specifications obtained from Delphi for the SOFC power conditioning unit (PCU), it is clear that a battery backup option needs to be explored for the PCU to satisfy stand-alone and uninterrupted power supply (UPS) modes of operation. In order to comply with these specifications, the converter topology shown in Figure 1 has been modified as shown in Figure 2.

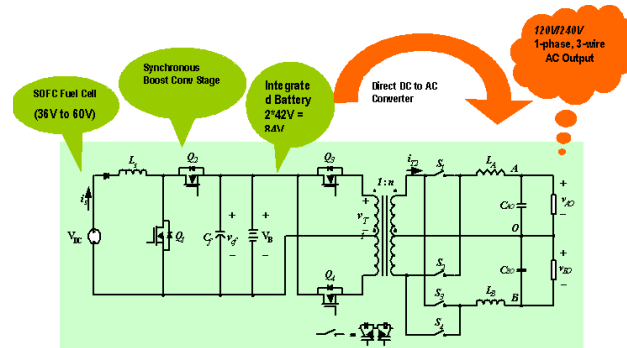


Figure 2. Proposed Voltage Source Type Direct DC-to-AC Converter for SOFC PCU with an Integrated Battery

Figure 2 shows the direct DC-to-AC converter topology with integrated battery backup concept suitable for operating modes Mode 1 and Mode 4. In this approach, the SOFC output (36 V to 60 V) is first processed via a synchronous boost converter and is converted to 84 V. Two 42-V batteries (connected in series to obtain 84 V) are connected at the output of the boost stage. The direct DC-to-AC converter stage then converts the 84-V DC to 120-V/240-V 1-phase 3-wire output. The push-pull stage of the direct DC-to-AC converter in this design (Figure 2) sees a fixed 84-V DC at its input, and its design is optimized for full-load operation of 5 kW. Comparing Figure 1 and Figure 2, one notes that the direct DC-to-AC converter along with the high-frequency transformer in Figure 2 will be smaller in size and more efficient than the converter design in Figure 1. This increase in conversion efficiency is expected to be offset by the addition of the synchronous boost stage in Figure 2. Therefore, the overall efficiency of Figure 1 and Figure 2 designs should be comparable. Integrating the battery within the power conversion stage has many advantages and can meet the Delphi-described PCU operating modes 1 and 4.

Results

Texas A&M University (TAMU) design for the proposed converter has centered around the specifications obtained from Delphi and General Electric. Table 1 and Table 2 show the converter component ratings to meet the specifications. Figures 3, 4, and 5 show the waveforms obtained from simulations.

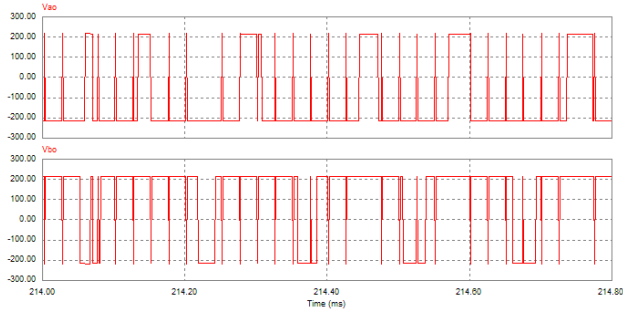


Figure 3. Unfiltered Output Voltage of the Direct DC-to-AC Converter Shown in Figure 1 and Figure 2

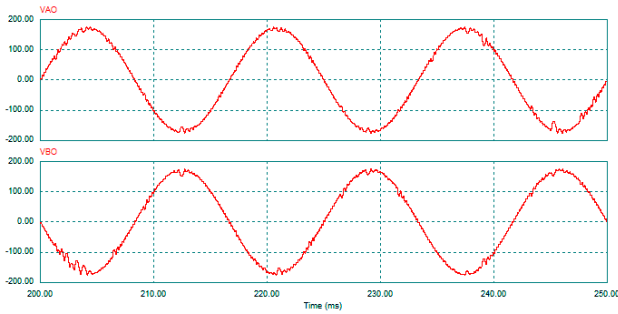


Figure 4a. Single-phase 120-V/240-V, 60-Hz, 3-wire Output Voltage of the Direct DC-to-AC Converter of Figure 1 and Figure 2

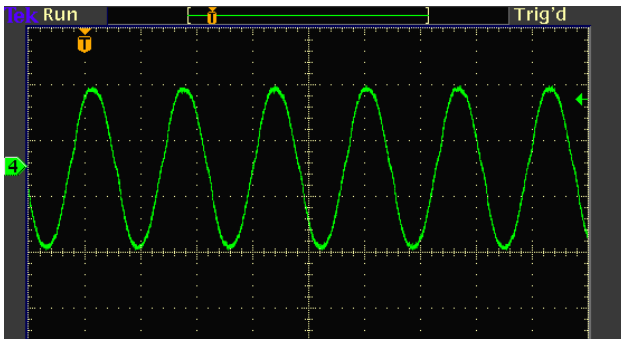


Figure 4b. Experimental Results (output ac voltage for phase A)

Output power: 5 kW (resistive)
 Output voltage: 120-V/240-V, 1-phase, 60-Hz, 3-wire output
 Output current: 20.7 A (rms.), 29.3 A (peak)
 Switching frequency: 20 kHz

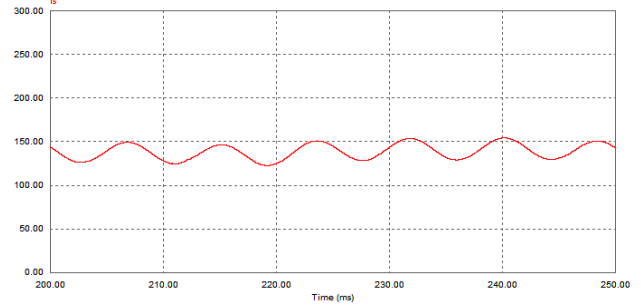


Figure 5. Fuel Cell Input Current Waveform

Table 1. Converter Component Ratings to Meet the Specifications

Input voltage Vdc [V]	Turn ratio N2/N1	L ₁ [uH]	L ₂ [nH]	C ₁ [F]	C ₂ [F]	L _A [mH]	C _{AO} [uF]
36	16/3	1	5	30	0.5	1	50

Table 2. Converter Component Ratings to Meet the Specifications (Con't)

V _i [V]	V _{Q3,rms} [V _{rms}]	I _{Q3,pk} [A]	V _{S1,rms} [V _{rms}]	I _{S1,pk} [A]	I _{A,rms} [A _{rms}]	I _{A,pk} [A]	I _{T2,rms} [A _{rms}]	I _{T2,pk} [A]
36	50.7 0.42p.u	365.5 12.5 p.u	270.8 2.3 p.u	32.1 1.1p.u	21.1 1 p.u	32.4 1.1 p.u	19.7 0.95p.u	33.6 1.1p.u

Conclusions

From the results obtained in Phase 1, it can be concluded that the topologies shown in Figure 1 and Figure 2 have several advantages compared to the prior state-of-the-art. A 3-kW converter has been successfully constructed and tested. An overall efficiency of 90% was measured. There is still room for improvement by reducing the transformer leakage and by improving the four-step switching strategy of the bidirectional switches. These approaches will be pursued in Phase 2 of the project. Due to absence of dc-link capacitors, a low-profile converter construction can be adopted, resulting in a higher-density package. Higher reliability is achievable because the control of the primary side push-pull converter is simple and operates at 50% fixed duty cycle. Zero voltage switching of the switching converter on the primary side can be achieved using magnetizing current inherent in the high-frequency transformer. This aspect is under further

investigation. An optimized 2nd order input filter at the input terminals guarantees the fuel cell input current to contain minimum input current ripple. The output of the converter can be altered from 1-phase to 3-phase by a simple change in software.

References

1. S. Kim, S. K. Sul and T. A. Lipo, "AC/AC Power Conversion Based on Matrix Converter Topology with Unidirectional Switches", IEEE Trans. IA, Vol. 36, No. 1, pp. 139-145, 2000
2. V. Kaura and V. Blasko, "Operation of a Voltage Source Converter at Increased Utility Voltage", IEEE Trans. PE, Vol. 12, No. 1, pp. 132-137, January, 1997

3. N. Mohan, T. M. Undeland and W. P. Robbins, "Power Electronics: Converters, Applications, and Design" 3rd Edition

FY 2004 Publications/Presentations

1. Yu Jin Song, P. Enjeti, "A High Frequency Link Direct DC-AC Converter for Residential Fuel Cell Power Systems", IEEE Power Electronics Specialist Conference, PESC 2004, June 2004

Special Recognitions & Awards/Patents Issued

1. Patenting process initiated via TAMU technology licensing office.

III.C.3 Low-Cost Soft-Switched DC/DC Converter for Solid Oxide Fuel Cells

Jih-Sheng (Jason) Lai (Primary Contact), Changrong Liu, Amy Johnson

Virginia Polytechnic Institute and State University

668 Whittemore Hall

Blacksburg, Virginia 24060

Phone: (540) 231-4741; Fax: (540) 231-3362; E-mail: laijs@vt.edu

DOE Project Manager: Don Collins

Phone: (304) 285-4156; E-mail: Donald.Collins@netl.doe.gov

Subcontractor: EPRI-PEAC Corp., Knoxville, Tennessee

Objectives

- Develop a low-cost DC/DC converter for low- to high-voltage power conversion as the standard interface between the solid oxide fuel cell (SOFC) source and the load-side DC/AC inverter.
- Achieve 97% DC/DC conversion efficiency for the Solid State Energy Conversion Alliance (SECA) 5-kW solid oxide fuel cells.
- Advance high-power DC/DC converter technology with high-efficiency soft switching and high-performance digital-controlled techniques.

Approach

- Develop an interleaved multiphase isolated DC/DC converter (V6 converter) that reduces the ripple going back to the fuel cell and the ripple appearing at the output.
- Develop a phase-shift modulated soft-switching technique to eliminate switching losses of the DC/DC converter.
- Develop a dynamic fuel cell model for strategizing the fuel cell energy management and the DC/DC converter control.
- Design a high-frequency planar transformer to reduce the size of the complete system.
- Design an intelligent digital controller for high-performance SOFC power conversions.
- Test the converter with a calorimeter to characterize the converter efficiency.

Accomplishments

- A novel multiphase isolated DC/DC converter has been developed for low-voltage input and high-voltage output, especially for SECA SOFC applications. A prototype 5-kW V6 converter has been designed, fabricated and tested to demonstrate 97% efficiency over a wide load range.
- An intelligent current sensor-less control technique has been developed for high-performance DC/DC converters.
- A dynamic fuel cell model has been developed and proven with a commercially available proton exchange membrane (PEM) fuel cell for converter simulation and for strategizing controller design and energy management. The model will be modified for solid oxide fuel cells with minor changes of the time constants.
- Two calorimeters have been built and characterized for DC/DC converter efficiency measurement.

Future Directions

- Continue testing the DC/DC converter to full power with the calorimeter.
- Address fuel cell current ripple reduction issue in the converter design.
- Design the package for the V6 DC/DC converter that incorporates a DC/AC inverter.
- Design the solid oxide fuel cell interface and communication.
- Test DC/DC converter electromagnetic interference (EMI) performance at EPRI-PEAC Corp.
- Test DC/DC converter with the solid oxide fuel cell.

Introduction

While the efficiency of the SOFC stack is crucial to the entire power plant efficiency, the inefficient power electronics can eat up all the gains in SOFC stack development. As shown in Figure 1, the SOFC-based power plant consists of multiple-stage power conversions including a DC/DC converter and a DC/AC inverter to obtain utility AC voltage. It is nontrivial to achieve high efficiency for multiple-stage power conversions. The most important power conversion stage in this SOFC power plant is the DC/DC converter, which takes low-voltage SOFC output DC and converts it to high-voltage DC through a 3-stage power conversion. Currently, the commercial off-the-shelf DC/DC converter is normally less than 90% efficient and is not available at 5-kW or higher power level.

Efficiency translates not only to fuel savings but also to cost reduction because a smaller membrane electrode assembly (MEA) can be used for the same power output. Thus, the primary focus of this project is to develop a low-cost DC/DC converter that achieves 97% efficiency at 5 kW for SECA SOFC power plants. Given that the SECA SOFC voltage output is as low as 20 V and the silicon bandgap is 0.7 V, any single junction voltage drop in silicon devices would drop the efficiency below 96.5%.

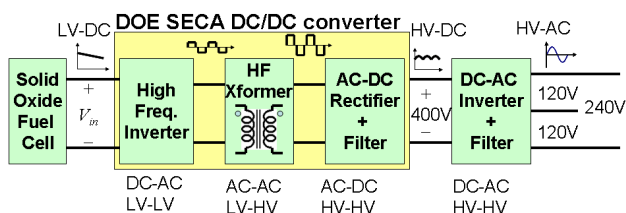


Figure 1. Block Diagram of a SOFC-Based Power Plant Showing a DC/DC Converter as the Most Important Power Conversion Stage

Thus, the design of the highly efficient DC/DC converter is very challenging and requires innovative ideas and substantial engineering effort.

Approach

A novel interleaved multiphase isolated DC/DC converter has been proposed and developed for cost reduction and efficiency improvement. This newly developed converter has been named as “V6 converter” because it resembles a V6 engine for high-horsepower vehicles. With 6-phase legs interleaved operation, the V6 converter significantly reduces the ripple going back to the fuel cell and the ripple appearing at the output. The structure of the converter also allows phase-shift modulation to eliminate the switching loss. An optimized transformer turns ratio has been designed to avoid device body diode conducting that generally consumes more than 7% of the total conduction loss.

In order to design a controller that matches the fuel cell dynamic response, a dynamic fuel cell model has been developed for the entire fuel cell power plant simulation to verify the fuel cell energy management and the DC/DC converter control strategy. An intelligent digital controller is being developed for high-performance power conversions to ensure system stability under any transient and dynamic conditions.

Results

Figure 2 shows the schematic circuit diagram and the 5-kW prototype of the proposed 6-phase leg (V6) isolated DC/DC converter. The schematic circuit diagram only shows one DC output; however, the actual prototype has two DC outputs that allow interfacing to a dual-output DC/AC inverter.

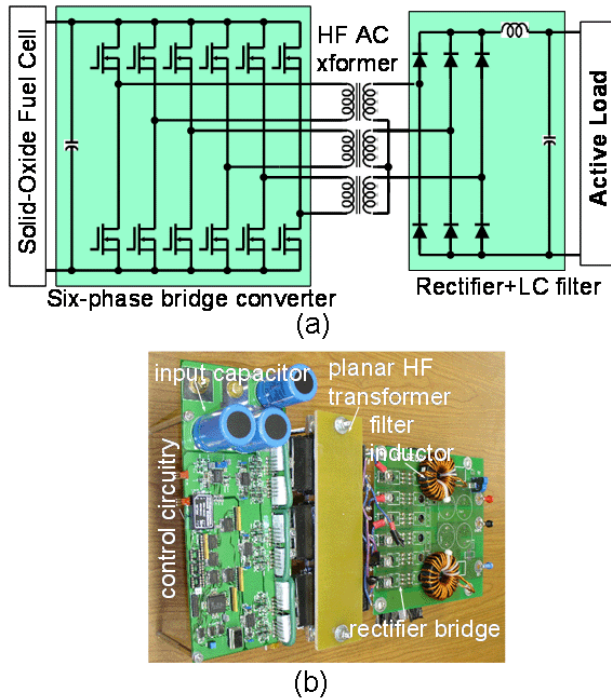


Figure 2. Circuit Diagram and Photograph of the Proposed V6 DC/DC Converter: (a) Schematic Circuit Diagram; (b) Photograph of the 5-kW Converter Prototype

For the 6-leg DC/DC converter, every two-phase leg pair forms a full-bridge converter that can be operated at zero-voltage switching condition with phase-shift-modulation control. Three full-bridge converters are phase-shifted 120° with transformer current interleaving each other to cancel the high-frequency ripple at both input and output; thus, the size of the input filter capacitor and output filter inductor can be largely reduced. These passive components reduce the size and cost by 6 times compared to the single-phase leg converter. The multiphase converter also avoids device paralleling associated parasitic losses and reliability degradation problems. The novel multiphase isolated V6 converter has been developed for low-voltage input and high-voltage output, especially for SECA solid oxide fuel cell applications. A prototype 5-kW converter has been designed, fabricated and tested to demonstrate 97% efficiency over a wide load range.

The DC/DC controller is implemented with a proprietary digital phase-shift controller. It produces very precise phase-shift angles between three full-

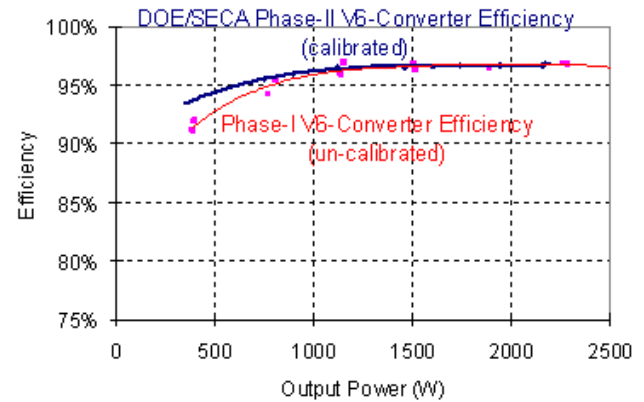


Figure 3. Measured Input and Output Voltage Waveforms for (a) Conventional Full Bridge Converter and (b) the Proposed V6 Converter

bridge converters to avoid the unbalanced output-induced circulating current. The transformer output is tied in Y-connection to double the output with a lower turns ratio, thus avoiding significant leakage inductance and its associated losses. The turns ratio is also optimized to avoid circulation current associated losses. The phase-shift modulation allows the devices turning on at zero voltage to eliminate the switching loss. Thus, the only major converter losses are in device conduction, and the system efficiency can be manipulated with proper selection of low-voltage-drop semiconductor devices.

Figure 3 compares measurement results of input and output voltage and current waveforms for the conventional full-bridge DC/DC converter and the proposed V6 converter. The full-bridge converter not only shows poor efficiency of about 87% at the 1-kW test condition, but also presents significant electromagnetic interference noise on the output voltage. The proposed V6 converter, however, shows very clean voltage and current waveforms and a high efficiency of 97% at the same power level.

The efficiency measurement has been very inconsistent during Phase I testing. The numbers were all over the place and occasionally exceeded 100%. Since the only trustable efficiency measurement is from thermal measurement, we built a calorimeter and calibrated all the sensors and data acquisition units in the Phase II effort. The calibration for thermal measurement is very time consuming, typically taking 8 hours to reach thermal

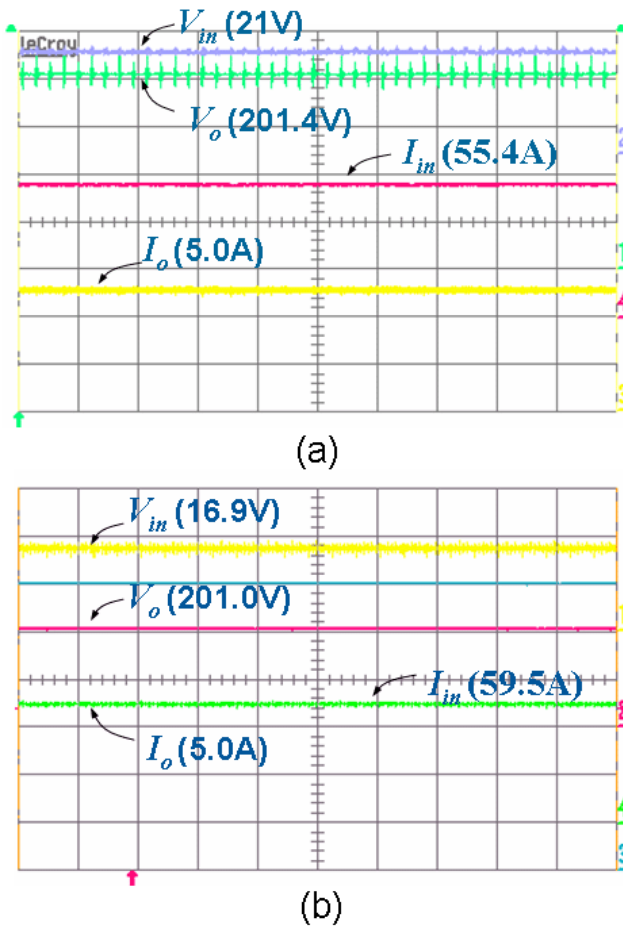


Figure 4. Efficiency Measurement Results of the V6 DC/DC Converter Showing Both Un-calibrated Phase-I and Calibrated Phase-II Results

equilibrium, but is the only way to have high confident level. Figure 4 shows the efficiency measurement results of the V6 DC/DC converter with both un-calibrated Phase-I and calibrated Phase-II results. The calibrated results were obtained from the average of 10 data acquisition points, while the un-calibrated results were obtained from human eye monitoring. The results agreed reasonably well with each other at most power levels. However, the Phase-II converter has better efficiencies at lower powers and is expected to show better results at higher power level as well. The reason we have not pushed to higher power is because the sensor has been calibrated only at 5 A for the two output current measurements, and the maximum output power can be measured at about 2 kW.

We also developed a dynamic fuel cell model and proved it with a commercially available PEM fuel cell for converter simulation and for strategizing controller design and energy management. The model will be modified for solid oxide fuel cells with minor changes of the time constant. To date, the converter control system design has been based on the PEM fuel cell dynamics and has been proven to be stable under load transient conditions. Once the SOFC dynamic model is known, we will modify the controller time constant accordingly to ensure stability.

Conclusions

The proposed V6 DC/DC converter shows superior performance and achieves the SECA efficiency goal in a wide power range. The major effort and achievements can be summarized as follows.

- Successful development of highly efficient DC/DC converter.
- Successful development of low-loss low-profile high-frequency transformer.
- Successful development of highly precised digital phase-shift modulation controller for the V6 converter.
- Calibration of loss measurement and calorimeters.
- Modeling of fuel cell dynamics for DC/DC controller and fuel cell energy management system designs.

The proposed V6 converter has been characterized with the following distinct features:

- High efficiency – 97% over a wide load range
- Low input current ripple – 6X reduction over conventional technologies
- Low output current ripple – 6X reduction over conventional technologies
- Small input filter capacitor – 6X reduction over conventional technologies
- Small output filter inductor – 6X reduction over conventional technologies
- Low cost – significant reduction on passive components (6X) and heat sink size

- Low EMI – soft switching over a wide load range and interleaving to cancel ripples
- High stability – controller design based on the fuel cell and converter dynamic models

FY 2004 Publications/Presentations

1. Changrong Liu, Amy Johnson, and Jih-Sheng Lai, “A Novel Three-Phase High-Power Soft Switched DC/DC Converter for Low Voltage Fuel Cell Applications,” in Proc. of IEEE Applied Power Electronics Conference, Anaheim, CA, February 2004, pp. 1365 – 1371.
2. Jih-Sheng (Jason) Lai, “A High-Efficiency Low-Cost DC-DC Converter for SOFC Performance and Control of V6 Converter,” Presentation at SECA Core Technology Program Review Meeting, May 13, 2004.

3. Jih-Sheng (Jason) Lai, “Fuel Cell Power Conditioning,” Keynote Speech at ASME International Conference on Fuel Cell Science, Engineering and Technology, June 14-16, 2004.
4. Changrong Liu, Amy Johnson, and Jih-Sheng Lai, “Modeling and Control of a Novel Six-Leg Three-Phase High-Power Converter for Low-Voltage Fuel Cell Fuel Cell Applications,” in Proc. of IEEE Power Electronics Specialists Conference, Aachen, Germany, June 2004, pp. 4715 – 4721.

Special Recognitions & Awards/Patents Issued

A Patent Disclosure is in the process of filing through Whitham, Curtis & Christofferson, RC Intellectual Property Law for the Multiphase Soft-Switched DC-to-DC Converter.

III.D Modeling & Simulation

III.D.1 An Integrated Approach to Modeling and Mitigating SOFC Failure

Jianmin Qu (Primary Contact), Andrei Fedorov, Comas Haynes and Sam Graham

Georgia Institute of Technology

Atlanta, GA 30332-0405

Phone: (404) 894-5687; Fax: (404) 894-0186; E-mail: jianmin.qu@me.gatech.edu

DOE Project Manager: Travis Shultz

Phone: (304) 285-1370; E-mail: Travis.Shultz@netl.doe.gov

Objectives

- To develop and demonstrate the feasibility of an integrated predictive computer-based tool for fuel cell design and reliability/durability analysis;
- To generate new scientific and engineering knowledge to better enable Solid State Energy Conversion Alliance (SECA) Industry Teams to develop reliable, low-cost solid oxide fuel cell (SOFC) power generation systems;
- To create technology breakthroughs to address technical risks and barriers that currently limit achievement of the SECA performance and cost goals for solid oxide fuel cell systems; and
- To transfer new science and technology developed in the project to the SECA Industry Teams.

Approach

- The Georgia Tech team is using a multi-physics modeling approach to collectively characterize the interdependency between structural issues and electrochemical/thermal transport phenomena in order to create high-fidelity thermo-mechanical failure analysis models.
- Experimental data from Oak Ridge National Laboratory (ORNL) will be utilized for model validation, and exploratory studies using these modeling tools will be performed to optimize cell and stack level designs.

Accomplishments

- A global/local analysis scheme was developed and illustrated on a 3D co-flow cell model that allows the integration of thermal/fluid simulation results directly combined with local stress analysis.
- Developed a domain integration formulation to evaluate crack tip parameters for fracture analysis.
- Developed a first-order design criterion for the maximum allowable crack size on the electrolyte/anode interface against delamination.
- Developed a first-order design criterion for the maximum allowable localized heating rate against microcracking in the anode.
- It was experimentally determined using a Fourier transform infrared (FTIR) spectrometer that the electrode (anode made of 40 vol% Ni, 60 vol% 8YSZ and cathode made of Sr-doped lanthanum ferrite) samples appear to be opaque over the entire near- and mid-infrared spectra.
- Experimentally determined the radiative properties of common SOFC electrode and electrolyte materials.

- Developed a general formulation (on a spectral basis) for the analysis of the radiative heat transfer in the optically thin electrolyte of the planer SOFC, and wrote and validated a code for implementation of the formulation.
- Developed constitutive models for creep deformation in reduced Ni/YSZ anodes.

Future Directions

- Develop a suitable constitutive model for viscoelastic behavior in Ni/YSZ cermet anode compositions. Incorporate this model into SOFC stress analyses.
- Develop and demonstrate a suitable finite element analysis (FEA) tool for analysis of fracture failure in the context of various pre-existing flaws within SOFC cells under transient and steady-state operating conditions.
- Develop fracture mechanics-based models for damage accumulation in SOFCs.
- Develop models for thermal shock-induced failure in SOFCs.
- Develop models for transient heating for start-up and cool-down analyses.

Introduction

In this work, the Georgia Tech team will take a multi-physics modeling approach to collectively characterize the interdependency between structural issues and electrochemical/thermal transport phenomena in order to create greater fidelity within thermo-mechanical failure analysis models. Once such models and computational algorithms are developed, they will be implemented into various commercial software codes for analysis and simulation. Software such as FLUENT, Star-CD, Marc, ANSYS, and ABAQUS will be used, as needed, for the purpose of validating the convergence and accuracy of the solutions. In addition, limited experimental tests will be conducted in the Phase II project. These tests will be primarily at the material level to understand materials behavior and to obtain certain materials properties needed in the models. Tests will also be conducted to validate the damage evolution models developed in Phase II.

Georgia Tech's Phase I project has demonstrated the feasibility of simulating thermo-mechanical failure in SOFCs using an integrated approach that takes into account the interdependency between structural issues and electrochemical/thermal transport phenomena. Building upon the success of Phase I, Georgia Tech will further develop and mature the multi-physics modeling approach to a level that can be utilized directly by the SECA Industry Teams.

Realizing the complexity and magnitude of technical challenges associated with modeling and simulating SOFC stack failure, the Georgia Tech team will focus on the specific critical tasks listed below. Computational algorithms and related computer codes for the models developed will be transferred to the SECA Industry Teams directly, as well as to Pacific Northwest National Laboratory (PNNL), the National Energy Technology Laboratory (NETL), and ORNL for integration into the Life Prediction and Structural Modeling Tools under development at these national labs.

Approach

Creep Models for Reduced Ni/YSZ Anodes

The Ni/YSZ anode is a mixture of Ni and yttria-stabilized zirconia (YSZ), or a cermet. Due to NiO reduction, the Ni/YSZ anode also contains a large number of voids, making it a porous cermet. In this complicated microstructure, creep deformation will occur predominately in the Ni phase. However, the creep behavior of the anode will be very different from that of bulk Ni due to the presence of YSZ particles and voids. A constitutive creep law needs to be developed for the anode. In this report, several distributions of Ni and YSZ in the anode are investigated in order to gain better understanding of how creep of Ni in the anode will affect the creep of

the mixture of Ni and YSZ. Based on the theories of micromechanics, it was derived that

$$\dot{\varepsilon} = c_N \frac{\mu_N}{\mu} \left[\frac{-3c_Y A \mu_N \mu_Y (1-n_c) t}{2\mu} \exp\left(-\frac{Q}{RT}\right) + \left(\frac{\mu^N}{\mu} \bar{\sigma}\right)^{1-n_c} \right]^{\frac{n_c}{1-n_c}}$$

This equation gives the strain rate (relaxation) of the entire Ni/YSZ mixture as a function of the overall effective stress. For Ni, n_c is typically greater than one. Thus, the exponent in the above equation is negative, and the quantity inside the brackets is positive and increases with time. Consequently, $\dot{\varepsilon}$ vanishes as time goes to infinity. That means that the overall relaxation will eventually cease.

Radiative Property Characterization

The measurement of transmittance of SOFC materials was carried out on an FTLA 2000-154 (ABB Bomem Inc.) Fourier transform infrared (FTIR) spectrometer. In order to measure the reflectance of the sample, the spectrometer was fitted with a 10 SPEC (Pike Technologies) 10-degree specular reflectance accessory.

Transmittance measurements are conducted by measuring the transmission of a beam of normal incidence through a sample as the wavenumber of the light is varied. An infrared detector measures the intensity of the transmitted beam, and this value is reported as a percentage of the source beam. The reflectance measurements are conducted in a similar manner. However, rather than shining normal and through the sample, the beam of light strikes the sample at 10 degrees from normal incidence and a mirror collects the reflected light. This reflected beam is then passed to the infrared detector, and the ratio of intensities of the reflected light to the source beam is the reflectance of the sample. Optical properties were then obtained for several SOFC materials.

Two-Medium Non-Equilibrium Heat Transfer in Porous Electrodes

The proposed two-equation, thermal non-equilibrium model is derived from conservation of energy in the gas and solid phases:

$$\nabla \cdot (\rho \vec{v} c_p T_g) = \nabla \cdot (k_{g,eff} \nabla T_g) - h_{sf} a_s (T_g - T_s) \quad (\text{Gas phase})$$

$$0 = \nabla \cdot (k_{s,eff} \nabla T_s) + h_{sf} a_s (T_g - T_s) + \sum \dot{Q}_{gen_i} \quad (\text{Solid phase})$$

where, h_{sf} is the solid-to-gas-phase heat transfer coefficient, a_s is the specific surface area of the media, and \dot{Q}_{gen}^m represents sources of volumetric heat generation within the solid phase. The magnitude of the difference in local temperatures between the gas and solid phases, $(T_g - T_s)$, is an indicator of how valid the assumption of local thermal equilibrium (LTE) might be. Thus, an order-of-magnitude analysis of the terms in the above equation was performed as a first step.

Effects of Mechanical Damage on Cell Stack's Electrical Performance

The electrochemical impact of a delamination crack (between electrolyte and electrode(s)) is that of an electrochemical obstacle. Specifically, the cracked area is a region through which little to no current is generated or flows. As an initial conservative (i.e., "safety factor") measure for quantifying a crack's impact on current flow, it can be assumed that delamination along the purposely thin electrolyte (on the order of microns) results in corresponding regions of nullified electroactivity and charge transport. Stated differently, the thin electrolyte promotes the approximation that delamination locations are effectively "masked" or "de-activated" locales along the cell. Current must thus be generated and conducted outside of the domains of delamination.

Results

Creep Models for Reduced Ni/YSZ Anodes

A representative cell model is used for the finite element analysis. Periodic boundary conditions are prescribed on all four sides of the cell. In other words, the cell element considered here can be viewed as a representative volume in a complete cell. Considering the symmetry of the structure, one only needs to consider a quarter of the representative cell.

In addition to the elastic properties of the cell materials, the creep properties of the anode, as listed

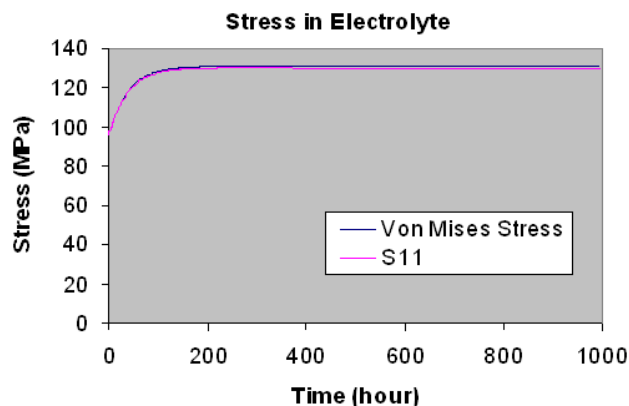


Figure 1. Stress Increment in the Electrolyte Due to Creep in the Anode

in Table 1, are used in the analysis. The electrolyte and cathode are assumed linear elastic without creep.

Table 1. Parameters of Creep Material Model

	A	n_c	Q
Ni/YSZ	$2.0e^{-6}$	1.2	550 kJ/mol

In the analysis, the cell is raised to 800°C rather rapidly. So, creep deformation is neglected during the heating of the cell. Once it reaches 800°C, the cell is kept at this temperature for 1000 hours. Because of creep, stresses in the anode start to relax and approach zero in about 200 hours. Contrary to popular belief, the stress in the electrolyte increases as creep relaxes the stresses in the anode. In the example shown in Figure 1, the in-plane stress in the electrolyte increased by over 30% in about 200 hours. This clearly increases the propensity for electrolyte cracking.

Radiative Property Characterization

Transmittance measurements were used in obtaining the following optical properties for SOFC materials.

Anode (Nickel-doped Yttria-stabilized Zirconia)

Composition: 40% (Ni), 60% ($Zr_{1-x}Y_xO_2$); (vol%) ($x = 0.08$)
 Porosity: 43 vol%
 Sample Thickness: 200 m

Cathode (Strontium-doped Lanthanum Ferrite, LSF)

Composition: $(La_{1-x}Sr_x)FeO_3$
 Porosity: 24 vol%
 Sample Thickness: 200 m

Electrolyte (Yttria-stabilized Zirconia)

Composition: $(Zr_{1-x}Y_xO_2)$ ($x = 0.08$)
 Sample Thickness: 330 m

The spectral region of interest for typical SOFC operating conditions (700°C) can be found from Planck's distribution [1], and Murthy and Fedorov [2] showed that 80% of the emissive power is contained within $1.4 < \lambda < 6.1$ m for emission from an object with refractive index $n = 1.8$. Although data was collected for the spectral range $2 < \lambda < 20$ m, data for $\lambda > 10$ m is of little interest for this application.

For the anode and cathode materials of given thickness, the transmittance measurement was essentially zero within the noise of the FTIR spectrometer (Figure 2). This implies that the absorptive index is very large, i.e. the electrodes are opaque in the mid-infrared region of the electromagnetic spectrum.

For the YSZ electrolyte, the FTIR data shows significant transmittance in the spectral region of interest, indicating that the electrolyte layer of the thickness typically used in SOFCs is optically thin. This transmittance and reflectance data (Figure 3) is used to calculate the absorption coefficient and refractive index as described above. The results of these calculations are shown in Figure 4.

Two-Medium Non-Equilibrium Heat Transfer in Porous Electrodes

An order-of-magnitude analysis of the energy equation for the solid phase of the porous medium was used to estimate the expected temperature difference between the gas and solid phases. This required an estimate of the volumetric heat transfer coefficient between the two phases and an estimate of the volumetric heat generation within the solid phase. The estimated temperature difference based on this analysis was negligible, indicating the validity of the assumption of local thermal equilibrium. Two other criteria found in the

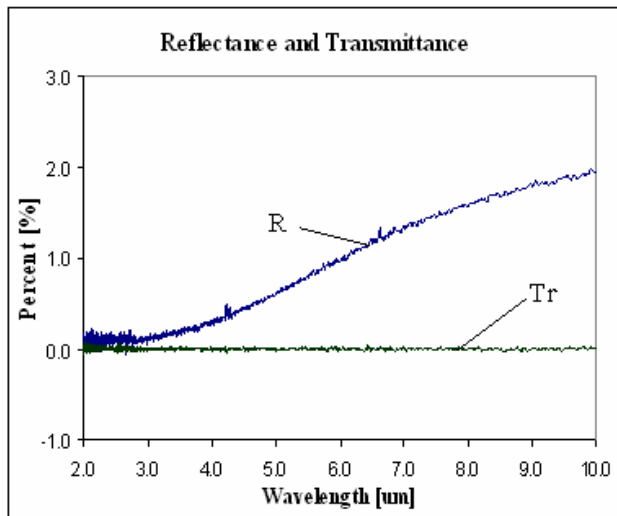
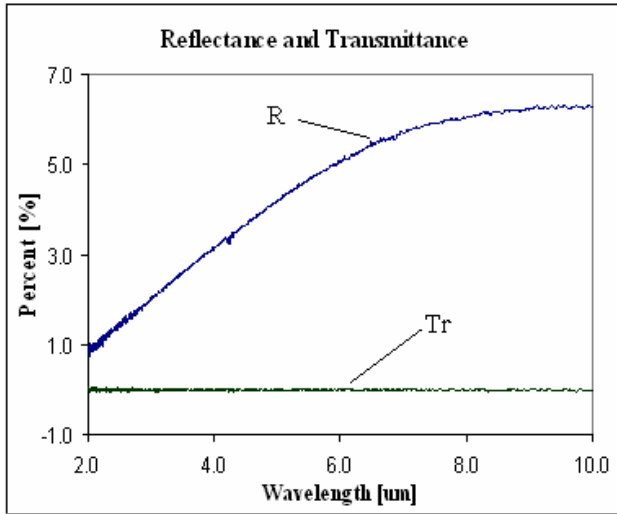


Figure 2. Plots of FTIR Data for LSF (a) and Nickel-doped YSZ (b), Showing Percentage of Reflectance and Transmittance of Samples

literature were applied, and both indicated that local thermal equilibrium in the porous electrodes of SOFCs is probably valid.

However, several critical simplifying assumptions were made concerning the nature of the porous microstructure, the cell operating conditions and heat generation processes, and the magnitude of the current density and heat generation zone. In particular, the local current density (at the microscale level) could be several orders of magnitude greater than the average cell current density depending on the size and distribution of catalytically active sites near the electrolyte/electrode interface.

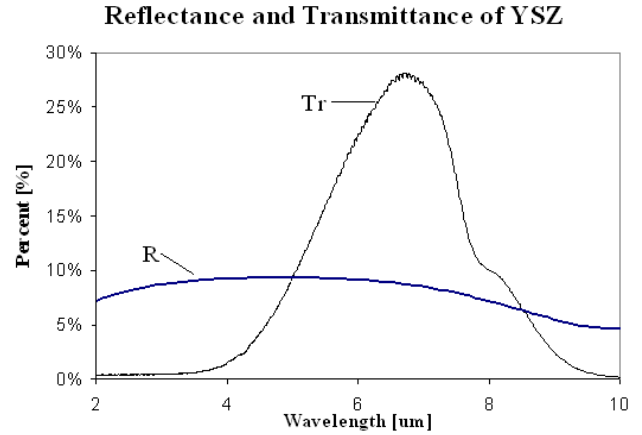


Figure 3. Plot of FTIR Data for YSZ, Showing Percentage of Transmittance and Reflectance

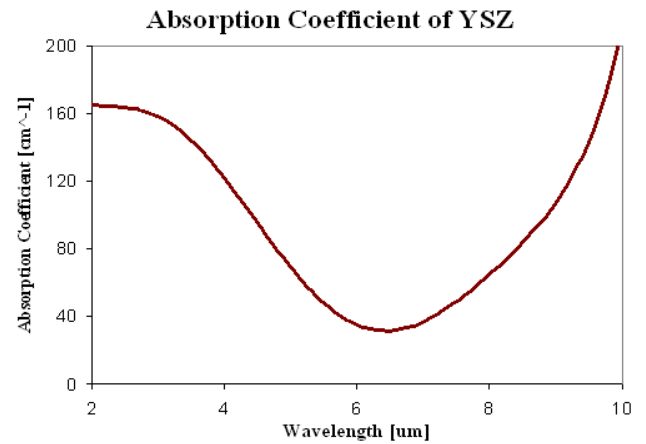


Figure 4. Absorption Coefficient of Electrolyte Material (YSZ)

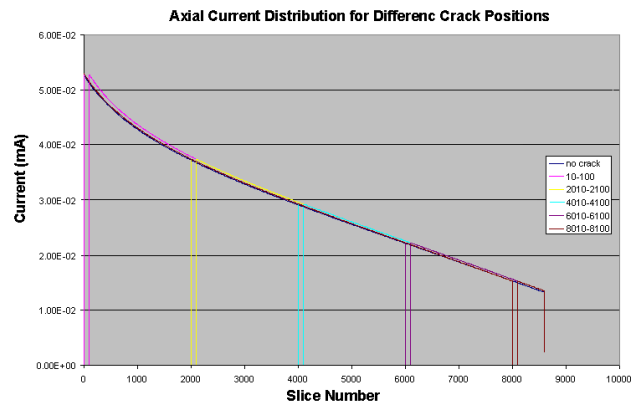


Figure 5. Impact of Crack Location

Effects of Mechanical Damage on Cell Stack's Electrical Performance

A conservative approach, from the standpoint of electrochemical impact of delamination, is the “masking” approximation whereby no current transport is presumed within the SOFC P-E-N segment that is vertically aligned with the delamination zone. In essence, the electroactive region is presumed to be “de-activated” due to separation of the classically considered *plane* of electroactivity, and no *charge transfer* (i.e., current generation) is presumed to occur within such region. Additionally, since the electrolyte thickness is conventionally on the order of microns, there is no in-plane component of ionic current presumed due to exorbitant sheet resistance effects. The result is that the “footprints” of the delamination zones are effectively presumed to become insulated or “*masked*” regions. Such zones are evident within such plots as in Figure 5.

Conclusions

It was experimentally determined using FTIR spectrometer that the electrode (anode made of 40 vol% Ni, 60 vol% 8YSZ and cathode made of Sr-doped lanthanum ferrite) samples appear to be opaque over the entire near- and mid-infrared spectra. The experimentally determined radiative properties of common SOFC electrode and electrolyte materials were made into a material database and delivered to the SECA team. Optical properties such as those obtained here can greatly add to our understanding of heat transfer mechanisms in SOFCs. It has long been debated whether radiation played any role in heat and mass transport

in a SOFC environment. Our studies, to a certain extent, have settled that issue.

Additionally, the developed general formulation (on a spectral basis) of the radiative heat transfer in the optically thin electrolyte of the planer SOFC can be used as an effective tool to simulate radiative heat transfer. A software code had been written and validated for implementation of the formulation. The SECA Industry Teams can use this code to analyze radiative heat transfer in their own designs.

Furthermore, the constitutive models developed here for creep deformation in reduced Ni/YSZ anodes enable us to calculate the stress evolution during SOFC operation. Using this model, one can simulate the stresses in the various layers of the SOFC stack as a function of time and temperature. This is a major step toward understanding performance degradation in SOFCs.

References

1. Modest, M., *Radiative Heat Transfer*, 1st Edition, McGraw-Hill, 1993.
2. Murthy, S. and Fedorov, A. G., 2003, "Radiation Heat Transfer Analysis of the Monolith-Type Solid Oxide Fuel Cell", *Journal of Power Sources*, Vol. 124, No. 2, pp. 453-458.

FY 2004 Publications/Presentations

1. Murthy, S. and Fedorov, A. G., 2003, "Radiation Heat Transfer Analysis of the Monolith-Type Solid Oxide Fuel Cell", *Journal of Power Sources*, Vol. 124, No. 2, pp. 453-458.

III.D.2 SOFC Model Development at PNNL

Mohammad A. Khaleel (Primary Contact), Brian J. Koepfel, Ba Nghiep Nguyen, Kenneth I. Johnson, Kurtis P. Recknagle, David Rector, John S. Vetrano

Pacific Northwest National Laboratory

P.O. Box 999, MS K9-95

Richland, WA 99352

Phone: (509) 375-2527; Fax: (509) 375-2438; E-mail: moe.khaleel@pnl.gov

DOE Project Manager: Travis Shultz

Phone: (304) 285-1370; E-mail: Travis.Shultz@netl.doe.gov

Objectives

- Develop, improve, and validate modeling tools for analyzing solid oxide fuel cell (SOFC) cells, stacks, and systems.
- Transfer the modeling technology to the Solid State Energy Conversion Alliance (SECA) vertical teams for their use in designing and building SOFC cells, stacks, and systems.
- Conduct training sessions that SECA vertical team members can attend to learn to use the customized modeling tools created.
- Identify degradation mechanisms critical to extended operation and performance of SOFCs, and implement into existing modeling tools.

Approach

- Microstructural level modeling analyzes the flow of chemical species and electrical current within the cell electrodes to determine the effect of microstructure and material defects on electrochemical performance.
- Stack level models investigate the stack geometry and stack component material properties for suitability in creating well-operating and long-lasting designs.
- System models use knowledge of the operating characteristics of cell and stack designs to create optimized environments that will ensure the longest possible life span.

Accomplishments

- Incorporated stack-electrochemistry models, developed at Pacific Northwest National Laboratory (PNNL), into the MARC and STAR-CD codes in the form of Graphical User Interface (GUI) Stack Modeling Tools.
- Validated STAR-CD model temperature predictions with experimental measurements.
- Benchmarked thermal-electrochemical results of the MARC EC implementation against STAR-CD results.
- GUIs presented at the SECA Modeling and Simulation Training Workshop.

Future Directions

- Focus will be on life prediction in the cell and stack level modeling efforts.
- Computational fluid dynamics (CFD) electrochemical (EC): Include submodels to predict the degradation of electrochemical performance over time.
- Finite element EC: Improve geometry options, flow field characterization, and structural evaluations in the MARC GUI.
- Evaluate seal damage and thermal cycling effects in stack level models.
- Evaluate transient response of the controls/system model.

Introduction

Modeling tools have been developed under the SECA Core Technology Program to aid industrial teams in design and analysis of their SOFC designs in several areas. The bulk of the work in SOFC modeling has centered primarily on flow-thermal-electrochemistry behavior using a computational fluid dynamics (CFD) approach. This has been very successful in design of flow fields for planar stacks, where critical metrics are power density and temperature distributions. These temperature results have then been used as inputs for structural models to assess stack mechanical stresses. These models have been useful in designing the physical support for the electrodes (e.g., edge-to-edge and frame-supported electrodes) and rigid glass seals for air and fuel gases. For example, the combined use of these tools demonstrated the advantage of the co-flow design, which is more structurally robust as a consequence of its lower temperature gradients. These modeling tools have been critical for developing a “working” product and evaluating relative performance of stack designs under steady-state conditions with virgin materials properties.

Approach

In the current year, work has been directed to 1) migrate tools for the CFD electrochemistry evaluation into a finite element framework, 2) extend tools to evaluate degradation, and 3) create tools for studying system integration. This first task uses finite element numerical procedures to obtain results adequate for engineering design of stacks. Specifically, by using assumed or approximated flow fields, a multi-physics solution for both electrochemistry and structural response can be obtained within a single software application, with less computational effort due to greater numerical efficiency. This is done using MSC’s MARC code. The second major task is building on the existing tools for short-term performance to address the potential degradation mechanisms in the stack. To address this subject, relevant degradation behaviors are identified and prioritized according to influence. These are implemented in the models at several levels. On the microscopic level, for example, the effects of fractures on electrochemical processes and mechanical integrity are being

investigated. At the macroscopic level, routines will be integrated to assess the influence of the degradation mechanisms at the stack level. Therefore, degradation behaviors can be treated at both a rigorous fundamental level to understand their rates, severity, mechanisms, etc., and also at the stack level to assess overall influence on performance of a particular design. The third thrust is at a higher system level. In field applications, the stack must now interact with accessory equipment and actual electrical loads. Coupled interactions of the fuel cell, the power electronics, and the loads are largely unknown but could potentially have significant effect on cell efficiency and lifetime. System models that capture these interactions will be needed to aid industrial teams with implementation into actual power systems.

Results

Electrochemistry models have long been used in stack level analysis at PNNL with the STAR-CD computational fluid dynamics code. Model results for stack temperatures were validated against experimental results with good correlation. A photo of a one-cell stack test setup is shown in Figure 1. During the stack tests, the inflow and outflow gas temperatures were monitored as the stack generated 44 watts of power at 0.7 volts. A 3-dimensional

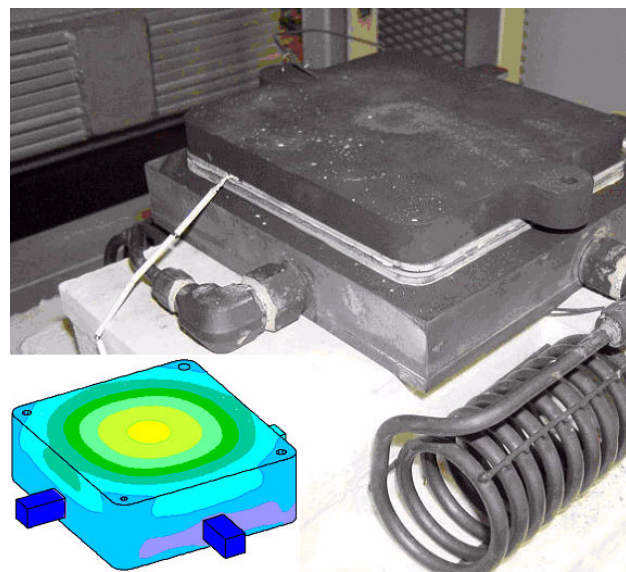


Figure 1. One-Cell Stack Experimental Setup, and the CFD Model Created to Simulate the Experiment (inset)

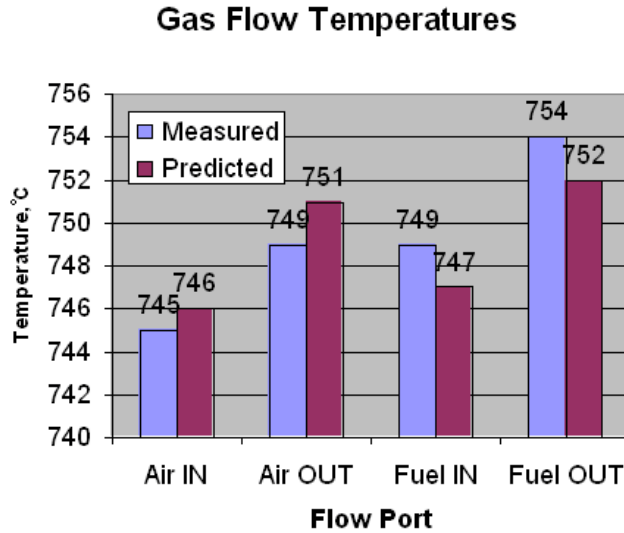


Figure 2. Comparison of Measured and Model-Predicted Inflow and Outflow Gas Temperatures

model of the stack containing 89,000 computational elements was created to mimic the experimental setup (Figure 1 inset). The model predicted inflow and outflow gas temperatures to within 2 degrees Celsius of those measured at the tested power and voltage. A graphic of the measured and predicted temperatures is given in Figure 2.

This modeling capability was successfully migrated into the finite element code MARC. The EC module was developed to calculate the current density distribution, heat generation, and fuel/oxidant species concentrations for a planar cell based on the thermal state, flow conditions, and user-defined electrochemical parameters (Khaleel et al 2004). The output heat generation profile from the EC module is input to MARC, which performs a thermal analysis and iteratively updates the temperature field until the steady-state solution is achieved. The steady-state temperature field can then be further used to obtain mechanical stresses in the stack.

Steady-state results from the MARC EC model were compared with similar STAR-CD simulation results. The case chosen was a cross-flow design with 116.6 cm² active area. The cell was operating at 40 watts and 0.7 volts. Fuel and air delivery rates were 4.236E-4 mol/s and 1.69E-4 mol/s respectively. The cell temperature distribution calculated by the STAR-CD stack modeling tool is shown in Figure 3. The cell temperature distribution calculated by the

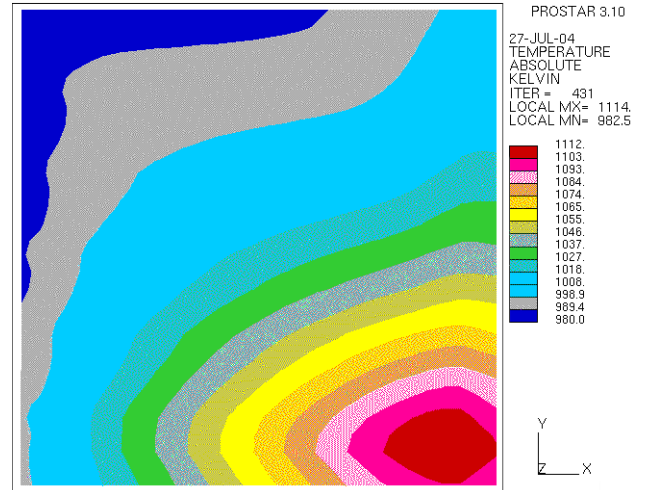


Figure 3. Cell temperature distribution calculated by the STAR-CD stack modeling tool. Cell with 116.6 cm² active area operating at 40 W and 0.7 V. Fuel and air delivery rates were 4.236E-4 mol/s and 1.69E-4 mol/s, respectively.

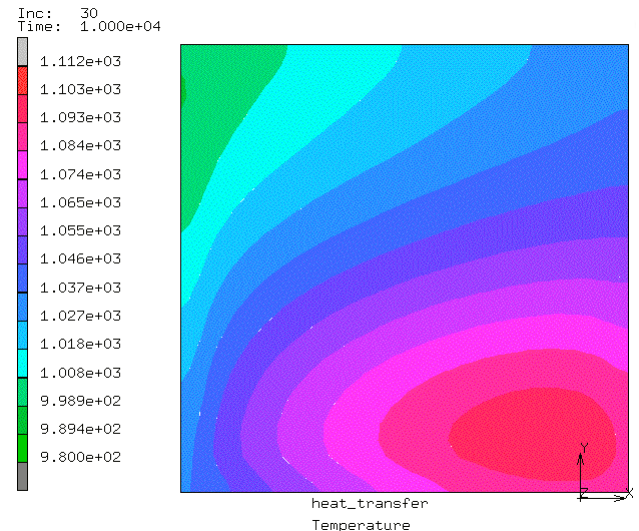


Figure 4. Cell temperature distribution calculated by the MSC stack modeling tool. Cell with 116.6 cm² active area operating at 40 W and 0.7 V. Fuel and air delivery rates were 4.236E-4 mol/s and 1.69E-4 mol/s, respectively.

MSC stack modeling tool is shown in Figure 4. Obtaining the close agreement shown in Figures 3 and 4 required adjusting the fuel concentrations in the MARC EC simulation to account for gas diffusion in the inlet fuel stream. The initial comparisons between MARC EC and Star-CD

showed considerable difference between the results until the inlet fuel concentrations were compared. The Star-CD solution includes diffusion of the fuel species in the flow simulation, whereas the MARC EC module assumes that the initial fuel concentrations exists at the inlet edge of the positive-electrolyte-negative (PEN). Closer review of the Star-CD results showed a significant diffusion gradient from the inlet manifold to the leading edge of the active area of the cell. A diffusion approximation (based on a path length from the inlet manifold to the cell, the fuel flow velocity, and the binary gas diffusion coefficients) is being developed to account for this effect.

Specialized GUIs to analyze electrochemical performance of multi-cell planar stacks were created in both the CFD and finite element analysis (FEA) frameworks. PNNL provided technical input to CD-Adapco as they created their customized GUI within STAR-CD and to MSC Software as they developed their customized GUI within MARC Mentat. Both implementations are based on the electrochemical routines developed at PNNL.

The STAR-CD stack modeling GUI has the capability to import user-defined model geometry or use templates to build custom planar cross-, co-, and counter-flow SOFC stack designs. The MARC GUI currently uses a template to build a customized planar SOFC stack design. Boundary conditions and electrochemical performance parameters can then be set and the fuel cell simulation performed. This capability enables the modeler/engineer to easily perform parametric studies of stack performance. Modelers from the SECA industrial partners and from universities were trained how to use this modeling capability by representatives of CD-Adapco (STAR-CD) and MSC Software (MARC) in July of 2004. The PNNL-hosted "SECA Modeling and Simulation Training Workshop" was organized to allow the software companies one full day to train the modelers how to use their "general purpose" baseline code as well as the SOFC-specific GUI. In the training workshop, the modelers had "hands on" use of the tools and provided direct feedback to the software company representatives about the functionality of the GUI as they worked through the training examples and manuals.

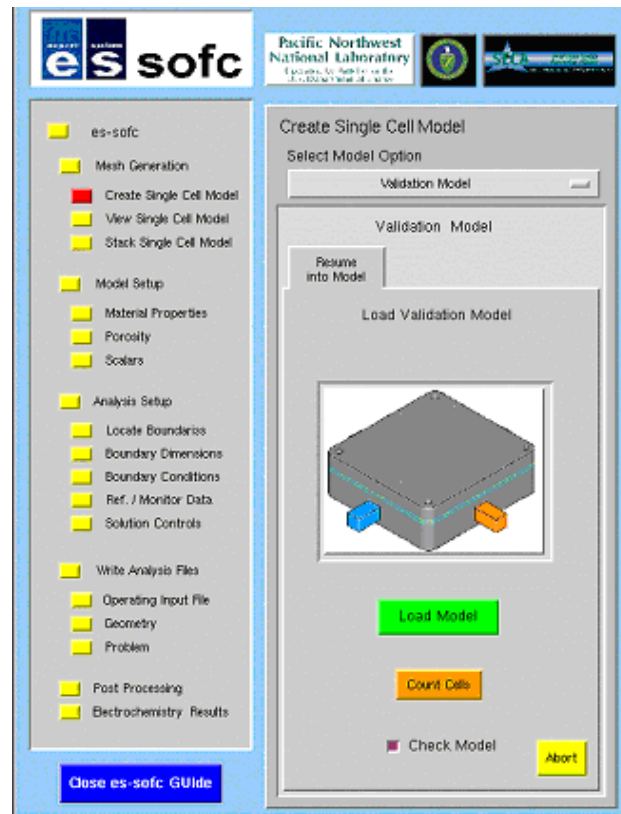


Figure 5. Main Model Setup Window of the STAR-CD GUI named ES-SOFC

The main model setup page for the STAR-CD GUI, named ES-SOFC, is shown in Figure 5. The models are set up step-by-step by working down through the list of tasks in the window shown. Each of the buttons on the list invokes popup windows that prompt the user for input. When the user completes the last step on the main page, the model setup is complete and is ready to run. The MARC GUI main window is shown in Figure 6. Similar to the ES-SOFC window, the models are set up step-by-step by following popup windows that prompt the user for model input. When input is completed, the model is saved and ready to run. In addition to the thermal-electrochemical performance, the MARC model can also be solved to evaluate the temperature-induced mechanical stresses in the cell.

In other activities, enhancements to existing modeling tools were made. On-cell steam methane reforming capabilities were added to the CFD electrochemistry model. This capability will be exercised to provide guidance for optimizing SOFC

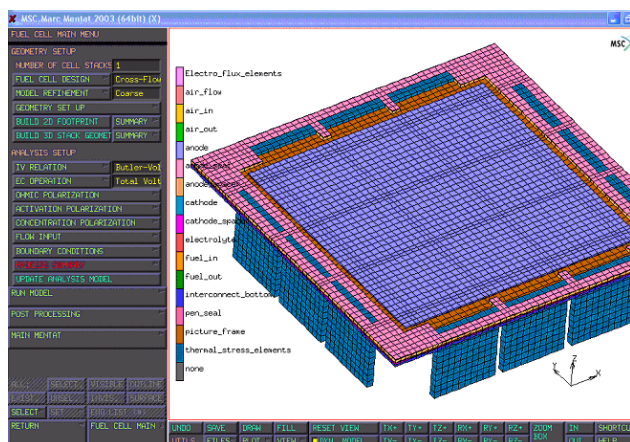


Figure 6. Main Model Setup Window of the MARC GUI

systems with respect to external reformer and blower sizes and the thermal load. For the structural model in MARC, compressive seal behavior was captured using specialized gasket elements and contact surfaces to evaluate the seal contact pressure distribution. Mechanical testing of seals was initiated to fill a void for fundamental material properties and provide mechanical properties and strengths for common seal materials. The data will also be included in the planned materials database. Testing of sealing glass is ongoing, but its inelastic response at cell operating temperatures has been observed.

New modeling efforts have also been initiated. As a basis for the study of cell/stack degradation, PNNL cataloged critical degradation mechanisms, physical parameters, and performance effects for SOFCs. The effect of fractures on electrochemical and mechanical behavior was one mechanism of interest. Microstructural electrochemistry models were used to determine the effect of anode cracks on

cell power density, and a continuum damage model was created in MARC to analyze structural integrity of rigid glass seals. These models will be integrated into the higher-level stack models. PNNL has also developed a Matlab/Simulink model of a complete SOFC power system, including the fuel cell, reformer, heat exchangers, battery, controllers, and power electronics. Transient stack behavior in the model was improved by experimental testing of electrical response to load switching.

Conclusions

Advanced computational modeling tools are being developed at PNNL and disseminated to SECA members to aid in meeting required SOFC performance targets.

FY 2004 Publications/Presentations

1. JE Deibler, KP Recknagle, and MA Khaleel, "Modeling of SOFC Stacks in Transition from Startup to Steady State Operation at PNNL," 2003 Fuel Cell Seminar Proceedings.
2. MA Khaleel, Z Lin, P Singh, W Surdoval, and D Collins, "A Finite Element Analysis Modeling Tool for Solid Oxide Fuel Cell Development: Coupled Electrochemistry, Thermal and Flow Analysis in MARC," *Journal of Power Sources*, Vol. 130, pp. 136-148 (2004).
3. MA Khaleel, KP Recknagle, Z Lin, BJ Koepfel, SJ Moorehead, KI Johnson, N Nguyen, D Rector, and G Grant, "SECA Core Program- Recent Development of Modeling Activities at PNNL," SECA CTP Program Review, May 11-13, Boston, MA (2004).

III.D.3 Solid Oxide Fuel Cell Manufacturing Cost Model: Simulating Relationships between Performance, Manufacturing, and Cost of Production

Eric J. Carlson (Primary Contact), Chandler Fulton, Yong Yang
TIAX LLC
Acorn Park
Cambridge, MA 02140-2390
Phone: (617) 498-5903; Fax: (617) 498-7295; E-mail: carlson.e@tiaxllc.com

DOE Project Manager: Shawna Toth
Phone: (304) 285-1316; Fax: (304) 285-4403; E-mail: Shawna.Toth@netl.doe.gov

Objectives

The objective of this project within the Solid State Energy Conversion Alliance (SECA) Core Technology Program (CTP) was to develop analysis methods and computational codes for analyzing solid oxide fuel cell (SOFC) production process issues in order to aid development of optimal production process methods, rates, and controls. The National Energy Technology Laboratory (NETL) sought development of a model with the capability to:

- Handle all key SOFC stack components, including ceramic cells and interconnects;
- Relate manufactured cost to product quality and likely performance, taking into account manufacturing tolerances, product yield, and line speed; and
- Address a range of manufacturing volumes ranging from tens to hundreds of megawatts per year.

Approach

- In Task 1, the overall project approach was presented to the SECA teams to solicit their inputs on how to tailor the cost model to their needs and what issues should be addressed in this phase of work
- In Task 2, the manufacturing cost model was linked to a performance/thermal/mechanical model and a statistical model of material failure to calculate process yields and performance as a function of electrode electrolyte layer thicknesses. The impact of economies of scale on the manufacturing cost was also modeled. The results of the analysis and the model assumptions were discussed with the SECA teams, and their feedback was incorporated into the analysis.
- In Task 3, a final report was prepared.

Accomplishments

- A manufacturing cost model developed in 1999 was updated and enhanced by linking it to a performance/thermal/mechanical model that calculated average power densities and stress distributions in the stack as a function of stack parameters and operating conditions. A more detailed analysis of quality control costs was incorporated in the model.
- The statistical material failure models developed by Oak Ridge National Laboratory (ORNL) were incorporated into the model to calculate yields as a function of stresses during manufacturing and power generation. The effect of electrode electrolyte assembly (EEA) defects on stack yield was estimated.
- The impact of economies of scale on stack cost was modeled.
- Several but not all of the SECA teams provided inputs to the project on an individual basis. The Teams preferred this mode of input versus the workshop format suggested in the proposal.

Future Directions

This project was not continued into Phase II; however, recommendations from the Teams and NETL for future cost analysis included:

- Alternative production techniques to tape casting and screen printing
- Coating processes for interconnects with 3-D flow channels
- Seal and manifold designs
- Balance-of-plant components, particularly any high-temperature components such as recuperators

Introduction

The National Energy Technology Laboratory (NETL) has a long history in high-temperature fuel cell technology development. The assessment of manufacturing technologies and cost has been an integral component of the technology development due to the criticality of both to the commercialization of fuel cells in a competitive marketplace. In 1999, TIAX [1] (as the Technology and Product Development sector of Arthur D. Little) conducted a technology and cost assessment of anode-supported planar SOFC technology with metallic interconnects. The cost of this lower-temperature (<800°C) SOFC technology was compared to a high-temperature (1000°C) planar all-ceramic design. For the low-temperature planar technology with metallic interconnects, a manufacturing cost projection of \$430/m² was obtained through an activities-based cost model. For an assumed power density of 500 mW/cm², this translates into a cost of \$86/kW for materials and processing, significantly less than the all-ceramic high-temperature stack with a cost of \$377/kW. Several factors contributed to the lower overall stack cost:

- Lower temperature permitted the selection of a much less expensive interconnect material, ferritic stainless steel.
- Anode support of the cell allows use of a thin electrolyte, leading to higher power density and much less yttria stabilized zirconia (YSZ) material.

The lower projected overall cost for low-temperature SOFC technology increases the likelihood of commercial success of SOFCs.

Using the previously developed cost model as the starting basis, NETL-SECA wished to develop

analysis methods and computational codes for analyzing issues in SOFC production. The methods and codes are ultimately to be used in development of optimal production process methods, rates, and controls.

Approach

In this phase of the project, the emphasis was on demonstrating the capabilities of the cost model to the SECA Industry teams and getting their inputs on critical issues. The proposed approach involved workshops to gather these inputs. However, after discussions with the SECA teams, we found that they preferred the use of individual meetings rather than collective workshops as a means of collecting information. In addition, the teams did not want to access the cost model through an internet-based user interface. For this project, only non-proprietary discussions were held, and the cost model demonstration was conducted using generic information in the public domain. Several of the SECA teams provided inputs on topics of interest for this analysis and feedback on the draft final presentation. After the initial face-to-face meetings, subsequent discussions were conducted at SECA meetings or over the phone.

For purposes of this project, a cost model developed in 1999 for planar metal-supported stacks was used as the basis. The results and assumptions of the 1999 project were updated, and the cost model was augmented with a SOFC performance model to calculate power density, utilization, temperature gradients, and mechanical stresses in the stack, the latter during steady-state operation and thermal cycling. Addition of this capability permits one to evaluate the impact of improvements in electrochemical performance, changes in power density as the stack design changes (e.g., thickness of

individual layers, changes in active area and flow field design), and changes in material properties. The model was also used to calculate maximum stresses on the materials, and it was compared with failure curves to estimate mechanical failures due to cracking. In contrast, the 1999 model simply selected an average power density and assumed that the utilization could be achieved and the materials would survive any stresses arising from thermal gradients.

Results

The analysis was based on the stack design assumed in the 1999 study (as a baseline to provide continuity) and a production volume of 250 MW per year. Conventional SOFC materials (i.e., nickel cermet anode, 8 YSZ electrolyte, and lanthanum strontium manganite cathode) with nominal anode/electrolyte/cathode thickness of 700/10/50 microns,

respectively, were used to develop a bill-of-materials. A rolled formed ferritic stainless steel was assumed for the interconnect; however, a stabilizing conductive coating was not used. In this demonstration, we focused only on the active materials and the interconnect. The seals and manifolds were excluded from this cost analysis.

For a fuel (reformed natural gas) utilization of 85%, cell voltage of 0.7 V, maximum temperature gradient of 150°C across the stack, maximum stack temperature of 800°C, and a contact resistance of 0.1 Ωcm^2 , the performance model calculated a baseline average power density of 470 mW/cm^2 . The model kinetic and diffusion parameters were calibrated using single cell kinetic data from the literature. For these operating conditions, the stress conditions resulted in less than 5% cracking of the materials based on failure data from ORNL. Power density increased when using thinner ceramic layers in the cell, reaching a maximum of 570 mW/cm^2 at the minimum thickness allowed for each layer.

Table 1. 2003 Total Stack Factory Cost on an Area Basis ($\$/\text{m}^2$). In the co-fire process, the electrodes and electrolyte are sintered in a single step. In the multi-fire process, the anode and electrolyte are sintered first and then the cathode is sintered.

Total Cost (Materials + Processes) (\$/m ²)			
Co-Fire		\$/m ²	
		Material	Process
Process Flow Steps	Anode	\$ 123.95	\$ 9.63
	Cathode	\$ 18.22	\$ 7.40
	Electrolyte	\$ 6.01	\$ 6.18
	Interconnect	\$ 118.70	\$ 19.25
	Fabrication	\$ -	\$ 100.99
Sub-Total		\$ 266.87	\$ 143.45
Total		\$410.32	

Total Cost (Materials + Processes) (\$/m ²)			
Multi-Fire		\$/m ²	
		Material	Process
Process Flow Steps	Anode	\$ 125.92	\$ 9.69
	Cathode	\$ 14.57	\$ 7.07
	Electrolyte	\$ 6.11	\$ 6.21
	Interconnect	\$ 118.70	\$ 19.25
	Fabrication	\$ -	\$ 126.72
Sub-Total		\$ 265.29	\$ 168.93
Total		\$434.22	

Table 2. 2003 Total Stack Factory Cost on a Power Basis ($\$/\text{kW}$)

Total Cost (Materials + Processes) (\$/kW)			
Co-Fire		\$/kW	
		Material	Process
Process Flow Steps	Anode	\$ 26.29	\$ 2.04
	Cathode	\$ 3.86	\$ 1.57
	Electrolyte	\$ 1.27	\$ 1.31
	Interconnect	\$ 25.18	\$ 4.08
	Fabrication	\$ -	\$ 21.42
Sub-Total		\$ 56.60	\$ 30.43
Total		\$87.03	

Total Cost (Materials + Processes) (\$/kW)			
Multi-Fire		\$/kW	
		Material	Process
Process Flow Steps	Anode	\$ 26.71	\$ 2.05
	Cathode	\$ 3.09	\$ 1.50
	Electrolyte	\$ 1.30	\$ 1.32
	Interconnect	\$ 25.18	\$ 4.08
	Fabrication	\$ -	\$ 26.88
Sub-Total		\$ 56.27	\$ 35.83
Total		\$92.10	

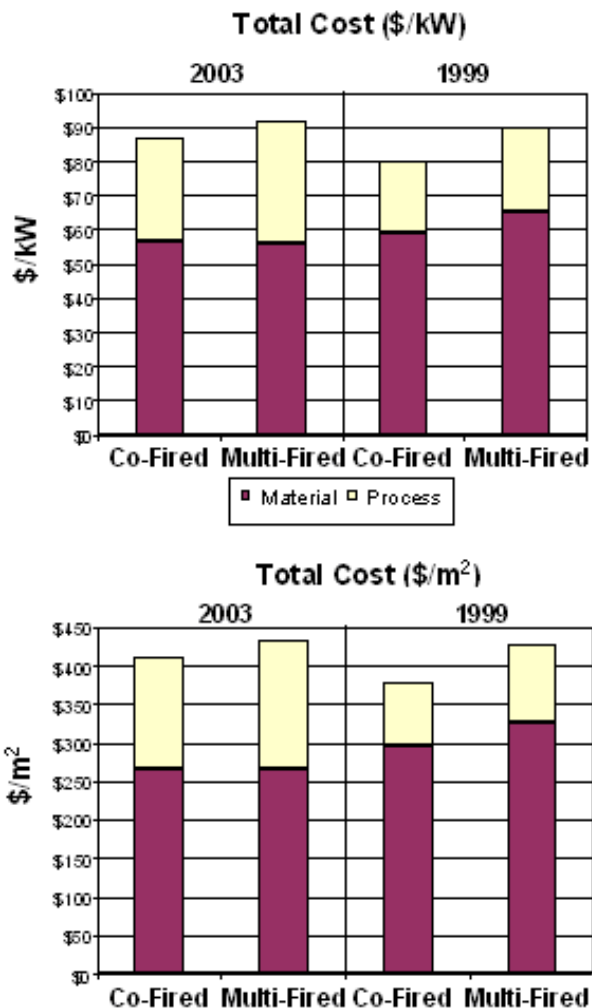


Figure 1. Comparison of 2003 and 1999 Total Stack Factory Cost Projections (250 MW per year production volume)

The updated analysis of stack cost showed that the 1999 cost projections for planar anode-supported SOFC stacks should still be achievable (Tables 1 and 2, Figure 1). In the present study, the net result of increases and decreases in factors influencing the cost resulted in approximately a 5% increase in cost of the baseline case to \$90/kW. Increases in processing costs, primarily driven by the addition of quality control steps, were greater than the reductions in material cost, primarily driven by lower assumed costs for YSZ. The lower power density of the 2003 baseline case further accentuated the increases in cost on per kW basis. The anode and interconnect dominated the stack cost, contributing approximately

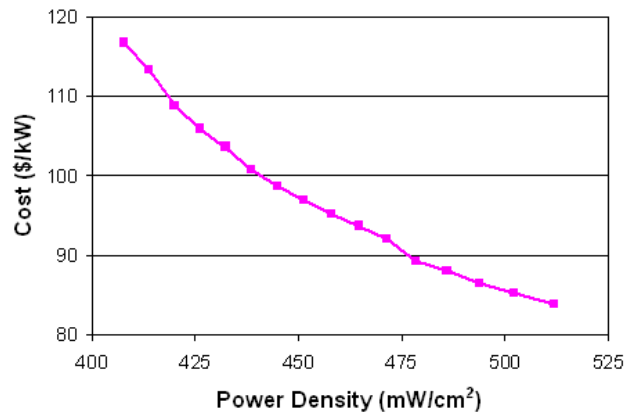


Figure 2. Cost Versus Power Density

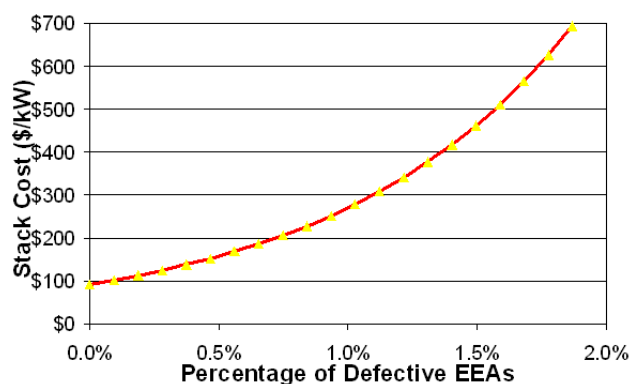


Figure 3. Plot of Stack Cost Versus Percentage of Defective EEAs Getting through Quality Control

90% of the cost. Tables 1 and 2 provide a breakdown of cost on an area and kW basis.

Achievement of high power densities will be important for low cost due to the large contribution (approximately 85% at high production volumes) of materials to the stack cost. The inclusion of a performance/thermal/mechanical model is important for analyses of this type because real kinetic data, ohmic losses, stack design parameters, mass transport limitations, and temperature gradients can be factored into the projected power density without violating utilization assumptions. Minimization of the thickness of the EEA layers will contribute to increased power density with the electrolyte being the most important factor. Figure 2 shows cost as a function of power density. Electrolyte thickness was varied from 5 to 20 μm with a fixed anode (700 μm)

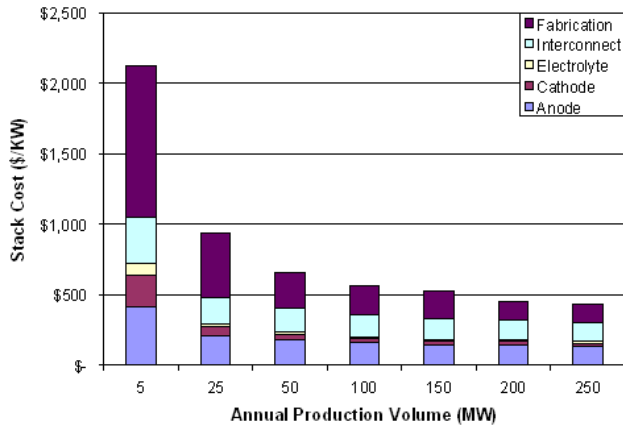


Figure 4. Breakdown of Stack Costs as a Function of Production Volume (\$/kW)

and cathode thickness to obtain this variation in power density.

Quality control will be critical to successful assembly of stacks with high yields. If defective EEAs pass through final inspections prior to stack assembly at even a 1 percent level, stack cost could increase by more than a factor of 2 above the baseline projection (Figure 3). The stack yield will be influenced by the number of cells, which can impact decisions on stack voltage and stack interconnect costs for a targeted system voltage.

Significant economies of scale will be realized in increasing the production volume from 5 MW to 250 MW, with approximately 60% of the cost reduction realized in stepping up to 25 MW (Figure 4). For this analysis, reductions in process costs due to higher utilization of capital equipment were a major factor in the decrease in cost.

Conclusions

- The stack costs estimated in 1999 are still achievable. Updating of the model, including process assumptions, material costs, and consideration of quality control processes, resulted in offsetting cost factors.

- The performance model showed that the power density assumed in 1999 was in fact reasonable and consistent with critical assumptions such as fuel utilization, inlet/outlet temperatures, contact resistance, and electrode dimensions. In a materials intensive technology, the realization of target power densities will be critical to meeting cost targets.
- Quality control of the EEAs going into stack assembly will be absolutely critical to achieving high yields and projected costs. Quality control processes must be included in cost projections to reflect important cost contributions.
- Economies of scale do play a significant role in reducing costs; however, 60% of the benefit is realized at one-tenth the maximum volume considered in this study, largely due to higher utilization of capital equipment.

References

1. E.J. Carlson, S.A. Mariano (1999), Assessment of Planar Solid Oxide Fuel Cell Technology, Arthur D. Little, Inc.

FY 2004 Publications/Presentations

1. SECA Core Technology Program Review Meeting, Sacramento (February 2003)
2. Final report presentation to NETL (February 2004)
3. Eric J. Carlson, Suresh Sriramulu, Peter Teagan, Yong Yang, "Cost Modeling of SOFC Technology", First International Conference on Fuel Cell Development and Deployment, University of Connecticut, Storrs (March 7-10, 2004).
4. Presentation accepted for Fuel Cell Seminar (November 2004)

III.D.4 Determination of Electrochemical Performance and Thermo-Mechanical-Chemical Stability of SOFCs from Defect Modeling

Eric D. Wachsman (Primary Contact), Keith L. Duncan, Fereshteh Ebrahimi

Department of Materials Science and Engineering

University of Florida

Gainesville, Florida 32611

Phone: (352) 846-2991; Fax: (352) 392-3771; E-mail: ewach@mse.ufl.edu

DOE Project Manager: Travis Shultz

Phone: (304) 285-1370; E-mail: Travis.Shultz@netl.doe.gov

Objectives

- Advance the fundamental understanding of the continuum-level electrochemistry of oxide mixed ionic-electronic conductors in relation to their performance in solid oxide fuel cells (SOFCs).
- Obtain, from experiments, fundamental constants required for implementing the continuum-level electrochemical model.
- Extend the models to multi-layer structures and incorporate microstructural effects.
- Verify the models through experiments.
- Develop a transient version of the continuum-level electrochemical model.
- Obtain time constants for various transport processes from electrical impedance spectroscopy to examine the effects of transients on SOFC performance.
- Develop and deliver software modules for incorporation of the continuum-level electrochemical model into SOFC failure analysis software used by the National Energy Technology Laboratory (NETL), Pacific Northwest National Laboratory (PNNL), Oak Ridge National Laboratory (ORNL) and the Solid State Energy Conversion Alliance (SECA) industrial teams.

Approach

- Develop a continuum-level electrochemical model for the generation, distribution and transport of defects in oxide mixed ionic-electronic conductors (MIECs).
- Extend model to thermo-mechanical properties, thermochemical stability and transient behavior of oxide MIECs.
- Extend model to multi-layer (anode-electrolyte-cathode) SOFCs.
- Incorporate microstructural effects into the continuum-level electrochemical model.
- Design and conduct experiments to explore the thermo-mechanical, thermochemical and transient behavior of oxide MIECs and verify the continuum-level electrochemical model.
- Analyze experimental results and interpret them in framework of model.
- Feed back experimental results into model and validate it.

Accomplishments

- Completed the continuum-level electrochemical model for *steady-state* conditions, using potential dependent boundary conditions and non-linear Galvani potential.
- Completed the continuum-level electrochemical model for *transient* conditions, using potential dependent boundary conditions and a linear Galvani potential.

- Compiled software modules for vacancy concentration and electron concentration in *n*-type and *p*-type mixed ionic-electronic conductors.
- Extended the continuum-level electrochemical model to thermo-mechanical and thermochemical properties of mixed ionic-electronic conductors.
- Extended the continuum-level electrochemical model to yttria-stabilized zirconia (YSZ)/lanthanum strontium manganate (LSM) bilayer.
- Measured the thermal expansion of ceria and samaria-doped ceria in air and reducing atmospheres.
- Measured the elastic moduli of pure ceria and gadolinia-doped ceria in reducing (H_2) and oxidizing (air) atmospheres using nondestructive and (nanoscale) destructive techniques; both showed that reducing conditions cause a ~30% decrease in the elastic modulus relative to air.

Future Directions

- Complete the extension of the continuum-level electrochemical model to multi-layer SOFC architecture.
- Incorporate microstructural effects into the continuum-level electrochemical model.
- Minimize uncertainty in the deconvolution of electrical impedance spectra for more accurate assessment of time constants for electrochemical processes.
- Obtain more data points for the elastic moduli of ceria, gadolinia-doped ceria and YSZ within the range of oxygen partial pressures (P_{O_2}) between air and H_2/H_2O using both nondestructive and (nanoscale) destructive techniques.
- Obtain data for the thermo-mechanical properties of polycrystalline YSZ as a function of P_{O_2} between air and H_2/H_2O .
- Obtain thermal expansion data for Ni-YSZ, LSM, YSZ and other MIECS in various (reducing or oxidizing) atmospheres.
- Experimentally determine effect of microstructure on transient behavior of SOFCs.

Introduction

SOFCs are the future of energy production. They offer great promise as a clean and efficient process for directly converting chemical energy from a fuel to electricity while providing significant environmental benefits (they produce negligible hydrocarbons, CO, or NO_x and, as a result of their high efficiency, produce about one-third less CO_2 per kilowatt hour than internal combustion engines). Moreover, SOFCs are fuel flexible, expanding the range of fuels that can be used in the conversion process from conventional fuels to hydrogen.

For extensive deployment of SOFCs into industrial and consumer markets to become a reality, some key hurdles need to be cleared. Three of these hurdles are the (i) thermo-mechanical, (ii) thermochemical and (iii) transient stability of SOFCs. In our research, we are tackling these hurdles by developing models to relate point defect (atomic-scale anomalies) population distribution and

microstructure (the fine structure of a material) to the electrochemical and mechanical properties of SOFC components, which are then the actual determinants of the thermo-mechanical, thermochemical and transient stability of SOFCs. These fundamental-level models can then be incorporated into system-level models to predict and analyze SOFC performance and response (transient and steady-state) to various inputs.

Approach

To develop models relating point defect population distribution and microstructure to the electrochemical and mechanical properties of SOFC components, first we modeled the generation of point defects in oxide MIECs as a function of atmosphere (P_{O_2}) and temperature. Since SOFCs operate in a P_{O_2} gradient, next we modeled the transport and distribution of defects in an MIEC in a P_{O_2} gradient by solving the Nernst-Planck, mass conservation and charge conservation equations for Laplacian and

non-Laplacian potential distributions. These two steps produced a continuum-level electrochemical model that relates point defect concentration to operating conditions (such as temperature, P_{O_2} gradient and load voltage) and material properties (such as the mass action constant for oxygen exchange between the oxide and the ambient, and ionic and electronic diffusivity). Hence, by modeling or applying relationships between point defects and indices for thermo-mechanical, thermochemical and transient stability, secondary relationships between these indices and the SOFC operating conditions and material properties can be derived.

An essential complement to the models developed in our research is experimental verification. To this end, experiments are being conducted to confirm the predictions of the models as well as to give more insight into the factors and mechanisms that play a role in the performance of the SOFC components and the overall stability of the SOFC.

Results

Continuum-Level Electrochemical Model-Defect Thermodynamics. To obtain defect concentration dependence on P_{O_2} requires the solution of a system of equations consisting of mass action equations from the defect equilibria and charge, mass and site balance equations. However, depending on the defect species involved, the system of equations can result in high order (>3) polynomials with no analytical solution. The traditional way of simplifying such equation systems is the Brouwer method, which divides the equilibria into separate Brouwer regimes where two species dominate [1]. This method generates defect concentration dependence on P_{O_2} in each Brouwer regime. However, it produces formulae that are discontinuous across the Brouwer regimes. This is a problem for some MIECs in a P_{O_2} gradient where the defect equilibria span more than one regime. Moreover, an electrical potential can drive an MIEC from one regime to the next. Conversely, by considering three defects instead of two, we have derived equations that are continuous across all regimes. Examples of these, for oxide MIECs, follow:

$$c_v(P_{O_2}) = \left[\frac{3}{4} K_r \frac{1}{2} P_{O_2}^{-1/2} + \left(\frac{1}{2} c_A \right)^{1/2} \right]^{2/3}$$

and

$$c_e(P_{O_2}) = K_r \frac{1}{2} P_{O_2}^{-1/2} \left[\frac{3}{4} K_r \frac{1}{2} P_{O_2}^{-1/2} + \left(\frac{1}{2} c_A \right)^{1/2} \right]^{2/3} \quad (1)$$

where c_v , c_e and c_A are the concentrations of vacancies, electrons and a trivalent acceptor dopant, respectively. K_r is the equilibrium constant for the oxygen exchange between the oxide and gaseous O_2 . The full derivation may be found in our earlier work [2]. Equation (1) is a low P_{O_2} simplification of more general equations we developed for fluorites and perovskites [2]. Finally, excellent results were obtained when these equations were fitted to experimental data [3] with K_r as the sole fitting parameter.

Continuum-Level Electrochemical Model-Defect Transport. To model defect transport in MIECs, we solved the Nernst-Planck, material balance, and current density equations [4]. To simplify the equations and make the derivations more tractable, previous researchers have assumed a linear, i.e., Laplacian, potential distribution. We have been able to relax that assumption and solve for the more general Poisson potential distribution where the Galvani potential is not forced to vary linearly with position inside the MIEC.

In steady-state conditions, the solutions for oxygen vacancy concentration as a function of distance (x), for n -type oxide MIECs, are as follows [2, 5]:

$$c_v(x) - c_{v_0} - \frac{(D_v \gamma - j_v) c_A}{z_v (z_v - z_e) D_v \gamma} \cdot \ln \frac{z_v (z_v - z_e) D_v \gamma c_v(x) - j_v c_A}{z_v (z_v - z_e) D_v \gamma c_{v_0} - j_v c_A} = -\gamma x \quad (2)$$

where z is charge equivalence, q is the elementary electronic charge, j is flux density, Φ is Galvani potential, u is electrical mobility, L is MIEC thickness and $\gamma = (\Delta\phi/\lambda - C_{vL} + C_{v0})/L$. The subscripts 0 and L refer to the boundary values of the MIEC, i.e., at $x = 0$ (anode side) and $x = L$ (cathode side). Also, from the local equilibrium approximation,

$$\Delta\phi = \Phi_{\text{ext}} - \Phi_{\text{th}} - k_B T (z_v q)^{-1} \ln(C_{vL}/C_{v0}),$$

and from the equivalent circuit of an SOFC,

$$\bar{t}_{ion} \Phi_{th} = \eta + \Phi_{ext}$$

where \bar{t}_{ion} is average transference number, Φ_{ext} is load voltage, Φ_{th} is the Nernst potential and η is cell overpotential [6].

Previous researchers [6-8] used fixed boundary values for the defect concentrations and linear potential distributions. *Fixed* boundary values are independent of the load voltage, Φ_{ext} . This implies that Φ_{ext} only affects the spatial distribution of defects inside the MIEC. In principle, this is not possible, since the activities of all the reacting chemical species cannot be held constant while changing the potential at the interface [4, 9]. Potential-dependent boundary conditions were obtained by including the effect of the load voltage on the boundary values of the defect concentrations [5]. Our results, exemplified in Equation (2), allow for the prediction of the transport properties of the MIEC components and SOFC performance. As an example, we will consider the current and power efficiency of an SOFC, which are given by $\zeta_J = J/J_V$ and $\zeta_P = \zeta_J \Phi_{ext} / \Phi_{th}$, respectively, where J is current density.

Figure 1 shows a comparison of current and power efficiencies calculated from models with different assumptions for a doped ceria electrolyte. The figure shows that using fixed boundary conditions and assuming a linear Galvani potential leads to an overestimation of both current and power efficiencies. Assuming a linear potential ignores the efficiency-sapping effects of mixed conduction, and using *fixed* (i.e., independent of potential) boundary concentrations reduces the effects of changing concentration gradients. Consequently, when these assumptions are removed, the calculated efficiencies are smaller. These results emphasize the importance of using the correct electrochemical model as the basis for computation of relevant properties.

Thermo-Mechanical Properties. We now seek to extend the model developed above to the thermo-mechanical properties of MIECs. The relationship between defect population and elastic modulus—which is related to another crucial property: fracture toughness—may be derived by considering that the bond energy, E , between atoms in a crystal may be

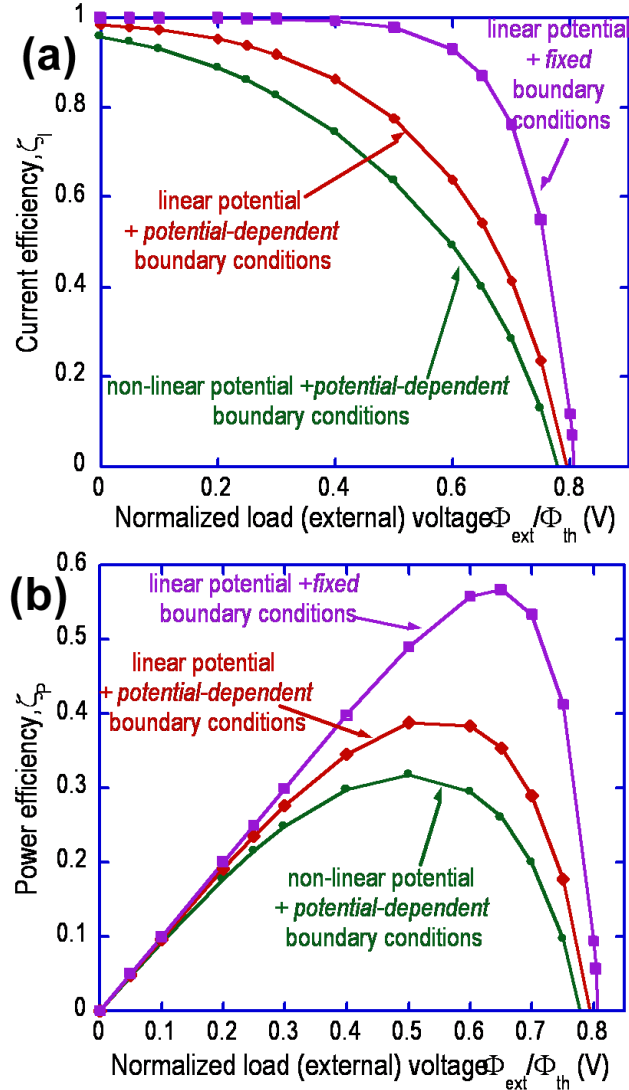


Figure 1. Comparison of current and power efficiency from various models for an SOFC.

approximated by $E = A/r^n - B/r^m$ [10], where r is the inter-atomic distance, and A , B , n and m are empirically determined constants ($m < n$). Thus, the elastic modulus for a perfect crystal, Y , may be approximated by: $1/r_0(d^2E/dr^2)_{r=r_0}$. In addition, the lattice constant, a , is proportional to r_0 (the average inter-atomic separation), and a has been shown to increase linearly with c_V [11, 12]. Thus, Y becomes

$$Y(x) \approx Y^*(\Theta c_V(x) + 1)^{-(m+3)} \quad (3)$$

where Θ is an empirically determined constant, and the superscript "*" refers to stoichiometric

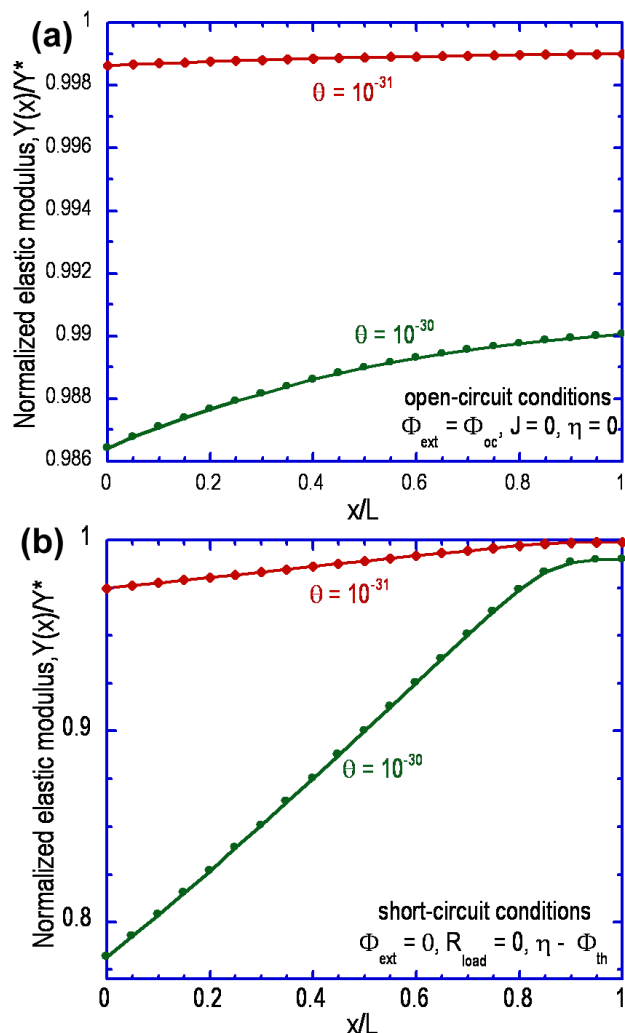


Figure 2. Elastic modulus profiles in (a) open-circuit and (b) short-circuit for samaria-doped ceria electrolyte, at 800 °C; anode is at $x = 0$ ($P_{O_2} = 10^{-20}$ atm), cathode at $x = L$ ($P_{O_2} = 0.21$ atm)

conditions-i.e., when $c_V = 0$. Similar expressions were also derived for fracture toughness.

Figure 2 shows the results of extending the continuum-level electrochemical model to mechanical properties such as the elastic modulus, Y , in this example. The plots show a general degradation of the elastic modulus towards the anode side ($x = 0$) of the electrolyte. Moreover, it is seen that the variation in the elastic modulus is much less in open-circuit conditions (smallest concentration gradients) than in short-circuit conditions (steepest concentration gradients) [6]. Thus, one may expect

that the electrolyte gets *weaker* as more current passes through the cell.

Using a Hysitron[®] Triboindenter, we have measured the elastic modulus of individual grains of pure ceria samples annealed in an H_2 atmosphere. Our results, Table 1, show that annealing in H_2 causes a ~30 % reduction in the elastic modulus of the samples. Also, the low standard deviation in our results indicates isotropy of the elastic modulus. These results were independently confirmed by our collaborators at ORNL, who obtained similar results using an acoustic resonance analyzer. Clearly, the continuum-level electrochemical model can facilitate the prediction of the thermo-mechanical properties of SOFCs.

Table 1. Elastic Modulus of Ceria before and after Hydrogen Anneal

		Modulus, Y_e (GPa)	Hardness, H (GPa)
On the surface	As sintered	220.22±7.08	9.52±1.15
	H_2 reduced	148.87±14.86	8.80±1.41
		Reduction (%)	7.56
At the center	As sintered	187.46±5.81	8.47±0.6905
	H_2 reduced	129.77±13.04	7.31±1.43
		Reduction (%)	30.77

In the near future, we will perform 3-point bend tests with a MTS instrument to obtain elastic modulus and fracture toughness data for polycrystalline samples. Fractured samples will also be examined with scanning electron microscopy and transmission electron microscopy to determine the sources of fracture.

Chemical Stability. The continuum-level electrochemical model has also been applied to the chemical stability of interfaces, e.g., YSZ/LSM. Not surprisingly, our early results indicate that for relevant insight into the stability of electrolyte-electrode interfaces, we will need to incorporate the microstructure of the electrode. We are in the process of doing just that.

Transient Response. The continuum-level electrochemical model has been extended to transient conditions (more detail may be obtained from the Phase 1 topical report of this project). To obtain solutions, we assumed a linear potential distribution. This assumption is best applied to predominantly

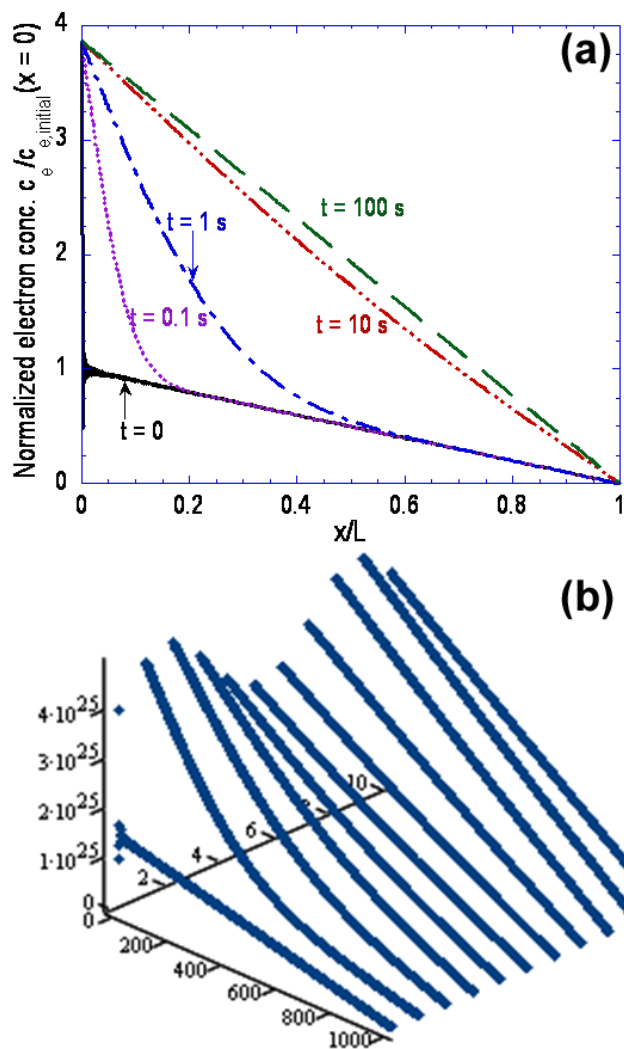


Figure 3. Time-dependent evolution of electron concentration profiles in a 1 mm thick YSZ electrolyte at 800 °C: (a) load voltage, Φ_{ext} goes from open-circuit value to $\Phi_{th}/4$ (b) Φ_{ext} has a 60 Hz sinusoidal *ripple*; anode is at $x = 0$ ($P_{O_2} = 10^{-22}$ atm), cathode at $x = 1$ ($P_{O_2} = 0.21$ atm).

ionic conductors, e.g., YSZ, or predominantly electronic conductors, e.g., LSM.

Figure 3 shows the evolution of the electron concentration profiles in a 1 mm thick YSZ electrolyte. In Figure 3a a load (of voltage $\Phi_{th}/4$) is introduced to the SOFC, which was initially (at time, $t = 0$) in *open-circuit* conditions. The results show that while the boundary concentrations are established *instantly*, the concentration in the bulk

lags behind, ostensibly limited by electron diffusivity and electrolyte thickness.

Figure 3b is a surface plot showing the spatial and temporal distribution of electron concentration, $c_e(x, t)$. In Figure 3b a load is again introduced to the SOFC, but this time it carries a 60-Hz sinusoidal *ripple* with it. The effect and presence of the *ripple* is evident in the plot, which shows an initial response similar to Figure 3a. However, after about 6 s, the lag is no longer evident even though the *ripple* persists. This is a result of the amplitude and frequency of the *ripple*. The amplitude is small enough not to cause great changes in the concentration gradient. The time constant of the electrolyte (~ 4.5 s) is ~ 270 times the period of the *ripple*. Hence, the electrolyte does not have enough time to respond to the *ripple* in the bulk, and the *ripple's* effect is seen only at the boundaries.

For transient defect transport, the total thickness of the MIEC, L , is a component of the time constant for the process such that the transient response of the MIEC depends exponentially on the electrolyte thickness. As the thickness of the electrolyte is reduced to 10 μm , the time scale decreases to ~ 0.05 s (approaching 60 Hz). This provides important criteria (impact of improved performance with thinner electrolytes versus susceptibility to higher transient voltages or fuel composition variations) if the SOFC is going to be used under transient conditions.

The challenge of accurately deconvoluting the significant transport mechanisms for electrical impedance spectra is proving to be formidable. Hence, we have been unable to test the model at this time. However, we anticipate this will be completed in the near future.

Software Development. The development of software modules for the continuum-level electrochemical model is in progress. We also intend to offer them to the teams at ORNL, NETL and PNNL for pre-testing to determine their compatibility with existing failure analysis software, and we will make them available to the SECA industrial teams shortly thereafter. At this point, the project for the *steady-state* continuum-level electrochemical model for defect generation and

transport has been completed. Two languages were used, C++, because it is the industry standard, and PHP, because of its web-oriented features.

Conclusions

- A continuum-level electrochemical model has been developed that improves on preceding efforts by including a non-linear potential distribution and by including potential-dependent boundary conditions.
- The continuum-level electrochemical model has been extended to describe thermo-mechanical, thermochemical and transient stability in MIECs.
- Experimental results concur with the predictions of the continuum-level electrochemical model for electrical conductivity.
- Experimental results concur with the predictions of the continuum-level electrochemical model for thermo-mechanical properties.
- The steady-state version of the continuum-level electrochemical model has been written in C++ and PHP.

References

1. H. L. Tuller, *Nonstoichiometric Oxides*, ed. O. Sorensen (Academic, N. Y., 1981) ch. 6.
2. K. Duncan, Ph. D. Thesis, University of Florida (2001).
3. K. Eguchi, T. Setoguchi, T. Inoue and H. Arai, *Solid State Ionics* 52 (1992) 265.
4. J. Newman, *Electrochemical Systems* (Prentice-Hall, 1991).
5. E. Wachman and K. Duncan, *Stable High Conductivity Bilayered Electrolytes for Low Temperature SOFCs*, DOE Final Report, Contract No. DE-AC26-99FT40712, 2002.
6. I. Riess, *J. Electrochem. Soc.* 128 (1981) 2077.
7. M. Liu, *J. Electrochem. Soc.* 144 (1997) 1813.
8. S. Yuan and U. Pal, *J. Electrochem. Soc.* 143 (1996) 3214.
9. P. J. Gellings, H. J. A. Koopmans and A. J. Burggraaf, *App. Catalysis* 39 (1988) 1.
10. M. Barsoum, in *Fundamentals of Ceramics* (McGraw-Hill, 1977).
11. D-J. Kim, *J. Amer. Ceram. Soc.* 72 (1989) 1415.
12. M. Zacatea, L. Minervinia, D. Bradfielda, R. Grimes and K. Sickafus, *Solid State Ionics* 128 (2000) 243.

FY 2004 Publications/Presentations

1. "Determination of Electrochemical Performance and Thermo-Mechanical-Chemical Stability of SOFCs from Defect Modeling," US Department of Energy, Solid State Energy Conversion Alliance Workshop, September 30 - October 1, 2003, Albany, NY.
2. "Low-Temperature Solid Oxide Fuel Cells Based on Stable High Conductivity Bilayered Electrolytes," Fuel Cell Seminar, November 3-6, 2003, Miami, FL.
3. "Determination of Electrochemical Performance and Thermo-Mechanical-Chemical Stability of SOFCs from Defect Modeling," US Department of Energy, Solid State Energy Conversion Alliance Workshop, May 11-13, 2004, Boston, MA.
4. "Effect of Tertiary Phase Formation at the LSM/YSZ Interface on the Cathodic SOFC Reaction," 6th International Symposium on Electrochemical Impedance Spectroscopy, May 16-21, 2004, Cocoa Beach, FL.

III.E Controls & Diagnostics

III.E.1 An Investigation to Resolve the Interaction between Fuel Cell, Power Conditioning System and Application Load

Prof. Sudip K. Mazumder (Primary Contact), Sanjaya Pradhan, and Kaustuva Acharya
Department of Electrical and Computer Engineering
University of Illinois, Chicago
851 S. Morgan Street, Science and Engineering Offices, M/C 15, Chicago, IL 60607
Phone: (312) 355-1315; Fax: (312) 996-6465; E-mail: mazumder@ece.uic.edu

Profs. Michael R. von Spakovsky and Doug Nelson, and Diego Rancruel
Energy Management Institute/Center for Automotive Fuel Cell Systems
Department of Mechanical Engineering
Virginia Tech.
Blacksburg, VA 24061
E-mail: vonspako@vt.edu

Dr. Comas Haynes and Robert Williams
Center for Innovative and Battery Technologies
Georgia Tech Research Institute
Atlanta, Georgia 30332-0853
E-mail: comas.haynes@gtri.gatech.edu

Drs. Joseph Hartvigsen and S. Elangovan
Ceramatec Inc.
2425 South 900 West
Salt Lake City, Utah 84119
E-mail: jjh@ceramatec.com

DOE Project Manager: Magda Rivera
Phone: (304) 285-1359; Fax: (304) 285-4638; E-mail: Magda.Rivera@netl.doe.gov

Objectives

- Develop nonlinear transient component and system models for tubular solid oxide fuel cell (TSOFC) power-conditioning system (PCS).
- Analyze the effect of load transients and switching, and low-frequency ripples on the performance and reliability of the TSOFC.
- Conduct parametric studies of balance-of-plant subsystem (BOPS) for TSOFC PCS optimization.
- Investigate the load-transient-mitigation effectiveness of two energy-buffering schemes (battery and pressurized hydrogen tank) on the performance and durability of the solid oxide fuel cell (SOFC).

Approach

- Initially a multi-software TSOFC PCS model was developed using the following scheme:
 - TSOFC temporal model [1, 2] was developed on a Visual Fortran platform.
 - BOPS model was developed using gPROMS, a powerful nonlinear solver.

- Power electronics subsystem (PES) and application load (AL) models were developed using SaberDesigner, a sophisticated and powerful circuit and system simulator.
- The overall TSOFC PCS model was realized by integrating the four component models (i.e., TSOFC, PES and AL, and BOPS) using iSIGHT, which is a powerful software management tool.
- TSOFC spatial model is implemented using TOPAZ [4], which is a powerful finite-element-analysis software originally provided by Lawrence Berkeley National Laboratory.
- Subsequently, on suggestion from Solid State Energy Conversion Alliance (SECA) industry members and the National Energy Technology Laboratory (NETL), the TSOFC component and system models have been implemented in a “low-cost” Matlab/Simulink environment for easy use by the SECA industry members. It is also anticipated that Matlab/Simulink will provide a better avenue for real-time simulation, which may be required for long-term analysis studies.
- Objective 1 has been accomplished; however, effort is being made to enhance the computational speed for long-term reliability studies. Detailed work on objectives 2 through 4 has been done.

Accomplishments

- Developed the TSOFC temporal model based on fundamental electrochemical equations [1, 2]. The transient modeling technique is based on the Lagrangian approach, which involves focusing attention on each fluid element of the SOFC and calculating the mass and energy balances for each individual element during the transient.
- Developed the temporal BOPS model consisting of the fuel-processing subsystem for conversion of natural gas to hydrogen and thermal-management and power recovery subsystems to maintain fuel and oxidant temperatures for efficient chemical reactions.
- Developed optimal PES topology for SOFC PCS, consisting of a DC-DC boost converter to step up the SOFC output voltage followed by a DC-AC inverter and residential load profile.
- Integrated all the models in MATLAB/Simulink platform to obtain a comprehensive transient TSOFC PCS model.
- Analyzed the effect of the load transient on the material of the TSOFC.

Future Directions

- Development of fully transient spatial model for planar SOFC (PSOFC) configurations.
- Development of enhanced BOPS model and investigation of additional BOPS component models consistent with possible configuration changes which accommodate fuel reforming and application loads.
- Optimal PES design and design methodology using updated PES transient models (including a variety of additional nonlinear topologies for stationary and mobile applications) for enhanced PSOFC performance.
- Detailed parametric studies to determine best-practice control strategies and component design and possible configuration changes based on NETL guidelines.
- Validation of the models and verification of simulation results.

Introduction

Differences in the response times of a solid oxide fuel cell (SOFC), its power-electronics subsystem (PES), and the balance-of-plant subsystem (BOPS) cause low-reactant conditions near the SOFC during load transients. Because the BOPS cannot instantaneously provide enough fuel

to the SOFC, load transients have a detrimental effect on the performance and durability of the fuel cell. To alleviate the degrading effects of load transients on the performance and durability of SOFC stacks, we investigate the effects of energy-storage devices, namely pressurized hydrogen storage tanks and batteries, and optimize their costs and size. Finally, using finite-element analysis, we

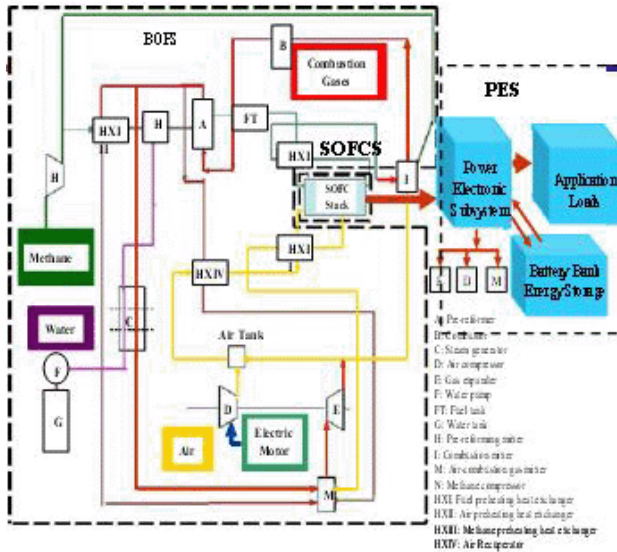


Figure 1. Block Diagram of a Complete SOFC PCS Comprising the SOFC Stack, PES, and the BOPS Supplying Power to the Application Load

compare the effectiveness of two inverter-modulation strategies (space-vector modulation and sinusoidal pulse-width modulation) during load transients by resolving their impacts on SOFC hydrogen utilization and current density.

Approach

The overall interaction analysis, to ascertain the efficacy of energy-buffering devices and control techniques on improving the performance of the SOFC stack during a load transient, is carried out in two steps. First, a time-domain analysis of the SOFC PCS is carried out using the comprehensive model as shown in Figure 1. Using such a temporal analysis, we obtain the change in SOFC stack output current and voltages before, during, and after a load transient. Next, to translate system-level electrical parameters of the SOFC stack to its cell-level electrochemical parameters (such as current-density and cell-temperature distributions), a detailed finite-element analysis (FEA) is conducted using the spatial model of the SOFC stack [4]. Because SOFC parameters like hydrogen depletion and cell temperature can directly affect the material properties of the SOFC and hence impact its performance and durability, it is important to study the spatial distribution of these parameters across its cross-section.

Using the FEA [4], thermal conduction effects are coupled with electrical conduction effects, and local electrical and chemical properties are rigorously computed across the SOFC cross-section. Temperature dependencies of material properties are also incorporated into the SOFC model. The effective resistance of each component (interconnect, anode, cathode, and electrolyte) is computed by FEA from actual cell geometry and temperature-dependent conductivity. Current density is calculated at each electrolyte element from the local electrode potential, overpotential function and local bulk gas chemical potential. Hydrogen utilization is directly proportional to the current drawn by the PES and can be defined as $U = I/n(\dot{n}F)$ where \dot{n} is the hydrogen flow rate which is determined by the BOPS and nF determines the charge flow between the anode and the cathode. Finally, SOFC temperature is obtained by using basic thermodynamic equations [2]. These results are used to relate the SOFC current to the cell temperature. Theoretical studies indicating interaction between the standard cathode, $(La_{0.85}Sr_{0.15})_{0.95}MnO_3$ (LSM), and the standard electrolyte (yttria-stabilized zirconia) above temperatures of $1000^\circ C$ [6] say that in long-term operation, an interlayer of $LaZr_2O_7$ forms whose conductivity is much less than that of LSM and, hence, has an impact on the output voltage and current supplied by the SOFC.

Results

The load transient causes a significant increase in the load current and hence the current density inside the cell. This causes a drop in the cell voltage (Figure 2(a)) because of higher polarization. Because the response time of the BOPS is significantly lower than the response time of the PES/SOFC, the input fuel flow rates of the SOFC stack do not change soon after the load transient. This leads to higher fuel utilization inside the SOFC stack for it to attain a new electrochemical steady state. Figure 3 shows that hydrogen (fuel) utilization and current density increase very sharply immediately after the load transient. As expected, hydrogen utilization is higher at the SOFC stack outlet than at the SOFC stack inlet.

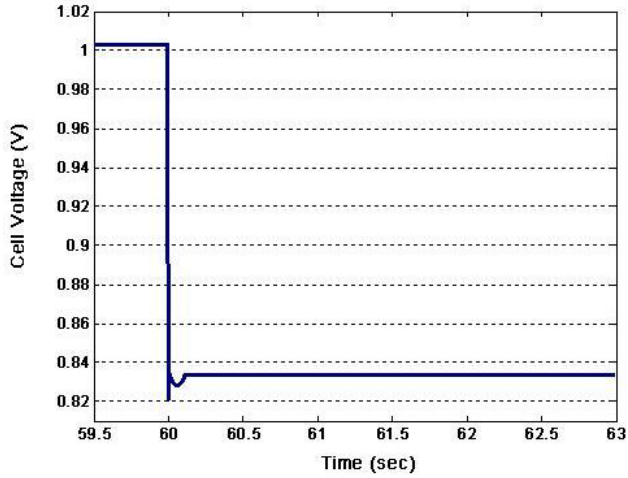


Figure 2(a). Response of the Fuel Cell Voltage Due to the Sudden Load Transient

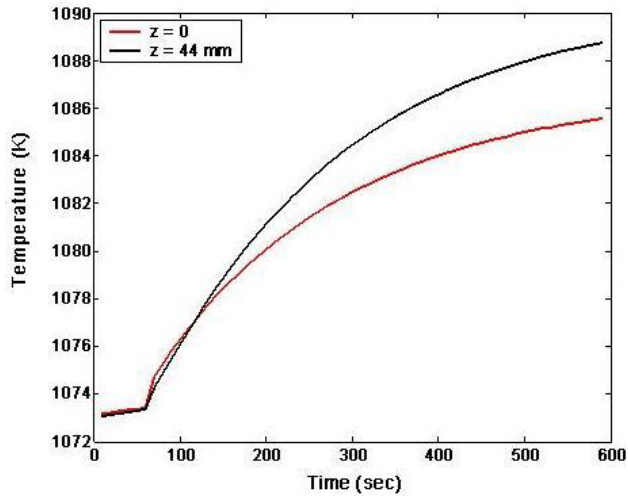


Figure 2(b). Variation of Temperature Due to Load Transients

The fuel-cell temperature increases with time for increased fuel utilization. However, the thermal time constant of the SOFC stack being much larger than that of the SOFC electrochemical or PES time constant [5], the cell temperature increases gradually, as validated in Figure 2(b), until the SOFC attains a new thermal equilibrium. Figure 4 shows the spatial variation of temperature across a cross-section of the SOFC. This indicates that, to protect the SOFC from the degrading effects of the load transients, the BOPS should be fast enough to prevent such an increase in the temperature. However, in reality, response time

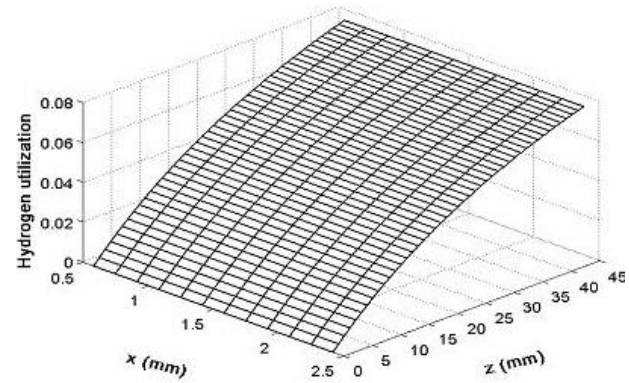
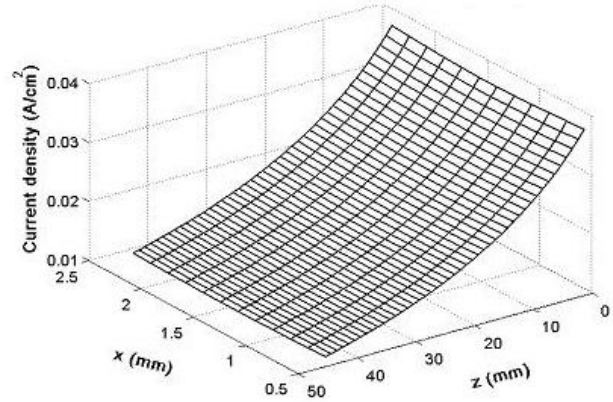


Figure 3. Spatial Variation of Current Density and Spatial Distribution of Hydrogen Utilization Inside the Fuel before the Load Transients

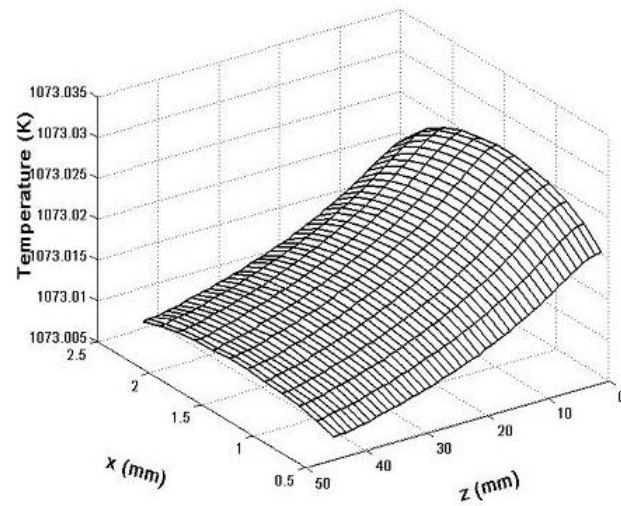


Figure 4. Spatial Variation of Temperature Inside the Solid Oxide Fuel Cell before Load Transients

of the BOPS is not fast and, as such, load-transient mitigation techniques are needed.

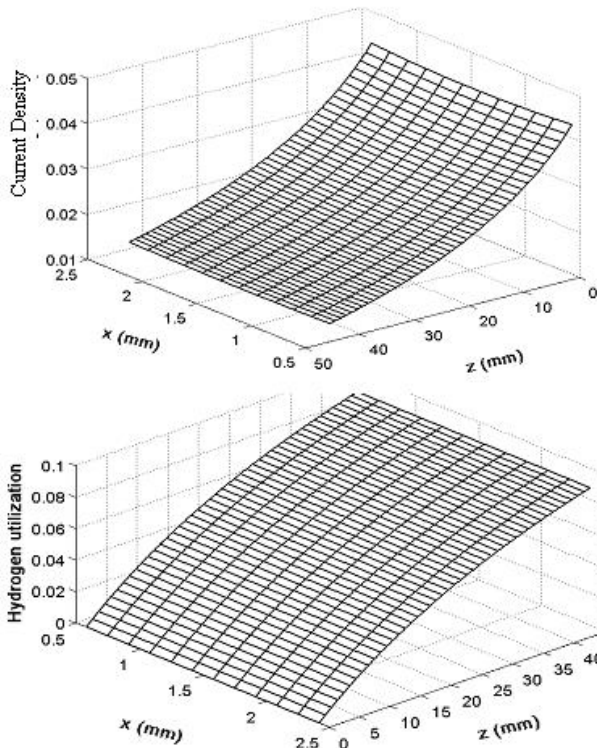


Figure 5. Spatial Variation of Current Density and Spatial Distribution of Hydrogen Utilization Inside the Fuel Cell during the Load Transients with Battery

During the load transient, the energy-buffering devices supply the additional energy requirements to the load; hence, the load demands of the SOFC are substantially reduced. Figure 5 shows the current density of the SOFC after the load transient. Clearly, the energy buffering ensures practically no change in the current density of the SOFC after the transient. Consequently, the increase in fuel utilization as well as the accompanying temperature rise is negligible.

The transient response of the SOFC using sine-wave pulse width modulation (SPWM) and bus-clamped space-vector modulation (SVM) has been analyzed. We observe an improved SOFC stack output current response as in Figure 6 but minimal effect on the hydrogen utilization when bus-clamped SVM is used as the modulation technique; this is attributed to the improved utilization of the DC bus by the inverter using bus-clamped SVM.

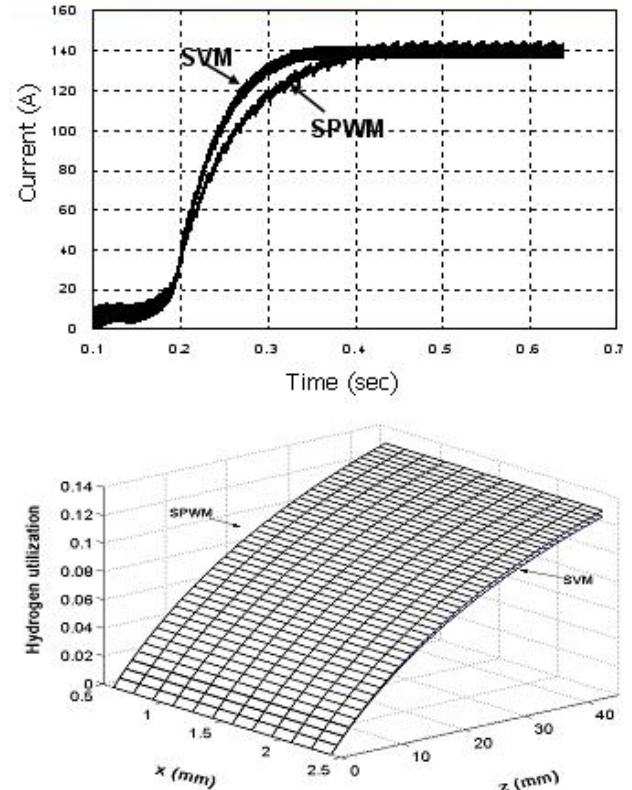


Figure 6. (a) SOFC Input Current during Load Transient Showing Difference between SPWM and Bus-Clamped SVM (b) Spatial Distribution of Hydrogen Utilization during the Load Transient

Conclusions

We investigate the effects of load transients on the performance and durability of SOFCs and how energy-buffering devices can be used to mitigate the detrimental effects of these load transients. The use of pressurized hydrogen tanks (PHTs) and batteries for load-transient mitigation are considered.

Using optimization techniques with cost and size as the constraints, optimal battery and PHT sizes are obtained for a particular response time while ensuring that the SOFC reliability is not compromised.

The impacts of advanced PES modulation and control strategies on SOFC reliability are investigated. We observe that bus-clamped SVM, as compared to SPWM, of the inverter yields faster

dynamic response under load transients. While the superior dynamic performance capability of (bus-clamped) SVM for three-phase inverters is well known, what is often overlooked in such analysis is the need for a stiff DC voltage source. As such, for SOFC, which is not a stiff DC voltage source, the enhanced performance of SVM comes at the cost of higher localized current densities and fuel flow rates, which may be detrimental to the SOFC stack. Non-uniformities during load transients will result in localized oxidization of SOFC electrolyte material, which could result in reduced conductivity because of the formation of LaZr_2O_7 .

However, the detrimental effects of SVM can be overcome if it is used in conjunction with energy storage devices because such energy storage devices can almost instantaneously supply the excess energy required during load transients; hence, such techniques can be used to maintain a stiff DC input voltage to the converters. Such a SOFC power-conditioning system (PCS) would ensure better load-following and hence lead to improved SOFC PCS performance.

References

1. C. Haynes, *Simulation of tubular solid oxide fuel cell behavior for integration into gas turbine cycles*, Ph.D. Thesis, Georgia Institute of Technology, Atlanta, 1999.
2. C.L. Haynes and W.J. Wepfer, "Design for power of a commercial-grade tubular solid oxide fuel cell," *Journal of Energy Conversion and Management*, vol. 41, pp. 1123-1139, 2000.
3. M.R. von Spakovsky, D. Rancruel, D. Nelson, S.K. Mazumder, R. Burra, K. Acharya, C. Haynes, R. Williams, and R.S. Gemmen, "Investigation of system and component performance and interaction issues for solid-oxide fuel cell based auxiliary power units responding to changes in application load", *Proceedings of the IEEE Industrial Electronics Conference*, pp. 1574-1580, November 2003.
4. J. Hartvigsen, "A transient model of solid-oxide fuel cell operation in a high cycle regime of inverter induced current variation", *Proceedings of the 8th International Fatigue Conference*, Stockholm, vol. 4, pp. 2187-2196, 2002.
5. E.A. Liese, R.S. Gemmen, F. Jabbari, and J. Brouwer, "Technical development issues and dynamic modeling of gas turbine and fuel cell hybrid systems," *Proceedings of the 1999 International Gas Turbines Institute*, 99-GT-360, 1999.
6. Y.C. Hsiao and J.R. Selman, "The degradation of SOFC electrodes", *Proceedings of Solid State Ionics*, vol. 98, pp. 33-38.

FY 2004 Publications/Presentations

1. S.K. Mazumder, K. Acharya, C. Haynes, R. Williams, M.R. von Spakovsky, D. Nelson, D. Rancruel, J. Hartvigsen, and R. Gemmen, "Solid-oxide-fuel-cell performance and durability: resolution of the effects of power-conditioning systems and application loads", *Special Issue, IEEE Transactions on Power Electronics*, 2004.
2. S.K. Mazumder, K. Acharya, S.K. Pradhan, J. Hartvigsen, C. Haynes, and M.R. von Spakovsky, "Energy-buffering and control techniques for load transient mitigation of solid-oxide fuel cell (SOFC) power conditioning system (PCS)", accepted for publication, *IEEE Power Electronics Specialists Conference*, 2004.
3. K. Acharya, S.K. Mazumder, R.K. Burra, C. Haynes, and R. Williams, "Solid-oxide fuel cell (SOFC) power-conditioning systems interaction analyses: Resolution of the electrical-feedback effects on performance and durability", *IEEE Applied Power Electronics Conference*, February 2004.
4. M.R. von Spakovsky, D. Nelson, D. Rancruel, S.K. Mazumder, K. Acharya, C. Haynes, and R. Williams, "Investigation of system and component performance and interaction issues for solid-oxide fuel cell based auxiliary power units responding to changes in application load", *IEEE Industrial Electronics Conference*, 2003.

**Special Recognitions & Awards/Patents
Issued**

1. Publication of interaction analysis work in a **Special Issue** of Distributed Generation of “prestigious” IEEE Transactions on Power Electronics.
2. **Invited Paper** (*please see paper #4 under ‘FY 2004 Publications/Presentations’*) in a Special Session on Fuel Cell Power Systems at the “prestigious” IEEE Industrial Electronics Conference, Roanoke, Virginia.

III.F Manufacturing

III.F.1 Tape-Calendering Manufacturing Processes for Multi-Layer Thin-Film Solid Oxide Fuel Cells

Nguyen Minh (Primary Contact), K. Montgomery, S. Gudlavalleti, J. Guan, S. Kamat, L. Supra
GE Hybrid Power Generation Systems
19310 Pacific Gateway Drive
Torrance, CA 90502-1031
Phone: (310) 538-7250; Fax: (310) 538-7260; E-mail: nguyen.minh@ps.ge.com

DOE Project Manager: Don Collins
Phone: (304) 285-4156; E-mail: Donald.Collins@netl.doe.gov

Objectives

- Develop a manufacturing process along with an advanced cell configuration that will contribute to significantly lowering cell first cost while improving cell robustness, life, reliability, and maintainability

Approach

- Examine and optimize cell fabrication process based on tape calendering
- Map cell fabrication process
- Identify critical process parameters for yield, performance, etc.
- Examine effects of cell footprint scale-up
- Modify fabrication parameters to produce multi-layer cells and unitized cells for characterization
- Assess the properties of the fabricated cells using modeling and electrochemical testing for screening
- Examine destructive and nondestructive testing requirements for various manufacturing process steps
- Develop unitized cells and demonstrate electrochemical performance under specified conditions of temperature, gas flow rate, utilization, and current density
- Model and validate flow field designs using computational fluid dynamics (CFD), electrochemical and physical testing
- Examine issues of fabricating stamped metallic interconnect sheets
 - Establish design limits
 - Evaluate manufacturing process

Accomplishments

- Cathode and anode improvements, such as modifications to powder morphologies and compositions, processing improvements and formulation changes, have led to significantly improved solid oxide fuel cell (SOFC) performance, especially in the 650 to 700°C range, for anode-supported cells manufactured by tape calendering
 - Cell power density was increased from 0.243 W/cm² to 0.892 W/cm² for 650°C operation
 - Cells were operated at greater than 70% fuel utilization

- Cells were fabricated that exhibited a 3x improvement in flexure strength while maintaining a peak power density of 0.914 W/cm²
- Flow field designs for unitized cells were analyzed and optimized for improved flow uniformity across the active area
 - 70% fuel utilization at a power density of greater than 0.2 W/cm² was demonstrated on a unitized cell operating on dilute hydrogen (64%)
- Several nondestructive evaluation techniques for flaw detection in multi-layer cells were evaluated; digital radiography was selected for further evaluation
- Developed forming models and investigated advanced joining methods, such as laser, electron-beam, and micro-TIG welding, for fabricating complex interconnect structures

Future Directions

- Work is completed on this project; appropriate process improvements will be incorporated in the work performed under the Solid State Energy Conversion Alliance SOFC Program (Cooperative Agreement DE-FC26-01NT41245)

Introduction

The overall objective of this project is to develop a low-cost tape-calendering process for manufacturing high-performance SOFCs using the unitized cell design. The innovative unitized cell concept has many attractive features, including simple stacking processes, ease of cell handling, improved maintainability, and high reliability. The tape-calendering process for cell manufacture has many desirable characteristics for low-cost and high-volume production: robustness, simplicity, scalability, automation, and simple quality control. For SOFC systems, the tape-calendering manufacturing process along with the unitized cell configuration will contribute to significantly lowering cell first cost while improving cell robustness, life, reliability, availability, and maintainability.

Approach

Two key aspects in developing a low-cost, high-performance SOFC technology are cell and interconnect fabrication. Any SOFC technology requires appropriate multi-layer ceramic fabrication and assembly methods to incorporate cell materials into a desired cell configuration. Appropriate methods are also required for making suitable interconnect structures that can be used to build a stack. The fabrication and assembly processes must ensure that no condition or environment in any process step destroys desired material characteristics

of any of the components. Fabrication and assembly methodologies must attain the desired structural integrity, shape, electrical conductivity, and electrochemical performance of single cells and interconnect structures in the stack.

The overall approach of this project integrates two key elements to achieve the program objective: (a) the development of a process based on tape calendering for manufacturing multi-layer fuel cell components and (b) an innovative unitized cell design concept. The manufacturing approach is based on tape calendering as a core technology for fabricating thin-electrolyte, anode-supported cells. Tape calendering is the formation of a continuous sheet of tape of controlled size by squeezing of a softened thermoplastic material between two rolls. Components can be fabricated by calendering to contain multifunctional multilayers to enhance cell performance. The cell configuration is based on a unitized cell concept in which an individual cell is contained within a metallic housing with its own gas channels and manifolds to form a complete cell package. The fabrication process and cell configuration have all the characteristics required for low-cost production of high-performance cell packages that can be easily used for building stacks.

Results

Cathode and anode improvements, such as modifications to powder morphologies and compositions, processing improvements and

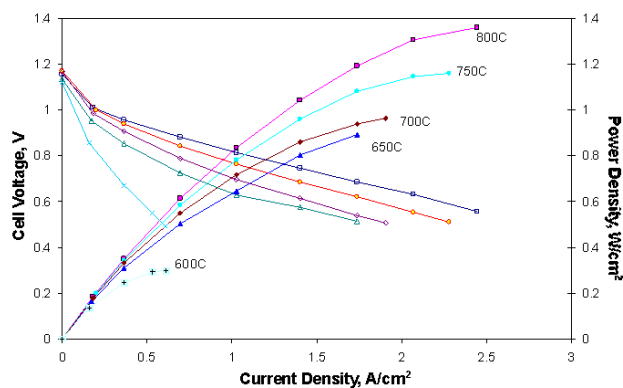


Figure 1. Polarization Curve from a Cell with an Improved Cathode; Pure hydrogen fuel with a fixed fuel flow rate of 67 cc/min and non-flowing air as oxidant

formulation changes, and cell configurations have lead to significantly improved SOFC performance, especially in the 650 to 700°C range, for anode-supported cells made by calendering. By modifying the particle size distribution of the cathode constituents and then optimizing the firing temperature, cells were fabricated that showed increased performance from 0.250 W/cm² to nearly 0.9 W/cm² for 650°C operation. This performance was world-leading at the time of its reporting. A polarization curve from a cell of this design is presented in Figure 1. Anode advancements resulted in cell designs that exhibited stable performance at increased fuel utilization; fuel utilization increased from 75% to greater than 80% while the cell performance nearly doubled (increased from 380 to 650 mW/cm²). These improvements were focused around improvement of the porosity in the anode electrode by engineering the pore-forming additives in the individual layers for size, shape, amount, and distribution. Reactant flow to the electrolyte was improved. To manage the possible loss in mechanical strength from pore-former engineering, strength-improving approaches were investigated. Again, through engineering the individual layers, a 3x improvement in flexure strength was demonstrated with only minimal loss in electrochemical performance.

The tape-calendering cell fabrication process was examined and optimized. Detailed process maps were developed, and process parameters critical for yield, performance, etc. were identified. Fabrication

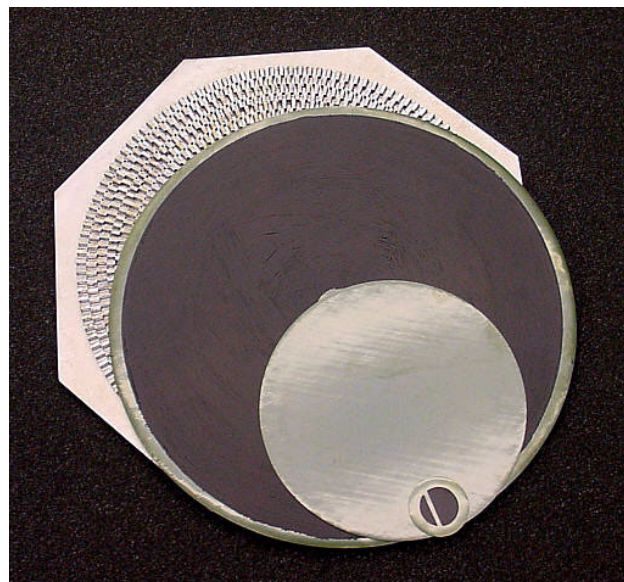


Figure 2. Photograph of a Tape-Calendered 8" Cell and Other Samples

of large-area cells was also attempted. Figure 2 shows as an example a photograph of an 8" cell made by calendering (along with an interconnect, a smaller bilayer, and a 1" button cell). The effects and issues related to cell footprint scale-up were explored.

Unitized cells were designed and tested to address the stacking issues of practical fuel cells. A significant number of cells were fabricated and tested to probe the many issues of stacking, including sealing, contact resistance, and flow distribution. Flow paths were designed that exhibited stable performance at high fuel utilizations (>70%) in electrochemical tests yet are expected to be formable with traditional stamping processes. Improved assembly processes led to unitized cell tests with maximum power densities of 0.3 W/cm² at fuel utilizations of 50%. This is nearly a 100% improvement in power density over the duration of the project.

In the area of non-destructive evaluation, several non-destructive imaging modalities, including infrared imaging, ultrasonic imaging, and digital radiography, were evaluated for their capabilities in defect recognition in SOFC materials in various stages of manufacture. Using radiography, a number of SOFC cells were followed through sequential stages of manufacture by tape calendering, from the

bilayer tapes all the way to the fired cathodes on the bilayer substrate. Many different inhomogeneities were identified, characterized and cataloged. The short acquisition time and high image fidelity showed that digital radiography was very well suited to screening, cataloging, and monitoring surface and structural defects that occur throughout the manufacturing phases of SOFC components. The level of detail has shown to be sufficient to identify defects and density inhomogeneities at the level of 200 microns in a tape or cell. Furthermore, the digital data enables fast quantitative estimates of material thickness and scales of the inhomogeneities.

Potential processes for interconnect fabrication were assessed. Analytical and experimental means were established to determine these manufacturing process capabilities, requirements and gaps. Data were generated in the following areas.

- Formability of metallic interconnects and current collectors
- Flatness of metallic interconnects and current collectors
- Methods to assemble metallic interconnects, cell support sheet

Detailed process capability assessments were conducted using the following approaches: (a) Paper studies: survey of industrial mass production lines—consumer appliances and high-performance heat exchangers; consultation with industrial experts;

- (b) Analytical: stack- and component-level stress analyses; finite element simulations;
- (c) Experimental: component-level fabrication and testing; fabrication of prototype interconnect components; assembly of prototype interconnect components; testing of interconnect components.

In addition to theoretical and experimental determination of process capability, a sheet metal interconnect was manufactured by manufacturing methods similar to those intended for use in a mass production environment. The interconnect pan was stamped, then assembled by laser welding. A glass-sealed tape-calendered cell was tested for performance using this interconnect.

Conclusions

- Improved cathode and anode compositions and processes for producing cells by tape calendering were identified and validated.
- Cell strength was characterized and improved.
- Non-destructive evaluation techniques for tape-calendered cells were examined and identified for further investigation.
- Unitized cells were designed and tested; these cells achieved high fuel utilizations while maintaining other performance characteristics.
- Interconnect metal forming properties were examined and potential processes for interconnect structure fabrication evaluated.

III.F.2 A Low-Cost Process for the Synthesis of Nanosize Yttria-Stabilized Zirconia (YSZ) by Molecular Decomposition

Anil V. Virkar

University of Utah

Department of Materials Science & Engineering

122 S. Central Campus Drive

Salt Lake City, UT 84112

Phone: (801) 581-5396; Fax: (801) 581-4816; E-mail: anil.virkar@m.cc.utah.edu

DOE Project Manager: Lane Wilson

Phone: (304) 285-1336; E-mail: Lane.Wilson@netl.doe.gov

Objectives

- To synthesize Y-BaZrO₃, Y-Na₂ZrO₃, and Y-CaZrO₃ starting with commercial-grade powders of precursors.
- To synthesize and characterize the nanosize YSZ formed. Characterization includes (a) surface area, (b) particle size, (c) agglomerate size, and (d) composition.
- To sinter YSZ discs and bars made from the nanosize YSZ powder, and characterize the sintered samples. Characterization includes (a) density, (b) grain size, and (c) conductivity.
- To conduct a preliminary design of a process for the synthesis of nanosize YSZ powder.

Approach

- Mix *macrosize*, inexpensive Y₂O₃, ZrO₂, and NaOH (or Ba(NO₃)₂) powders in the desired proportions to form Y-doped Na₂ZrO₃ (or Y-doped BaZrO₃).
- Calcine at ~1100°C in air to form Y-doped Na₂ZrO₃ (or Y-doped BaZrO₃). The reactions are as follows:

$$2\text{NaOH} + x/2\text{Y}_2\text{O}_3 + (1-x)\text{ZrO}_2 \rightarrow \text{Na}_2\text{Zr}_{(1-x)}\text{Y}_x\text{O}_{(3-x/2)} + \text{H}_2\text{O}$$
 or

$$\text{Ba}(\text{NO}_3)_2 + x/2\text{Y}_2\text{O}_3 + (1-x)\text{ZrO}_2 \rightarrow \text{BaY}_x\text{Zr}_{(1-x)}\text{O}_{(3-x/2)} + \text{N}_2 + 5/2\text{O}_2$$
 In what follows, we will denote Na₂Zr_(1-x)Y_xO_(3-x/2) by Y-Na₂ZrO₃ and BaY_xZr_(1-x)O_(3-x/2) by Y-BaZrO₃.
- Leach in water to form and dissolve away NaOH by the following reaction:

$$\text{Y-Na}_2\text{ZrO}_3 + (n+1)\text{H}_2\text{O} \rightarrow \text{Y-ZrO}_2 + 2\text{NaOH} + n\text{H}_2\text{O}$$
 The NaOH formed is dissolved in water, and Y-ZrO₂ (YSZ) is a nanosize residue.
 or
 Leach in HNO₃ to form and dissolve Ba(NO₃)₂ by the following reaction:

$$\text{Y-BaZrO}_3 + 2\text{HNO}_3 + n\text{H}_2\text{O} \rightarrow \text{Y-ZrO}_2 + \text{Ba}(\text{NO}_3)_2 + (n+1)\text{H}_2\text{O}$$
 The Ba(NO₃)₂ formed is dissolved in water, and Y-ZrO₂ (YSZ) is a nanosize residue.
- Dry the NaOH (or Ba(NO₃)₂) solution, and recycle NaOH (or Ba(NO₃)₂).

Accomplishments

- From the two selected precursors, namely Y-doped BaZrO₃ and Y-doped Na₂ZrO₃, selection of Y-doped Na₂ZrO₃ was made for the synthesis of nanosize (or fine) YSZ. This was based on the potential cost of the precursor, the need to use only water for leaching, and the short time required for the process.

- For the synthesis of calcia-stabilized zirconia (CSZ), which has the potential for use in place of YSZ in the anode of the SOFC, Ca-doped Na_2ZrO_3 was demonstrated as a suitable precursor.
- Synthesis of Y-doped Na_2ZrO_3 and Ca-doped Na_2ZrO_3 was achieved using a conventional calcination process. The corresponding surface area was ~ 1 to $2 \text{ m}^2/\text{g}$.
- By leaching with water, nanosize (very fine) YSZ and CSZ powders were synthesized. The corresponding surface area was $\sim 65 \text{ m}^2/\text{g}$. This demonstrates the molecular decomposition (MD) concept, namely macroscopic precursor \rightarrow leaching \rightarrow very fine (nanosize) product.
- Anode-supported cells, with YSZ and CSZ made by the MD process, were successfully made by a conventional pressing and sintering process.
- A single cell (Sr-doped LaMnO_3 (LSM) + YSZ cathode) was tested at 800°C with H_2/air , with maximum power density of $\sim 1.2 \text{ W}/\text{cm}^2$.
- Preliminary cost analysis, based on materials cost only, showed that the cost of YSZ powder made by the MD process should be considerably lower than that of YSZ powder made by either chemical co-precipitation or combustion synthesis.

Future Directions

The funded project has been completed, and no more work is planned. However, the following work is necessary for full evaluation of the process.

- Fabricate and test large-area (100 cm^2) cells in short stacks to evaluate performance.
- Design, construct and demonstrate a lab-scale reactor for the synthesis of CSZ and YSZ by molecular decomposition.
- Conduct a detailed cost analysis of the process.

Introduction

In order to facilitate the fabrication of solid oxide fuel cells by ceramic processing methods, it is necessary to use high-quality powders that are fine and not agglomerated. If the powders are fine (nanosize) and also de-agglomerated, processing temperature can be lowered, thus lowering the cost of energy and also minimizing materials interactions. One of the important materials is yttria-stabilized zirconia, or YSZ. At the present, commercially available powders of high quality sell for $\sim \$100/\text{kg}$, which is too expensive to be practical. One of the main reasons for the high cost is the cost of water-soluble salts used in the conventional fabrication process. This process is based on *molecular synthesis*, which involves an atom-by-atom or a molecule-by-molecule addition to a growing particle.

The University of Utah has invented a novel process for the synthesis of nanosize powders based on the concept of *molecular decomposition (MD)*, which is a radical departure from the traditional approach. This approach has numerous

technological advantages over the traditional approaches. This method is based on forming an insoluble but reactive precursor which has a fugitive constituent along with the desired constituent. The precursor synthesis does not require expensive water-soluble salts, but can use inexpensive oxides, carbonates, hydroxides, and the like.

Approach

The basic premise of the process of MD is that by decomposing a larger molecule (or structure) and leaching away fugitive constituents, fragments of the remaining constituents are formed at the atomic or nano level. These fragments then arrange themselves in the most stable structure so as to minimize the net free energy. For the process to work, the following conditions must be satisfied. (1) The precursor must contain the desired constituents of the final product and a fugitive constituent, in a chemically combined form. (2) The precursor must be insoluble in the liquid reagent used, but must react with it. (3) The fugitive constituent must form a soluble compound upon reacting with the reagent. (4) The final product

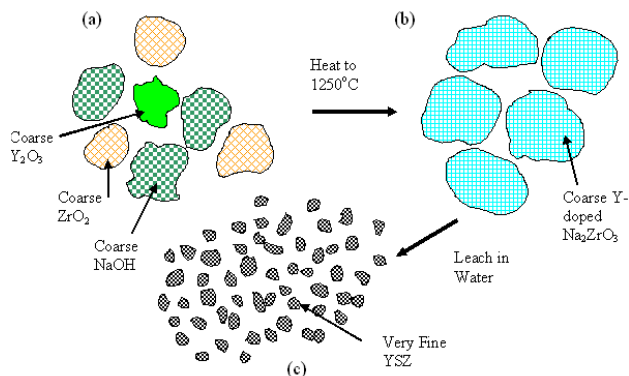


Figure 1. A schematic of the MD process: (a) Mixing of raw materials: Y₂O₃, ZrO₂, and NaOH, all of particle sizes in the micron to tens of microns range. (b) Calcination to form Y-Na₂ZrO₃ of several tens of microns in size. (c) Leaching in water to form nanosize YSZ.

must neither react with the reagent, nor dissolve in it. This prevents the occurrence of particle growth by dissolution-re-precipitation (Ostwald ripening).

The approach is described below by way of an example for the formation of nanosize ZrO₂ (n-ZrO₂). (1) A possible precursor is Na₂ZrO₃, which can be formed by reacting macrosized NaOH and macrosized ZrO₂, both of which are inexpensive. Na₂O is the fugitive constituent. (2) Na₂ZrO₃ reacts with water (reagent), but does not dissolve in it. (3) The fugitive constituent reacts with water to form NaOH, which is readily soluble in water. (4) The final product is n-ZrO₂, which does not react (although there is some tendency to form hydroxides) or dissolve in water. For the synthesis of YSZ, the stabilizer Y₂O₃ can be incorporated into the precursor. Alternative precursors and reagents can be used to obtain n-ZrO₂—for example, BaZrO₃ and HNO₃.

Results

Figure 1 shows a schematic of the MD process, wherein the precursor can be formed using inexpensive raw materials of large particle sizes (well into the microns or several tens of microns). Once a precursor is formed and reacted with a suitable reagent, the product phase forms fragments at the nanosize level. This method was used to make nanosize powders of YSZ and CSZ. The precursors used were Y-doped Na₂ZrO₃ and Ca-doped



Figure 2. A bright field TEM image of nanosize YSZ formed by the MD process. The crystallite size is ~5 nm. The agglomerate size in this TEM image is about 50 to 200 nm. The agglomerates are soft and can be broken with ease, down to a few tens of nm.

Na₂ZrO₃. Figure 2 is a transmission electron micrograph (TEM) bright field image of nanosize YSZ formed by MD. The precursor specific surface area was about 1 to 2 m²/g. However, the specific surface area of the nanosize YSZ was about 67 m²/g. The actual surface area should be larger. However, the particles were agglomerated (to form clusters of 50 to 100 nm in size, still in the nano range). X-ray diffraction (XRD) using CuKα radiation (Scherrer formula) showed that the crystallite size is about 3 to 4 nm. The YSZ powder, once properly ball-milled, could be readily sintered to form full dense parts. Figure 3 shows a scanning electron micrograph (SEM) of a sintered sample of YSZ made by MD. Note that the microstructure is equiaxed and that there is negligible porosity. While the nanosize powder made by this process can be used to make dense parts, its principal anticipated use is in the anode support of an anode-supported solid oxide fuel cell (SOFC). Cells were made using n-YSZ made

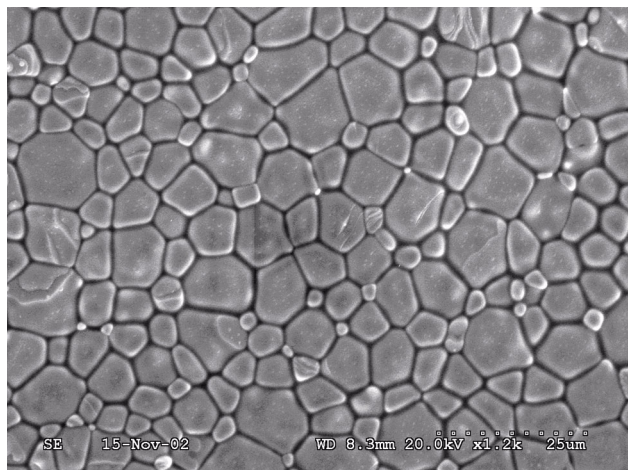


Figure 3. An SEM micrograph of a sintered sample of YSZ made by the MD process. The sample was sintered at 1400°C.

during the course of this project, and cells were tested using hydrogen as fuel and air as oxidant. Figure 4 shows the performance curves for a cell. Note that power density of $\sim 1.2 \text{ W/cm}^2$ was achieved at 800°C. A preliminary cost analysis was performed. It showed that powders made by MD should be less expensive than those made by chemical co-precipitation. The projected cost was less than \$10/kg for large batches. Cells were also made using CSZ powder made by MD.

Conclusions

The principal objective of the work was to demonstrate the synthesis and densification characteristics of very fine (nanosize) YSZ made by novel molecular decomposition, a potentially low-cost process. This principal objective was achieved.

In addition to the stated objective of developing very fine YSZ powders by the MD process, other significant results were obtained. These included the fabrication and testing of an anode-supported button cell using YSZ and CSZ made by the MD process as a constituent in the anode. At 800°C, the maximum power density of the cell with MD-YSZ in the anode was about 1.2 W/cm^2 . The other significant achievement was the synthesis of calcia-stabilized

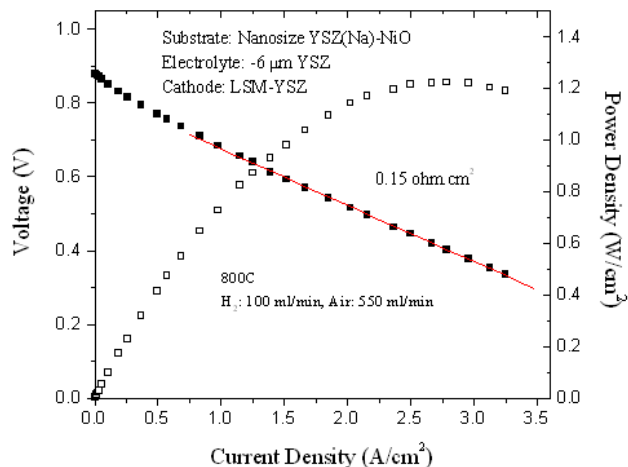


Figure 4. Voltage and power density vs. current density plots for the cell made using YSZ made by the MD process in the anode. In this initial trial, there were a few pinholes in the YSZ film (which was actually made using co-precipitated powder from a commercial source). As such, the open circuit voltage (OCV) is lower than had there been no pinholes. Nevertheless, it can be seen that the cell area specific resistance is quite low ($\sim 0.15 \text{ } \Omega\text{cm}^2$ at 800°C). The corresponding maximum power density is $\sim 1.2 \text{ W/cm}^2$. Had there been no pinholes and the OCV had been $\sim 1.15 \text{ V}$, the maximum power density would have been $\sim 1.9 \text{ W/cm}^2$.

zirconia (CSZ) by the MD process. The potential use of CSZ in the anode support is expected to have a beneficial effect of further lowering the cost.

FY 2004 Publications/Presentations

1. “Synthesis of Nanosize Oxide Powders by Molecular Decomposition”, by Anil V. Virkar, Invited talk presented at CHEMCON-2003, Bhubaneswar, India, December 2003.

Special Recognitions & Awards

1. Anil V. Virkar received the ‘Alkyl Amines Distinguished Speaker Award’ of the Indian Institute of Chemical Engineers, December 2003.

IV Fuel Cell Systems

IV Fuel Cell Systems

IV.1 Molten Carbonate Fuel Cell Product Design Improvement

Hans C. Maru (Primary Contact), M. Farooque

FuelCell Energy, Inc.

3 Great Pasture Road

Danbury, CT 06813

Phone: (203) 825-6006; Fax: (203) 825-6273; E-mail: hmaru@fce.com

DOE Project Manager: Norm Holcombe

Phone: (412) 386-4557; E-mail: Norman.Holcombe@netl.doe.gov

Objectives

The overall program objective is to advance the direct carbonate fuel cell technology to commercial entry level. The specific objectives to attain the overall goal are:

- Define power plant requirements and specifications;
- Design low-cost, modular, market-responsive DFC[®] (direct fuel cell) power plants;
- Resolve power plant manufacturing issues and design the commercial-scale manufacturing facility;
- Define the stack and balance-of-plant (BOP) equipment packaging arrangement and the stack module designs;
- Acquire capability for developmental testing of stacks and critical BOP equipment to support product design; and
- Resolve stack and BOP equipment technology issues, and design, build and field test prototype power plants to demonstrate readiness for commercial entry.

Approach

- Select product definition and specifications with input from potential users and define the commercialization plan;
- Design sub-MW and MW-class standard DFC[®] products for market entry;
- Acquire manufacturing capability for market-entry products;
- Develop stack module design(s) and establish product packaging configuration;
- Acquire capabilities for (1) stack development testing, (2) product stack and BOP design verifications, and (3) stack module conditioning and performance verification;
- Develop stack and BOP equipment technology (commercial design) to achieve market entry cost and performance goals; conduct prototype modular power plant field trial(s).

Accomplishments

- Defined and designed 250-kW (DFC300), 1000-kW (DFC1500) and 2000-kW (DFC3000) products, and established distribution alliances for worldwide marketing.
- Placed 32 sub-MW plants in operation; tested one MW plant at factory.
- Developed single-stack sub-MW and 4-stack MW stack modules.
- Expanded manufacturing facility to 50 MW/yr manufacturing capacity.
- Increased full-size stack power output capacity to 275 kW net AC.

- Achieved product entry life and stability goals; reduced stack module cost by 2.5 times.
- Developed enabling BOP equipment technologies: natural gas (NG) clean-up, preconverter, oxidizer, humidifying heat exchanger, and controls.

Future Directions

- Complete full-size Stack FA-100-3 test and improve full-size stack design based on the test results.
- Reduce power plant cost further by 10%; improve materials stability to extend DFC life.
- Initiate MW-class field trials.

Introduction and Approach

The Product Design Improvement project sponsored by government and private-sector cost-share draws on the manufacture, field test, and post-test experience of a 1.9-MW proof-of-concept power plant operated by FuelCell Energy (FCE) at a utility site in 1996-97. The efforts are focused on stack technology, manufacturing facility, and system developments leading to DFC[®] product designs and prototype system field trials.

Market entry commercial power plant products were defined in consultation with potential buyers. A standard power plant design applicable to most site conditions was selected. Optional features are provided for non-standard conditions. Manufacturing process lines were expanded to 50 MW/yr capacity as an intermediate point. Further expansion will be timed based on product order backlogs. Compact and truck-transportable fuel cell and BOP modules were selected for packaging the power plant. The configuration approach was aimed at reducing the fabrication cost and field installation time. It was decided to perform fuel cell stack module conditioning and performance verification testing at the factory. A conditioning facility for MW-class modules was built for this purpose. Stack and BOP technology improvement to define the commercial design is focused on cost reductions and performance and life enhancements. Product designs are verified in field trials.

Results

Products – Definition, Design, Verification and Marketing Plan

In collaboration with potential users, FCE has defined three modular products: MW-class

products rated at 1 MW (single module) and 2 MW (two modules), and a sub-MW-class product with a rating of 250 kW. Final design of the 2-MW product has been developed. Early market entry versions of the system will have 2 MW net AC output. If high-quality waste heat is utilized for cogeneration, overall thermal efficiency will be >70%. The 1-MW product is configured in a similar fashion as the 2-MW product. The DC power section is a 4-stack cylindrical module. FCE's technology partner, MTU, has developed the sub-MW power plant design. FCE has upgraded the design for conformance with U.S. codes and regulations. Currently there are 26 sub-MW units in operation throughout the world. Over 35 million kWh of electricity have been generated at customer sites. DFC1500 (1 MW) plant was performance tested at rated load in the Torrington facility (Figure 1) before shipment to site. The plant installation has been completed and field operation has started. Fuel cell modules for the DFC3000



Figure 1. MW-Class Module Performance Testing at Torrington Facility (Operation at rated load, on natural gas, verified.)

(2 MW) plant were conditioned and shipped to site. The field installation is in progress.

FCE has established commercial distribution alliances for worldwide marketing with MTU CFC Solutions in Europe; Marubeni Corporation in Asia; Enbridge, Inc. in Canada; and Caterpillar, PPL Energy Plus, Chevron Energy Solutions and Alliance Power in the U.S. FCE has been actively participating in the efforts to develop codes and standards for acceptance of fuel cell power plants in the marketplace. FCE's DFC300A power plant became the first fuel cell power system to be certified for operation, construction and performance under the new ANSI/CSA America FC 1-2004, Stationary Fuel Cell Power Systems standard.

Product Manufacturing and Power Plant Packaging

FCE's overall manufacturing strategy includes assembly of the BOP equipment skid at the equipment manufacturer and/or packager sites and stack manufacturing, conditioning and performance verification at the FCE factory. The sub-MW plant will be integrated at the factory, whereas the MW-class power plant modules will be integrated in the field. FCE manufactures fuel cells in Torrington, Connecticut. The stack manufacturing capability has been significantly enhanced at Torrington. The equipment necessary to produce 50 MW/yr of fuel cells has been installed. Each of the process lines has been tested and has achieved the 50 MW run rate. Equipment and processes have been developed to allow for assembling multiple horizontal- and vertical-type power plants simultaneously. FCE's product packaging approach has been defined. The MW-class products will include the truck-transportable stack, and mechanical, electrical and instrumentation skids. These skids will be field installed and interconnected. The sub-MW product will comprise of a single skid.

Test Facilities

Four subscale (10-kW, 20-kW, and two 30-kW) stack test facilities were made available for technology development testing. An existing 100-kW-class facility was modified to represent the commercial power plant, incorporate Santa Clara Demonstration Program (SCDP) BOP experience, and accept 9000-cm² cell area stacks with a capacity

of up to 400 kW. The 400-kW facility has been used for system-integrated operation of BOP equipment, product building-block stack design evaluation, and verification of power plant control and operational parameters. These test results have provided the basis for design of full-size stack and key BOP equipment incorporated in the DFC[®] products.

FCE has also acquired facilities for conditioning and performance verification (acceptance) test of sub-MW- and MW-class products. The MW-class facility can have one module in operation while the other module is being connected/disconnected. The sub-MW facility can accommodate eight modules. These two facilities together can provide 50 MW/yr total stack conditioning and performance verification capability.

Technology Development

FCE has made significant advances in the area of cell technology improvement directed towards commercial products. The cell area has been scaled up 50%. Stack performance improvement achieved included the areas of cell conversion efficiency, thermal management, thermal cycleability and high-power operation. The reformer unit design has been optimized using a hydrodynamic fuel cell stack computer model. The stack temperature distribution has been improved significantly. The full-size stack capacity has been increased to 275 kW net AC. The improved end cell design has shown excellent performance stability through numerous repeated thermal cycles.

The material development activities were focused on extending stack life to >40,000 h and product cost reduction. Low-cost bipolar plate material offering substantial cost savings was implemented in product stacks. The advanced corrosion-protected cathode current collector reduced corrosion and electrolyte loss, thereby offering a 2+ year increase in stack life. Significant improvements in direct internal reforming (DIR) catalyst performance, stability and cost were made.

Full-size Stack FA-100-3 test results have shown that the performance decay rate has been reduced significantly, meeting the stability goal. Value-engineered low-cost stack hardware components have been qualified. Manifold gas-seal design has

been improved, resulting in an effectiveness greater than two times that of the baseline design.

BOP equipment development included progress in the areas of sulfur removal, fuel humidifier, preconverter and DC-to-AC inverter. A 2-layer sorbent design for NG cleanup has increased adsorption capacity to 10 times that for the baseline design. The fuel humidifier design has been made compact, offering high effectiveness, reliability and 50% reduction in cost compared to the baseline design. The advanced preconverter design developed is capable of processing fuels containing O₂, such as digester gas, coal mine methane and peak shave NG, and secure fuels such as commercial-grade propane (HD-5). Four inverter vendors have been qualified, leading to 36% cost reduction concurrent with higher efficiency. Also, grid-to-island transfer capability has been demonstrated.

Conclusions

Three DFC[®] low-cost, modular, environment-friendly power plant products for distributed power generation have been defined, offering approximately 50% electrical efficiency and >70% system efficiency with cogeneration. The corresponding fuel cell stack module and BOP equipment designs, including the power plant packaging arrangements, have been developed based on testing at the subscale level and

verification testing in a 250-kW integrated system. Commercial product distribution alliances for worldwide marketing have been established. In parallel, the manufacturing technology has been developed, acquiring 50 MW/yr production capacity. Field trials of sub-MW products are ongoing in the U.S., Europe and Japan. Field trials of MW-class products are being initiated. A 1-MW plant (DFC1500) was performance tested at the rated load. Operation in the field has been initiated. Installation of a 2-MW plant (DFC3000) in the field is in progress. The product designs are upgraded based on power plant construction and field trial experiences. Parallel efforts to develop technology for further improving fuel cell performance and reducing power plant costs continue, to bolster the launching of the commercial products.

Publications

1. Molten Carbonate Fuel Cell Product Design Improvement, Technical Progress Report 1 (Dec. 1995) to 7 (Dec. 2001), submitted to DOE by FCE, Contract No. DE-FC21-95MC31184.
2. Molten Carbonate Fuel Cell Product Design Improvement, Semiannual Technical Progress Reports (June 2002, Dec. 2002, June 2003, Dec. 2003), submitted to DOE by FCE, Contract No. DE-FC21-95MC31184.

IV.2 High-Temperature Solid Oxide Fuel Cell Development

Joseph F. Pierre

Manager, Tactical Marketing

Siemens Westinghouse Power Corporation

Stationary Fuel Cells

1310 Beulah Road

Pittsburgh, PA 15235

Phone: (412) 256-5313; Fax: (412) 256-2012; E-mail: joseph.pierre@siemens.com

DOE Project Manager: Don Collins

Phone: (304) 285-4156; E-mail: Donald.Collins@netl.doe.gov

Objectives

- To complete the development of the tubular solid oxide fuel cell (SOFC) technology to the point of acceptable risk for private sector commercialization

Approach

- Verification of cell performance and durability
- Development, qualification, and implementation of cell manufacturing processes at rates commensurate with commercial production
- Development, qualification, and implementation of lower-cost bundling techniques
- Development of a reduced-cost module
- Design of cost-effective balance-of-plant systems and components

Accomplishments

- Established the 125-kWe combined heat and power system (CHP125) as the commercial product
- Achieved more than 10,000 hours of operation with minimal degradation for an atmospheric plasma spray (APS)-manufactured SOFC
- Completed more than 10 thermal cycles with negligible voltage loss for an APS-manufactured cell
- Improved the yield rate for the air electrode tube extrusion process
- Qualified less severe processing conditions for the densification of the plasma spray interconnection/interlayer
- Demonstrated that cells manufactured by the latest techniques have electrical performance equal to or superior to that of cells manufactured via the electrochemical vapor deposition (EVD) process
- Demonstrated the mechanical and structural integrity of a new cell-to-cell connection
- Demonstrated an advanced bundle-to-bundle welding technique that is amenable for automation
- Optimized the design and reduced the cost of certain module components, including air feed tubes, stack reformer boards, and high-purity insulation
- Developed, optimized, and designed advanced, cost-effective balance-of-plant concepts

Future Directions

- Develop a lower-cost air electrode tube making process
 - Identify and qualify low-cost cell materials
 - Qualify the plasma spray cell manufacturing processes and equipment
 - Demonstrate control and reproducibility of the bundling process
 - Qualify lower-cost bundling processes
 - Define and evaluate advanced module design concept
 - Initiate fabrication of the first CHP125 power system
 - Complete the first CHP125 Factory Acceptance Test
-

Introduction

The objective of the Cooperative Agreement between the U.S. Department of Energy (DOE) and Siemens Westinghouse Power Corporation (SWPC) is to complete the development of SWPC's tubular solid oxide fuel cell (SOFC) to the point of acceptable risk for commercialization. Our efforts are focused primarily on cost-reduction activities in order to drive down the cost of the CHP125 to commercially acceptable levels. In support of this commercial focus, our technology development and cost-reduction efforts are categorized into five main areas: cells, bundles, the SOFC module, balance-of-plant (BOP), and systems. Within each of the main areas, we have prioritized our development efforts to focus on those activities that have the greatest impact on product cost and have a high potential for success without compromising system performance, reliability, or safety.

The Cooperative Agreement will culminate in the field test of a commercial design SOFC combined heat and power system (identified as the CHP125) and the commissioning of a non-federally funded manufacturing facility for the production of CHP125 systems.

Approach

The goal of achieving commercially competitive SOFC power systems requires low-cost cell manufacturing and cost-effective fabrication and assembly of SOFC bundles, modules, and BOP systems. Activities under the cell manufacturing and development task are directed to improve and optimize the raw materials, simplify cell processing

conditions, and develop and qualify lower-cost manufacturing techniques. New materials and the latest manufacturing techniques and processes are qualified via a series of electrical performance and mechanical stability tests.

In the bundling area, our efforts are focused on the development of commercially viable cell-to-cell and bundle-to-bundle connections that are amenable to automation. Qualification and verification of the latest cell and bundle connections, improved bundling processes and process conditions, and enhanced bundling techniques are accomplished via multi-cell and bundle tests.

Our SOFC module design process ensures that all objectives related to the functionality and performance, cost, ease of assembly, and serviceability are incorporated early in the design process. Extensive use of computational fluid dynamics is employed to validate the designs, and where appropriate, the latest module design concepts are incorporated into and validated via bundle tests.

Many of the components in the CHP125 power system BOP have unique functional requirements that often require a one-of-a-kind component or subsystem. These items are considered to be strategic because an SOFC power system cannot be viably configured without them. When strategic equipment items are identified and/or developed, we verify them by testing their functionality and cost implications on the CHP125.

Finally, the latest cell and module technology and the most recent cost reduction features are incorporated into fully integrated SOFC power system field tests for verification and validation.

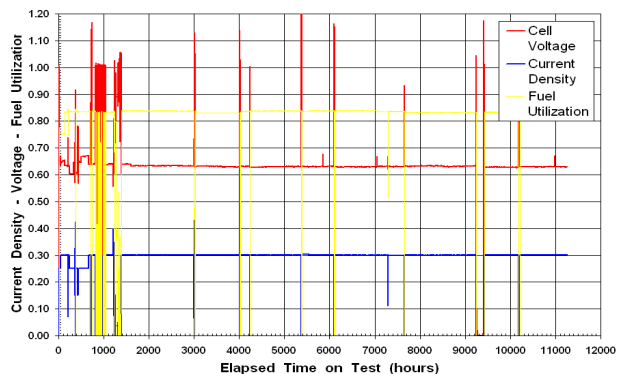


Figure 1. APS Cell Electrical Performance Without Degradation After 11,000 Hours of Operation

Results

Our standard product was defined to be a 125-kWe combined heat and power system (CHP125). At its nominal rating, the CHP125 will deliver a net 125 kWe AC to the grid at an electrical efficiency of ~45% (lower heating value). Thermal output in the form of hot water is anticipated to be ~100 kWt, thus achieving an overall efficiency of ~80%. In support of the singular commercial focus, our development and cost reduction efforts are categorized into five areas: cells, bundles, the SOFC module, balance-of-plant, and systems.

Significant progress in the cell manufacturing and development area was made in the past year as evidenced by the following:

- The air electrode tube extrusion process was simplified, resulting in a reduced rejection rate and, thus, an improved tube-making yield rate.
- Less severe processing conditions for the plasma spray interconnect/interlayer densification were qualified.
- Specifications and preparation techniques for lower-cost plasma spray electrolyte and plasma spray fuel electrode powders, respectively, were developed, tested, verified, and documented.

Cells manufactured using these latest specifications and techniques demonstrated electrical performance equal or superior to that of cells manufactured via the EVD process. Figure 1 shows the long-term electrical performance of a cell

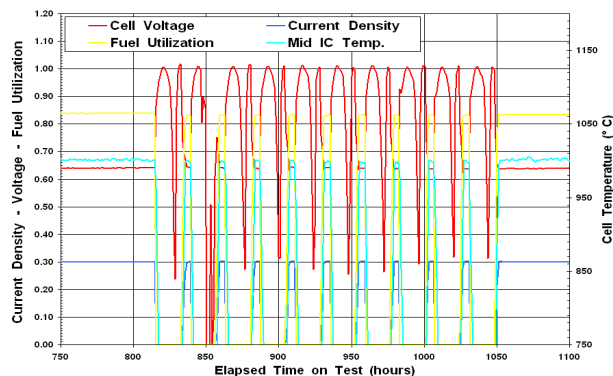


Figure 2. APS Cell Electrical Performance Without Degradation After Ten Thermal Cycles

manufactured via the preferred processes. After more than 11,000 hours of operation, the cell is demonstrating superior performance and voltage stability, displaying a degradation rate of less than 0.01% per thousand hours. Mechanical stability is also excellent, as shown in Figure 2. After ten thermal cycles there was no measurable loss in cell performance.

In the bundling area, efforts were directed to the development of cell-to-cell and bundle-to-bundle connections that are amenable to automated production. These efforts resulted in the following:

- The development of a second-generation cell-to-cell connection
- The successful demonstration, via multi-cell and bundle tests, of the mechanical and structural integrity of the new cell-to-cell connection
- The development of an advanced bundle-to-bundle welding technique that shows great promise for future automation.

Tensile tests to measure the mechanical viability and integrity of the cell-to-cell connections were conducted on numerous multi-cell and full-sized bundles and produced encouraging results. High bond strengths were consistently measured in a statistically significant number of tensile tests. In addition to possessing satisfactory mechanical and structural integrity, the cell-to-cell connections must satisfy criteria related to dimensional stability and electrical performance to ensure the cell-to-cell connections are suitable for the bundle manufacturing

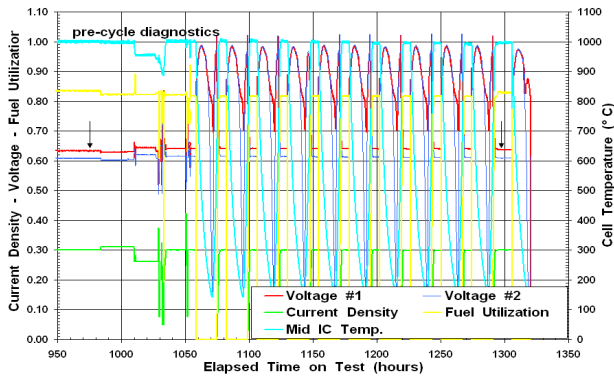


Figure 3. Cell-to-Cell Connection Performance Without Degradation After Ten Thermal Cycles

process. The electrical performance and thermal stability of this second-generation cell-to-cell connection are shown in Figure 3. After ten thermal cycles and more than 1,300 hours of operation, there is no measurable decline in cell performance.

Significant effort was also focused on the development and qualification of the bundle-to-bundle connection. A unique welding process was developed for the inter-bundle connection that lends itself to automated bundle fabrication. Initial tensile and electrical performance tests indicate it is a technically viable process.

The design of the SOFC module is a work in progress. To date, we have incorporated numerous innovative concepts that will result in a lower-cost, more reliable module. The concepts under development include reduced-cost air feed tubes; lower-cost, high-purity insulation; optimized stack reformer boards; enhanced designs of the fuel, air, and exhaust plena; stack support structures; and the fuel feed system. Significant stack and module configuration changes occurred in the past year, all directed to more cost-effective designs of the stack and module. The major changes affected components such as the positioning boards, power leads, power takeoffs and busbars, instrumentation, and stack insulation. Extensive use of computational fluid dynamics was employed to validate the designs. Where appropriate, module improvements are verified in 5-kWe bundle tests.

Many of the components in the CHP125 power system BOP have unique functional requirements that often require a one-of-a-kind component or subsystem. These items are considered to be strategic because an SOFC power system cannot be viably configured without them. The integration of these components and subsystems within the balance-of-plant and with the SOFC module requires optimization of the interfaces between the two systems. The functional specifications of the BOP subsystems and components were revised based on the new conceptual design of the SOFC module. As the SOFC module design matures, these functional specification and interface requirements will be revised accordingly. Other accomplishments in the BOP area include the following:

- Definition of a safe, cost-effective, and functional BOP
- Optimization of the orientation of the BOP relative to the SOFC module
- Conceptual and detailed designs of the respective systems, subsystems, and components comprising the BOP
- Development of advanced system and subsystem concepts that enable elimination of previously required components
- Identification of low-cost, high-performance desulfurizing reagents.

Efforts to achieve cost-effective strategic equipment for the BOP are continuing. As new components or system concepts are developed, their functionality will be verified by testing and their impact on system cost will be evaluated.

Conclusions

Our continued and increased efforts to reduce the cell, module, and BOP costs are well-defined and progressing according to schedule. The latest cell, module, and BOP technology available and the most recent cost-reduction features will be incorporated into the appropriate field test for verification and validation.

V Hybrids

V Hybrids

V.1 Direct Fuel Cell/Turbine Power Plant

Hossein Ghezel-Ayagh

FuelCell Energy, Inc.

3 Great Pasture Road

Danbury, CT 06813

Phone: (203) 825-6048; Fax: (203) 825-6273; E-mail: hghezel@fce.com

DOE Project Manager: Norm Holcombe

Phone: (412) 386-4557; E-mail: Norman.Holcombe@netl.doe.gov

Subcontractors:

Capstone Turbine Corporation, Chatsworth, California

Montana State University, Bozeman, Montana

CTA Architects Engineers, Billings, Montana

Objectives

The overall project goal is to develop ultra high efficiency power plants based on Direct FuelCell/Turbine[®] (DFC/T[®]) Technology. The specific objectives are:

- Develop the conceptual design of multi-MW hybrid DFC/T systems with efficiencies approaching 75% (natural gas fuel) and with sulfur and nitrogen oxide emissions < 0.01 lb/million BTU.
- Verify commercial viability of the DFC/T systems for near-term deployment.
- Design a packaged sub-MW DFC/T system for distributed power generation.
- Verify the potential benefits of hybrid technology and show its readiness by a grid-connected field demonstration at a customer site.

Approach

- Conduct proof-of-concept tests of the DFC/T system in a sub-MW class power plant configuration.
- Evaluate the design of the key system components, including gas turbine, heat recuperators and high-temperature catalytic oxidizer.
- Develop the preliminary design of a 40-MW DFC/T power plant representative of the multi-MW hybrid systems. Estimate the cost of the power plant to verify its commercial competitiveness with alternate technologies.
- Conduct experimental investigation to evaluate alternative designs for anode gas delivery to fuel cells to further increase fuel cell efficiency.
- Design, fabricate, and test two sub-MW class DFC/T units to assess the efficiency potential of the power plants and to demonstrate the technology.

Accomplishments

- Completed the construction of a sub-MW DFC/T power plant facility by integration of a full-size 250-kW DFC stack with a Capstone C60 Micro-turbine.

- Completed the proof-of-concept demonstration tests by successful operation of the world's first grid-connected hybrid system (Pre-alpha DFC/T).
- Completed the preliminary design of a 40-MW DFC/T hybrid system, including site plan and fuel cell module layouts. Estimated plant capital cost (preliminary) and performance characteristics of the 40-MW power plant.
- Completed experimental investigation to evaluate alternative designs for anode gas delivery to fuel cells to further increase fuel cell efficiency.
- Investigated alternative designs for the micro-turbine, recuperators, and anode gas oxidizer for the sub-MW hybrid system. Completed the preliminary process design and instrumentation configuration of the packaged sub-MW class DFC/T.
- Performed a preliminary review and survey of the potential demonstration sites in Montana for the Beta sub-MW unit.

Future Directions

- Complete cost estimation and system optimization for the multi-MW scale DFC/T hybrid power plant.
- Conduct collaborative research with Montana State University to develop guidelines for heat exchangers and load monitoring equipment.
- Complete the packaging design and equipment layouts for the Alpha sub-MW DFC/T power plant.
- Conduct tests of the first sub-MW (Alpha) unit at FuelCell Energy (FCE) facilities in Danbury, Connecticut. Implement the design improvements in a second sub-MW (Beta) DFC/T unit.
- Complete site preparation in Montana for testing the Beta sub-MW DFC/T unit.
- Fabricate the Beta DFC/T unit and conduct field demonstration of the unit in Montana.

Introduction

FCE's DFC/T hybrid system concept is based on integration of the company's Direct FuelCell[®] with a gas turbine. The power plant design utilizes a heat recovery approach for extraction of heat from the balance-of-plant. The fuel cell plays the key role by producing the larger share of the power (>80%). The gas turbine is utilized for generation of additional power by recovering the fuel cell byproduct heat in a Brayton cycle, as well as for providing the air for the fuel cell operation.

Features of the DFC/T system include electrical efficiencies approaching 75% on natural gas (60% on coal gas), direct reforming internal to the fuel cell, minimal emissions, reduced carbon dioxide release to the environment, simple design, and cost competitiveness with existing combined cycle power plants.

Approach

The DFC/T system concept was implemented in a power plant test facility (pre-alpha power plant) by



Figure 1. Sub-MW DFC/T Hybrid Power Plant Showing Full-Size DFC Stack Integrated with a Capstone Micro-turbine

integration of a 250-kW DFC stack and a Capstone microturbine. Figure 1 shows a picture of the DFC/T

power plant facility. The focus of the pre-alpha testing was the verification of the DFC/T concept, development of critical system components, and acquisition of design information for development of power plant products. Initially, a Capstone Simple Cycle Model 330 micro-turbine was used for the proof-of-concept tests. The micro-turbine was built with a compressed air exhaust port and expander inlet pipe to provide flow connections to the fuel cell system. The power plant was capable of operating in dual modes: fuel cell/turbine integrated mode and fuel cell only mode. The dual mode capability was used to evaluate the benefits of the DFC/T cycle over the fuel cell only cycle. The pre-alpha power plant was later modified to accommodate a Capstone 60-kW micro-turbine. The inclusion of the 60-kW micro-turbine extended the range of operation of the hybrid power plant to current densities (power) higher than those achieved in previous tests using the 30-kW micro-turbine.

Test results from the proof-of-concept tests are being used in the design of the packaged sub-MW units. The hybrid technology development plan includes the design, construction, and testing of two sub-MW DFC/T units, which will demonstrate grid-connected operations, help assess the efficiency potential of the sub-MW plants, and provide valuable data on integration and operation of DFC/T power plants under laboratory and field conditions. The first unit, "alpha," will be factory tested at FCE headquarters in Danbury, Connecticut. The test results and experience from the alpha unit will be used to refine the design for the "beta" unit, which will undergo one year of demonstration testing in Montana.

The design of a large-scale hybrid power plant is focused on scalable products. FCE has developed the fuel cell cluster concept in order to upscale product capacities in a short design time cycle. Presently, FCE has completed preliminary design of a 40-MW hybrid power plant.

Results

Proof-of-Concept Tests: The "pre-alpha" proof-of-concept tests verified the DFC/T concept by demonstrating that a substantial gain in efficiency is feasible in small power plants by integrating a

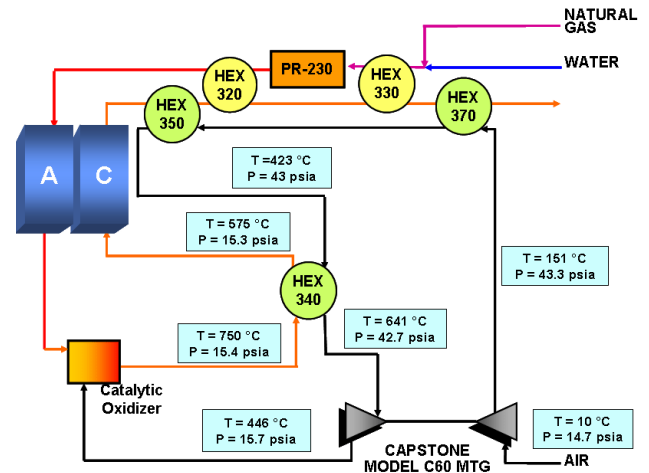


Figure 2. Sub-MW DFC/T Power Plant Facility Process Flow Diagram Represented by a Typical Set of Operational Data

microturbine with the fuel cell. The operation of the integrated power plant benchmarked a near 5% increase in efficiency. Figure 2 shows a simplified process flow diagram for the sub-MW DFC/T power plant, including a typical set of plant operating conditions. Three heat recuperators for indirect heating of air from the compressor side of the micro-turbine were included. The anode exhaust oxidizer included a high-temperature catalytic section.

The proof-of-concept test was completed, verifying the DFC/T concept. The tests established the stable and well-controlled operation of the DFC/T power plant. Thermal management of the system was confirmed by increasing micro-turbine expander inlet temperature while controlling the fuel cell operating temperature. The tests successfully demonstrated the ability of the control system to follow prescribed load ramps and to respond to abrupt utility grid outages. NO_x emission levels of less than 0.25 ppm were achieved.

Sub-MW Power Plant Design and Demonstrations: The design of the sub-MW packaged demonstration unit is in progress. Steady-state mass and energy balances for the power plant were completed for various modes of operation, including start-up, standby, and full load operation. Data sheets and specifications were prepared for balance-of-plant equipment, including instrument and control equipment. A process flow diagram and

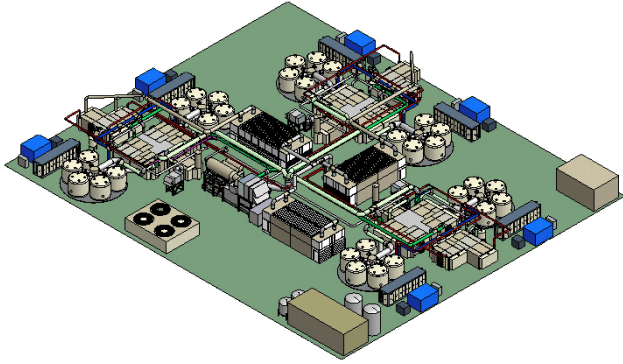


Figure 3. 40-MW Hybrid DFC/T Power Plant Layout and Site Plan for Near-Term Very Efficient Power Generation

a set of piping and instrumentation diagrams (P&IDs) have been prepared.

A preliminary review of potential demonstration sites in Montana for the beta sub-MW unit was completed. Two venues in Montana, including the Engineering/Physical Science Building at Montana State University (Bozeman, Montana) and the Deaconess Billings Clinic (Billings, Montana), were investigated. Both sites were found to be suitable for the demonstration.

Multi-MW Power Plant Design:

The preliminary design of a 40-MW Power Plant hybrid system concept was completed. An overall layout/plot plan of the 40-MW plant is shown in Figure 3. The site is approximately 273' x 325' in size. The arrangement of equipment on the site is designed to provide easy access to the equipment for maintenance and replacement, and to minimize the length for the largest process piping. The design is based on a scalable approach using FCE's existing M-10 (MW-scale) fuel cell modules in a cluster arrangement. The fuel cell cluster design has five M-10 modules in a cluster with common distribution piping for the fuel and oxidant gases. Based on the scalable overall plant design concept, the plant is arranged in three sections (power blocks) in addition to the centralized equipment. Each power block consists of two clusters of fuel cell modules together with supporting equipment. The centralized equipment, which supports all three sections, includes a gas turbine, an anode gas oxidizer and

other common site equipment such as a fuel clean-up subsystem and a water treatment subsystem. The gas turbine incorporated in the 40-MW plant design is a Man Turbo Model 1304-11 (MAN Turbomachinery Inc). Key characteristics of the gas turbine include pressure ratio of 8 and turbine inlet temperature of about 1800°F.

Conclusions

The DFC/T concept was verified in the world's first grid-connected hybrid fuel cell/gas turbine sub-MW class power station. The test results showed that the DFC/T concept has potential for achieving very high efficiencies. The operation of the first-of-a-kind power plant resulted in resolution of key technical challenges. The thermal management of the system was confirmed. The control strategies were developed. System trip/emergency shutdown scenarios were tested successfully. Power plant operation, using a micro-turbine as the only source of fresh air supply to the system, was demonstrated. Based on the proof-of-concept test results, design of the sub-MW DFC/T units is being finalized.

A scalable approach for the multi-MW plant design based on fuel cell clusters of the existing 1-MW (M-10) modules has been developed. Preliminary design of a 40-MW hybrid system for near-term deployment was completed.

Publications

1. H. Ghezal-Ayagh, J. M. Daly and Z. Wang, "Advances In Direct Fuel Cell/Gas Turbine Power Plants", Proceedings of ASME/IGTI Turbo Expo 2003, ASME paper GT2003-38941.
2. Direct Fuel Cell/Turbine Power Plant, Semi-Annual Technical Progress Report (November 2003 to April 2004), submitted to DOE by FCE, Contract No. DE-FC26-00NT40798.

Patents Issued

1. H. Ghezal-Ayagh, A. J. Leo, and R. Sanderson, "High-Efficiency Fuel Cell System", U.S. Patent No. 6,365,290, April 2002

V.2 Solid Oxide Fuel Cell Hybrid System for Distributed Power Generation

Nguyen Minh (Primary Contact), Ray Andrews, Faress Rahman

GE Hybrid Power Generation Systems

19310 Pacific Gateway Drive

Torrance, CA 90502-1031

Phone: (310) 538-7250; Fax: (310) 538-7250; E-mail: nguyen.minh@ps.ge.com

DOE Project Manager: Norm Holcombe

Phone: (412) 386-4557; E-mail: Norman.Holcombe@netl.doe.gov

Objectives

- Develop and demonstrate the feasibility of highly efficient hybrid systems, integrating a planar solid oxide fuel cell (SOFC) and a gas turbine (GT).
- Identify and assess highly efficient coal power plant system configurations integrating a coal gasifier and gas clean-up train with a planar SOFC and bottoming cycle.
- Develop scale-up strategies for large SOFC-GT systems, and identify system architectures that minimize SOFC stack scale-up and technology development risks.

Approach

- Develop conceptual design for high-efficiency SOFC-GT hybrid systems based on the results of preliminary analysis and trade studies on a variety of system concepts. These trade studies are done for a variety of plant applications, sizes, and fuels, including 500-kW distributed power generation fueled with natural gas and 25-MW and 300-MW centralized power generation fueled with natural gas and coal. Evaluate the expected performance for these systems and establish the requirements of the SOFC subsystem.
- Fabricate and test laboratory-scale SOFCs to investigate their operating characteristics under hybrid conditions and identify key technical barriers.
- Assess SOFC stack technology, especially that currently under development in the Solid State Energy Conversion Alliance (SECA) program, with a focus on critical near-term issues that are necessary to demonstrate feasibility to support the development of large hybrid and coal-based systems. Namely, demonstrate the potential of SOFC cell scalability for tape-calendered cells, operate SOFC stacks of increasing size under hybrid conditions, and assess the scalability of stack designs.
- Identify key technology gaps for SOFC-GT hybrid systems.

Accomplishments

- The structural integrity of 6-inch cells up to a pressure differential of 5 psid was demonstrated using the half-sealed SECA stack design. The level of control of the differential pressure across the stack is currently unknown for pressurized hybrid systems. It is estimated that hybrid systems require that the cell be capable of withstanding at most 5 psid pressure across the cell. This demonstration indicates that a 6-inch cell has sufficient strength to withstand the stresses for hybrid systems with the current stack design.
- Tests were completed to quantify the impact of pressure on carbon deposition using an operational cell. Pressure was found not to have a significant impact on the carbon boundary under the tested conditions (290 mA/cm², 30% fuel utilization, and steam reformed fuel inlet composition). These tests were performed on a sealless radial test vehicle having 4 3/8-inch cells at pressures up to 4 atm.
- Tests were completed to quantify the impact of pressure on the performance degradation of SOFC cells operating under pressurized conditions. Pressurized operation was found to have a significant impact on

cell conditioning and degradation. Cell performance degradation was observed to increase substantially with pressure. Potential mechanisms responsible for this degradation have been suggested. No work on the performance degradation of planar stacks under pressurized conditions was done prior to this effort.

- The conceptual design of a 300-MW coal-fired SOFC hybrid system is estimated to be 53% (higher heating value) efficient (based on current technologies with an assumed performance for the SOFC), a 10% efficiency improvement over a current 220-MW state-of-the-art baseline Integrated Gasified Combined Cycle (IGCC) system. The downselected system consists of 40 SOFC modules, each generating 4.8 MW; two General Electric (GE) frame-5 gas turbines; a British Gas Lurgi (BGL) oxygen-blown gasifier; and a two-pressure reheat steam cycle. It is assumed to use Pittsburgh 8 coal. This system is anticipated to cost \$1650/kW, approximately \$150/kW less than the baseline IGCC system. No technology gaps are foreseen for the gas turbine or gasifier, although engineering challenges exist. The major technical hurdle is the development of the large-scale stacks, assumed to operate at SECA phase 3 levels.
- The addition of 85% carbon dioxide isolation on the 300-MW coal-fired Integrated Gasified Fuel Cell (IGFC) system has been analyzed. It is expected to reduce system efficiency by 2.5% and increase system cost by \$350/kW.
- The functional product specification for a 25-MW natural gas plant for centralized power applications has been completed. This product specification was developed based on requirements of competing technology.
- Different system concepts have been brainstormed for 25-MW natural gas SOFC-GT systems for centralized power applications. Performance, cost, and reliability analysis models have been developed. These models have been used to complete the preliminary analysis of the four downselected system concepts.

Future Directions

- Evaluate the performance of subscale SOFC stacks as a function of temperature, pressure, and gas composition. Stacks of increasing size (footprint and height) will be tested.
- Analyze SOFC stack design features that have impact on stack reliability, cost, and performance. Designs and operating procedures to facilitate stack scale-up will be identified.
- Demonstrate cell area scale-up. This effort will include theoretical assessment of the sintering process to establish a framework for scale-up improvements and performance testing of large-area cells.
- Conduct a system trade study to examine the trade-off in cost and reliability of the stack subsystem with the goal of identifying the combination of cell size, stack size, and stack subsystem configuration that best meets the functional product specification of the 25-MW natural gas plant.
- Identify stack performance and scale-up technology gaps.

Introduction

The overall objective of this project is to develop and demonstrate the feasibility of highly efficient SOFC-GT hybrid systems. The hybrid system concept has several attractive features: (i) efficiencies can be over 65% depending on system size, design, and operating conditions; (ii) the combination of planar SOFC and commercial gas turbine leads to low-cost solutions; (iii) high efficiency will result in low greenhouse gas emissions; and (iv) the hybrid is a low-noise system with siting flexibility for distributed

power generation. Many of these benefits stem from the integration of the SOFC stack with the gas turbine. The hybrid environment is distinguished from the simple cycle system by the pressurized operation of the SOFC, the general requirement for larger stacks and systems, and the fuel compositions entering the stack.

The work in this project focuses on defining and optimizing suitable system concepts for various size plants operating on different fuels, conducting experiments to resolve identified technical barriers,

and demonstrating the scalability and operation of the SOFC in a hybrid environment.

Approach

System concepts and configurations are developed via a series of trade studies and performance and cost analyses. The feasibility of selected SOFC-GT hybrid systems is demonstrated through a comparison of the top-down requirements with the bottom-up estimates and technology demonstrations. This comparison results in identification of the technology gaps that must be addressed for commercialization. The top-down requirements are established through the conceptual design of the different plants, and the necessary operating requirements of the various subsystems, especially the SOFC stack subsystem, are defined to meet the performance needs of the plant. The bottom-up estimates represent the current technology capability. Several technology gaps identified through this process are then evaluated through laboratory testing and demonstrations.

Laboratory testing of the SOFC mainly concentrates on evaluating the effects of pressure on the performance and operating characteristics of the fuel cell. Due to the current development status of the SOFC stack technology, many of the SOFC tests are performed on test vehicles that are not optimized for hybrid systems. Such tests identify the design considerations that would be necessary to accomplish high-efficiency hybrid systems and, in many cases, identify the approach by which to optimize the design.

Results

In FY 2004, the conceptual design of an Integrated Gasification Fuel Cell (IGFC) system was completed. The IGFC system combines the current advantages of the Integrated Gasification Combined Cycle (IGCC) system with the high efficiency of SOFC technology. The IGCC system with two GE 6FA+e gas turbines and a bottoming cycle was modified so that one of the gas turbines was replaced with the SOFC system. The evaluation of the IGFC system was driven by the use of near-term available commercial technology wherever possible, the use of projected large (MW-size) planar SOFC technology,

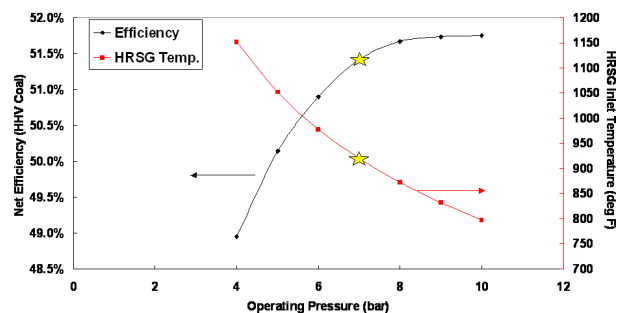


Figure 1. Effect of fuel cell operating pressure on the efficiency of the 300-MW baseline integrated gasification fuel cell system assuming 10 stack modules operating with a fuel utilization of 80%. The impact of operation pressure on the HRSG inlet temperature is also shown. The stars in the graph represent the chosen optimum design condition.

and system optimization aiming for overall system efficiencies of 50% in the short-term and 60% in the long-term. Based on these design constraints, the IGFC system was designed around the British Gas Lurgi (BGL) oxygen-blown gasifier, and the system trade studies focused on the design of the fuel cell modules and integration of the fuel cell with the gasifier and fuel integration system.

After preliminary analysis and evaluation of several brainstormed system concepts, two concepts were downselected for further analysis. Several sensitivity analyses were performed on these concepts to optimize their performance. These studies included the effect of fuel cell operating pressure, SOFC fuel utilization, and the number of SOFC stages on the system efficiency and system cost. Figure 1 shows as an example the performance for the baseline system design as a function of fuel cell operating pressure. The impact on the heat recovery steam generator (HRSG) inlet temperature is also shown in this figure.

The optimized system was then analyzed to understand the impact of carbon dioxide isolation from the exhaust stream. Two methods for isolating carbon dioxide were evaluated: (1) Selexol-based physical absorption and (2) combustion of spent fuel with pure oxygen from the air separation unit rather than the cathode exhaust. The latter method ideally creates a fuel exhaust that is almost pure carbon

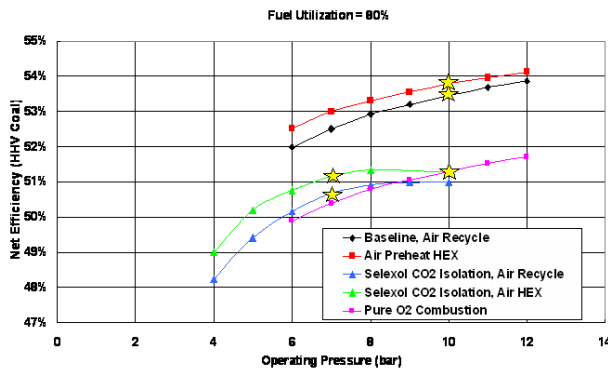


Figure 2. Efficiency of 300-MW baseline and alternate baseline integrated gasification fuel cell systems versus fuel cell inlet pressure assuming 10 stack modules operating with a fuel utilization of 80%. The reduction in plant performance that is expected with the addition of Selexol-based carbon dioxide isolation is also shown for the two system concepts. The stars in the graph represent the chosen optimum design points.

dioxide and water vapor. The water vapor is condensed out easily to isolate the carbon dioxide. The sensitivity of the two downselected systems to operating pressure with and without carbon dioxide isolation is shown in Figure 2.

The resulting conceptual design of the 300-MW IGFC system clearly demonstrates a significant benefit over current IGCC technology as indicated by the substantial gains in efficiency. No technology gaps are foreseen for the gas turbine and gasifier systems to achieve this level of performance, although engineering challenges are expected. However, these systems assume stack performance consistent with SECA Phase 3 goals and therefore require significant technology development in this area, including SOFC scale-up.

The operation of planar SOFCs in hybrid conditions is key in the feasibility demonstration of SOFC hybrid systems. The impact of differential pressure across the cell (anode-to-cathode and cathode-to-anode) was investigated experimentally using the current SECA stack design. A single-cell stack was held at operating temperature while the pressure differential across the cell was varied from +5 psid to -5 psid. The leakage across the cell was measured periodically through this test and was

found to be unaffected by the differential pressure. This result, in conjunction with the physical observation of the cell, clearly indicates that the thin cell has adequate strength and is adequately supported to withstand 5 psi differential pressure across it. The control scheme of a hybrid system is likely to be sufficient to maintain the differential pressure across the cell to within this limit under normal operating conditions.

The impact of pressure on the long-term cell performance degradation was also investigated. Several cell samples were operated over long periods of time at ambient and pressurized conditions. The results of these tests indicate that the performance degradation over time increases with pressure. The degradation at a pressure of 4 atmospheres is roughly twice that at ambient conditions. However, the exact magnitude is uncertain since significant cell-to-cell variability was observed in these experiments.

The operation of a cell with steam-reformed fuels showed no additional issues and, in fact, demonstrated a potential method for increasing system efficiencies. Steam is added to the fuel stream to prevent the formation of carbon at the inlet of the cell. The system design point is at a steam-to-carbon ratio of 1.5. Lowering this ratio would increase the system efficiency but also increase the potential for carbon deposition. Tests were conducted to understand the boundary at which carbon formation is initiated. It was found that cells could operate stably at steam-to-carbon ratios as low as 1.0 but that carbon deposition would occur at 0.5. This is the first time planar SOFC cells have been operated under pressurized conditions with simulated fuels.

Conclusions

- The integration of a SOFC in a 300-MW IGCC system has the potential to increase overall system efficiency by 10% and lower cost by \$150/kW. This result assumes SECA Phase 3 SOFC performance and current technology gas turbines, gasifiers, air separation units, and balance of plant.
- The addition of 85% carbon dioxide isolation on the IGFC system reduces the efficiency of the plant by approximately 2.5% and increases the cost by \$350/kW.

- Pressurized operation of planar SOFC fuel cells has been demonstrated for the first time. While the performance degradation of the cell is observed to be higher than that at ambient conditions, no other operational issues have been observed. Further work is necessary to quantify the degradation rate and the mechanisms responsible for increased degradation.
- Pressurized operation of SOFCs on simulated steam reformat indicated that carbon formation occurred at steam-to-carbon ratios less than 1.0 at 4 atm and 800°C. The design point for pressurized systems is at steam-to-carbon ratio of

1.5, leaving adequate margin for stable operation and potential for reducing the necessary steam and therefore potentially increasing the performance of the system.

FY 2004 Publications/Presentations

1. Presentation made at American Society of Mechanical Engineers conference (AIAA/ASME 2nd Annual Northeast Aerospace/Mechanical Engineering Mini-Symposium) in Albany, NY, on April 14, 2004.

VI Advanced Research

VI Advanced Research

VI.1 Enhanced Power Stability for Proton-Conducting Solid Oxide Fuel Cells

William Goddard III (Primary Contact), Sossina Haile, Boris Merinov, Adri van Duin
California Institute of Technology
1200 East California Blvd.
Pasadena, CA 91125
Phone: (626) 395-2731; Fax: (626) 585-0918; E-mail: wag@wag.caltech.edu

DOE Project Manager: Lane Wilson
Phone: (304) 285-1336; E-mail: Lane.Wilson@netl.doe.gov

Objectives

- Develop modified electrolytes that exhibit both high proton conductivity and excellent chemical and mechanical stability. Doped BaZrO₃ has been selected as a basic material for further modifications.
- Develop a fundamental understanding of the mechanisms and barriers of proton transport in a proton ceramic fuel cell (PCFC).
- Develop highly efficient electrocatalysts for the anodes and cathodes of PCFCs based on the above-mentioned relatively new electrolytes.
- Develop rapid synthesis methodologies for both candidate electrolytes and candidate electrodes (or electrocatalysts).

Approach

- Obtain equations of state (EOS) for relevant metals, metal oxides, pure and Y-doped BaZrO₃.
- Determine equilibrium positions for protons in doped BaY_xZr_{1-x}H_xO₃ (BYZ).
- Calculate transition barriers for proton migration in doped BYZ.
- Develop Reactive Force Fields (ReaxFF) based on *ab initio* quantum mechanical (QM) calculations on relevant metals and metal oxides.
- Perform ReaxFF molecular dynamics (MD) simulations on large systems to investigate physico-chemical processes in the electrolyte and electrode/electrolyte interfaces.
- Synthesize and characterize dense BYZ ceramics with desired grain size.
- Screen potential cathode materials among transition metal perovskites.
- Fabricate complete membrane electrode assembly (MEA) and establish baseline fuel cell performance.

Accomplishments

- A series of QM calculations of EOS was performed on various bulk metals (Pt, Zr, Y, Ba), metal alloys (Y/Zr, Y/Ba, Zr/Ba), metal oxides (ZrO₂, Y₂O₃, BaO) and BYZ.
- Based on the QM data, ReaxFF were developed for Pt-metal clusters, various bulk metals (Pt, Zr, Y, Ba), metal alloys (Y/Zr, Y/Ba, Zr/Ba), metal oxides (ZrO₂, Y₂O₃, BaO) and initial ReaxFF potentials for BYZ.
- Fabrication protocols have been developed for high-density BYZ, both with and without transition metal modifiers, and for thin film membrane fuel cells. NiO, CuO and ZnO are the most effective additives for enhancing barium zirconate densification. The enhanced densification for modified BYZ was improved to 95% with refined mixing techniques.

- Characterization of Zn-, Cu- and Ni-modified BYZ was performed. The conductivities and ionic transport numbers of high-density pellets have been measured, and preliminary fuel cell polarization curves obtained from BYZ-based MEAs.

Future Directions

- Continue developing ReaxFF based on the interaction between QM and ReaxFF results. Adding diffusion barriers to the ReaxFF training will allow MD simulations of diffusion processes in the BYZ electrolyte and electrode/electrolyte interface to be performed.
- Perform QM calculations on stable BaZrO₃ surfaces for further modeling grain boundaries.
- Start applying ReaxFF on the realistic electrolyte structures to study proton transport in BYZ grains and grain boundaries.
- Potential cathode materials (transition metal perovskites) will be screened for reactivity with BYZ. Total conductivity of viable cathode materials will be measured for further screening.
- Optimal cathode catalyst in terms of reactivity and conductivity will be identified.

Introduction

Many acceptor-doped perovskite-type oxides show high protonic conductivity at elevated temperatures. In addition to their reduced temperature operation relative to traditional oxide ion conductors such as Y-stabilized ZrO₂, these perovskites, due to their proton transport properties, offer the possibility of application in a number of arenas including hydrogen sensors for molten metals, H₂/D₂ separators, and hydrogen pumps. However, at present only electrolytes based on BYZ combine high bulk proton conductivity with excellent chemical and mechanical stability. The current limitation for application of BYZ in PCFCs is the extremely high grain boundary resistance, which leads to the relatively poor total conductivity. To understand the conduction process and the role of defects and dopants in transport at the molecular level, we are developing the multi-scale strategy based on accurate QM calculations of the relevant materials which are then used to derive a First Principles-based ReaxFF allowing large-scale MD simulations that enable the study of proton transport under realistic conditions as well as the role of grain boundaries, defects, dopants, etc. Follow-up experiments are used to validate the computational predictions and to formulate new problems and tasks.

Approach

A series of QM calculations of EOS, based on Density Functional Theory [1] using Generalized

Gradient Approximation [2] to treat the exchange-correlation energy functional, has been performed on various bulk metals (Pt, Zr, Y, Ba), metal alloys (Y/Zr, Y/Ba, Zr/Ba), metal oxides (ZrO₂, Y₂O₃, BaO) and BYZ. Most of the QM calculations were carried out using the pseudo-potential local basis set code SeqQuest [3], jointly being developed between Sandia National Laboratories and California Institute of Technology. The obtained QM data were then used to develop ReaxFF for the Pt-metal clusters, the bulk metals, the metal alloys, the metal oxides and the initial ReaxFF potentials for BYZ. ReaxFF MD simulations might help to find ways to optimize the grain-boundary properties.

To accelerate the densification process of BYZ ceramics at lower temperature, we have performed an initial screening of all transition elements in the series Sc to Zn. It turned out that NiO, CuO and ZnO are the most effective additives for enhancing barium zirconate densification. The enhanced densification for modified BYZ was improved to 95%. We also carried out characterization (X-ray diffraction, scanning electron microscopy, and impedance spectroscopy) of Zn-, Cu- and Ni-modified BYZ. The temperature dependence of the bulk conductivity, grain boundary conductivity, and specific grain boundary conductivity were measured. The bulk conductivity of BYZ-Zn₄ is slightly lower than that of unmodified BYZ. Preliminary fuel cell polarization curves were obtained from BYZ-based MEAs.

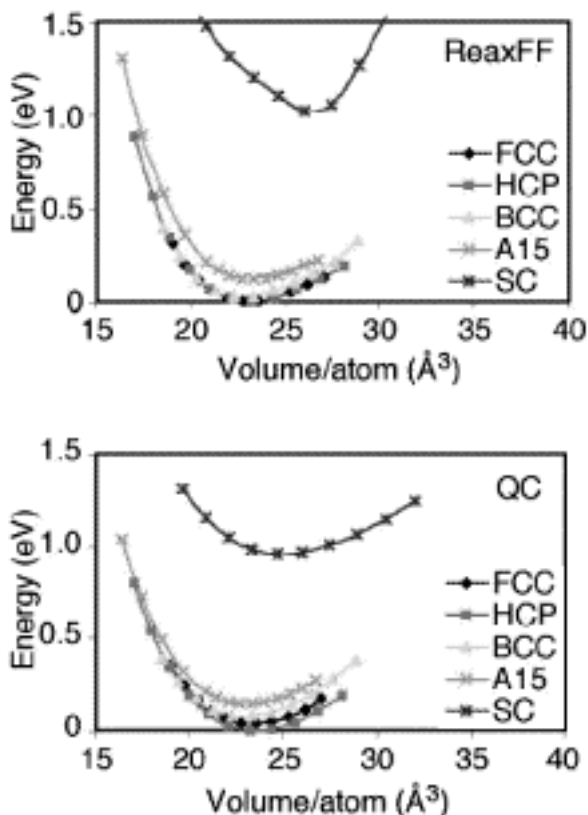


Figure 1. QM and ReaxFF Results for EOS of Various Zr-Polymorphs

Results

Theory. In the ReaxFF parameter optimization, most weight was given to the low-energy phases. For the high-energy phases, like simple cubic, we gave little weight to the QM EOS but rather focused on making sure that ReaxFF gets the correct energy with respect to the low-energy phases. Figure 1 shows an example of the QM data and the ReaxFF results for the Zr-metal. The figure demonstrates that ReaxFF provides a good reproduction of the QM EOS and relative energies for the stable metal polymorphs and properly predicts the unstable polymorphs to be higher in energy. Further optimization of the ReaxFF parameters will be performed, in particular, for better description of the EOS of the high-energy simple cubic metal phases.

We also performed QM calculations of EOS on the relevant metal oxides, such as ZrO_2 , Y_2O_3 , and BaO . ReaxFF should be completely defined in terms

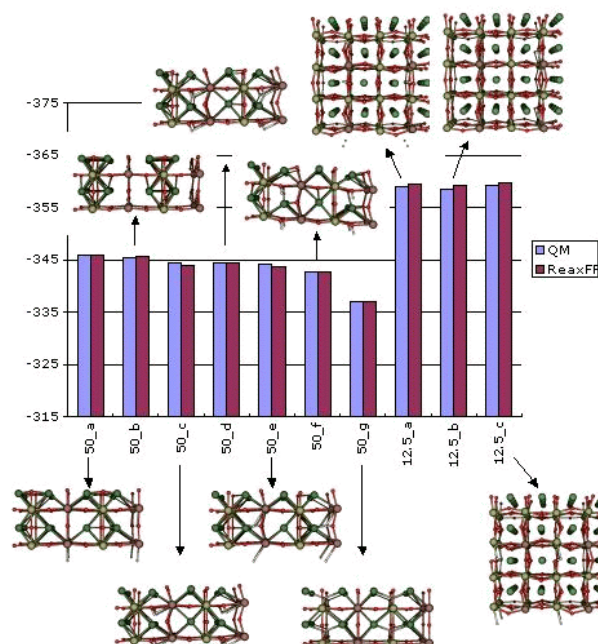


Figure 2. Heats of Formation (in kcal/mol) for Various Y-doped (50% and 12.5% mol) $BaZrO_3$ Structures

of geometry, i.e., each metal must be described in different polyhedral environments (tetrahedral, octahedral, cubic, etc.). Therefore, ReaxFF needs QM data not only for experimentally observed phases but also for some hypothetical phases, for instance, the rutile and BaF_2 phases for ZrO_2 , or the corundum phase for Y_2O_3 . Different phases have very different densities, and ReaxFF reproduces all these densities and energies very well.

In our development of initial ReaxFF potentials for BYZ, the main focus was to reproduce the QM relative energies and geometries for various structural configurations of BYZ in which the hydrogen atoms occupied various possible positions. As it is seen from Figure 2, we obtained good agreement between the QM and ReaxFF data for BYZ.

Experimental. Addition of 4 mol% ZnO in the form of a dispersed powder to an aqueous solution of barium, yttrium and zirconium nitrates then converted to oxides by the glycine-nitrate combustion process results in samples with 95% of theoretical density after sintering at only 1300°C for 4 hours. The bulk conductivity of Zn-modified BYZ is slightly lower (by about a factor of three) than that

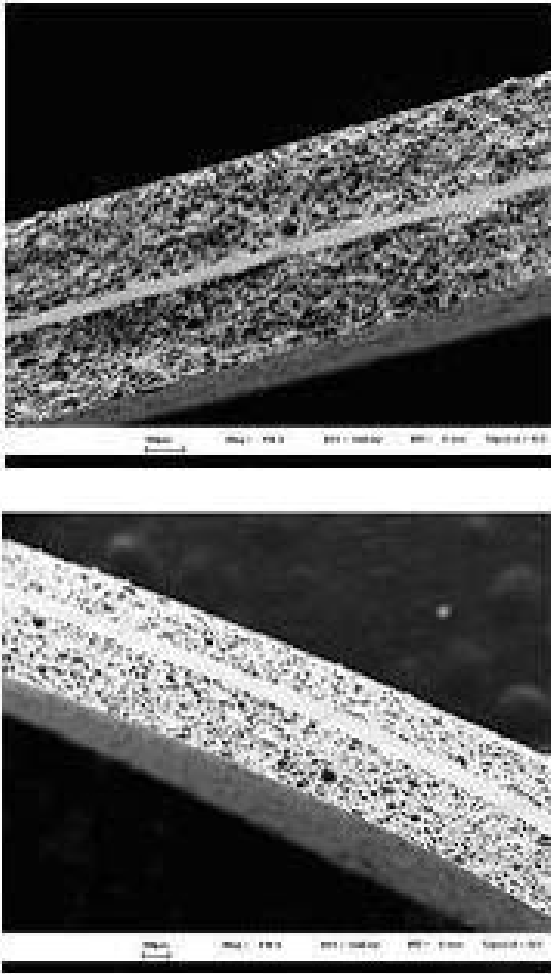


Figure 3. Cross Section of (left) 80 μm and (right) 40 μm BYZ Electrolyte Sandwiched between Porous BYZ Supports

of unmodified BYZ [4], whereas the specific grain boundary conductivities of the two types of materials are equivalent.

With BYZ densification protocols in hand, the next step has been to fabricate MEAs (membrane electrode assemblies) with thin electrolytes. A number of alternative approaches were attempted, including use of different metal oxides such as FeO , and even the direct use of metals such as Ni, Fe and NiAl in the anode support layer during the fabrication step. Ultimately, these attempts at direct incorporation of the metallic catalyst into the electrode layer were abandoned in favor of an approach in which a dense layer of BYZ is supported in between two porous layers of BYZ and the catalyst

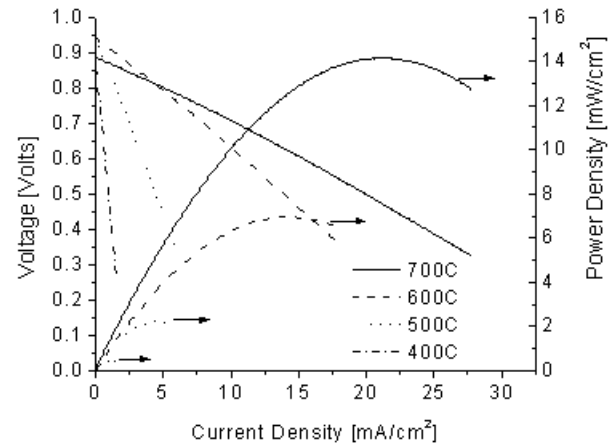


Figure 4. Polarization and Power Density Curves Obtained from a Pt | BYZ-4%ZnO | Pt Fuel Cell Exposed to Air at the Cathode and Water-Saturated Hydrogen at the Anode

material is deposited in a subsequent step. This fabrication route is particularly attractive for the investigation of a wide variety of electrocatalyst materials, as only the final deposition step need be modified for any new catalyst. Images of tri-layer structures obtained to date are shown in Figure 3.

Preliminary, 'proof of concept' fuel cell measurements have been conducted using 4 mol% Zn modified BYZ as the electrolyte. The MEA was comprised of a dense electrolyte, 400 μm in thickness, with Pt paste deposited on both faces to serve as the electrodes. The electrode active area was 0.71 cm^2 . MEAs were exposed to water-saturated hydrogen [$P(\text{H}_2\text{O}) = 0.03 \text{ atm}$] at the anode and air at the cathode. The results (see Figure 4) show that indeed reasonable power densities can be attained from BYZ cells, and as expected for this MEA configuration, the voltage losses are dominated by the thick electrolyte. In addition, the open circuit voltage (OCV) drops as temperature is increased, although the overall performance improves. The drop in OCV is a result of the increasing electronic conductivity of BYZ at elevated temperatures. It is also noteworthy that the presence or absence of water at either anode or cathode played a dramatic role in fuel cell performance, suggesting a catalytic role for H_2O in the electro-oxidation and reduction processes.

Conclusions

- QM calculations of EOS have been performed on various bulk metals (Pt, Zr, Y, Ba), metal alloys (Y/Zr, Y/Ba, Zr/Ba), metal oxides (ZrO_2 , Y_2O_3 , BaO) and BYZ. The obtained QM data were then used to optimize ReaxFF that allows large-scale MD simulations to study proton transport and the role of grain boundaries, defects, dopants, etc. in the BYZ electrolyte and the electrode/electrolyte interfaces.
- Fabrication protocols have been developed for high-density BYZ, both with and without transition metal modifiers, and for thin film membrane fuel cells. NiO, CuO and ZnO are the most effective additives for enhancing barium zirconate densification. The enhanced densification for the modified BYZ ceramics has been improved to 95% with refined mixing techniques.
- The conductivities and ionic transport numbers of high-density pellets have been measured. For the BYZ system with an average grain size of 1 μm , the total conductivity is dominated by the grain boundary until approximately 590°C, at which the total grain boundary and bulk conductivities intercept. Preliminary fuel cell polarization curves have been obtained from BYZ-based MEAs.

References

1. W. Kohn and L. J. Sham “Self-consistent equations including exchange and correlation effects” *Phys. Rev.* **140**, 1133A (1965).
2. J. P. Perdew, K. Burke and M. Ernzerhof “Generalized gradient approximation made simple” *Phys. Rev. Lett.* **77**, 3865 (1996).
3. D. Raczkowski, C. Y. Fong, P. A. Schultz, R. A. Lippert, and E. B. Stechel “Unconstrained and constrained minimization, localization, and the Grassmann manifold: Theory and application to electronic structure” *Phys. Rev.* **B64**, 155203 (2001).
4. H. G. Bohn and T. Schober “Electrical conductivity of the high-temperature proton conductor $BaZ_{0.9}Y_{0.1}O_{2.95}$ ” *J. Am. Ceram. Soc.* **83**, 768 (2000).

VI.2 Optimization and Demonstration of Solid Oxide Regenerative Fuel Cell (SORFC)

Jim McElroy (Primary Contact), Darren Hickey, Fred Mitlitsky

Ion America Corporation

Bldg. 543 NASA Research Park

PO Box 97

Moffett Field, CA 94035

Phone: (650) 964-6444 ext. 205; Fax: (650) 964-9474; E-mail: jmcelroy@ionamerica.com

DOE Project Manager: Lane Wilson

Phone: (304) 285-1336; E-mail: Lane.Wilson@netl.doe.gov

Objectives

- Development of electrode materials that can perform adequately in both the electrolyzer (charge) and fuel cell (discharge) modes, have long life, and are affordable.
- Development of novel thermal control schemes that allow for a high overall efficiency for the system by proper utilization of the heat generated.

Approach

- Establish a baseline SORFC performance with platinum-based electrodes in a button-sized cell.
- Perform screening tests on SORFC button cells with various non-noble metal-based electrodes.
- Perform lifetime tests on SORFC button cells having the best screening test results.
- Study thermal management approaches for storing exothermic fuel cell mode waste heat for use in endothermic electrolysis mode operation.

Accomplishments

- Established a baseline SORFC performance with platinum-based electrodes in a button cell at 71.6% initial electrochemical cycle efficiency (fuel cell voltage / electrolysis voltage) with a degradation rate (change in cycle efficiency) of 4% per 1000 hours after 800 operating hours and 26 charge/discharge cycles while operating at 100 mA/cm².
- Performed screening tests on a series of SORFC button cells with non-noble metal electrodes, establishing initial electrochemical cycle efficiency of 85% on the best variant.
- Performed lifetime tests on 14 SORFC button cells with non-noble metal electrodes and established performance stability within 0.5% per 1000 hours in the best variant.
- Downselected two candidate molten salt materials from a literature search^[1,2] and developed a thermodynamic model in ASPEN Plus for their use as phase change materials in planned thermal storage experiments.

Future Directions

- Attempt to optimize the selected SORFC button cells to obtain improved performance.
- Change to an electrolyte with higher ionic conductivity to resolve small differences in electrode catalysts.
- Design a larger footprint cell for stack testing.
- Conduct thermal storage experiments using one of the selected molten salts as a phase change material.

Introduction

The SORFC is a unique device that can efficiently produce and store energy. A single unit operates alternately as a fuel cell to produce electrical power and as an electrolyzer to split water into hydrogen and oxygen. Such an SORFC can be used for:

- Distributed electrical power peak shaving
- Remote off-grid energy storage combined with intermittent energy sources (wind, photovoltaic)
- On-grid energy management when combined with intermittent energy sources

In order to bring this concept closer to practical use, we are developing electrodes that can operate in both charge (electrolyzer) and discharge (fuel cell) modes. The cells are operated on diurnal cycles, and the electrodes that display the best combination of cycle efficiency and degradation will be selected for future stack testing. The project goal is to demonstrate electrochemical cycle efficiencies of 70% at 100 mA/cm². For operation at 200 mA/cm² in charge mode and 100 mA/cm² in discharge mode, the goal is 61.5% energy storage efficiency. Degradation rates are to be not more than 2% per 1000 hours in either operating condition.

SORFC system efficiency can be improved by storing exothermic fuel cell mode waste heat for use in endothermic electrolysis mode operation, which requires heat to maintain operating temperature. Novel approaches for thermal storage will be considered using molten salts that have high heat capacity and a melting temperature that occurs between the fuel cell and electrolysis operating temperatures. The project goal is to demonstrate a total system round-trip efficiency, which includes the thermal losses, of 67% at 100 mA/cm².

Approach

Electrode catalysts are tested using a platform that has demonstrated many thousands of hours of solid oxide fuel cell testing with very low failure rates. The electrolyte substrate consists of a 300 micron thick 8YSZ wafer 50 mm in diameter. The electrodes are applied onto the electrolyte using standard high-volume techniques with a total active area of 10 cm². The cells are sealed between

SORFC	100mA/cm ²		200mA/cm ²		300mA/cm ²	
Test	Cycle Efficiency	Degradation	Cycle Efficiency	Degradation	Cycle Efficiency	Degradation
Number	%	%/hrs	%	%/hrs	%	%/hrs
2 ^{Pt}	71.6	4				
5	81.8	20				
6	82.4	4				
7	82.5	1				
8	75.4	0.7				
9	78.0	1				
11	83.2	0.3				
13	81.6	0.5			52.3	0.5
14	81.8	0.8	66.2	2		
15	82.8	2	67.2	3		
16	82.2	2	66.5	2		

Figure 1. Degradation and Performance Results from the SORFC Life Cycle Tests. SORFC-014 was a repeat of SORFC-011. ^{Pt} Platinum baseline cell.

manifolds and compressed. Each cell is ramped up to temperature, and once the initial characterization experiments have been completed, the cell automatically cycles at 12-hour intervals. A complete polarization curve is automatically produced at every cycle change-over.

A variety of cells are produced with different combinations of electrode catalysts. All cells are initially screen tested over a short time to determine cycle efficiency and degradation trends. Cells that display acceptable performance parameters continue testing up to 750 hours and undergo 30 charge/discharge cycles. Once an optimum candidate is identified that meets the project goals, it will be repeated and possibly operated at higher current densities in order to examine its stability.

Results

The first two cells were tested using baseline platinum electrodes on both sides of the cell. SORFC-002 went through life cycle testing with initial cycle efficiency of 71.6% and a degradation rate of 4% per 1000 hours. All life cycle testing results are reported in Figure 1.

SORFC tests 003–016 have demonstrated the effects of various non-noble metal electrode catalysts. SORFC-007 operated for more than 1400 hours at high efficiency with a low degradation rate of 1% per 1000 hours. A very low degradation rate of 0.7% per 1000 hours was seen for SORFC-008 from start to finish; however, it performed at a lower efficiency.

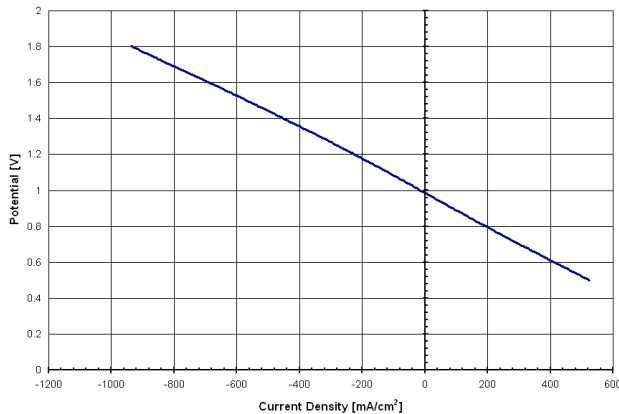


Figure 2. SORFC-016 Initial Polarization Curve at 120 Hours. The test conditions were 850°C, 30% steam under flooded conditions. Positive current represents the discharge or fuel cell mode, negative current represents the charge or electrolysis mode.

SORFC-011 produced the highest cycle efficiency to date with initial values of 85%. However, electrochemical stability was not obtained until 300-400 hours of operation, at which point the efficiency had dropped to 83.2%. After such time, the degradation rates were extremely good at less than 0.5% per 1000 hours. Because this catalyst configuration showed very good promise, it was repeated in SORFC-014, which again showed similar behavior at 100 mA/cm². At 500 hours, the current density was increased to 200 mA/cm² with a slight increase in degradation rate to approximately 2% per 1000 hours.

It has been encouraging to note that the degradation rate does not increase substantially with an increase in current density for certain catalyst combinations. The steady-state current density of SORFC-013 was tripled without any noticeable impact on the degradation rate. The latest cell tested was SORFC-016, which displayed a very good combination of performance and degradation. The initial polarization curve is shown in Figure 2; it exhibits almost a straight line characteristic from 0.5-1.8 V across the range from charge to discharge mode. It is this highly reversible characteristic which makes the solid oxide technology an ideal choice for regenerative applications. The life cycle plot can be seen in Figure 3, which indicates that

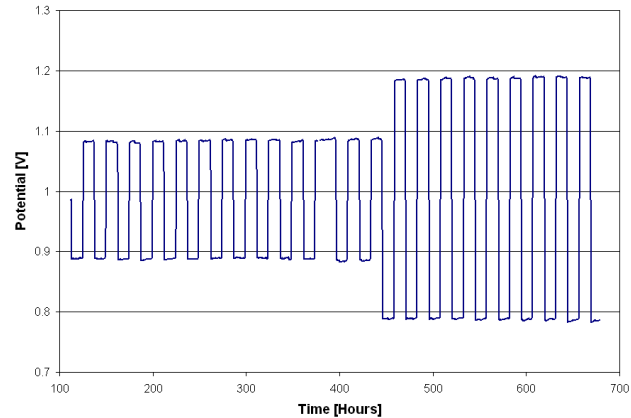


Figure 3. SORFC-016 Life Cycle Test at 850°C. The cell was operated at 100 mA/cm² from 120-450 hours, then at 200 mA/cm² from 450-680 hours. Potential above 1.0 V represents the charge or electrolysis mode, below 1.0 V represents the discharge or fuel cell mode.

doubling the current density to 200 mA/cm² did not increase the degradation rate.

Conclusions

- All cells tested have exceeded the project goal of 70% cycle efficiency at 100 mA/cm².
- All cells tested have exceeded the project goal of 61.5% cycle efficiency at 200 mA/cm² in both charge and discharge modes.
- Demonstrated one cell with a degradation rate that met the goal of 2% per 1000 hours operating at 200 mA/cm² in both charge and discharge modes.
- Demonstrated one cell with a degradation rate that exceeded the goal of 2% per 1000 hours operating at 300 mA/cm² in both charge and discharge modes.
- Seven cells have demonstrated degradation rates of not more than 2% per 1000 hours operating at 100 mA/cm² in both charge and discharge modes.

References

1. J.D. Whittenberger, "Tensile properties and structure of several superalloys after long-term exposure to LiF and vacuum at 1173 K," *J. Mater. Eng. Perf.* 4 (1995) 657-73.

2. U. Herrmann, M. Geyer, and D. Kearney,
“Overview on thermal storage systems,”
Workshop on Thermal Storage for Trough Power
Systems, February 20 - 21, (2002); [http://
www.eere.energy.gov/troughnet/pdfs/
uh_storage_overview_ws030320.pdf](http://www.eere.energy.gov/troughnet/pdfs/uh_storage_overview_ws030320.pdf)

VI.3 Direct Carbon Conversion Fuel Cell

John F. Cooper

Lawrence Livermore National Laboratory

PO Box 808, L-352, Livermore CA 94550

Phone: (925) 423-6649; Fax: (925) 422-0049; E-mail: cooper3@LLNL.gov

DOE Project Manager: Travis Shultz

Phone: (304) 285-1370; E-mail: Travis.Shultz@netl.doe.gov

Objectives

- Determine voltage and utilization efficiencies of carbon anodes, in the form of pastes and rigid plates, and define conditions necessary for high efficiencies.
- Examine feasibility of 80% efficient fuel cell conversion of de-ashed coal chars.
- Develop a single-unit process for coal thermal decomposition to chars and high-BTU gas and electrochemical conversion of the chars at 80% efficiency.

Approach

- Construct experimental cells for determining polarization and offgas composition.
- Measure conversion efficiency of chars from decomposition of non-agglomerating coal powders that have been chemically de-ashed to <0.3% ash.
- Devise and analyze a simple process for pyrolysis of non-agglomerating coal powder and electrochemical conversion of chars using industrial data for component costs and published literature for pyrolysis rates and products.

Accomplishments

- Measured CO₂/CO ratios in anode offgas, finding agreement with published studies for planar carbon anodes, indicating CO₂ product for >0.1 V polarization.
- Measured electrode polarization in carbon/air cells using porous Ni cathodes and chemically de-ashed non-agglomerating coal, finding 0.8 V at 1 kA/m².
- Developed a fuel cell design providing for decomposition of coal particles producing H₂-rich gas and anode fuel char, with stack cost <\$500/kW.

Future Directions

- Model current/potential distribution within porous carbon blocks and pastes, and predict CO₂/CO ratios and utilization efficiencies of direct carbon fuel cells (DCFCs) for powdered coal beds as function of compaction and scale; test predictions experimentally.
- Determine techno-economic potential for conversion of chars from chemically de-ashed non-agglomerating sub-bituminous coal, and for conferring such properties to higher ranks of coal by modifying surface functional groups.
- Construct and test a 100-W segment of an advanced configuration for simultaneous pyrolysis of de-ashed coal (producing high-BTU, H₂-rich offgas) and conversion of the residual coal char to electric power at 80% efficiency.

Introduction

We are continuing studies of the direct carbon fuel cell (DCFC) that consumes elemental carbon (or coal chars) and oxygen to generate electric power.¹⁻³ Figure 1 shows a promising configuration that combines coal pyrolysis (to form a high-BTU gas and a conductive carbon char) and power generation into a single-unit process.^{4,9} The DCFC operates at 750-800°C using alkali carbonate eutectics and a cathode similar to that of the molten carbonate fuel cell (MCFC). The porous separator is a melt-saturated ceramic. Neither rate nor efficiency depends on composition of the carbon anode. Rather, structural disorder is required. A total efficiency of 80% (ref. HHV of carbon, 33 MJ/kg-C, -94.05 kcal/mol) is achievable at 30-500 mA/cm² for more than 20 diverse carbon materials having disordered nanostructure and small domain sizes of micro-crystallinity. Such “turbostratic” properties are often found with products of low-temperature hydrocarbon pyrolysis and with coal or biomass chars. Reaction mechanisms on planar carbon anodes yield CO₂ (not CO) when anode overpotential exceeds roughly 0.1 V.^{7,3} The efficiency of the DCFC derives from two thermodynamic aspects of the net cell reaction:



The entropy change is nearly zero, allowing theoretical efficiency ($\Delta G_T/\Delta H^\circ_{298}$) of 100%. Activities of the carbon and CO₂ in the anode chamber are invariant, fixing anode potential independent of position in cell or extent of conversion. This simplifies thermal management and allows full utilization of the carbon fuel in a single pass.

Hauser⁶, Weaver⁷, and Vutetakis⁸ studied graphite and coke plates or slurries of particles of coal. They found current densities (at fixed polarization $E_a = -0.8\text{ V vs. Au/CO}_2, \text{O}_2$) to vary by factors of up to 10⁴ between specular graphite anode rods and porous coal or lignite chars. Hauser and Weaver found that the coulombic efficiency for CO₂ evolution approaches 100% at overpotentials >0.1 V for graphite and coke, despite the equilibrium of the Boudouard reaction ($\text{C} + \text{CO}_2 = 2\text{CO}$) that predicts predominately CO at $T > 730^\circ\text{C}$. We related reactivity to a crystallinity factor measuring disorder,

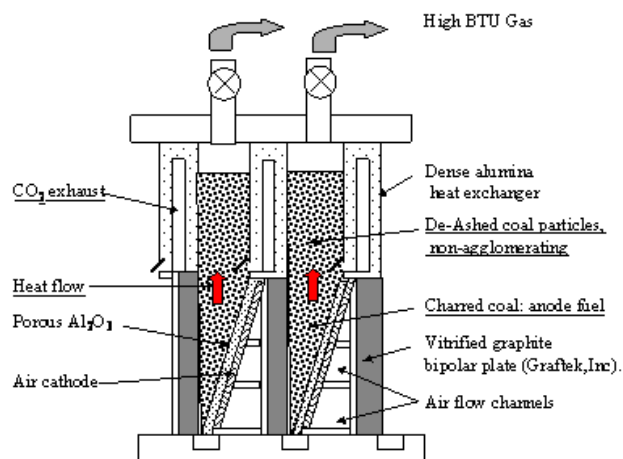


Figure 1. Conceptual Design of a Carbon Fuel Cell that Thermally Decomposes De-Ashed, Non-Agglomerating Coal Particles in an Overlying Chamber Using Waste Heat from the Cell

and CO₂ product to the potential-dependent adsorption of CO onto reactive sites.³

Approach

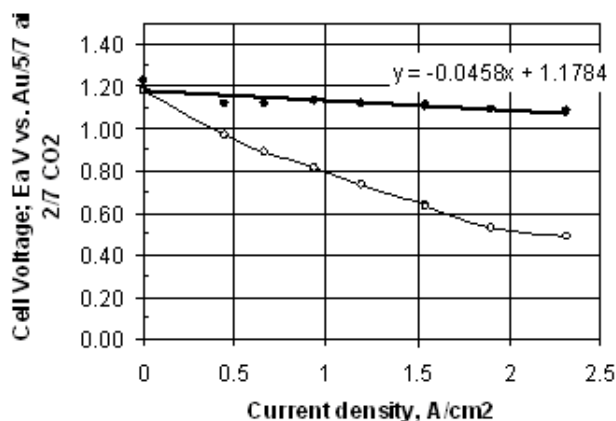
(1) We determine coulombic efficiency for paste anodes by collection and analysis of offgas and compare with planar electrodes. (2) We measure polarization and decomposition rates on samples of low-cost chemically de-ashed coal particles that may be pneumatically distributed. (3) We formulate a simple configuration that both thermally decomposes non-agglomerating coal (to produce a high-BTU gas) and converts the char product to electric power. (4) We estimate costs from industrial suppliers of the components.

Results

Table 1 presents CO/CO₂ ratios for planar carbon electrodes (baked pitch smelter anode, Alcoa) and a solvent extract powder electrode (WVU/SECO; low ash; calcined 800°C). These preliminary results indicate predominant CO₂ product at high polarizations, but primarily CO at low polarizations. These results support findings of suppression of Boudouard corrosion at high polarizations,^{6,7} but show that achieving high utilizations on pastes is impeded because of the lower local current density and polarization on a

Table 1. CO/CO₂ Ratios for Planar and Powdered Forms of Coal-derived Pitch

Sample	T (°C)	Overpotential (V)	CO/CO ₂
Baked pitch anode (Alcoa smelter anode)	754	0.159	0.038
Same as above	775	0.149	0.037
WVU/SECO, low ash extract, 800°C calcine; fine particles	774	0.036	13.7
Same	773	0.01	29

**Figure 2.** Typical Cell Performance of Non-Agglomerating Sub-Bituminous Coal Char, Chemically De-Ashed by Bayer Process Digestion of the Ash Impurities

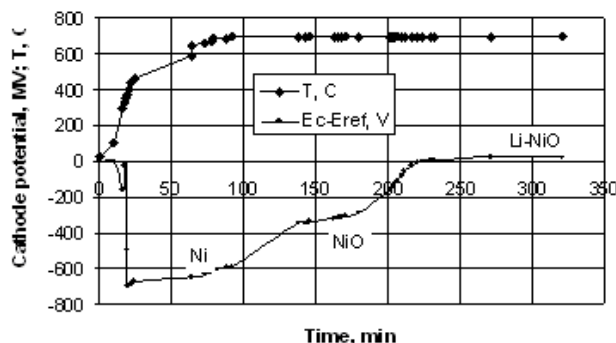
fine particle bed. In the remainder of this project, we will attempt to increase particle bed polarization by various means (see below).

The cell polarization is given in Figure 2 for sub-bituminous coal that is chemically de-ashed to 0.17-0.27%, non-agglomerating (non-tarring), and low in cost (\$3/GJ, \$96/ton).⁵ These properties facilitate distribution of fuel to multiple cells, *in situ* decomposition to high-BTU gas, and extended electrolyte life (>1 year). Table 2 decomposes the cell voltage with a pyrolyzed powdered coal sample. The majority of cell losses are associated with the air electrode, which does not show the performance achieved in the MCFC.¹⁰ Poor performance may result from too-rapid and incomplete activation of the 1-mm Ni porous cathode (Figure 3), compared with.

Table 2. Distribution of Potentials in Current Cell Tests and Required Modifications for Acceptable Total Voltage Efficiency (>0.8 V) at 0.1 A/cm² and 750°C

	UCC coal ^a	Goal ^b	Maximum ^c
Current density, A/cm ²	0.1	0.1	0.1
Anode loss, V	0.046	0.134	0.11
Cathode loss, V	0.15	0.06	0.03
IR loss in separator (calculated)	0.022 ^d	0.02	0.008
Sum of cell losses	0.218	0.214	0.148
Cell voltage	0.8	0.81	0.87
Total efficiency, % HHV	--	81	87

^a UCC, Pty. Ltd. deep de-ashed sub-bituminous coal⁴, pyrolyzed at 650°C for 45 min; tested at 754°C; utilization not measured.
^b Performance to meet goal of 80% HHV efficiency at 0.1 A/cm².
^c Projected efficiency: cathode loss = 0.03 V, 1 mm separator 50% void, $k = 2.5 \Omega^{-1}\text{cm}^{-1}$.
^d 2 mm separator, 50% void, $k = 1.8 \Omega^{-1}\text{cm}^{-1}$.

**Figure 3.** Activation of Porous Nickel Air Cathode by Sequential Film Formation and Lithiation

the 100 hour activation procedure employed elsewhere.¹¹

Conclusions

While tests with chemically de-ashed coal and other pyrolyzed coal chars yielded acceptable current densities at 0.8 V, the anode polarization was too low to achieve a full conversion to CO₂ when the anode was a thick paste. Relative contributions of separator, cathode and anode to total voltage

indicated that the cathode has a loss in our tests of about 0.15 V—far higher than the 0.03-0.06 V losses reported for nickel cathodes elsewhere.^{10,11} Anode overpotential (at cell voltages of 0.8 V) may also be increased to >0.1 V by partial compaction of the particles, limiting the thickness of the anode, back current collection, and improved cathode polarizations enabling higher total currents—techniques to increase the flux to the reacting surface. Our focus is on chemically de-ashed non-agglomerating coal because of ease of pneumatic feed, minimal impact on electrolyte and low cost. The most favorable configuration for a DCFC for coal conversion appears to be a single-unit process that pyrolyzes non-agglomerating coal *in situ* using kinetic heat, producing a H₂-rich offgas and a coal char anode that is then fully converted. Costs are estimated below \$500/kW based on components. An independent study of the economics of DCFC indicated competitive applications for large industrial users of DC and in distributed power, when efficiency is enhanced by simplicity and cost is low.⁹

References

1. J. F. Cooper, N. Cherepy, G. Berry, A. Pasternak, and T. Surles, "Direct Carbon Conversion: Application to the Efficient Conversion of Fossil Fuels to Electricity," (Proc. Global Warming Conference, PV 20-2000, The Electrochemical Society April 2001).
2. John F. Cooper, "Direct Conversion of Coal and Coal-Derived Carbon in Fuel Cells," Keynote Address, Fuel Cell Science, Engineering and Technology, ASME, June 14, 2004; No. 2495. FuelCell2004-2495.
3. N. Cherepy, J. F. Cooper, et al., "Direct Conversion of Carbon in Molten Carbonate Fuel Cells," paper accepted by J. Electrochemical Society; preprint UCRL-JRNL-202412, February 25, 2004.
4. John F. Cooper, "Conversion of raw carbonaceous fuels," US patent pending, July 23, 2004.
5. Supplied by UCC Energy Pty. Ltd. (N. Sydney, NSW Australia) and marketed as a non-abrasive particulate turbine fuel; UCC Energy uses Bayer process chemistry for digestion of solid ash inclusions.
6. Hauser, Victor Emerald, 1964, A study of carbon anode polarization in fused carbonate fuel cells, Ph.D. Thesis, Oregon State University, June 1964.
7. Weaver R. D., S. C. Leach, A. E. Bayce and L. Nanis, 1979, Direct Electrochemical Generation of Electricity from Coal, Report May 16, 1977-Feb. 15; SRI, Menlo Park, CA 94025; SAN-0115/105-1.
8. Vutetakis, D. J., 1985, Electrochemical oxidation of carbonaceous materials dispersed in molten salt, Ph.D. Dissertation, Ohio State University, Columbus, OH.
9. Ron Wolk, "Direct Carbon Fuel Cells: Assessment of their Potential as Solid Carbon Fuel Based Power Generation Systems", Wolk Integrated Services, San Jose, CA; reported UCRL-SR-203880, April 9, 2004.
10. K. Kinoshita, *Electrochemical Oxygen Technology* (p. 213, UTC data; John Wiley & Sons, 1992).
11. Mehmet Suha Yazici, Oxidation and corrosion of metals and alloys by molten carbonate: electrochemical studies and in-situ observation, Ph.D. Thesis IIT 1996 (Selman).

FY 2004 Publications/Presentations

1. John F. Cooper, "Direct Conversion of Coal and Coal-Derived Carbon in Fuel Cells," Keynote Address, Fuel Cell Science, Engineering and Technology, ASME, June 14, 2004; No. 2495. FuelCell2004-2495.
2. N. Cherepy, et al., "Direct Conversion of Carbon in Molten Carbonate Fuel Cells," paper accepted by J. Electrochemical Society; preprint UCRL-JRNL-202412, February 25, 2004.
3. John F. Cooper, "Direct Conversion of Carbon and Fossil Fuel Chars in Fuel Cells and Batteries," Invited seminar, The Gordon Conference; Roger Williams University, Bristol, RI, July 24-30, 2004.

Special Recognitions & Awards/Patents Issued

1. Invited Keynote Address at 2nd International Fuel Cell Conference, American Society of Mechanical Engineers, Rochester, NY, June 14-17, 2004. Session Chair.
2. Invited Paper on Direct Carbon Conversion Fuel Cell, the Gordon Conference, July 24-30, 2004.
3. Patent allowed, John F. Cooper, R. Krueger, and N. Cherepy, "Fuel Cell Apparatus and Method Thereof," 2004. Four additional patent applications or preliminary applications filed.
4. US patent pending, "Conversion of raw carbonaceous fuels," July 23, 2004.

VI.4 High Temperature Electrochemistry Center

LR Pederson (Primary Contact), GW Coffey, A Marina, GL McVay, CD Nguyen, PC Rieke, P Singh, SC Singhal, and EC Thomsen

Pacific Northwest National Laboratory

PO Box 999

Richland, Washington 99352

E-mail: larry.pederson@pnl.gov

DOE Program Manager: Lane Wilson

Phone: (304) 285-1336; E-mail: Lane.Wilson@netl.doe.gov

Subcontractors:

Montana State University

Lee Spangler (Primary Contact)

207 Montana Hall

Bozeman, Montana 59717

University of Utah

AV Virkar (Primary Contact)

201 South Presidents Circle

Salt Lake City, Utah 84112

Objectives

- In collaboration with university partners, provide crosscutting, multidisciplinary research that supports the FutureGen Initiative to improve efficiency and minimize the environmental consequences of electric power generation from coal.
- Develop reversible solid oxide fuel cell (SOFC) technology capable of efficiently producing hydrogen in an electrolyzer mode as well as producing electrical power from stored hydrogen in the fuel cell mode.
- Develop high-temperature membranes aimed at separation of hydrogen from gasified coal and other complex mixtures.
- Improve fundamental understanding of reactions and processes that occur at the electrode-electrolyte-gas interface, critical to the operation of a wide range of electrochemical technologies including fuel cells, electrolyzers, sensors, and gas separation membranes.
- Develop corrosion-resistant thin films to extend the lifetime of metallic fuel cell interconnects (Montana State University).
- Develop tools necessary to monitor and model the response of fuel cells to transient electrical loads, and design power electronics modules to improve the performance and efficiency of fuel cells integrated with multiple power sources (Montana State University).

Approach

- Develop alternative fuel and air electrodes for use in reversible fuel cells that minimize overpotential losses, a major source of inefficiency in fuel cells and electrolyzers.
- Develop cerate-based ceramic-ceramic and cermet composite electrodes and forms to separate hydrogen from gasified coal at high temperatures and pressures.
- Utilize micropatterned electrode structures as a means of probing fundamental electrocatalytic reaction mechanisms.

- Assess the efficacy of multilayer nitride films in improving the corrosion resistance of metallic interconnect materials.
- Employ unique load monitoring and modeling methods to enhance a fuel cell system to respond to specific transient electrical loads.

Accomplishments

- Cerate-titanate composite fuel electrodes were developed that provide better reversible performance than standard nickel/zirconia compositions.
- A stable defect structure was shown to be an important consideration in selecting an air electrode composition for reversible fuel cells.
- Cerate-ceramic and cerate-metal composite membranes were fabricated and hydrogen permeability evaluated. The materials show promise for the separation of hydrogen from gasified coal.
- A model was developed that allows a fuel cell system to recognize and react to specific transient electrical loads.
- Multilayer chromium nitride/aluminum nitride coatings have been developed that inhibit the oxidation of steel interconnect materials and provide improved area-specific resistances.

Future Directions

- Construct and demonstrate a planar, reversible fuel cell stack constructed with optimized air and fuel electrode compositions and forms to minimize overpotential losses.
- Demonstrate the separation of hydrogen from gasified coal using a cerate-based, asymmetric composite membrane.
- Demonstrate the efficacy of cluster training methods in enhancing the transient load-following of a solid oxide fuel cell system.
- Evaluate the efficacy of multilayer nitride coatings on metallic interconnect materials in a planar solid oxide fuel cell stack.
- Employ advanced x-ray techniques to probe interfacial defect chemistry at the air electrode of an operating high-temperature electrochemical cell.

Introduction

The High Temperature Electrochemistry Center (HiTEC) was created in 2002 to provide crosscutting, multidisciplinary research that supports the Office of Fossil Energy's FutureGen Initiative. The National Energy Technology Laboratory (NETL), Montana State University (MSU), and the Pacific Northwest National Laboratory (PNNL) currently are the principal contributors to HiTEC. Collaborative research has also been established with the University of Utah in the study of fundamental reaction mechanisms involving the air electrode, the University of Missouri at Rolla on electrode microstructure changes due to defect chemistry gradients, and the University of Karlsruhe (Germany) on reversible fuel cells. Research topics

expected to be addressed by this project include energy conversion, hydrogen production, gas separation and purification, electrolysis, energy storage, emissions reduction, sensors, and low-cost materials processing technologies. Additional collaborations with other universities are planned, focusing on specific topical areas where new scientific knowledge and innovations are needed to overcome the technical challenges being addressed by the FutureGen Initiative.

Current research activities being conducted at PNNL include the development of low-loss electrodes for reversible solid oxide fuel cells, the development of high-temperature membranes for hydrogen separation, and studies of fundamental electrochemical processes at interfaces. Research

activities at MSU include the development of dynamic models of fuel cell systems for distributed generation applications, development of adaptive power controllers for fuel cells, the development of multilayer thin-film coatings to improve the corrosion resistance of interconnect materials, and advanced x-ray studies of buried interfaces. Because of the high priority given to the development of reversible fuel cell technology, this portion of the research is emphasized.

Approach

The reversibility of the fuel electrodes, nickel/zirconia cermet and lanthanum-doped strontium titanate/ceria composite, on an yttria/zirconia electrolyte was examined using electrochemical impedance spectroscopy and current interrupt methods. Lanthanum-doped SrTiO_3 is an n-type semiconductor under reducing conditions. When combined with the doped ceria, it exhibits excellent electrocatalytic activity towards hydrogen [1]. It has also been shown to possess good dimensional and chemical stability when exposed to oxygen [1] [2]. Here, the ceria phase was doped with La as well as Group 5a metals Nb and Ta to enhance the electrical conductivity. The reversibility of lanthanum ferrite, lanthanum copper ferrite, lanthanum cobalt ferrite and lanthanum manganite air electrodes was also evaluated using similar techniques.

To develop an adaptive power control scheme that would allow fuel cell systems to react to rapid transient loads, non-intrusive load monitors were employed to disaggregate currents measured at a central location. Such monitors are capable of associating disaggregated current transients with individual loads. Characteristic transient loads emanating from common devices were established, providing the basis for adaptive power control through pattern recognition.

Multilayer coatings consisting of alternating layers of chromium nitride and aluminum nitride were deposited onto 304 and 440 stainless steels and onto Crofer grade APU 22. After exposure to air at 800°C for varying periods, the corrosion layer was analyzed by Rutherford backscatter, nuclear reaction analysis, x-ray photoelectron spectroscopy, analytical electron microscopy, and atomic force microscopy.

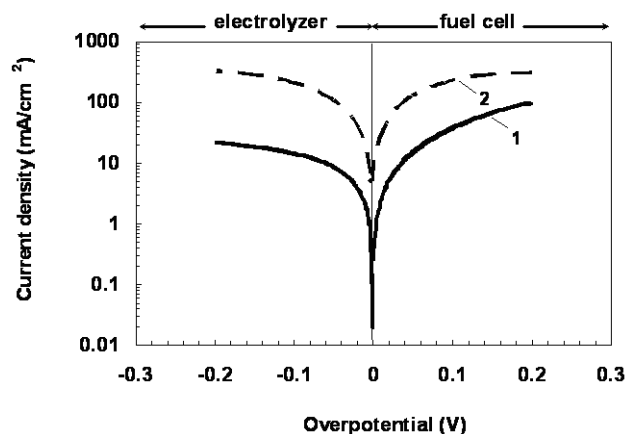


Figure 1. A cerate-titanate composite electrode provided higher reversible current densities than a standard Ni-YSZ fuel electrode in dilute hydrogen/steam mixtures. Current-potential characteristics were obtained for Ni-YSZ (1) and $\text{La}_{0.35}\text{Sr}_{0.65}\text{TiO}_3\text{-Ce}_{0.5}\text{La}_{0.5}\text{O}_{1.75}$ (2) electrodes at 900°C and $\text{H}_2/\text{H}_2\text{O}/\text{N}_2 = 2.75/3/94.5$.

Changes in area specific resistance due to exposure to air at high temperatures were also assessed.

Results

A ceramic composite electrode was shown to have better reversible activity than standard Ni-YSZ (yttria-stabilized zirconia) electrodes. Current-potential characteristics were obtained on Ni-YSZ and titanate/ceria composite electrodes at 900°C at a steam-to-hydrogen ratio of around 1, as is shown in Figure 1. Both electrodes can catalyze not only hydrogen oxidation, but the reverse reaction, electrochemical decomposition of water, as well. Under the experimental conditions studied, the titanate/ceria electrode is noted to perform substantially better than state-of-art Ni/YSZ in both the fuel cell and electrolysis modes. The nickel-based electrode shows somewhat better performance in the fuel cell mode compared to that in the electrolyzer mode. The ceramic composite shows slightly higher activity for water electrolysis compared to hydrogen oxidation.

The cerate-titanate composite fuel electrode operates at higher capacity in the electrolyzer mode than in the fuel cell mode. High hydrogen partial pressures also resulted in higher electrode activity.

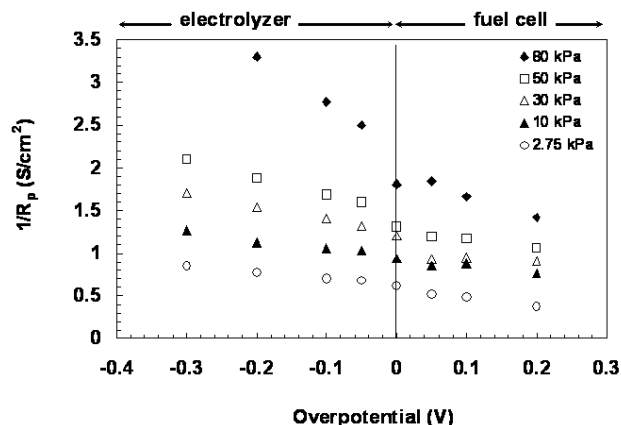


Figure 2. Effect of overpotential on polarization resistance of $\text{La}_{0.35}\text{Sr}_{0.65}\text{TiO}_3\text{-Ce}_{0.6}\text{La}_{0.4}\text{O}_{1.8}$ oxide electrode vs. Pt/air at 850°C at different hydrogen partial pressures and a $p\text{H}_2\text{O} = 31$ kPa. The cerate-titanate composite electrode shows slightly better activity when operated as an electrolyzer than as a fuel cell

Figure 2 illustrates the effect of electrode overpotential on the reciprocal polarization resistance, R_p , of the titanate/ceria electrode in the wide range of hydrogen partial pressures, $p\text{H}_2$. It is seen that the R_p increases slightly in the fuel cell mode and decreases in the electrolyzer mode for all $p\text{H}_2$ analyzed. It is apparent that the ceramic composite demonstrates good reversibility in the wide range of hydrogen partial pressures.

High steam partial pressures diminished the activity of the cerate-titanate composite electrode, as shown in Figure 3. A gradual increase in the steam partial pressure resulted in increased electrode polarization losses in both electrolyzer and fuel cell modes. It should be noted that hydrogen partial pressure was somewhat decreased in this test as well, which might contribute to the outcome. For the highest steam pressure given (80 kPa), only rather poor electrode performance was observed. This could be due to too low $p\text{H}_2$ in the feed gas resulting in partial loss of electrical conductivity of the titanate/ceria composite. Indeed, subsequent increasing hydrogen partial pressure improved electrode performance, although the initial activity value has not been achieved.

Most air electrodes are found to perform considerably less well in the electrolysis mode than

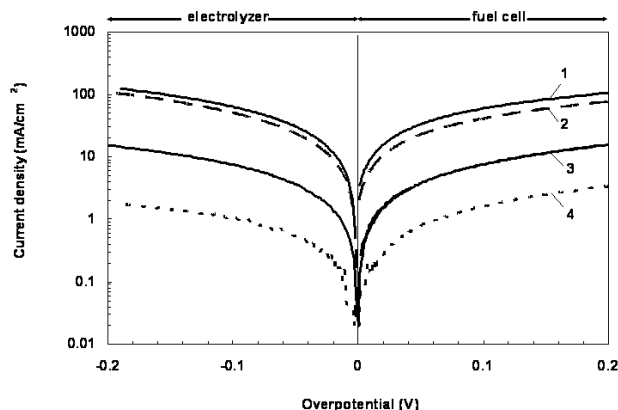


Figure 3. Overpotentials measured for the cerate-titanate composite electrode were found to increase with increased steam content in both fuel cell and electrolysis modes. Similar behavior was observed for Ni-YSZ fuel electrodes, though at lower current density. Current-overpotential dependencies obtained on ceramic $\text{La}_{0.35}\text{Sr}_{0.65}\text{TiO}_3\text{-Ce}_{0.98}\text{Ta}_{0.02}\text{O}_2$ electrode at 900°C in $\text{H}_2/\text{H}_2\text{O}/\text{N}_2 = 2.7/3/94.3$ (1), $\text{H}_2/\text{H}_2\text{O}/\text{N}_2 = 2/24/74$ (2), $\text{H}_2/\text{H}_2\text{O}/\text{N}_2 = 1.7/40/58.3$ (3), and $\text{H}_2/\text{H}_2\text{O}/\text{N}_2 = 0.8/80/19.2$ (4).

in the fuel cell mode. As such, the air electrode may be the major cause of inefficiencies in a reversible fuel cell. Results for lanthanum ferrite with 20 percent strontium substitution for lanthanum (LSF-20), a very active SOFC electrode, are given in Figure 4. Under electrolysis conditions, where the local oxygen partial pressure can be very high, oxygen vacancy populations and therefore mixed conductivity are substantially lessened, leading to diminished electrocatalytic activity. Oxygen defect stability is thus an important characteristic in choosing a reversible air electrode.

A novel adaptive power control scheme is under development at MSU that would allow a fuel cell system to recognize and respond to characteristic transients introduced by various appliances. Non-intrusive load monitors developed at MSU were employed to disaggregate currents associated with a specific load. These transient recognition techniques were shown to substantially stabilize fuel cell stack output currents and potentials, typically in less than 10 milliseconds. Without this approach, significant oscillations in current and voltage levels from the same stack continued to hundreds of milliseconds.

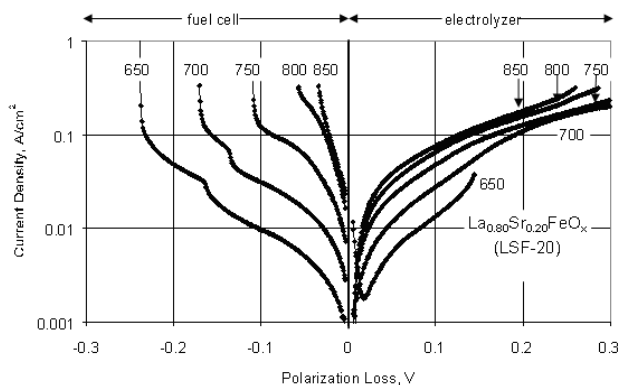


Figure 4. Cathodic and anodic overpotentials versus current density for LSF-20 on YSZ with a 3 micron thick samaria-ceria interlayer. Decreased oxygen vacancies under locally high oxygen partial pressures in the electrolyzer mode are responsible for lowered electrode performance.

This research is intended to address the inherently slow response of fuel cell systems due to slow internal chemical reactions.

Multilayer chromium nitride/aluminum nitride coatings have been shown at MSU to substantially improve the area specific resistance (ASR) of metallic interconnect materials compared to uncoated interconnects. The absolute ASR as well as the rate of growth in that parameter were found to be improved by the presence of the coating. The parabolic ASR growth rate constant (units of $m^2\text{-cm}^2\text{-h}^{1/2}$) was measured at 0.169 for an uncoated Crofer 22 APU steel specimen, 0.024 for a chromium nitride/aluminum nitride coating composed of 1.1-nanometer bilayers with a total coating thickness of 1.2 microns, and 0.037 for a similar coating composed of 4.5-nanometer bilayers with a total coating thickness of 1.6 microns. Though a corrosion scale still formed on coated steel specimens following prolonged exposure to air at high temperature, the scale was thinner and less resistive than that which is formed when coatings are not present.

Conclusions

- Ceramic fuel electrode compositions have been identified that exhibit improved reversible behavior compared to standard materials.

- The performance of air electrodes is diminished in an electrolyzer compared to a fuel cell due to defect structure instability.
- An adaptive power control approach has been developed that allows fuel cell systems to better respond to load transients.
- Multilayer coatings have been developed that substantially improve the corrosion resistance of metallic interconnect materials.

References

1. O.A. Marina, N. Canfield, J.W. Stevenson, *Solid State Ionics* 149:21 (2002).
2. O.A. Marina, L.R. Pederson, in 5th European Solid Oxide Fuel Cell Forum, Vol. 1 (J. Huijsmans, ed.), European Fuel Cell Forum, Lucerne, Switzerland, 2002, p. 481.

FY 2004 Publications/Presentations

1. Zheng F, Bordia RK, and Pederson LR. "Phase constitution in Sr and Mg doped LaGaO₃ system." *Mater. Res. Bull.* 39 (1): 141-155 JAN 3 2004.
2. Coffey GW, Pederson LR, and Rieke PC. "Competition between bulk and surface pathways in mixed ionic electronic conducting oxygen electrodes." *J. Electrochem. Soc.* 150 (8): A1139-A1151 2003.
3. Williams MC, Marina OA, Coffey GW, Pederson LR, Rieke PC, and Thomsen EC. "Electrode development for reversible solid oxide fuel cells." *J. Electrochem. Soc.* 2004 (submitted).
4. Radhakrishnan R, Jiang Y, Marina OA, Virkar AV, and Singhal SC. "Determination of cathodic polarization resistance of LSM/YSZ using patterned electrodes." *Solid State Ionics* 2004 (in press).
5. Shaw SR, Keppler M, and Leeb SB. "Pre-estimation for better initial guesses. *IEEE Trans. Instrumentation and Measurement* 53 (3): 762-769 2004.

6. Smith RJ, Tripp C, Knospe A, Ramana CV, Kayani A, Gorokhovskiy V, Shuffhanandan V, and Gelles DS. "Using CrAlN multilayer coatings to improve oxidation resistance of steel interconnects for solid oxide fuel cell stacks." J. Materials Engineering and Performance 13 (3): 295-302 JUN 2004.

Special Recognitions & Awards/Patents

Issued

1. Patent Application 190527/2. "Copper-Substituted Perovskite Compositions for Solid Oxide Fuel Cell Cathodes and Oxygen Reduction Electrodes in Other Electrochemical Devices." Pederson LR, Coffey GW, Marina OA, Rieke PC, Singh P, and Thomsen EC.
2. Patent Application 12776-E. "Novel Composite Solid Oxide Fuel Cell Anode Based on Ceria and Strontium Titanate." Marina OA and Pederson LR.

VI.5 Active Cathodes for Super-High Power Density Solid Oxide Fuel Cells through Space Charge Effects

Anil V. Virkar

University of Utah

Department of Materials Science & Engineering

122 S. Central Campus Drive

Salt Lake City, UT 84112

Phone: (801) 581-5396; Fax: (801) 581-4816; E-mail: anil.virkar@m.cc.utah.edu

DOE Project Manager: Lane Wilson

Phone: (304) 285-1336; E-mail: Lane.Wilson@netl.doe.gov

Objectives

- To synthesize doped CeO₂ and ZrO₂ nanosize powders containing several dopants chosen for the purpose of manipulating space charge effects.
- To synthesize nanosize powders of mixed ionic electronic conducting (MIEC) electrocatalysts.
- To form partially sintered, porous compacts and fully dense compacts, and determine their transport properties (conductivity) as a function of temperature and grain size.
- To identify suitable materials combinations for prospective composite cathodes comprising two-phase mixtures of an ionic conductor and an electrocatalyst.
- To develop a theoretical model embodying space charge effects in polarization resistance, R_p .
- To fabricate and test performance of anode-supported single cells with composite cathodes, based on space charge effects, over a range of temperatures from 500 to 800°C.
- To measure and characterize cathode polarization. Relate R_p to space charge effects.

Approach

- Synthesize nanosize, doped CeO₂ and ZrO₂ powders. Fabricate dense and porous samples of doped materials. This is to be accomplished by varying sintering and annealing temperatures.
- Select and synthesize electrocatalysts for composite cathodes.
- Fabricate anode-supported cells with composite cathodes.
- Investigate dependence of conductivity of porous and dense samples on grain size: space charge effects. Conductivity will be measured using four-probe DC technique.
- Develop a model for conduction through porous bodies by taking into account grain boundary transport, morphology (neck size between particles) and space charge layer.
- Test anode-supported cells; characterize cathodes.
- Analyze the effects of space charge on cathodic polarization.

Accomplishments

- A theoretical model was developed which relates ionic conduction through porous bodies to morphology, grain boundary transport, grain size, and space charge layer thickness. It was demonstrated that the relative neck size has a profound effect on ionic conduction.
- Two processes were developed for the fabrication of porous samples with widely varying porosities and widely varying neck sizes. Process 1: Sintering of samarium-doped ceria (SDC) powder compacts over a range of temperatures to obtain porosity levels between ~4% and ~52%, the latter with narrow necks.

Process 2: Sintering of NiO + SDC samples, followed by reduction of NiO to Ni and subsequent leaching of Ni to generate porosity levels between ~31% and ~54%, with wide necks.

- Ionic conductivity of porous SDC samples made by the two different processes was measured. It was demonstrated that samples with porosity ~52% made by process 1 were a hundred times smaller than samples with porosity ~54% made by process 2. This difference is attributed to wide necks (process 2) vs. narrow necks (process 1).

Future Directions

- Incorporate the temperature and composition dependence of space charge layer on transport through porous bodies into model.
- Incorporate space charge effects and porous body morphology into the cathodic polarization model for composite and single-phase MIEC cathodes.
- Fabricate single cells with cathodes made using two processes: Process 1: Firing on cathodes directly on the electrolyte layer to generate large porosity but narrow necks; Process 2: Firing a mixture of NiO + SDC, reducing NiO to Ni, leaching away Ni, and then infiltrating the pores with the electrocatalyst. The cathode made with the first process is expected to exhibit poor performance relative to the one made by the second process.

Introduction

It is now well known that electrode morphology has a profound effect on electrode polarization and thus on solid oxide fuel cell (SOFC) performance. Recent work has shown that a large part of the activation polarization loss is associated with the cathode. In addition to the morphological effect, it is also known that ionic conductivity of the cathode has a large effect on cathodic polarization. The grain size has a large effect on conductivity. It is desired that the cathode microstructure close to the electrolyte be as fine as possible. However, when the particle size is very fine, there can be a significant effect of space charge on transport. Space charge could either increase conductivity, or could decrease it. It is desired that the space charge be such that it enhances ionic conductivity of porous bodies. These two factors, grain size and space charge, can substantially influence conductivity, and hence cathodic polarization. If the space charge effect is naturally adverse, such as is the case with yttria-stabilized zirconia (YSZ) and doped ceria, then the objective is to lower the space charge layer thickness by appropriate sintering/annealing procedures.

Approach

The following describes the general approach used.

- (1) Theoretical analysis of the effect of neck size in contacting spheres on the conductivity of porous bodies. The approach is analytical, with focus on obtaining an analytical equation in a parametric form.
- (2) Synthesis of nanosize powders of Sm-doped CeO₂ (SDC) for the fabrication of dense and porous bodies. Sm(NO₃)₃ and Ce(NO₃)₃ were mixed corresponding to a composition Sm - 20% and Ce - 80% and dissolved in de-ionized water. Di-gluconic acid (DGA) was used as fuel in combustion synthesis.
- (3) Powder characterization using x-ray diffraction (XRD) and transmission electron microscopy (TEM).
- (4) Formation of powder compacts by die-pressing, followed by sintering: Process 1.
- (5) Mixing of SDC powder with NiO, formation of powder compacts, sintering to form two-phase samples, reduction of NiO to Ni at 800°C in flowing hydrogen, and removal of Ni by leaching with nitric acid.
- (6) Measurement of total conductivity of the samples of varying porosity levels as a function of temperature using a four-probe DC method.

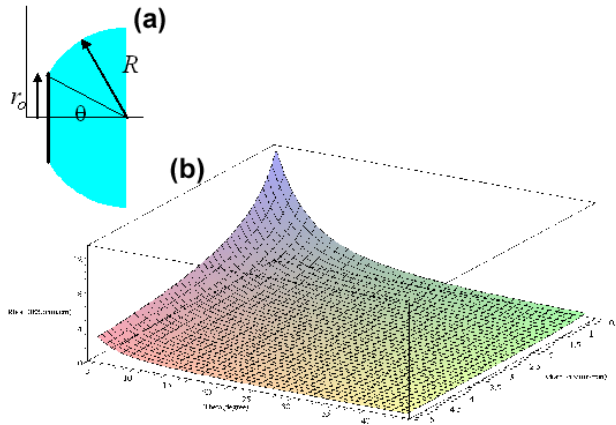


Figure 1. (a) Schematic of a Grain in a Porous Body Used for Calculation of the Effect of Morphology and Space Charge on Conductivity (Resistivity) of Porous Bodies; (b) Resistivity as a Function of Grain Size and Neck Size (angle theta)

Results

Figure 1(a) shows the geometry of the idealized porous body used for the model development. In this figure, the neck size is r_0 and the grain size is R . The calculation includes the estimation of resistance through three regions. Region 1: Conduction through the grain, including space charge layer along the spherical surface. Region 2: Conduction through the space charge layer adjacent to the grain boundary (neck). Region 3: Conduction through the core of the grain boundary. Figure 1(b) shows the results of resistivity calculations as a function of grain size and neck size, the latter defined in terms of the angle subtended by the neck with respect to the center. Note that resistivity sharply increases at small grain sizes and small neck sizes, especially significant being the effect of neck size (angle theta) on resistivity. Figure 2 shows the results of four-probe DC conductivity measurements as a function of relative density on samples made by the two different processes. Note that the conductivity of the sample made by process 2 with a porosity level of ~54% is about a hundred times greater than that of the sample of porosity ~52% made by process 1. The difference is attributed to differences in morphology and space charge effects. Figure 3 shows performance curves for three anode-supported cells made with different ratios of Sr-doped LaCoO_3 (LSC) to SDC. Note that power densities in excess of 1.8 W/cm^2 can be achieved. Figure 4 shows performance curves

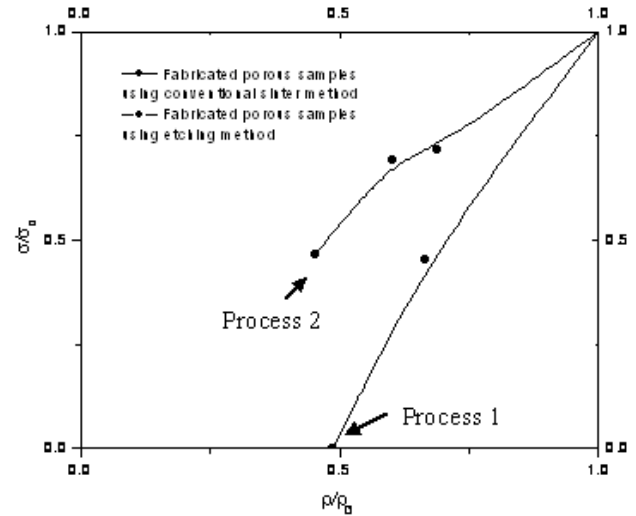


Figure 2. Measured Conductivity of Porous SDC as a Function of Relative Density on Samples Made by the Two Processes

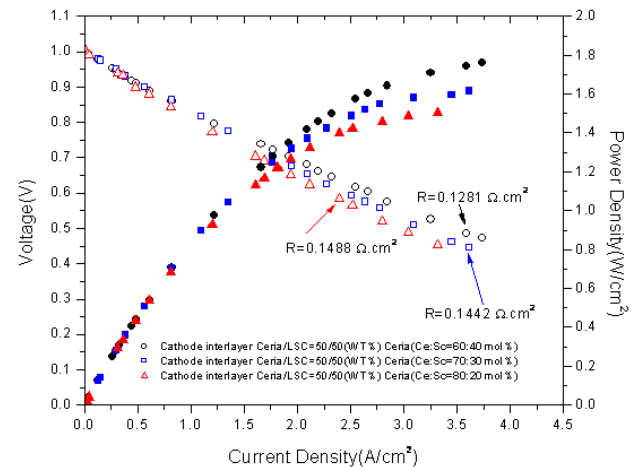


Figure 3. Performance Curves for Three Anode-Supported Cells with Hydrogen as Fuel and Air as Oxidant at 800°C ; The Ratio of LSC to SDC Was Varied

wherein the SDC layer was first made by using process 2. The cells were annealed at different temperatures. After leaching away Ni, a solution of water-soluble salts corresponding to LSC was introduced. Note that in the cell annealed at 1200°C , the performance is lower. This is attributed to larger space charge layer, lower conductivity, higher cathodic polarization, and effectively lower performance. Experiments are underway to make

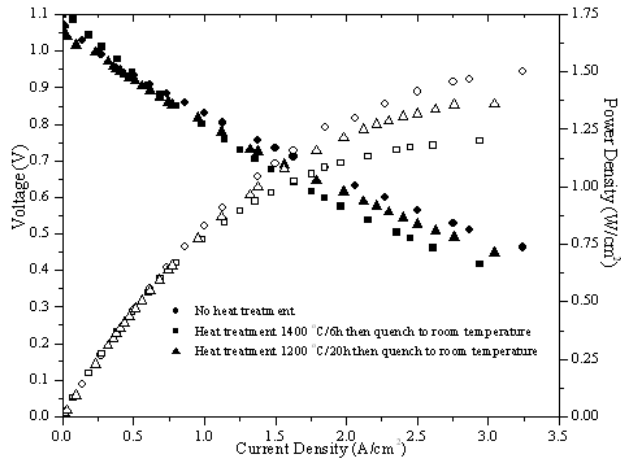


Figure 4. Performance Curves of Cells Wherein the Porous SDC Layer Was Annealed at Various Temperatures; As the Annealing Temperature Was Lowered, the Performance Decreased

cells at higher temperatures so that performance at lower temperatures will be improved.

Conclusions

The principal objective of the work was to demonstrate the roles of morphology of porous bodies and space charge on ionic conduction, and their implications on cathodic polarization. The results have shown that the morphology and space charge have a profound effect on conductivity. Specifically, for samples of identical porosities, the ionic conductivity varies by over two orders of magnitude. The effect of electrode morphology on cathodic polarization is also profound. The present study for the first time shows why a vast difference in cell performance can occur due to different cathode preparation procedures.

FY 2004 Publications/Presentations

1. “Effect of Space Charge and Morphology on Conduction through Porous Bodies: Electrode Polarization” by Anil V. Virkar, Invited talk presented at Dokiya Memorial Symposium in Tokyo, Japan, June 25, 2004.

VII SBIR, HBCU, & UCR Projects

VII SBIR, HBCU, & UCR Projects

VII.1 Bi-Layer p-n Junction Devices for Coal-Based SOFC Interconnections

Srikanth Gopalan and Wenhua Huang

Department of Manufacturing Engineering, Boston University

15 St. Mary's Street

Boston, MA 02215

Phone: (617) 358-2297; Fax: (617) 353-5548; E-mail: sgopalan@bu.edu

DOE Project Manager: Lane Wilson

Phone: (304) 285-1336; E-mail: Lane.Wilson@netl.doe.gov

Objectives

- Develop a stable, high-conductivity bi-layer interconnection (IC) for lower operating temperature solid oxide fuel cells (SOFCs).

Approach

- Analyze and model a bi-layer IC comprising of a p-type and an n-type semiconducting layer using literature data for well-known materials.
- Develop design criteria for a bi-layer IC based on the model.
- Investigate techniques for fabricating a bi-layer IC.

Accomplishments

- Analyzed bi-layer IC structures using species transport models and developed design criteria for fabrication of such structures.
- Conducted preliminary investigations into fabricating bi-layer IC structures.

Future Directions

Future work in this project will focus on combining detailed measurement of partial conductivities of various p- and n-type oxides with a study of various fabrication techniques to identify the most appropriate technique to fabricate bi-layer ICs.

Introduction

Current research on solid oxide fuel cells (SOFCs) is focused on reducing the operating temperature from a nominal temperature of 1000°C to 600-800°C. Reducing the operating temperature allows the use of low-cost stack and manifolding materials, reduces heat-up time, and enables use in small-scale residential and transportation applications. However, reducing the operating temperature also has the unintended negative consequences of higher electrode polarization and

higher area specific electrolyte and interconnection resistances. In particular, doped LaCrO_3 , a high-temperature p-type semiconductor which is used as the interconnection material in state-of-the-art high-temperature SOFCs, is a very poor choice for an interconnection material in the 600-800°C temperature regime for two different reasons. First, the conduction mechanism in doped- LaCrO_3 is small polaron hopping, which is a thermally activated process. Thus, the p-type conductivity of this material decreases exponentially with decreasing temperature. Secondly, the interconnection material,

like the solid electrolyte in the SOFC, is exposed to highly oxidizing conditions on the cathodic side ($pO_2 = 0.21$ atm) and highly reducing conditions on the anode side (10^{-18} to 10^{-21} atm). Thus, a gradient in the electronic conductivity exists across the interconnect, with a high conductivity on the cathode side and poor conductivity on the anode side leading to an overall low average electronic conductivity across the interconnect. In this project, we are studying a novel concept for an improved SOFC interconnection structure with a high average conductivity across the entire thickness.

Approach

The approach being explored in the current project utilizes a bi-layer IC with a p-type layer (electronic conductivity proportional to $pO_2^{1/n}$) exposed to the cathode gas (air or oxygen) and an n-type layer (electronic conductivity proportional to $pO_2^{-1/n}$) exposed to anode gas (mixture of H_2 , H_2O , CO and CO_2). By designing the thickness of the layers appropriately, one can in principle maintain thermodynamic stability of the layers while at the same time retaining a high average electronic conductivity across the IC.

Results

The principal result from Phase 1 of this project is a detailed analysis of a model bi-layer SOFC IC culminating in definitive design criteria for such a structure. The results have given a firm direction for future work in this area. The analysis of the bi-layer IC structure and the design criteria ensuing from the analysis are described in what follows.

Figure 1 shows a schematic of the bi-layer interconnection and associated transport directions of oxygen ions (O^{2-}), holes (h^+) and electrons (e^-). The generalized current density of species 'k' is given by

$$J_k = -\frac{\sigma_k}{z_k e} \nabla \eta_k \quad (1)$$

Applying equation (1) to transport of O^{2-} , h^+ , and e^- , the species current densities can be written as,

$$J_i = \frac{\sigma_i}{2e} \nabla \eta_i \quad (2a)$$

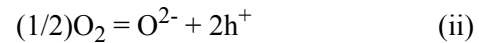
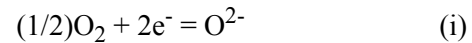
$$J_p = -\frac{\sigma_p}{e} \nabla \eta_p \quad (2b)$$

$$J_n = \frac{\sigma_n}{e} \nabla \eta_n \quad (2c)$$

The sum of the species' current densities can then be equated to the total current density through the bi-layer interconnection under SOFC operating conditions, i.e.

$$J = J_i + J_p + J_n \quad (3)$$

The next step in the analysis is the assumption that local thermodynamic equilibrium prevails between neutral oxygen gas, oxygen ions and electrons/holes, i.e. the following reactions are in thermodynamic equilibrium everywhere across the interconnection structure.



Assumption of thermodynamic equilibrium of the above reactions gives,

$$\frac{1}{2} \nabla \mu_{O_2} + 2 \nabla \eta_n = \nabla \eta_i \quad (4)$$

$$\frac{1}{2} \nabla \mu_{O_2} + 2 \nabla \eta_n = \nabla \eta_i \quad (5)$$

$$\nabla \eta_n + \nabla \eta_p = 0 \quad (6)$$

(1): p-type (2): n-type

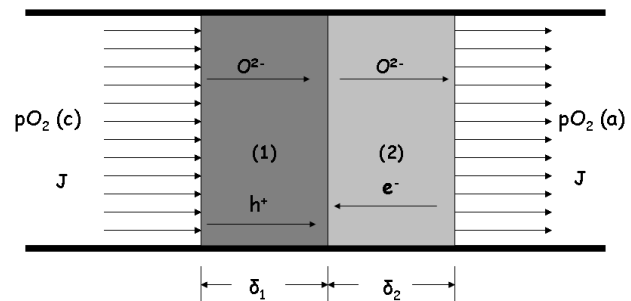


Figure 1. Schematic of a Bi-layer IC

$$J_{el} = J_n + J_p = \frac{\sigma_n + \sigma_p}{\sigma_i + \sigma_n + \sigma_p} J - \frac{1}{2e} \frac{\sigma_i (\sigma_n + \sigma_p)}{\sigma_i + \sigma_n + \sigma_p} \nabla \mu_{O_2} \quad (7a)$$

$$J_i = \frac{1}{2e} \frac{\sigma_i (\sigma_n + \sigma_p)}{\sigma_i + \sigma_n + \sigma_p} \nabla \mu_{O_2} + \left(\frac{\sigma_i}{\sigma_i + \sigma_n + \sigma_p} \right) J \quad (7b)$$

Substituting equations (2), (4), (5) and (6) in (3), it can be shown that

Each of the above equations – (7a), which represents the total electronic current density (electron and hole current density), and (7b), which represents the total ionic current density – has two terms, one associated with J , the total external current density, and the other $\nabla \mu_{O_2}$, the neutral oxygen chemical potential gradient. The transport coefficient multiplying $\nabla \mu_{O_2}$, namely,

$$\frac{\sigma_i (\sigma_n + \sigma_p)}{\sigma_i + \sigma_n + \sigma_p}$$

is easily recognized as the ambipolar conductivity of the individual layers. In general, the conductivities σ_i , σ_n and σ_p will be functions of temperature and composition. Since the composition is both a function of the local electrostatic potential and the oxygen partial pressure, the conductivities are expected to vary as a function of position. Relevant simplifying assumptions to derive analytical expressions can now be made that can guide design of the bi-layer interconnection.

First, we assume that the ionic conductivity in the two layers is invariant with pO_2 . Second, we assume that the ionic conductivity is much smaller in magnitude than the sum of the electron and hole conductivities, i.e. $\sigma_i \ll (\sigma_n + \sigma_p)$. The first assumption is true of most p-type and n-type oxide electronic conductors. In these materials, the oxygen ionic conductivity is determined extrinsically, i.e. it is a stronger function of the aliovalent dopant level than of pO_2 . The second assumption is a necessary condition to be satisfied of any candidate interconnection material. With the second of these assumptions, equations (7) can be simplified to

$$J_{el} = J - \frac{1}{2e} \sigma_i \nabla \mu_{O_2} \quad (8a)$$

$$J_i = \frac{1}{2e} \sigma_i \nabla \mu_{O_2} \quad (8b)$$

These assumptions imply that at steady state, the current passing through the bi-layer interconnection is substantially electronic in nature. Furthermore, the rather small oxygen ionic current through the bi-layer given by equation (8b) does not depend on the total current through the interconnection but only on the cathodic and anodic side pO_2 's. Assuming that the chemical and electrostatic potential gradients are one-dimensional and integrating equation (8b) over both layers, it can be shown that,

$$J_{i1} = \frac{k_B T \sigma_{i1}}{2e \delta_1} \ln \left[\frac{pO_2(c)}{pO_2(i)} \right] \quad (9a)$$

$$J_{i2} = \frac{k_B T \sigma_{i2}}{2e \delta_2} \ln \left[\frac{pO_2(i)}{pO_2(a)} \right] \quad (9b)$$

The interfacial oxygen partial pressure $pO_2(i)$, which is an important design parameter as will be seen shortly, can be derived by equating the ionic current densities through the two layers at steady state, i.e. $J_{i1} = J_{i2}$, i.e. Equation (10) gives the

$$pO_2(i) = \left[\{pO_2(c)\}^{\left(\frac{\sigma_{i1}}{\delta_1}\right)} \{pO_2(a)\}^{\left(\frac{\sigma_{i2}}{\delta_2}\right)} \right]^{\frac{1}{\left(\frac{\sigma_{i1}}{\delta_1} + \frac{\sigma_{i2}}{\delta_2}\right)}} \quad (10)$$

interfacial oxygen partial pressure as a function of the oxygen partial pressure on the cathodic and anodic sides, the oxygen ionic conductivities in the two regions and the thickness of the two layers. The principal criterion is for $pO_2(i)$ to remain above the decomposition oxygen partial pressure for the p-type layer. Figure 2 shows as a function of p-type layer thickness for an assumed n-type layer thickness of 500 μm and SOFC operating temperature of 900°C, using literature data for two prototypical materials, namely, Sr-doped LaMnO₃ or LSM (p-type) and Y-doped SrTiO₃ or YST (n-type). Since LSM has a decomposition oxygen partial pressure of roughly 10⁻⁶ atm, it can be concluded for this configuration that the LSM layer thickness has to be about 5 μm . Figure 3 shows the variation of pO_2 as a function of

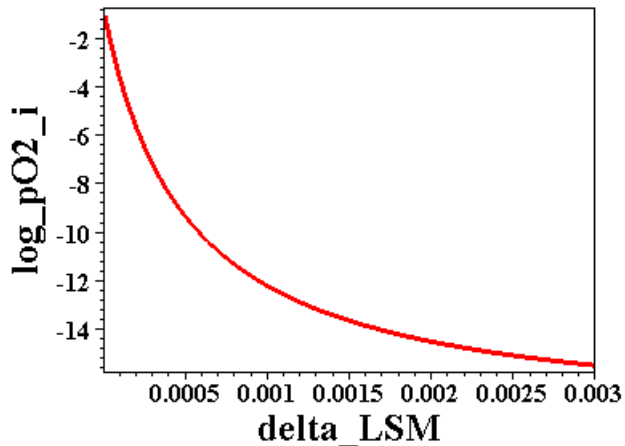


Figure 2. Variation of pO_2 in atm with varying LSM layer thickness in cm. Assumed fixed YST thickness is 500 microns. Ionic conductivity of YST is 10^{-5} S/cm and that of LSM is 10^{-7} S/cm; operating temperature is 900°C . Air side pO_2 is 0.21 atm and fuel side pO_2 is 10^{-18} atm.

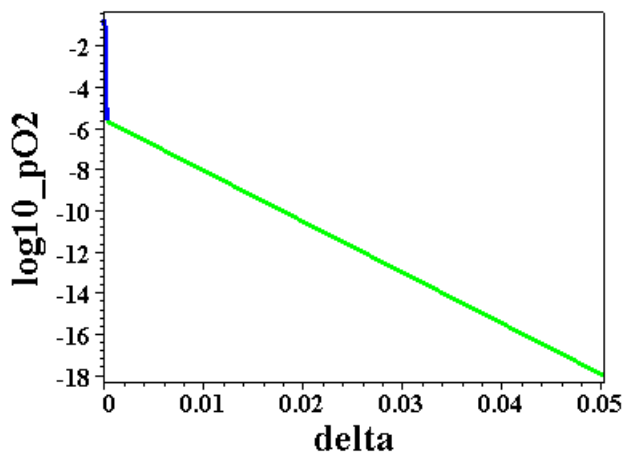


Figure 3. Variation of pO_2 across a bi-layer IC comprising a 5 micron thick LSM layer and 500 micron thick YST layer. Ionic conductivities of the layers and the air side and fuel side pO_2 's are as in Figure 2.

position across the thickness for the same pair of materials and same operating conditions as in Figure 2.

Thus, a simple rule of thumb for design of the bi-layer IC is: ***the layer with the higher oxygen ionic conductivity has to be fabricated with a greater thickness.***

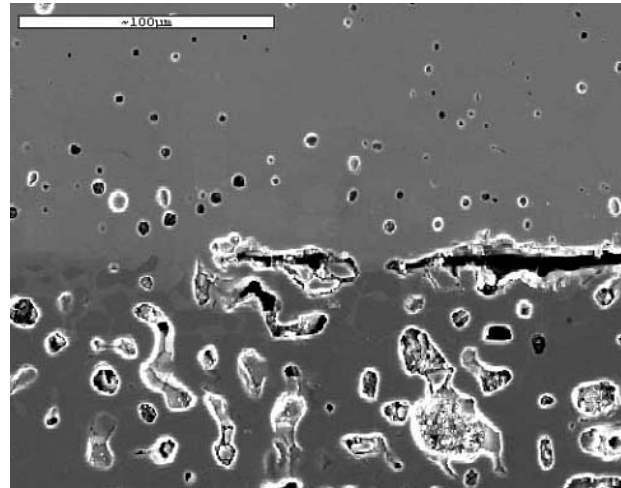


Figure 4. Micrograph of a bi-layer IC fabricated by contacting sintered pellets of LSM and YST at elevated temperature. Note the uneven bonding.

Similar design criteria can be developed for other pairs of materials if detailed partial conductivities of the p- and n-type materials are known as a function of temperature and pO_2 .

Preliminary experiments have been performed to fabricate bi-layer structures by contacting sintered compacts of LSM and YST at elevated temperatures. Microstructures of the interface of bi-layers obtained using this method indicate discontinuous contact between the layers (Figure 4). Fabrication techniques including electrophoretic deposition, screen printing and thermal spray deposition are presently being investigated.

The focus of future work in this area will be:

- To obtain detailed partial conductivity data on various p-type and n-type perovskites as a function of pO_2 and temperature.
- To identify the most appropriate fabrication technique to fabricate bi-layer IC structures.

Conclusions

- Design criteria have been developed for design of bi-layer ICs.
- A general rule of thumb for bi-layer IC design is to fabricate the layer with the higher oxygen ion conductivity with a greater thickness.

References

1. A.V. Virkar, *J.Electrochem.Soc.*, (138) 5 (1991) 148
2. T. Kawada, T. Watanabe, A. Kaimai, K. Kawamura, Y. Nigara and J. Misuzaki, *Solid State Ionics*, 108 (1998) 391
3. <http://www.netl.doe.gov/publications/proceedings/02/SECActp/TuePM/wachsman.pdf>

FY 2004 Publications/Presentations

1. W. Huang and S. Gopalan, "Bi-layer Structures as SOFC Interconnections", *J.Power Sources* (Submitted)
2. W. Huang and S. Gopalan, "Bi-layer Interconnections for Coal Based Solid Oxide Fuel Cells (Innovative concepts – phase I), DOE UCR Contractors Review Meeting, Pittsburgh, PA, 6/19/04
3. W. Huang and S. Gopalan, "Bi-Layer Structures for Interconnections in SOFCs", to be presented in MRS Fall meeting, November 2004

VII.2 Materials System for Intermediate-Temperature SOFC

Uday B. Pal (Primary Contact), Srikanth Gopalan, Wenquan Gong

Department of Manufacturing Engineering, Boston University

15 St. Mary's Street

Brookline, MA 02446

Phone: (617) 353-7708; Fax: (617) 353-5548; E-mail: upal@bu.edu

DOE Project Manager: Lane Wilson

Phone: (304) 285-1336; E-mail: Lane.Wilson@netl.doe.gov

Objectives

- Synthesize and evaluate materials system for intermediate-temperature (600-800°C) solid oxide fuel cell (SOFC).
- Demonstrate feasibility of manufacturing multi-layered SOFC structures utilizing the intermediate-temperature materials system.

Approach

- From literature data, selected the electrolyte, anode, and cathode materials for the intermediate-temperature SOFC system: lanthanum gallate ($\text{La}_{0.9}\text{Sr}_{0.1}\text{Ga}_{0.8}\text{Mg}_{0.2}\text{O}_3$, or LSGM) as electrolyte, nickel-gadolinium doped ceria ($\text{Ce}_{0.85}\text{Gd}_{0.15}\text{O}_{2-x}$, or Ni-GDC) cermet as anode, and LSGM-lanthanum cobaltite ($\text{La}_{0.6}\text{Sr}_{0.4}\text{Co}_{0.8}\text{Fe}_{0.2}\text{O}_3$, or LSCF) composite as cathode.
- Synthesized and confirmed the suitability of the LSGM electrolyte for intermediate-temperature operation.
- Measured the interfacial polarizations of the candidate electrodes for the LSGM electrolyte utilizing impedance spectroscopy.
- After determining optimum electrode composition, structure and thicknesses of the cathode and the anode, complete planar cells will be fabricated and evaluated in terms of their current-voltage (I-V) characteristics and stability.

Accomplishments

- LSGM electrolyte was synthesized. It was found to be stable under fuel cell operating conditions and had the required conductivities to function as an electrolyte for the intermediate-temperature SOFC (Figure 1).
- Optimum active cathode that resulted in the least polarization resistance (0.1 ohm-cm² at 800°C) and good thermal expansion match with the LSGM electrode was determined to be a 50-50 volume-% LSCF-LSGM composite having a thickness of 30-40 micrometers.
- Optimum active anode was found to be Ni-GDC cermet having a barrier layer of $\text{Ce}_{0.6}\text{La}_{0.4}\text{O}_{2-x}$ (LDC) between the anode and the LSGM electrolyte.

Future Directions

- Effects of Ni-GDC anode composition, structure and thickness on interfacial polarization will be investigated.
- After determining the composition, structure and thickness of the anode, complete anode-supported planar cells will be fabricated and evaluated at intermediate temperatures in terms of its I-V characteristics and stability.

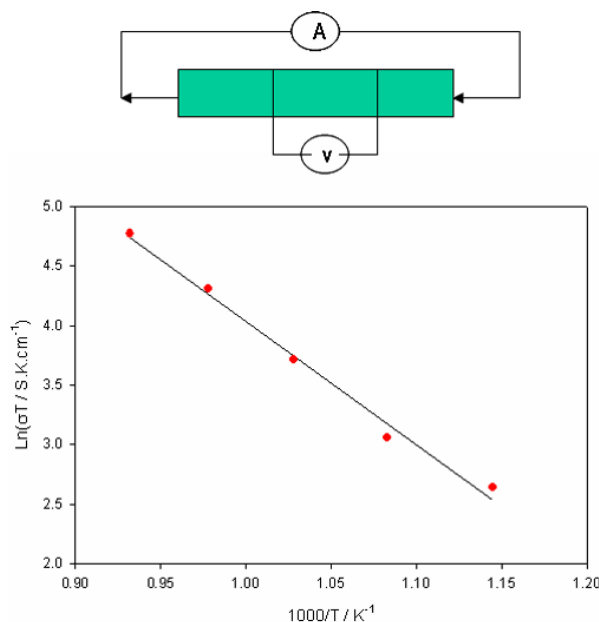


Figure 1. Conductivity of LSGM Electrolyte as a Function of Temperature Measured Using a Four-Probe Technique

Introduction

Solid oxide fuel cells offer the possibility of very high efficiency power generation. They are noiseless, emit far lower quantities of greenhouse gases such as CO₂ compared to conventional power generation systems, and cause virtually zero NO_x and SO_x emissions. They are also fuel cell candidates for enabling the hydrogen economy. Despite their many advantages, SOFC power systems are not yet cost-effective to merit large-scale deployment in the power generation industry. Of the approaches currently being investigated to decrease the cost of SOFCs, improving power density while decreasing operating temperature is perhaps the most promising option. Improvements in power density will result in decreased system size, which in turn will have the effect of decreasing the size of the balance of plant (BOP). Decreasing operating temperature will lead to the deployment of cheaper manifolding and interconnection materials. However, decreasing operating temperature has the effect of increasing all types of polarization losses in the cell. Thus, the simultaneous goals of improving power density and lowering the operating temperature are at odds with each other. Therefore, the focus of recent research is aimed at development of more active electrodes and

more conductive electrolyte materials that can efficiently operate at lower temperatures (600-800°C).

A large fraction of the total polarization losses is known to occur at the electrode-electrolyte interface manifesting itself as the kinetic barrier to charge-transfer reactions. Great advances have been made in reducing electrode polarization related to the charge-transfer reaction through the use of two-phase porous composite electrodes [1-4] and mixed conducting electrodes [5]. Much of this work has been aimed at developing electrodes for SOFCs based on the conventional yttria-stabilized zirconia (YSZ) electrolyte and not on researching a materials system that can be employed to manufacture intermediate-temperature SOFCs. The focus of this work is an investigation of electrode materials for SOFCs based on the perovskite electrolyte La_{1-x}Sr_xGa_{1-y}Mg_yO₃ (or LSGM). LSGM has received a lot of interest in recent years after it was first reported by Goodenough et al. [6] to have significantly higher oxygen-ion conductivity than YSZ.

Approach

Powders of the composition La_{0.9}Sr_{0.1}Ga_{0.8}Mg_{0.2}O₃ (LSGM) were synthesized by mixing high-purity precursors of lanthanum carbonate, strontium carbonate, gallium oxide and magnesium oxide in appropriate stoichiometric ratios and calcining at a temperature of 1200°C for 4 hours in air. Electrode materials such as La_{0.9}Sr_{0.1}MnO₃ (LSM), La_{0.6}Sr_{0.4}Co_{0.8}Fe_{0.2}O₃ (LSCF), Ce_{0.85}Gd_{0.15}O₂ (GDC), and Ce_{0.6}La_{0.4}O₂ (LDC) were also made using a similar procedure.

Calcined and milled LSGM powders at room temperature were die-pressed with 10,000 psi pressure into pellets and sintered in air at 1450°C for 4 hours. The sintered LSGM pellets were 1.4 mm thick and 2 cm in diameter. The LSGM pellets were then all finely ground to a uniform 1 mm thickness using diamond grinding discs. LSM-LSGM, LSCF-LSGM, NiO-GDC, and NiO-LDC composite electrodes were prepared by thoroughly mixing controlled amounts of powders. The electrode powders (LSM, LSM-LSGM, LSCF, LSCF-LSGM, NiO-GDC, NiO-LDC) were each dispersed in terpenol solvent to form a paste. The ground LSGM

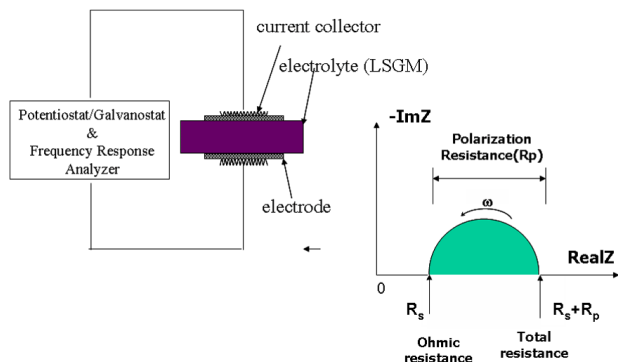


Figure 2. Schematic Diagram of the Experimental Setup Employing Symmetrical Cell for Measuring Electrode Polarization through Impedance Spectroscopy

electrolyte pellets were masked with Scotch™ tape to form an outer ring on both sides, and the electrode pastes were painted smoothly on the open circular surfaces. The painted electrolyte pellets were air-dried, the masks were removed, and the pellets were fired in air at elevated temperature for 2 hours. The firing temperature was 1100°C for all the cathodic samples and 1100-1300°C for the anodic samples. When platinum electrodes were used, commercial platinum paste (6926 Engelhard) was painted over a similarly masked LSGM electrolyte pellet, air-dried, and fired (with masks removed) at 950°C for 2 hrs. All electrodes had the same effective area of around 1.33 cm². For the cathode materials, two pieces of platinum mesh were co-sintered on both electrode surfaces at the same time to act as current collectors. Lead wires of Pt were used to connect the platinum mesh current collectors to the measuring instrument. For the anode materials, Nickel mesh was pressed over the electrode surfaces in a reducing atmosphere, and lead wires of Nickel were used. The experimental setup used for AC impedance characterization is shown in Figure 2. In this setup, the symmetrical cell was exposed to the same oxidizing (cathodic) or reducing (anodic) atmosphere on both sides, and a two-probe configuration was used to measure the impedance spectra. During measurement, a constant flow rate of air was maintained for experiments involving the cathode materials, and a constant flow rate of forming gas, i.e. 95% argon-5% hydrogen bubbled through water at 25°C, was maintained for experiments involving the anode materials. The measurements were made

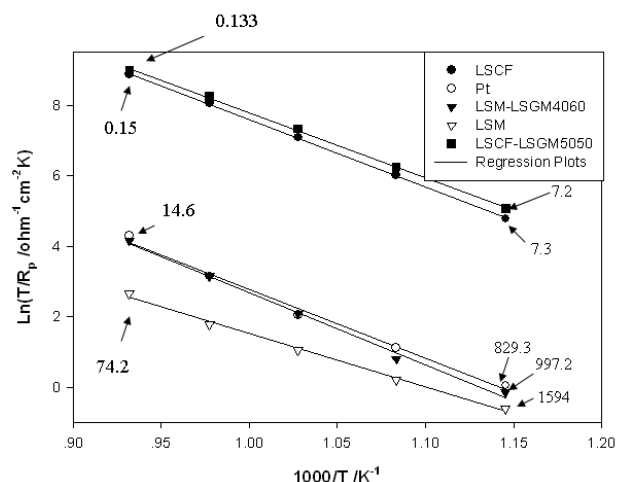


Figure 3. Temperature Dependence of the Polarization Resistance for Various Cathode Materials Measured in Air

in the temperature range of 600 to 800°C by applying a small-amplitude AC voltage (10 mV) to the cell and monitoring the response current as a function of the AC frequency (from 1 mHz to 65 KHz). A plot of the imaginary part of the measured impedance versus the real part reveals details of the individual ohmic and polarization contributions to the total resistance of the cell. After electrochemical testing, the samples were epoxy mounted and polished in cross section; both scanning electron microscopy (SEM) and optical microscopy were used to measure the grain size, porosity and thickness of the electrodes and confirm the consistency of the microstructure.

Results

Among the cathode materials [LSM ($\text{La}_{0.9}\text{Sr}_{0.1}\text{MnO}_3$) and LSCF], the pure LSM electrode had the worst polarization performance. The addition of LSGM electrolyte material to the LSM electrode increased the mixed-conducting boundary with the gas phase and lowered the overall polarization. Although LSM-LSGM composite electrodes are better than just pure LSM, the performance of the best LSM-LSGM (40:60) electrode was similar to that of platinum. Single-phase mixed-conducting LSCF electrode had three orders lower polarization resistance than the LSM-LSGM composite electrodes (Figure 3). Addition of

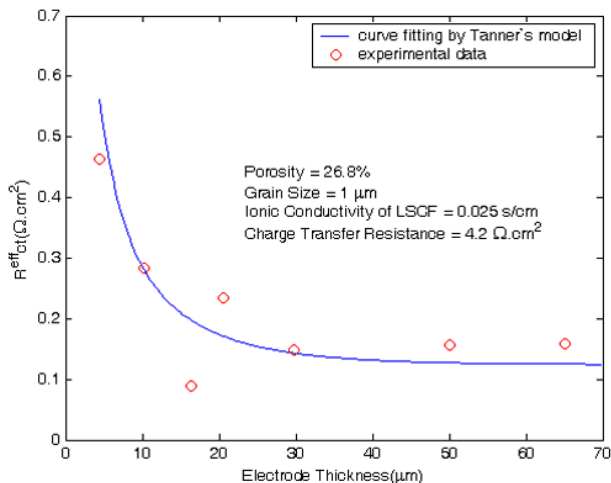


Figure 4. A Plot of Polarization or Charge Transfer Resistance as a Function of Electrode Thickness for Symmetrical LSCF/LSGM/LSCF Cells Measured in Air at 800°C

LSGM to LSCF did not significantly alter (lower) the polarization resistance of the LSCF electrodes (Figure 3). However, a composite LSCF-LSGM electrode is preferred over a plain LSCF electrode in order to match the coefficient of thermal expansion with the LSGM electrolyte. It is also observed that the interfacial polarization resistance of the LSCF electrode decreased asymptotically as the electrode thickness increased. An optimum thickness of 30 to 40 microns is required to minimize the cathodic polarization resistance (Figure 4).

The anode material investigated was Ni-GDC. It was observed that the LSGM electrolyte reacts with the Ni during processing and also at the operating temperature and increased both the ohmic and the polarization resistances. A buffer layer of GDC between the LSGM electrolyte and the Ni-GDC composite anode could not completely prevent this interaction due to lanthanum diffusion when sintering temperature was above 1200°C. The La diffusion also resulted in increasing the ohmic resistance. It is possible to prevent the La diffusion from the LSGM electrolyte by changing the buffer layer from GDC to lanthanum-doped ceria (LDC). It is to be noted that the lanthanum in the LDC does not react with the Ni. Since the ionic conductivity of the LDC is lower than that of GDC, it is desirable to employ a Ni-GDC cermet anode above the LDC barrier layer to lower the polarization resistance.

Effects of Ni-GDC anode composition, structure and thickness on interfacial polarization are being investigated.

Conclusions

Single-phase mixed-conducting LSCF cathodes have much lower polarization resistance than the LSM-LSGM composite cathodes. The polarization resistance of the LSCF cathodes decreases asymptotically as the electrode thickness is increased. Adding LSGM electrolyte material to the LSCF electrode does not improve the cell performance very much, but buffers the larger thermal expansion coefficient of LSCF compared to the LSGM electrolyte. Ni in the anode material reacts with LSGM electrolyte and lowers the overall cell performance. A dense layer of an appropriate buffer oxide (LDC) is needed between the LSGM electrolyte and the Ni-GDC anode.

References

1. T. Kawada, N. Sakai, H. Yokokawa, M. Dokiya, M. Mori and T. Iwata: "Characteristics of slurry coated nickel zirconia cermet anodes for solid oxide fuel cell," *J. Electrochem. Soc.*, 1990, 137, pp. 3042-3046.
2. T. Kenjo and M. Nishiya: "LaMnO₃ air cathodes containing ZrO₂ electrolyte for high temperature solid oxide fuel cells," *Solid State Ionics*, 1992, 57, pp. 295-302.
3. M. J. L. Østergård, C. Clausen, C. Bagger and M. Mogensen: "Manganite-zirconia composite cathodes for SOFC: Influence of structure and composition," *Electrochim. Acta*, 1995, 40, pp. 1971-1981.
4. V. Dusastre and J. A. Kilner: "Optimisation of composite cathodes for intermediate temperature SOFC applications," *Solid State Ionics*, 1999, 126, pp. 163-174.
5. M. T. Colomer, B. C. H. Steele and J. A. Kilner: "Structural and electrochemical properties of the Sr_{0.8}Ce_{0.1}Fe_{0.7}Co_{0.3}O_{3-δ} perovskite as cathode material for ITSOFCs," *Solid State Ionics*, 2002, 147, pp. 41-48.

6. M. Feng, and J. B. Goodenough: "A superior oxide-ion electrolyte," *Eur. J. Solid State Inorg. Chem.*, 1994, 31, pp. 663-672.

FY 2004 Publications/Presentations

1. Wenquan Gong, Srikanth Gopalan and Uday B. Pal, "Polarization Study on Doped Lanthanum Gallate Electrolyte Using Impedance Spectroscopy," *Journal of Materials Engineering and Performance*, Vol. 13, No. 3, June 2004, pp. 274-281.
2. Wenquan Gong, Srikanth Gopalan and Uday B. Pal, "Cathodic Polarization Study on Doped Lanthanum Gallate Electrolyte Using Impedance Spectroscopy," Accepted for Publication in the *Journal of Electroceramics*, March 2004.
3. June 2003, "Cathode Materials for Intermediate Temperature SOFCs," Department of Materials Science and Engineering Graduate Seminar, SUNY Stonybrook.
4. November 2003, "Polarization Study on Doped Lanthanum Gallate Electrolyte Using Impedance Spectroscopy," ASM Fall Meeting, Pittsburgh, PA.
5. June 2004, "Materials System for Intermediate Temperature Solid Oxide Fuel Cell," DOE-UCR Meeting, Pittsburgh, PA.

VII.3 Spouted Bed Electrodes for Direct Utilization of Carbon in Fuel Cells

J.M. Calo

Brown University

Division of Engineering, Box D

Providence, RI 02912

Phone: (401) 863-1421; Fax: (401) 863-9120; E-mail: Joseph_Calo@brown.edu

DOE Project Manager: Travis Shultz

Phone: (304) 285-1370; E-mail: Travis.Shultz@netl.doe.gov

Objectives

- Explore the extension/application of spouted bed electrode (SBE) systems to direct carbon fuel cell (DCFC) applications.
- Simulate anticipated hydrodynamics of DCFCs.
- In a rectangular spouted vessel hydrodynamics apparatus (SVHA) with simulated mixtures containing carbon particles, explore fluid-particle circulation as a function of particle size, loading, fluid velocity, density, viscosity, geometry, etc.

Approach

- Adapt and apply computational fluid dynamics (CFD) code originally developed to simulate particle circulation in spouted bed electrolytic reactors to carbon particle circulation in candidate geometries for DCFC systems.
- Experimentally investigate the hydrodynamics of carbon slurry circulation in DCFC systems using simulated slurry mixtures.

Accomplishments

- A CFD hydrodynamics model of a rectangular spouted bed has been adapted to the DCFC application.
- Preliminary results involving particle loading and flow rate have been used to identify conditions for good particle contact with the inclined vessel bottom (e.g., anode), as well as particle recirculation.
- Both two-phase (liquid-solid) and three-phase (liquid-solid-CO₂ gas) hydrodynamics have been examined.
- The rectangular spouted vessel hydrodynamics apparatus has been retrofitted for simulated molten carbonate/carbon slurry experiments. Experiments are ongoing.

Future Directions

- The CFD model will continue to be developed to explore the behavior of the spouted bed DCFC.
- The experimental apparatus will be used to conduct experiments using additives in water, simulate molten carbonate viscosity and density under expected DCFC operating conditions, and study carbon particles of varying sizes as a function of loading and flow rate.

Introduction

Carbon-oxygen fuel cells have been demonstrated that operate on very fine particles (10-1000 nm) of low-ash, turbostratic carbon. As impressive as these devices are, however, a number

of problems remain to be solved before this technology can successfully operate on many different carbon sources on a large scale. The use of coal- and biomass-derived carbons, for example, requires a fuel cell design that can handle high amounts of ash and larger particles. It is proposed to

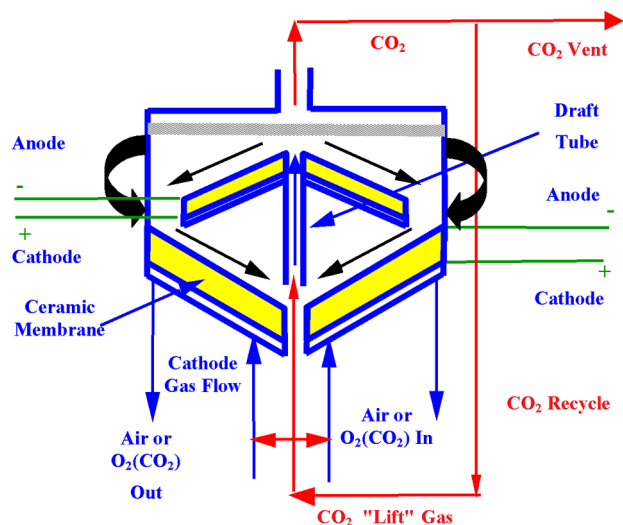


Figure 1. Schematic of Spouted Bed Direct Carbon Fuel Cell

adapt the concept of particulate spouted bed electrodes (SBEs) to the carbon-oxygen fuel cell.

In our laboratory, we have developed SBEs for point source metals recovery. In these devices, an aqueous solution containing metal ions is introduced as a high-velocity jet at the bottom of a conical vessel *via* a central draft tube. This liquid jet entrains particles that disengage from the jet in a region above the draft tube known as the "fountain." The particles are then distributed radially by the distributor to the bed periphery, where they fall onto the cathodic "feeder cone" at the reactor bottom and are directed back to the inlet of the draft tube for re-entrainment. Metal is deposited on the particles when they are in contact with the cathodic bottom cone. The "pumping action" of the spout continually circulates the particles through the vessel: upwards in the spout and downwards in the annular region. We have successfully recovered Ag, Au, Cu, Ni, Sn, and Cd from various aqueous solutions with this system at high current densities and high current efficiencies.

The objective of this project is to explore the extension/application of SBE-like systems to direct carbon fuel cells. More specifically, the approach is to (1) adapt SBE CFD codes to simulate the expected hydrodynamics of a DCFC and (2) perform simulated experiments of fluid-particle circulation in a rectangular spouted vessel hydrodynamics apparatus.

Approach

A conceptual schematic of the spouted bed DCFC (SBDCFC) is presented in Figure 1. Carbon/molten carbonate slurry flows continuously through the system in a toroidal fashion – upwards in the draft tube and then centripetally back down along inclined, bipolar anode/cathode stacks. Two such stacks are shown in Figure 1 (one at the vessel bottom and the other serves as a slurry distributor); however, it is anticipated that a number of these stacks will be arranged in a single vessel in chevron-like arrangements.

The slurry can be circulated through the fuel cell either mechanically or by gas-lift created by injecting CO_2 produced in the carbon oxidation reaction into the slurry below the draft tube entrainment region (e.g., as in a gas-lift riser).

Fuel cell operation requires continuous carbon feed and removal of spent, ash-rich particles. The flow in the SBDCFC provides a few possibilities for accomplishing this. For example, the slurry can be circulated in an external circuit to remove spent, ash-rich particles (e.g., by filtration with metallic or ceramic media), and to feed fresh carbon particles to the SBDCFC. These operations can also be performed within the cell either at the draft tube inlet or outlet.

In order to become a viable system, the SBDCFC must be capable of operation on a large scale. The SBDCFC has some significant advantages in this regard: (1) it is readily scalable (e.g., by "stacking" units and inclined bipolar elements); and (2) continuous flow provides the means for performing removal and recovery of spent particles, continuous "self-cleaning" of electrodes that can be easily fouled in other systems, and facile temperature control *via* convective heat removal. In particular, the "self-cleaning" nature of the electrodes tends to minimize the effects of contaminants on performance and aging. In addition, the continuous feed of carbonaceous material tends to reduce electrode sintering that can be a problem for fixed solid electrodes.

As a result of our spouted bed electrolytic reactor work, we have developed numerical Eulerian CFD

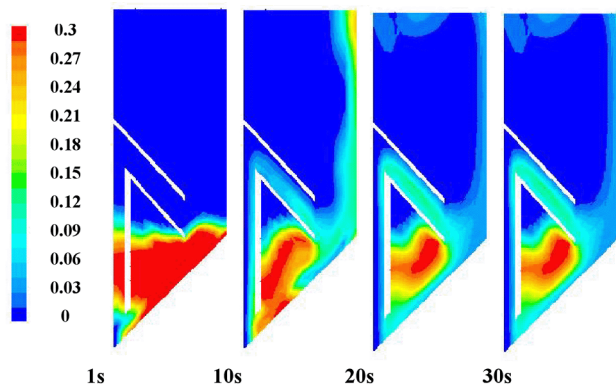


Figure 2. Simulation Results Using an Eulerian CFD Model Solved with FLUENT™ of Time Evolution of Carbon Particle Volume Fraction in One Quadrant of a Rectangular Spouted Vessel; $\text{Li}_2(\text{CO}_3)$ at 810°C ; 200 g, 0.1 mm Particles; 0.3 m/s Inlet Velocity

models for simulating the performance of SBE systems. For electrowinning, these models were validated with hydrodynamic data from a rectangular SVHA. We are pursuing a similar approach for the SBDCFC concept, i.e., simulation of carbon slurry flows with the CFD model, and model validation *via* hydrodynamics experiments with simulated carbon/molten carbonate slurries in the SVHA.

Results

Simulations. A number of carbon/molten carbonate slurry flow conditions have been simulated in a domain of the same size as one quadrant of the SVHA experimental system. An example of these results is presented in Figure 2. The geometry in this case includes a draft tube with a “cap.” Molten carbonate is injected at the inlet at 0.3 m/s. As shown, even though the densities of the carbon particles and molten carbonate are practically the same, under these conditions there is good contact of the carbon with the inclined vessel bottom, as well as the top and bottom of the distribution channel; all these inclined surfaces can potentially serve as anodes in a SBDCFC “chevron-type” bipolar electrode system.

Another simulation result is presented in Figure 3 with just an open draft tube in which CO_2 is used as a lift-gas to circulate the carbon/molten carbonate slurry in the SBDCFC. Two things are apparent in

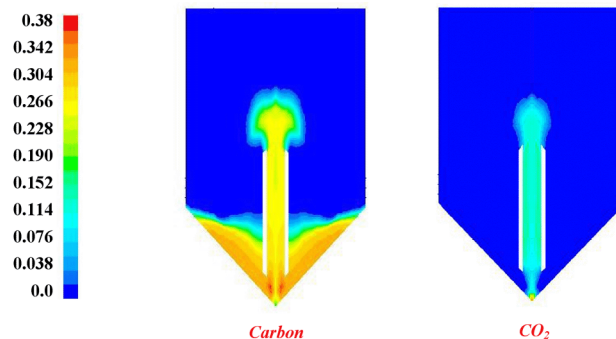


Figure 3. Simulation Results Using an Eulerian CFD Model Solved with FLUENT™ of Carbon Particle and CO_2 Gas Volume Fractions in Molten Carbonate at 29 s after Start-up with Pure CO_2 at Atmospheric Pressure at the Inlet, in a Rectangular SBDCFC; Li_2CO_3 at 810°C ; 200 g, 0.1 mm Particles

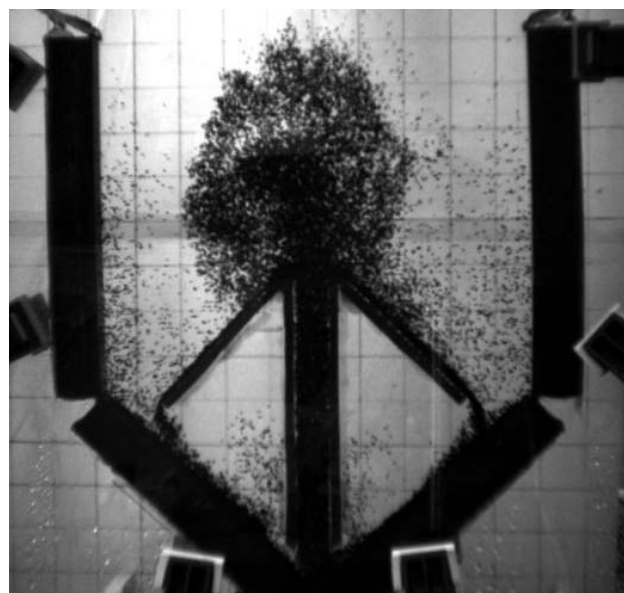


Figure 4. Carbon-Water Slurry Flow in SVHA; 2.6 gpm Water, 75 cm^3 , 1 mm Carbon Particles

this simulation: (1) CO_2 injection does provide “lift” of the slurry through the draft tube; and (2) the transient start-up process is much slower than in Figure 2, where molten carbonate is being injected directly into the cell. This is undoubtedly due to the fact that the gas provides less force than the injected fluid, and it takes longer to develop the momentum required to circulate the slurry. Since this is a more complex, three-phase calculation, the solution

diverges at about 29 s, so we have yet to determine the eventual steady-state condition.

Experimental. Simulated carbon slurry experiments are being conducted in the SVHA. An image of the apparatus is presented in Figure 4. A 5-hole Pitot probe is used to determine the velocity field at selected points within the vessel. Fluid profile properties will be varied with additives to simulate carbon/molten carbonate slurry flow.

Conclusions

- Hydrodynamics can be used to control the circulation, residence time, and distribution of carbon within the spouted bed.
- Function of relative densities, viscosity, particle loading and particle size.
- Carbonate slurry circulation can be provided by pumping the slurry or by gas-lift.
- Gas-lift more favorable – no moving parts.
- Good carbon particle contact with inclined anodes can be achieved with low inlet velocities and with larger particles with greater relative density.

FY 2004 Publications/Presentations

Conference Presentations

1. “Hydrodynamic Reaction Model of a Spouted Bed Electrolytic Reactor,” P.A. Shirvanian, and J.M. Calo, Paper No. 190a, presented at the AIChE 2003 Annual Meeting, San Francisco, CA, November 17, 2003.
2. “A Kinetic-theory Analysis of the Scale-up for the Hydrodynamics of a Rectangular Slot, Spouted Fluidized Vessel,” P.A. Shirvanian and J.M. Calo, Paper No. 292g, presented at the AIChE 2003 Annual Meeting, San Francisco, CA, November 17, 2003.
3. “Spouted Bed Electrodes (SBE) For Direct Utilization of Carbon in Fuel Cells,” J.M. Calo, DOE NETL UCR/HBCU Contractors’ Review Meeting, Pittsburgh, PA, June 9-10, 2004.

Papers

1. “An Experimental Investigation of the Hydrodynamics of a Rectangular, Spouted Vessel with a Draft Duct,” P.A. Shirvanian, J.M. Calo, and G. Hradil, submitted to *Chem. Eng. Sci.*, 2004.
2. “Numerical Simulation of Fluid-Particle Hydrodynamics in a Rectangular Spouted Vessel,” P.A. Shirvanian, J.M. Calo, and G. Hradil, in press, *Int. J. Multiphase Flow*, 2004.
3. “Hydrodynamic Scaling of a Rectangular Spouted Vessel With a Draft Duct,” P.A. Shirvanian and J.M. Calo, submitted to *Chem. Eng. J.*, 2003.

VII.4 Lanthanum Gallate Electrolyte Based Intermediate-Temperature Solid Oxide Fuel Cell Development

S. (Elango) Elangovan (Primary Contact), Shekar Balagopal, Dennis Larsen
Ceramatec, Inc.
2425 South 900 West
Salt Lake City, UT 84119-1517
Phone: (801) 978-2162; Fax: (801) 972-1925; E-mail: Elango@ceramatec.com

DOE Project Manager: Lane Wilson
Phone: (304) 285-1336; E-mail: Lane.Wilson@netl.doe.gov

Subcontractors: Sandia National Laboratory, Albuquerque, New Mexico; New Mexico Tech, Socorro, New Mexico

Objectives

- Evaluate alternative anode materials in order to reduce anode-electrolyte reactivity
- Develop tape cast process to fabricate thin electrolyte cells
- Fabricate single cells using a supported structure
- Demonstrate intermediate-temperature fuel cell operation
- Test short stacks using 10x10 cm cells

Approach

- Modify the anode composition and verify reduction in reactivity using x-ray diffraction of reacted anode-electrolyte powder mixture
- Perform tape sintering studies to fabricate supported single cells
- Test single cells at 700-800°C for short-term and long-term performance

Accomplishments

- Determined that the modification introduced into the nickel-based anode reduced the reactivity between nickel and lanthanum gallate
- Fabricated single cells using thin supported electrolyte with electrolyte thickness ranging from 30 to 75 microns
- Demonstrated single cell performance with an area specific resistance of 0.5 ohm-cm² at 700°C
- Demonstrated stable 1,000-hour performance at an operating temperature of 700°C

Future Directions

- Fabricate full-size (10x10 cm) thin electrolyte cells
- Perform stack tests to verify performance and stability benefits demonstrated in single cells

Introduction

Reducing the operating temperature of solid oxide fuel cells (SOFCs) offers several benefits:

improvement in long-term stability by slowing physical and chemical changes in the cell materials; lower-cost systems by the use of less expensive balance-of-plant components; compatibility with

hydrocarbon reformation process allowing partial internal reformation, which in turn reduces the heat exchanger duty; and finally, the potential to improve thermal cycle capability. In addition, the use of stainless steel interconnects is also facilitated by the lower operating temperature. A temperature range of 650 to 700°C is ideally suited to derive the performance stability, system integration and cost benefits.

In order to derive the advantages of the lower operating temperature, two factors that limit the cell performance, namely the electrolyte resistance and electrode polarization, must be addressed. Lanthanum gallate compositions have shown high oxygen ion conductivity when doped with Sr and Mg. Unlike other oxygen ion conductors such as ceria and bismuth oxide, the Sr- and Mg-doped lanthanum gallate (LSGM) compositions are stable over the oxygen partial pressure range of interest. The combination of stability in fuel gas environments and high oxygen ion conductivity makes the LSGM material a potential choice for intermediate-temperature SOFCs. However, challenges in the development of electrode materials and cell fabrication processes need to be overcome to make use of the potential of the LSGM electrolyte.

Approach

Nickel-based anodes have been successfully demonstrated to be catalytic for fuel oxidation in zirconia electrolyte-based SOFC systems. A modified nickel anode composition was evaluated using powder mixtures of the anode and LSGM electrolyte. The reacted powder mixture was analyzed using x-ray diffraction technique. Additionally, an 8-cell stack was tested for over 1,000 hours, and the anode-electrolyte interface was analyzed using scanning electron microscopy for evidence of nickel diffusion into the electrolyte.

Tape cast process development was performed to cast LSGM tape of various thicknesses to provide sintered electrolyte thicknesses ranging from 75 to 300 microns. The process variables included powder surface area, organic content in the tape slip, and sintering temperature. The primary objectives of the activity were to achieve sintered electrolyte density and flatness required for stacking. Single cells with

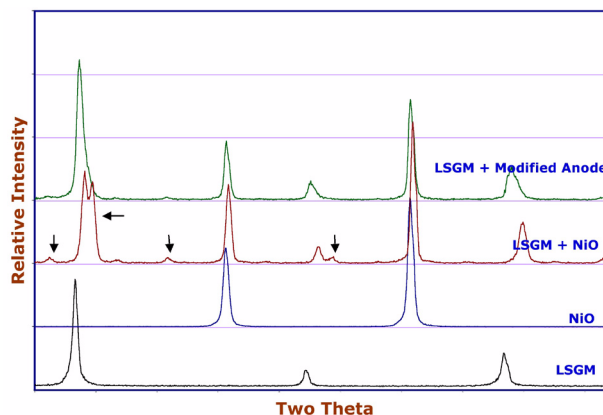


Figure 1. Powder X-ray of Baseline and Reacted Electrolytes, Anode Powders

1 to 2.5 cm² active area were tested for performance characteristics and long-term stability.

Results

The modification to the nickel anode was found to significantly reduce the reactivity with the LSGM electrolyte. X-ray diffraction pattern for the powder mixture of the anode-electrolyte calcined at 1300°C is shown in Figure 1. Diffraction pattern for the baseline LSGM, NiO, and a mixture of the two are also shown in the figure. It can be seen that the reaction phase peaks prominent in the baseline mixture are significantly reduced in their intensities for the modified anode.

In order to verify the long-term stability of the anode-electrolyte interface, a stack was built and tested for 1200 hours. Although performance degradation was observed, attributable to chromium evaporation from the interconnect, scanning electron microscopy of the anode-electrolyte interface showed no detectable diffusion of nickel into the electrolyte, nor were any interfacial reaction products observed. The nickel x-ray map is shown in Figure 2.

Thin electrolyte single cells were fabricated using the tape lamination technique. Both anode and cathode structures were evaluated as the support for the electrolyte. The performance of a cathode-supported cell is shown in Figure 3. The thin, 75-micron LSGM electrolyte cells showed an area specific resistance of 0.5 ohm-cm² at an operating

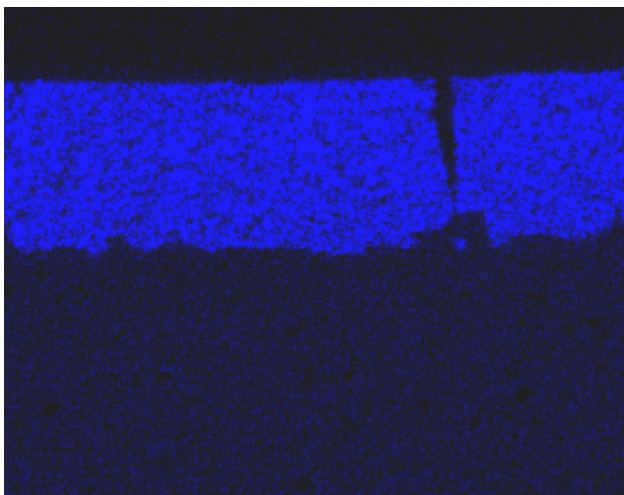


Figure 2. Nickel Map of Anode-Electrolyte Interface after 1200-hr Stack Test

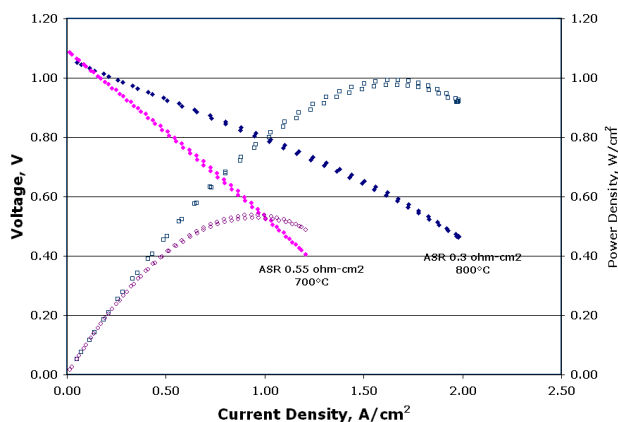


Figure 3. Performance of a Cathode-Supported LSGM Cell; Electrolyte Thickness of 75 Microns Was Used

temperature of 700°C. The long-term performance of selected cells is shown in Figure 4. Similar performance and stability results were also obtained using cells with the anode-support configurations. Thus, the performance benefits of using high-conductivity LSGM electrolyte and the stability improvement by using the modified anode were established in single-cell tests.

Conclusions

- Sr- and Mg-doped lanthanum gallate compositions show exceptionally high oxygen ion conductivity and stability in SOFC operating

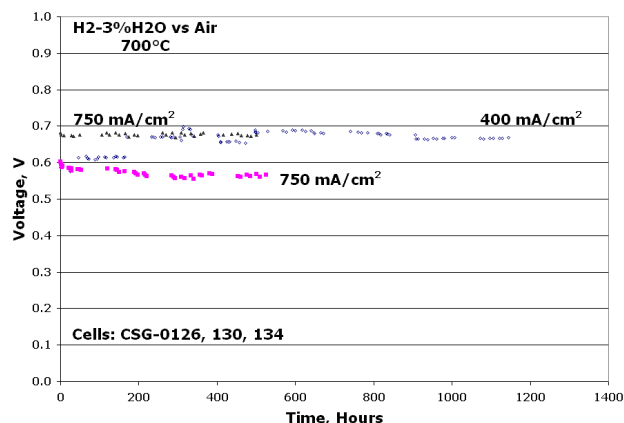


Figure 4. Long-term Stability of Cathode-Supported Cells at an Operating Temperature of 700°C

conditions for use at the intermediate temperatures of 650-700°C.

- The anode reactivity that is known to cause long-term instability has been addressed by introducing a modification to the nickel-based anode composition.
- A 1000-hour stack test provided additional confirmation on the effectiveness of the anode modification.
- Thin, supported cells meet the performance target of 0.5 ohm-cm² resistance at 700°C.
- Long-term tests of single cells show stable performance.

FY 2004 Publications/Presentations

1. Lanthanum gallate electrolyte for intermediate temperature SOFC operation, S. Elangovan, B. Heck, S. Balagopal, D. Larsen, M. Timper and J. Hartvigsen, Presented at the International Symposium on "Solid Oxide Fuel Cell (SOFC) Materials and Technology," 28th International Cocoa Beach Conference and Exposition of the American Ceramic Society, January 25-30, 2004 at Cocoa Beach, FL.
2. Intermediate temperature stack operation using lanthanum gallate electrolyte system, S. Elangovan, B. Heck, S. Balagopal, Insoo Bay, R. Merrill, and D. Larsen, Proc. Sixth European SOFC Forum, Lucerne, Switzerland, p. 97, June 28 - July 2, 2004.

VII.5 Advanced Net-Shape Insulation for Solid Oxide Fuel Cells

Balakrishnan Nair (Primary Contact), Akash Akash, Kerri Cameron, Mark Timper, Jesse Nachlas and S. Elangovan

Ceramatec, Inc.

Salt Lake City, UT 84119

Phone: (801) 956-1019; Fax: (801) 972-1925; E-mail: bnair@ceramatec.com

DOE Project Manager: Travis Shultz

Phone: (304) 285-1370; E-mail: Travis.Shultz@netl.doe.gov

Objectives

- Demonstrate the feasibility of using a proprietary material – CERCANAM[®] (Ceramatec Castable Nano Material) – as a functional insulation material in high-temperature solid oxide fuel cell (SOFC) operational environments.
- Fabricate 6" × 6" × 1/4-1/2" CERCANAM plates with minimal post-machining.
- Demonstrate appropriate thermal shock resistance and thermal cycling resistance for 6" × 6" × 1/4-1/2" CERCANAM plates at temperatures up to 1000°C.
- Demonstrate the intermediate-term (100 h) thermochemical stability of CERCANAM materials in high-temperature air and fuel environments.
- Demonstrate the short-term (100 h) stability of SOFC electrodes and electrode/electrolyte interfaces in fuel/air passed over CERCANAM at 850°C.
- Demonstrate adequately low thermal conductivity and tolerable cost for application as SOFC insulation.

Approach

- Fabricate 6" × 6" × 1/4-1/2" CERCANAM plates using modified processing routes amenable to low-cost bulk fabrication of custom shapes.
- Perform thermogravimetric analysis (TGA) of CERCANAM specimens in air, hydrogen and carbon dioxide, as well as weight change measurements after exposure to syngas.
- Perform testing of solid oxide fuel cells with CERCANAM in the air and fuel streams and monitor fuel cell performance during the test.
- Measure thermal conductivity using conventional laser flash diffusivity analysis (LFA) as well as a guarded hot-plate apparatus.
- Perform a preliminary cost analysis to estimate production costs of CERCANAM in large-scale production.

Accomplishments

- 6" × 6" CERCANAM parts were fabricated with minimal warpage.
- These parts showed excellent resistance to aggressive thermal cycling and thermal shock exposures.
- Lightweight (0.9 g/cc), low thermal conductivity (0.3-0.4 W/m/K), high purity (<0.1% SiO₂) compositions were developed. CERCANAM specimens exposed to flowing air and fuel on the cathode and anode side, respectively, of both yttria-stabilized zirconia (YSZ) and lanthanum strontium magnesium gallate (LSGM; La_{1-x}Sr_xGa_{1-y}Mg_yO₃; lanthanum gallate doped with Sr on the A-site and Mg on the B-site) based SOFC button cells resulted in no degradation in SOFC performance in intermediate-term (100-200 hour) tests.

- CERCANAM specimens showed excellent resistance to significant temperature gradients; excellent resistance to coking in reformed natural gas (and no change in thermal conductivity); and excellent chemical stability in hydrogen, CO₂ and syngas.
- Raw-materials cost for CERCANAM production were shown to be below \$125/ft³, and since the production processes are similar to conventional ceramics, it is clear that production cost targets will easily be below the insulation cost target set by the Solid State Energy Conversion Alliance (SECA) of \$345/ft³.

Future Directions

- Establish detailed processing-microstructure-property-cost correlations for CERCANAM and optimize materials processing to achieve the lowest possible thermal conductivity and cost in CERCANAM materials.
- Demonstrate long-term stability (>2000 hours) of YSZ and LSGM button cells with selected CERCANAM compositions in the fuel and air sides.
- Demonstrate application of CERCANAM to insulate a simulated full-scale SOFC stack.
- Fabricate and evaluate tubular high alumina sintered porous/dense layered structure for net-shape insulation in tubular SOFCs.
- Perform detailed manufacturing cost analysis for CERCANAM and the porous/dense laminated structures to provide data that can be utilized in global SOFC cost models by SECA teams.
- Identify specific insulation requirements for SOFC designs of various SECA vertical teams and identify appropriate CERCANAM compositions with the optimal combination of thermal conductivity, strength, and cost.

Introduction

As solid oxide fuel cell (SOFC) technology matures, cost considerations are becoming the primary barriers to commercialization. The cost threshold for commercialization of SOFCs is believed to be \$400/kW, a target set by SECA, a consortium of government, industrial partners and national laboratories/universities focused on development of cost-effective fuel cell-based power generators. As the cost of other components of the system (electrodes, electrolytes, and interconnects) become lower due to increased production and improved yield through technology maturation, the cost of insulation as a percentage of the total cost is becoming higher. SECA has identified a cost target for SOFC insulation of about \$16-20/kW (based on \$400/kW for the overall system), which translates to \$300-350/ft³ of insulation material. For comparison, the cost of high-purity microporous insulation is around \$1200/ft³, and the current status of insulation cost for the stack is about \$30-40/kW.

There are major technological issues associated with use of the currently available low-cost insulation materials. Most current materials are

processed from aluminosilicate fibers, aluminosilicate-based reaction bonded ceramics or low-grade alumina, all of which have significant silica content. It is now well known that materials with substantial silica contents are poor choices for SOFC systems where spent fuel recirculation is used as an option for increasing fuel efficiency, such as in the tubular design employed by Siemens-Westinghouse Power Corporation. Testing of SOFC performance, when operated with partially reformed natural gas blown through a porous silica-rich insulation, has shown that SOFC performance starts to decline after 1000 h of testing. Some types of high-purity alumina (low silica) insulation are commercially available and have been shown to have good performance in SOFC environments. However, the sintered, porous insulation materials generally have relatively high thermal conductivity (>0.6 W/mK) and density to make them practical for SOFC applications on a weight/kW basis. In addition, sintered materials generally need substantial post-machining to form the desired shapes, which increases processing costs. Fibrous insulation materials, on the other hand, can be cut and shaped easily, but the high-purity fiber-based materials are



Figure 1. An L-shaped CERCANAM Specimen That Showed No Significant Damage after 9 Thermal Cycles from Room Temperature to 850°C, Followed by an Aggressive Thermal Shock Test

cost-ineffective for SOFC applications. Therefore, there is a current and pending need for low-cost, high-performance insulation for SOFC systems.

Approach

Over the past three years, Ceramtec has been developing castable alumina-based nano- and sub-micron ceramics for micro-components that require very high dimensional tolerances. The new family of materials, called CERCANAM, is based on the idea that precision components can be fabricated through reaction bonding. In 2003, Ceramtec was awarded a Phase I Small Business Innovation Research (SBIR) Grant by the Department of Energy (DOE) to develop SOFC insulation. The goal of Phase I was to demonstrate that the process and material were suitable for fabricating larger parts with sufficient thermomechanical and thermochemical stability in SOFC operating environments and could meet SOFC commercialization cost targets. Based on the substantial progress achieved in Phase I, Ceramtec was recently notified of a Phase II grant to continue development of CERCANAM SOFC insulation to near commercial scale.

Results

The Phase I project was highly successful in meeting all of the technical targets. CERCANAM

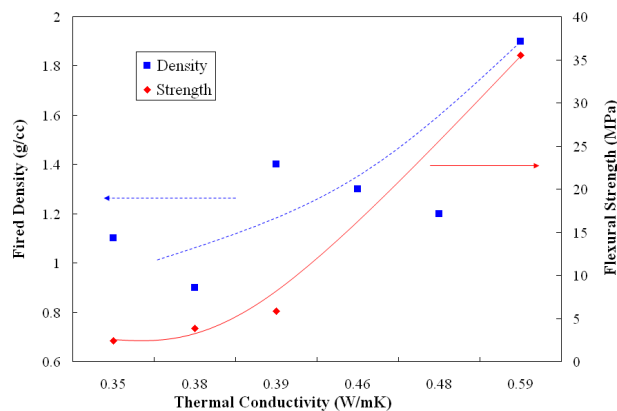


Figure 2. Plot Showing a Trade-off Between Thermal Conductivity and Strength of CERCANAM Materials

parts with dimensions 6" × 6" could be fabricated with minimal warpage, and parts of these dimensions showed excellent resistance to aggressive thermal cycling and thermal shock exposures from typical SOFC operating conditions to ambient temperature. Figure 1 shows an L-shaped CERCANAM slab subjected to thermal cycling and thermal shock. No degradation was seen after 9 cycles to 850°C followed by in-furnace air cooling. After the thermal cycling tests, the same part was subjected to an aggressive thermal shock test which involved rapid air cooling from 850°C to room temperature at ~3600°C/hr. The part survived this test also with no significant damage. CERCANAM specimens also showed excellent resistance to significant temperature gradients, excellent resistance to coking in reformed natural gas (with no change in thermal conductivity), and excellent chemical stability in hydrogen, CO₂ and syngas.

CERCANAM compositions with bulk density lower than 0.9 g/cc and thermal conductivities as low as 0.3-0.4 W/m/K (which meet SECA targets) were developed. As expected, a trade-off between thermal conductivity and flexural strength was observed – both flexural strength and thermal conductivity decrease with decreasing density as shown in Figure 2. CERCANAM specimens exposed to flowing air and fuel on the cathode and anode side, respectively, of SOFC button cells (both YSZ- and LSGM-based) resulted in no degradation in SOFC performance in intermediate-term (100-200 hour) tests. An example is provided in Figure 3 which indicates that there is

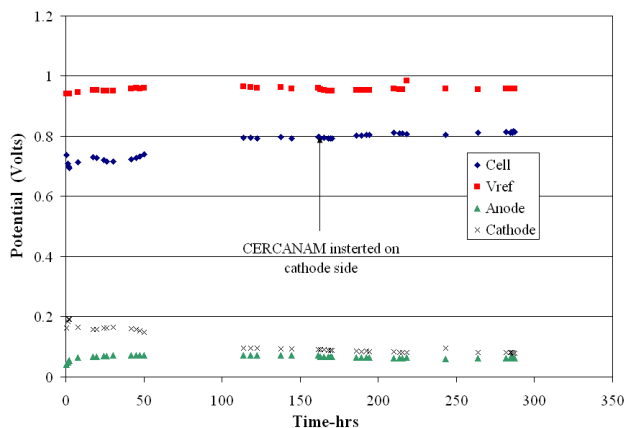


Figure 3. An Example of Cell Test Data Showing No Effect of Introducing CERCANAM on the Cathode Side of a YSZ-based SOFC Button Cell

no degradation in fuel cell performance when CERCANAM is introduced on the cathode side of YSZ-based SOFC button cells. Similar tests have also shown no effect when CERCANAM is introduced on the anode or cathode side of YSZ- or LSGM-based button cells.

In addition, raw-materials cost for CERCANAM production was shown to be about \$125/ft³ (assuming a density of 0.9 g/cc). Since the production processes are similar to conventional ceramics, it is clear that production cost targets will easily be below the SECA targets. Figure 4 shows the results of a preliminary production cost analysis carried out in the Phase I project utilizing some simplifying assumptions. The analysis shows that the cost starts to approach the DOE cost target at an annual production volume of over 3,800 ft³/year.

Conclusions

To ensure commercially viable SOFC systems, it is critical to develop low-cost, high-performance insulation materials. CERCANAM materials were shown to have sufficiently low thermal conductivity, sufficiently low cost, sufficiently high thermal/

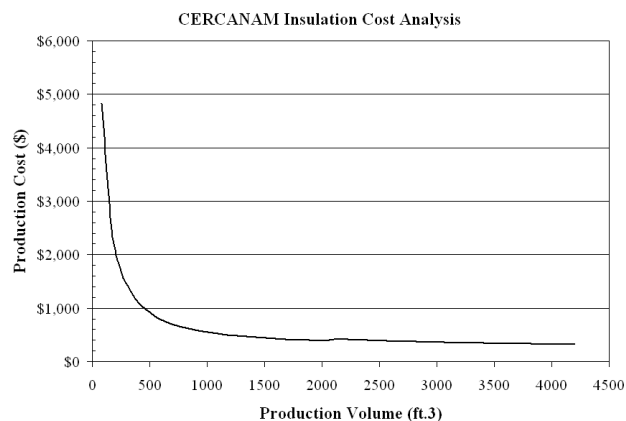


Figure 4. Preliminary Production Cost Analysis for CERCANAM Insulation Materials Which Indicates That the Cost Approaches the SECA Target of \$345/ft³ at a Production Volume over 3,800 ft³/year

chemical stability and sufficiently high thermal cycling/thermal shock resistance for application as SOFC insulation. Clearly, CERCANAM is a promising option for SOFC insulation from both technical and commercialization perspectives. Future work in the Phase II project will be directed at developing low-cost, high-yield manufacturing routes and demonstrating long-term operation of SOFC button cells and simulated stacks with CERCANAM insulation.

Patents

No patent applications have been submitted yet. It is anticipated that a provisional patent will be filed in the first year of the Phase II project.

VII.6 Carbon Ionic Conductors for Use in Novel Carbon-Ion Fuel Cells

F. H. Cocks (Primary Contact), W. N. Simmons, P. A. Klenk

Duke University

Pratt School of Engineering

Box 20300

Durham, NC 27708

Phone: (919) 660-5301; Fax: (919) 660-8963; E-mail: hadley01@duke.edu

DOE Project Manager: Lane Wilson

Phone: (304) 285-1336; E-mail: Lane.Wilson@netl.doe.gov

Objectives

- To evaluate the possibility that ionic carbides could act as superionic membrane materials for carbon ions, allowing the development of a radically new fuel cell based on the transport of carbon ions rather than hydrogen or oxygen ions.

Approach

- Stabilization of the fluorite crystal structure via combining at least two lanthanides having substantially different ionic radii.
- Preparation of pseudo-binary ionic carbide compounds using carbon-13 together with the diffusion of carbon-12 vapor-deposited layers.
- Analysis of the in-diffusion profiles of carbon-12 into pseudo-binary ionic carbide compounds using SIMS (secondary ion mass spectrometry) to determine carbon ion diffusivities in these materials.
- Use of the Nernst-Einstein equation to estimate ionic mobilities from the measured diffusion data.

Accomplishments

- Successfully developed a novel method of preparing lanthanide carbides by sintering lanthanum oxide/carbon admixtures heated to very high (>2500°C) temperatures using electron beam heating.
- Successfully stabilized La-Er carbide, La-Ce carbide and La-Y carbide produced with carbon-13 so that these compounds retain the cubic fluorite structure in the temperature range from 300 K - 2800 K.

Future Directions

- Complete the carbon-12 in-diffusion heat treatments.
- Determine the in-diffused carbon-12 depth profile using secondary ion mass spectrometry.
- Calculate the carbon ion mobility using the Nernst-Einstein equation.

Introduction

Carbon-consuming fuel cells have many potential advantages, including increased efficiency and reduced pollution. A large amount of work has already been done on coal fuel cells which utilize yttria-stabilized zirconium carbide as an oxygen-ion superionic membrane material. However, no superionic membrane material for carbon ions is yet

known. Such a solid-state superionic membrane material would enable an entirely new class of carbon fuel cell to be developed that would use coal directly as the fuel source, without any intervening combustion process. A carbon-ion superionic conductor would be an enormous step forward because it would allow the direct conversion of coal to electricity without the formation of any of the pollutants (SO₂, etc) other than CO₂ that can

accompany coal combustion. Fuel cells utilizing yttria-stabilized zirconium may require combustion of coal to carbon monoxide prior to final oxidation to carbon dioxide with the oxygen-ion membrane. The objective of this research is to investigate specific ionic lanthanide carbide and ionic lanthanide carbide pseudo-binary solid solutions as possible superionic carbide-ion conductors. The discovery of such a material would have the potential of ushering in a truly revolutionary new coal technology.

Rare earth carbides have the fluorite structure when they are above their transition temperatures, which vary from 350°C (EuC₂) to 1450°C (LuC₂). This structure is perhaps the crystal structure most widely found in superionic materials. These cubic lanthanide carbide compounds could potentially be good ionic conductors for carbon.

Approach

Rare earth carbides of the form LnC₂ (where Ln refers to any element of the lanthanide series) are being investigated as potential superionic membrane materials. These compounds have the fluorite structure when they are above their transition temperatures. The carbon atoms in these compounds reside as anions in tetragonal positions equivalent to the positions of the mobile ions F⁻ and O₂⁻ in the known superionic conductors CaF₂ and Zr_{0.8}Y_{0.2}O₂. Rare earth carbides represent perhaps the most favorable class of superionic carbon membrane materials. However, it is necessary to stabilize the cubic fluorite structure which these compounds exhibit at elevated temperature so that this structure is stable down to room temperature. Such stabilization is being sought by alloying rare earth carbides with substantially different lattice parameters. Measurement of carbon ion diffusivity will be measured via the in-diffusion of carbon-12 into the base carbide compound produced with carbon-13.

Results

The lanthanide dicarbides have been synthesized by reacting mixtures of Ln₂O₃ and amorphous ¹³C under vacuum at high temperatures (>1600°C), using a newly developed synthesis technique which we have termed the reactive oxide electron beam

(REOB) synthesis technique. These dicarbides were subsequently densified at high temperatures (<2500°C) using electron beam heating. Direct production of these materials by means of direct melting of lanthanide-series metals and carbon using water-cooled copper hearth arc-melting was found to be ineffective due to the uncontrollable dispersion of the carbon as a result of the arc blow generated by the high arc current.

La-Er carbide, La-Ce carbide and La-Y carbide have been successfully produced using the REOB procedure. Powder x-ray diffraction was used to confirm that their crystal structures remained stable in the fluorite structure in the temperature range of 300-2800 K. These compounds have been produced with carbon-13 in order that vapor-deposited carbon-12 coatings could be used in the diffusion measurements, since carbon-13 arcing electrodes or sputtering targets do not appear to be available from any source world-wide. Either arc evaporation or sputtering is needed to produce an adherent film for the high-temperature in-diffusion treatment.

Semi-thick coatings (>10 m) of ¹²C were deposited on these samples using the arc-evaporation of high-purity, commercially available graphite electrodes. Natural graphite contains ~1.11% carbon-13 and 99% carbon-12. The small (1%) amount of carbon-13 contained in the graphite can be readily accounted for mathematically in the deconvolution of the measured carbon-12 in-diffusion profile. To produce these samples, coated samples are heated at 850°C, 950°C, and 1150°C in a custom-built high-vacuum furnace. Prolonged SIMS sputtering will be used to determine the complete carbon-12 diffusion profile from surface to baseline. From these measurements, together with semi-infinite diffusion equations, the carbon-12 diffusion constant can be determined, which can then be used in the Nernst-Einstein equation to calculate carbon ion mobilities.

Conclusions

- A novel method for preparing lanthanide carbides by sintering lanthanum oxide/carbon admixtures heated to very high (>2500°C) temperatures using electron beam heating has been developed.

- Stabilized La-Er carbide, La-Ce carbide and La-Y carbide have been produced with carbon-13 so that these compounds retain the cubic fluorite structure in the temperature range from 300 – 2800 K.
- Diffusion measurements together with the Nernst-Einstein equation will be used to determine the carbon-ion mobility in these fluorite structure stabilized lanthanide carbides.

FY 2004 Publications/Presentations

1. *Carbon Ionic Conductors for Use in Novel Carbon-Ion Fuel Cells*, Presented at the University Coal Research Contractors Review Conference, June 9-10, 2004, Pittsburgh, PA

VII.7 Novel Electrode Materials for Low-Temperature Solid Oxide Fuel Cells

Meilin Liu (Primary Contact), Shaowu Zha, Yin Liu, Luis Aguilar, Yuelan Zhang

School of Materials and Engineering, Georgia Institute of Technology

771 Ferst Drive

Atlanta, GA 30332-0245

Phone: (404) 894-6114; Fax: (404) 894-9140; E-mail: meilin.liu@mse.gatech.edu

DOE Project Manager: Lane Wilson

Phone: (304) 285-1336; E-mail: Lane.Wilson@netl.doe.gov

Objectives

- Characterize the microscopic features of composite anodes and correlate them with the ionic and electronic transport properties as well as the catalytic activities for oxidation of fuels.
- Minimize interfacial polarization resistances of anodes through processing modifications, microstructure improvements, and new materials development.
- Develop new catalysts for pre-reforming of hydrocarbon fuels to smaller molecules or for *in-situ* reforming.
- Gain a profound understanding of the principles of composite anodes for fuel cells to be operated at low temperatures.

Approach

- Synthesize and optimize NiO-GDC (gadolinium-doped ceria) composites as anode materials.
- Develop low-temperature solid oxide fuel cells (SOFCs) with active electro-catalyst for hydrocarbon fuels.
- Test catalyst consisting of 1 wt.% Pt supported by Gd-doped ceria for pre-reforming of propane at low steam/carbon ratio.
- Fabricate highly porous and nano-structured electrodes using combustion chemical vapor deposition (CVD) and characterize their performance as electrodes for low-temperature SOFCs.

Accomplishments

- Four types of anodes with two kinds of NiO and GDC powders were investigated. By carefully adjusting the anode microstructure, the GDC electrolyte/anode interfacial polarization resistances were reduced dramatically. The interfacial resistance at 600°C decreased from 1.61 $\Omega \text{ cm}^2$ for the anodes prepared using commercially available powders to 0.06 $\Omega \text{ cm}^2$ for those prepared using powders derived from a glycine-nitrate process.
- Anode-supported SOFCs with an electrolyte of 20 μm -thick GDC were fabricated by co-pressing, and both Ni- and Cu-based anodes were prepared by a solution impregnation process. At 600°C, SOFCs fuelled with humidified H₂ and methane reached peak power densities of 602 and 519 mW/cm², respectively.
- A catalyst (1 wt.% Pt dispersed on porous Gd-doped ceria) for pre-reforming of propane was developed with relatively low steam to carbon (S/C) ratio (~0.5), coupled with direct utilization of the reformat in low-temperature SOFCs. Propane was converted to smaller molecules during pre-reforming, including H₂, CH₄, CO, and CO₂. A peak power density of 247 mW/cm² was observed when pre-reformed propane was directly fed to an SOFC operated at 600°C.
- Highly porous, excellently bonded and nano-structured electrodes fabricated by combustion CVD exhibit extremely high surface area and remarkable catalytic activity.

Future Directions

- Fabricate anode-supported SOFCs based on yttria-stabilized zirconia (YSZ) electrolyte and further modify anode surfaces for low-temperature (500-800°C) operation.
- Further minimize interfacial resistances through processing modifications and microstructure improvements using combustion CVD technology.

Introduction

It is the interfacial resistances that limit the performance of SOFCs at temperatures below 550°C. The overall objective of this project is to develop novel electrode materials for SOFCs to be operated at low temperatures in order to significantly reduce the cost of SOFC technology, thus achieving the goals of the Vision 21 coal-based power plants. More specifically, in this work we will (1) characterize the microscopic features of composite mixed-conducting electrodes and correlate with the ionic, electronic, and ambipolar transport properties as well as with the catalytic activities for pertinent electrochemical reactions; (2) minimize interfacial polarization resistances through processing modifications, microstructure improvements, and new materials development; and (3) gain a profound understanding of the principles of composite mixed-conducting electrodes.

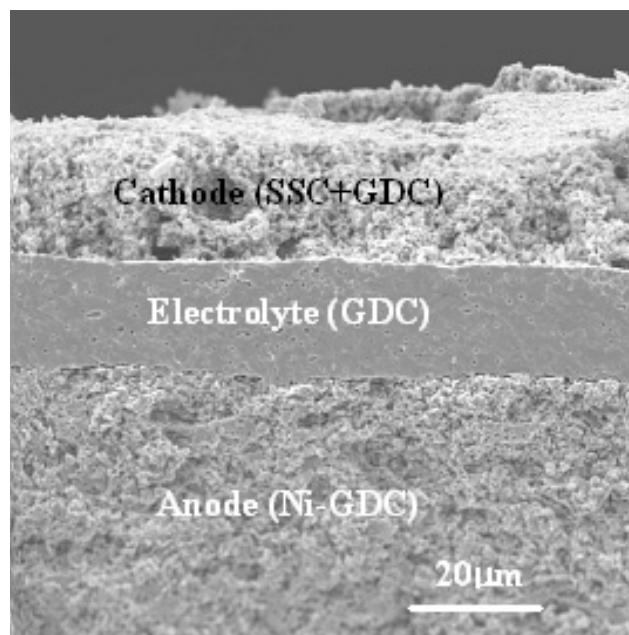


Figure 1. A Cross-Sectional View (SEM photograph) of a Ni-GDC Anode-Supported SOFC with a Thin GDC Electrolyte Layer

Approach

It has been demonstrated that the length of the triple-phase boundary (TPB) correlates well with the reaction rate for electrochemical oxidation of hydrogen; thus, the extension of the TPB becomes a determining factor in improving anode performance. This can be achieved mainly by optimizing the microstructure of the cermet anode through the adjustment of powder morphologies and particle sizes for the precursor NiO and ceria, and/or developing a favorable electroding process.

Carbon deposits can be suppressed by using anode compositions that do not catalyze hydrocarbon cracking, especially when running SOFCs at relatively low temperatures. In this study, we developed new anode materials for direct oxidation of methane and propane in low-temperature SOFCs. Anode-supported SOFCs with thin Gd-doped ceria electrolyte were fabricated by co-pressing, and both Ni- and Cu-based anodes were prepared by a solution impregnation process. We also developed novel catalysts for pre-reforming of propane, coupled with direct utilization of the reformat in low-temperature SOFCs.

We employed the combustion CVD technique to fabricate nano-structured electrodes for low-temperature SOFCs. These combustion CVD-derived electrodes exhibit extremely high surface area and remarkable catalytic activity.

Results

Four types of anodes with two kinds of NiO and GDC powders were investigated. It was found that fuel cell performance depends strongly on the anode microstructure, which is determined by the anode composition and fabrication conditions. By carefully adjusting the anode microstructure, the GDC electrolyte/anode interfacial polarization resistances were reduced dramatically. The interfacial resistance

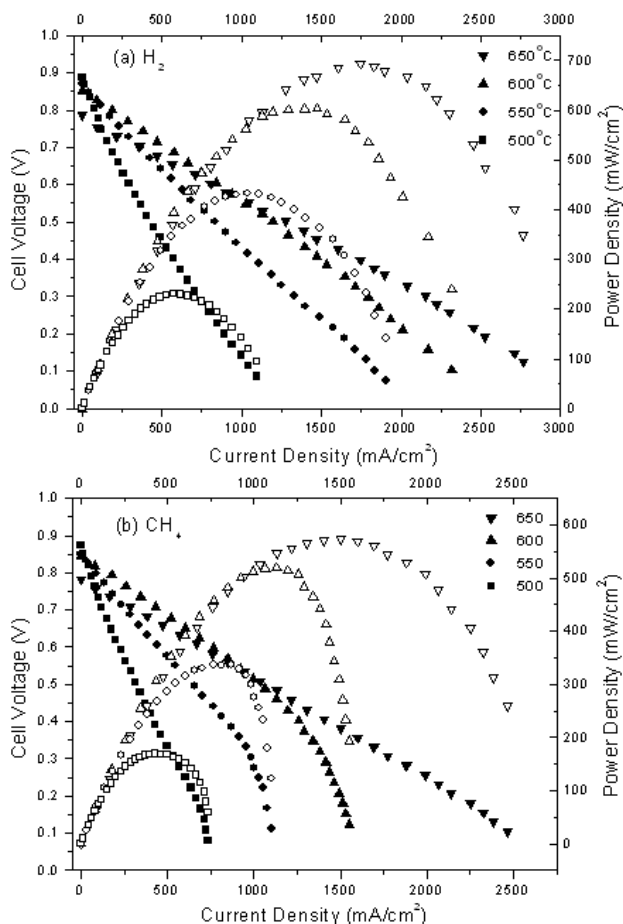


Figure 2. Cell Voltages and Power Densities as a Function of Current Density for a Cell with Ni-GDC Anode Fabricated by Co-Pressing Operated at Different Temperatures (500 - 650°C) with Different Fuels: (a) H_2 and (b) CH_4

at 600°C decreased from $1.61 \Omega \text{ cm}^2$ for the anodes prepared using commercially available powders to $0.06 \Omega \text{ cm}^2$ for those prepared using powders derived from a glycine-nitrate process.

The critical issues facing the development of economically competitive SOFC systems include lowering the operation temperature and creating novel anode materials and microstructures capable of efficiently utilizing hydrocarbon fuels. Anode-supported SOFCs with an electrolyte of 20 μm -thick GDC were fabricated by co-pressing (Figure 1), and both Ni- and Cu-based anodes were prepared by a solution impregnation process. Figure 2 shows that SOFCs fuelled with humidified H_2 and methane reached peak power densities of 602 and 519

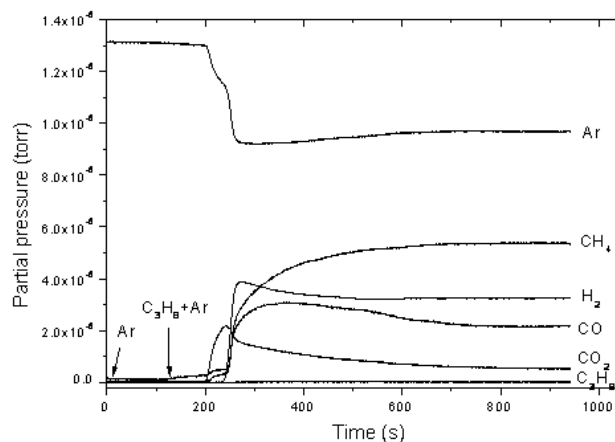


Figure 3. A Typical Mass Spectrum of the Reformed Propane on Catalyst Pt-GDC at 650°C (S/C = 0.5)

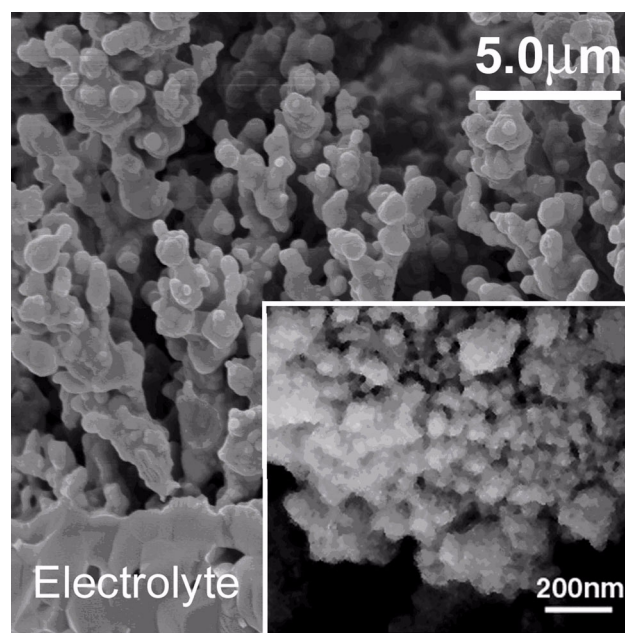


Figure 4. Cross-Sectional Views of an SOFC with Cathode Fabricated Using Combustion CVD

mW/cm^2 , respectively, at 600°C. Both microstructure and composition of the anodes, as fabricated using a solution impregnation technique, greatly influence fuel cell performance.

A catalyst (1 wt.% Pt dispersed on porous Gd-doped ceria) was tested for pre-reforming of propane with relatively low steam to carbon (S/C) ratio (~ 0.5), coupled with direct utilization of the reformat in low-temperature SOFCs. Figure 3

shows that propane is converted to smaller molecules during pre-reforming, including H₂, CH₄, CO, and CO₂. A peak power density of 247 mW/cm² was observed when pre-reformed propane was directly fed to an SOFC operated at 600°C. No carbon deposition was observed in the fuel cell for a continuous operation of 10 hours at 600°C.

The development of a nano-structured cathode yielded interesting results. Highly porous, excellently bonded and nano-structured electrodes for low-temperature SOFCs have been successfully fabricated using the combustion CVD approach, as shown in Figure 4. These combustion CVD-derived electrodes consisting of nano-grains less than 50 nm in length exhibit extremely high surface area and remarkable catalytic activity.

Conclusions

The performance of SOFCs at low temperatures depends strongly on the interfacial resistances between the electrodes and the electrolyte. By carefully controlling the microstructures of the electrodes, relatively high performances have been achieved at temperatures below 650°C due to a significant reduction in interfacial polarization resistances. Nano-structured electrodes fabricated by combustion CVD show extremely high surface area and remarkable catalytic activity.

Ni-GDC anode-supported fuel cells are capable of running on methane directly at low temperatures. A catalyst (1% Pt-GDC) was developed for pre-reforming of propane at low steam/carbon ratio to smaller molecules such as H₂, CH₄, CO, and CO₂.

FY 2004 Publications

1. Y. Liu, S. Zha, M. Liu, Nanostructured Electrodes for SOFCs Fabricated by Combustion CVD, *Advanced Materials*, 16 (2004) 256.
2. S. Zha, A. Moore, H. Abernathy, M. Liu, GDC-Based Low Temperature SOFCs Powered by Hydrocarbon Fuels, *J. Electrochem. Soc.*, 151 (2004) A1128.
3. S. Zha, W.L. Rauch, M. Liu, Ni-GDC Anode for GDC Electrolyte-Based Low-Temperature SOFCs, *Solid State Ionics*, 166 (2004) 241.
4. F. Chen, S. Zha, J. Dong, M. Liu, Pre-reforming of Propane for Low-Temperature SOFCs, *Solid State Ionics*, 166 (2004) 269.
5. Y. Liu, W.L. Rauch, S. Zha, M. Liu, Fabrication of Nano-structured Sm_{0.5}Sr_{0.5}CoO_{3-δ} – Sm_{0.1}Ce_{0.9}O_{2-δ} Cathodes for Solid Oxide Fuel Cells Using Combustion CVD, *Solid State Ionics*, 166 (2004) 261.
6. C. Xia, Y. Zhang, M. Liu, Composite Cathode Based on Ytria Stabilized Bismuth Oxide for Low-Temperature SOFCs, *Appl. Phys. Lett.*, 82 (2003) 901-903.
7. L. Aguilar, S. Zha, Z. Cheng, J. Winnick, M. Liu, A Solid Oxide Fuel Cell Operating on Hydrogen Sulfide (H₂S) and Sulfur-Containing Fuels, *J. Power Sources*, in press.
8. L. Aguilar, S. Zha, S. Li, M. Liu, J. Winnick, Sulfur Tolerant Materials for Hydrogen Sulfide (H₂S) Solid Oxide Fuel Cell, *Electrochem. Solid-State Lett.*, in press.

VII.8 LSGM-Based Composite Cathodes for Anode-Supported, Intermediate-Temperature (600-800°C) Solid Oxide Fuel Cells

Tad J. Armstrong (Primary Contact), Anil V. Virkar, Roger Smith, Yimei Gao

Materials and Systems Research, Inc.

5395 West 700 South

Salt Lake City, UT 84104

Phone: (801) 530-4987; Fax: (801) 530-4820; E-mail: tarmstro@MSRIhome.com

DOE Project Manager: Lane Wilson

Phone: (304) 285-1336; E-mail: Lane.Wilson@netl.doe.gov

Objectives

- Develop Sr- and Mg-doped LaGaO₃ (LSGM)-based composite cathodes for anode-supported solid oxide fuel cells (SOFCs) capable of operating at 600-800°C.
- Develop and optimize a powder synthesis process that produces single-phase, nanosized powders of LSGM and Co- and Fe-doped LSGM for cathode use.
- Optimize composite cathode interlayer with regards to microstructure and composition for low-temperature SOFC operation.
- Perform electrochemical testing on single cells at temperatures between 500 and 800°C and estimate electrode overpotentials and ohmic losses.
- Construct and demonstrate the operation of an internally manifolded stack, comprised of cells with LSGM-based cathodes, capable of delivering 1 kW of power while operating on partially reformed natural gas at 800°C.

Approach

- Identify mixed ionic-electronic conducting (MIEC) electrocatalytic materials compatible with LSGM for use in composite cathodes.
- Synthesize single-phase and nanosized powders of both electrocatalytic materials (MIEC) and LSGM by a glycine-nitrate combustion technique.
- Fabricate anode-supported SOFC with thin-film yttria-stabilized zirconia (YSZ) electrolytes for testing and evaluation of composite cathodes.
- Fabricate LSGM-based composite cathodes onto SOFC by screen printing. Optimize cathode with regards to thickness, particle size, composition, firing temperature, and firing time.
- Perform electrochemical testing of single SOFC at temperatures between 600 and 800°C.
- Characterize microstructure of the starting powders and the as-fabricated composite cathodes by scanning electron microscopy (SEM) and x-ray diffraction (XRD).

Accomplishments

- Successfully synthesized single-phase, nanosized powders of LSGM (La_{0.9}Sr_{0.1}Ga_{0.8}Mg_{0.2}O₃) and various electrocatalytic materials including La_{0.8}Sr_{0.2}MnO₃, La_{0.6}Sr_{0.4}CoO₃, La_{0.6}Sr_{0.4}Co_{0.2}Fe_{0.8}O₃, La₂NiO₄, and La_{1.7}Sr_{0.3}NiO₄.
- Fabricated and tested SOFCs with active areas of 2 cm² and 30 cm² with LSGM-based composite cathodes. Cell performance measured at temperatures between 600 and 800°C.

- Demonstrated that reduction in particle size and refinement of composite cathode interlayer microstructure can reduce the average area specific resistance (ASR) of the cell by as much as 25% for a given cathode composition.
- High performance in single cells with LSGM-based cathodes has been demonstrated. Power densities of 1.2 W/cm² at 0.7 V at 800°C, and 0.7 W/cm² at 0.7 V at 700°C, have been achieved.

Future Directions

- Incorporate nanosized powders into composite cathode interlayer and optimize with respect to microstructure and processing conditions.
- Investigate the long-term stability of LSGM-based cathodes with respect to interdiffusion and secondary phase formation at operating temperatures.
- Further optimize the microstructure of LSGM-based cathodes containing Sr- and Fe-doped LaCoO₃ (LSCF), Sr-doped LaCoO₃ (LSC), and Sr-doped LaFeO₃ (LSF).
- Fabricate internally manifolded SOFC with LSGM-based cathodes and an active area of 100 cm². Evaluate the performance of the cells in short stacks.

Introduction

Previous work has shown that the largest polarization loss of an anode-supported SOFC with a thin-film electrolyte operating at 600 to 800°C is from the cathode. The polarization at the cathode can be substantially reduced by the use of composite cathodes that typically consist of a solid electrolyte, such as YSZ, and an electrocatalyst, such as La_{1-x}Sr_xMn_{3-δ} (LSM). The performance of the composite cathode depends on 1) oxide ion conductivity of the solid electrolyte (in the cathode), 2) the electronic and catalytic properties of the electrocatalyst, and 3) the microstructure of the composite cathode. Therefore, one approach to reducing the activation polarization of the composite cathode is to use a solid electrolyte phase that exhibits high oxide ion conductivity.

The perovskite oxide ion conductor LaGaO₃ doped with Sr and Mg (LSGM) exhibits higher oxide ion conductivity as compared to YSZ. Therefore, replacing the YSZ phase in the composite cathode with LSGM can substantially reduce the polarization losses at the cathode, especially at lower operating temperatures. In this work, composite cathodes comprised of LSGM and an electrocatalyst phase, such as LSC, LSF, or LSCF, have been developed and tested on anode-supported SOFCs. In addition, work is being done to develop and employ nanosized LSGM in the cathode interlayer to further reduce the polarization losses at the cathode.

Approach

Anode-supported SOFCs were fabricated with composite cathodes comprised of LSGM and a number of electrocatalytic phases, including LSC, LSF, and LSCF. The cells consist of five distinct layers: a porous Ni/YSZ composite anode support (~1 mm), a porous Ni/YSZ anode interlayer (~15 μm), a dense thin-film YSZ electrolyte (~6-8 μm), a porous composite cathode interlayer (LSGM with either LSM or LSC) (~20 μm), and a porous current-collecting layer (LSM or LSC) (~50 μm). In the case of the LSGM + LSC composite cathode, a barrier layer (~2 μm) of Gd-doped CeO₂ was deposited between the dense YSZ electrolyte and the composite cathode interlayer in order to prevent deleterious chemical reactions between the YSZ and LSC (Figure 1). Anode-supported cells with an active area of 2 cm² (button cells) and internally manifolded cells with an active area of 30 cm² have been fabricated and tested. Anodes were fabricated from NiO and YSZ mixtures by standard ceramic powder processes and tape casting. The dense electrolyte and barrier layers were fabricated by spraying powder suspensions followed by sintering. The composite cathodes were deposited by screen printing inks comprised of La_{0.9}Sr_{0.1}Ga_{0.8}Mg_{0.2}O_{3-δ} (LSGM) and an electrocatalyst phase, such as La_{0.85}Sr_{0.15}MnO_{3-δ} (LSM) or La_{0.5}Sr_{0.5}CoO_{3-δ} (LSC). A number of processing parameters have been varied in order to optimize the cathode microstructure and ultimately cell performance.

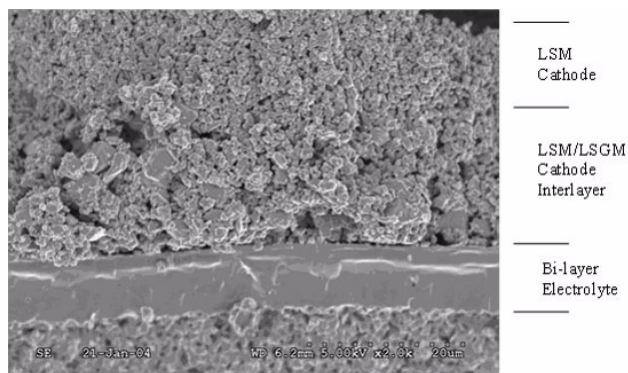


Figure 1. SEM Micrograph Showing a Cathode Interlayer Composed of LSGM and LSM

For instance, a parametric study of cathode interlayer thickness, particle size, composition, firing temperature, and firing time is being conducted. Single cells were tested at temperatures between 600 and 800°C with flowing H₂ as the fuel and air as the oxidant. Currently, cells with an active area of 30 cm² and with LSGM-LSCF composite cathodes are being evaluated in SOFC stacks operating at 600 to 800°C.

The polarization losses at the cathode are largely a function of the microstructure, with a finer microstructure generally reducing the activation polarization. The development of a highly refined cathode microstructure is being conducted via the use of nanosized starting powders. The nanosized powders were synthesized by a combustion technique wherein the maximum measured temperatures were controlled and kept below 600°C to reduce effects of coarsening. An optimization of the processing parameters, including firing time and temperature, results in a finer microstructure with increased three-phase boundaries in the composite cathode layer.

Results

Anode-supported cells with LSGM and the electrocatalyst phases LSM, LSC, LSF, and LSCF have been fabricated and tested. For each material combination, various parameters including composition of the cathode, particle size of the starting materials, firing times, and firing temperatures were systematically varied in order to optimize the performance of the composite cathode.

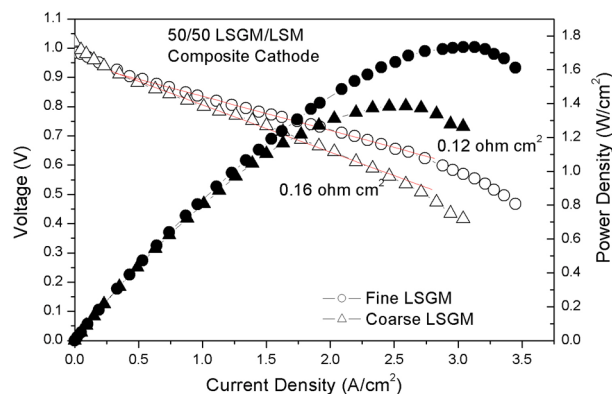


Figure 2. Performance of Two Cells with LSGM-LSM Cathodes Tested at 800°C, Showing the Effects of Particle Size on Cell Performance

The performance of the composite cathode is largely dictated by microstructural parameters of the interlayer, including three-phase boundary (TPB) length, porosity, and contiguity of the electrocatalyst and solid electrolyte phases. The performance of the cathode is highly sensitive to the microstructure of the 15-20 μm composite interlayer. For instance, a reduction in particle size of the LSGM in the cathode interlayer can substantially increase the performance of the cell. Figure 2 shows the performance of two cells tested at 800°C with two different cathode layers, one having a cathode interlayer prepared with fine (submicron) LSGM powder and one prepared with coarse (2-3 μm) LSGM powder. In both cases, the anode substrates were prepared from the same batch and the cathode interlayer was the same composition, 50% LSGM and 50% LSM; thus, the only difference was particle size. The decrease in starting powder size produced a more refined cathode microstructure, resulting in a decrease in the ASR of the cell from 0.16 to 0.12 Ωcm². This decrease in cell ASR translates into a power density of 1.4 W/cm² at 0.7 V at 800°C. Further refinement of the cathode microstructure and improvements in cell performance are expected with the use of nanosized powders. Nanosized powders of LSGM and various electrocatalyst phases, including La_{0.8}Sr_{0.2}MnO₃, La_{0.6}Sr_{0.4}CoO₃, and La_{0.6}Sr_{0.4}Co_{0.2}Fe_{0.8}O₃, have been synthesized and characterized. The development and optimization of composite cathodes utilizing nanosized starting powders is currently being conducted.

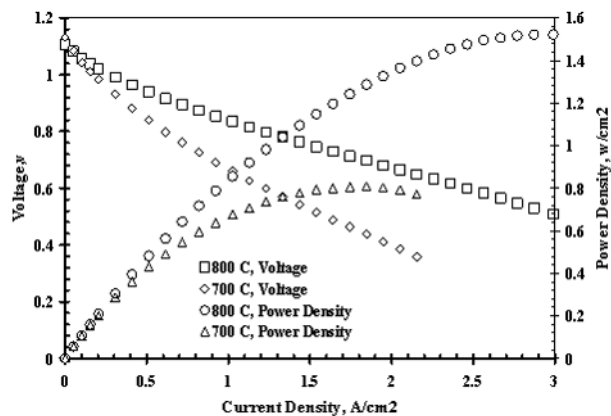


Figure 3. Performance of a Single Cell with a LSGM-LSCF Cathode Tested at 700 and 800°C

In addition to the microstructural effects, the intrinsic properties of the electrocatalytic phase play an important role in the activation polarization and ohmic losses of the cathode layers, especially at lower temperature. Although low cathode polarizations have been demonstrated with LSGM-LSM composite cathodes while operating at 800°C, the low electronic conductivity and semiconducting nature of LSM prohibits its use in the temperature range 600 to 700°C. In an effort to decrease the operating temperature of the SOFC, LSGM-based cathodes using the electrocatalytic phases LSC, LSF, and LSCF have been developed. The Fe- and Co-perovskite phases exhibit much higher electronic and ionic conductivity than LSM. However, these perovskite phases react with the YSZ electrolyte and, thus, a doped-ceria barrier layer is necessary to prevent the deleterious formation of any secondary phases. The performance of a cell with a LSGM-LSCF composite cathode layer tested at 700 and 800°C is shown in Figure 3. At 800°C, the power density of the cell is ~ 1.4 W/cm² at 0.7 V, and at 700°C, the power density is ~ 0.6 W/cm² at 0.7 V. The microstructure and starting powder particle size have not been fully optimized for this material system; thus, further increases in cell performance

are expected with more refinement. After testing, the microstructure, composition, and crystal chemical properties of the composite cathode are characterized by SEM and XRD in order to detect formation of secondary phases and interdiffusion. To date, no secondary phases have been found, but some interdiffusion between LSGM and the other perovskite phases (electrocatalysts) can be detected after the cathode firing step. Further investigation of the effects of this interdiffusion on the performance and polarization losses of the composite cathode is underway.

Conclusions

LSGM-based composite cathodes have been developed for anode-supported SOFCs with thin-film electrolytes, for operation in the temperature range 600 to 800°C. Cells with LSGM-LSM composite cathodes tested at 800°C have exhibited power densities as high as 1.4 W/cm² at 0.7 V.

The performance of the composite cathode interlayer is highly sensitive to microstructure and processing. For instance, a reduction in particle size of 50% in the cathode interlayer alone can decrease the ASR of the cell by as much as 25%. The incorporation of nanosized powders into the LSGM-based composite cathodes is currently underway. LSGM composite cathodes with the electrocatalysts LSC, LSF, and LSCF have been developed for lower temperature operation. Cells with LSGM-LSCF cathodes have delivered power densities of 0.6 W/cm² at 0.7 V at 700°C. In addition to cell-level testing, future work will include the testing of cells with LSGM-based cathodes in short stacks at temperatures between 600 and 800°C.

FY 2004 Publications/Presentations

1. Poster presented at SECA Core Technology Program Review Meeting, September 30 - October 1, 2003. Albany, New York.

VII.9 A Metallic Interconnect for Intermediate-Temperature Planar Solid Oxide Fuel Cells (SOFCs)

Tad J. Armstrong (Primary Contact), Anil V. Virkar, Micha Smith, Mike Homel

Materials and Systems Research, Inc.

5395 West 700 South

Salt Lake City, UT 84104

Phone: (801) 530-4987; Fax: (801) 530-4820; E-mail: tarmstro@MSRIhome.com

DOE Project Manager: Lane Wilson

Phone: (304) 285-1336; E-mail: Lane.Wilson@netl.doe.gov

Objectives

- Develop coatings for metallic interconnects for use in intermediate-temperature planar SOFC stacks, with the intent to increase oxidation resistance and electrical conductivity of the interconnect.
- Develop consumptive coatings wherein a metallic coating reacts with the chromium in the alloy to form a stable chromite phase. Examples include Mn and La metal.
- Develop protective coatings, based on spinel and perovskite phases, which are deposited directly onto the alloy substrate and function to decrease the oxidation kinetics of the alloy and suppress the evaporation of chromium species.
- Investigate the oxidation kinetics and electronic properties of coated alloy foils ex-situ (out of stack) and in-situ (in SOFC stack) over a range of temperatures between 600 and 800°C, in air and fuel, over various periods of time.
- Evaluate the performance of internally manifolded SOFC stacks with coated metallic interconnects operated between 600 and 800°C.

Approach

- Identify commercially available alloys, including stainless steels and Ni-Cr super alloys, suitable for use as metallic interconnects in SOFC. Identify spinel and perovskite oxide phases that are potential candidates for coatings, based on the criteria of low ion conductivity but high electronic conductivity.
- Demonstrate consumptive coatings by depositing thin layers of a metal, such as Mn, by physical vapor deposition (PVD) onto a metallic substrate. Upon oxidation, the metal reacts with the chromium in the alloy, promoting the formation of a spinel (or perovskite) phase and suppressing the formation of Cr₂O₃.
- Fabricate protective coatings wherein a dense layer of a spinel (Mn,Cr)₃O₄ or perovskite La(Cr,Mn)O₃ phase is deposited onto the alloy by sputtering.
- Measure the oxidation kinetics of coated and uncoated metallic interconnects at temperatures between 600 and 800°C. Develop a model of the oxidation kinetics and fit to the experimentally obtained data.
- Measure the area specific resistance (ASR) of coated and uncoated interconnects as a function of oxidation time and temperature.
- Assemble short stacks of internally manifolded SOFCs with coated interconnects and evaluate the performance under system conditions operating between 600 and 800°C.
- Characterize the crystal chemistry, composition, and assemblage of the phases that form on the alloy interconnects and at the coating interfaces during oxidation.

Accomplishments

- Protective and consumptive coatings have been developed for SOFC metallic interconnects. The coatings suppress formation of Cr_2O_3 , reduce Cr vaporization at high temperature, decrease the oxidation kinetics of the alloy, and increase the electronic conductivity of the oxide layer.
- Protective coatings of the perovskite Sr-doped LaMnO_3 (LSM) and the spinel Mn_2CrO_4 were shown to be effective in reducing the oxidation kinetics. In both cases, the oxidation kinetics exhibited linear behavior with the rate dictated by oxide ion diffusivity in the protective coating.
- The ASR of Cr_2O_3 -forming alloys including Haynes 230 was reduced by over an order of magnitude with the use of consumptive coatings including La, Co, and Mn.
- Coated interconnects were evaluated in internally manifolded, planar SOFC stacks. As compared to uncoated interconnects, the coated interconnects reduced the ASR of the stack by a factor of two, resulting in a doubling of the power density.

Future Directions

- No additional work is planned under this project; however, a large amount of future work and opportunities exist based on the developed methodology.
- Dope the A and B sites of the spinel and perovskite phases to optimize the effectiveness of the coatings with regard to decreasing the ion transport and increasing the electronic conductivity.
- Identify other oxide phases that may be suitable as coating candidates based on their stability in both oxidizing and reducing atmospheres, ionic and electronic conductivity, and thermal expansion coefficient.

Introduction

Chromium-containing alloys are of interest for use as metallic interconnects in planar solid oxide fuel cell stacks due to their good oxidation resistance at temperatures from 600–800°C. However, the Cr-based alloys naturally form a Cr_2O_3 oxide layer which is highly resistive and thus not suitable for interconnect applications. One approach to reducing oxidation kinetics of the alloy and increasing the electronic conductivity of the oxide layer is with the use of coatings. In this work, coating materials were identified and coating methods were developed that significantly improve the oxidation properties of commercially available alloys. Two types of coatings for metallic interconnects were developed: 1) protective coatings and 2) consumptive coatings. The protective coatings were formed by depositing a dense oxide layer directly onto the metallic interconnects. The consumptive coatings were formed by depositing a thin layer of metal onto the interconnect, which upon oxidation would react with the Cr in the alloy to form the desired oxide layer. The chromium-based oxides strongly adhere to the metal, exhibit excellent electronic conductivity, suppress the vaporization of Cr, and serve as a barrier

to oxidation. The coated interconnect samples were oxidized in both fuel and air atmospheres, at different temperatures, and for various periods of time. The oxidation kinetics and electronic conductivity of the coated interconnects were measured and compared to oxidation kinetics models that were developed for both types of coatings. The most promising coated interconnects were tested in planar SOFC stacks.

Approach

Numerous commercially available substrate alloys were investigated in this study, including Haynes 230, Inconels, and various stainless steels. The selection of suitable coating materials was based on the criteria of oxidation resistance and electronic conductivity. Two coating methods were developed: 1) protective coatings and 2) consumptive coatings. The protective coatings were formed by depositing coatings of the desired spinel and perovskite phases directly on the metal substrates by sputtering. Two of the oxides investigated were the perovskite phase $\text{La}_{0.85}\text{Sr}_{0.15}\text{MnO}_{3-\delta}$ and the spinel phase Mn_2CrO_4 . Oxide layers with a range of thickness between 0.2 and 2 μm were deposited onto the metallic interconnect foils. The consumptive coatings were

fabricated by depositing thin films of various metals onto the interconnect surface before oxidation. Upon heating, the deposited metal oxidized, reacted with the chromium from the interconnect alloy, and subsequently formed Cr-based oxides other than Cr_2O_3 . For example, a coating of Mn metal on an alloy containing Cr will result in the formation of the more conductive spinel phase $(\text{Mn}, \text{Cr})_3\text{O}_4$, while a coating of La metal will promote the formation of the perovskite phase LaCrO_3 .

In order to study the oxidation kinetics, sample coupons with the consumptive and protective oxide coatings were heated in air and fuel atmospheres (wet and dry) at temperatures between 600 and 800°C for various periods of time and subsequently analyzed with scanning electron microscopy (SEM), electron dispersive spectroscopy (EDS), and x-ray diffraction (XRD). Models of the oxidation kinetics of both protective and consumptive coatings were developed and fitted to the experimental data. The electronic conductivity of coated and uncoated samples at various degrees of oxidation was measured in various atmospheres as a function of temperature with a two-probe fixture. Coated and uncoated interconnects were tested in short stacks at temperatures between 600 and 800°C.

Results

Models of the oxidation kinetics of both protective and consumptive coatings were developed for a number of different cases. For the case of the protective coating, the formation of an oxide layer under the protective coating can be modeled in terms of the chemical diffusivity of the participating species. In this case, it is assumed that the oxide ion diffusivity is faster than the cation diffusivity in the coating layer and that the cation diffusivity is faster than the oxide ion diffusivity in the formed oxide layer. For this given scenario, two limiting cases of oxidation kinetics of interconnects with coatings exist: (a) coating limited: with linear growth rate with time, this is the desired case wherein the coating is effective in reducing the oxidation kinetics, and (b) diffusion limited: with parabolic growth rate with time, the coating is ineffective and the growth rate is a function of diffusion in the native oxide. These oxidation kinetics models were validated with experimentally obtained kinetics data.

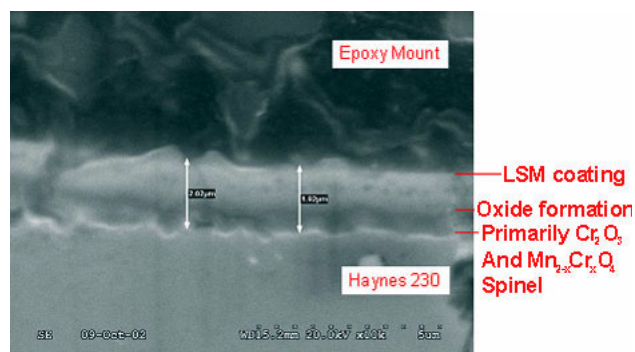


Figure 1. SEM Micrograph Showing a LSM-Coated Haynes 230 Sample after Being Oxidized for 14 Days at 800°C in Air; Secondary Electron Image

The oxidation studies of Haynes 230 samples coated with a dense, protective coating of either LSM or the spinel phase Mn_2CrO_4 were conducted in air at 800°C for various periods of time. Before oxidation, the coatings were $\sim 1.3 \mu\text{m}$ thick and were continuous, dense, and well adhered to the metallic substrate. At various points during the oxidation study, the oxide layers were examined with SEM and characterized for elemental analysis with EDS. A cross-section of a LSM-coated Haynes 230 sample after oxidation for 14 days at 800°C in air is shown in the SEM micrograph in Figure 1. The oxide coating is comprised of two distinct layers: the original deposited LSM coating on the top and a layer of oxide that has formed under the protective LSM coating. The oxide that has formed under the LSM is primarily comprised of Cr_2O_3 and the spinel phase $\text{Mn}_{2-x}\text{Cr}_x\text{O}_4$, which are the native oxides that normally occur on oxidized Haynes 230. The formation of an oxide layer under the protective coating indicates that oxide ions are diffusing through the LSM layer and oxidizing the Cr and Mn contained in the Haynes 230. This is in agreement with one scenario depicted in the proposed kinetics model for a protective coating.

The oxidation kinetics of LSM- and Mn_2CrO_4 -coated Haynes 230 samples were studied at 800°C in air. Initially, a dense layer of oxide coating with a thickness, X_c , of $1.3 \mu\text{m}$ was deposited onto the metal substrates by sputtering. During oxidation, an oxide layer formed under the protective coating with a thickness, X_d . The rate of oxidation is shown in Figure 2 where the total thickness ($X_c + X_d$) is

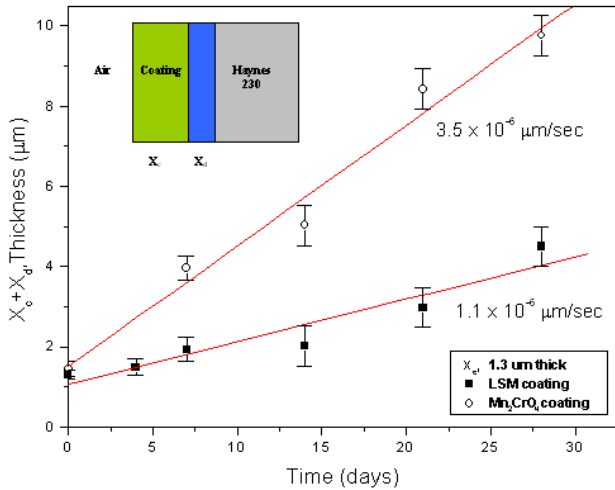


Figure 2. Total Oxide Thickness (X_c and X_d) as a Function of Time for LSM- and Mn_2CrO_4 -Coated Haynes 230 Oxidized at $800^\circ C$ in Air

plotted as a function of oxidation time for samples with both types of protective oxide coatings. The oxidation rates for samples with both coatings are linear with time, thus indicating a surface rate limiting process. Thus, the oxidation kinetics are dictated and controlled by the protective coating. Based on these growth rates, the chemical diffusivities of the participating species can be estimated by the kinetics model. The chemical diffusivity of oxide ions is $\sim 6 \times 10^{-16} \text{ cm}^2/\text{s}$ in the LSM and $\sim 2 \times 10^{-15} \text{ cm}^2/\text{s}$ in the spinel phase. The thickness of the oxide coating can be predicted for longer times with the model. For an LSM coating of $1.3 \mu\text{m}$ and a chemical diffusivity of oxide ions in LSM of $6 \times 10^{-16} \text{ cm}^2/\text{s}$, the oxide thickness as a function of time at $800^\circ C$ with and without an LSM coating was calculated for the Cr diffusivity of $10^{-13} \text{ cm}^2/\text{s}$, shown in Figure 3. The results show that the coating significantly decreases the oxidation kinetics of the alloys and thus reduces the total thickness of the oxide layer.

Consumptive coatings were developed by depositing thin films of various metals onto the interconnect surface before oxidation. A coating of Mn metal on the Ni-Cr alloys resulted in the formation of the spinel phase $(Mn, Cr)_3O_4$, while a coating of La metal resulted in the formation of the perovskite phase $LaCrO_3$. Of the materials studied, the spinel formers Mn and Co and the perovskite

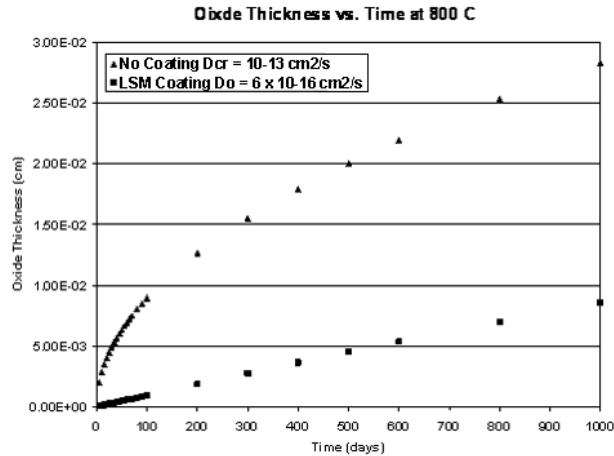


Figure 3. Calculated Oxide Thickness as a Function of Time at $800^\circ C$ for an Uncoated and LSM-Coated Alloy That Exhibits a Cr Diffusivity of $10^{-13} \text{ cm}^2/\text{s}$

former La were most effective in reducing the ASR of the oxidized interconnect. The Co- and La-coated samples repeatedly and routinely exhibited an ASR one order of magnitude lower than that of the uncoated Haynes 230 samples at $800^\circ C$. Coated interconnects were evaluated in short SOFC planar stacks tested at $800^\circ C$ with air as the oxidant and hydrogen as the fuel. The results of testing 4-cell stacks with this configuration with coated and uncoated interconnects is shown in Figure 4. The

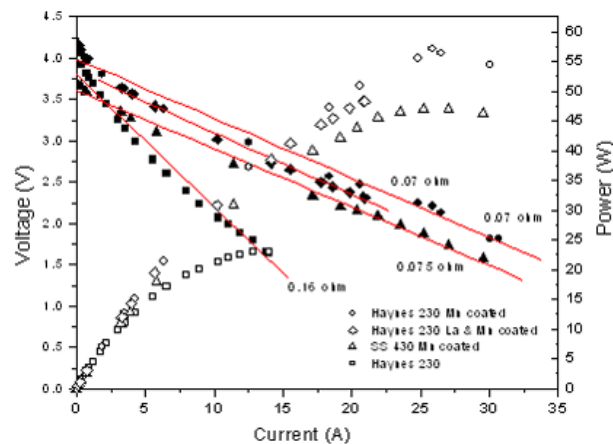


Figure 4. Comparison of the Voltage-Current and Power-Current Characteristics of 4-Cell Planar SOFC Stacks Operating at $800^\circ C$ with Uncoated Haynes 230, Mn-Coated Haynes 230, Mn-Coated SS 430, and La- & Mn-Coated Haynes 230 Interconnects

ASR of the stacks with the coated Haynes 230 interconnects was one half that of the stacks with the standard uncoated interconnects. Therefore, the coated interconnects reduced the stack resistance and increased the stack power by a factor of two.

Conclusions

Protective and consumptive coatings have been developed for SOFC metallic interconnects. The coatings suppress formation of Cr_2O_3 , reduce Cr vaporization at high temperature, decrease the oxidation kinetics of the alloy, and increase the electronic conductivity of the oxide layer. Oxidation models for both protective and consumptive coatings were developed. Based on the models, two limiting cases of oxidation kinetics of interconnects with coatings exist: (a) coating limited (linear) and (b) diffusion limited (parabolic). Protective coatings of the perovskite LSM and the spinel Mn_2CrO_4 were shown to be effective in reducing the oxidation kinetics. In both cases, the oxidation kinetics

exhibited linear behavior, with the rate dictated by oxide ion diffusivity in the protective coating.

Consumptive coatings that promote the formation of desired oxide phases and suppress the formation of Cr_2O_3 were developed and demonstrated. The ASR of Cr_2O_3 -forming alloys including Haynes 230 was reduced by over an order of magnitude with the use of consumptive coatings including La, Co, and Mn. Coated interconnects were evaluated in internally manifolded, planar SOFC stacks. As compared to uncoated interconnects, the coated interconnects reduced the ASR of the stack by a factor of two, resulting in a doubling of the power density.

FY 2004 Publications/Presentations

1. Poster presented at SECA Core Technology Program Review Meeting, September 30 - October 1, 2003. Albany, New York.

VII.10 Advanced Thermal Spray Fabrication of Solid Oxide Fuel Cells

J. Brogan (Primary Contact), R. Gambino, R. Greenlaw, J. Gutleber
MesoScribe Technologies, Inc.
25 East Loop Road
Stony Brook, NY 11790
Phone: (631) 444-6455; Fax: (631) 444-6234; E-mail: jbrogan@mesoscribe.com

DOE Project Manager: Shawna Toth
Phone: (304) 285-1316; Fax: (304) 285-440; E-mail: Shawna.Toth@netl.doe.gov

Subcontractors: Boston University, Boston, MA; SUNY-Stony Brook, Stony Brook, NY

Objectives

- Optimize thermal spray parameters to produce dense deposits on cathode and anode supports.
- Minimize electrolyte thickness and ensure gas tightness.
- Maximize materials utilization.
- Determine microstructure and porosity evolution during spraying. Minimize porosity in electrolyte layer.
- Determine performance characteristics of solid oxide fuel cells (SOFCs) using electrolytes fabricated by High Definition Thermal Spray.

Approach

- Critically assess requirements for present and future SOFC systems and develop a realistic assessment of needs and capabilities.
- Identify and fabricate cathodic and anodic substrates for MesoScribe's deposition experiments.
- Deposit both yttria-stabilized zirconia (YSZ) and strontium-doped lanthanum gallate (LSGM) electrolytes on cathodic and anodic substrates using High Definition Thermal Spray.
- Characterize the cross-sections of deposited splats and electrolyte layers using optical and scanning electron microscopy (SEM).
- Measure the gas tightness of the as-sprayed deposited and post heat-treated electrolytes using a gas leak tester.
- Obtain the open circuit potential for cells characterized during this project phase and conduct impedance spectroscopy to reveal information about the cell ohmic resistance and interfacial polarizations.

Accomplishments

- High definition spray strategy was demonstrated for both YSZ and LSGM to meet DOE's goal of effective material utilization.
- High density, water-tight YSZ deposits were produced on both anodic and cathodic substrates in as-sprayed state. In general, YSZ layers in as-deposited state show intra-splat microcracks arising from relief of quenching stresses associated with solidification. This can be reduced or eliminated by a short heat treatment cycle. One goal is to lower this treatment temperature and to carefully design the anode/electrolyte/cathode manufacturing process to reduce steps.
- High density, water-tight LSGM deposits can be produced as-deposited, but they generally contain some degree of amorphicity. Again, this can be manipulated by controlling the degree of melting of the particles and/or through a low temperature sintering operation.

Future Directions

- Demonstrate advanced high definition thermal spray process as a means to deposit leak-tight YSZ and LSGM electrolyte on both anode- and cathode-supported cells in tubular, planar and Siemens Westinghouse HPD configurations.
- Identify the most appropriate means, compatible with thermal spray deposition of electrolyte, to engineer electrode-electrolyte interfaces with the goal of enabling the cell to undergo multiple thermal cycles (>100) and perform at high power densities (1 to 2 W/cm² on single cells).
- Demonstrate stoichiometric control of LSGM powders as a means to achieve single-phase perovskite phase in the as-sprayed state.
- Develop thermo-mechanical modeling methods to allow design of interfaces so as to aid in thermal mismatch management of the multilayer during either processing or service. Examine appropriate graded porosity concepts at the interface to achieve this requirement.
- Demonstrate high materials utilization (>70%) through high definition thermal spraying, particularly MesoPlasma process.
- Demonstrate atmospheric and MesoPlasma thermal spray processes as means to achieve high density, leak-tight YSZ electrolyte with minimal post spray heat treatment (<1200°C) through the application of advanced feedstock and processing strategies.

Introduction

Solid oxide fuel cell (SOFC) technology is expected to revolutionize power generation in the coming decades, given its higher energy efficiency, improved environmental performance and cost. The main impediment to SOFC implementation on a large scale is cell manufacturing cost. The challenge to lower the cost of SOFC manufacturing is being addressed through the development of advanced thermal spray methods for the fabrication of the electrolyte and, possibly, electrodes/interconnects. Thermal spray is a versatile, efficient, and cost effective approach to produce the ceramic fuel cell multilayers; however, conventional thermal spray may not be suited to meet the requirements of a modern fuel cell design. This is due to lack of effective microstructural control, interconnected porosity in electrolytes, and poor material utilization during deposition. MesoScribe Technologies Inc, in conjunction with program partners Center for Thermal Spray Research-SUNY-Stony Brook and Boston University, addressed these issues during the Phase I project. The research and development program addresses key DOE Small Business Innovation Research (SBIR) requirements in terms of effective material utilization, improved material characteristics and an integrated approach towards sequential fabrication of solid oxide fuel cells.

Approach

The basis of the effort lies in a breakthrough extension to modern day thermal spray technology through a *high definition* plasma spray capability and the ability to insert and deposit fine powders. This is coupled with use of advanced process map concepts to operate in parametric regimes that control specific microstructural features. Phase I effort concentrated on identifying key technical issues with respect to thermal spray fabrication of fuel cells. The processing effort concentrated on electrolyte deposition onto both anodic and cathodic substrates made by conventional powder processing routes. Both yttria-stabilized zirconia (YSZ) and strontium-doped lanthanum gallate (LSGM) have been deposited. Microstructural characterization was conducted in as-deposited and thermally treated materials. Water and gas leak tests were conducted to qualitatively assess the attributes of the sprayed layers to function as a high performance electrolyte. Finally, open circuit voltage and I-V measurements were made on the samples. The Phase I results demonstrate the potential of the technology and also identify key challenges and potential mitigating strategies. MesoScribe has communicated and discussed these developments with DOE National Energy Technology Laboratory (NETL) personnel as well as with our industrial partners. MesoScribe's goal is to develop and commercialize these advanced

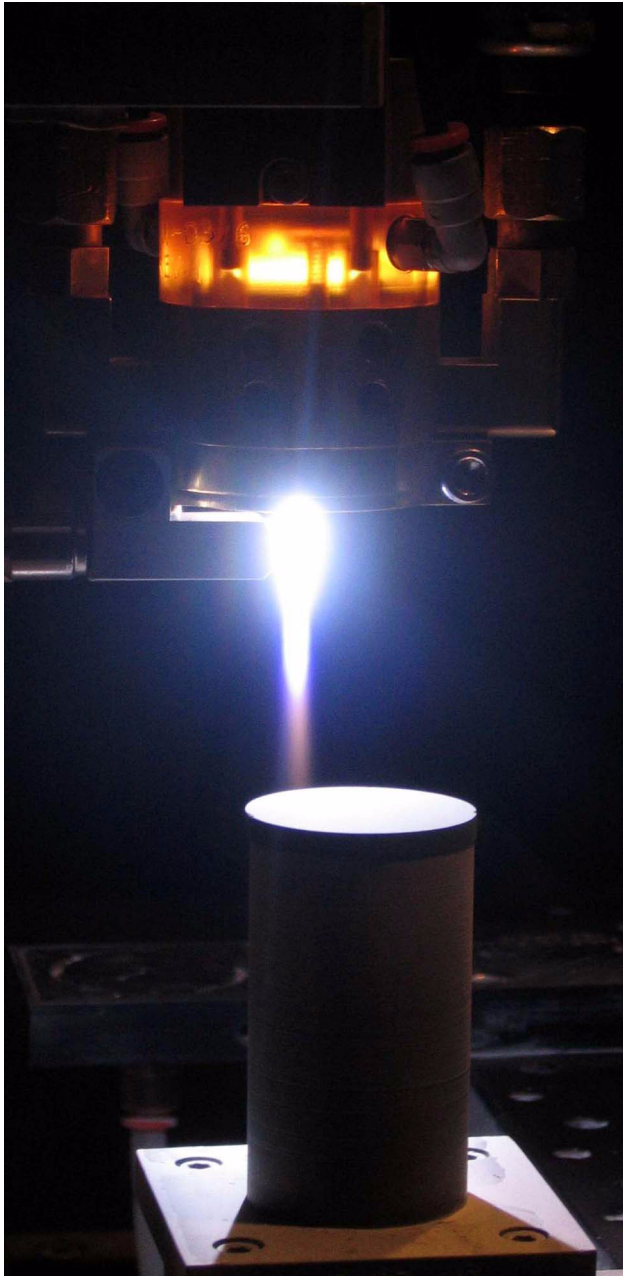


Figure 1. Demonstration of a High Definition Spray Deposition Process (Material: LSGM)

fabrication systems for implementation in fuel cell manufacturing. If successful, this approach has the potential to lower cell manufacturing cost while increasing throughput, both outcomes being key drivers in widespread fuel cell implementation.

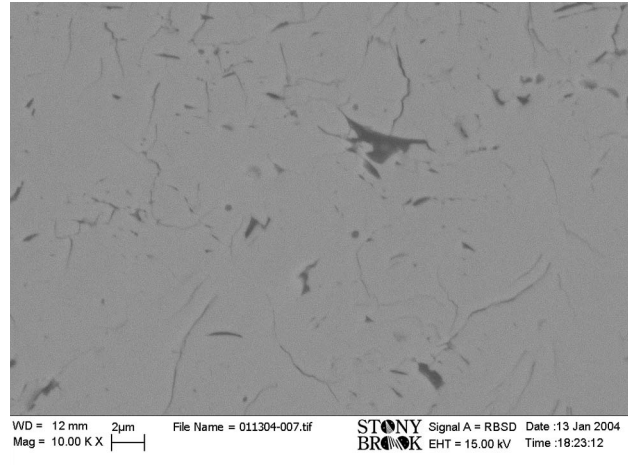


Figure 2. Cross-Sectional Micrograph of YSZ Showing Reduced Porosity in As-Deposited State

Results

MesoScribe, in conjunction with program partner Boston University, evaluated the important materials and processing requirements associated with thermal spray processing of SOFC electrolytes. System level considerations were also taken into account with respect to cathode, anode and interconnect materials. MesoScribe has successfully demonstrated that high definition spray deposition of both YSZ and LSGM can be achieved using the new technologies. Figure 1 illustrates the spray-plume substrate interaction on a disk that is approximately 1 inch (25 mm) in diameter. The plume size is in the range of 4-6 mm and can be scaled upwards. The research clearly shows that high target efficiency deposits can be achieved in planar or tubular cells with dimensions of 15 mm or more. For larger systems, the process can be appropriately rastered or scaled depending on the optimum processing ability.

A series of splat studies were conducted to evaluate the underlying characteristics of fragmentation and microcracking based on materials and processes. It was observed that LSGM splats did not undergo microcracking. Additionally, we were successful in obtaining fragmentation-free splats. Finer particle size and increased Reynold's number through MesoPlasma approaches yielded thinner

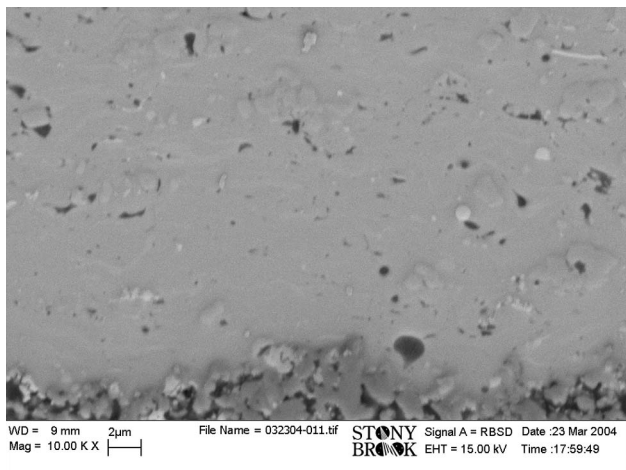


Figure 3. Mesoplasma-Deposited LSGM on Nio-GDC Anode. No Interfacial Layer Was Applied At This Stage (The as-deposited sample was water-tight)

splats, although quantitative studies need to be completed to assess reduction in splat thickness. Significant improvements in deposit density were achieved in the case of YSZ using the strategies outlined above (Figure 2).

Considerable effort in feedstock and parameter development enabled the fabrication of dense, water-tight LSGM electrolytes on Ni-GDC anodes. The deposit thickness was about 30 microns. A cross-sectional micrograph of the LSGM deposit in the as-sprayed state is shown in Figure 3, and a micrograph of the heat-treated LSGM is shown in Figure 4. Note the excellent interface between the LSGM layer and the anode. At this stage, we have not incorporated the interfacial barrier layer, but it is planned for Phase II.

As-sprayed and annealed LSGM layers were also characterized using x-ray diffraction (XRD) analysis. XRD traces obtained from as-sprayed LSGM layers can be indexed to a predominant perovskite phase with a broad low-angle, low-intensity peak which could not be identified conclusively. It is likely that this broad low-angle peak is indicative of an amorphous second phase. Upon annealing at 800°C for 30 minutes, two other phases were identified in the XRD trace of the annealed sample in addition to the original LSGM phase. They were indexed to a binary oxide with the stoichiometry $\text{La}_4\text{Ga}_2\text{O}_9$ and

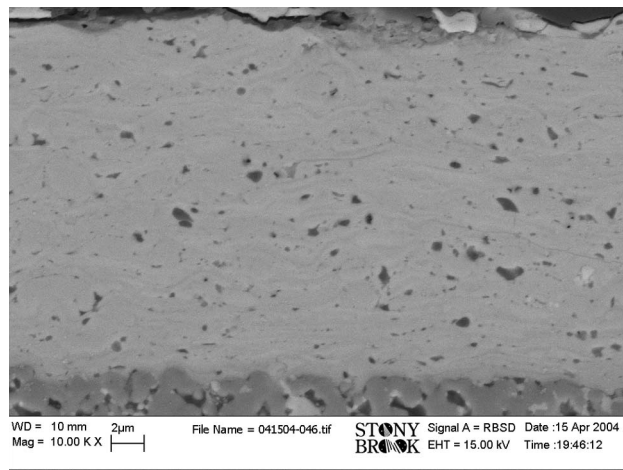


Figure 4. Mesoplasma-Sprayed LSGM on Nio-GDC after Low Temperature Heat Treatment for 30 Minutes (The sample shows increasing density but underwent macrocracking.)

Ga_2O_3 . A future goal is to obtain stoichiometric LSGM in the as-sprayed state.

Selected bi-layers of anode-YSZ electrolyte structures were post-spray annealed at 1300-1350°C. A two-layer cathode consisting of a lanthanum strontium manganese (LSM)-YSZ inner layer and a LSM outer layer was applied to the electrolyte through painting and firing at 1100°C for 2 hours. Prior to firing, platinum mesh current collectors were attached to the anode and cathode sides of the specimens. The completed cell was placed in a dual atmosphere test setup. Voltage-current density characteristics were obtained with flowing air on the cathode side and hydrogen humidified by bubbling through water at room temperature (composition of ~97% H_2 /3% H_2O) on the anode side. The open-circuit potential was a little lower than the theoretically predicted value of 1.085 V but did not vary with flow rate once the flow rates of both air and humidified hydrogen were above 30 cc/min. This is indicative of a finite leak through the electrolyte which can be compensated by adding extra fuel. In the Phase I program, we have not performed detailed evaluation of the effects of leaks through 'unhealed' microcracks in the electrolyte. However, one of the tasks in Phase II will be to obtain more precise estimates of the effect of leaks through remaining microcracks on cell performance. The voltage-current density and power density-

current density characteristics were obtained at 850°C. The maximum power density obtained was only ~45 mW/cm². Far higher power densities are expected once the electrode microstructure and porosity are carefully engineered, particularly near the interfaces.

Conclusions

The Phase I results demonstrate the potential capability of MesoScribe's advanced thermal spray process. The high definition plasma spray process was demonstrated to fabricate both YSZ and LSGM electrolytes onto both cathodic and anodic supported cells to meet DOE's goal of effective material utilization. High density, water-tight YSZ deposits were produced on both anodic and cathodic substrates in as-sprayed state. In general, YSZ layers in as-deposited state show intra-splat microcracks arising from relief of quenching stresses associated with solidification. This can be reduced or

eliminated by a short heat treatment cycle. One goal is to lower this treatment temperature and to carefully design the anode/electrolyte/cathode manufacturing process to reduce steps. High density, water-tight LSGM deposits can be produced as-deposited, but they generally contain some degree of amorphicity. Again, this can be manipulated by controlling the degree of melting of the particles and/or through a low temperature sintering operation.

MesoScribe has effectively engaged both DOE NETL personnel and end use industrial partners for a successful transition of its efforts. MesoScribe's goal is to develop and commercialize advanced concepts and fabrication systems for implementation in fuel cell manufacturing. Together with DOE support and guidance from our industrial partners, a *concerted, integrated* effort is being made to innovate and enhance thermal spray technology for fuel cell manufacturing.

VII.11 Novel Ceria-Based Materials for Low-Temperature SOFCs

Matthew M. Seabaugh (Primary Contact), Sergio A. Ibanez, Katarzyna Sabolsky

NexTech Materials, Ltd.

404 Enterprise Dr.

Lewis Center, OH 43035

Phone: (614) 842-6606; Fax: (614) 842-6607; E-mail: seabaugh@nextechmaterials.com

DOE Project Manager: Lane Wilson

Phone: (304) 285-1336; E-mail: Lane.Wilson@netl.doe.gov

Objectives

- Develop single-phase cathodes, composite cathodes, and/or two-layer cathode structures that provide efficient low-temperature electrochemical performance and are adaptable to different solid oxide fuel cell (SOFC) materials systems and different SOFC cell/stack designs.
- Evaluate the effects of composition and synthesis conditions on thermal expansion and high-temperature electrical conductivity of perovskite electrode powders in the B-site doped lanthanum strontium ferrite (LSXF) system.
- Evaluate the effects of composition of LSXF perovskite materials on their high-temperature reactivity with electrolyte materials (yttria-stabilized zirconia, YSZ, and gadolinium-doped ceria, GDC) that are being considered for low-temperature solid oxide fuel cells.
- Evaluate the effects of composition, thickness and morphology on sheet resistance and area specific resistance of screen-printed coatings of LSXF perovskite and LSXF/GDC composite cathode materials, and correlate results with characterization data.

Approach

- Synthesize and characterize a matrix of single-phase electrode (LSXF) powders selected for their low-temperature electrochemical performance in SOFC systems.
- Measure high-temperature electrical conductivity and evaluate interfacial resistance of the single-phase LSXF materials.
- Synthesize and characterize a matrix of composite cathode (LSXF/GDC) powders to further improve low-temperature electrochemical performance of SOFCs.
- Measure high-temperature electrical conductivity and evaluate interfacial resistance of the composite cathode materials.
- Prepare fuel cell samples with most promising cathode materials and test their performance at low operating temperatures (YSZ-based cells at 600-850°C and GDC-based cells at 500-700°C).

Accomplishments

- Synthesized and characterized over 30 highly conductive single-phase cathode materials.
- Developed and characterized composite cathode materials based on above analysis.
- Demonstrated improved performance of the composite cathode materials over the single-phase materials.

Future Directions

- Evaluate interfacial resistance of other LSXF cathode materials from the characterized set in composite cathode form.
- Analyze interfacial resistance of composite cathode materials with different LSXF:GDC ratios.
- Demonstrate SOFC performance on ceria- and zirconia-based cells.

Introduction

We have investigated several new single-phase cathodes and composite cathode materials with the goal to reduce the interfacial resistance between the cathode and the electrolyte. We have evaluated the effect of processing route and composite electrolyte component characteristics on the interfacial resistance. The initial analyses determined that the composite cathode materials outperform the single-phase lanthanum strontium ferrite (LSF) and B-site doped LSF materials.

Approach

LSXF perovskite system was identified as having promising electrochemical performance, and a set of LSXF compositions was synthesized and characterized for phase purity and conductivity. Upon evaluation of the single-phase materials, the most promising material was selected for study in the composite form with GDC powders. The study of the composite materials focused on determining the surface area effect on the electrochemical performance of the cathode. The composites were prepared by milling LSXF powder with two different GDC powders, with high and low specific surface area (SSA), at LSXF:GDC volume ratio of 60:40. The composites were made into inks and screen printed symmetrically onto two faces of GDC and YSZ electrolyte discs. The interfacial resistance was analyzed using a Solartron SI 1260 Impedance Analyzer.

Results

In previous work in this system, the LSXF compositions have been evaluated and found to have excellent performance on GDC electrolytes. Demonstration of low area specific resistances is shown in Figure 1. These bulk resistances of symmetric sandwich cells have been very low for a number of compositions at temperatures above 600°C.

In this phase of the study, a number of LSF-based cathodes have been evaluated in contact with YSZ to determine processing parameters and composite fabrication processes that provide the best interfacial resistance behavior. LSF-40 was selected for

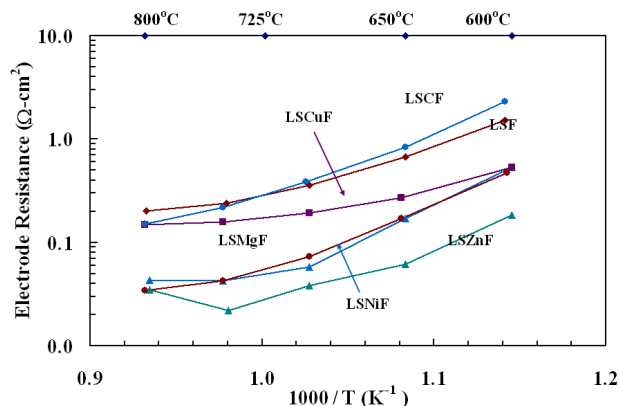


Figure 1. Interfacial resistance data for LSXF materials on GDC electrolyte substrates measured by DC resistance on symmetric samples. The resistance of the GDC electrolyte has been subtracted from the data.

evaluation of its performance versus processing technique. LSF-40 was prepared by three different techniques. The oxide and carbonate forms of lanthanum, strontium, and iron were milled together and calcined at 1300°C to ensure formation of single-phase perovskite. The calcined powders were then either attrition milled for one to six hours or ball milled for 12 hours. The three milling techniques allowed for evaluation of the powder at different surface area values. The ball-milled powder achieved surface area of 2.776 m²/g; the attrition-milled powder achieved surface area of 3.423 and 7.700 m²/g for one- and six-hour milling time, respectively. Each powder was made into an ink. The inks were screen printed and annealed on YSZ disks. The annealing temperature for the ball-milled powder was 1050°C. The attrition-milled powders were annealed at 1050°C and 1000°C for one- and six-hours milling time, respectively. The samples were then tested for interfacial resistance using 1260 Impedance Analyzer. Figure 2 shows the impedance spectra for the three LSF-40 powders measured at 600°C. The data shows that the interfacial resistance decreases with the increasing surface area and decreasing adhesion temperature. The reason for this trend could be explained by the formation of resistive phase at the interface of cathode and electrolyte. The lanthanum- and praseodymium-containing materials have a tendency to form pyrochlore compounds with ZrO₂ such as La₂Zr₂O₇, which is highly resistive.

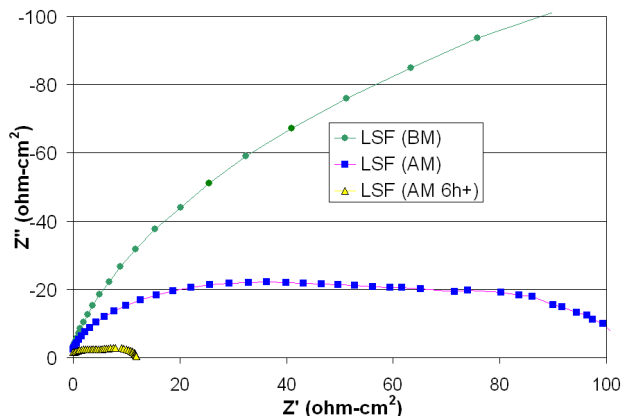


Figure 2. Interfacial resistance data for LSF-40 processed by either ball milling or attrition milling for one and six hours measured on YSZ electrolyte substrates at 600°C.

The probability of reaction between YSZ substrate and cathode materials increases with higher annealing temperature. The high surface area powder adheres to the YSZ substrate at lower temperature; hence, the pyrochlore materials are not formed at the interface and the interfacial resistance is low.

LSF-40 attrition milled for six hours was used to evaluate composite cathode materials with GDC as the electrolyte component of the composite. Two GDC powders were mixed with LSF-40: a nano-scale material with surface area of $>100 \text{ m}^2/\text{g}$ (high SSA) and a ceramic grade material with surface area of $<10 \text{ m}^2/\text{g}$ (low SSA). The composite powders were mixed at 60:40 ratio of LSF:GDC. The powders were then calcined to achieve surface area similar to the pure LSF-40 ($7.700 \text{ m}^2/\text{g}$). Upon calcination, the composite with high-SSA GDC achieved surface area of $7.572 \text{ m}^2/\text{g}$, and the composite with low-SSA GDC achieved surface area of $7.619 \text{ m}^2/\text{g}$. Each powder was made into an ink. The inks were screen printed and annealed on YSZ disks. The samples were adhered at 1000°C. The interfacial resistance of the samples was measured at 600°C. Figure 3 shows the impedance spectra for the LSF-40 and the composite powders.

The data shows that the performance of the cathode can be improved by addition of the electrolyte material such as GDC to the pure perovskite powder. However, it is essential that

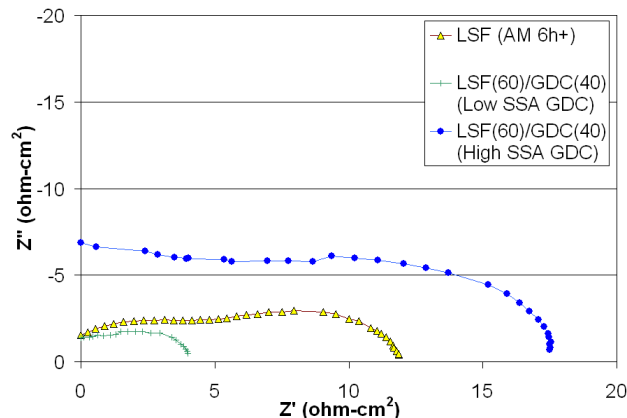


Figure 3. Interfacial resistance data for LSF-40 and composite cathode materials made with two different surface area GDC powders measured on YSZ electrolyte substrates at 600°C.

components of the composite are carefully selected based on their initial surface area. The impedance results show that the high-SSA GDC composite cathode has higher interfacial resistance, while the low-SSA GDC composite cathode has a lower interfacial resistance than the pure LSF-40 material. The low SSA-GDC composite cathode showed an improvement over the LSF-40 powder by increasing the triple point boundary area of the cathode. However, in the case of the high-SSA GDC composite cathode, it is believed that due to the extreme difference in surface area between the LSF-40 and nano-scale GDC materials, the particles of LSF were completely covered by the fine GDC powder, in effect decreasing the overall triple point boundary area of the cathode.

Conclusions

- Within the evaluated set of single-phase materials, LSF-40 achieved the highest conductivity, while PSF-40 appears to have the lowest interfacial resistance.
- The processing technique of the cathode powders is an important factor in cathode performance. Higher surface area powders lead to lower adhesion temperatures and lower interfacial resistance.
- LSF/GDC cathode composites outperform single-phase LSF material when the surface area of the components is carefully taken into consideration.

VII.12 Low-Cost Spray Deposition for SOFC Manufacturing

Matthew M. Seabaugh (Primary Contact), Michael J. Day

NexTech Materials, Ltd.

404 Enterprise Dr.

Lewis Center, OH 43035

Phone: (614) 824-6606; Fax: (614) 842-6607; E-mail: seabaugh@nextechmaterials.com

www.nextechmaterials.com

DOE Project Manager: Shawna Toth

Phone: (304) 285-1316; E-mail: Shawna.Toth@netl.doe.gov

Phase One Objectives

In Phase I, NexTech Materials established the feasibility of low-cost manufacturing processes for solid oxide fuel cells that are highly flexible with respect to layer composition and morphology as well as cell geometry. The overall objectives of this proposed program are listed below:

- Demonstrate the applicability and versatility of aerosol spray deposition as a low-cost alternative to plasma spray and dip coating methods for the production of functional film layers for solid oxide fuel cells (SOFCs).
- Demonstrate the potential for process simplification by validation of low-temperature co-sintering of protocols of multilayer components including electrode interlayers, electrodes and electrolyte.
- Demonstrate the above processes on both anode- and cathode-supported SOFC designs that include different geometries and differing substrate pre-conditions.

Approach

The approach conducted at NexTech included the following salient points:

- Investigation of both aqueous and non-aqueous spray suspensions deposited by low-cost aerosol deposition techniques.
- Development of ink/slurry dispersion and manufacture techniques appropriate to large-scale manufacture and standard quality control protocol.
- Control of porosity/density and sinter activity of co-sintered materials by appropriate selection of surface area and particle size distribution, and green film density control by ink solids/organic loading.
- Analysis by microstructural assessment including optical and scanning electron microscopy (SEM) investigation.
- Electrolyte densification and defect analysis by vacuum leak testing.

Accomplishments

- Demonstrated aerosol deposition process that enables the uniform electrode and electrolyte coating of both anode- and cathode-supported SOFC tubular designs.
- Demonstrated a single-step deposition and co-firing regime that results in a dense electrolyte layer validated by Siemens-Westinghouse Power Corporation (SWPC).
- Demonstrated a full cell (electrodes + electrolyte) deposition and single co-fire protocol for anode-supported structure resulting in fully dense electrolyte microstructure between porous electrode films.
- Scaled the process to reproducibly coat tube lengths up to 60 cm.

Future Directions

The Phase I Program is complete. NexTech is currently seeking commercial partners for further development.

Introduction

The objective of this Phase I Small Business Innovation Research (SBIR) project was to demonstrate the feasibility of a low-cost aerosol spray process for the deposition of electrochemically active layers for solid oxide fuel cells. Currently, processes that include electrochemical deposition and plasma spray amongst others are being used for the production of the SOFC functional components. These processes are inherently expensive as they require considerable capital investment, use expensive precursors and require several thermal processing sequences for each layer in the multi-layered structure.

This project aimed to demonstrate that using the aerosol deposition method, a multi-layer structure could be formed using minimized thermal processing steps and that the microstructure of these layers could be optimized for electrochemical performance.

This project focused on two types of SOFC designs currently under development by Solid State Energy Conversion Alliance (SECA) team leaders: the cathode-supported tubular design of Siemens-Westinghouse Power Corporation and the tubular anode-supported design of Acumentrics.

Results

Initial attempts to produce dense electrolyte structures on SWPC fully sintered cathode tubes were based on aqueous solvent systems. The most promising results were obtained when slurries with low solids contents were utilized. This was due to the highly porous nature of the substrate that readily absorbed the water solvent and tended to prevent the flow, rearrangement and relaxation of the film on the substrate. It is expected that it was this ability of the substrate to rapidly extract solvent from the slurry that limited the packing density of the film and resulted in high drying stresses. As the SWPC tubes are fully sintered, there is no further shrinkage that occurs during electrolyte densification; therefore,

maximization of the film green density is critical. Our second approach utilized a non-aqueous solvent system, which has enabled a much higher slurry and film density to be achieved.

The drying rates of films deposited using the non-aqueous solvent system are controlled by volatilization of the solvent, which typically takes 15 minutes at a temperature of 100°C. After drying and approximately 5 minutes cooling, secondary layers can be applied with no observed detrimental interactions with the initial layers. During this stage of Phase I, subsequent film sintering temperatures of 1250-1350°C were investigated. In total, some 80 samples have been manufactured in lengths up to 45 cm for microstructural and gas leak analysis. Several samples with leak rates lower than can be detected by our apparatus have been supplied to SWPC for analysis.

Figure 1a demonstrates the greater utility of the non-aqueous system in depositing multiple films of varying composition. The backscatter image shows that the fine scale porosity near the electrolyte surface is associated with an electrochemically active cathode layer, a composite of lanthanum strontium manganese (LSM) and gadolinia-doped ceria (GDC)-10 powders. This layer was initially sprayed and dried, then immediately over-coated with the electrolyte layer. This type of multi-component coating was unachievable in the aqueous coating systems; intermediate calcination steps were required to maintain the integrity of the electrolyte and active electrode layers. The coating layers shown in Figure 1b were co-fired on the dead-sintered tube at 1300°C for two hours. Top-down views of the two coating surfaces revealed the improved quality the interlayer material produced in the electrolyte by moderating the surface roughness of the as-produced tube.

Based on the interlayer results achieved in Figure 1, the logical extension of the approach was to incorporate anode layer deposition and co-sintering to eliminate as many firing steps as possible. While this approach has yet to be demonstrated on the

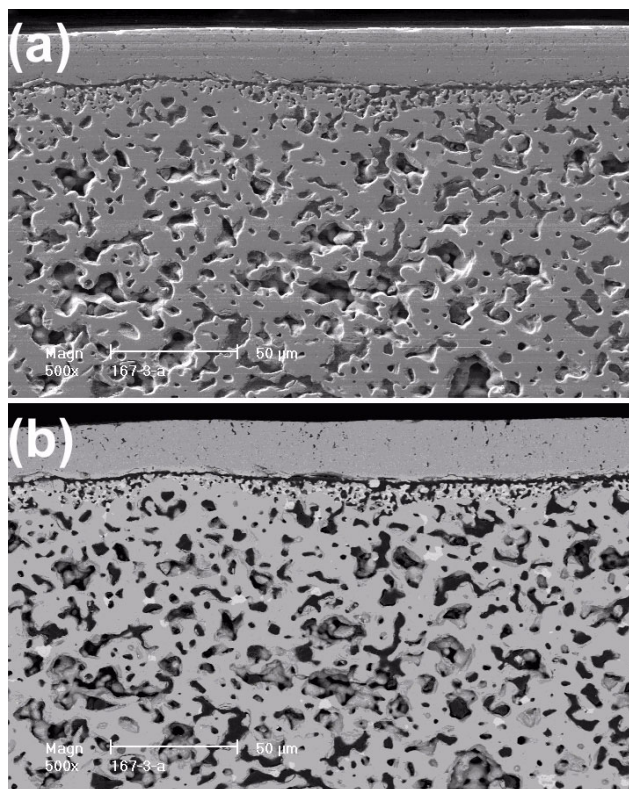


Figure 1. Zirconia-coated sample with LSM/GDC interlayer sintered at 1350°C. The picture on the top (a) is a secondary electron image; the picture on the bottom (b) is taken in backscatter mode.

SWPC tubes, it has been successfully completed in parallel work on anode supports. Figure 2 shows an aerosol-coated anode tube in which the interlayer and co-sintering processes have been taken to the next level of complexity. The tube shown in Figure 2 has four layers applied to the initial surface. An active anode layer, electrolyte, active cathode and current-carrying cathode layer have been applied and all sintered in a single step.

Conclusions

The technical achievement from this Phase I SBIR project is the demonstration of the feasibility of the aerosol spray deposition process for the producing electrochemically active layers in a solid oxide fuel cell. In addition to producing dense electrolyte films on SWPC cathode support tubes, greater levels of cell fabrication and process integration have been demonstrated on anode-supported tubes provided by Acumentrics, thereby

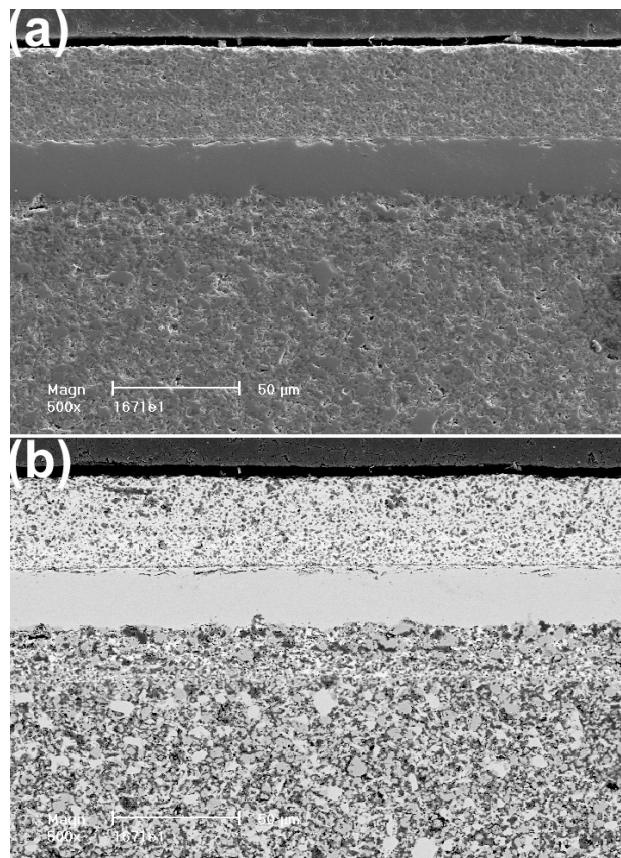


Figure 2. Zirconia-coated NiO-YSZ anode tube with active-anode interlayer, active cathode and current collector cathode layer, sintered at 1350°C. The picture on the top (a) is a secondary electron image; the picture on the bottom (b) is taken in backscatter mode.

demonstrating the applicability of the process multiple designs. In Phase I, a range of electrolyte spray formulations have been evaluated, improving coating deposition while maintaining low cost and low environmental impact. Alternative solvents have provided enhanced utility of the spray process and provided the opportunity for sequential depositions without intermediate calcination steps.

The successful manipulation of ink formulation for each of the functional layers, including electrode interlayer, current collectors and electrolyte, has resulted in the demonstration of a single sintering procedure for the electrochemical system for anode-supported cells. Co-firing temperatures as low as 1250°C appear to be feasible using this novel coating system.

VII.13 Highly Textured Composite Seals for SOFC Applications

Matthew M. Seabaugh (Primary Contact), Amy Trujillo, Michael J. Day

NexTech Materials, Ltd.

404 Enterprise Dr.

Lewis Center, OH 43035

Phone: (614) 824-6606; Fax: (614) 842-6607; E-mail: seabaugh@nextechmaterials.com

www.nextechmaterials.com

DOE Project Manager: Travis Shultz

Phone: (304) 285-1370; E-mail: Travis.Shultz@netl.doe.gov

Subcontractors: University of Missouri-Rolla, Rolla, Missouri

Objectives for Glass Composite Seal

- Develop glass composite seal with the following properties:
 - Low operating temperature (600°C-800°C)
 - Chemically stable with anode, cathode, electrolyte, interconnect materials, in both reducing and oxidizing environment over long periods of time
 - Thermally stable to cycle at operating temperatures
 - Mechanically durable to withstand thermal cycling
 - Flexible configuration to become compatible with the Solid State Energy Conversion Alliance (SECA) stack design and materials
- Demonstrate high seal performance in user-specific test cells and testing conditions
- Perform adhesion study of the glass composites on anode, cathode, electrolyte, and interconnect materials

Accomplishments

- Formulated glass compositions that soften below 900°C
- Glass compositions are chemically non-reactive and adhere to the surface of the anode, cathode and electrolyte materials
- Processed crystalline particulates into glass matrix for added strength
- Completed several successful seal leak tests of glass/crystalline composite structures
- Performed seal lifetime tests to 100 hours

Future Directions

- Provide seals that serve as ‘drop-in’ components for existing SECA designs and materials
- Perform lifetime study of 10,000 hours with thermal cycling
- Reduce seal costs
- Approach commercialization of SOFC seal materials tailored for the current SECA cell designs and materials

Introduction

To achieve the high power densities promised by planar stacks in solid oxide fuel cells (SOFC), reliable seal technology must be developed. Current seal technology has been successful in laboratory stack testing, but in practice is plagued by reliability and lifetime issues, particularly with respect to thermal cycling. Current seal materials are dependent upon glass and glass-ceramic technologies with significant alkali, borate, and phosphate contents, constituents that are known to be highly mobile at the cell operating temperatures. The volatilization of these species can degrade cell performance and ultimately limit cell life. Many of the reported seal formulations have been designed to operate near 1000°C, using ceramic interconnect materials, rather than the 600-800°C range, where the use of metallic interconnects are envisioned. A composite approach, in which a crystalline ceramic phase is oriented in a compliant viscous matrix, achieves good thermal, mechanical, and chemical stability through the stress relief and self-healing character of the viscous seal material and the interlocking nature of the crystalline phase.

Approach

A prospective seal material must be chemically and mechanically robust. Additionally, it must demonstrate highly tailored and often contradictory properties. Seals must be chemically inert, with negligible interaction with the electrodes, electrolyte, and interconnecting materials, but still form an intimate interface with the materials. The seal material must be compliant enough during manufacture and use to conform to irregularities in the component surfaces, but rigid enough during service to prevent creep and cell collapse. Finally, the seal must withstand tensile and compressive stresses that develop during thermal cycling of the fuel cell. Such resilience is particularly important for transportation applications. This project has targeted SOFCs operating at 750-850°C. Seal evaluation experiments are designed to bond electrode, electrolyte, and interconnect materials appropriate to the 750-850°C temperature range. In this project, the crystalline component materials were identified and incorporated into prototype seals, which were evaluated for leak-tightness and

stability to thermal cycling in contact with representative SOFC materials.

Results

Four potential crystalline phases were evaluated. Talc powder, mica powder and alpha-alumina platelet were selected based on reported use in the literature, observed anisotropy of particle shape or both. As powders were received, they were evaluated by scanning electron microscopy to confirm morphology and incorporated into tape casting slurries both with and without glass formers. While talc was observed to be very platy, all powders were easily incorporated into tapes.

Seals with up to twenty-five volume percent glass former were produced by tape casting. The dried tapes were cut and laminated to produce seals approximately one millimeter thick, and the seal quality was tested. The talc-based seals had the highest leak rate, while the alumina and mica seals showed superior performance. Tape casting was used to produce all the samples. The process was used to produce green tapes that were then laminated and used directly in sealing experiments. This direct implementation of the tape-cast seal materials allows a very high materials utilization, assures template particle orientation in the seal, and relies on inexpensive forming approaches, keeping production costs low. The seal materials have been directly used in SOFC testing without intermediate binder burnout—a potentially significant advantage of the forming process and materials selection.

For the seal test station, recording the time it takes for the pressure to decay from 2 psi to 0 psi will provide a repeatable procedure for testing. This pressure gradient is expected to be somewhat higher than that experienced in an SOFC. As a consequence of this pressure selection, the flow rates observed are higher than would be expected for SOFCs operating at atmospheric pressures and low pressure gradients.

As shown in Figure 1, the talc seals showed much higher flow rates than the mica or alumina seals and a different dependence on glass content. It is theorized that this difference is related to the relatively isotropic orientation and properties of the talc powder as compared to the more anisotropic and

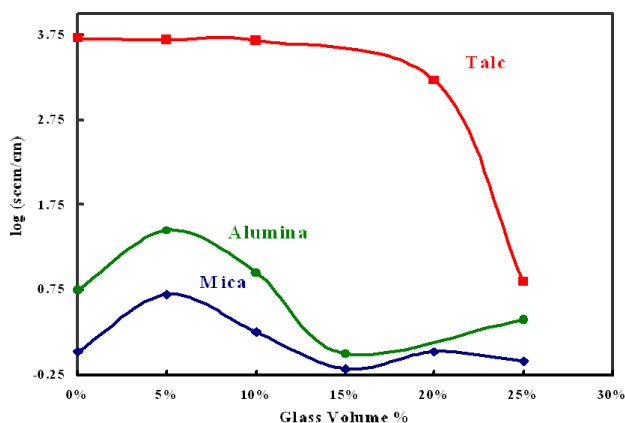


Figure 1. Effect of Crystalline Phase Selection on the Leak Rate of Composite Seal Materials

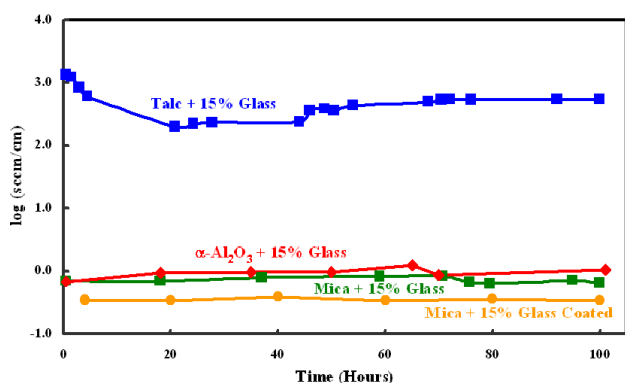


Figure 2. Flow Rates as a Function of Operating Time at 800°C for Four Textured Composite Seals

orientable mica and alumina platelets. The correlation between seal performance improvement with heating and the softening temperature of the glass is also significant, and it shows that the redistribution of the glass phase is critical to achieving good seal performance. This result underscores the importance of developing low-melting, low-viscosity glasses.

As processing of the seal materials has improved and the distribution of glass in the seal materials has been optimized, seal performance has also improved. To evaluate seal stability, 100-hour-long seal tests at 800°C were performed, and the data from four of these tests are shown in Figure 2. Particularly interesting is the improvement of the mica-based seals with the improved distribution of the glass

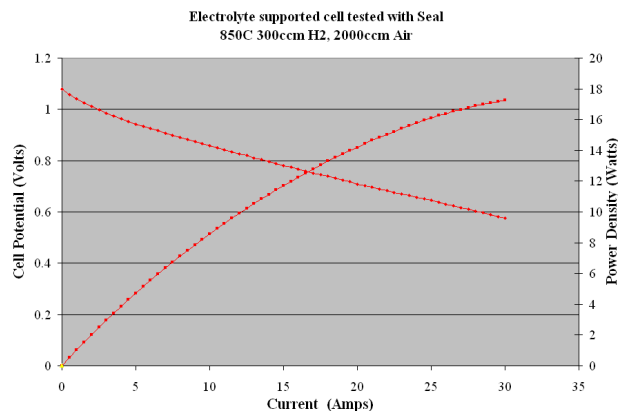


Figure 3. A Solid Oxide Fuel Cell Performance Test Using a Glass Seal

phase, re-emphasizing the importance of glass distribution to seal performance.

The seal must be tested in working conditions. Figure 3 shows the SOFC performance test of a working cell using a glass seal. A small load (current) was electrically placed on the cell to extract performance data, which isn't possible without a reliable and durable seal. This test was performed at a constant temperature while varying the current load. The seal held against a positive air pressure of both the oxygen-rich as well as the reducing atmosphere while at a high operating temperature.

Conclusions

The overall achievement of the project was the successful demonstration of compliant, low-temperature seals for SOFC applications using the textured composite approach. The performance of seal materials was demonstrated at SOFC operating temperatures for over 100 hours and through more than five thermal cycles. Materials selection was performed by a systematic evaluation of component properties and long- and short-term tests of seal performance, using test facilities constructed expressly for this project. The flexibility of the textured composite architecture was demonstrated in seal materials with a range of properties, which were produced using a single, low-cost, scalable tape casting approach. These results demonstrate that the textured composite architecture provides a robust design that is highly tailorable. These glass

composites have performed well in leak rate testing as well as preliminary lifetime studies.

FY 2004 Publications/Presentations

1. Materials Solutions 2003 Conference and Exposition, October 15, 2003, “Textured Composite Seals and Cathode Materials for Intermediate Temperature SOFC”
2. SECA Core Technology Program Meeting Seals 2004, “Materials Development for SOFCs: Seals and Electrolytes

VII.14 A Novel Integrated Stack Approach for Realizing Mechanically Robust SOFCs

Scott A. Barnett (Primary Contact), Tammy Lai, Jiang Liu

Northwestern University

Dept. of Materials Science

2220 Campus Drive

Evanston, IL 60208

Phone: (847) 491-2447; Fax: (847) 491-7820; E-mail: s-barnett@northwestern.edu

DOE Project Manager: Lane Wilson

Phone: (304) 285-1336; E-mail: Lane.Wilson@netl.doe.gov

Objectives

- Develop a screen print process for fabricating integrated solid oxide fuel cells (SOFCs).
- Demonstrate that the process can provide the resolution and alignment required to fabricate integrated SOFCs with dimensions in the millimeter range.
- Determine the performance of integrated SOFC arrays, and make initial attempts to optimize them via materials processing.
- Predict the optimal dimensions for segmented-in-series SOFCs.

Approach

- Ceramic processes including powder pressing, screen printing, and high-temperature sintering were used to prepare zirconia supports and cell active layers with desired structures.
- Standard materials characterization techniques such as scanning electron microscopy (SEM) and x-ray diffraction (XRD) were utilized to determine if the desired phases and structures were achieved.
- Electrical testing methods such as impedance spectroscopy, commonly used for characterizing fuel cells, were employed.
- Electrical modeling was carried out using equations describing the resistance losses in individual cells and current flows in the supports, and equations were solved using the program MatLab.

Accomplishments

- Developed and demonstrated screen printing of all fuel cell components with the required resolution of <0.1 mm, desired microstructures (dense electrolytes and electrodes with porosity >30%), and desired electrical properties.
- Demonstrated for the first time the successful operation of integrated solid oxide fuel cells with repeat periods of 1-2 mm, compared with 10 mm in prior work, and power densities in excess of 200 mW/cm².
- Developed a detailed electrical model useful for design and optimization of segmented-in-series SOFCs. The model accounts for cell characteristics, electrode resistance losses, and substrate shunting currents. Optimal cell widths were predicted to be in the range of 2-3 mm, depending on the above factors.

Future Directions

No other work is planned on this project, but work is ongoing on other projects:

- We are continuing to evaluate different ceramic interconnect materials in order to achieve low resistance losses and high density using a process where the interconnect is co-sintered with the other key cell

components. This is a key for achieving simple processing, low materials cost, and optimal cell performance.

- Work is still ongoing to analyze cell test results as a function of electrode sheet resistance in terms of the model. This will allow us to validate the model, make more quantitative predictions, and better predict optimal geometries/materials. At the same time, component processing and structure are being improved in order to achieve better stack performance.
- The work should also be extended to larger area devices with larger numbers of integrated cells. There are no fundamental issues here, but this will require detailed attention to processing in order to achieve flat surfaces and uniform properties across large wafers.

Introduction

While great success has been achieved with high-performance individual planar solid oxide fuel cells (SOFCs), problems remain with interconnecting, stacking, and sealing these devices to make full-scale generators. Some of these problems may continue, for some time to come, to be significant barriers to achieving reliable, low-cost, long-lived SOFC generators. Thus, other approaches should be explored that have the potential to circumvent these problems. This was the rationale behind the present project, in which we explored a novel segmented-in-series stack geometry. The segmented-in-series design is shown schematically in Figure 1. The geometry features an integral ceramic interconnect that avoids oxide scale problems with metallic interconnects, a flattened tubular design that provides for easier sealing while maintaining high power densities, and small-width cells that minimize current collection losses.

Considerable progress was made during this project. The entire materials processing sequence was developed and successfully implemented. Initial devices were fabricated, characterized, and successfully tested. A model was developed to explain the device performance results and to allow

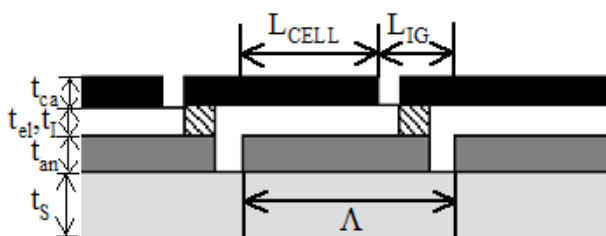


Figure 1. Cross-Sectional Schematic of the Segmented-in-Series Geometry

for prediction of optimal device design for future work. The results of this preliminary work are extremely promising, and we believe that this approach merits increased development efforts. The approach should provide for much better sealing than planar designs, and thus should be very useful for hydrogen generation schemes such as steam electrolysis.

Approach

Our approach combined experimental work and modeling. The experimental work was mainly to demonstrate the feasibility and utility of the novel stack geometry and to provide initial process and materials development for future work. The modeling was to help understand the experimental device performance and to provide a design tool for future development.

Experimental Results

Baseline studies were carried out to determine materials processing conditions that yielded the desired material structures and properties. A design-of-experiments study of partially-stabilized zirconia (PSZ) supports was carried out to obtain optimal strength for desired porosity levels of 30-40%. Based on the results, cell fabrication was done on PSZ supports with a filler content of 15 wt%, with strengths of ≈ 150 MPa.

In order to achieve low ohmic losses in mm-wide devices, the sheet resistance of electrodes should be $< \approx 10$ /square. The sheet resistance of single Ni-YSZ (yttria-stabilized zirconia) screen-printed layers (≈ 10 m thick) was 0.2–0.25 Ω /square from 600°C-800°C, well below the desired value. Thus, single Ni-YSZ

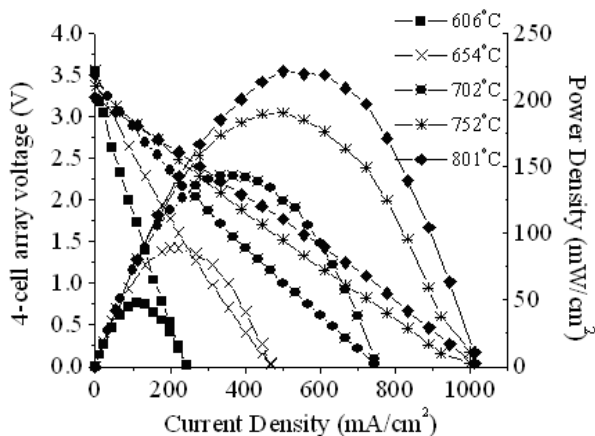


Figure 2. Voltage and Power Density versus Current Density for a Four-Cell SOFC Array Tested in Air and Humidified Hydrogen at Various Temperatures

printed layers provide negligible contribution to the array resistance.

The Ni-YSZ conductivity was ≈ 1000 S/cm, in fairly good agreement with literature values.¹

The cathodes consist of an LSCF-GDC layer printed directly on the electrolyte followed by a strontium- and iron-doped lanthanum cobaltite (LSCF) layer, both fired at 950°C . The LSCF-GDC layer provides good electrochemical performance,² but the low electronic conductivity of the gadolinium-doped ceria (GDC) component results in a high sheet resistance. The LSCF layer is used to provide an acceptable sheet resistance. LSCF sintered at 950°C yielded $r_s = 12$ /square at 800°C , corresponding to a conductivity of ≈ 70 S/cm in the $10\text{-}15$ μm thick layer. This is considerably lower than literature values for dense LSCF,³ perhaps due to the porous structure. Nonetheless, the single LSCF layer sintered at 950°C yielded a sheet resistance near the desired range of ≈ 10 /square.

Cross-sectional SEM was used to view the microstructures of the various layers after cell testing. In general, the microstructures were as expected. The Ni-YSZ layer was typically ≈ 15 μm thick and was porous with an average particle size of ≈ 1 μm . The YSZ layer was a double print, reasonably dense but with some closed porosity, typically $\approx 20\text{-}30$ μm thick. Thinner electrolytes can

presumably be used when a denser electrolyte structure is achieved. The cathode bi-layer was ≈ 30 μm thick with a porous structure (≈ 0.5 μm particle size), good adhesion to the electrolyte, and no clear evidence of the interface between the LSCF-GDC and LSCF layers.

Cell tests were carried out with air at the cathode and humidified hydrogen fed through the tube to the anode. The results of a typical four-cell array test are given in Figure 2. Open circuit voltages (OCV) ranged from 3.22-3.55 V, well below the theoretical value of ≈ 4.4 V. The porosity in the electrolyte and interconnect layers (SEM observation of the Pt and Au interconnects showed large porosity) is likely the dominant cause of the low OCV. Our calculations, described below, indicate that the PSZ support shunting current was too small to significantly reduce the OCV. The maximum power density calculated using the full array area was >200 mW/cm^2 at 800°C .

Both Au and Pt interconnects were tested, as well as $\text{Sr}_{0.94}\text{Y}_{0.04}\text{TiO}_3$ and $\text{Sr}_{0.55}\text{La}_{0.30}\text{TiO}_3$. The metallic interconnects yielded similar results as shown above. The La-doped interconnect was tested and gave almost no power output. The Y-doped interconnect gave only ~ 12 mW/cm^2 . It appears that the air conductivity of the doped SrTiO_3 is very low, preventing sufficient current flow through the interconnect. Other ceramic interconnect compositions are under investigation under other funding, and the results are very promising.

Calculation Results

Resistance-loss calculations were applied to realistic segmented-in-series geometries. The surface can be divided into active cell width L_{CELL} and interconnect/gap width L_{IG} . We have assumed interconnect/gap widths that are fixed by processing considerations. For example, in screen printing, there are limitations on resolution and print-to-print alignment. Relatively generous widths were chosen to provide easy alignment, i.e. wide gap widths (0.25 mm for the anode and 0.5 mm for the cathode) and relatively wide interconnects (0.5 mm), yielding a total inactive area $L_{\text{IG}} = 1.25$ mm. These values are well above the limits achievable by screen printing: ≈ 0.1 mm. The interconnect conductivity used was

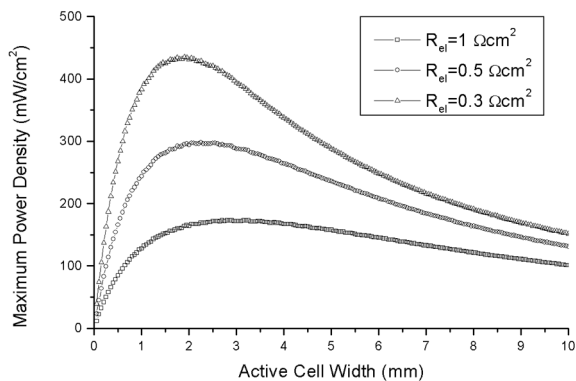


Figure 3. Maximum Power Density versus Active Cell Width L_{CELL} for a Segmented-in-Series Array

1 S/cm, a conservative value for typical ceramic interconnect materials such as doped LaCrO_3 . The cathode was taken to have a sheet resistance of 4 cm^2 .

Figure 3 shows the maximum power density versus active cell width for each of three different assumed area specific resistance (ASR) values. The curves each show a maximum power density at a different optimal L_{CELL} value. For cells with a relatively low ASR of $0.3 \text{ } \Omega\text{cm}^2$, the maximum power is 0.43 W/cm^2 at $L_{CELL} = 1.75 \text{ mm}$. For cells with a relatively high ASR of $1.0 \text{ } \Omega\text{cm}^2$, the maximum power is 0.17 W/cm^2 at $L_{CELL} = 2.9 \text{ mm}$. Note that if a smaller gap width L_{IG} is assumed, then the optimal cell widths shift to lower values and the maximum power densities to higher values. In general, the maximum results from the competition of two factors. First, at large cell widths, the electrode lateral resistance becomes large, yielding very low power densities. Second, as the cell width decreases to low values, the fraction of the total area taken up by the interconnect/gap area dominates, yielding low power.

We also carried out a detailed calculation of the shunting current in a mildly conducting support material for the segmented-in-series geometry. In order to provide a specific example of the shunting current expected in a typical segmented-in-series SOFC, we have assumed PSZ supports. Resistivity values for dense PSZ range from 1075-415 cm between 600-1000°C, respectively. These values were corrected to reflect the actual resistivity of the real supports, accounting for the typical porosity of

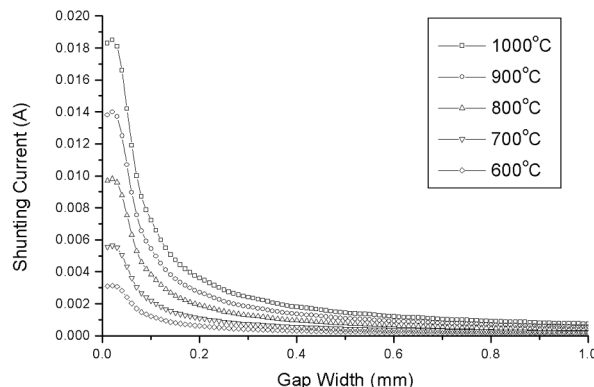


Figure 4. Shunting Current in a Porous PSZ Support versus Anode Gap Width for Different Operating Temperatures

$\approx 40 \text{ vol}\%$. Since PSZ is ionically conducting and the Ni-YSZ electrodes are electronically conducting, current flow through the support must involve electrochemical reactions at each of the interfaces and an associated polarization resistance. This resistance is neglected in the present calculation because its value may vary greatly depending on exact electrode composition and structure. Thus, the shunting current values given below must be regarded as upper limits.

Figure 4 shows a plot of the normalized current across a gap as a function of the gap width. Note that the current increases with decreasing gap width because of the increasingly high local current density as the gap narrows. Average shunting currents decreased rapidly for gap widths increased from 0 to 0.1 mm, after which they decreased more gradually. Taking the anode gap width of 0.25 mm assumed above, the shunting current should not be more than 2 mA at 800°C, or less than 2% of the total cell current (see Figure 4). Even for the smallest anode gap widths one might use, e.g. 0.1 mm, the shunting current is relatively small at 800°C. It is only at higher temperatures and small widths that the shunting current can become important. Shunting currents of this magnitude will not significantly affect the open-circuit voltage or maximum power density.

Summary and Conclusions

Millimeter-scale segmented-in-series SOFC arrays have been fabricated and tested. Optimization of the substrate processing, structure, and strength

were carried out, and screen printing inks and printing conditions were developed to achieve desired component structures. Fabrication of all patterned active layers by screen printing and co-sintering was successfully demonstrated. Electrical testing of four-cell arrays showed reasonable power densities for an initial study. There is considerable potential to improve upon this performance by increasing the fractional active cell area, increasing the OCV values, and reducing electrode polarization losses via improved active layer structures. The devices demonstrated here, containing only four cells in series on planar supports, are just an initial demonstration. When these devices are implemented on flattened tubes, they will combine most of the advantages of tubular SOFCs, i.e. integral interconnect and minimal sealing issues, with those of planar SOFCs, i.e. high power-to-volume ratio and ease of fabrication.

Calculations of the losses in segmented-in-series arrays, including electrode resistances, interconnect resistance, and shunting by a weakly conducting support material, show that millimeter-scale devices have advantages compared with the typical centimeter-wide cells. The results show that for $\approx 20 \mu\text{m}$ thick electrodes and interconnects and lateral print accuracy of $\approx 200 \mu\text{m}$, maximum power densities are achieved for cell widths of 2.9 to 1.75 mm as the cell resistance is decreased from 1 to $0.3 \Omega\text{cm}^2$. Shunting currents were found to have little effect on power density assuming partially-stabilized zirconia supports at temperatures below $\approx 800^\circ\text{C}$.

References

1. N.Q. Minh, *J. Am. Ceram. Soc.* **76**, 563-88 (1993).
2. E.P. Murray, M.J. Sever and S.A. Barnett, *Solid State Ionics* **148**, 27-34 (2002).
3. S.J. Skinner, *Intl. J. Inorg. Mater.* **3**, 113-121 (2001).

FY 2004 Publications/Presentations

1. T.S. Lai, J. Liu, and S.A. Barnett, "Patterned series-connected SOFCs," in *Solid Oxide Fuel Cells VIII*, Ed. By S.C. Singhal and M. Dokiya, (Electrochem. Soc., Pennington, NJ, 2003) p. 1068-1076.
2. T.S. Lai, J. Liu, and S.A. Barnett, "Effect of cell width on segmented-in-series solid oxide fuel cells," *Electrochem. Solid State Lett.* **7**, A78-A81 (2004).

Special Recognitions & Awards/Patents Issued

1. "Direct Hydrocarbon Fuel Cells" 6,479,178 (CIP covers basic cell design).

VII.15 Dense Membranes for Anode-Supported All-Perovskite IT-SOFC

Rambabu Bobba (Primary Contact), Samrat Ghosh (Research Associate)

Solid State Ionics Laboratory, Department of Physics

Southern University and A&M College

Baton Rouge, Louisiana 70813

Phone: (225) 771-2493; E-mail: rambabu@grant.phys.subr.edu

DOE Project Manager: Lane Wilson

Phone: (304) 285-4156; E-mail: Lane.Wilson@netl.doe.gov

Objectives

- Synthesize fine, homogeneous, phase-pure perovskites in the form of bulk (powders) and thin films to be used as components for developing zero-emission solid oxide fuel cells (SOFCs) capable of operating at reduced temperatures (~800°C).
- Study the effect of composition on the microstructure (grain size, grain boundaries, surface texture), magnitude of oxygen permeation, O₂ exchange rates and long-term stability.
- Measure the AC impedance at higher temperatures and investigate the effect of electrical conductivity on the electronic structure using x-ray absorption near edge spectroscopy (XANES) and extended x-ray absorption fine structure spectroscopy (EXAFS).
- Assemble all-perovskite SOFCs made from dense ceramic electrolyte membranes (LSGM: La_{0.8}Sr_{0.2}Ga_{0.875}Mg_{0.125}O_{3-x}) sandwiched between porous electrodes (based on Ni as anode and electronically conducting LaNi_{0.6}Fe_{0.4}O₃ and/or La_{0.8}Sr_{0.23}CoO₃ ceramic cathode).
- Evaluate the cost, performance, power generation capabilities, and emissions of the above SOFCs while optimizing the reduced-dimensionality structures needed to demonstrate a zero-emission unit by the end of the three-year period.
- Create an interest among African American undergraduate and graduate students to develop theses related to the development of all-perovskite anode-supported intermediate-temperature SOFCs (IT-SOFCs).

Introduction

To make solid oxide fuel cells (SOFCs) commercially viable for environment-friendly energy generation, it is of considerable interest to develop new techniques for large-scale, cost-effective preparation of perovskite-based multicomponent materials for application as cathode, anode and electrolyte. Preparation of perovskites using conventional solid-state sintering powder preparation routes is inconvenient when the requirement is for a fine, homogeneous, and phase-pure powder. Conventional processes have limitations due to the high temperature and prolonged period of heating involved, as highlighted by the following examples:

- Solid-state synthesis of LaCrO₃ often leads to volatilization of CrO₃.

- Cathode materials need to be porous for easy diffusion of O₂ to the electrode-electrolyte interface, but conventional solid-state technique does not result in porous materials.
- Formation of undesirable phases like La₄Ni₃O₁₀ in the synthesis of LaNi_{1-x}Fe_xO₃ can result in mismatch of thermal expansion coefficients.

Approach

For efficient performance of the LaCrO₃ interconnector, its sintered density should be close to its theoretical density (within =96%) or the porosity should be negligible to avoid interdiffusion of H₂ and O₂. High sintered density is usually achieved by high-temperature treatment (=1200°C) for prolonged duration. But in the case of LaCrO₃, large-scale synthesis of the pure phase is challenging because

loss of CrO_3 occurs during extreme conditions prevalent during conventional solid-state synthesis routes normally employed in industry. Fast synthetic techniques can prevent the loss of CrO_3 . The microwave-assisted route is a quick and efficient method for synthesis and sintering of materials. Recently, K.J. Rao et. al. reported synthesis of monophasic LaCrO_3 in a short time by microwave irradiation of a heterogeneous mixture of La_2O_3 and Cr_2O_3 embedded in graphite. The synthesis is fast because both graphite and Cr_2O_3 are good microwave susceptors. Although their results are interesting, it was felt that the porosity in LaCrO_3 prepared by microwave route can be further decreased. Porosity depends on the microstructure, which in turn is influenced to a great extent by the precursor chemistry and the synthetic conditions. Our approach to the minimization of porosity is to explore a combination of sol-gel and microwave techniques. The results from this investigation will clarify the following:

- (1) Whether or not there is any advantage of starting with a homogeneous mixture of La_2O_3 and Cr_2O_3 instead of a heterogeneous mixture as reported earlier. The homogeneous amorphous mixture is being generated using Pechini-type sol-gel route.
- (2) The correlation between the morphology of the precursor mixture obtained from the sol-gel route and the porosity of the final product after irradiating with microwaves. Systematic variation of the sol-gel parameters like nature of the ligand, metal-ligand ratio, thermal treatment etc. is being carried out to generate different morphologies of the precursor mixture.
- (3) The effect of duration of microwave irradiation on porosity.

Unlike interconnectors, cathodes for SOFC application need to be highly porous to facilitate oxygen diffusion to the electrode-electrolyte interface. One of the problems associated with cathodes is that they tend to lose their porosity at high fuel cell operating temperatures. This phenomenon is related to the microstructure. It has been shown that desired microstructures can be obtained by employing synthetic techniques such as hydro/solvo-thermal and template-based routes.

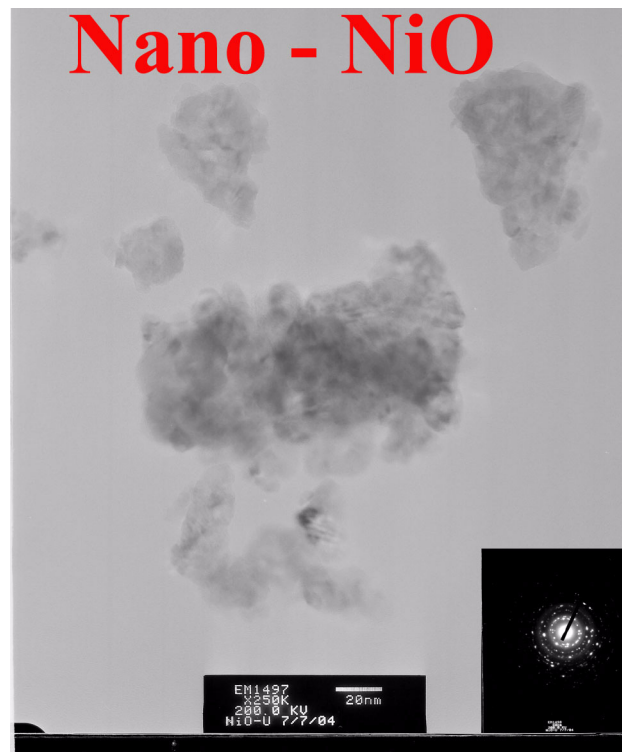


Figure 1. HRTEM Micrograph of Nanocrystalline NiO

In such synthetic routes, yield is very low and not suitable for large-scale synthesis. Hence there is a need for a synthetic technique which results in material where porosity is retained and can be prepared at a large scale. We are approaching this issue by adopting a combination of the Pechini-based method and scalable microwave processing.

Results and Discussion

We are employing a microwave-assisted solution combustion, mechano-assisted (ball milling), and pulsed laser deposition techniques to fabricate **dense ceramic membranes** on porous crystalline substrates. We have developed a combustion synthesis method using inexpensive, safe, water-soluble dimethyl urea (DMU), which is ignited at a temperature much lower than the actual phase-formation temperature. This fuel is new and has not been reported earlier. We have demonstrated the utility of this fuel and successfully prepared nanocrystalline NiO. The particle size of the NiO is ~ 50 nm, as determined by high-resolution transmission electron microscopy (HRTEM), shown in Figure 1.

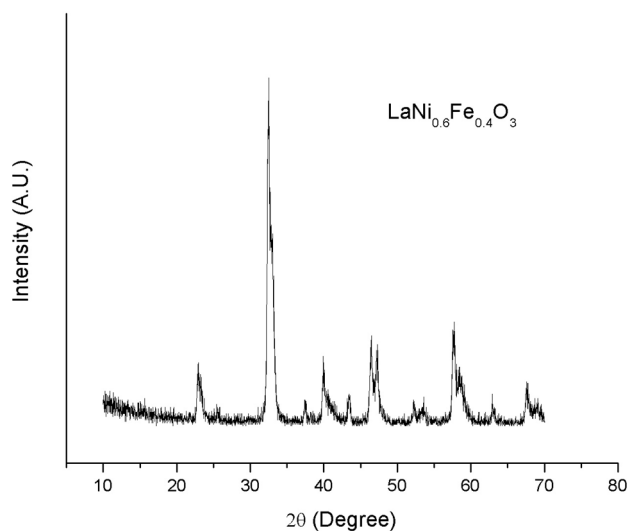


Figure 2. XRD Plot of $\text{LaNi}_{0.6}\text{Fe}_{0.4}\text{O}_3$ Powder Sample

The utility of this fuel further was extended to synthesize sub-micron sized mixed-perovskite-based oxides to be used in the fabrication of SOFCs. The properties of the SOFC components synthesized with DMU will be compared with those obtained by using other common fuels like glycine, citric acid, etc.

$\text{LaNi}_{1-x}\text{Fe}_x\text{O}_3$ was synthesized using the novel fuel developed in our laboratory. Figure 2 shows the x-ray diffraction (XRD) plots of the powder sample. The crystal structure was rhombohedral, and there were some impurities seen in the XRD. HRTEM, shown in Figure 3, reveals that the particle size is ~ 100 nm. We are now optimizing the synthesis procedure to further reduce the particle size and to get single phase at 800°C .

We have also successfully prepared these materials in a very short time (10-15 minutes) by subjecting sol-gel generated amorphous precursors to microwaves of 2.45 GHz in a multimode microwave oven coupled with suitable microwave susceptors. The cathode (that is the electrode at the air side of the fuel cell) has to reduce the oxygen molecules (O_2) of the air to oxygen ions (O^{2-}), which then migrate to (and through) the electrolyte. The cathode must have a porous structure to enable gas transport to the cathode's surface.

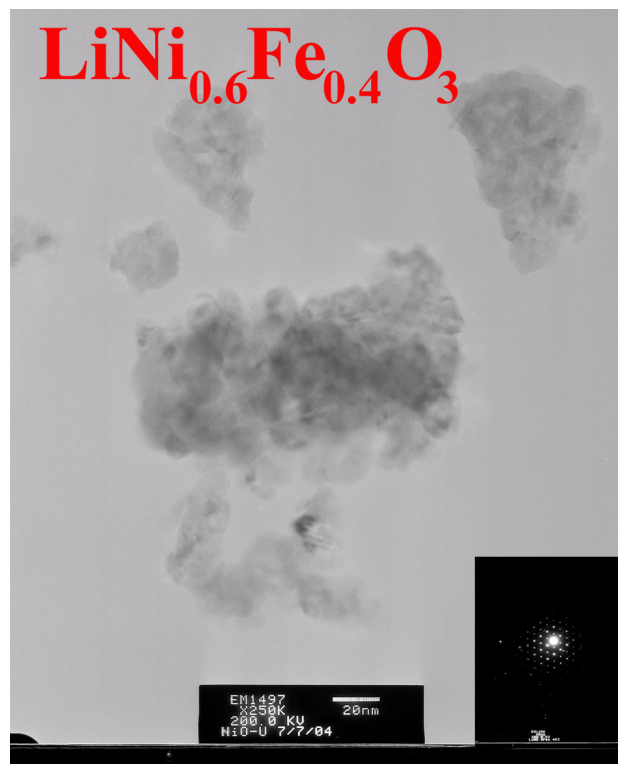


Figure 3. HRTEM Micrograph of $\text{LaNi}_{0.6}\text{Fe}_{0.4}\text{O}_3$

We have successfully prepared LaCrO_3 to be used as an interconnect in a very short time (10-15 minutes) by subjecting sol-gel generated amorphous precursors to microwaves of 2.45 GHz in a multimode microwave oven coupled with suitable microwave susceptors. No apparent loss of CrO_3 has been observed for LaCrO_3 . Products have been characterized by XRD and scanning electron microscopy. Conductivity measurements are in progress. The products are largely monophasic and stoichiometric. The oxide particles are of submicron size. LaCrO_3 has been microwave sintered to a remarkably high crack-free density of 96% in 10 minutes.

We are trying to evaluate valency of each transition metal in these perovskites using XANES, and to explore the relation between electrical conductivity and changes in electronic structure.

Summary

1. Combustion and mechano-chemical (ball milling) synthesis experimental stations were acquired and installed.
2. Research microwave system for high-temperature (1700°C) synthesis was acquired and installed.
3. Promising perovskite cathode, electrolyte, and interconnect were identified and synthesized.
4. The electrochemical impedance spectroscopy, EXAFS, XANES, and dilatometry measurements and fabrication development are in progress.

Future Plans

1. Once the synthetic parameters are optimized for LaCrO_3 and $\text{LaNi}_{0.6}\text{Fe}_{0.4}\text{O}_3$, the electrical conductivities of the samples will be measured.
2. Attempt synthesis of lanthanum strontium magnesium gallate (LSGM) electrolyte by regenerative sol-gel synthesis and carry out impedance measurements.
3. Attempt deposition of thin layer of LSGM electrolyte on $\text{LaNi}_{0.6}\text{Fe}_{0.4}\text{O}_3$ cathode.
4. We plan to carry out electrophoretic deposition of the dense LSGM samples on $\text{LaNi}_{1-x}\text{Fe}_x\text{O}_3$ porous cathodes presently being developed in our laboratory. To realize thin, dense O_2 -semipermeable membranes on single crystalline substrates, we are preparing thin films using pulsed laser deposition (PLD). The technique of PLD seems very well suited to deposit prototype thin perovskite films with various compositions.

VII.16 Sorbents for the Removal of Odorants from Natural Gas

Gokhan Alptekin

TDA Research

12345 W. 52nd Ave

Wheat Ridge, CO 80033

Phone: (303) 940-2349; Fax: (303) 422-7763; E-mail: galptekin@tda.com

DOE Project Manager: Norm Holcombe

Phone: (412) 386-4557; E-mail: Norman.Holcombe@netl.doe.gov

Objectives

- Identify the sorbent composition that maximizes the sorbent's capacity for organosulfur compounds
- Identify the sorbent's pre-breakthrough absorption and saturation capacity for organosulfur compounds
- Identify optimum operating conditions (i.e. temperature, pressure, contact time)
- Identify the effect of other natural gas contaminants such as CO₂, humidity and heavier hydrocarbons on sorbent performance

Approach

- Develop two types of sorbents: a high-temperature chemical sorbent and a low-temperature physical sorbent
- Screen the sorbents to rank their ability to remove odorants from simulated natural gas and liquefied petroleum gas (LPG)
- Optimize the conditions and demonstrate the effects of potential natural gas and LPG impurities on sorbent performance

Accomplishments

- Two types of sorbents were developed: a high-temperature chemical sorbent with an optimum operating temperature of 240°C and an ambient-temperature physical sorbent
- Both sorbents can reduce the sulfur content to less than 20 ppbv, achieving greater than 99.99% sulfur removal efficiency
- Both sorbents can remove all common organic sulfur species as well as H₂S
- Neither sorbent catalyzes any undesirable side reactions
- The absorption capacity for removing dimethyl sulfide from natural gas is 5.51% for the chemical sorbent and 2.52% for the physical sorbents
- For LPG, the chemical sorbent has a 0.47% wt. sulfur absorption capacity while the physical sorbent has 1.23% wt. sulfur adsorption capacity
- We showed that our ambient-temperature physical sorbent can also be regenerated by applying a mild temperature swing

Future Directions

- Develop a fundamental understanding of the removal process and the nature of the active sites so that we can optimize and improve the sorbent formulations
- Carry out long-duration tests where the regeneration potential of the physical adsorbent is demonstrated over multiple adsorption/regeneration cycles

- Carry out field tests to demonstrate the performance of our desulfurization sorbents integrated with a fuel cell system (with fuel cell stacks, fuel processor and all auxiliary items)
- Carry out an independent engineering study to assess the impact of TDA's novel desulfurization technologies on overall system efficiency, weight and cost

Introduction

Chemical odorants made with sulfur-containing compounds are added to natural gas and liquefied petroleum gas (LPG) to facilitate leak detection. However, these compounds contaminate the catalysts used in fuel cell fuel processing systems and degrade the performance of the fuel cell stacks.

We developed low-cost, high-capacity sorbents that can remove sulfur-bearing odorants from natural gas and LPG. We also demonstrated the technical and economic feasibility of processes using these sorbents, which dramatically reduce the cost of odorant removal.

Approach

The overall objective of the Phase I research was to determine the technical and economic feasibility of using a sorbent to remove sulfur-bearing odorants from natural gas and liquefied petroleum fractions such as propane. To accomplish this objective, we developed two different types of sorbents: a low-temperature physical adsorbent and a high-temperature chemical absorbent.

To prepare both types of sorbents, we first identified several precursors for the active phase and substrate matrix. A large number of these preparations (both physical and chemical sorbents) were first pre-screened based upon their physical properties (i.e., crush strength, surface area, porosity). Only the best samples were tested in the bench-scale reactor to determine their sulfur absorption capacity.

We built a testing system and developed an analytical method to allow us to measure the performance of both types of sorbents (high- and low-temperature) with a sulfur detection capability of 20 ppbv. We screened over 40 samples and identified the samples with the highest sulfur absorption capacity under representative conditions (using natural gas blends and LPG). We tested the

effect of different operating parameters on the sulfur absorption capacity of the sorbents and showed that we can develop sorbents with a very high sulfur absorption capacity. We showed the effectiveness of the sorbents for removing different odorant species, including dimethyl sulfide (DMS), tetrahydrothiophene (THT), tert-butyl mercaptan (TBM), and isopropyl mercaptan (IPM) at representative concentrations from natural gas and LPG blends. In all cases, dimethyl sulfide was found to be the hardest odorant to remove.

Results

In our research, we first recognized that a chemically active sorbent that works at high temperatures (240°C) could effectively remove more sulfur-bearing odorants from natural gas than a room-temperature sorbent. We developed a very active chemical absorbent that effectively removes even the most difficult to react organic sulfur species (such as dimethyl sulfide). Figure 1 shows the breakthrough profiles for a test done with multiple odorants. As the test starts, there are no odorants present in the exit gas stream, as they are all absorbed by the sorbent. During absorption, the sorbent forms a stable sulfide phase while reducing sulfur content of the natural gas to less than 20 ppbv (the detection limit of our Phase I apparatus). The DMS then

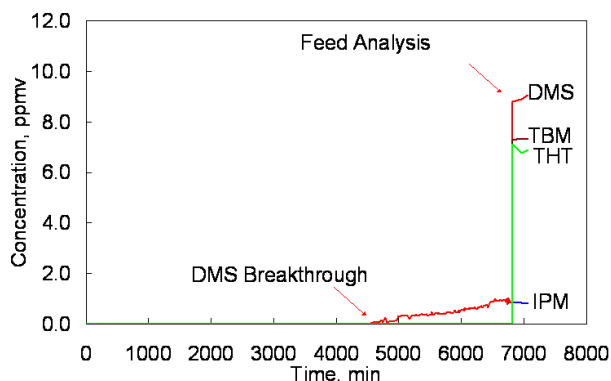


Figure 1. Adsorption Profile for the High-Temperature Sorbent Using a Mix of Odorants

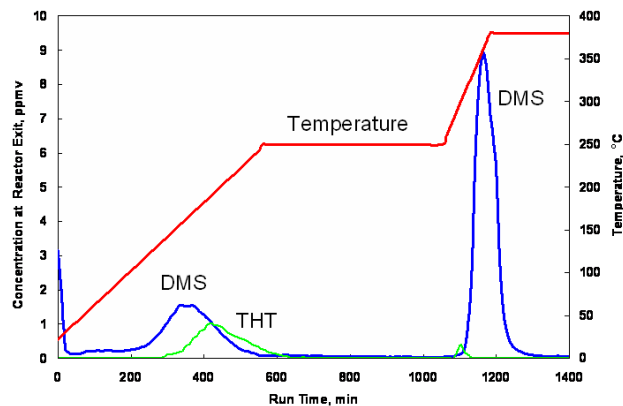


Figure 2. Regeneration of a Low-Temperature Physical Sorbent

breaks through. After the test was finished, the inlet gas stream was run through the analyzers to show that all of the sulfur compounds were present still in the correct proportions in the feed. The chemical absorbent we developed in the Phase I work achieves 5.51% wt. absorption capacity (lb of sulfur removed per lb of sorbent), nearly an order of magnitude higher than can be achieved by conventional sorbents. We also demonstrated that the operating temperature of the sorbent does not catalyze any undesirable side reactions (e.g., oxidation of natural gas or reactions among the organic sulfur species).

Based on the feedback from the fuel cell manufacturers, we also developed an ambient-temperature adsorbent that removes the odorants by physical adsorption. TDA's physical adsorbent achieved 2.52% wt. sulfur adsorption capacity, a great improvement in capacity over state-of-the-art room-temperature adsorbents (the best result reported in the literature to date is ~1.2% wt. by King and coworkers using copper and cerium exchanged zeolites). TDA's physical adsorbent was also very effective in removing organic sulfur compounds from LPG. We showed that our ambient-temperature sorbent can be regenerated by applying a mild temperature swing. Figure 2 shows a profile of a regeneration cycle. The sample was originally tested in a mixture of 17 ppmv DMS, 5 ppmv THT, 7 ppmv TBM. After testing, the sample was regenerated in

nitrogen. As the temperature was raised, the off-gas was monitored for sulfur compounds. The figure shows that at 150°C, some DMS and THT were released, and at 350°C, more DMS was released.

Conclusions

In our research, we developed very effective sorbents for desulfurization of natural gas and LPG. We first developed a very active chemical absorbent and showed that the sorbent forms a stable sulfide phase. The sorbent achieves 5.51% wt. sulfur absorption capacity for removing dimethyl sulfide from natural gas and can desulfurize LPG with 0.47% wt. sulfur absorption capacity.

We also developed a low-temperature adsorbent that removes the odorants by physical adsorption. The sorbent achieves 2.52% wt. sulfur adsorption capacity for removing dimethyl sulfide from natural gas and can desulfurize LPG with 1.23% wt. sulfur adsorption capacity. We showed that our ambient-temperature sorbent can be regenerated by applying a mild temperature swing.

References

1. King, D.L., Birnbaum, J.C., Singh, P., "Sulfur Removal from Pipe Line Natural Gas Fuel: Application to Fuel Cell Power Generation Systems", Proceedings of the 2002 Fuel Cell Seminar, Palm Springs, CA.

FY 2004 Publications/Presentations

1. Alptekin, G.O., Wright, J., Monroe, J., Amalfitano, B., and DeVoss, S.; "Sorbents for the Removal of Odorants from Natural Gas"; U.S. Department of Energy National Energy Technology Laboratory SECA Annual Workshop and Core Technology Peer Review Workshop, Boston, MA, May 11-13, 2004.
2. Alptekin, G.O., Amalfitano, B., Copeland, R., "Sorbents for Natural Gas Clean-up", Fuel Cell Seminar, Miami Beach, FL, 2003.

VII.17 Carbon-based Fuel Cell

Steven S. C. Chuang

Department of Chemical Engineering, The University of Akron

200 East Buchtel Commons

Akron, OH 44325-3906

Phone: (330) 972-6993; Fax: (330) 972-5856; E-mail: schuang@uakron.edu

DOE Project Manager: Travis Shultz

Phone: (304) 285-1370; Fax: (304) 285-4638; E-mail: Travis.Shultz@netl.doe.gov

Objectives

- Determine the technical feasibility of using coal as the fuel for solid oxide fuel cells.

Approach

- Develop an anode catalyst to promote the electrochemical oxidation of coal.
- Employ mass spectrometer and infrared spectrometer to monitor the effluent of the coal fuel cell.

Accomplishments

- Demonstrated that the use of coal as the fuel to the solid oxide fuel cell is technically feasible.
- Showed that the coal fuel cell gave 80 mA/cm² at 0.7 V.

Future Directions

- Increase the current density of the coal fuel cell above 200 mA/cm² at 0.7 V.

Introduction

The direct use of carbon from coal as a fuel for the solid oxide fuel cell to generate electricity is an innovative concept for power generation. This type of C-fuel cell (carbon-based fuel cell) could offer significant advantages in (i) minimization of NO_x emissions due to the operating temperature range of 700 - 1000°C, (ii) high overall efficiency because of the direct conversion of carbon to CO₂, and (iii) low investment and maintenance cost due to simplicity of the process. The objective of this study is to investigate the performance of a highly active anode catalyst for the electrochemical oxidation of coal. The performance of this C-fuel cell will be determined by measuring the voltage output and current density as a function of temperature, time, anode catalyst compositions, concentration of SO₂, and composition of carbon black and coal slurry. The results of this study will allow us to evaluate the limitations and potential of the carbon-based fuel cell for practical applications.

Approach

A number of solid oxide fuel cells were fabricated and tested at 950°C. The yttria-stabilized zirconia (YSZ) electrolyte was purchased from Tosoh Corp; its thickness is 1 mm. Both current and voltage output data from the fuel cell were acquired by a PC with an interface and Labview™ software. The gaseous product was analyzed by a SRI 8610C gas chromatograph and a Pfeiffer QMS 200 mass spectrometer. The analysis of gaseous products, such as CO and CO₂, allows determination of the fuel conversion efficiency and byproduct formation.

Results

Figure 1 shows the performance (I-V curves) of our fuel cell with a highly active oxidation catalyst using CH₄ and Ohio No. 5 coal as fuels. Ohio No. 5 coal contains 2% sulfur, 84% fixed carbon, and 5% ash. Coal was loaded on the anode side and gradually heated to 950°C. The coal fuel cell at

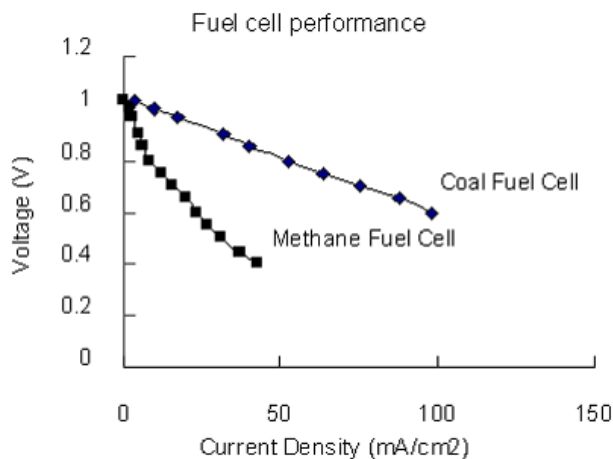


Figure 1. Fuel Cell Performance

950°C produced higher current density than did the CH₄-fuel cell. It is remarkable to observe that the current-voltage (I-V) curve for coal is higher than that for methane. Comparison of the CH₄ I-V curve in Figure 1 with those in literature (1-4) shows that the current density for CH₄ is about 35% of the best reported data for the direct methane solid oxide fuel cell. This is due to the use of thicker solid YSZ electrolyte (i.e., 1 mm in thickness) in our fuel cell as compared with 50 microns in the literature.

The analysis of the gaseous stream showed that the major product produced from the coal fuel cell is CO₂ with less than 5% of CO. CO concentration can be further decreased by decreasing the flow rate of Ar which was used to bring out the gaseous product for the analysis. SO₂ was only observed during heating of coal. SO₂ and CO, H₂ and CH₄ begin to form at 400°C. The SO₂ concentration in the fuel

cell effluent reached a peak at 650°C and then declined with temperature. Repeated runs on the same fuel cell gave the same level of electric power as that in the first run.

Conclusions

- The use of coal as the fuel to the solid oxide fuel cell is technically feasible.

References

1. S. Park, J. M. Vohs, R. L. Gorte, *Nature* 404 (2000) 265.
2. T. Ishihara, T. Yamada, T. Akbay, Y. Takita, *Chem. Eng. Sci.* 54 (1999) 1535.
3. T. Horita, N. Sakai, T. Kawada, H. Yokokawa, M. Dokiya, *J. Electrochem. Soc.* 143 (1996) 1161.
4. S. A. Barnett in *Handbook of Fuel Cells*, eds: W. Vielstich, A. Lamm, and H. A. Gasteiger, Wiley, 2003.

FY 2004 Publications/Presentations

1. "Coal-based Fuel Cell," Ohio Hydrogen from Coal Forum, April 2, 2004.

Special Recognitions & Awards/Patents Issued

1. Steven S. C. Chuang and Rajesh Khatri, U.S. Patent Application 60,520,455, The University of Akron, December 2003.

VII.18 Modeling and Design for a Direct Carbon Fuel Cell with Entrained Fuel and Oxidizer

Alan A. Kornhauser (Primary Contact), Ritesh Agarwal
Virginia Tech, Mechanical Engineering
Mail Code 0238
Blacksburg, VA 24061-0238
Phone: (540) 231-7064; Fax: (540) 231-9100; E-mail: alkorn@vt.edu

DOE Project Manager: Travis Shultz
Phone: (304) 285-1370; E-mail: Travis.Shultz@netl.doe.gov

Objectives

- Develop a fuel cell concept in which the anode and cathode are electrically-connected porous beds through which electrolyte flows with fuel and oxidizer entrained.
- Develop preliminary solutions to design problems such as electrode construction, gas-solid-electrolyte separation, and balance-of-plant design.
- Model overall plant mass and energy balances.
- Model processes within the electrodes.
- Develop to a stage where potential can be evaluated and research needs determined.

Approach

- Develop cell design.
- Develop balance-of-plant design.
- Model mass and energy balances for the plant.
- Model mass transfer, charge transfer, and chemical kinetics within the cell.
- Determine performance of cell and plant designs. Compare with alternate systems.
- Determine sensitivity to mass transfer, charge transfer, and chemical kinetic models. Evaluate research needs.

Accomplishments

- Developed cell design that provides circulation and separation of solid fuel, liquid electrolyte, supplied gases, and product gases with short ionic current paths.
- Developed balance-of-plant design that optimizes cell performance for power output and waste heat production.
- Modeled plant mass and energy balances. Determined that anode carbon dioxide/carbon monoxide balance was critical in overall plant performance.
- Reviewed literature to find correlations for mass transfer, reaction rates, and electronic and ionic electrical resistances.
- Modeled performance of cell electrodes with a set of simultaneous differential equations.

Future Directions

- Use electrode models to determine performance of cell designs.
- Use electrode models for first-cut optimization of cell designs.
- Compare performance with alternate systems.
- Determine model sensitivity to mass transfer, charge transfer, and chemical kinetic sub-models.
- Develop designs for experimental electrodes.

Introduction

Modern fuel cell development has concentrated on compact fuel cell designs in which immobile electrolyte is contained between porous membrane electrodes. Fuel and oxidizer are supplied to the electrodes on opposite sides of the electrolyte, and all reactions take place on the electrolyte-wetted surfaces of the electrode membrane. This design is effective for a compact cell using gaseous fuel, but it has serious limitations for utility-scale power generation using coal.

An alternate concept is proposed. In this concept, the anode and cathode are electrically-connected porous beds. Molten salt electrolyte, with carbon fuel and oxidizer entrained, is pumped through the porous beds.

This fuel cell design can use impure solid fuel (coal or coke) and offers economies of scale for utility-size plants.

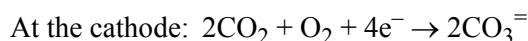
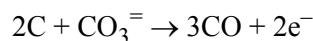
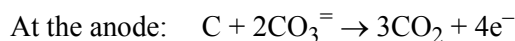
Approach

The technology is more like a chemical refinery or an electrochemical plant than like a membrane electrode fuel cell. Accordingly, design techniques are those used for chemical reactors and electrochemical plants.

Initial designs for the cells and for the balance-of-plant have been developed. Techniques from the chemical engineering literature are being used to model these designs. The models will be used to predict the performance of the designs and to optimize them. Sensitivity analysis will show which processes have the greatest effects on performance and thus merit further study.

Results

Because molten carbonate fuel cells show promise for direct generation of electricity from coal, cells of this type were the basis for the design. The reactions for a molten carbonate cell using coal are:



Chemical equilibrium and kinetics determine the amounts of CO and CO₂ produced at the anode. If CO is produced, it can be burned in an external burner. Anode exhaust gas is used to supply CO₂ to the cathode.

A major design challenge was to devise a cell that would allow for proper solid-liquid-gas separation and have short ionic conduction distances. After several iterations, the cell shown in Figure 1 was conceived.

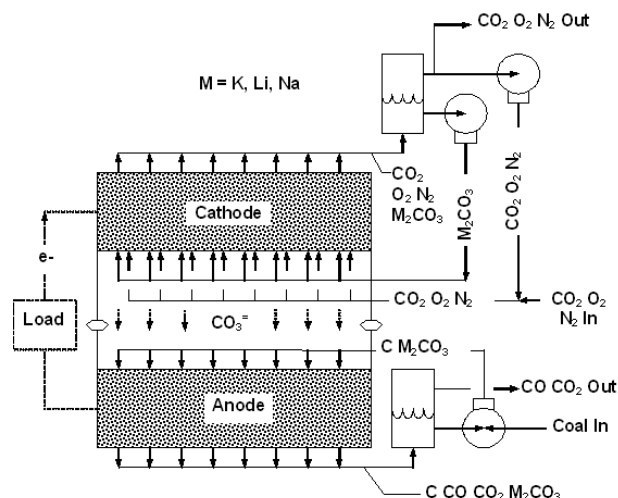


Figure 1. Coal-Fueled Molten Carbonate Fuel Cell with Porous Bed Electrodes

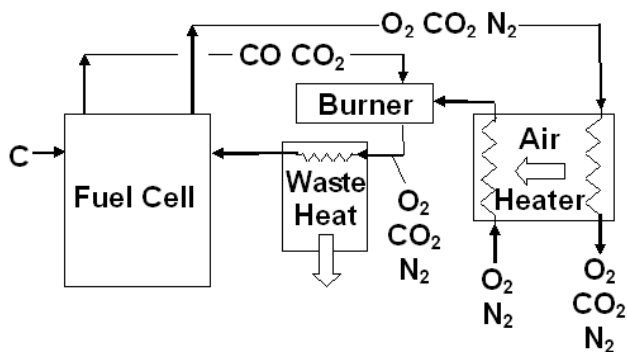


Figure 2. Balance-of-Plant Components for Coal-Fueled Molten Carbonate Fuel Cell

Molten carbonate salt, with carbon particles entrained, is pumped downward through the anode bed. It reacts with CO_3^- ions diffusing from the cathode to form CO and CO_2 , sending electrons to the load. Downward velocity of the salt ensures that both carbon particles and gas bubbles are entrained downwards. Salt, evolved gases, and excess carbon exit the bottom of the anode and gases are separated from the liquid/solid slurry. The slurry is enriched with more carbon and recirculated through the anode, while the gases supply CO_2 to the cathode.

Molten carbonate salt is pumped upward through the cathode bed, with O_2 , N_2 , and CO_2 entrained. O_2 and CO_2 molecules receive electrons from the load and react to form CO_3^- ions, which diffuse to the anode. Excess gases exit the top of the anode and are separated from the liquid. The liquid and part of the gas stream are enriched with O_2 and CO_2 and recirculated, while the remainder of the gas stream is exhausted.

It was also necessary to develop a design for the “balance-of-plant” components necessary for fuel cell operation. The balance-of-plant design is shown in Figure 2. CO and CO_2 generated in the anode are supplied to a burner, where they are combusted with excess air. The resulting O_2 - N_2 - CO_2 mixture is supplied to the cathode. The air supplied to the burner is preheated by the N_2 , CO_2 , and excess O_2 leaving the cathode, and waste heat is recovered from the gases leaving the burner.

Based on this plant concept and assuming uniform temperatures within the fuel cell itself, mass

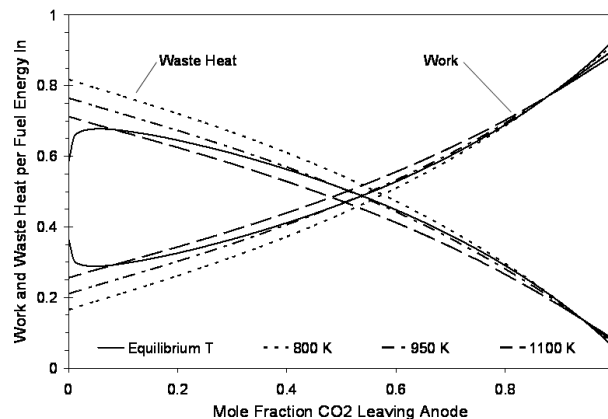


Figure 3. Work and Waste Heat Output vs. CO_2 Fraction Leaving Anode – Various Cell Temperatures

and energy balances were used to determine overall plant performance as a function of cell temperature, cell internal efficiency, excess air, air heater temperature difference, and CO- CO_2 ratio leaving the anode. This last was important because research has shown that the fraction of CO_2 produced in a carbon-fueled molten carbonate cell is much higher than predicted by chemical equilibrium.

The modeling showed that the CO- CO_2 ratio leaving the anode was dominant in determining plant efficiency. The effect of excess air was negligible, and the effect of heat exchanger temperature difference was small. Cell temperature and cell internal efficiency were significant, but less important than CO- CO_2 ratio.

Figure 3 shows work per fuel energy in (efficiency) and waste heat per fuel energy in, plotted against the volume fraction CO_2 leaving the anode. Cell temperature is a parameter, with curves shown for fixed values and also for cell temperature corresponding to the CO_2 fraction for chemical equilibrium. Cell internal efficiency is 100%, air heater minimum temperature difference is zero, and there is no excess air. Plant performance is a strong function of CO_2 fraction and a weaker function of cell temperature.

Figure 4 also shows work per fuel energy in and waste heat per fuel energy in plotted against the volume fraction CO_2 , but with cell internal efficiency as a parameter. Cell temperature is 950 K, air heater minimum temperature difference is zero, and there is

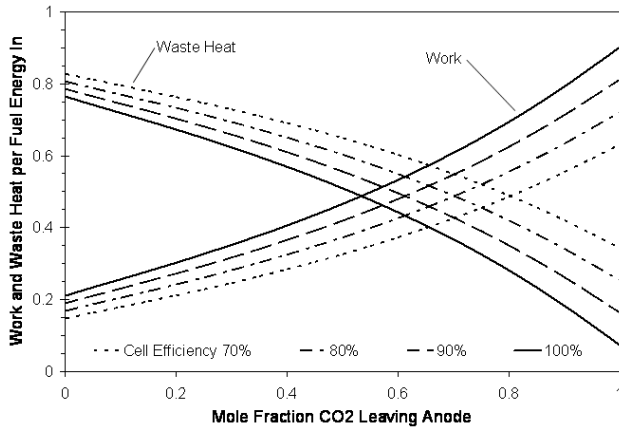


Figure 4. Work and Waste Heat Output vs. CO₂ Fraction Leaving Anode – Various Cell Internal Efficiencies

no excess air. Cell internal efficiency variation has a greater effect on performance than cell temperature, but its effect is less important than that of CO₂ fraction.

A model for the internal processes within the fuel cell is now close to completion. This model calculates the rates of mass transfer between gas and liquid, mass transfer between liquid and solid, ion diffusion through the electrolyte, and chemical reactions at the surfaces to determine a cell design for given voltage and current requirements. Results from this model are expected in the near future.

Conclusions

The most important conclusions from the work to date are:

- The fuel cell design shown in Figure 1 allows effective handling of solid, liquid, and gas phases within the cell while maintaining a short ionic conduction path.
- The balance-of-plant design shown in Figure 2 effectively maintains the cell at proper operating temperature, controlling cell temperature by controlling the temperature of the gaseous feed stream.
- The most important factor for good performance of the carbon-fueled molten carbonate fuel cell is high production of carbon dioxide (as opposed to carbon monoxide) in the anode.

FY 2004 Publications/Presentations

1. “Energy Balance for a Direct Carbon Molten Carbonate Fuel Cell,” R. Agarwal and A. Kornhauser, ASME Heat Transfer / Fluids Engineering Summer Conference, July 11-15 2004, Charlotte NC, Paper HT-FED2004-56887.
2. “Modeling and Design for a Direct Carbon Fuel Cell with Entrained Fuel and Oxidizer,” A. Kornhauser and R. Agarwal, DOE University Coal Research Contractors Review Meeting, June 9-10 2004, Pittsburgh PA.

VIII Novel Generation

VIII Novel Generation

VIII.1 Development and Testing of a Rotating Supersonic Shock Compressor

*Aaron Koopman (Primary Contact), Dr. John Hinkey, Peter Baldwin
Ramgen Power Systems, Inc.
11808 Northrup Way Suite W-190
Bellevue, WA 98005
Phone: (425) 828-4919 ext. 235; Fax (425) 828-7756; E-mail: hq@ramgen.com*

*DOE Project Manager: Tom George
Phone: (304) 285-4825; E-mail: Tom.George@netl.doe.gov*

Objectives

- Demonstrate a supersonic shock compression rotor (Rampressor™) to show feasibility of high-efficiency shock compression technology for stationary devices

Approach

- Design, manufacture and test a laboratory rig that will facilitate the understanding of the aerodynamic features of the shock compression rotor
- Analyze the performance data from the compression rig test to evaluate the technical potential of the novel compression technique

Accomplishments

- The supersonic shock compression rotor demonstrated several important milestones
- Achieved full rotor speed of ~20,000 RPM with all mechanical systems working properly
- Shock structures were established in all of the supersonic shock inlets on the rotor (3 inlets per rotor)
- The rig operated near design pressure ratio (~2.2:1) and mass flow (~1.8 lbm/sec)
- The rig achieved ~75% rotor efficiency without the optimization of the geometry, bleeds, tip clearance, etc.
- The technical design and analysis tools have been validated

Future Directions

- Analyze the performance data from the first Rampressor test rig and compare to computational fluid dynamics (CFD) data to develop our design and analysis tools
- Design the second Rampressor test rig to run at higher pressure ratio (10:1) and higher mass flow (1500 cfm), and achieve higher efficiency through optimization of the tip clearance and rotor geometry

Introduction

Since the sound barrier was broken in the late 1940s, ramjet engines have been widely used as a means to propel aerospace vehicles at supersonic speeds. The underlying supersonic aerodynamic shock theory and technology is very well

understood and fully characterized. Ramgen Power Systems' ("Ramgen's") primary innovation has been to apply ramjet engine concepts as a stationary "shock" compressor. The principal advantage of shock compression is that it can achieve exceptionally high compression efficiency at very high compression ratios.

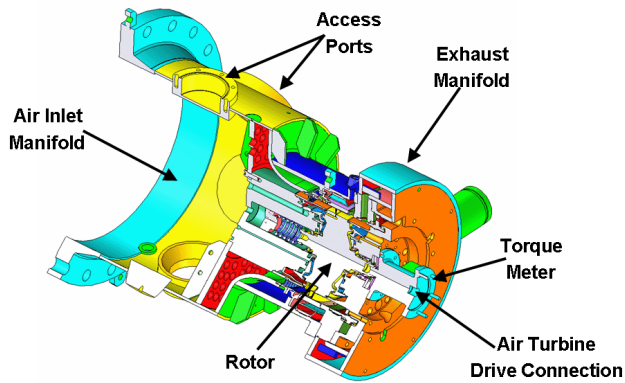


Figure 1. Test Rig

The importance of a breakthrough compression technology cannot be overstated. The air and gas compression industry is often referred to as the Fourth Utility. Compressed air is one of the most important utility requirements of industrial manufacturing. Air compression is also a critical element in determining the efficiency of all types of combustion engines, including gas turbines, internal combustion engines and hybrid fuel cells. Gas compression is the key to the transportation of natural gas, air conditioning and refrigeration, and efficient compression of CO₂, which is increasingly seen as pivotal to effectively dealing with greenhouse gas emissions.

Approach

In April, 2002, the DOE conducted a two-day Design Review of the Company's technology at the National Aeronautics and Space Administration (NASA) Glenn facility outside Cleveland, Ohio. This Design Review involved approximately 20 prominent scientists from the DOE, Department of Defense, and NASA, as well as a team of Ramgen scientists. At the time of this Design Review in Cleveland, Ramgen estimated that the development costs to demonstrate an advanced Ramgen engine were in excess of \$30 million. As a result of that Design Review, Ramgen management concluded that most of the advantages and value of the technology could be realized at a fraction of this cost (and within probable DOE support levels), in a shorter time period and with less technical risk. Consequently, Ramgen has focused its resources on demonstrating

the Rampressor and designing the Rampressor Turbine in the near-term.

The technology development path for the Rampressor starts with a rotor test rig at relatively low pressure ratio and performance. The next step is a higher (commercially desirable) pressure ratio and performance rotor test rig - the 2nd Rampressor Test Rig. The next test rig (Alpha rig) will be a compressor demonstrator including all the major components of a functional compressor package (drive, supporting systems, controls, etc.). Following the Alpha rig there are four Beta pre-production test units planned to complete the development of the compressor.

Results

During FY 2004, Ramgen succeeded in completing testing of the first Rampressor compressor test rig; see Figure 1. Testing was run at the Boeing Nozzle Test Facility in Seattle, Washington. The test was successful in many ways.

One of the testing accomplishments achieved by Ramgen was the successful establishment of a shock structure within the inlet that permits compression of the air by supersonic compression waves – the inlet has been “started.” Inlet “starting” is a significant milestone in any supersonic inlet test program, whether it is for supersonic air breathing missiles or aircraft (high speed military jet fighters, SR-71, or the Concord). Inlet starting is defined as stable supersonic flow throughout the converging/contracting portion of the inlet geometry. The minimum flow area of a fixed geometry inlet is sized for the design operating Mach number. As the inlet velocity (rotor tip speed) approaches Mach 1 (speed of sound), a fixed geometry inlet cannot swallow all of the air approaching the inlet. As a result, a normal shock wave is formed in front of and diverts flow away from the inlet. This normal shock wave results in subsonic flow into the inlet, an “unstarted” condition, which is not an efficient operating condition for an inlet designed for supersonic flow.

To eliminate the problem of unstarted inlets – i.e., to “start” the inlet – many conventional applications use variable geometry or mass bleed. Our Rampressor uses mass bleed. Because of the

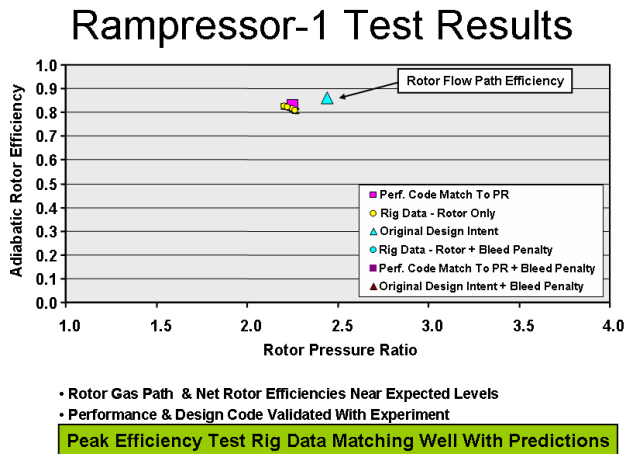


Figure 2. Rampressor Efficiency vs. Pressure Ratio

tremendous centripetal forces acting on the rotating structure, variable geometry (moving parts) is impractical. Mass bleed allows the flow to remain supersonic in the inlet at all times. Once the inlet has been started, the rate of mass removal is drastically reduced to levels that have a small impact on overall efficiency.

Another significant test success was the self-aspiration capability that the Rampressor compressor rig exhibited with no significant decrement in performance. The rig was normally run with supply air above atmospheric pressure to control and monitor flow into the inlet. In one set of experiments, the rig was run disconnected from the pressurized supply source and performance data was taken. The data indicates that no pre-fan stage is required to operate the Rampressor, which will greatly simplify the mechanical and aerodynamic flow path design.

During the test, many different test conditions were run from low pressure ratio/low mass flow to higher pressure ratios/mass flows. The collection of these data points forms the basis for a preliminary compressor map. A key conclusion from our testing was that our performance prediction tools matched the experimental results. The rotor efficiency, pressure ratio, rotor exhaust Mach number and flow angle all closely aligned with the analysis tools. See Figure 2. In addition, our compressor mapping showed that the Rampressor rotor does not exhibit

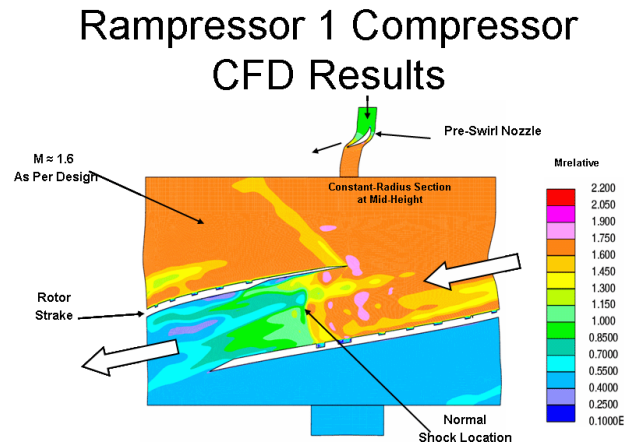


Figure 3. Sample CFD Run of Rampressor Flow Path

any violent surge (or failure to hold pressure ratio) characteristics. In fact, the surge characteristics were quite benign and reversible without having to go to great lengths to re-start the inlets.

After the testing was concluded, the test data was used to anchor or calibrate our CFD models. Once we established that CFD could duplicate the test conditions and results, we could use the CFD models to design the next-generation test rig. Full flow path 3-dimensional viscous modeling was used. See Figure 3. Data from these models agreed with the test data with reasonable assumptions.

Conclusions

Ramgen Power Systems Inc. has completed a series of tests that validate the technological base for a compressor product and for a small gas turbine (800 kW to 5 MW) to generate electricity. Recent compressor tests have successfully demonstrated a number of the fundamental technical requirements that are critical to achieving high efficiency supersonic inlet compression as required for industrial gas compression and engine applications, like fuel cell hybrids. Ramgen will continue to validate the engineering design tools needed to move towards a successful product. These products will leapfrog current technology in terms of higher efficiency, lower cost and lower emissions.

FY 2004 Publications/Presentations

1. Presentation made to AGTSR on the Development of the Rampressor Turbine Concept; Clemson University; Ramgen Document 0900-1069; October 2003
2. Presentation on Ramgen Technology Early Test Results made to DOE Contracting Officers Representative; Ramgen document 0900-1072; December 2003
3. Presentation on Opportunities for Ramgen Technology in Integrated Gasification Combined Cycles made to Ed Parsons - DOE; Ramgen document 0900-1075; presented February 2004
4. Opportunities for Ramgen Technology to Improve the Performance of a Coal Gasification Plant; Ramgen Document 0900-1075; February 2004
5. Paper for Purdue Conference on Ramgen Technology Potential for Refrigeration; Ramgen Document 0800-1093; May 2004
6. Paper for ASME conference; Ramgen Document 0800-1094; May 2004
7. Ramgen Business Plan; Ramgen Document 0800-1089; June 2004

Special Recognitions & Awards/Patents Issued

1. Provisional Patent application submitted for Supersonic Gas Compression with Integrated Heat Recovery; Ramgen Case Number RPS-3101; April 30, 2004

Acronyms & Abbreviations

°C	Degrees Celsius	BTU	British thermal unit
°F	Degrees Fahrenheit	BYZ	Barium zirconium yttrium oxide
1-D	One-dimensional	C	Carbon
3-D	Three-dimensional	Ca	Calcium
8YSZ	8% Doped yttria-stabilized zirconia	CaF ₂	Calcium fluoride
A	Ampere	cc/min	Cubic centimeters per minute
A/cm ²	Amps per square centimeter	CCVD	Combustion chemical vapor deposition
AC	Alternating current	Cd	Cadmium
AES	Auger electron spectroscopy	Ce	Cerium
AFM	Atomic force microscope	CeO ₂	Ceric oxide
Ag	Silver	CERCANAM	Ceramatec Castable Nano Material
AGTSR	Advanced Gas Turbine Systems Research	CFD	Computational fluid dynamics
AICHE	American Institute of Chemical Engineers	cfm	Cubic feet per minute
AL	Application load	CH ₄	Methane
Al ₂ O ₃	Alumina, aluminum oxide	CHEX	Cathode air heat exchanger
ANSI	American National Standards Institute	CHP	Combined heat and power
APS	Atmospheric plasma spray	cm	Centimeter
APU	Auxiliary power unit	cm/s	Centimeters per second
Ar	Argon	cm ²	Square centimeter
ASME	American Society of Mechanical Engineers	cm ³	Cubic centimeter
ASR	Area specific resistance	CO	Carbon monoxide
ASTM	American Society for Testing and Materials	Co	Cobalt
atm	Atmosphere	CO ₂	Carbon dioxide
ATR	Autothermal reforming	CO ₃ ⁻	Carbonate ion
Au	Gold	COR	Contracting Officer's Representative
AVC	Advanced vortex combustor	CPG	Cummins power generation
Ba	Barium	CPOX	Catalytic partial oxidation
BaF ₂	Barium flouride	Cr	Chromium
BaO	Barium oxide	Cr ₂ O ₃	Chromic oxide
BaZrO ₃	Barium zirconate	CrO ₃	Aluminum oxide
BGL	British Gas Lurgi	CSZ	Calcia-stabilized zirconia
BOM	Bill of material	CTE	Coefficient of thermal expansion
BOP	Balance of plant	CTP	Core technology program
BOPS	Balance of plant subsystem	Cu	Copper
		CuO	Cupric oxide
		CVD	Chemical vapor deposition
		DC	Direct current

DCFC	Direct carbon fuel cell	GE	General Electric
DFC	Direct Fuel Cell	GHSV	Gas hourly space velocity
DFC/T [®]	Direct Fuel Cell/Turbine [®]	GHz	Gigahertz
DGA	Di-gluonic acid	GJ	Gigajoule
DIR	Direct internal reforming	GPa	Gigapascal
DMS	Dimethyl sulfide	gpm	Gallons per minute
DMU	Dimethyl urea	GT	Gas turbine
DOE	U.S. Department of Energy	GTI	Gas Technology Institute
e ⁻	Electron	GUI	Graphical user interface
EC	Electrochemical	h	Hours
EDS	Energy dispersive x-ray	H ₂	Diatomic hydrogen
EDX	Energy dispersive x-ray	H ₂ O	Water
EEA	Electrode electrolyte assembly	H ₂ O/C	Ratio of steam to carbon
EIS	Electrochemical impedance spectroscopy	H ₂ S	Hydrogen sulfide
EMI	Electromagnetic interference	He	Helium
EOS	Equation of state	HF	High frequency
EPRI	Electric Power Research Institute	HHV	Higher heating value
Er	Erbium	HPD	High power density
EuC ₂	Europium dicarbide	hr	Hour
eV	Electron volts	hrs	Hours
EVD	Electrochemical vapor deposition	HRSRG	Heat recovery steam generator
EXAFS	Extended x-ray absorption fine structure	HRTEM	High-resolution transmission electron microscopy
F	Fluorine	HTXRD	High-temperature x-ray diffraction analysis
FCE	FuelCell Energy, Inc.	HV	High voltage
FCT	Fuel Cell Technologies	Hz	Hertz
Fe	Iron	I	Current
FEA	Finite element analysis	IC	Interconnection
FeO	Ferrous oxide	ICM	Integrated Component Manifold
FID	Flame ionization detector	IEEE	Institute of Electrical and Electronics Engineering
ft ³	Cubic feet	IGCC	Integrated Gasified Combined Cycle
FTIR	Fourier transform infrared	IGFC	Integrated Gasified Fuel Cell
FTIRES	Fourier transform infrared emission spectroscopy	IPM	Isopropyl mercaptan
FY	Fiscal year	IR	Infrared
g	Gram	IR-SOFC	Intermediate-temperature solid oxide fuel cell
g/cc	Grams per cubic centimeter	i-V	Current-voltage
Ga ₂ O ₃	Gallium oxide	J	Current density
Gd	Gadolinium	K	Kelvin
GDC	Gadolinia-doped ceria		

kA/m ²	Kiloamperes per square meter	LSNF 6419	((La _{0.6} Sr _{0.4})(Ni _{0.1} Fe _{0.9})O _{3-δ})
kcal	Kilocalorie	LSXF	((La _{1-X} Sr _X)(Fe _{1-Y} M _Y)O _{3-δ})
kcal/mol	Kilocalories per mole	LSZF 6419	((La _{0.6} Sr _{0.4})(Zn _{0.1} Fe _{0.9})O _{3-δ})
keV	1000 electron volts	LTE	Local thermal equilibrium
kg	Kilogram	LuC ₂	Lutetium dicarbide
khrs	1000 hours	LV	Low voltage
KHz	Kilohertz	m	Meter
kW	1000 ohms	m/s	Meters per second
kW	Kilowatt	m ² /g	Square meters per gram
kWe	Kilowatt electric	M ₂ CO ₃	Carbonate salt electrolyte. Lithium carbonate (Li ₂ CO ₃), potassium carbonate (K ₂ CO ₃), sodium carbonate (Na ₂ CO ₃), or a mixture of these.
kWh	Kilowatt-hour		
kWt	Kilowatt thermal		
La	Lanthanum		
LaAlO ₃	Lanthanum aluminite	mA/cm ₂	Milliamperes per square centimeter
LaCoO ₃	Lanthanum cobaltite	MCFC	Molten carbonate fuel cell
LaCrO ₃	Lanthanum chromite	MD	Molecular Dynamics
LaMnO ₃	Lanthanum manganite	MEA	Membrane electrode assembly
lb	Pound	Mg	Magnesium
lbm/sec	Pound mass per second	MgO	Magnesium oxide
LBNL	Lawrence Berkeley National Laboratory	MIEC	Mixed ionic and electronic conduction
LDC	Ce _{0.6} La _{0.4} O ₂ - Lanthanum-doped ceria	MJ	Megajoules
LF	Low frequency	ml/min	Milliliters per minute
LFA	Laser flash diffusivity analysis	μm	Micrometer, micron
LHV	Lower heating value	mm	Millimeter
Li ₂ CO ₃	Lithium carbonate	mm ²	Square millimeters
Li ₂ O	Lithium oxide	Mn	Manganese
LnC ₂	Lanthanide, where Ln is any element in the lanthanide series	Mn ₂ O ₃	Manganese oxide
LP	Liquefied petroleum	mol	Mole
LPG	Liquefied petroleum gas	mol%	Molar percent
LSC	Lanthanum strontium cobaltite	mol/s	Moles per second
LSCF	Lanthanum strontium cobalt ferrite	MOSFET	Metal-oxide-semiconductor field-effect transistor
LSF	Lanthanum strontium ferrite	MPa	Megapascal
LSF 40	((La _{0.6} Sr _{0.4})(FeO _{3-δ}))	MRS	Materials Research Society
LSGM	Lanthanum strontium magnesium gallate	MRSI	Materials and Systems Research, Inc.
LSGMF	Lanthanum strontium magnesium gallate ferrite	mV	Millivolt
LSM	Lanthanum strontium manganate	MW	Megawatt
		mW	Milliwatt
		mW/cm ²	Milliwatts per square centimeter

N ₂	Diatomic nitrogen	ppbv	Parts per billion by volume
N ₂	Nitrogen	ppm	Parts per million
N ₂ O	Nitrous oxide	Pr	Praseodymium
Na	Sodium	PSF 40	((Pr _{0.6} Sr _{0.4})(FeO _{3-δ}))
NaOH	Sodium hydroxide	psi	Pounds per square inch
NASA	National Aeronautics and Space Administration	psia	Pounds per square inch absolute
Nb	Niobium	psid	Pounds per square inch differential
NETL	National Energy Technology Laboratory	PSNF 6419	((Pr _{0.6} Sr _{0.4})(Ni _{0.1} Fe _{0.9})O _{3-δ})
NG	Natural gas	PSOFC	Planar solid oxide fuel cell
Ni	Nickel	PSZ	Partially stabilized zirconia
NiO	Nickel monoxide	Pt	Platinum
NLEIS	Nonlinear electrochemical impedance spectroscopy	PVD	Physical vapor deposition
nm	Nanometer	Q1	First quarter
NO _x	Oxides of nitrogen	Q2	Second quarter
O ₂	Diatomic oxygen	Q3	Third quarter
O ₂ /C	Oxygen to carbon ratio	Q4	Fourth quarter
OCP	Open circuit potential	QM	Quantum mechanics
OCV	Open circuit voltage	ReaxFF	First Principles-Based Reactive Force Fields
ORNL	Oak Ridge National Laboratory	Rh	Rhodium
P	Pressure	ROEB	Reactive oxide electron beam
P&IDs	Piping and instrumentation drawings	RPM	revolutions per minute
PAM	Process air module	RUS	Resonant ultrasound spectroscopy
PC	Personal computer	s	Second
PCFC	Proton ceramic fuel cell	S	Sulfur
PCS	Power conditioning system	S/C	Steam to carbon ratio
PCU	Power conditioning unit	S/cm	Siemens per centimeter
PD	Power density	SBDCFC	Spouted bed direct carbon fuel cell
PEAC	Power Electronics Applications Center	SBE	Spouted bed electrode
PEM	Proton exchange membrane	SBIR	Small Business Innovation Research
PEN	Positive-electrolyte-negative	Sc	Scandium
PES	Power Electronics subsystem	sccm/min	Standard cubic centimeters per minute
PLD	Pulsed laser deposition	SDC	Samaria-doped ceria
PNNL	Pacific Northwest National Laboratory	sec	Second
PO ₂	Partial pressure of oxygen	SECA	Solid State Energy Conversion Alliance
POH	Partial oxidation of hydrocarbons	SEM	Scanning electron microscopy
POX	Partial oxidation	Si	Silicon
		SiC	Silicon carbide
		SIMS	Secondary ion mass spectrometry

SiO _r	Silicon dioxide	Ti	Titanium
Sm	Samarium	TIG welding	Gas Tungsten Arc welding
Sn	Tin	TPB	Triple-phase boundary
SO ₂	Sulfur dioxide	TPD	Temperature-programmed desorption
SOFC	Solid oxide fuel cell	TSOFC	Tubular solid oxide fuel cell
SOFCo	SOFCo-EFS Holdings LLC	UCC	Ultra Clean Coal
SORFC	Solid oxide regenerative fuel cell	UU	University of Utah
SPU	Stationary power unit	V	Vanadium
SPWM	Sinusoidal pulse width modulation	V	Volt
SR	Steam reforming	vol%	Volume percent
Sr	Strontium	W	Watt
SrTiO ₃	Strontium titanate	W/cm ²	Watts per square centimeter
SS	Stainless steel	W/m/K	Watts per meter per Kelvin
SSA	Specific surface area	wt	Weight
SSC	Strontium samarium cobalt oxide	wt%	Weight percent
SUNY	State University of New York	WVU	West Virginia University
SV	Space velocity	XANES	X-ray absorption near edge spectroscopy
SVHA	Spouted vessel hydrodynamics apparatus	XPS	X-ray photoelectron spectroscopy
SVM	Space vector modulation (modulation strategy for DC AC inverter)	XRD	X-Ray diffraction
SWPC	Siemens-Westinghouse Power Corporation	Y	Yttrium
T	Temperature	Y ₂ O ₃	Yttrium oxide
TBM	Tert-butyl mercaptan	yr	Year
TCD	Thermal conductivity detector	YST	Y-doped SrTiO
TEC	Thermal expansion coefficient	YSZ	Ytria-stabilized zirconia
TEM	Transmission electron microscopy	ZnO	Zinc oxide
TERS	Tip-enhanced Raman scattering	Zr	Zirconium
Tg	Glass transition temperature	ZrO ₂	Zirconium dioxide
TGA	Thermogravimetric analysis	Ω	Ohm
THT	Tetrahydrothiophene	Ωcm ²	Ohm centimeter squared

Primary Contact Index

A

Adler, Stuart B. 119
 Alptekin, Gokhan 318
 Armstrong, Tad J. 285, 289

B

Barnett, Scott A. 147, 309
 Berry, David A. 135
 Bessette, Norman 11
 Bobba, Rambabu 314
 Borup, Rodney L. 128
 Brogan, J. 294

C

Calo, J. M. 267
 Carlson, Eric J. 178
 Chou, Yeong-Shyung "Matt" 81
 Chuang, Steven S. C. 321
 Cocks, F. H. 278
 Cooper, John F. 240

E

Elangovan, S. (Elango) 44, 271
 Enjeti, Prasad 157

G

Gardner, Todd H. 138
 Gemmen, Randall 66
 Ghezel-Ayagh, Hossein 219
 Goddard, William III 231
 Gopalan, Srikanth 257

K

Khaleel, Mohammad A. 173
 Kim, Ilwon 47
 King, David L. 85
 Koopman, Aaron 329
 Kornhauser, Alan A. 323
 Krumpelt, Michael 39, 125

L

Lai, Jih-Sheng (Jason) 161
 Lanning, Bruce 105
 Lara-Curzio, Edgar 75

Liu, Meilin 55, 281
 Loehman, Ronald E. 101

M

Marina, Olga 90
 Maru, Hans C. 209
 Mazumder, Sudip K. 191
 McElroy, Jim 236
 Meier, Gerald H. 109
 Minh, Nguyen 27, 51, 199, 223

N

Nair, Balakrishnan 274
 Norrick, Daniel 15

O

Ozpineci, Burak 153

P

Pal, Uday B. 262
 Patel, Pinakin 23
 Pederson, LR 245
 Pierre, Joseph F. 213

Q

Qu, Jianmin 167

S

Seabaugh, Matthew M. 299, 302, 305
 Shaffer, Steven 19
 Shekhawat, Dushyant 141
 Simner, Steve 93
 Swartz, Scott L. 71

V

Virkar, Anil V. 115, 203, 251
 Visco, Steven J. 61
 Vora, Shailesh D. 33

W

Wachsman, Eric D. 183

Y

Yang, Zhenguo "Gary" 97

